Controlling surface mediated insulin aggregation by peptides and light

Karim Chouchane

Communauté
UNIVERSITÉ Grenoble Alpes

THÈSE

Pour obtenir le grade de

DOCTEUR DE LA COMMUNAUTÉ UNIVERSITÉ GRENOBLE ALPES

Spécialité : Physique pour les Sciences du Vivant

Arrêté ministériel : 25 mai 2016

Présentée par

Karim CHOUCHANE

Thèse dirigée par **Franz BRUCKERT** et
codirigée par **Marianne WEIDENHAUPT**

Préparée au sein du **Laboratoire des Matériaux et du Génie Physique (LMGP)**
dans **l'École Doctorale de Physique**

Contrôler l'agrégation de l'insuline à la surface des matériaux via des interactions avec des peptides et la lumière

Thèse soutenue publiquement le **« 20 Octobre 2017 »**,
devant le jury composé de :

Mme. Christelle Hureau
Laboratoire de Chimie de Coordination, Rapporteur
Mr. André Matagne
Université de Liège, Rapporteur
Mr. Olivier Gallet
Universite de cergy pontoise, Président
Mme. Anja Böckmann
Institut de Biologie et Chimie des Protéines, Examinateur
Mr. Alain Buisson
Grenoble-Institut des Neurosciences, Examinateur
Mr. Vincent Forge
Institut de Biosciences et Biotechnologies de Grenoble, Examinateur
Mr. Alexandre Specht
Laboratoire de conception et application de molécules Bioactives, Examinateur
Mr. Arnaud Ponche
Institut de Science des Matériaux de Mulhouse, Examinateur

Table of contents

List of abbreviations

HI: Human Insulin
LIA: Light Induced Aggregation
ThT: Thioflavin T
GISAXS: Grazing Incidence Angle Small Angle X-ray Scattering
TAMRA: tetrametylrhodamine
FRET: Forster Resonance Energy Transfer
LMGP: Laboratoire des Matériaux et du Génie Physique
AFM: Atomic Force Microscopy
rpm: revolutions per minute
λ_{ex} : fluorophore excitation wavelength at peak fluorescence
λ_{em}: fluorophore emission wavelength at peak fluorescence
A_{λ}: Absorbance at the wavelength λ
Aβ: Amyloid beta
ANS: 8-Anilinonaphthalene-1-sulfonic acid
GFP: Green Fluorescent Protein
DMDCS: Dimethyldichlorosilane
WCA: Water Contact Angle

Vector notation: in this thesis the vectors are not represented in bold but accented by a right arrow. In the text bold is used to note the variables used in the equations regardless of their tensor order.

1 Introduction

1.1 General introduction

Before the 1980's, protein extraction from living organisms was the only way to obtain proteins. Biotechnology now provides ways to produce, purify and engineer proteins at large scale benefiting both research and the pharmaceutical industry. The development of protein based drugs allows the multiplication of novel treatments presenting improved efficiency and reduced side effects.

The problematics of protein stability and aggregation are complex issues addressed in numerous scientific, industrial, and medical fields. If the cost of proteins have been tremendously reduced, their value is still high, explaining the need for a minimization of protein losses during their processing. In vitro studies on protein aggregation are not only means to understand and improve therapeutic protein stability, they are also invaluable ways of understanding the more complex aggregation phenomena occurring in vivo. In this work we will focus on the amyloid aggregation of human insulin at material surfaces. This protein is an invaluable model because of its considerable therapeutic value, the large amount of literature available and the possible exploitation of its fibrils for nanotechnology[1].

1.2 Protein prolegomenon

1.2.1 Amino acids and peptides

Amino acids are organic molecules possessing both a carboxylic acid and an amine group, the first being the reference group for the denomination of the carbons in the chain. The first carbon in the chain attached to the carboxylic group is therefore named the α-carbon, the second the β-carbon, etc. Since the amine (or secondary amine in the case of proline) function of all proteogenic amino acids is attached to the alpha carbon they are referred as alpha amino acids. The α-carbon of all proteogenic amino acids except glycine are stereogenic centers, these amino acids can therefore exist under two enantiomers referred by convention as L or D by analogy with respectively the levorotatory and dextrorotatory enantiomers of glyceraldehyde:

(Chem. Eq. I)

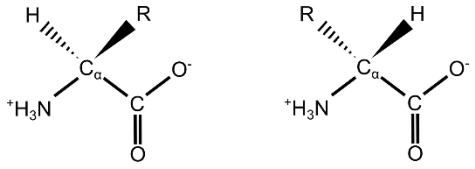

L amino acid D amino acid

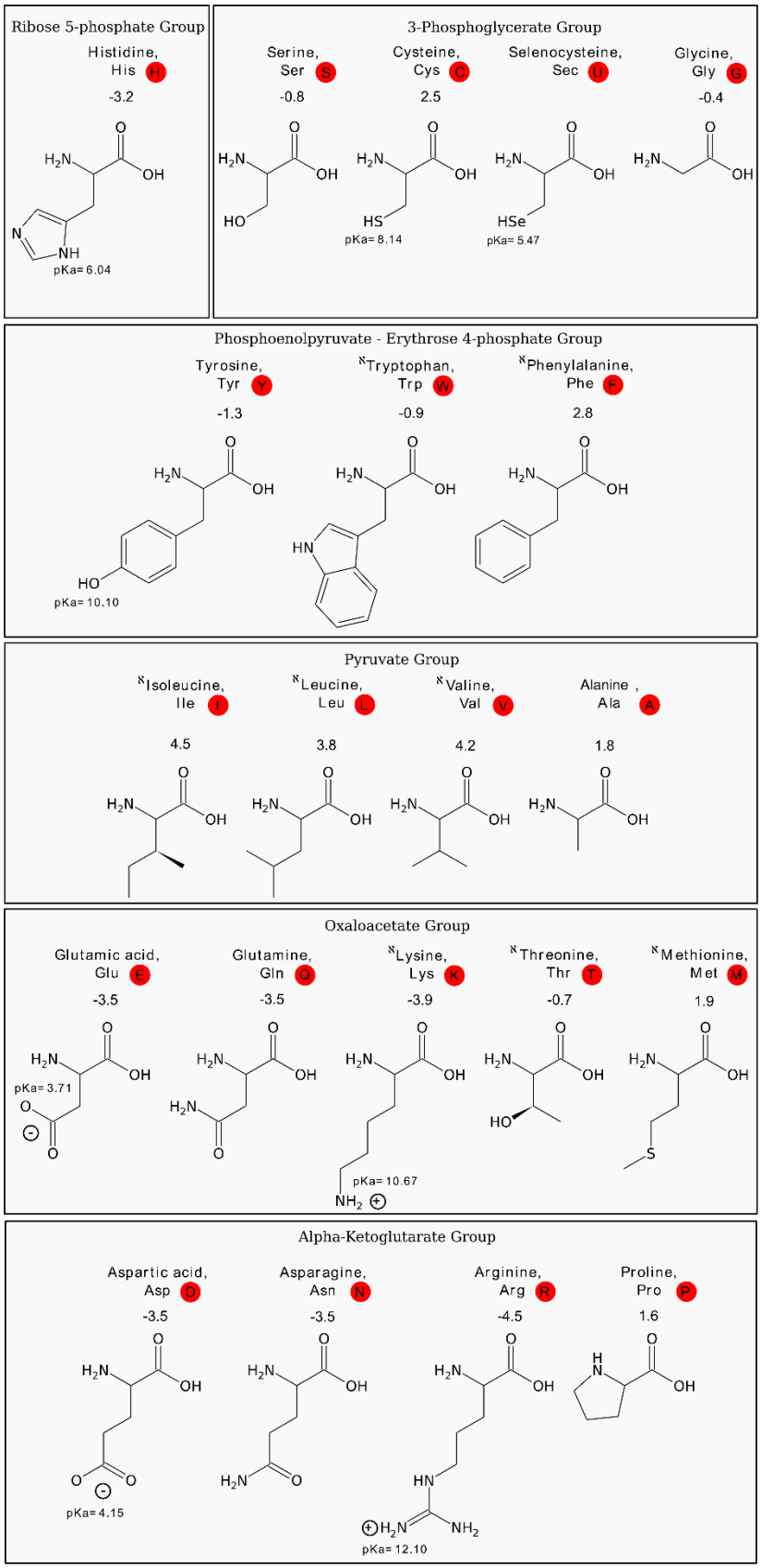

Figure 1. The 21 proteinogenic amino acids. Classified according to their anabolic pathway in animals, including hydrophobicity index[2], pKa of side chains, ϰ: essential amino acids for *Homo sapiens*[3]**.**

This system is more relevant in biology than the Cahn–Ingold–Prelog sequence rules which gives group priorities based on their atomic number and therefore affects the opposite conformation to cysteine and selenocysteine[4].

Only L enantiomers can be inserted into proteins even though some D amino acids can be formed in proteins by post translational modifications[5].

In vivo, individual amino acids play roles in a wide range of biological functions (neurotransmitters, toxins[6], nitrogen metabolism, etc.) and are used as building blocks for the synthesis of peptides and proteins via the formation of peptide bonds. This peptide bond consists in the condensation of the carboxylic group of amino acid n with the amine group of amino acid n+1 liberating one H_20 and forming a covalent bond:

(Chem. Eq. II)

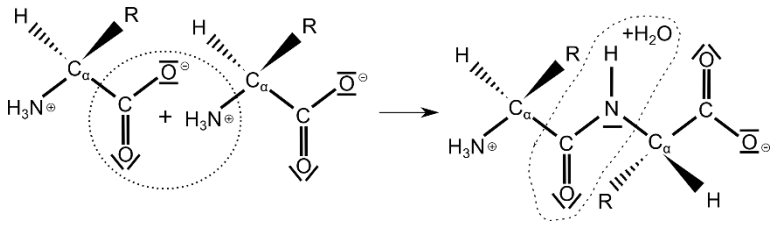

The resulting heteropolymeric chain of amino acids is referred to as a peptide. The diversity of peptides arisen from the combination of multiple and diverse amino acids results in the multiplication of the biological functions in which peptides are involved (toxins, cell wall, hormones, neurotransmitters, etc.). In water the peptide bond formation is thermodynamically disfavored and is spontaneously hydrolyzed even if this reaction rate is very slow under physiological conditions. In living organisms, peptides can be synthesized in multiple ways usually classified as the ribosomal and the non-ribosomal ways. But peptides can also be synthesized in vitro, particularly thanks to solid-phase synthesis[7] allowing the design of specific peptides for research or industrial applications.

1.2.2 Protein description and structure

Proteins are biological macromolecules, consisting in at least one linear heteropolymeric chain of L-α-amino acids linked together by peptide bonds. They are synthetized in vivo by the ribosomes[3,8] from the 21 proteogenic amino acids (22 including Pyrrolysine limited to some methanogenic eubacteria and archaea or 23 including N-Formylmethionine) which are represented in Figure 1. Protein structure can be described at 4 different levels. The primary structure, consisting in the raw sequence of the amino acids, is conventionally written from the N terminus to the C terminus corresponding to the translation order of the protein.

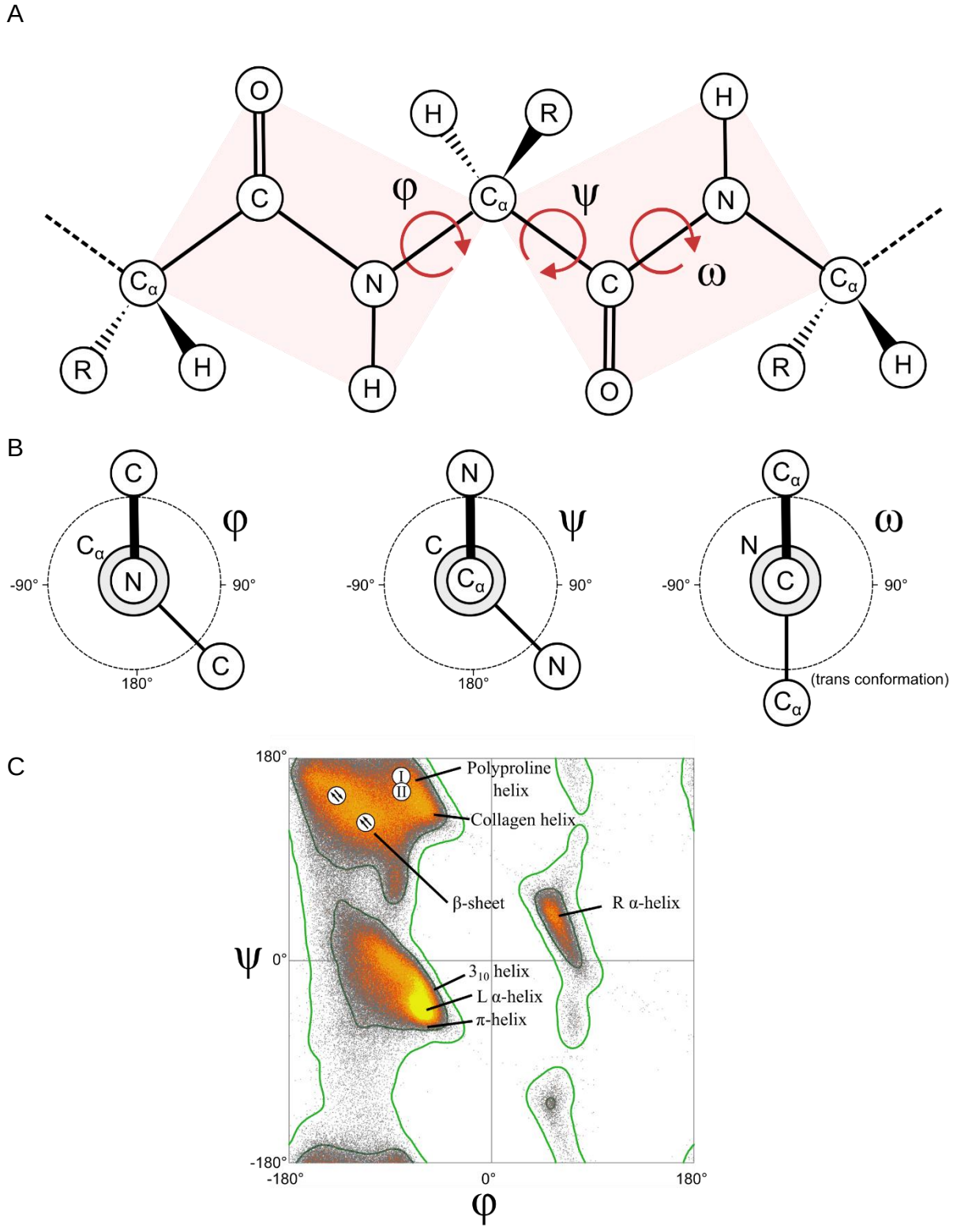

Figure 2. Principle of protein secondary structure. A: Definition of the rotation axes for the angles φ, ψ and ω; B: Convention usually used for the values of φ, ψ and ω angles; C: Ramachandran plot showing domains of specific secondary structures: parallel beta-sheet Ⓢ, antiparallel beta-sheet Ⓢ, polyproline I helix Ⓘ, polyproline II helix Ⓘ. In α-sheet the dihedral angles are not constant but alternate between R α-helix and D α-helix. (C: Modified from Jane S. Richardson, Proteopedia url: http://proteopedia.org/wiki/index.php/Ramachandran_Plots).

The secondary structure consists in the 3 dimensional arrangement of the dihedral angles between the atoms in the backbone of the chain. There are 3 dihedral angles defined for each residue as φ, ψ and ω (except for the C-terminal amino acid, lacking an ω dihedral angle)[9]. The peptide bond is planar because of its stabilization by mesomerism, resulting from the delocalization of the lone pair of electrons of the nitrogen atom:

(Chem. Eq. III)

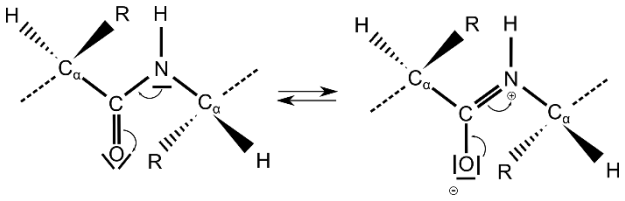

This bond is therefore not free to rotate but isomerizes between cis (ω =0°) and trans (ω =180°) conformations. On the other hand φ and ψ angles are not fixed and are free to adopt preferential values. A Ramachandran plot [10] represents the distribution of the combination of angles φ and ψ adopted by each amino acid in protein structures (Figure 2).

The most common secondary structures found in proteins are α-helices and β-sheets which are described in Figure 3. In the α-helix all the backbone forms a helical motif with 3.6 residues per turn, while all the side chains are exposed on the outer side. The structure is stabilized by the formation of hydrogen bonds between the C=O group of the amino acid *i* and N-H group of the amino acid *i+4* ($N_{i+4} \rightarrow O_i$). In the R_h nomenclature (where **R** is the number of residue per turn and **h** is the number of atoms in the ring formed by the atoms around each hydrogen bond), this motif is called a 3.6_{13} helix. Other less common similar helices include the 3_{10} helix and the π-helix (or 4.4_{16} helix) with respectively $N_{i+3} \rightarrow O_i$ and $N_{i+5} \rightarrow O_i$ hydrogen bonding. Due to the steric constraints of the side chains, α-helices must be left-handed except for polyglycine helices, which can seldom adopt the right-handed conformation.

In the β-strands the backbone forms a planar structure with the side chains exposed alternatively towards the upper side and towards the down side corresponding in an approximative 180° angle change in the orientation of the side chain between each residue. This motif is laterally stabilized by the formation of hydrogen bonds, perpendicular to the side chains, between β-strands. The structure formed by this assemblage of beta strands is referred to as a β-sheet. As the two β-strands can belong to distant parts of the peptide chain or even to different peptide chains (**intermolecular β-sheet**) the orientation of the two strands ($N_{term} \rightarrow C_{term}$) can either be identical (**parallel β-sheet**) or in opposite direction (**antiparallel**

β-sheet). As a result the hydrogen bonding between the amino acids of the two strands can either be regular in the case of an antiparallel β-sheet (meaning that each amino acid is bound only to one amino acid of the opposite strand) or in quincunx for a parallel β-sheet meaning that each amino acid is bound to two amino acids of the opposite strand.

Beside these two common strand motives an atypical and energetically unfavorable motif deserves here a description, the polar pleated sheet or simply α-sheet consisting in an assemblage of strands somewhat similar to the beta strand but in which all the C=O are exposed in the same direction with N-H towards the opposite direction inducing a polarity of the sheet. Although seldom found in native proteins, the alpha-strand has been proposed as an intermediate conformation between the helices and intermolecular β-sheets in the amyloidogenesis process and is present in the native structure of the lysozyme of hen egg white[11] (The fully reduced form of hen egg white lysozyme can form amyloid fibrils[12] and homologous proteins are amyloidogenic).

Other specific or local secondary structures can also be found such as turns, polyproline I helix or polyproline II helix and their polyglycine analogue. Secondary motives can even assemble into super-secondary structures such as coiled coils, beta helix, etc.

The tertiary structure represents the overall 3-dimensional structure of the protein including the orientation of the side chains and the arrangement into structural domains. Eventually, the functional proteins often consist in an assemblage of several protein subunits. This assemblage into multimeric complexes is described by the quaternary structure.

1.2.3 Proteins in a biological context

Proteins are the principal class of biologically active macromolecules, and play a wide range of roles in vivo. They are with the ribozymes the only biological molecules able of biocatalysis (enzymes), they compose the cytoskeleton, the (animal) extracellular matrix as well as the membrane channels (for a review see [13]). In eukaryotes, the genes encoded in the nuclear DNA are transcribed into messenger RNA which are then exported from the nucleus via nuclear pores to the cytoplasm where they are translated into protein by the ribosomes.

Post-translational modifications are all the modifications that newly synthetized proteins undergo. They can affect the sequence by peptide cleavage (in particular signal peptides), amino acid modifications, cross-linking of amino acids (essentially disulfide bonds between two cysteine residues), termini modifications and even the rare event of chromophore formation (in the green fluorescent protein family).

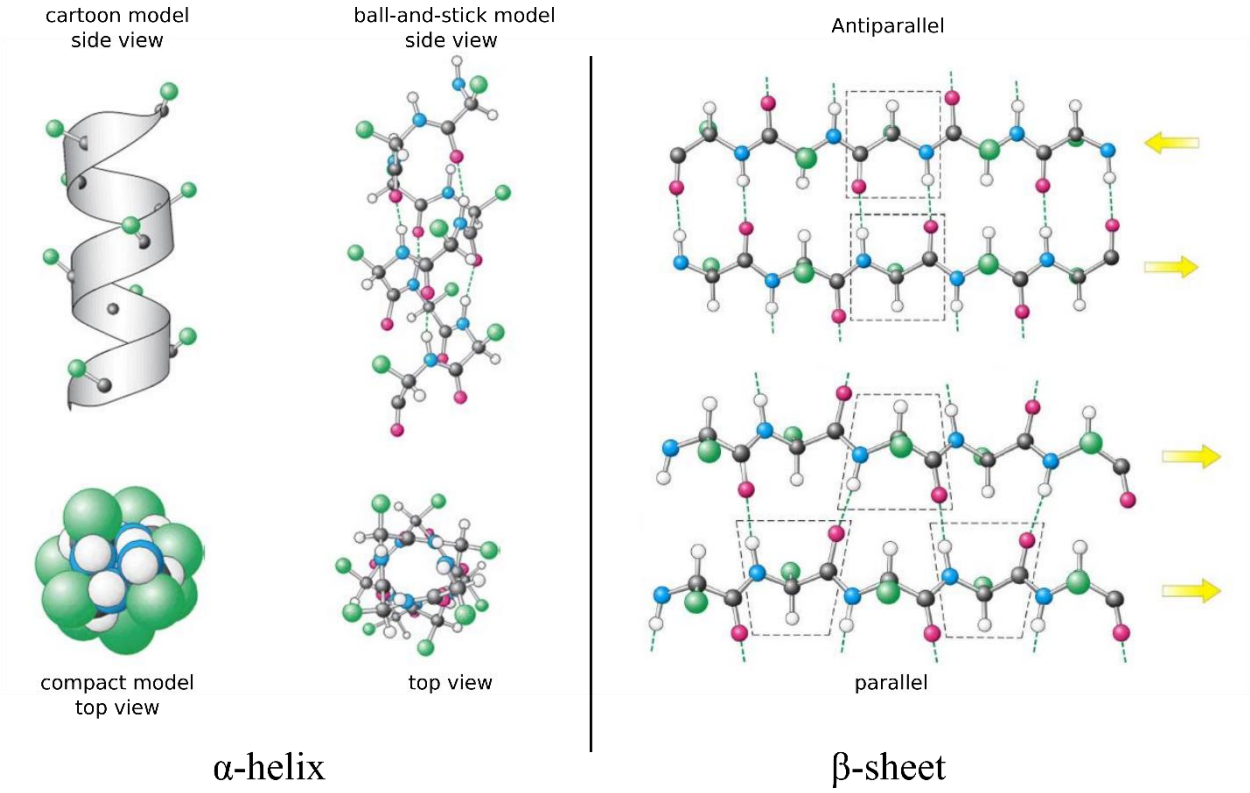

Figure 3. Structure of the α-helix and β-sheet. CPK atom coloring (modified from Berg et al.[14]).

1.2.4 Proteins in solution

The behavior of proteins in solution apart from their structural conformation, can be affected by the physico-chemical conditions of the solution (temperature, pH, ionic strength, etc.). Macromolecules in solution diffuse in random walk by Brownian motion[15]. Fick's first law describes the flux of a solute of local concentration φ as:

$$J = -D \cdot \nabla\varphi$$

With D representing the diffusivity of the macromolecules. The Stokes–Einstein equation defines the diffusivity for spherical particles in low Reynolds number liquids as:

$$D = \frac{k_b T}{6\pi\mu r}$$

Were $\mathbf{k_b}$ is the Boltzmann constant, **T** is the temperature and **μ** is the dynamic viscosity and **r** is the radius of the diffusing sphere. The diffusivity defines the rate at which a particular molecule can interact with other molecules in solution. In solution, protein assembly can lead to the formation of high molecular weight species. If the Brownian motion is not sufficient to maintain these oligomers in solution, they sediment.

At high protein concentration (typically concentrations observed in living cells ∽ 300 mg/ml)[16], the high exclusion volume in the solution leads to a drastic reduction of the volume accessible to a protein and therefore to an increase of their thermodynamic activity*, a phenomenon known as **macromolecular crowding**. These conditions, present in the living cell, can enhance protein aggregation[17–20].

1.3 Protein folding

1.3.1 Non covalent interactions in proteins

Functional groups from the side chains as well as the backbones of proteins are subject to intramolecular and intermolecular non covalent interactions. These interactions can be either electrostatic interactions, steric interactions or effects resulting from the solvent properties. They can be defined by their energy and by the way this energy varies as a function of the distance between interacting atoms[21].

Force and energy of interactions

The work (**W** in joules) of a force ($\vec{F}$ in Newton) applied to an object corresponds to the contribution of this force to the displacement of this object.

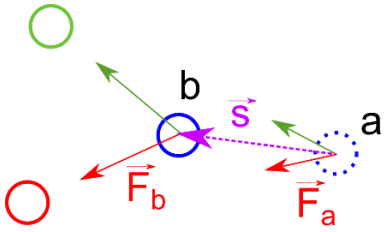

Figure 4. Scheme of the forces exerted by a green and a red particle on a blue particle throughout its displacement $\vec{s}$ from the point a to the point b. $\vec{F}_a$ and $\vec{F}_b$ represent the force exerted by the red particle on the blue particle at the position a and b, respectively.

On the example presented in Figure 4, the amount of work exerted by the red particle on the blue particle during its displacement from the point **a** to the point **b** corresponds to the scalar product of the force by the infinitesimal displacement vector (in meters) integrated over the displacement:

$$W_{red\ on\ blue} = \int_a^b \vec{F}_i \cdot d\vec{s}$$

* **Thermodynamic activity:** Effective concentration of a chemical species in solution

The energy of the red-blue interaction (in J) corresponds to the amount of work of the $\vec{F}$ force during a displacement of the blue particle from infinity to the point b:

$$E_{red-blue} = \int_{\infty}^{b} \vec{F}_i \cdot d\vec{s}$$

The total energy of the interaction represented in Figure 4 therefore corresponds to the amount of energy necessary to displace the blue particle from b to infinity given the present force field:

$$E_{tot} = E_{red-blue} + E_{green-blue} = \int_{\infty}^{b} \vec{F}_i \cdot d\vec{s} + \int_{\infty}^{b} \vec{F}_i' \cdot d\vec{s}$$

The force field of a system hence defines its energy state.

State functions

A state function represent a property of a system which is independent from the path by which the system gets to the current position. Here we will briefly review 4 important state functions for protein folding thermodynamics: internal energy, enthalpy, entropy and Gibbs free energy.

The variation of **internal energy** (**ΔU**) of a system is the difference between heat (**Q**) absorbed by this system and work (**W**) done by this system:

$$\Delta U = Q - W$$

All quantities are expressed in joules. **U** is a state function of all the energy contained in the system, in particular it contains the energy defined by internal force fields but not the energy defined by external force fields nor the kinetic energy of the whole system. Another state function the Enthalpy (H in joules) is defined by

$$H = U + PV$$

With **P** the pressure in $J.m^{-3}$ and **V** the volume in m^3 of the system.

Entropy (**S**) which is not expressed in joules but in $J.K^{-1}$ is a state function related to the number of available configurations for a system at that state:

$$S = k_B \cdot \ln(\Omega)$$

With **Ω** the number of equiprobable states and k_B the Boltzmann constant in $J.K^{-1}$.

In thermodynamics one fundamental question is to address whether a chemical process is spontaneous in given conditions, we will therefore use the **Gibbs free energy** (**G**) defined by:

$$G = \mathrm{H} - \mathrm{T}\,\mathrm{S}$$

The change in Gibbs free energy is the variation of energy observed through a transformation at constant pressure and temperature which is relatively appropriate for biological systems. It is given by:

$$\Delta G = \Delta \mathrm{H} - \mathrm{T}\,\Delta S$$

where **ΔH** is the change in enthalpy (expressed in J), **ΔS** is the change in entropy (expressed in $J.K^{-1}$) and **T** the absolute temperature in Kelvin. A negative **ΔG** is necessary for a process to be spontaneous at constant temperature and pressure.

Electrostatic interactions

The electrostatic interaction is one of the 4 fundamental interactions. The Coulomb's law describes forces between two static charges as:

$$\overrightarrow{\mathrm{F}_{ij}} = \frac{1}{4\pi\varepsilon_0}\frac{Z_i \cdot Z_j}{r^2}\vec{r}$$

Were $\overrightarrow{\mathbf{F_{ij}}}$ is the electrostatic force of a charged particle ***i*** presenting a charge $\boldsymbol{Z_i}$ on a charged particle ***j*** presenting a charge $\boldsymbol{Z_j}$, $\boldsymbol{\varepsilon_0}$ is the vacuum permittivity. The amount of work required to bring the charged particle from infinity to the point ***r,*** is the energy of the interaction.

Electrostatic interactions include: hydrogen bonds (in part), charge-charge interactions, charge-induced dipole interactions, π–π stacking, dipole-dipole interactions, dipole-induced dipole interactions and London dispersion forces.

Hydrogen bonds are a particular type of dipole-dipole interaction between a donor and an acceptor group in which the energy of bonding is mainly the output of electrostatic interaction but also, to a lesser extent (typically 10% of total energy), of the sharing of the hydrogen atom[22]. The donor group consist in a hydrogen atom covalently bound to an electronegative atom (typically O or N in proteins) and the acceptor group is another electronegative atom. Hydrogen bonds are stronger as the distance between the two groups is reduced, this distance can be shorter than the sum of the Van Der Waals radii of the two atoms. In proteins, H-bond interaction energy is usually considered to be comprised between 1 and 5 $kcal.mol^{-1}$.

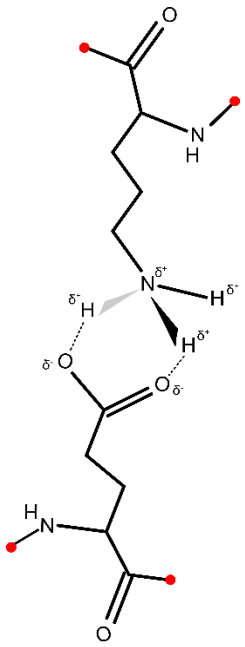

Figure 5. Salt bridge between glutamate and lysine. The global charges (respectively -1 and +1) of the two charged groups are distributed as partial charges between the different atoms leeding to the formation of hydrogen bonds as well as electrostatic interactions between oposite charges. The red dots corespond to the rest of the peptide chain.

Salt bridges are another particular bond found in proteins which involve both a hydrogen bond and an electrostatic interaction between charges. A typical example is the interaction between a primary ammonium group and a carboxylate group (Figure 5). First the global opposite charges of the two groups allow long range interactions, the bridge is then stabilized by one or more H bonds.

	Interaction	Energy	Order of magnitude (kcal.mol^{-1})
	Ion-ion	$E \propto \frac{Z_i \cdot Z_j}{\varepsilon r}$	10-100
	Ion-induced dipole	$E \propto \frac{Z_i \cdot \alpha_j}{\varepsilon r^4}$	1-10
Van Der Waals	Dipole-Dipole (Keesom)	$E \propto \frac{\mu_i \cdot \mu_j}{\varepsilon r^6}$	1
	Dipole induced dipole (Debye)	$E \propto \frac{\mu_i \cdot \alpha_j}{\varepsilon r^6}$	1
	Dispersion (London)	$E \propto \frac{\alpha_i \cdot \alpha_j}{\varepsilon r^6}$	1

Table 1. Orders of magnitude and relation to distance of the energy involved in electrostatic interactions. With Z_i and Z_j the permanent charge of the particles i and j; μ_i and μ_j the partial charges of the particles i and j; α_i and α_j the polarizabilities of the particles i and j; ε is the vacuum permittivity; E the energy of the interaction and r the interparticle distance.

Steric effects

Steric effects result from the overlapping of the electron orbitals of two atoms. As electrons are fermions, they obey to the **Pauli exclusion principle**. Hence each atom occupies its own space volume repulsing other atoms at close distance, a phenomenon known as **steric clash**.

Solvent interactions and hydrophobic effect

As water is a **polar** solvent, water molecules interact with each other via the formation of hydrogen bonds, explaining the strong **cohesion** between them. Similarly polar groups on a macromolecule will also form electrostatic interactions with the surrounding water molecules increasing its **solvation** i.e. the stabilization of the solute species in the solution. The **solvation shell** or hydration shell of a macromolecule is the ensemble of all the water molecules involved in the aqueous interface with this macromolecule.

Nonpolar chemical groups on the other hand do not usually form high energy interactions with the surrounding water molecules, which, as a result, tend to minimize their contact with these groups.

Apart from the enthalpy effect resulting from liquid cohesion, the reduction of entropy associated to the loss of degree of freedom by water molecules, has been proposed as the main source of the hydrophobic effect[23]. The lack of hydrogen bonds between water molecules forming the solvation shell and the nonpolar chemical groups of the macromolecule in solution results in a loss of some degree of freedom for these water molecules and therefore a reduction of entropy[24].

The chemical groups, moieties, molecules or surfaces with which water minimizes contacts are designed as **hydrophobic;** by opposition, charged or polar molecules forming more energetic interactions with water molecules are referred to as **hydrophilic**.

In native protein conformation non-polar side chains tend therefore to be buried in the structure to minimize their contact with water, forming a **hydrophobic core.** The interfacial tension, or **epistructural tension** in the specific case of macromolecules, is defined as the change in free energy per unit area required to envelop a macromolecule with its solvation shell. The computing of the epistructural tension of a protein surface can provide information for the identification of the binding sites or protein interaction sites[25]. Another thermodynamic benefit of dehydration is the protection of electrostatic interaction from water, the energy involved in electrostatic interactions being significantly higher in anhydrous environments[26–28]. In particular the notion of **protein wrapping** and **dehydron** are interesting in order to understand

and predict intermolecular interactions. A dehydron is a part of a protein presenting an electrostatic bond which is in contact with water. As a consequence it will have a tendency to bind ligands in order to increase the wrapping around this electrostatic interaction and therefore minimize its free energy[29].

1.3.2 Protein conformation

In solution, protein conformations are usually defined by the physico-chemical conditions of their environment as their functional groups interact with each other and with the surrounding water. The stability of a protein structure is defined by the energy involved in its internal interactions as well as its interaction with the solvent. Moreover the number of disulfide bonds have a great influence on the protein conformational stability. Proteins with high conformational stability are sometimes referred to as **hard proteins** whereas proteins that are easily deformable upon intermolecular contact or adsorption are referred to as **soft proteins**[30].

1.3.3 Energy landscape and Native folding: Anfinsen's dogma and the Levinthal paradox

One can represent the enthalpy of a protein i.e. the ensemble of the sterically available conformations of this protein for a given free energy level as an energy landscape[31] (Figure 6). In this view the number of available conformations for a protein decreases and these conformational states become separated by energy barriers as the free energy decreases. According to **Anfinsen's thermodynamic hypothesis**, the unfolded proteins emerging from the ribosome fold spontaneously into their native state corresponding to the thermodynamically accessible conformation possessing the lowest free energy[32]. Notable exceptions to this dogma are the **intrinsically disordered proteins**[33–35] which conformations remain unfolded and unstable in physiological conditions.

The **Levinthal's paradox** underlines the tremendous number of conformational possibilities and the impossibility for a protein to screen them all before reaching the most stable one (the lowest in energy). Since the proteins fold spontaneously into their native conformation in relatively short timescales this folding must occur by preferential pathways resulting in the formation of structural domains via **folding intermediates**. The hydrophobic collapse theory then states that intermediate states presenting native-like secondary structures acquire their tertiary conformation through the clustering of nonpolar side chains in the hydrophobic core[36–38]. **Molten globules** are a metastable conformational state in which the proteins conserve a

native-like secondary structure while maintaining dynamic side chains. This state is similar to the intermediate state in protein folding.

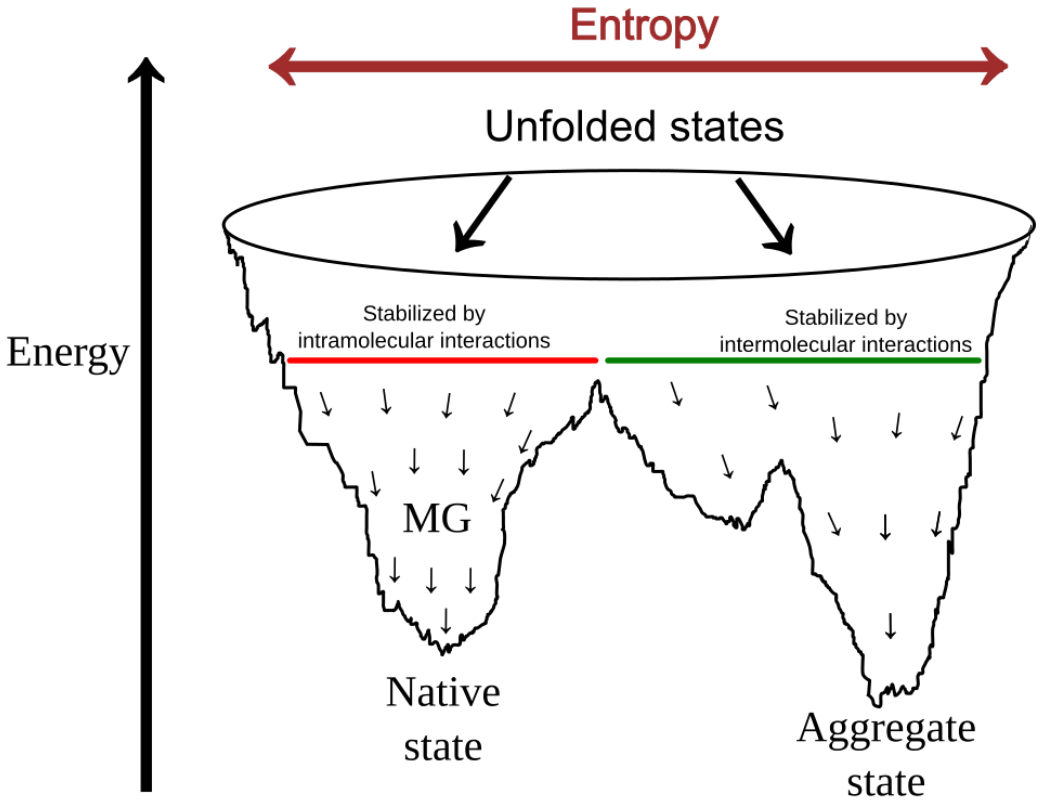

Figure 6. Protein folding funnel. MG: molten globule.

1.4 Protein Stability and Aggregation

Protein stability is the propensity of a protein to maintain its native chemical or conformational structure in a given environment. Stability can be defined at 3 different levels, chemical stability, conformational stability and solution stability. A loss of chemical structure can induce a loss of conformation (partial or total protein denaturation) which can in turn affect the solution stability leading to protein aggregation.

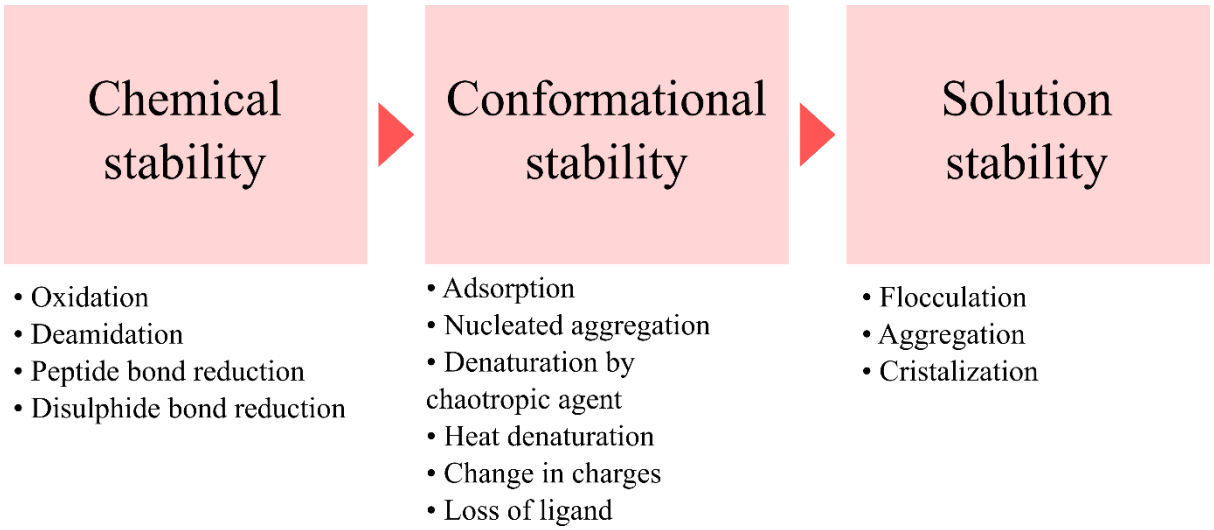

Figure 7. Main mechanisms of stability loss in proteins.

1.4.1 Chemical denaturation

Organic molecules are subject to **chemical degradation**, proteins in particular can undergo oxidation and deamidation of their side chains. These degradations can result in structural instability and aggregation. Moreover the reduction of disulphide bonds or the hydrolysis of peptide bonds is extremely destabilizing for the protein structure. This chemical alteration usually results in a disturbance of the protein conformation.

1.4.2 Protein structural denaturation

Denaturation is the loss of the native structure of a macromolecule. Protein denaturation can occur when the physico-chemical conditions of the environment no longer stabilize the conformational state of the protein. At high temperature denaturation occurs mostly by disruption of the hydrogen bonds. At low temperature, cold denaturation [39,40] can also occur mostly driven by entropic effects such as the hydrophobic effect.

The conformational changes of proteins can be monitored by fluorescence techniques relying on dyes binding preferentially to hydrophobic regions of the proteins such as 8-Anilinonaphthalene-1-sulfonic acid (ANS) or SYPRO orange. This approach is particularly used in the monitoring of amorphous aggregation, particularly thermal denaturation and has applications in drug screening by thermal shift assays. Moreover changes in a protein structure can affect its aromatic amino acids auto-fluorescence intensity in particular tyrosine (insulin does not contain tryptophan) auto-fluorescence has been used to monitor insulin conformational changes[41].

1.4.3 Protein aggregation

If the structure of a protein is no longer stabilized by the solvent, other stabilizing interactions can take place between different proteins. These intermolecular interactions are usually driven by hydrophobic effects between the newly exposed non polar amino acids[42–44]. Wang et al.[45] proposed a general classification of aggregation pathways (Figure 8). The pathways are divided in 3 categories (1) aggregation through an intermediate state, (2) direct protein aggregation from native (2a and 2b) or denatured (2a' and 2b') proteins and (3) chemical degradation inducing subsequent aggregation.

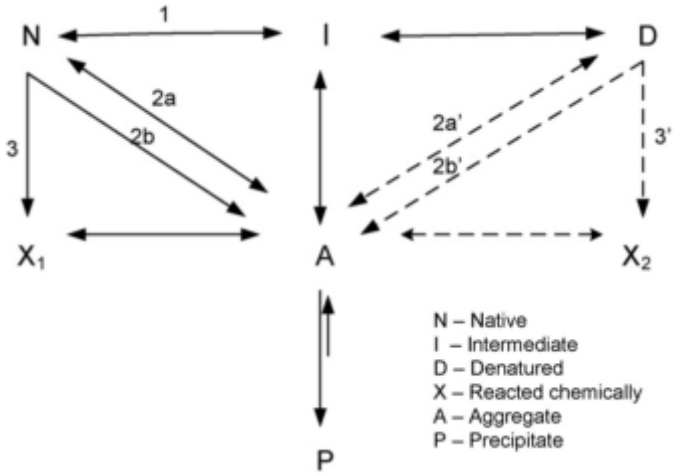

Figure 8. Pathways of protein denaturation (from Wang et al. 2010[45]). This pathway classification distinguishes reversible aggregation from native (2a) or denatured (2a') proteins and irreversible aggregation (2b and 2b').

Spontaneous aggregation

A spontaneous aggregation (pathway 2 in Figure 8) is usually the result of a sudden loss of Solution stability after a change in the physico-chemical condition of the solution (temperature, pH, denaturant, etc.) or a denaturation of the protein (by heating or high denaturant concentration). Aggregates formed under these conditions usually present a low ordered structure: precipitates or amorphous aggregates. They can also be composed of several protein species.

Figure 9 presents the solubility of a protein according to its concentration and to another parameter (such as the concentration of a precipitating agent). In the **solubility domain**, i.e. at low protein concentration or at low solubility reducing conditions, direct aggregation can only occur by denaturation of the protein (pathway 2a' and 2b'). Above supersaturation the proteins are no longer soluble and **flocculate** (pathway 2a and 2b).

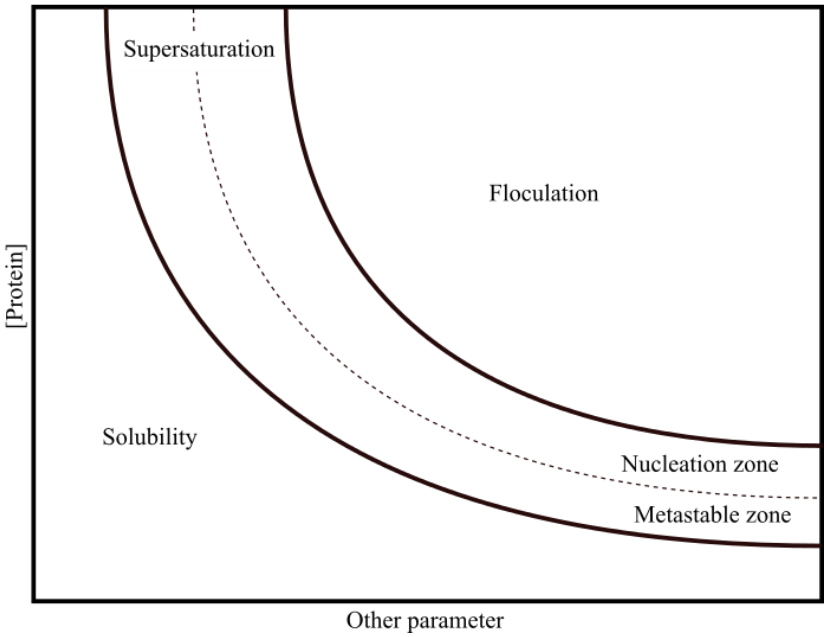

Figure 9. Protein solubility profile showing the 3 major domains. In the solubility domain aggregation can occur by loss of stability, in the supersaturation domain protein cristals can grow (although they can only nucleate in the nucleation zone) and in the floculation domain, proteins spontaneously precipitate.

Mechanisms of flocculation

The propensity of proteins to flocculate can be estimated using their osmotic **second virial coefficients** as well as their zeta potential[46]. The virial expansion of the osmotic pressure[47] is :

$$\Pi = \mathrm{RT}\left(\frac{1}{Mw}\cdot \mathrm{c}_p + B_{22}\cdot {\mathrm{c}_p}^2 + B_{23}\cdot {\mathrm{c}_p}^3 + \cdots\right)$$

Where **R** is the ideal gas constant, **T** is the absolute temperature in Kelvin, $\mathbf{M_w}$ is the protein molecular weight in Da, $\mathbf{c_p}$ the concentration of protein in M and B_{22} the osmotic second virial coefficient[48] is given by:

$$B_{22} = \frac{2\pi}{{M_w}^2}\int_0^\infty {r_{12}}^2\left(1 - e^{-\frac{W(r_{12})}{k_B T}}\right) dr_{12}$$

Were $\mathbf{r_{12}}$ is the intermolecular center-to-center distance, $W(\mathbf{r_{12}})$ is the potential of mean force , k_B is the Boltzmann constant, T the absolute temperature in Kelvin. The osmotic virial coefficients are responsible for the deviation from an ideal solution. In the case of positive coefficients, the osmotic pressure is higher than the ideal solution with a dominance of repulsive intermolecular interactions. Highly negative coefficient usually drive rapid formation of amorphous aggregates.

Morphology of aggregates superstructures

The morphology of larger aggregates can be shaped by specific aggregation mechanisms: diffusion-limited aggregation (Figure 10) produces lower fractal dimension patterns than reaction-limited aggregation[49–53]. The determination of the fractal dimension of an aggregate is therefore informative on the aggregation mechanism for instance by comparison with aggregates obtained by computer simulation.

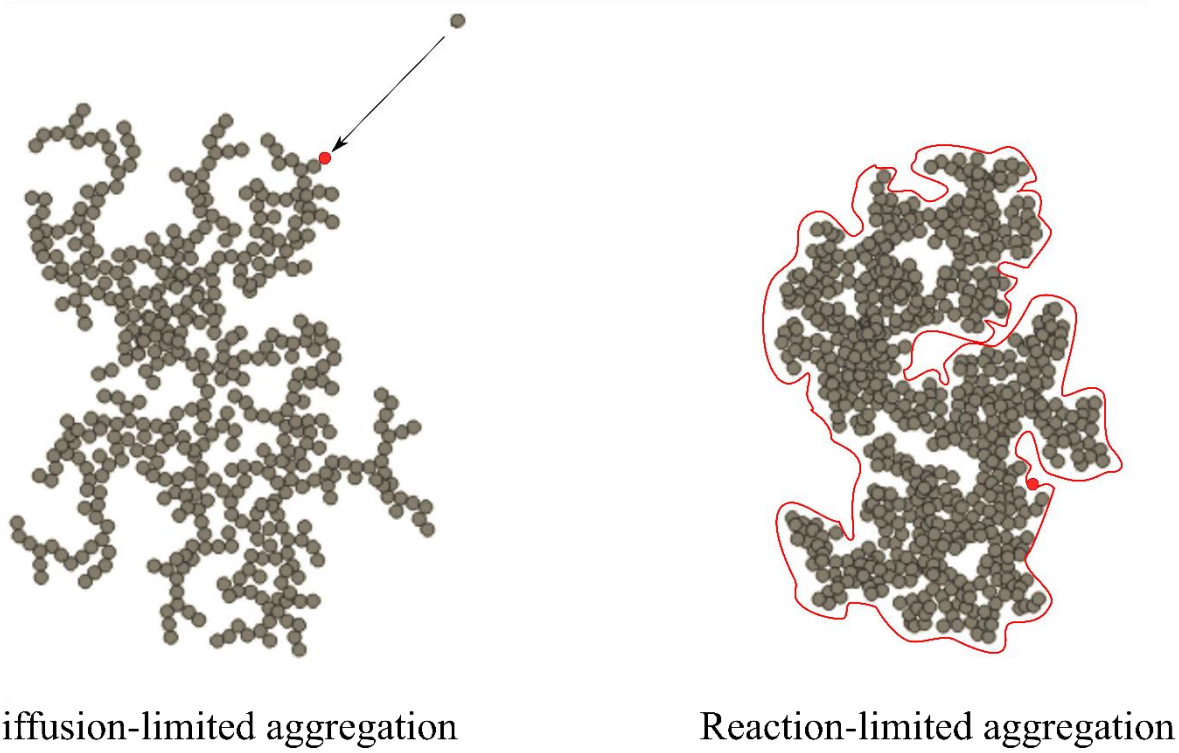

Figure 10. Reaction-limited aggregation (RLA) and diffusion-limited aggregation (DLA) mechanisms. In DLA particles diffusing from infinity are incorporated immediately upon contact with the aggregate. On the other hand, in reaction limited aggregation every point of the aggregate is accessible surface is equiprobable for particle incorporation. (modified from wikimedia commons : https://commons.wikimedia.org/wiki/File:ParticleAggregationDLCAvsRLCA1.png)

Aggregation through intermediate state

Aggregation involving an intermediate step (type 1 aggregation pathway in the Wang et al. classification) can be encountered in the solubility domain. The high energy barrier between the native and the aggregated form of the protein (Figure 6) allow both forms to be stable (or relatively stable) in the same conditions. Aggregates formed via intermediary states can be extremely ordered (Table 2). In the present work the focus is made on amyloid aggregation in the solubility domain by such type 1 aggregation mechanisms in particular via the formation of intermediates via nucleation.

Crystallization

When the concentration of the protein increases or its solubility decreases, the solution enters in the **supersaturation domain (**Figure 9**)**. Under high supersaturation and usually high protein purity, protein crystals can nucleate. These crystals are monospecific and highly ordered and the proteins retain most of their native structure under this state[54,55]. Contrary to the amyloid nucleation occurring in the solubility domain, nucleation of the protein crystals only takes place in the nucleation zone of the supersaturation domain. The growth of these crystals is then thermodynamically supported in the whole supersaturation domain.

		Wang et al.	Nucleation	Domain	Structure
Aggregation	Crystallization		Usually nucleated	Supersaturation	Ordered
	Via intermediate	1		Solubility	Ordered
	Flocculation	2a, 2b	Direct	Flocculation	Amorphous
	By denaturation	2a', 2b'		Solubility	Amorphous
	By chemical degradation	3		Solubility	Amorphous

Table 2. Summary of protein association mechanisms. With coresponding pathways in Wang et al. clasification, nucleation dependancy, solubility domain of occurance and level of order of their structures.

1.4.4 Amyloid aggregation

Amyloid aggregates are a specific case of **monospecific** and highly organized fibrillar protein aggregates, which are characterized by their unique structural properties[56] (Figure 11). The main feature of amyloid fibers is the stacking of a protein along the axis of the fiber maintained together by a backbone of intermolecular β-sheets[57]. The hydrogen bonds of these intermolecular β-sheets being oriented along the fibril axis. The amyloid fibrils intermolecular β-sheets usually present lower dispersion of φ and ψ angles than the β-sheets in native proteins[58]. Despite this stabilization by the backbones of proteins, the amyloid aggregation is highly sequence specific as only closely related sequences can be inserted into the same fibrils[59]. There is a large consensus that amyloid aggregation occurs mostly via oligomeric and conformational intermediates through a phase of nucleation. The morphology of the final fibrils is regular and unbranched (or usually unbranched[60]). Charges are believed to play important roles in the formation of the fibrils as well as in their stability[61].

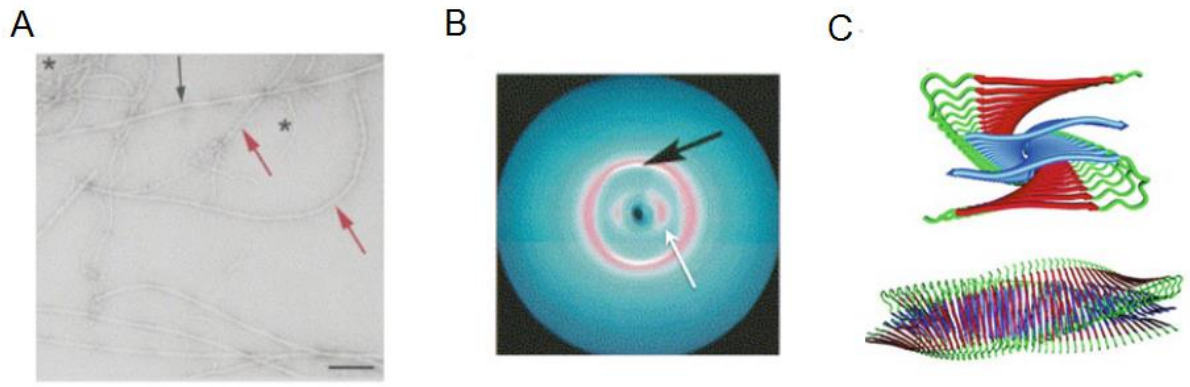

Figure 11. Structural characterization of amyloid fibrils by 3 biophysical methods. A: Transmission electron micrograph of $A\beta_{1-40}$ imaged after uranyl formate staining, the asterisk indicates a proto-fibril while the arrows indicate fibrils, B: Synchrotron X-ray diffraction pattern of amyloid fibrils from a patient presenting familial amyloidosis; this pattern presents a typical 4.7 Å inter-strand spacing (white arrow) and a 10 Å inter-sheet spacing (black arrow), C: Model of $A\beta_{1-40}$ fibril derived from magic angle solid state NMR data. Modified from Martin et al.[56] originally adapted from Goldsbury et al.[62] (A), Sunde et al.[63](B) and Petkova et al.[64] (C).

Detailed structural data on fibrils are scarce owing to the incapacity to obtain amyloid crystals, the detailed structure are usually obtained by NMR (in particular magic angle spinning solid-state nuclear magnetic resonance[65–67]) often conjugated with cryo-electron microscopy and computer-aided energy minimization[68].

Thioflavin T (ThT) is a dye consisting of a benzothiazol moiety and a dimethylaminobenzyl moiety which is able to bind specifically the amyloid fibrils in the groove formed by the intermolecular beta sheets [69]. In protic solvent† ThT presents an absorption peak at 342nm and a fluorescence emission peak at 430nm[70]. However, once bound to an amyloid fibril, ThT molecules undergo a fluorescence switch to a maximum absorption peak at 450nm and an emission peak at 480nm as well as an increase in their fluorescence quantum yield[71–75]. Protein aggregates inducing such a fluorescence transition are called ThT-positive in the literature.

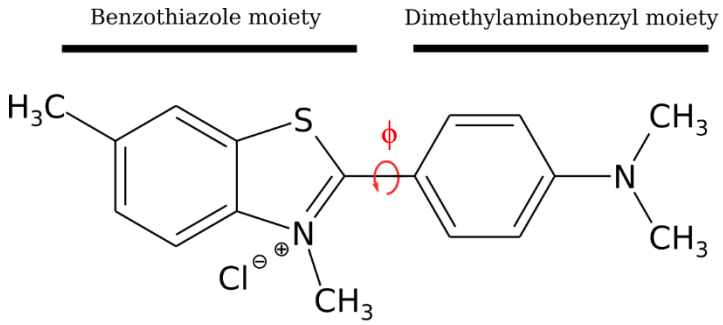

Figure 12. Structure of Thioflavin T showing the torsional angle between the two moieties (ϕ angle).

† **Protic solvent**: a solvent able to donate H+ (e.g. H_2O)

Some studies suggest the formation of a ThT excimer[76] (i.e. a dimer of excited Thioflavin T) in cavities able to bind two ThT molecules[77,78]. Such a system would allow intermolecular conjugation resulting in a fluorescence shift. Such dimers of collinearly stacked ThT molecules have been found in crystal structures[69,70] but the absence of associated red shifts in emission wavelength[70] plus the non-cooperative binding of ThT to the amyloid fibril[73] show that the excimer formation is unlikely to be at the origin of the ThT positive-state.

The energy barrier for the rotation of the bond between the two moieties is 2.2 kcal/mol. [79] In a rigid microenvironment, preventing this rotation, the fluorescence of the ThT shifts from short wavelength and low quantum yield to long wavelength and high quantum yield. The grooves formed between the side chains of beta sheets provide such a rigid environment preventing the free rotation of the ThT ϕ torsional angle and therefore increase the fluorescence at λ_{ex}=450nm. The incorporation of ThT inside the fibril might be limited by the accessibility to the binding site; indeed the presence of ThT during the elongation phase results in higher fluorescence compared to the addition of ThT at the end of the aggregation.

ThT is considered as a dye, specific of the amyloid structure, however ThT-positive states have been observed in aggregates lacking fibrillary structure under electron microscopy and therefore qualified as amorphous, albeit possessing an increased β-sheet content[80]. To a lesser extent, increased quantum yield and minor fluorescence wavelength shifts have been observed in micelles and membranes[81].

Other chemicals are known to stain amyloid aggregates, **Congo red** in particular is a long known amyloid-specific dye that presents apple green birefringence under polarized light upon insertion into amyloid fibrils[82].

The term amyloid (amylum + oid “starch like”) was introduced by Rudolf Virchow in 1854 in reason of the positive iodine staining of these extracellular aggregates[83]. This purely histological definition is now extended to the structural property of the proteins forming these aggregates. The common structure of amyloid aggregates allow the exploitation of data acquired on one protein to enlighten the amyloid aggregation of other proteins.

Since the amyloid fibril structures rely on a stabilization by the protein backbone and not restricted to a particular sequence, and with the findings of widespread amyloid aggregation in numerous proteins, it has been suggested that amyloid aggregation is a common property of polypeptide chains[84–86].

If the inter-protein interactions by intermolecular β-sheet in the direction of the fibril axis are well known, it is not the case for the interactions perpendicular to this axis. And why are amyloid aggregates so sequence-specific, despite this stabilization by the protein backbone? Numerous evidences obtained on small amyloid forming peptides show lateral interaction of their side chains by the formation of a dehydrated interface called a steric zipper[87–89]. This close interaction of the side chains is mainly stabilized by the hydrophobic effect or electrostatic interactions. Furthermore the dehydration of the fibril core increases the energy of electrostatic interactions[26]. Under high hydrostatic pressure the anisotropic voids created by such dehydrated interfaces can lead to the fibril deformation. These voids contribute to reduce the thermodynamic potential of their formation under high pressure [90,91].

The steric zipper may therefore explain the sequence specificity of amyloid aggregation and nuance the universality of amyloid aggregation. Furthermore it suggests that only a specific portion of the protein is involved in fibril formation. Therefore for each amyloidogenic protein a minimum peptide able to form amyloid fibrils on its own must exist. Attempts have even been made to predict the propensity of aggregation of polypeptide sequences. For instance arginine-rich regions are known for their propensity to form amyloid aggregates[92–95].

1.4.5 Amyloid aggregation kinetics

The amyloid aggregations usually follow a typical nucleated aggregation kinetics which is divided into three different phases (Figure 13): At first the aggregation rate remains null for an extended period of time (typically hours). This **lag-time** preceding the appearance of the first aggregates is the **nucleation phase** during which proteins overcome the energy barrier between their soluble form and their aggregate form via the formation of unstable oligomeric structures called nuclei. The appearance of the first fibrils then initiates an exponential aggregation soon attenuated by the depletion of native proteins in solution resulting in a logistic‡ **growth phase**. Eventually the aggregation reaches a **plateau** when all the native proteins in solution have been converted to amyloid aggregates.

The addition of amyloid fibrils at the beginning of a kinetic abolishes the lag-time and induces a rapid transition to the growth phase, this action is known as seeding[96].This seeding and the

‡ **Logistic growth**: An exponential growth in a limited environment, here a limited number of native protein, results in a sigmoid kinetic.

elongation of the fibril are sequence-specific[59]. Genuine cross-seeding between unrelated peptide sequences have although been reported which has high medical significance[97].

A simple way to deal with amyloid kinetics is to separate the **primary nucleation** i.e. the process leading to the appearance of the first aggregate from **secondary processes** or **seeded aggregation** which occur during the growth phase. Since amyloid aggregates are remarkably efficient seeds, these secondary processes become predominant as soon as the first aggregates appear in solution.

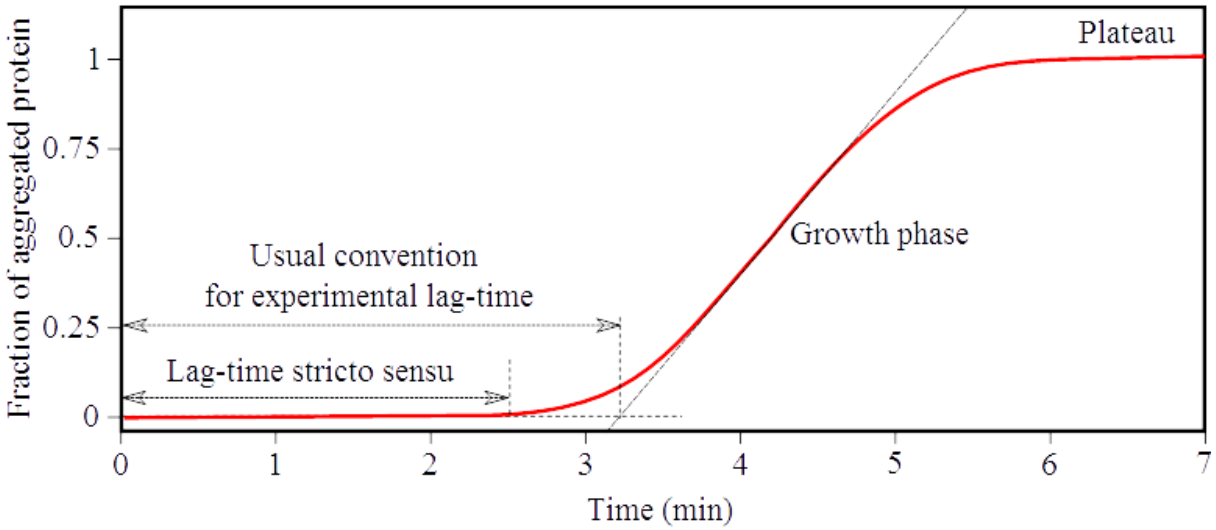

Figure 13 Theoretical kinetic of an amyloid aggregation in vitro with limited amount of native proteins.

The kinetics of amyloid aggregation is usually monitored by fluorescence quantification using the specific fluorescent dye Thioflavin T. Experimental time points do not systematically and sufficiently cover the rapid transition between lag-phase and growth phase to allow the determination of the appearance point of the first ThT positive amyloid fiber (lag-time stricto sensu). Experimental lag times are therefore usually defined as the intersection of the steepest tangent of the growth phase with the abscissae (Figure 13).

Amyloid kinetic, and protein aggregation kinetic in general have received great attention since they allow the deduction of aggregation mechanisms[98]; these mechanisms will receive particular attention in the following sections.

1.4.6 Principles of nucleation

Nucleation is the process leading to the first formation of a new phase or structure from individual particles. It differs from a spontaneous assembly in the presence of a **lag-time** preceding the assembly itself. Nucleation is therefore known in numerous processes involving self-assembly such as ice formation or crystallization [99]. A distinction is made between

heterogeneous nucleation which occurs in contact with a surface and **homogeneous nucleation** which occurs in a homogenous medium (e.g. in solution). Protein nucleation has been observed both in solution and on surfaces. **Classical nucleation theory (CNT)** is the main model used to describe a thermodynamic phase change and has also been used in order to understand protein nucleation[100].

CNT focuses on the change in the free energy associated with the surface and with the bulk of a spherical nucleus of radius r[101–103]. The outcome of the interfacial tension (σ) of this nucleus will be a surface free energy proportional to its surface ($4\pi r^2$). This positive contribution to the total free energy of the nucleus will therefore disfavor nucleation. On the other hand, the free energy released in the transfer of a volume of monomers from solution to the bulk of the nucleus (Δg_{trans}) creates a bulk energy term proportional to the volume of the nucleus ($4\pi r^3/3$). This negative contribution to the total free energy will favor nucleation. The balance between these two antagonist contributions to the total free energy defines the critical size of the nucleus and its variation of free energy as:

$$\Delta G = \Delta G_{bulk} + \Delta G_{surf}$$

$$\Delta G = \frac{4}{3}\pi r^3 \Delta g_{trans} + 4\pi r^2 \sigma$$

For small nuclei the increase of the surface energy associated with the addition of a new monomer exceeds the release of energy resulting from bulk interactions. The nucleus growth is therefore thermodynamically disfavored in the first place. But since the surface contribution is proportional to r^2, this instability will soon be compensated by the bulk contribution which is proportional to r^3. The nucleus then reaches a critical radius corresponding to the radius where ΔG reaches a maximum, $\frac{d}{dr}\Delta G\Big|_{r^*} = 0$

at:

$$r^* = \frac{-2\sigma}{\Delta g_{trans}}$$

Where the addition of monomer no longer increases its free energy but begins to stabilize it (Figure 14).

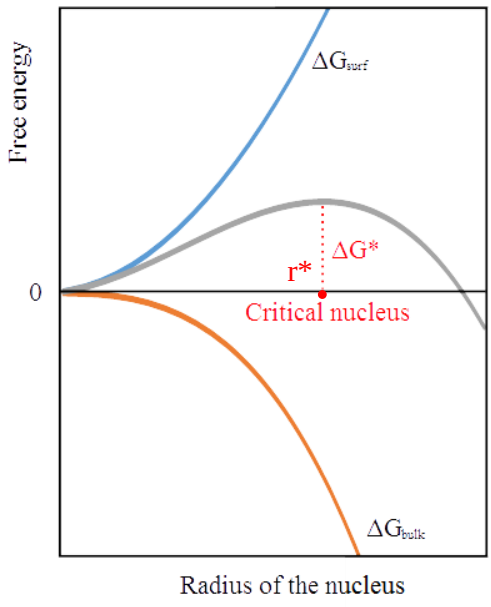

Figure 14. Evolution of the contribution of bulk and surface free energy to the free energy of the nucleus.

CNT however does not take into account the conformational transitions of the proteins nor the change in ΔG associated with these transitions. Furthermore this model considers the nuclei as a sphere having both a bulk energy and a surface energy which can be an uncertain assumption for small nuclei comprising a discrete number of molecules. Nevertheless this theory enables us to visualize the basic concept of nucleation: the first oligomers are unstable and the nuclei will only gain stability after the reaching of a critical state after a certain number of transition states.

Furthermore the dominance of heterogeneous nucleation over homogenous nucleation in the presence of a surface for which the monomers have affinity is obvious: nuclei growing on a physical interface will have lower surface exposed to the liquid, and therefore a lower $\Delta G_{surf.}$.

1.4.7 Amyloid nucleation mechanism

Because proteins are complex molecules including numerous functional groups having specific interaction energies with each other and because the conformation of the proteins is able to change especially upon external stabilizing interactions, the stability of protein nuclei is not restricted to simple considerations of bulk versus surface energy. Moreover the assembly of structures as complex as a mature amyloid fibril is divided into several intermediary states with at least one of them being thermodynamically limiting.

Similarly to the CNT model, the critical nuclei represent the oligomeric form with the highest free energy in the pathway to an amyloid fibril. From a kinetic point of view the nucleation rate

is the rate of apearance of the first oligomer for which the addition of a monomer is more favorable than its disassembly.

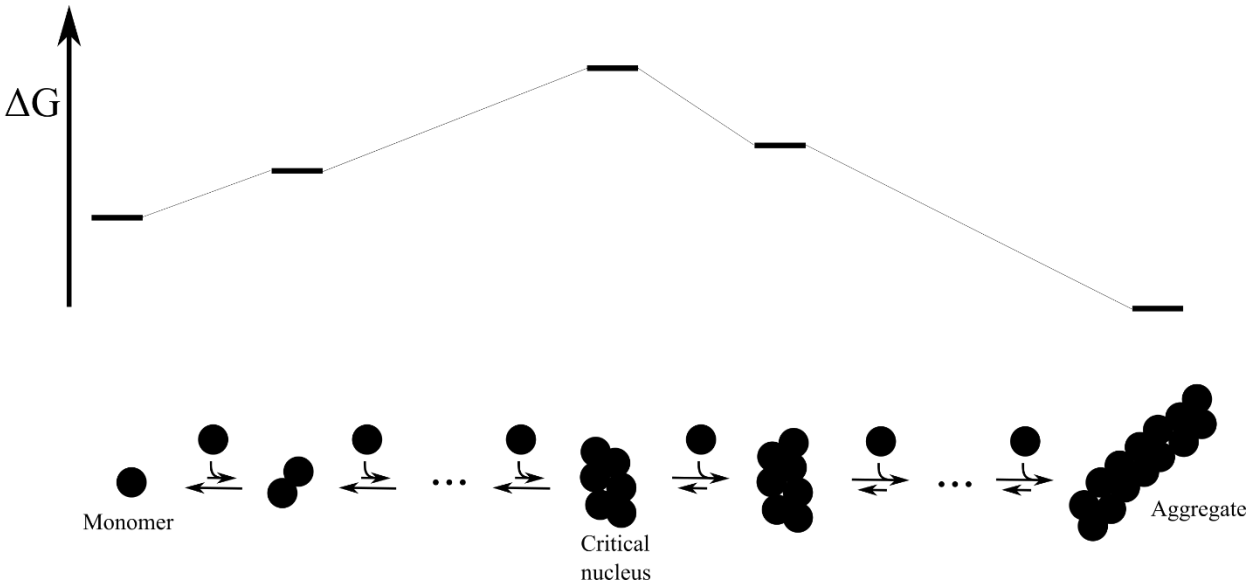

Figure 15. Simplest themodynamic model of amyloid nucleation.

Amyloid kinetics has received much attention in recent years,[104–109] resulting in the production of numerous thermodynamic and kinetic models: template-assembly model[110,111], nucleated polymerization, monomer-directed conversion[112], nucleated conformational conversion [113] (Figure 16) and off-pathway folding model[114].

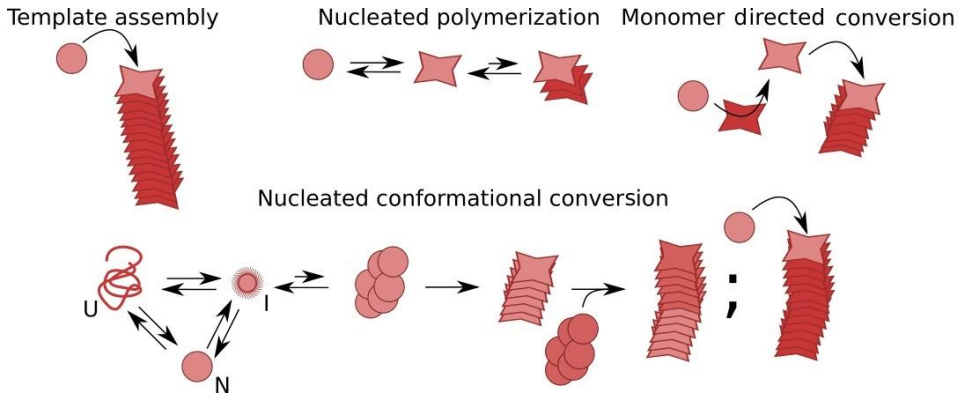

Figure 16. Models of amyloid mechanisms (adapted from Serio et al.[113])

In the **template assembly** model (Figure 16), the native monomers undergo conformational changes directly upon their assembly into the amyloid aggregate. This conformational change constitutes the rate-limiting step. This model does not include a nucleation step but can apply to the mechanism of fibril elongation. Alternatively in the **monomer-directed conversion**

model, the rate limiting step is the conversion in solution of a native protein by an amyloid state monomer; the amyloid monomers subsequently aggregating in a non-limiting step. In the **nucleated polymerization** model an equilibrium exists in solution between native and amyloid monomer, then the limiting step consists in the association of the rare amyloid monomers in solution.

Nucleated conformational conversion was then proposed by Serio et al. [113] after experiments on the fungal prion sup 35 protein. They have shown that conformational conversion is rate-limiting imposing a maximum rate. In this model the nuclei originate from partially unfolded monomers, they then grow by addition of native or partially unfolded monomers which will undergo a structural transition leading to an amyloid state. From this point, the growth by nucleus assembly or monomer addition will be prevalent over disassembly.

With nucleated conformational conversion the mechanism of nucleation does not rely on a mass action effect but on conformational changes. The transition of the thermodynamic constant associated with monomer addition is therefore explained by a qualitative rather than a quantitative increase of intermolecular interaction inside the nucleus. Indeed the final amyloid fibrils are rod like objects with high surface/volume ratio.

A general model for amyloid nucleation kinetic is:

$$(1) \qquad N \rightleftharpoons I$$

$$(2) \qquad \left(I_{n-1} + N \rightleftharpoons I_n\right)_{n \text{ times}}$$

$$(3) \qquad I_n \rightleftharpoons A_n$$

$$(4) \qquad N + A_n \rightleftharpoons A_{n+1}$$

Where N is a native monomer in solution, I is an intermediate state protein and A is an amyloid state protein. Intermediate state protein is here a term that may apply to several states that are distinct from the native state, unfolded state and the amyloid state. Notably, the proteins forming the nucleus are here referred as intermediates but are not necessarily all under the same conformation. Analogously to the model proposed by Serio et al. the native protein **(1)** undergoes a transition to an intermediate state (for instance by adsorption on a surface), then this intermediate state protein is able to act as a thermodynamically unstable center of oligomerization **(2)** forming a nucleus $\mathbf{I_n}$ composed of n monomers. This nucleus presents a high propensity to disassemble until it reaches a critical state **(3)** of conformational transition $\mathbf{A_n}$ above which the propensity of monomer incorporation will be greater than the propensity to disassemble **(4)**.

Due to the high conformational instability of the nuclei, nucleation events are extremely rare: typical nucleation times (i.e. appearance of the first amyloid aggregate in solution) range from several minutes to several days. Nucleation events exhibit a pronounced stochastic behavior with high variation between similar samples in the duration of the lag-time.

However the path from monomer to amyloid fibril usually belongs to a wider aggregation network[115] where more than one pathway can lead to the formation of amyloid fibrils and in which the reactions of monomer addition can be in competition. An additional obstacle to nucleation can therefore consist in its kinetic inhibition by the formation of competing oligomeric structures off the amyloid formation pathway.

One model of the amyloid nucleus is a micelle-like structure, stabilized by the hydrophobic effect. Molecular dynamics simulations in particular have emphasized the importance of hydrophobic cooperativity in amyloid nucleation[116]. Then conformational changes occur in this nucleus stabilized by intermolecular interactions. The α-sheet has been proposed as a conformational intermediate between the native conformation and the amyloid intermolecular β-sheet[117]. This intermediate conformation has been proposed for lysozyme and is alleged to be involved in the cellular toxicity of amyloid aggregates[11].

Amyloid nucleation depends on the concentration of monomer and therefore increasing concentration of monomer will increase the nucleation rate. However, contrary to protein crystallization, amyloid nucleation is mainly described as not requiring a supersaturation.[99,118,119]

1.4.8 Amyloid growth phase

The **elongation** phase consists in the fast incorporation of monomers at the extremities of the amyloid fibrils (Figure 17). According to the template model, native monomers (or native dimers) are readily converted and incorporated into the fibril's extremities. In other proposed models however, the elongation proceeds by incorporation of transition state proteins or transition state nuclei.

Amyloid fibrils are unbranched, meaning that their elongation can only proceed by incorporation of proteins at one or both of their extremities. Assuming that primary nucleation events are extremely infrequent and for $\mathbf{k_{inc}}$, the rate constant of protein incorporation at one site, the elongation rate $\frac{dA}{dt}$ can be written as:

$$\frac{dA}{dt} = a \cdot k_{inc} \cdot S \cdot [P_{inc}]$$

Where ***a*** is the stoichiometric coefficient corresponding to the number of protein units in the incorporated form (1 for monomer, 2 for dimer, etc.) **$[P_{inc}]$** is the concentration of protein in the state which can be incorporated into the fibril and **S** the number of incorporation sites. **S** is constant in the absence of primary nucleation and secondary processes. At high protein concentration and under the constant **S** hypothesis, this rate law results in a linear aggregation kinetic. On the other hand, in conditions where the concentration of precursor protein is limited, this rate law gives an aggregation kinetic in the form:

$$A(t) = [P]_0 \cdot (1 - e^{-a \cdot k_{inc} \cdot S \cdot t})$$

Where A(t) is the number of mole of proteins in the aggregate state and $[P]_0$ is the initial concentration of protein (assuming a rapid conversion between the different protein forms in solution).

On the other hand if primary nucleation is not so scarce and occurs at a significant rate then the number of elongation sites will increase with time. Leading to an aggregation kinetic following $A(t) \propto t^n$.

The exponential behavior of aggregation during the growth phase can therefore only result from a multiplication of the elongation sites by secondary processes. These secondary processes include monomer independent phenomena such as fiber fragmentation or monomer concentration-dependent rate processes such as secondary nucleation[108] (Figure 17).

If elongation occurs by incorporation of intermediary or oligomeric protein forms (for instance elongation by nuclei addition) then the formation rate of these intermediates can become a limiting factor slowing elongation.

The rate of primary and secondary nucleation can be obtained from the kinetic data of aggregation at different concentrations using the following formula[108]:

$$T_{1/2} \propto [Monomer]^{\gamma}$$

Were $\mathbf{T_{1/2}}$ is the time necessary to achieve the aggregation of half the initial protein concentration **[Monomer]** and **γ** is the exponential scaling coefficient. Depending on the dominant mechanisms the scaling coefficient allows the determination of nucleation rates: (n_c: the primary nucleation rate and n_2: the secondary nucleation rate)

(Primary nucleation) $\gamma = -\frac{n_c}{2}$

(Secondary pathways) $\gamma = -\frac{1+n_2}{2}$

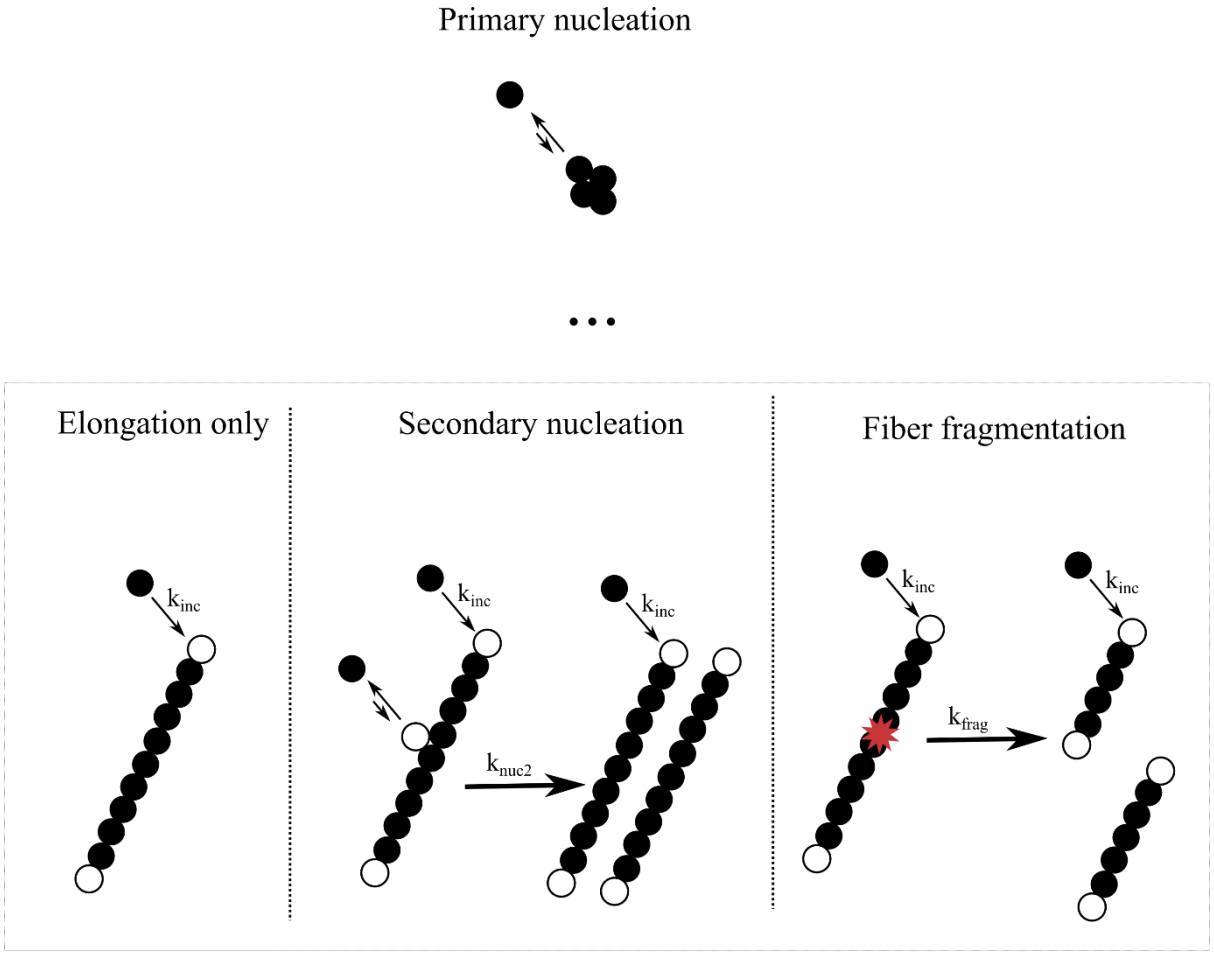

Figure 17: Kinetic model presenting the primary nucleation step leading to the appearance of the first fibril, and the subsequent growth mechanisms observed in amyloid kinetics. Filed circle represent protein, open circles represent the protein incorporation sites in amyloid fibrils.

Among the diversity of amyloid aggregation mechanisms described in the literature (Figure 18) the prevalence of each individual mechanism can greatly differ depending on the protein.

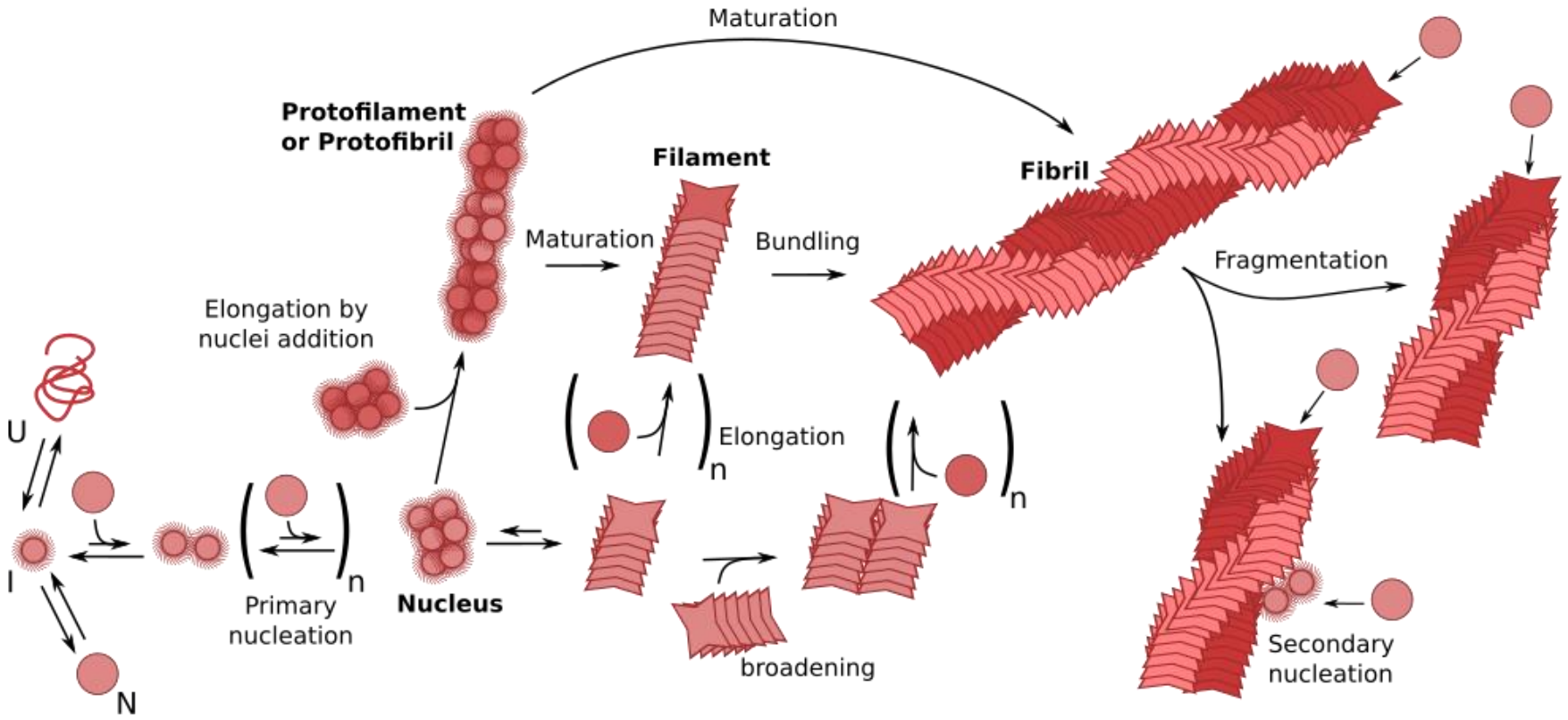

Figure 18: Summary of amyloid aggregation mechanisms described in the literature. The role of each individual mechanism varies among specific cases and in most cases is still discussed. Here the nucleus represents a critical nucleus from which the addition of monomer becomes thermodynamically favored over its disassembly. Fibrils can include more than two filaments (typically 2 to 4), in order to keep the network as simple as possible the secondary pathways are detailed in Figure 19**.**

A summary of amyloid secondary processes with an emphasis on processes that could lead to a branching of amyloid fibrils has been proposed by Andersen et al. (Figure 19).

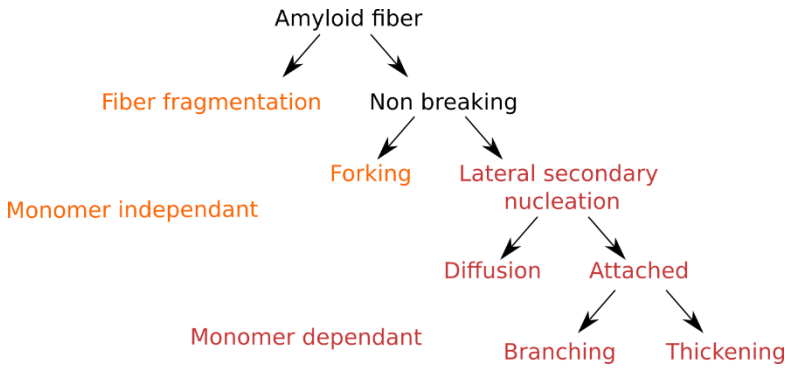

Figure 19. Classification of 5 secondary processes according to Andersen et al.[60] In the monomer-independent processes (here in orange) the rate of creation of new aggregation sites only depends on the amount of aggregates. On the other hand, in the monomer-dependent processes (here in red) the rate of the creation of new aggregation sites depends on both the amount of aggregates and the concentration of monomers in solution.

1.5 Parameters influencing protein stability

In this section we will review the major sources of protein instability with an emphasis on amyloid aggregation phenomena. First the physico-chemical conditions of the solution such as pH, temperature, ionic strength, concentration of chaotropic or kosmotropic agents, Red/Ox potential, protein concentration, etc.[45] are determinant for protein solution and chemical stability. Moreover absorbed photons provide supplementary energy to the proteins or their surrounding which can induce a loss of chemical or solution stability.

Stress resulting from agitation or formation of air-liquid interfaces such as: drying, shearing, formation of bubbles or emulsions are well known to trigger protein aggregation and poses major challenges to the pharmaceutic industry. Eventually unspecific interactions with small molecules, macromolecules or surfaces and specific interactions with peptides and proteins control the formation of protein multimeric structures[120].

1.5.1 Physicochemical parameters of the solution

Temperature

Temperature affects the stability of proteins in multiple ways: increased temperature increases diffusion, reaction rate, and the mean energy of particles. Therefore both the kinetics and thermodynamics of chemical reactions are affected by temperature. According to Arrhenius equation, the rate constant of a chemical reaction is:

$$k = A \cdot e^{\frac{-E\ddagger}{k_B T}}$$

Were A is the pre-exponential factor, **E‡** is the activation energy per molecule, $\mathbf{k_B}$ is the Boltzmann constant and **T** is the temperature. But both the pre-exponential factor and the activation energy can be influenced by temperature. Notably the hydrophobic interactions strongly depend on the temperature as higher temperatures induce higher dynamics in the hydrogen bond network, increasing the solubility of non-polar groups and, as a consequence, lowering the importance of hydrophobic effects and in turn protein stability[121].

pH

The solution pH defines which chemical group will or will not be charged according to their pKa. This will therefore affect the global charge of the protein. Besides the flocculation effect driven by the reduction of the zeta potential, the change in charge at specific groups can allow otherwise impossible interactions, hindered due to repulsion. In particular the amyloid aggregation of several proteins is influenced by the pH especially in acidic conditions, (e.g. transthyretin (L55P)[122], insulin[123] and immunoglobulin light chain[124]). One explanation lies in the fact that charge repulsion can prevent the formation of the steric zipper and therefore prevent amyloid fibril appearance.

Ionic strength and electric fields

The ionic strength denotes the ability to form an "ionic atmosphere" of counter ions around charged groups in a solution. It is defined as:

$$I = \frac{1}{2}\sum_{i=1}^{n} c_i \cdot z_i^2$$

Where c_i and z_i are the concentration and the charge of the ion ***i,*** respectively. Ionic strength is responsible for the shielding of the charges in solution, consequently reducing the effect of these charge in macromolecular interactions. Ionic strength and the net charge of the protein is involved in the Zeta potential which is the potential of a particle and its associated ions at the slipping plane (i.e. the interface between the stationary solution layer around the particle and the bulk solution). As the Zeta potential is involved in solution stability, flocculation can occur if it approaches zero. But as described in the next section, ions are also able to affect more specifically the solubility and conformation of proteins.

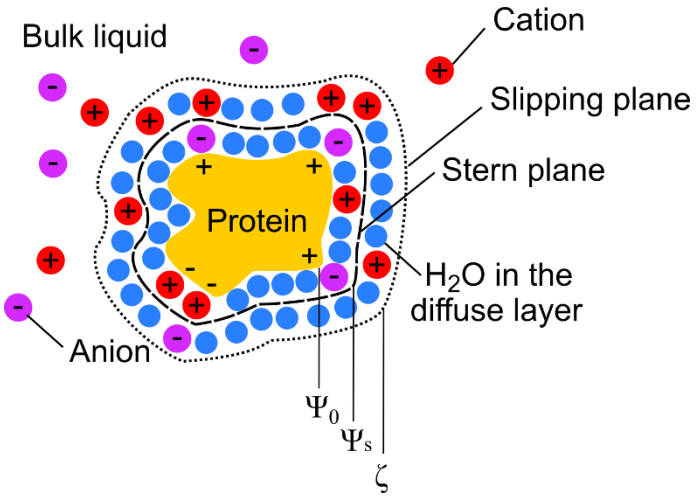

Figure 20. Definition of the planes and potentials around a solute protein. The surface potential (Ψ_0), Stern potential (Ψ_s) and Zeta potential (ξ) of the protein are defined at the protein surface, at the Stern plane and at the slipping plane respectively.

Proteins are charged molecules and therefore migrate under the influence of electric fields by electrophoresis. Electric fields can also induce conformational changes in a protein structure. Within human PDZ domain crystals the electric-field-induced conformation mimics the conformation of the domain upon binding of a ligand[125]. However such effects remain rare in physiological conditions apart from membrane proteins[126] .

1.5.2 Chaotropic and kosmotropic agents

Chaotropic molecules are chemical species destabilizing the conformational structure of macromolecules[127] for instance by lowering the hydrophobic effect. On the other hand kosmotropic molecules lower the solubility of non-polar groups.

The Hofmeister effect describes the ability of ions to affect protein solubility and structural stability[128]. Ions interact with water molecules of the solvation shell and directly with the macro-molecules, modifying their interfacial tension and in turn hydrophobic interactions. The Hofmeister series classifies the anions and cations from the most out salting to the most in salting (**Figure 21**). Out salting ions increase the hydrophobic effect, increasing therefore the proteins tendency to aggregate. But these ions will also stabilize the protein structure probably through the stabilization of the hydrophobic core.

On the other hand in salting ions enhance the solubility of nonpolar groups, increasing protein solubility but also stabilizing the unfolded form of the protein.

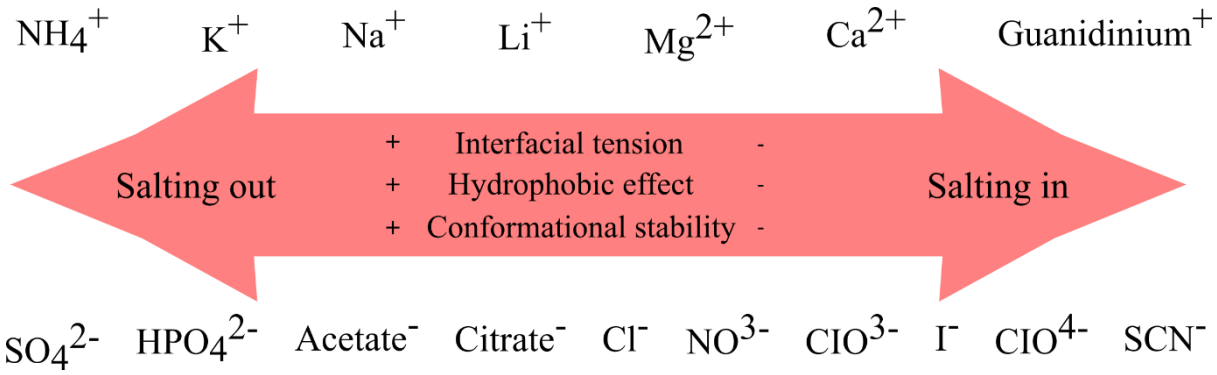

Figure 21: Hofmeister series presenting the anionic and the cationic series.

Apart from ions, other soluble molecules exhibit chaotropic and kosmotropic behavior, urea for instance is long known to denature proteins. On the other hand trehalose, betaine and citruline are perhaps the most known examples of kosmotropic compounds. Some kosmotropic molecules are sometimes referred as chemical chaperones by analogy with chaperone proteins.[129] Ferulic acid for instance has been shown to inhibit the nucleation of insulin[130].

1.5.3 Electromagnetic radiations

Electromagnetic radiation can be absorbed by the electrons of molecules increasing their energy by the level of energy of the photon:

$$E = h \cdot \nu$$

Where h is the Planck's constant and ν the frequency of the photon. Molecules are able to absorb a photon presenting an energy corresponding to the difference between an occupied molecular orbital and an unoccupied orbital of higher energy (Figure 22).

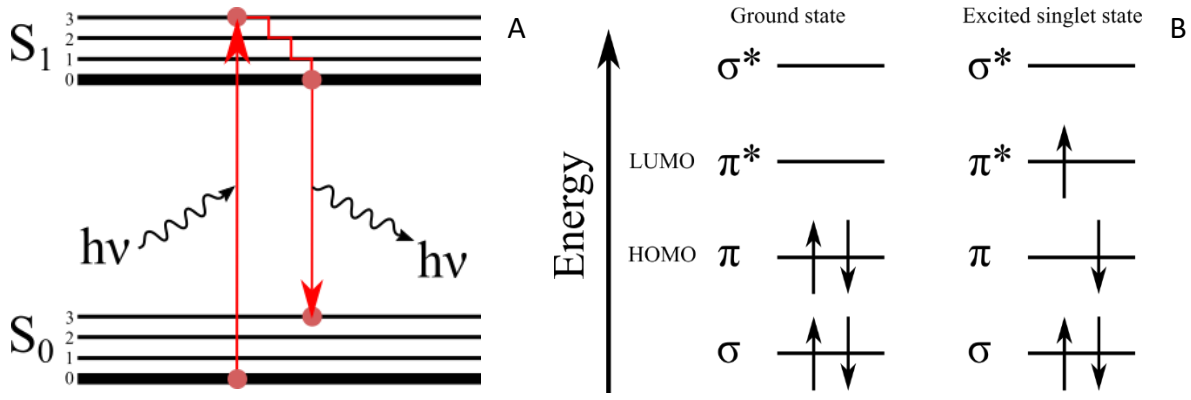

Figure 22. Jablonski diagram (A) and diagram of electron orbital ocupancy before and after a $\pi \rightarrow \pi^*$ transition induced by a photon absorbtion (B).

The frontier molecular orbital theory describes the transition from the highest occupied molecular orbital to the lowest unoccupied molecular orbital by the absorption of a photon of

the corresponding energy. The π electrons in particular have the higher propensity to absorb electromagnetic radiation due to the low energy gap between their ground and excited state. After internal vibrational relaxation resulting in the dissipation of energy as heat, the electron gains its ground state by emitting a photon of lower energy than the excitation photon. But this radiative relaxation is not the only way to release the absorbed energy. First the excited molecule can react in particular via oxidation reactions leading to its chemical degradation. Non-radiative relaxation ways include the release of energy as heat to the solvent molecules. Within a nanometric range, Förster resonance energy transfer (FRET) allows the direct transfer of the energy to a molecule presenting an excitation energy corresponding to the emitted energy.

In proteins, aromatic amino acids (Phe, Trp, Tyr) as well as His are able to absorb photons in the UV range. The energy absorbed by proteins or nearby molecules can result in local heating allowing conformational changes or can lead to their chemical degradation.

1.5.4 Mechanical stress

Mechanical stress is known to be an accelerating factor in protein aggregation: stirring can increase the diffusion and as a consequence increase the reaction rate especially in the case of localized reactions on surfaces. Shear stress is usually associated with protein aggregation despite its incapacity to denature proteins[131]. The mechanical fragmentation of aggregates especially fibrils leading to an increase of incorporation sites for native proteins is another explanation for the stirring requirement observed in protein aggregation kinetic. Alternatively mechanical stress could lead to the successive wetting and drying of proteins adsorbed on material surfaces at the material-air-liquid triple interface (cf. section 1.5.5).

1.5.5 Protein interaction with surfaces and interfaces

Protein adsorption is the process leading to the bonding of a protein to the surface of a material or an interface with another phase (e.g. liquid-air interface, organic-aqueous interface, etc.). Upon contact with a surface, especially hydrophobic or charged surfaces, the non-covalent interactions between the protein and the surface can lead to a dehydration of the protein-material interface[132]. The difference in energy of this interfacial interaction compared to the protein solvent interaction defines the stability of this adsorption. Due to the diversity of their chemical groups and their amphiphilic character, proteins are able to interact with a wide range of surfaces and physical interfaces.

Usually the adsorption of proteins on material surfaces and at the air-liquid interface are reported as forming monolayers. In this case, the adsorption of a protein on a surface can be modeled using the following equation:

$$\theta = \frac{1}{1 + \left(\frac{K}{[P]}\right)^{n}}$$

Where the fraction of the occupied surface **θ** depends on the protein concentration **[P]**, the affinity constant **K** and the cooperativity index **n** of the protein. The cooperativity index reflects the stabilization of a protein on the surface by other adsorbed protein molecules. Indeed protein-protein interactions can stabilize adsorbed proteins and facilitate the adsorption of new proteins (Figure 23). This positive cooperativity would be reflected by a cooperativity index higher than 1.

However if the pH is distant from the protein isoelectric point, then the resulting electrostatic repulsion might disfavor its adsorption close to other proteins on the surface. In such a case known as negative cooperativity, where the adsorption of a first protein disfavors the adsorption of another protein at proximity**, n** is lower than 1. For a cooperativity index equal to 1, the equation is identical to the Langmuir equation.

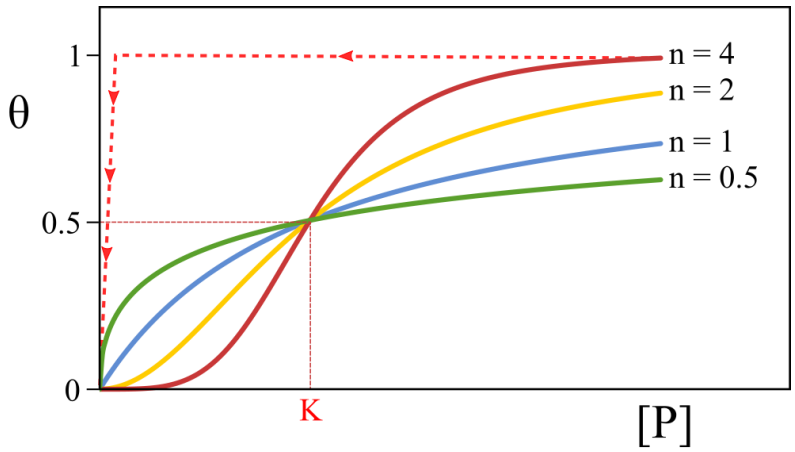

Figure 23. Adsorption isotherm for cooperative (n=2 and n=4), non-cooperative (n=1) and anti cooperative adsorption(n=0.5). The red doted curve also shows desorption hysteresis after the sudden reduction of protein concentration in solution.

The energy involved in the noncovalent protein-surface interaction defines the affinity **K** of the protein for the surface. These interactions will, like the protein internal interactions and the protein solvent interactions, influence the protein conformation (as described in section 1.3.1). Upon adsorption, the conformation of the macromolecules undergoes rapid transitions in order to match the surface, increasing the contact area and stabilizing the interaction. Notably an

increase of random coils and a modified thermal stability of the adsorbed proteins are often observed[133,134]. This state can represent the first intermediate leading to the formation of protein aggregates[134]. The affinity for the surface and the formation of conformational intermediates explains why heterogeneous nucleation pathways dominate in the presence of suitable surfaces (as seen in section 1.4).

The **Vroman effect** explains the succession of adsorbed molecules on a surface, newly exposed to the solution. The smallest proteins or peptides are the first to adsorb on the surface due to their higher mobility. They are later followed and often replaced by larger proteins which have therefore lower diffusion constants but usually higher affinity for the surface[135].

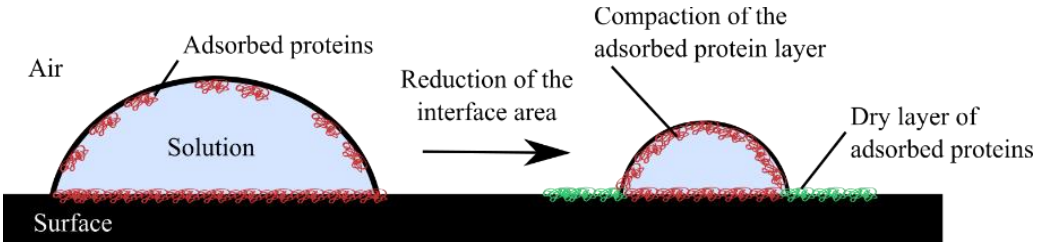

Figure 24. Effect of triple interface point variation and surface reduction on the interfacial layer of proteins.

The air-liquid interface is also of great significance for protein aggregation and in particular for amyloid aggregation. Aβ peptides for instance form monolayers of high β-sheet content at this interface[136]. The triple interface region is often pointed out as critical for protein stability for several reasons. First the air liquid interface area can be rapidly contracted or extended, leading to rapid variations of the protein density at the interface. Furthermore the triple interface line can vary along the material surface possibly exposing adsorbed protein to the air.

1.5.6 Specific interactions

First the binding of a ligand increases the number of interactions in the whole complex and therefore tends to stabilize the protein structure, in particular the protein-ligand complex is expected to remain stable at higher temperatures than the protein alone. This general property is the foundation of drug screening by thermal shift assays in which the denaturation temperature of a protein (protein melting temperature, at which 50% of the proteins are unfolded) is evaluated in the presence of different potential ligands[137].

Then, in the specific amyloid context, numerous small molecules have been shown to interfere with amyloid aggregation or to interact specifically with amyloid fibrils including metals, glycosaminoglycan and other proteins[138].

This is particularly true in the case of the Aβ(1-42) aggregation for which several cases of interactions with metals ions are well documented [139]. In particular Cu^{2+} binds amino-terminal copper and nickel binding motif (Nterm-X-X-H-) of the Aβ(11-23) peptide[140,141] which reduces the number of inter-strand H bonds and as a consequence inhibits aggregation[142].

If the introduction of amyloid seeds of a protein into a fresh solution of this specific protein is well known to induce a rapid transition to a fast aggregation phase, other polypeptide chains can also specifically interfere with amyloid kinetics. Alpha 1-antichymotrypsin for instance is known to either promote Aβ aggregation at a low molar ratio (1/200)[143] or inhibit it at a 1/10 molar ratio[144] and even disaggregates β-amyloid fibrils. This protein can also form amyloid aggregates on its own in specific conditions[145]. Similarly apolipoprotein E accelerates Aβ aggregation at a 1:100 molar ratio[143,146] but kinetically inhibits the nucleation step at lower concentrations[147]. Besides the dual effect of these two proteins, numerous molecules are known either as inhibitors or as enhancers of Aβ aggregation including proteins, phospholipids, gangliosides, etc.[148]

It is usually believed that only a short sequence of the protein is responsible for this seeding effect observed in amyloid aggregation: the section of the protein involved in the formation of the intermolecular β-sheet. Ivanova et al.[123] have shown that small peptides originating from the insulin sequence were able to significantly interfere with insulin aggregation. Either accelerating both nucleation and growth phase at sub stoichiometric concentrations (1/40 and 1/25 molar ratios) or preventing aggregation at equimolar ratios.

We therefore observe mechanisms of aggregation enhancement which, in contrast with chaotropic agents, operate at sub-stoichiometric concentrations. This indicates an interaction of these peptides with a rate-limiting intermediate in the amyloid aggregation pathway and strongly points toward a stabilization of the nucleation phase. On the other hand inhibition near equimolar concentrations suggests a thermodynamic competition with the native proteins.

1.6 Scientific context and approach

In the present thesis we focus on the issues of the amyloid aggregation of insulin induced by hydrophobic surfaces.

1.6.1 Insulin

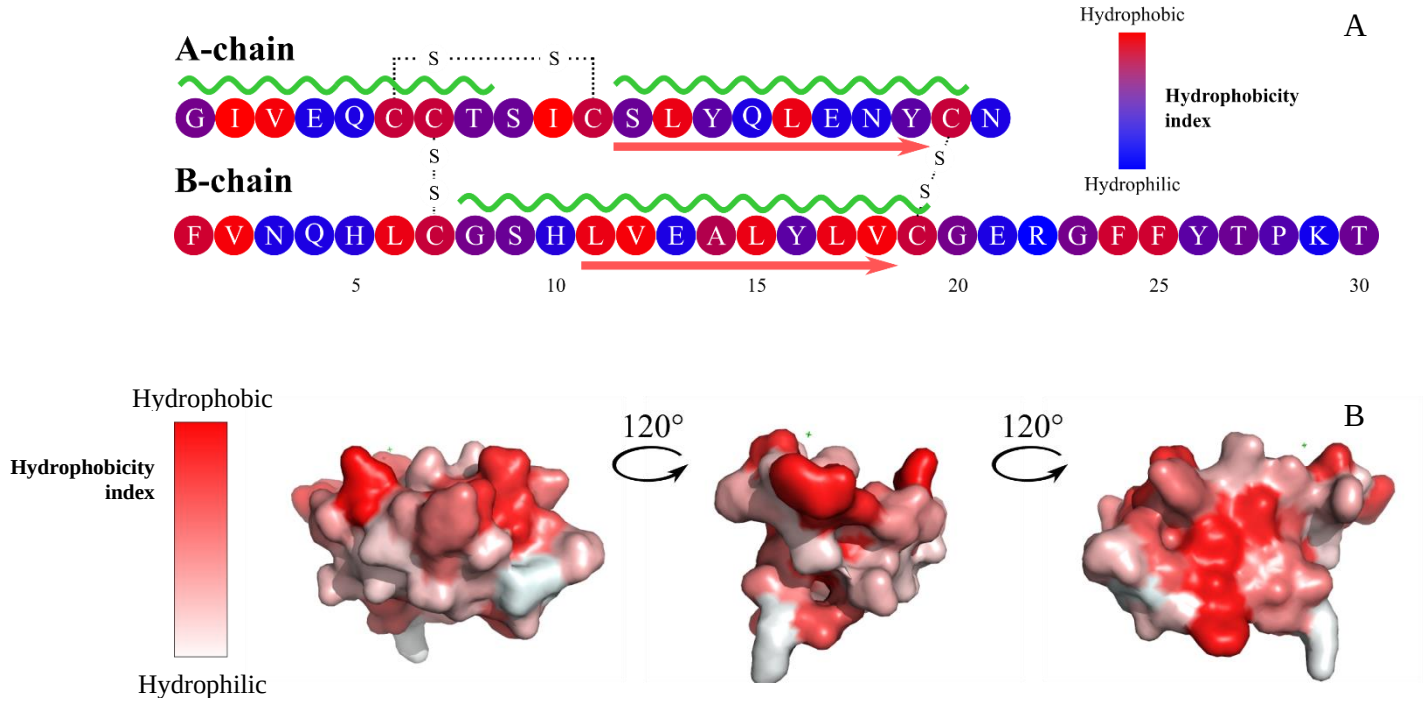

Figure 25. A: Sequence of human insulin A and B chains and hydrophobicity[2] of their amino acids. The green undulating line marks the alpha helices in the native structure. Red arrows mark the β-sheets in the amyloid structure. B: Surface model of native *Sus scrofa* insulin coloured using hydrophobicity scale (PDB acces number 4INS).

Insulin is a protein hormone secreted by the β-cells of the islets of Langerhans in the pancreas (hence its name from *insula* lat. "island") which exhibits important effects on metabolism regulation and glycaemia and is therefore used as a therapeutic protein in the treatment of diabetes mellitus[149].

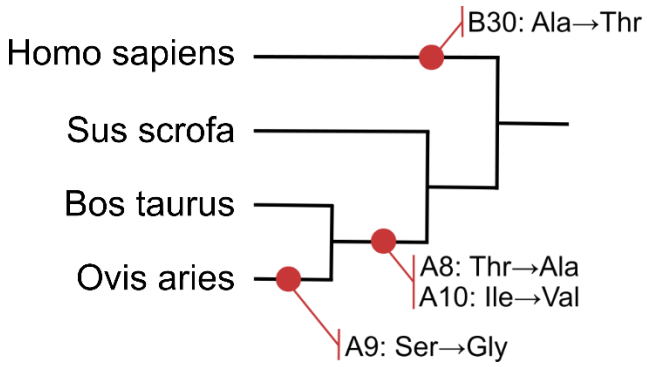

Figure 26. Evolution of the insulin amino acid sequence from the four most used species in the insulin literature.

Insulin is a small globular protein of approximately 5800 Da. Its structure is mainly globular and includes 3 disulfide bonds which are the conserved characteristic element of the insulin-like protein family. Two of these bonds link the two peptide chains plus one intra-chain disulfide bridge in the A chain (Figure 25).

Its sequence is highly conserved among vertebrates[150]: insulin from distantly related species can therefore induce clinical responses. Porcine and human insulin only differ from one amino acid (Figure 26) allowing the widespread use of insulin from *Sus scrofa* in diabetes therapy before the emergence of recombinant DNA biotechnology. More recently, protein engineering has led to the development of insulin analogs presenting modified absorption, distribution, metabolism and excretion profiles. In particular these analogs have been developed in order to obtain designed association constants and corresponding pharmacokinetic properties.

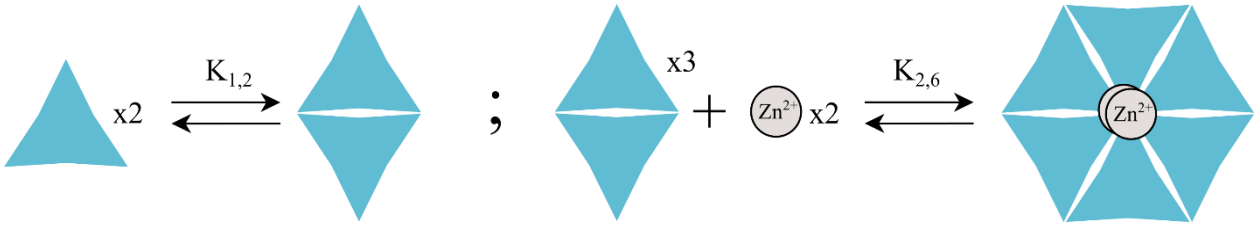

Figure 27. Insulin monomer self-association into dimer and dimer self-association into hexamer by association with 2 Zn^{2+} ions.

Insulin can form dimers and hexamers in solution increasing its conformational stability by inter-molecular interactions. Insulin hexamers are formed by the association of 3 dimers via the formation of a complex with 2 Zn^{2+} ions (Figure 27). Human insulin isoelectric point is 5.3-5.35 [151] (Figure 28).

Insulin form	$K_{1,2}$ (M^{-1})	$K_{2,6}$ (M^{-2})
Sus scrofa Zn-free[152]	$14 \cdot 10^4$	$4 \cdot 10^8$
Bos taurus Zn-free[153]	$1 \cdot 10^4$	$1 \cdot 10^8$
Sus scrofa Zn[154]	$14 \cdot 10^4$	$15 \cdot 10^{10}$

Table 3: Equilibrium constant for dimer ($K_{1,2}$) and hexamer ($K_{2,6}$) formation of different insulin molecules.

1.6.2 Insulin amyloid aggregation

Two main conditions are known to induce the formation of insulin amyloid aggregates: (i) in solution at high temperature and low pH (>70°C; pH 2) and (ii) on hydrophobic surfaces under physiological conditions (37°C; pH 7) and mechanical stress.

Fibrous aggregation of insulin at low pH and high temperature in solution has been known for a long time[155,156]. Most of the mechanistic data available on insulin aggregation comes from

these conditions. These resulting fibrils were found to be unbranched and characterized by intermolecular β-shets[157].

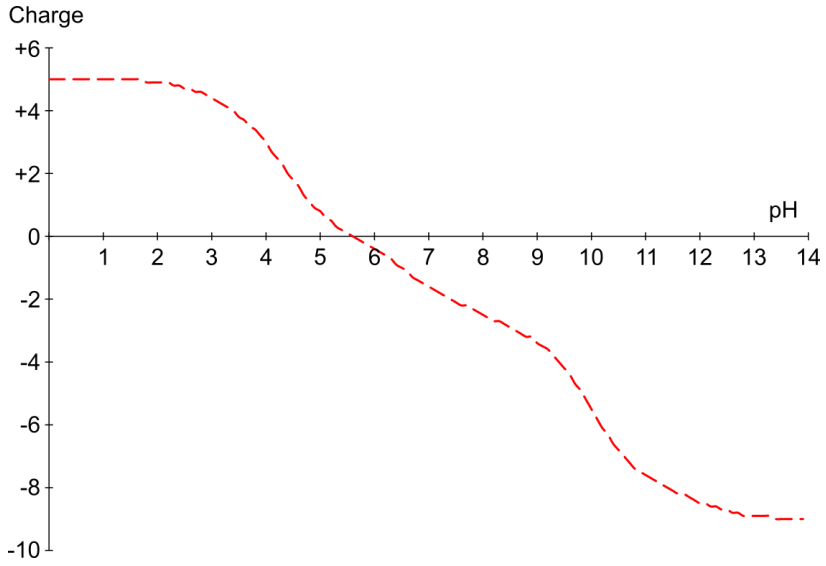

Figure 28. Theorical net charge of human insulin as a function of pH.

Lee et al. have presented a kinetic model divided into three phases: misfolding, nucleation, and elongation [158]. According to this model which is similar to the general model developed in the section 1.4.7, the hexamer dissociates into monomers, which, after a conformational change, will oligomerize into nuclei in an unfavorable association process. Beyond a critical nucleus size, monomer addition becomes thermodynamically favorable allowing the fast elongation of the fibrils.

The early steps of bovine insulin fibrillation can be monitored through tyrosine intrinsic fluorescence (bovine insulin presents four tyrosines located at the same positions as human insulin cf. Figure 25). This approach combined with ThT and ANS fluorescence has shown that dimer dissociation, unfolding (ANS positive state) and coalescence preceded the ThT positive state.[41]

Small angle X-ray scattering in solution has yielded low resolution structures of the monomer, the fibrils and an oligomer composed of 5-6 insulin monomers[159]. The authors present these oligomers as structural nuclei, also representing the elongation unit of the insulin fibril.

Nielsen et al [160] conducted a screening of the effect of environmental factors on insulin aggregation, presenting a model in which partially folded monomeric intermediates form nuclei which eventually mature into amyloid fibrils. They observe a high temperature dependency for insulin fibrillation which they attribute to the formation of fibrillation-competent intermediates

representing the rate-limiting step. Moreover they underline the positive role of mechanical agitation on nucleation which they explain by the formation of an extended air-water interfacial area.

The steps of insulin amyloid aggregation investigated by circular dichroism and electron microscopy are first the formation of non-fibrillar aggregates, leading to the development of protofilaments which subsequently assemble into fibrils, and eventually rearrange into the well-ordered highly twisted structures presenting a 450 Å helical repeat [161]. Meanwhile the FTIR spectrum reveals a progressive increase of the 1628cm^{-1} peak characteristic of β-sheets.

Dutta et al. consider ThT-positive insulin aggregates obtained after seeding in neutral pH and in the presence of disulfide-reducing agents as amorphous [162]. They monitored the aggregate morphology by electron microscopy as well as atomic force microscopy and their ability to seed a fresh insulin solution.

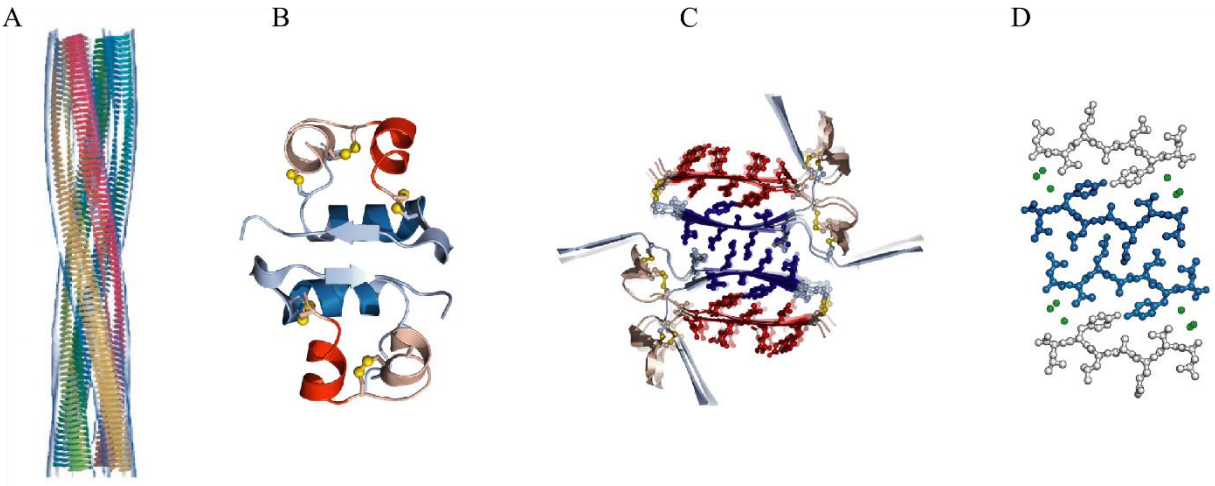

Figure 29. Structure of insulin amyloid fibril. A fibril, B structure of the native insulin dimer, C model of amyloid insulin dimer, D structure of region involved in the beta sheet formation with formation of a steric zipper. Modified from Jimenez et al.[163] (A) and Ivanova et al.[123] (B, C, D).

In 2002 Jimenez et al.[163] have investigated the structure of the insulin amyloid fibrils by cryo-electron microscopy, once again at high temperature and low pH. They observed fibrils containing either 2, 4 or 6 protofilaments (Figure 31). Manno et al. characterized the growth kinetic from a morphological point of view and described the growth phase as a combination of elongation and broadening by secondary nucleation[164,165]. Ivanova et al [123] have further investigated the mechanisms of the insulin amyloid fibril formation and provided a model for conformational changes of insulin during fibrillation. They have characterized the protein section involved in the formation of the intermolecular β-sheet by investigating the minimum

peptide from insulin the human sequence able to aggregate on its own. These peptides involved in the cross β-sheet were able to affect the kinetics of insulin aggregation.

Nayak et al.[166] observed the correlation between hydrophobicity and roughness of the surfaces and their ability to reduce the lag time of insulin aggregation. Even at pH 1.6, hydrophobic and rough surfaces were able to significantly enhance nucleation. On the other hand they did not observe an influence of the surface on the growth rate of the aggregates.

All these data are of great interest to our research question but are not readily referable. First even if the nucleation (and not growth) is the only step requiring high temperature[167], the low pH modifies the charges on the insulin allowing interactions otherwise physiologically unfavorable.

Another known condition causing insulin aggregation is **upon agitation at material surfaces**. The development of insulin therapy in diabetes mellitus rapidly pointed towards issues of its adsorption on the surface of storage and delivery systems[168] and subsequent aggregation[169,170]. The role of mechanical stress on this loss of stability was also pointed out[169,171], raising obstacles to the development of insulin delivery devices[172–175] and microparticulate insulin powder[176]. Furthermore localized iatrogenic amyloidosis was observed at the sites of regular insulin injection[177,178]. Both amorphous and amyloid aggregates of insulin have been found to present cytotoxicity to cultured rat insulinoma cells[179]. This cytotoxicity is higher for amyloid aggregates and increases through the aggregation time.

Sluzky et al. [171,180] have studied the kinetics and mechanisms of insulin aggregation under mechanical stress and upon hydrophobic surfaces. They proposed a model in which monomeric insulin adsorbs on hydrophobic surfaces, where it undergoes structural transitions to an unfolded state. This unfolded state monomers are then released in solution where they subsequently aggregate (Figure 32). They also observed that insulin hexamers were able to participate to the solution stability by interacting with the hydrophobic surface. Insulin aggregation at 37°C is promoted by agitation, surface hydrophobicity and increases with the area of hydrophobic surface in contact with the solution.

More recently our team focused (in particular through two PhD thesis by Thomas Ballet and Laurent Nault) on the conformational change undergone by insulin upon adsorption at material surfaces[181]. Fast insulin adsorption is associated with a first conformational change (Figure 30) which is followed by a second and much slower conformational change presenting an alleged increase of its β-sheet content and a ThT-positive signal. The β-sheet content of Nault

"amyloid" stage (Figure 30) based on the increase of a 1700cm^{-1} peak, has been questioned by mauri et al.[181,182] . It remain however clear from the infrared signature that important conformation change occurs after HI adsorption. Mollmann et al. and Mauri et al. have reported a loss of the α-helix content and an increase of random coils[182,183] upon insulin adsorption.

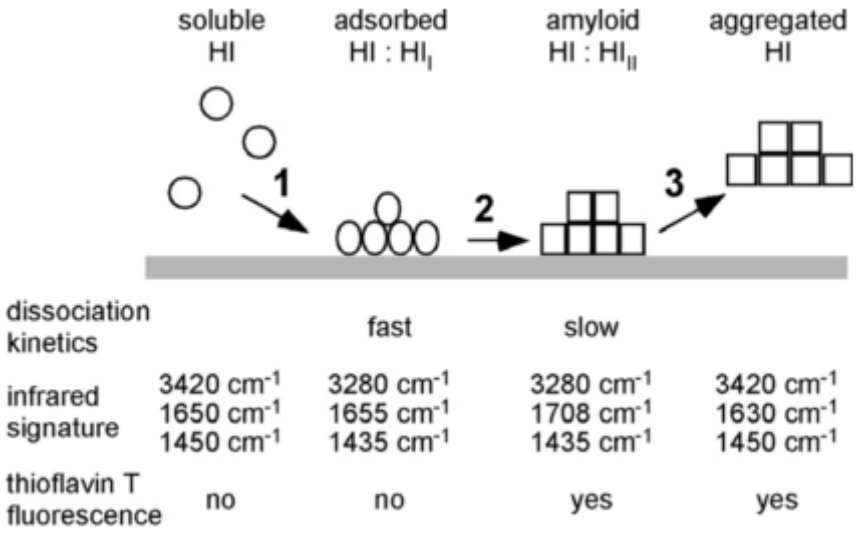

Figure 30. Nault's model for insulin surface-induced conformational changes. With FTIR signatures and ThT fluorescence.

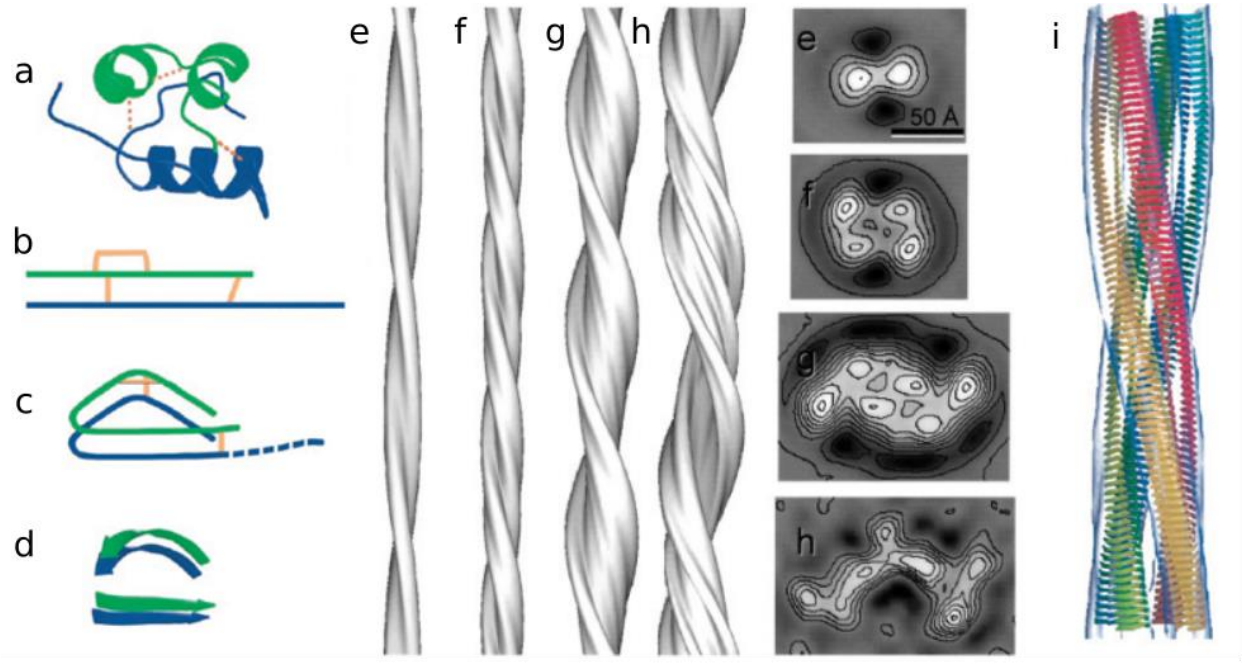

Figure 31. Structure of the insulin fibril from Jimenez et al.[163] (a) native structure of insulin showing the A chain in green and the B chain in blue; b) plain structure; c) proposed amyloid insulin model; d) β-sheet in the insulin amyloid model. Structure and cross section of observed fibril containing either 1 filament (e), 2 filaments (f), 4 filaments (g) or 6 filaments (h). Model of the insulin amyloid fibril presenting the cross β-sheet structures (i).

A

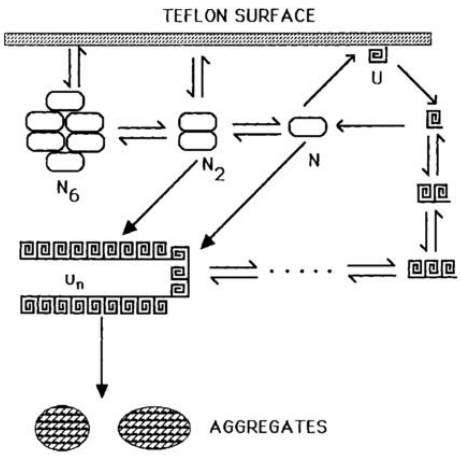

Sluzky et al.

1980

B

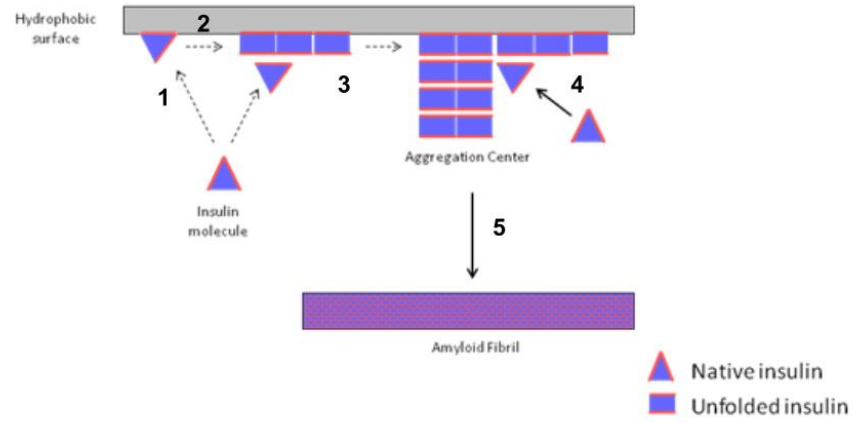

Ballet et al.

2010

C

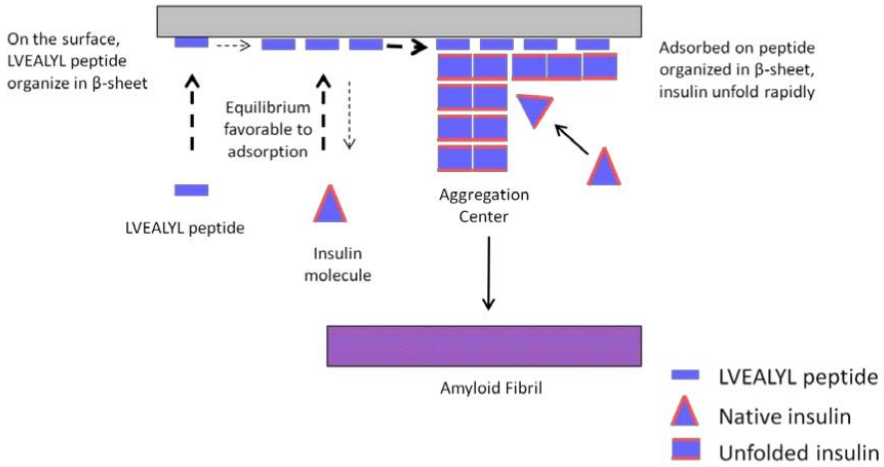

Nault et al.

2012

Figure 32. Model of surface-induced human insulin aggregation proposed by Sluzky et al. (A), Ballet et al. (B) and Nault et al. (C). According to Sluzky's model, insulin molecules unfold at hydrophobic surfaces and are released in solution where they oligomerize until forming large oligomers able to incorporate native monomers. According to Ballet's model, insulin adsorbs and unfolds on hydrophobic surfaces, where they nucleate to form aggregation centers incorporating native monomers. Amyloid fibrils are then released in solution. In Nault's model the peptides act as enhancers of nucleation and unfolding of insulin on the surface.

During his PhD Ballet reported the reduction of insulin aggregation lag-time at pH 2 and 60°C by seed formed either in the same conditions or on hydrophobic surface at pH 7.4 and 37°C. With seeds formed in the latter condition, the lag-time was even completely abolished which would indicate a direct seeding even though aggregates formed at pH 2 and 60°C presented a lag-time of about 1H 30[184]. These cross seeding results shows that HI aggregates formed on hydrophobic surfaces and subsequently released in solution in physiological conditions are amyloid aggregates similar to those formed in acidic conditions and at high temperature.

1.6.3 Peptide interaction with insulin aggregation

In order to determine the sections of human insulin involved in the formation of the β-sheets, spine of the amyloid fibrils, Ivanova et al[123] have searched for the minimum peptide able to both self-aggregate into amyloid fibrils and enhance insulin amyloid aggregation. They have shown that two peptides SLYQLENY and LVEALYLV, present in the sequence of the insulin A chain and B chain respectively, formed such amyloid fibrils. Moreover LVEALYLV was able to modify the kinetics of the insulin aggregation (Figure 33). At sub-stoichiometric (1/40) concentrations, it accelerates insulin aggregation, however at 1/10 or equimolar ratio the peptide inhibits this aggregation. From the presented kinetics (Figure 33) the LVEALYLV peptide likely seeds insulin amyloid fibrils as the lag-time seems abolished at low peptide concentrations. But both nucleation and growth seem impacted at inhibiting concentrations. The authors proposed a structural model for the amyloid insulin aggregation (Figure 29 C and D) in which these two peptide sections form a steric zipper at the core of the amyloid fibril spine. Nevertheless this study neither focuses on the role played by surfaces on insulin aggregation nor on the interactions of insulin with the adsorbed peptides.

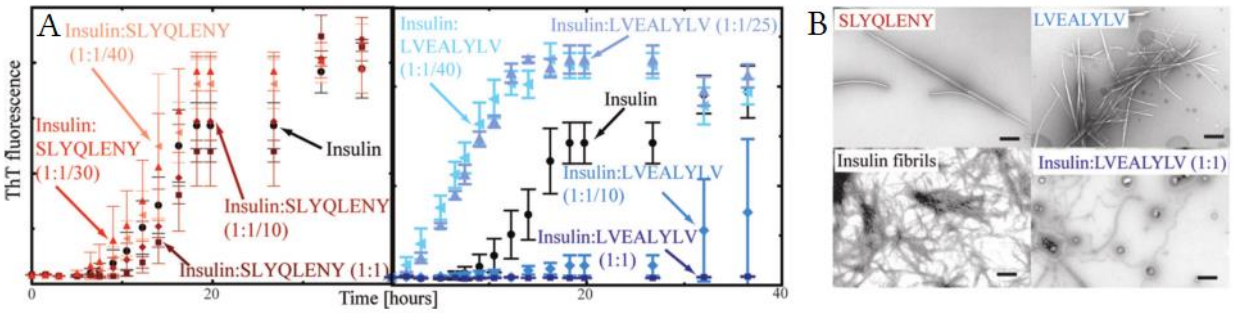

Figure 33. Two peptides extracted from the insulin sequence are able to self-aggregate into amyloid fibrils. A: effect of SLYQLENY and LVEALYLV on insulin aggregation kinetics, B: fibers of SLYQLENY and LVEALYLV (top) and reduction of insulin fibrillation at equimolar HI/ LVEALYLV ratio (bottom). (Figure from ivanova et al.[123])

Recently our team[185] investigated the effect of peptides on insulin aggregation with an emphasis on phenomena occurring at the material surface. Nault used various sequences of small peptides and monitored their effects on the kinetics of insulin aggregation. He has shown

that peptides forming β-sheets over hydrophobic surfaces were able to significantly accelerate the nucleation of insulin aggregation triggered by surfaces in sub-stoichiometric concentrations. Surface plasmon resonance revealed that such peptides once adsorbed on the surface, increase the mass of adsorbed insulin. Moreover by comparing the infrared spectrum of peptides in solution by transmission FTIR and peptides adsorbed on the surface by ATR FTIR, he has shown that the peptides presenting a β-sheet conformation on hydrophobic surfaces, were able to reduce the lag time of insulin aggregation whatever their sequence. As these peptides were designed by alternating hydrophobic and hydrophilic amino acids, their adsorption results in the formation of a β-sheet on the surface by the contact of one (the hydrophobic chains) in every two lateral chains with the surface (Figure 34). This phenomenon suggest that the lateral hydrogen bonds are responsible for the nucleation effect. On the other hand peptides forming alpha helices on hydrophobic surfaces exhibited a completely different behavior, dramatically delaying the first appearance of ThT positive insulin aggregates.

1.6.4 **Present work**

The present work consists in understanding the different effects on insulin aggregation of peptides containing a sequence with alternating hydrophobic and hydrophilic amino acids and their behavior either in solution or at hydrophobic surfaces. Moreover attempts were made to characterize and observe the location of insulin nucleation on hydrophobic surfaces.

In the first part (chapter 3), we investigate the effect of peptides with a sequence alternating between hydrophobic and hydrophilic amino acids, in particular $(LK)_nL$ peptides, on insulin aggregation kinetics. We demonstrate that the $(LK)_nL$ peptides cooperatively adsorb on hydrophobic surfaces, where they enhance insulin nucleation. A second antagonistic effect was observed with the longest peptides ($(LK)_4L$ and $(LK)_5L$): the peptides remaining in solution prolong the lag-time of insulin aggregation.

In the second part (chapter 4), we characterize the mechanisms of this inhibiting effect in detail, and the nature of the peptide-aggregate interaction in solution. The LK11 peptide was found to bind with high affinity the insulin aggregates, and prevents their growth likely by steric effects. This binding is mediated by the charges of the peptide's side chains, and inhibits both nucleation and growth of insulin aggregates.

In the last part (chapter 5) we investigate the location of insulin nucleation sites at the surface, in particular the triple interface between material, air and solution maximizing the shear stress

as well as the dehydration stress. We observe a maximal presence of early ThT positive objects at this triple interface.

On illuminated surfaces, a different aggregation mechanism was discovered: in the presence of ThT the light locally induces surface insulin aggregation. We have shed light on the dependency of this aggregation mode to surfaces allowing insulin adsorption as well as its dependency to strong agitation. Furthermore we investigate the role of ThT as an energy mediator between light at 436nm and insulin. This localized induction of ThT-positive growth, in conditions, where the location and the aggregation rate can be fully controlled, is of particular interest to test (or even screen) the effect of chemical compounds on protein aggregation.

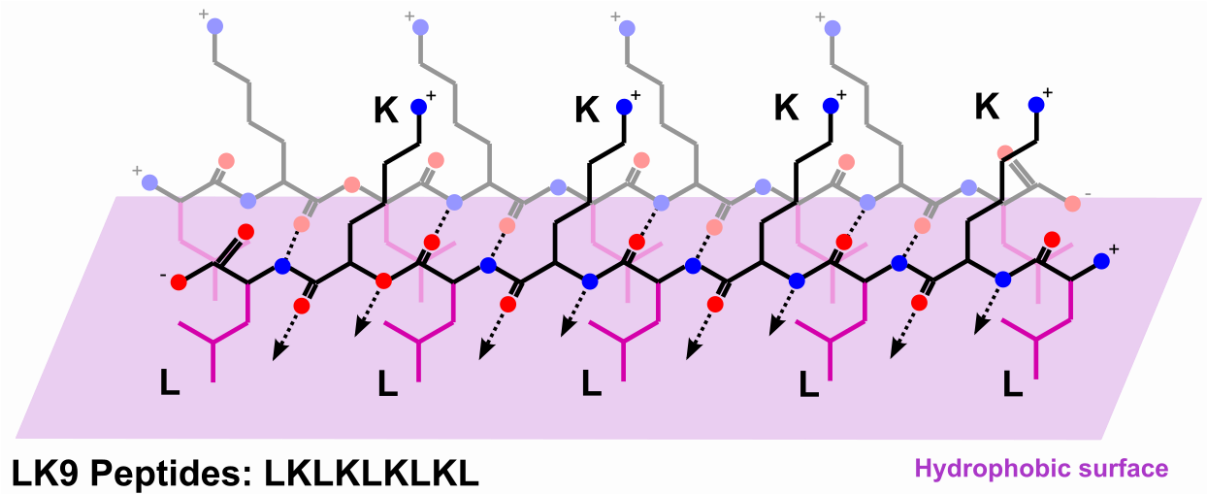

Figure 34. Alternate hydrophilic/hydrophobic peptide LK9 forming an antiparallel β-sheet on a hydrophobic surface. The dotted lines represent the intermolecular hydrogen bonds. We use CPK coloring with purple coloration of the apolar side chains in contact with the hydrophobic surface.

2 Material and Methods

2.1 Materials

2.1.1 Chemicals and Proteins

Buffers

The buffers were prepared as 10-fold concentrated solutions (10X buffer). The buffers used were either TN (NaCl 125 mM, Tris-HCl 25 mM, pH 7.4) for light induced aggregation or TMN (NaCl 125 mM, $MgCl_2$ 2 mM, Tris-HCl 25 mM, pH 7.4) in the kinetic assays. The presence of magnesium in the TMN buffer results from previous work of the team with a chaperone protein requiring Mg^{2+} as cofactor. The desired mass of salt were weighed as powders and dissolved in Milli-Q® pure water (resistivity =18 MOhm·cm at 25 °C). The pH of the tris buffer was eventually lowered to 7.4 by addition of HCl and the solutions were filtered and stored at 4 °C. In specific cases; SDS 20% (v/v) was added in the 1X filtered buffer solution prior to the experiment.

Insulin

We purchased recombinant human insulin (HI) produced in Saccharomyces cerevisiae from Sigma-Aldrich (ref: I2643). HI solutions were solubilized either in TN buffer or in TMN buffer. In order to solubilize insulin, the pH of the solution was lowered to 3.2 using 1 M HCl then adjusted to pH 7.4 with 1 M NaOH using a pH electrode. The HI concentration was then precisely adjusted to 86 µM, measuring the absorbance at 280nm ($\varepsilon_{280\ nm}$(HI) = 5.53 mM^{-1} cm^{-1}). Once adjusted at the proper concentration, the solution was filtered through a 0.22 µm Millex-GV filter unit (ref: SLGV033SS). The solutions were stored at T = 4 °C for less than 2 weeks and re-filtered before use.

Peptides

Selected chemically synthesized peptides were ordered from Genecust. They were solubilized in 10 mM NaOH or 1 mM NaOH to a concentration of approx. 430 µM, then filtered with a 0.22 µM filter (Millex-GV ref: SLGV033SS), aliquoted and stored at T = −20°C. As these peptides lack aromatic groups, their concentration cannot be determined by UV spectroscopy. In order to adjust their concentration, peptide solutions were therefore quantified by the bicinchoninic acid assay.

	Sequence		pH(I)	ΔG adsorption (Kcal.mol^{-1})	Mean concentration (µM)	Buffer
LK5	$(LK)_2L$	LKLKL	10.73	-8.4	84 ± 6	10µM NaOH
LK7	$(LK)_3L$	LKLKLKL	10.99	-11.2	76 ± 5	10µM NaOH
LK9	$(LK)_4L$	LKLKLKLKL	11.16	-14	75 ± 3	10µM NaOH
LK11	$(LK)_5L$	LKLKLKLKLKL	11.28	-16.8	115 ± 11	10µM NaOH
TAMRA-LK11	TAMRA$(LK)_5L$	TAMRA-LKLKLKLKLKL		-16.8	140 ± 28	10µM NaOH
LD9	$(LD)_4L$	LDLDLDL	0.39	-14	60 ± 7	1µM NaOH
LN9	$(LN)_4L$	LNLNLNL	3.63	-14	Non solubilized	
IS5	(IS)I	ISISI				
IS7	(IS)I	ISISISI				

Table 4. Measured concentration of peptides used in this thesis. Determined by quantipro BCA.

The estimation of the energy involved in the adsorption of a peptide on a hydrophobic surface is obtained by summing the transfer energy of its hydrophobic residues from an aqueous to a non-polar phase:

$$\Delta G_{adsorption} = \sum_{i=1}^{N_{Hydrophobic}} \Delta G_{Hydrophobic}$$

As only one type of hydrophobic residue is present per sequence:

$$\Delta G_{adsorption} = N_{Hydrophobic} \cdot \Delta G_{Hydrophobic}$$

Where $N_{Hydrophobic}$ is the number of hydrophobic amino acid residues in the peptide chains and $\Delta G_{Hydrophobic}$ is the energy transfer of the hydrophobic residues in question from the aqueous phase to the non-polar phase.

These transfer energy, corresponding to the transfer of the amino acid from water to benzene, were taken from Engelman *et al.*[186]: $\Delta G_{Leu} = -2.8\ Kcal.mol^{-1}$.

Thioflavin T

When bound to amyloid fibers, Thioflavin T (ThT) undergoes a fluorescence shift from (λ_{ex}= 342 nm; λ_{em}= 430 nm) to (λ_{ex}= 450 nm; λ_{em}= 482 nm). This property allows the direct quantification of amyloid fibers by fluorescence since the fluorescence of bound ThT is proportional to the amount of amyloid fibers. Thioflavin T (from Sigma-Aldrich, ref: T3516) was solubilized in TMN or TN buffer. The ThT concentration was then adjusted to 1 mM by absorbance measurement in 99% ethanol ($\varepsilon_{416\ nm}$ (ThT) = 26.6 $mM^{-1}.cm^{-1}$ in ethanol). Finally, solutions were filtered through a 0.22 µm Millex-GV filter (ref: SLGV033SS) and stored protected from light at 4°C for less than 2 weeks.

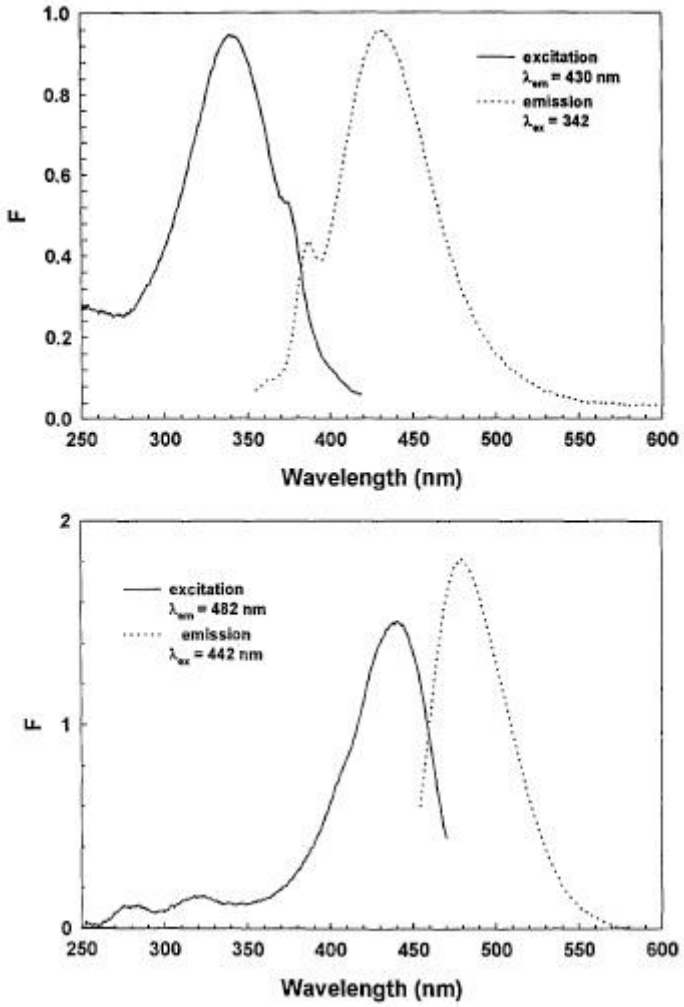

Figure 35. Thioflavin T excitation (solid line) and emission spectra for free ThT (top) and ThT bound to the fibrils (bottom) from Levine et al. [187]

2.1.2 Material surfaces

Glass surfaces

Borosilicate glass coverslips (from VWR international, ref: 631-0162) were either used untreated (water contact angle ~ 70°) or etched in NaOH 14M for 30 min which lowers their water contact angle to 30°. In order to obtain hydrophobic glass surfaces we silanized them with dimethyldichlorosilane (DMDCS) to obtain a water contact angle of 100°.

Glass functionalization with silanes

Borosilicate cover glass ϕ = 32 mm (from VWR international, ref: 631-0162) was washed successively in NaOH 14M for 30 min, soapy water and ethanol, then oxidized in oxygen plasma for 4 minutes. The silanization was performed during 2h with dimethyldichlorosilane 10% (v/v) in toluene. The coverslips were then washed in toluene and absolute ethanol and eventually incubated at 110°C in order to cross link silane functions by the formation of ether

group between silicon atomes. The proper functionalization of the glass was controled by water contact angle analysis (with a 20µL drop of pure H_20). The resulting functionalized glass presented a contact angle of 100 ± 5° compared to 70° for untreated glass (a contact angle superior to 90° indicates hydrophobicity).

Hydrophilic glass

In order to obtain hydrophilic glass surfaces, we incubate Borosilicate cover slips ϕ = 32 mm (from VWR international, ref: 631-0162) in NaOH 14M for 30 min after successive cleaning in soapy water, ethanol and Milli-Q water. The rotating glass rod used in light-induced aggregation assays was treated in the same conditions in order to avoid protein adsorption and aggregation on its surface.

Polystyrene beads

Fluorescent carboxylate-modified polystyrene beads (diameter = 0.5µm) purchased from Sigma-Aldrich (ref: L3280-1ML) were diluted 100 times in TN buffer. Then 10 µL of the diluted solution was added per well and observed at the beads fluorescence wavelength (λ_{ex}~575 nm; λ_{em}~610 nm) for 10 min until enough beads were stably adsorbed to the surface (~10 by field of view). The aggregation assay was then performed as described above.

2.2 Protein and peptide quantification techniques

Protein quantification by UV absorbance

Tryptophan, tyrosine and to a lesser extent disulfide bonds absorb ultra violet light at 280nm. This absorbance allows the determination of a pure protein concentration in solution knowing the protein molar extinction coefficient at 280nm (ε_{280nm}). This ε_{280nm} can be estimated with satisfying accuracy, provided the protein sequence is known, by the Pace et al.[188] formula:

$$\varepsilon_{280} = \sum_i \varepsilon_i \cdot n_i \approx 5500 \cdot n_{Trp} + 1490 \cdot n_{Tyr} + 125 \cdot n_{cystine}$$

Where $\boldsymbol{\varepsilon_i}$ represents the molar extinction coefficient of the amino acid ***i*** and $\boldsymbol{n_i}$ represents the number of ***i*** residues in the polypeptide chain. In practice tryptophan and tyrosine and disulfide bond contribute mostly to the protein extinction coefficient.

Protein concentration in solution can then be calculated using the Beer-Lambert law:

$$A_{280} = -log\frac{I}{I_0} = \varepsilon_{280} \cdot l \cdot [Prot]$$

Where $\mathbf{I_0}$ represents the incident light intensity, and **I** the transmitted light intensity, A_{280} is the absorbance at 280nm, $\boldsymbol{\varepsilon_{280}}$ is the molar extinction coefficient (in $M^{-1}.cm^{-1}$), ***l*** is the path length of the light beam through the solution (in cm), and [Prot] is the concentration of proteins in solution (in M).

For insulin the extinction coefficient ε is 5.53 $mM^{-1}.cm^{-1}$ (eq. 0.953 $L.g^{-1}.cm^{-1}$).

Bicinchoninic acid assay

At alkaline pH peptide bonds can reduce Cu(II) into Cu(I). The rate of this reduction by a particular polypeptide in solution is proportional to its mass. Bicinchoninic acid then forms complexes with Cu^+ ions absorbing light at a wavelength of 562 nm. The absorbance at 562nm is measured on a Tecan Infinite® plate reader. A calibration curve is done with BSA over a 0 to 30 µg/ml concentration range (QuantiPro BCA Sigma).

Quantification of adsorbed peptides

As the peptides used in this study do not contain aromatic residues, we used a fluorescently labelled LK11 peptide, in order to determine the amount of LK peptides adsorbed on surfaces. This peptide was incubated in the wells of a 96 well plate in a 200µL volume in the desired conditions for typically 10 minutes and 1200 rpm agitation on a Titramax 100 at 37°. The wells were then washed with filtered TN buffer. The remaining adsorbed TAMRA-LK11 peptides were quantified after desorption in 200µL TN 0.5% SDS by TAMRA fluorescence (λ_{ex}= 557 nm; λ_{em}= 585 nm) measurement on a Tecan Infinite® plate reader and comparison to a calibration curve (Figure 36).

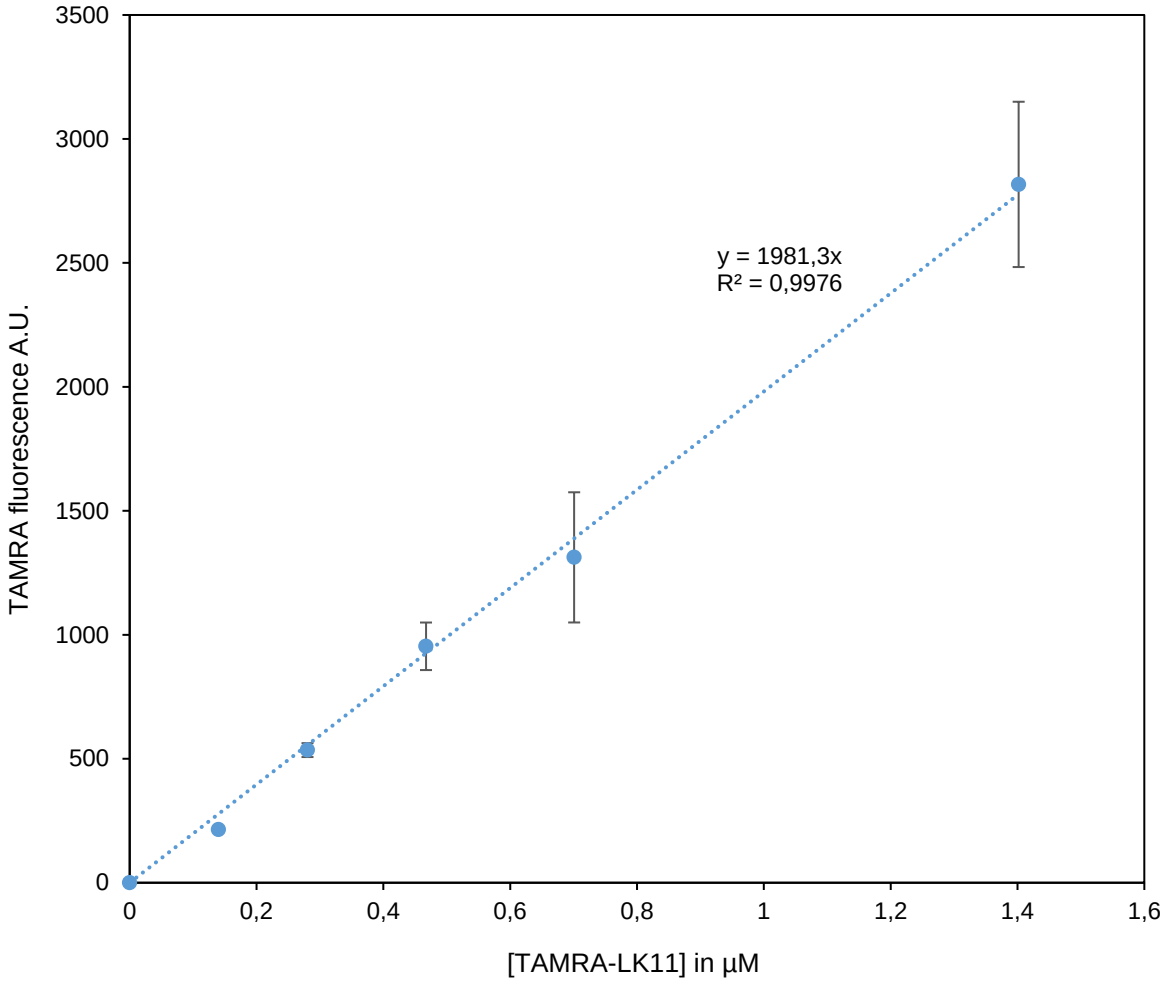

Figure 36. Calibration curve of the TAMRA fluorescence (λ_{ex}= 557 nm; λ_{em}= 585 nm) of the TAMRA-LK11 peptide in the 0.5% SDS.

2.3 Aggregation kinetic

2.3.1 HI aggregation kinetic assays in 96 well plates

The kinetic assay consist in the monitoring of the formation of ThT positive insulin aggregates. These kinetics were typically performed by measuring ThT fluorescence in 200µL wells on a Tecan Infinite® plate reader at 480 nm.

In the multi-well plates assay, the wells presenting the desired surface were incubated with TMN buffer containing the desired concentration of peptide and/or HI. The plates were then incubated under a constant temperature of 37°C on a Titramax 100® rotating at 1200 rpm unless differently specified.

Either hydrophobic (Nunc™ ref: 237105) or hydrophilic (Nunc™ ref: 237101) 96-well plates were used. The solution contained human insulin (HI) at a concentration of 0,5 mg.mL^{-1} (eq 86µM), Thioflavin T at a concentration of 20µM and the desired peptide at concentrations

ranging from 0 to 12 µM. For the standard conditions these plates were incubated at T = 37° and 1200 rpm on a plate agitator (Heidolph, Titramax 100) and covered by a Parafilm M to prevent evaporation. Every 15 min, amyloid aggregates were quantified by fluorescence measurement of the ThT bound to the amyloid fibers (excitation 450 ± 5 nm, emission 482 ± 5 nm.). For this, the plates were removed from the incubator and from agitation in order to read their fluorescence on a Tecan Infinite M1000 plate reader. The resulting fluorescence intensity are here considered to be proportional to the mass of HI amyloid aggregates in a 200µL volume and can be compared between similar conditions as verified by dilution.

Determination of the lag-times

The conventional lag-times (Cf. 1.4.5) were determined from the raw kinetic of each individual well as the abscissa of the steepest tangent to the amount of aggregate in solution with the baseline. These calculations were performed using a R script. This script first identifies the points belonging to the growth phase according to their fluorescence derivative in A.U. min^{-1}. The point is included in to the growth phase dataset if its derivative exceeds a threshold value (which can be adjusted according to the concentration of the solution, for instance). Then the growth phase dataset from each individual well is used in a linear regression, the result of which is controlled both graphically and by the regression residuals. The conventional lag-times are then directly determined by the intersection of the fluorescence baseline with the regression line.

On the other hand the slope of the regression line in A.U. min^{-1} determines the growth rate (Except in the Article III where the growth rate is determined according to a specific procedure).

Shear stress

As demonstrated by previous works[171] strong agitation is paramount for insulin aggregation on surfaces. The consequences of this agitation are an improved diffusion and a mechanical stress.

Difference of liquid velocity between points in space result in shear stress. For Newtonian fluids such as water, the shear stress is proportional to the liquid dynamic viscosity:

$$\tau = \mu \frac{\partial u}{\partial z}$$

Were $\boldsymbol{\tau}$ is the shear stress in Pa, $\boldsymbol{\mu}$ the dynamic viscosity in Pa.s, $\boldsymbol{u}$ is the liquid velocity in $m.s^{-1}$ and $\mathbf{z}$ the height perpendicular to the flow in m. Since the plate agitation results in the formation of a liquid vortex inside the well, the determination of the liquid velocity near the

surface and the corresponding shear stress are difficult to estimate. It is however clear that this shear stress increases with the rotation speed and the radius of the plate agitator.

In this work the rotation speed was fixed at 1200 rpm. According to Nault et al. work (unpublished) a minimal rotation speed (700 rpm) is required in order to induce aggregation in our multiwell plate set-up. The optimal rotation speed for aggregation (i.e. presenting the shortest lag-time) being approx. 900 rpm.

Surfaces of the wells

Since the observed aggregation phenomenon exclusively takes place on the surfaces of the well a detailed physico-chemical description of the well surface is necessary. The plate used in standard aggregation assays were polystyrene plates, presenting a hydrophobic surface. The wells have a diameter of 6.4mm, which (considering them as a perfect cylinder) corresponds to a surface of the well bottom of 32.1 mm². The volume of liquid in all assays performed is 200µL which corresponds to a height of 6.2mm and a parietal surface in contact with the liquid of 125mm². In total the surface in contact with the liquid represents 157.16 mm². Due to the centrifugal effect observed during agitation at 1200 rpm the height of the liquid on the side of the well can however increase slightly during the experiments.

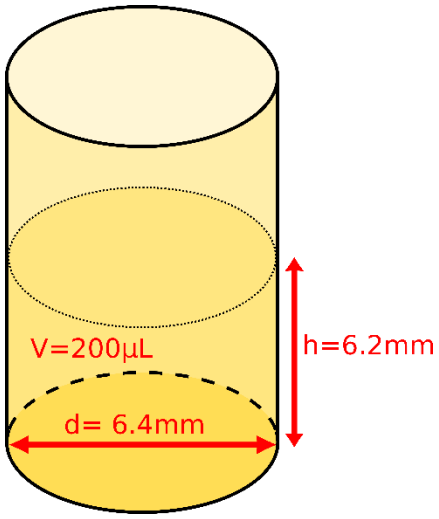

Figure 37. Scheme of a standard 96-well plate well, showing the surface in contact with the solution for a 200µL volume.

2.3.2 Seeding

Seeding consists in bypassing the nucleation step by introducing insulin amyloid fibrils into a fresh insulin solution. The aggregation will therefore proceed by growth and secondary pathways from the introduced fibrils and not via primary nucleation which presents orders of magnitude lower rates. In our standard aggregation kinetic assays (cf. supra), seeding was

performed by transferring 1µL of solution from a well in the plateau phase of aggregation into a fresh insulin well.

2.3.3 Surface pre-incubation

To test the role played by molecular complexes of proteins and/or peptides adsorbed at material surfaces, surfaces of the well (or in specific cases microscope coverslips) were pre-incubated with the desired concentration of peptides or protein during 10min (at 37°C under 1200 rpm agitation on a Titramax). After the desired pre-incubation time, these surfaces were then separated from the solutions and rinsed with TMN buffer for 30 seconds agitation (at 1200 rpm on a Titramax at 37°C). Eventually a fresh insulin solution was incubated in standard conditions in the rinsed wells.

The following diagram describes the successive steps in surface pre-incubation. In typical peptide pre-incubation assays, 200µl of 5µM LK9 or LK11 in TMN buffer were incubated in the wells for typically 10 min at 37°C. This procedure ensures a short lag-time with extremely low dispersion.

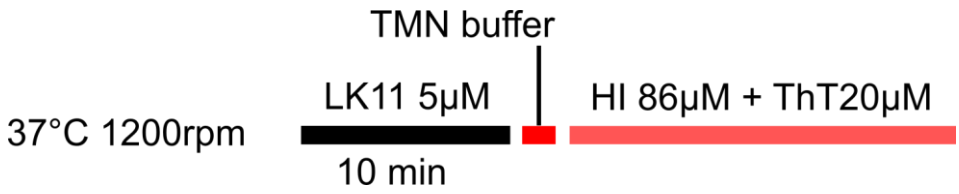

Figure 38. Diagram of surface pre-incubation protocol

2.3.4 Microscopic observations of surface aggregates.

Principle of fluorescence microscopy

In order to localize and characterize the amyloid aggregates, we observed them under an inversed fluorescence microscope. As presented on the scheme (Figure 39), the illumination is provided by a mercury lamp from which the desired excitation wavelength is selected by an excitation filter. The beam is then reflected by a dichroic mirror towards the objective which focalizes it on the sample. The fluorescence emitted by the fluorophores in the sample is then observed by the objective through the dichroic mirror and an emission filter selecting the wavelength resulting from the sample fluorescence and stopping the light resulting from scattering. This fluorescence light is then redirected towards the eyepieces or a CCD camera. In the experiments the filter of excitation, emission and the dichroic mirror are joined in a same fluorescence cube which is selected according to the fluorophore of interest.

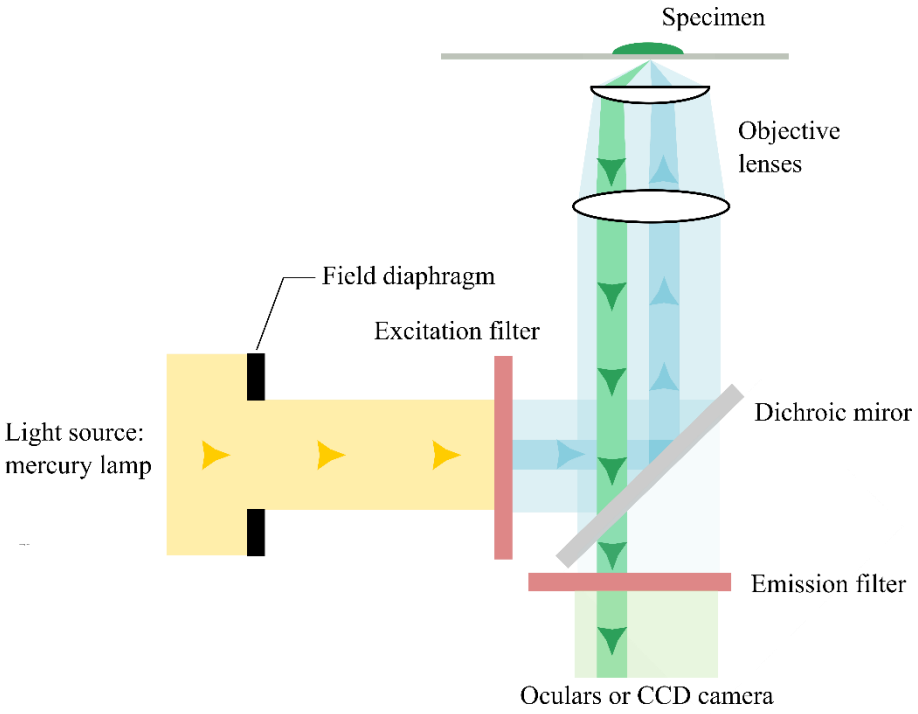

Figure 39. Principles of episcopic fluorescence microscopy.

2.3.5 Fluorescence Microscopy of ThT positive aggregates

Fluorescence microscopy was commonly used to observe ThT-positive aggregates. For glass coverslips, a 60X oil immersion objective (1.25 numerical aperture) was used on an Olympus IX71 fluorescence inverted microscope.

For the characterization of the size and number of amyloid particles through time, the fluorescence microscopy observations of the fibers were conducted in transparent flat bottom 96 well plates (Greiner bio-one, ref: 655101). The aggregation procedure was similar to that for the kinetic measurement. At selected time point the plate was removed from agitation and the wells were imaged using an Olympus IX71 fluorescence microscope and an Olympus U-CMAD3 camera (Japan) under a 20X magnification objective.

Name	*Reference*	*Excitation filter*	*Emission filter*	*Dichroic mirror cutoff wavelength*
DAPI	EO439072 U-N31036v2 DEAC C142286 Chroma	436 nm Bandwidth: 20 nm	480 nm Bandwidth: 30nm	455 nm
FITC	UMWIB2 olympus japan	460-490nm	510 nm (interference filter)	505 nm
Cy3	U-MWIG2 OLYMPUS JAPAN Green Wide 565 Interference	520-550nm	580 nm (interference filter)	565 nm

Table 5. Fluorescence cubes used in this study

2.3.6 Atomic Force Microscopy

Sample preparation for the observation of insulin amyloid fibers by AFM

DMDCS-functionalized borosilicate coverglasses ϕ = 32 mm (from VWR international ref: 631-0162) were incubated in 6-well Nuclon Delta surface plates (Thermo scientific, ref: 140675) under previously established standard conditions ([HI]=86 μM, T=37°C, 1200 rpm, [LK9] = 1μM). Their aggregation states were monitored using multiple fluorescence measurements per well with a Tecan Infinite M1000 apparatus (excitation: 342 nm, emission: 430 for the free ThT and excitation 450 nm, emission 482 nm for the fibril-bound ThT).

Atomic force Microscopy

Samples were imaged in TN buffer using a Dimension Icon AFM (Bruker SAS, Palaiseau, France), equipped with a 150 μm scanner in the intermittent-contact mode. We used a Scanasyst-air Si_3N_4 cantilever (Bruker) with a resonance frequency of 70 kHz and a spring constant of 0.4 N m^{-1}. Images were obtained in the center of the coverslips, where the nuclei density was highest. We show representative 2 × 2 μm^2 topology images. The analysis of the topologies was performed using the NanoScope Analysis software (Bruker).

2.4 Light induced amyloid aggregation

2.4.1 Experimental set-up

In order to localize the appearance of the first fibrils and the nucleation area, we developed a homemade device, allowing the direct observation of the surface in contact with a continuously agitated solution. The phenomenon of light-induced insulin aggregation localized at the surface of this chamber was later observed and imaged in similar conditions.

The experimental setup consists of a home-made chamber installed on the microscope stage of an inverted microscope (Figure 40). The microscope provides both the illumination for the photoactivation process and the monitoring of ThT fluorescence. The chamber was built using a 5 mm diameter tube cut from the top of a 1200 µL polypropylene pipette tip (Sorenson a34000), sealed over a borosilicate glass coverslip using melted Parafilm M®. It was filled with 750 µL of a HI and ThT solution, continuously stirred with a 1.5mm diameter cylindrical glass rod rotating at 1200 rpm thanks to a 6mm diameter DC gear motor (Nano Planetary 16mm Type ref: 206-102). The chamber was then placed on the stage of an Olympus IX71 inverted microscope and illuminated by episcopic illumination at the ThT excitation wavelength through a 60 x magnification objective (1.25 numerical aperture). The microscope is fitted with a mercury short arc bulb (Osram cb1915239) and a Chroma DEAC filter cube (ref. U-N31036v2 C108867). The spectroscopic parameters of the illumination and the fluorescence recording were: excitation wavelength λ_{ex} = 436 nm, bandwidth 20 nm, long-pass dichroic mirror cutoff wavelength λ_{cutoff} = 455 nm, emission wavelength λ_{em} = 480 nm, bandwidth 30 nm. The illuminating light intensity was modulated using neutral density (ND) filters and the area of illumination was delimited using the field diaphragm. For all standard assays (except for the aggregation on the nano-beads) this field diaphragm aperture was set to its minimum resulting in an illumination area at the surface under the form of a focused 50 µm-wide octagon (Figure 40.C).

The illumination was continuous during the time lapse unless differently specified. In these specific cases, a shutter (Unibliz VCM-D1) controlled the short illumination of the surface for the exposure time, typically 1s. The time lapse imaging of the ThT fluorescence distribution at the surface was performed with an Olympus DP30BW camera (256 grey levels). The exposure time is set depending on the illumination irradiance.

The illumination irradiance was determined in the following manner. The radiant flux falling on the illuminated area (1725 µm²) was measured at 440nm using a photodiode detector (18I27 Lasermate Q, Coherent, USA) with each ND filter used in this study. The radiant flux in the illuminated area was experimentally determined to be given by $P = 3.3187 \cdot \tau$ (mW), where τ is the ND filter transmittance, which corresponds to an irradiance $I = 1920 \cdot \tau$ kW.m^{-2} = $1920 \cdot \tau$ nW.µm^{-2}.

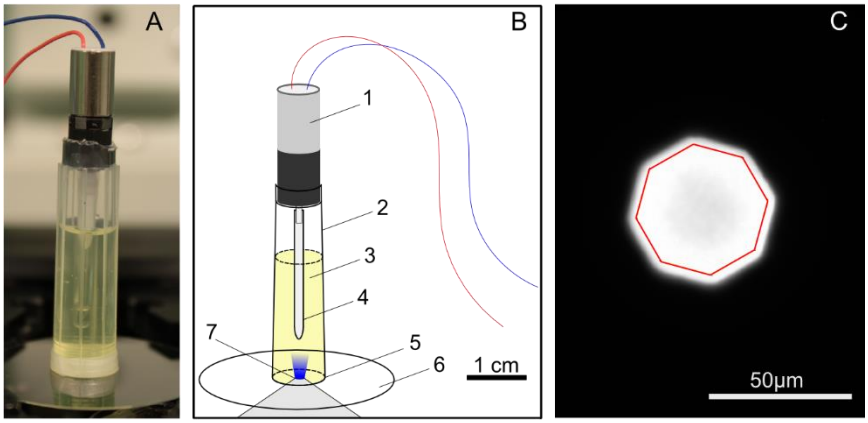

Figure 40. Experimental setup for light induced aggregation. A, photograph of the experimental setup on the fluorescence microscope while the motor is under tension (exposure time = 160ms). B, Scheme of the experimental setup: electrical motor (1), polypropylene well (2), protein solution (3), rotating glass rod (4), Parafilm gasket (5), glass coverslip (6), inverted microscope objective (7). C, Microscope image taken during a representative light induced insulin amyloidal aggregation assay using the minimum aperture of the field diaphragm. The red polygon defines the area of interest used for image analysis.

The same rod was used for different experiments so as to produce identical shear stress and solution agitation between assays. The glass rod was therefore rinsed successively with NaClO 10% (m/v) to remove any adsorbed protein and then in NaOH 14M in order to reduce its hydrophobicity by surface etching and prevent aggregation on its surface.

Light-induced amyloidal aggregation assays

For insulin aggregation assays on plain surfaces, the protein solution contained 86 µM HI and 20 µM ThT in TN buffer. The field diaphragm aperture was set to its minimum resulting in an octagonal illumination area (50 µm diameter). The illumination was continuous, at different light intensities, and the surface fluorescence was measured every 30 sec.

Beads assay

For insulin aggregation assays on beads, red fluorescent carboxylate-modified polystyrene beads (0.5 µm diameter, $4.87 \cdot 10^7$ beads.mL^{-1}) were purchased from Sigma-Aldrich (L3280) and diluted 100 times in TN buffer. Then 10 µL of the diluted suspension was added to the protein solution containing 86 µM HI and 20 µM ThT in TN buffer. The suspension was observed under red fluorescence conditions (λ_{ex} = 575 nm; λ_{em} = 610 nm) for about 10 min, until about 10 beads had been stably adsorbed on the surface in the field of view. The illumination was then switched to the ThT fluorescence conditions and the aggregation kinetics was recorded as described above.

Peptide injection assays

In order to test the effect of the $(LK)_nL$ in solution on the kinetic of light induced aggregation, we constructed a chamber fitted with an injection hole allowing direct addition of 5µM LK11 peptide in solution during the imaging process.

Image processing and data analysis

In order to avoid counting the fluorescence of aggregates resulting from edge effects we defined an area of interest (AOI) located in the center of the illumination field (Figure 40.C). The fluorescence intensity of each image was obtained by averaging the value of the pixels in this region: average raw fluorescence intensity. The saturation of the CCD camera limits the linear range of fluorescence recordings. We therefore excluded from analysis images presenting saturated pixels. In addition, we observed, after sufficient time, that amyloidal objects grow rapidly extending in height above the coverslip surface. This results in defocusing of the fluorescent zone and therefore a reduction of its measured fluorescence intensity. Images that were not well focused were therefore removed from the quantitative analysis.

To compare fluorescence intensities measured under different exposure times t_{exp} (s), different irradiances $I = 1920 \cdot \tau$ (nW.µm^{-2}), where τ is the ND filter transmittance, and at different ThT concentrations [ThT] (µM), the average raw fluorescence intensity is divided by the following coefficient $H = \tau \cdot t_{exp} \cdot [ThT] \cdot 0.6^{-1}$, resulting in F, the normalized surface fluorescence intensity. The kinetics of amyloidal aggregate growth under continuous agitation and illumination are then fitted with a first order exponential using a non-linear least squares method (Gauss-Newton algorithm) to determine A, k_{app} and B.

$$F = Ae^{k_{app}t} + B$$

To analyze the fluorescence increase on beads surface, an AOI was defined around the beads, large enough to encompass the largest exploitable fluorescence spot recorded. Another AOI was defined in the background region, to measure the (very slow) fluorescence increase at the coverslip surface. The initial values were subtracted from the fluorescence levels to obtain a normalized fluorescence.

2.4.2 Confocal microscopy

Principle of fluorescence confocal microscopy

In confocal microscopy, the scanning of the sample with a focused laser beam allows the observation of a sample in 3 dimensions and with high resolution in the focal plane. A pinhole

restricts the observed light to the fluorescence light originating in the focal plane. This is of particular interest for the observation of tridimensional objects spanning beyond the focal plane which in traditional microscopy are often responsible for an important **background noise.** Moreover the superposition of these focal plane slices allows the visualization of an object in 3 dimensions.

Observation of light-induced aggregates by scanning laser confocal microscopy

For confocal microscopy, the protein solution contained 86 µM HI and 130 µM ThT in TN buffer. The field diaphragm aperture was set to its maximum resulting in a circular illumination area (425 µm diameter). The illumination was continuous, at 960 $nW.\mu m^{-2}$ irradiance during 1 hour. The sample was then imaged using a 60x / 1.4 numerical aperture oil immersion objective on a LSM700 ZEISS confocal microscope, z steps= 0.4µm.

2.4.3 Electron microscopy

Observation of light-induced aggregates by Scanning electron microscopy

For electron microscopy, the protein solution contained 86 µM HI and 20 µM ThT in TN buffer. The field diaphragm aperture was set to its maximum resulting in a circular illumination area (425 µm diameter). The illumination was continuous, at I = 57.7 $nW.\mu m^{-2}$ irradiance during 1 hour.

The coverslip was then separated from the chamber, rinsed in pure H_2O, fixed 1hour in glutaraldehyde (2.5% in 0.1 M sodium cacodylate buffer pH=7.2) rinsed 3 times in 0.1M sodium cacodylate buffer pH 7.2 and eventually dehydrated in successive ethanol baths of increasing concentrations (70%, 90%, 95% 100%). The sample was then observed on a Quanta FEG 250 (FEI) scanning electron microscope using an Everhart-Thornley detector (HV= 5.00kV; magnification 20 000 X; Width 9.2mm; spot size: 3.0).

3 Cooperative induction of insulin aggregation by $(LK)_nL$ peptides

3.1 Introduction

The fundamental principles behind the quest for the minimal peptide, able to both self-aggregate and act as a seed for the aggregation of the full-length protein from which it is extracted, are based on the assumption that this sequence forms the β-strand of the amyloid fibril spine. However as illustrated by the works of Nault et al. there are differences between pure seeding (in which aggregation takes place from pre-existing fibrils) and enhanced nucleation (in which the primary nucleation rate is increased) especially when interaction with interfaces are involved.

At physiological pH, the LVEALYLV peptide is unable to form amyloid fibrils[185] on its own. Nault et al. have however shown that it is nevertheless able to accelerate insulin aggregation, specifically at hydrophobic surfaces. The experiments were however only conducted at a single peptide concentration.

Trials with variations of this peptide sequence proved that, in contrast to the seeding experiment performed by Ivanova et al.[123] at low pH, the sequence is not involved in this mechanism. Only the ability of peptides to form β-sheets upon adsorption on hydrophobic surfaces determined their ability to reduce (but not to abolish) the lag-time of insulin aggregation[185]. In surface-mediated aggregation, peptides are therefore unlikely to form the seed for amyloid fibrils but rather play a role in insulin nucleation.

The most efficient of Nault's peptides was $(IS)_3I$, a peptide exhibiting an alternate sequence between hydrophobic (isoleucine) and hydrophilic (serine**)** amino acids. Such peptides can adsorb on hydrophobic surfaces where they adopt a β-sheet conformation resulting from the exposure of hydrophobic side chains towards the surface and hydrophilic side chains towards the solution[189]. The first experiments that we performed with this peptide and the shorter $(IS)_2I$ peptide have shown their ability to cooperatively reduce the lag-time for insulin aggregation. The lowest critical concentration was found for the $(IS)_3I$. Similar, but charged peptides alternating L and K have been described in the literature as forming anti-parallel β-sheets on hydrophobic surfaces[189](Figure 41).

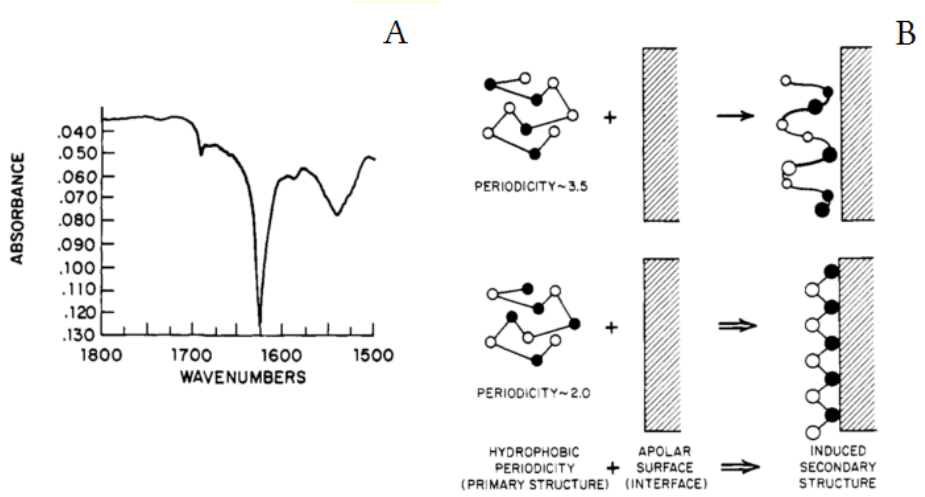

Figure 41. Conformation of peptides with alternate hydrophobic and hydrophilic amino acids on hydrophobic surfaces. A: ATIR Infrared spectrum of a monolayer of adsorbed LK7 peptide showing the 1700 cm^{-1} peak characteristic of antiparallel β-sheet, B: adsorption-induced secondary structure on hydrophobic surface according to the hydrophobic periodicity of peptides. Hydrophobic amino acids are represented with filled circles and hydrophilic residues with open circles. Modified from Degrado and Lear [189].

This interpretation of the spectrum is coherent with the scientific literature[190–192] defining the amide I region for antiparallele β-sheets as follow: "In antiparallel β-sheet structures, the amide I region displays two typical components. The major component has an average wavenumber located at ~1630 cm^{-1}, whereas the minor component, approx. 5-fold weaker than the major one, is characterized by an average wavenumber at 1695 cm^{-1}." Cerf et al. 2009[191]. However this interpretation has been contested by members of the PhD defence jury on the basis of (i) the broadness of the main peak at ~1625 cm^{-1}, and (ii) the absence of another peak.

In the following article, we used LK peptides to demonstrate that these small charged peptides have two opposed effects on insulin aggregation kinetics, depending on their concentration. The first effect consists in the acceleration of insulin amyloid nucleation on hydrophobic surfaces by adsorbed peptides. On the other hand, peptides remaining in excess in solution inhibit insulin aggregation. Several points not mentioned in the article are also developed below.

3.2 Article I

THE JOURNAL OF PHYSICAL CHEMISTRY B

Article

pubs.acs.org/JPCB

Dual Effect of (LK)nL Peptides on the Onset of Insulin Amyloid Fiber Formation at Hydrophobic Surfaces

Karim Chouchane, Charlotte Vendrely,[‡] Myriam Amari, Katie Moreaux, Franz Bruckert, and Marianne Weidenhaupt*

[†]University Grenoble Alpes, CNRS, LMGP, F-38000 Grenoble, France

[‡]Cergy Pontoise University, ERRMECe, I-MAT FD4122, F-95302 Cergy Pontoise, France

ABSTRACT: Soluble proteins are constantly in contact with material or cellular surfaces, which can trigger their aggregation and therefore have a serious impact on the development of stable therapeutic proteins. In contact with hydrophobic material surfaces, human insulin aggregates readily into amyloid fibers. The kinetics of this aggregation can be accelerated by small peptides, forming stable beta-sheets on hydrophobic surfaces. Using a series of (LK)nL peptides with varying length, we show that these peptides, at low, substoichiometric concentrations, have a positive, cooperative effect on insulin aggregation. This effect is based on a cooperative adsorption of (LK)nL peptides at hydrophobic surfaces, where they form complexes that help the formation of aggregation nuclei. At higher concentrations, they interfere with the formation of an aggregative nucleus. These effects are strictly dependent on the their adsorption on hydrophobic material surfaces and highlight the importance of the impact of materials on protein stability. (LK)nL peptides prove to be valuable tools to investigate the mechanism of HI aggregation nuclei formation on hydrophobic surfaces.

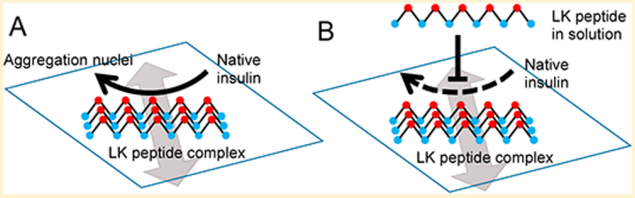

INTRODUCTION

Protein stability is a crucial parameter, foremost because it is a prerequisite for cellular function but also for safety and economic reasons in the production, storage, and delivery of therapeutics. Alteration of the protein structure usually entails the formation of aggregates, among which the amyloid fiber is widely studied. Amyloid aggregation of proteins in vivo is linked to major diseases, like Alzheimer's or Parkinson's.[1] Insulin, the most produced therapeutic protein, is known for decades for its propensity to aggregate into fibers, which is a serious drawback for the development of novel diabetes therapies.[2] Understanding the mechanisms involved in protein fibrillation is therefore essential to be able to control protein stability.

The transition from the soluble protein to the aggregated amyloid fiber is generally described in three successive steps: (1) a conformational change triggered by improper folding or environmental conditions, (2) stabilization of partly unfolded protein monomers by intermolecular interactions to form nucleation sites, and (3) association of successive unfolded monomers with the nuclei to promote fiber growth. Accordingly, a lag phase (steps 1 and 2) and a growth phase (step 3) are characteristically defined to describe protein fibrillation. For human insulin (HI), fibrillation can be triggered in vitro by low pH, high temperature, high ionic strength, and hydrophobic surfaces.[3−5] We have shown that at pH 7 and 37 °C, all three steps of the fibrillation process are strictly dependent on the presence of hydrophobic surfaces.[6] This finding highlights an aspect that is generally overseen in protein aggregation studies: the impact of the container material used for the experiments. In most cases, plastic containers are used and their hydrophobic surface represents both the site and trigger for insulin aggregation. In the following, we define nuclei as the surface-bound structures, able to trigger fibril growth (seeds). All complexes present during the maturation of these nuclei are termed prenuclei.

In an attempt to understand protein aggregation into amyloid fibers, multiple studies have been aimed at identifying minimal peptide sequences, inhibiting, or accelerating the aggregation kinetics of the parent protein. For example, an 8 amino-acid prion peptide segment (residues 113−120: AGAAAAGA), a 6 amino-acid modified peptide from Aβ (residues 16−20: KLVFF) and a 5 amino-acid segment from IAPP (residues 22−27: NFGAIL) can delay fibril formation of their respective full-length protein.[7−10] Such peptides are often hydrophobic, adopt a beta-sheet conformation, and fibrillate by themselves. The inhibitory effect is generally obtained at high concentrations, ranging from equimolar to concentrations exceeding ten times the protein concentration. On the other hand, amyloidogenic peptides, accelerating the aggregation lag phase, were also discovered.[11−13] They are often effective at low concentrations compared to the protein. Interestingly, many peptides have both accelerating and inhibiting effects on protein aggregation, depending on their relative concentrations. Ivanova et al. have shown that the HI B-chain peptide LVEALYL (residues B11 to B17) is able, at substoichiometric

Received: July 30, 2015
Revised: August 1, 2015

DOI: 10.1021/acs.jpcb.5b07365
J. Phys. Chem. B XXXX, XXX, XXX−XXX

concentrations to reduce the HI aggregation lag-time significantly and, at higher concentrations, to inhibit fibril growth.[12]

Using the same LVEALYL peptide and mutants thereof, we could demonstrate that the amyloidogenic effect described by Ivanova et al.[12] depends on the adsorption of the peptide in beta-sheet conformation on a hydrophobic surface.[14] Moreover, we could show that the secondary structure and not the sequence of the adsorbed peptide was crucial.[14,15]

Amyloidogenic peptides thus represent a tool to elucidate how a hydrophobic surface can trigger the formation of aggregation nuclei and hence amyloid fiber growth. They can be customized in sequence and chemical properties (functional groups, fluorescent labels). In this way, they are at the same time amyloid aggregation inducers and tools to investigate the aggregates they trigger. In order to get insight into the underlying molecular phenomena, we decided to use peptides adopting well-defined beta-sheet structures on hydrophobic surfaces. Such peptides were described by De Grado and Lear[16] and consist of alternating leucine (L) and lysine (K) residues to create a hydrophobic repeat, matching a beta-sheet. Using circular dichroism (CD) and Fourier-transform infrared spectroscopy (FTIR), they demonstrated that the synthetic peptide LKLKLKL adopted beta-sheet-stabilized monolayers at apolar interfaces, the hydrophobic leucine residues segregating toward the hydrophobic surface, and the lysine residues toward the water. On the basis of these findings, we reasoned that LK-repeat peptides of variable length were ideal tools to investigate the formation of nuclei, presenting an aggregation-triggering, surface-adsorbed beta-sheet structure to incoming HI molecules.

Here we present a thorough study of the mechanism of formation of HI aggregation nuclei on hydrophobic surfaces, using a series of (LK)nL peptides with varying length and a fluorescent tag. We investigate the dual concentration-dependent effect that these peptides have on HI aggregation kinetics. We demonstrate that their accelerating effect is based on their cooperative and stable adsorption properties, increasing the efficiency of formation of surface-bound prenuclei and that their inhibitory effect is due to an excess of peptide in solution.

EXPERIMENTAL AND THEORETICAL METHODS

Human Insulin. Recombinant human insulin (HI) produced in *Saccharomyces cerevisiae* was purchased from Sigma-Aldrich (ref: I2643). HI solutions TMN buffer (NaCl 125 mM, $MgCl_2$ 2 mM, Tris-HCl 25 mM, pH 7.4). In order to solubilize insulin, the pH of the solution was lowered to 3.2 using 1 M HCl then adjusted to pH 7.4 with 1 M NaOH using a pH electrode. The HI concentration was then precisely adjusted to 86 μM, measuring the 280 nm absorbance [ε_{280}(HI) = 5.53 mM^{-1} cm^{-1})]. The resistivity of the pure water used was 18 MOhm cm at 25 °C. Once adjusted at the proper concentration, the solution was filtered through a 0.22 μm Millex-GV filter unit (ref: SLGV033SS). The solutions were stored at T = 4 °C for less than 2 weeks and refiltered (if not fresh) before use.

Thioflavin T. When linked to amyloid fibers, Thioflavin T (ThT) undergoes a fluorescence shift from (λ_{ex} = 342 nm; λ_{em} = 430 nm) to (λ_{ex} = 450 nm; λ_{em} = 482 nm). This property allows the direct quantification of amyloid fibers by fluorescence since the fluorescence of linked ThT is proportional to the amount of amyloid fibers. Thioflavin T (from Sigma-Aldrich, ref: T3516) was solubilized in TMN buffer. Then the ThT concentration was adjusted to 1 mM by absorbance measurement (in ethanol ε_{416}(ThT) = 26.6 mM^{-1} cm^{-1}). Finally, solutions were filtered through a 0.22 μm Millex-GV filter (ref: SLGV033SS) and conserved protected from light at T = 4 °C for several months.

Peptides. Chemically synthesized (LK)nL peptides as well as the tetramethyl rhodamine-labeled (LK)5L peptide (TAMRA-LK11) (Table 1) were ordered from Genecust (Luxembourg), solubilized in 10 mM NaOH to a concentration between 75 and 115 μM then filtered through a 0.22 μm filter (Millex-GV ref: SLGV033SS) and stored at T = −20 °C. The concentration of unlabeled peptides was determined using the Quanti Pro Bicinchoninic acid assay (Sigma-Aldrich ref QPBCA). The concentration of TAMRA-LK11 was determined using the molar extinction coefficient of tetramethyl rhodamine, ε = 65 200 M^{-1} cm^{-1}.[17] A linear correlation curve linking fluorescence at 585 nm to the amount of TAMRA-LK11 peptide was established (data not shown).

Table 1. (LK)nL Peptides

peptide name	peptide sequence
LK5	LKLKL
LK7	LKLKLKL
LK9	LKLKLKLKL
LK11	LKLKLKLKLKL
TAMRA-LK11	^{TAMRA}LKLKLKLKLKL

Quantification of TAMRA-LK11 Adsorption on Hydrophobic Surfaces. TAMRA-LK11 was incubated at different concentrations (up to 2.8 μM) in hydrophobic 96-well plates (in triplicate) and shaken at 1200 rpm for 10 min. The solution was then discarded and the well washed with 200 μL of filtered TMN buffer. After discarding the buffer, the adsorbed peptide was desorbed using 0.5% SDS in TMN buffer (1 min at 1200 rpm and 37 °C). The peptide TAMRA-LK11 was then quantified using a calibration curve (see above).

Measurement of Insulin Aggregation Kinetics. Aggregation kinetics were done in a 200 μL reaction volume in hydrophobic black 96-well plates (Nunc TM ref: 237105). In each well, aggregation assays were performed in the following conditions: [HI] = 86 μM, [ThT] = 20 μM, [LK peptide] = 0−5 μM, at T = 37 °C and agitation of 1200 rpm on a plate agitator (Heidolph instrument, Titramax 100). The amount of amyloid fibers has been monitored by fluorescence measurement of ThT bound to amyloid fibers (λ_{ex} = 450 nm, λ_{em} = 482 nm). The plates were removed from the incubator/agitator in order to read their fluorescence in a Tecan infinite M1000 plate reader, every 15 min. The bandwidth of the monochromators at the excitation and emission wavelengths was 5 nm. Data were obtained with three independent experiments using five replicates for each experimental condition. Lag times and growth rates were obtained by fitting data points of individual replicates.[14] These were then used to calculate mean values and standard deviations.

Cooperativity Calculations. To calculate the Hill coefficient of the cooperative effect of the peptides on the lag time, the experimental data points of the lag times (τ) as a function of peptide concentration (see also Figure 1) were fitted to the following equation:

$$\tau = \tau_{max} - (\tau_{max} - \tau_{min}) * \frac{[LK]^n}{[LK]^n + [LK]_c^n} \quad (1)$$

DOI: 10.1021/acs.jpcb.5b07365
J. Phys. Chem. B XXXX, XXX, XXX−XXX

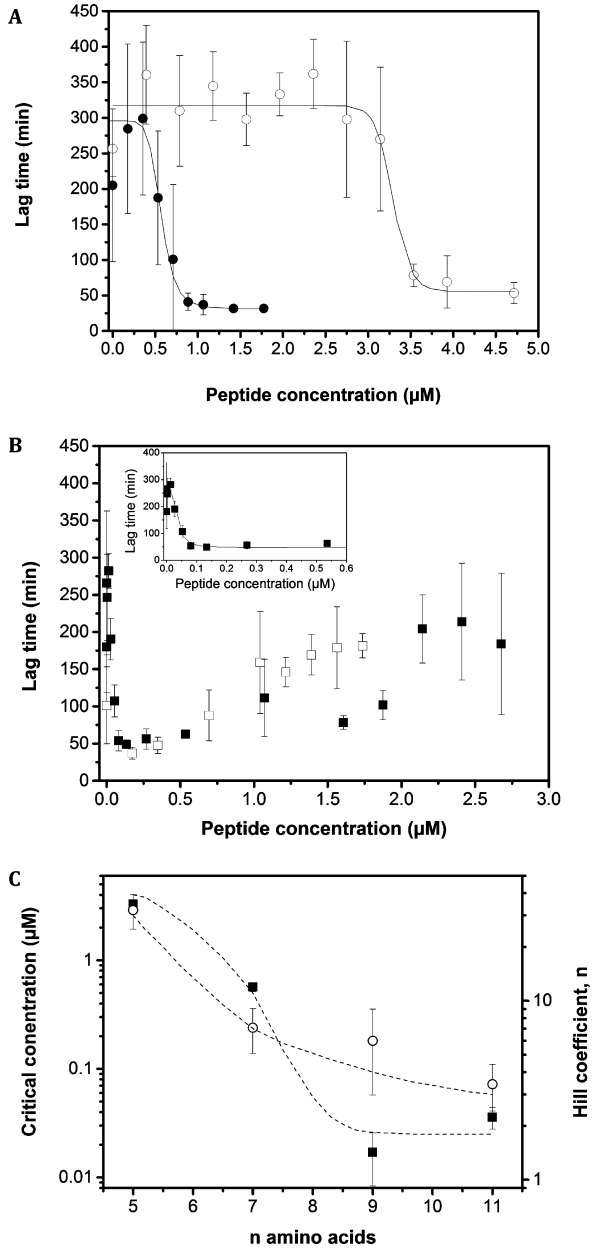

Figure 1. Different effects of LK peptides on the lag time of fibrillation. HI and ThT have been mixed with LK5 (A, ○), LK7 (A, ●), LK9 (B, □) and LK11 (B, ■) peptides at different concentrations and HI fibrillation has been monitored by ThT fluorescence. The solid line represents the fit of the experimental data with the Hill equation (see Experimental and Theoretical Methods). (C) The Hill coefficient (circles) and the critical concentration (squares), corresponding to the one at which 50% of the reduction of the maximal lag time was obtained, are plotted versus the number of LK amino acids. For easier reading, symbols are joined by a hand-drawn dashed line.

where τ_{max} represents the lag time (min) without peptide, τ_{min} the minimal lag time (min) obtained for a given peptide, [LK] the peptide concentration (μM), $[LK]_c$ the critical peptide concentration, corresponding to the concentration at which the lag time is half maximal and n the Hill coefficient. The fit was obtained by minimizing the quadratic error between experimental and calculated τ, weighted by the standard deviation of the lag time.

For the cooperative adsorption of TAMRA-LK11 on the hydrophobic surface of 96-well plates, the following equation was used to fit the experimental data:

$$[LK11]_{ad} = [LK11]_{max} * \frac{[LK11]_{sol}^{n}}{[LK11]_{sol}^{n} + [LK11]_{c}^{n}} \quad (2)$$

where $[LK11]_{ad}$ represents the concentration (in μM) of the TAMRA-LK11 peptide adsorbed on the well walls, $[LK11]_{sol}$ represents the concentration (in μM) of the TAMRA-LK11 peptide remaining in solution (i.e., $[LK11]_{sol} = [LK11]_{initial} - [LK11]_{ad}$), and $[LK11]_{max}$ represents the equivalent maximum concentration (in μM) of TAMRA-LK11 peptide adsorbed on the well surface for a given initial TAMRA-LK11 concentration, $[LK11]_{initial}$. $[LK11]_c$ represents the critical [LK11] concentration (in μM), corresponding to the half-maximal concentration of adsorbed TAMRA-LK11, and n represents the Hill coefficient of cooperative peptide surface adsorption. The fit was obtained by minimizing the quadratic error between experimental and calculated peptide concentration, weighted by the standard deviation of the measured concentrations.

Atomic Force Microscopy. *Glass Functionalization.* Borosilicate coverslip glasses (ϕ = 32 mm, from VWR international ref: 631-0162) were washed successively in SDS, ethanol, water, dried, and then activated in oxygen plasma for 4 min, and treated (t = 2 h) with dimethyldichlorosilane 5% (v/v) in toluene. This process covalently couples the silane to the glass by reacting with exposed Si−OH groups on the glass. The coverslips were then washed in toluene and absolute ethanol, and incubated at T = 100 °C (2 h) (curing) in order to cross-link silane oxides. Functionalization of the glass was controlled by water contact angle analysis (20 μL droplets of pure H_2O). The resulting glass presented a contact angle of 100° ± 5°, indicating a significant hydrophobicity.

Sample Preparation for the Observation of Insulin Aggregation Nuclei by AFM. Functionalized borosilicate coverslips were incubated in 6-well Nuclon Delta surface plates (Thermo scientific, ref: 140675) under the following conditions: T = 37 °C, 1200 rpm, [HI] = 43 μM, [LK9] = 0 or 0.2 μM, [ThT] = 20 μM in TN (NaCl 125 mM, Tris-HCl 25 mM, pH 7.4). The aggregation state was monitored using fluorescence measurements with a Tecan infinite M1000 apparatus (λ_{ex} = 450 nm; λ_{em} = 482 nm for bound ThT). Before AFM imaging, the samples were washed briefly by dipping in 0.1 μm-filtered TN buffer and dried. Mg was omitted from the buffer to avoid crystal formation during drying.

Visualization of Insulin Amyloid Aggregation Nuclei by Atomic Force Microscopy. Samples were imaged in TN buffer using a Dimension Icon (Bruker SAS, Palaiseau, France), equipped with a 150 μm scanner in the intermittent-contact mode. We used a Scanasyst-air Si_3N_4 cantilever (Bruker) with a resonance frequency of 70 kHz and a spring constant of 0.4 N m^{-1}. Images were obtained in the center of the coverslips, where nuclei density was highest. We show representative 2 × 2 μm^2 topology images. The analysis of the topologies was performed using the NanoScope Analysis software (Bruker).

Fluorescence Microscopy. *Sample Preparation for the Observation of Insulin Amyloid Aggregates by Fluorescence Microscopy.* Fluorescence microscopy observations of HI aggregates were conducted in transparent polystyrene flat-bottom 96 well plates (Greiner bio-one, ref: 655101). The aggregation procedure was the same as for the kinetic measurements. At selected time points, the plate was removed

DOI: 10.1021/acs.jpcb.5b07365
J. Phys. Chem. B XXXX, XXX, XXX−XXX

from agitation, and the wells were imaged using an Olympus IX71 fluorescence microscope equipped with an Olympus U-CMAD3 camera, with an objective magnification of 20×.

Particle Analysis. Particle counting and measurement of particle area (in pixels) from 16 images (covering 0.53 mm^2) at each time point were performed with ImageJ, using a fluorescence intensity threshold adjusted to the background for each image set. The selection of the particles was done using the particle analysis command and defining 10 pixels as the minimal particle area. The areas were then converted into μm^2 using the rate of 0.023 μm^2 $pixel^{-1}$.

RESULTS

LK Peptides Show Concentration-Dependent Effects on the Lag Time of HI Fibrillation but Have No Influence on the Fibril Growth Rate. As described in our previous work, HI fibrillation was monitored using ThT fluorescence emission at 482 nm in polystyrene 96 well plates at 37 °C with an orbital agitation of 1200 rpm.[14] In order to study the effect of LK peptides on HI amyloid formation, the peptides, at concentrations between 0.01 and 4.7 μM, were mixed with the HI solution, and the fibrillation kinetics were recorded defining the lag time, elongation, and plateau phases. As a control, no ThT fluorescence increase was observed in wells containing 2.6 μM of peptide alone without HI, showing that the LK peptides do not assemble into amyloid fibers by themselves.

Our results show that, upon incubation with LK5, the shorter peptide, at concentrations up to 3 μM, the lag times of HI fiber formation were not modified and remained similar to those obtained in the absence of peptide (i.e., about 300 min) (Figure 1A, ○). By mixing HI with LK5 at concentrations equal or higher than 3.5 μM, the lag times of HI self-aggregation were decreased about six times to around 75−50 min. The LK7 peptide also shortens the lag times for peptide concentrations higher than 0.7 μM (Figure 1A, ●). For LK7 concentrations from 0.9 to 1.7 μM, the lag times were about 6 times decreased. No effect of the peptide is observed for LK7 concentrations lower than 0.7 μM. Using peptides of longer sequences, LK9 and LK11, the accelerating effect occurs at very low peptide concentrations, lower than 0.3 μM (Figure 1B). The lag time decrease became evident for LK11 concentrations of 0.03 μM, and the minimum lag time, equal to 50 min, was reached for 0.1 μM of LK11 (Figure 1B, inset). Moreover, for LK9 and LK11, a second effect was seen at concentrations higher than 0.3 μM: the lag times increased and reached a value similar to the one obtained without peptide. At 1.5 to 3 μM, LK9 and LK11 seemed to delay the nucleation, as the lag times were higher than the one observed without peptide (see also Figures 3 and 5, white bars). HI fibrillation kinetics is known to be highly variable, and this phenomenon is reflected by the large standard deviations obtained at high peptide concentrations (Figure 1B). In contrast, in the presence of LK peptides in accelerating conditions, the variability is strongly reduced.

For each peptide, the variations of the lag times with their concentration showed a sigmoidal shape suggesting a cooperative effect of the peptides on the acceleration of the nucleation step. Indeed, a critical concentration, corresponding to the one with which the accelerating effect obtained was 50% of the maximum, could be determined. For longer LK peptides, lower concentrations were enough to shorten the lag phase, suggesting that the accelerating effect of the LK peptides is more efficient with increasing peptide length. To assess this point, we plotted the correlation between the length of the peptides and the logarithm of their critical concentration (Figure 1C). This plot shows that the critical concentration decreases sharply with the length of the LK peptide until 9 amino acids. For LK11 a Hill coefficient of 2.5 and a critical concentration of 0.035 μM are observed (Figure 1C).

In order to check if LK peptides could influence the growth of HI fibrils (elongation phase), the variations of the growth rates in function of the peptide concentration have been investigated (Figure 2). At the different peptide concentrations

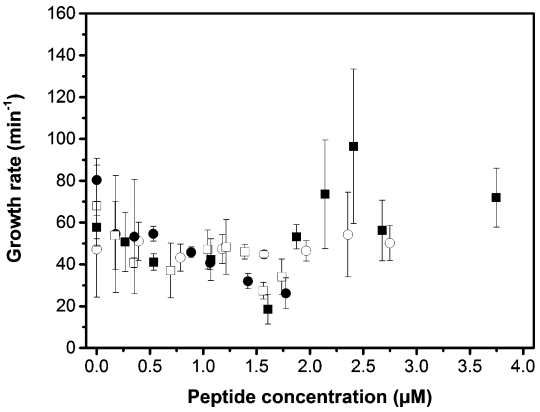

Figure 2. No influence of LK peptides on the growth rate of HI fibrillation. HI and ThT were mixed with LK5 (○), LK7 (●), LK9 (□), and LK11 (■) peptides at different concentrations, and HI fibrillation was monitored by ThT fluorescence.

tested, the growth rates of HI fibrillation remained stable at a value similar to the rate observed without peptide (i.e., about 60 AU min^{-1}), suggesting that the four peptides LK5, LK7, LK9, and LK11 have no significant effect on the elongation step of HI fibrillation. The plateau values recorded during fibrillation experiments remained also unchanged in the presence of LK peptides. Hence LK peptides play a critical role only in the nucleation step. The length of the LKnL peptides in amino acids is important for this process.

Accelerating HI Fibrillation: LK Peptides Form Complexes Facilitating the Formation of Seeds on the Hydrophobic Surface. In order to gain insight into the role of the peptides on the hydrophobic surface, we investigated the effect of preadsorption of the peptides on the surface, on the formation of HI aggregation nuclei.

The LK11 peptide was preadsorbed onto hydrophobic surfaces by incubation at 37 °C with rotation at 1200 rpm during 10 min. After the incubation, nonadsorbed peptides were removed by a buffer wash. Then HI solution (86 μM) containing ThT (20 μM) was added to the wells and incubated at 37 °C and 1200 rpm. The lag times of the fibrillation curves, obtained in the presence of preadsorbed peptides, have been compared to the lag times obtained by mixing HI and LK11 simultaneously in the hydrophobic wells. Three concentrations of peptide, 0.01, 0.3, and 3 μM, correlated to three different effects seen on Figure 1B, were compared.

No shortening of the lag time was observed at a peptide concentration of 0.01 μM in comparison with the condition without peptide (Figure 3). In contrast, when mixed with HI, 0.3 μM of LK11 decreased the lag time, and this effect was inversed with a 3 μM concentration of peptide (Figure 3, white bars). These results confirmed the concentration dependency

DOI: 10.1021/acs.jpcb.5b07365
J. Phys. Chem. B XXXX, XXX, XXX−XXX

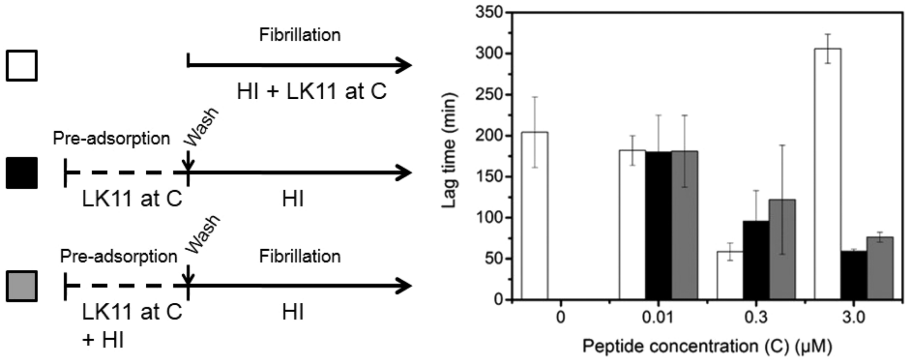

Figure 3. Preadsorption of LK11 peptide onto hydrophobic surfaces is enough to decrease the lag time of HI fibrillation. The peptide was incubated with the surface and rinsed before adding HI with ThT to monitor the aggregation kinetics by ThT fluorescence. The influence of different peptide concentrations on the lag time is shown. The effect of the peptide directly mixed with HI (white bars) is compared with the preadsorbed peptide (black bars) and with the preadsorbed peptide in the presence of an HI solution (gray bars).

of the effect of the peptide when mixed with HI as previously shown on Figure 1B.

The preincubation of the peptide at a concentration of 0.01 μM did not influence the HI aggregation kinetics (Figure 3, black column). In contrast, the lag time was greatly shortened when 0.3 or 3 μM of peptide were preadsorbed on the surface before triggering HI fibrillation, when compared to the experiment without peptide (Figure 3, black columns). Indeed, preadsorption of LK11 at 0.3 μM leads to a lag time of about 100 min, while preadsorption of LK11 at 3 μM resulted in a very similar lag time to the one obtained by directly mixing 0.3 μM of LK11 with HI (about 50 min). These results suggest that the accelerating effect of the peptide depends on the amount of adsorbed peptide remaining on the hydrophobic surface and not on the peptide in solution.

Thanks to their high adsorption energy, the peptides could form stable complexes on the surface favoring the growth of amyloid nuclei. This could be achieved in two possible ways: the aggregative complexes could (1) be made of peptides alone and form seeds for HI fibrillation or (2) consist in assemblies of peptides together with HI molecules. In order to assess this point, the influence of HI on the preadsorption of the peptides has been investigated. By adding HI to the peptide solution during the preadsorption step, the decrease of the lag times of fibrillation observed at the peptide concentrations of 0.3 and 3 μM was less pronounced (Figure 3, gray columns). Indeed, for 0.3 μM of preadsorbed LK11, the lag time obtained was about 125 min when HI was added during preadsorption, instead of 100 min for preadsorption of the peptide alone. Similarly, a lag time of about 125 min was also observed, when HI alone was preadsorbed then washed before triggering the formation of the fibrils by adding the peptide at 0.3 μM with HI. These results show that the peptide and HI have no synergistic effect in assembling aggregative prenuclei on the surface in these conditions and that both species, HI and LK peptides, compete for adsorption at the surface.

LK Peptides Adsorb in a Cooperative Manner on Hydrophobic Surfaces and Remain Stably Adsorbed. Because the accelerating effect of LKnL peptides on HI aggregation kinetics is linked to their preadsorption on hydrophobic surfaces, we investigated the adsorption properties of the LK11 peptide in more detail using a fluorescently tagged TAMRA-LK11 peptide (see Experimental and Theoretical Methods). As represented in Figure 4A, this peptide shows a similar accelerating effect on the HI aggregation lagtime at low concentrations (0.07−0.28 μM). Likewise, at high concentrations (>0.7 μM) TAMRA-LK11 strongly inhibits HI aggregation.

To obtain a closer insight into the binding of the TAMRA-LK11 peptide on hydrophobic surfaces, we plotted the concentration of adsorbed peptide after 10 min of incubation as a function of the total peptide concentration (Figure 4B) and the peptide concentration remaining in solution (Figure 4B inset). The results indicate that the TAMRA-LK11 peptide cooperatively adsorbs to the hydrophobic surface and reaches a maximum adsorption after 10 min incubation at 0.07 nMol (eq 0.35 μM in a 200 μL well). Using the Hill equation, described in Experimental and Theoretical Methods, we have determined a Hill coefficient of 2.1 and a critical concentration of 0.14 μM for the TAMRA-LK11 peptide adsorption.

We then used this peptide to analyze the stability of its adsorption on hydrophobic surfaces in the presence of HI. TAMRA-LK11 was incubated at 1.4 μM in hydrophobic 96-well plates and shaken at 1200 rpm for 10 min. The solution was then discarded, the well washed with TMN buffer and incubated with 86 μM HI. After the indicated times, the well was rinsed and the adsorbed peptide was desorbed in TMN buffer containing 0.5% SDS before quantification as described in Experimental and Theoretical Methods. As can be seen in Figure 4C, the amount of adsorbed peptide decreases slowly over 120 min. Indeed fitting the data points to an exponential function shows that the TAMRA-LK11 peptide has a $t_{1/2}$ of 99 min on the hydrophobic well surface. We can therefore assume that less than 30% of the peptide desorbs from the surface during the lag time.

These results strongly indicate that the cooperative accelerating effect of LK peptides at low concentrations on the lag time of HI aggregation kinetics is driven by a cooperative adsorption mechanism of these peptides on the hydrophobic surface and sustained by the stability of their surface-binding over time.

Inhibiting HI Fibrillation: LK Peptides in Excess in Solution Block Fibril Formation. In solution, LK peptides showed inhibitory effects at high concentrations. Indeed, when an excess of LK11 peptide remained in solution, it delayed the fibrillation kinetics (Figure 3, white bar at 3 μM, Figure 1B for LK11 > 2 μM, and Figure 4A for TAMRA-LK11 > 0.7 μM).

To gain insight into the effect of the peptide in solution, LK11 has been preadsorbed on the hydrophobic surface at three relevant concentrations C (0.01, 0.3, and 3 μM) and

DOI: 10.1021/acs.jpcb.5b07365
J. Phys. Chem. B XXXX, XXX, XXX−XXX

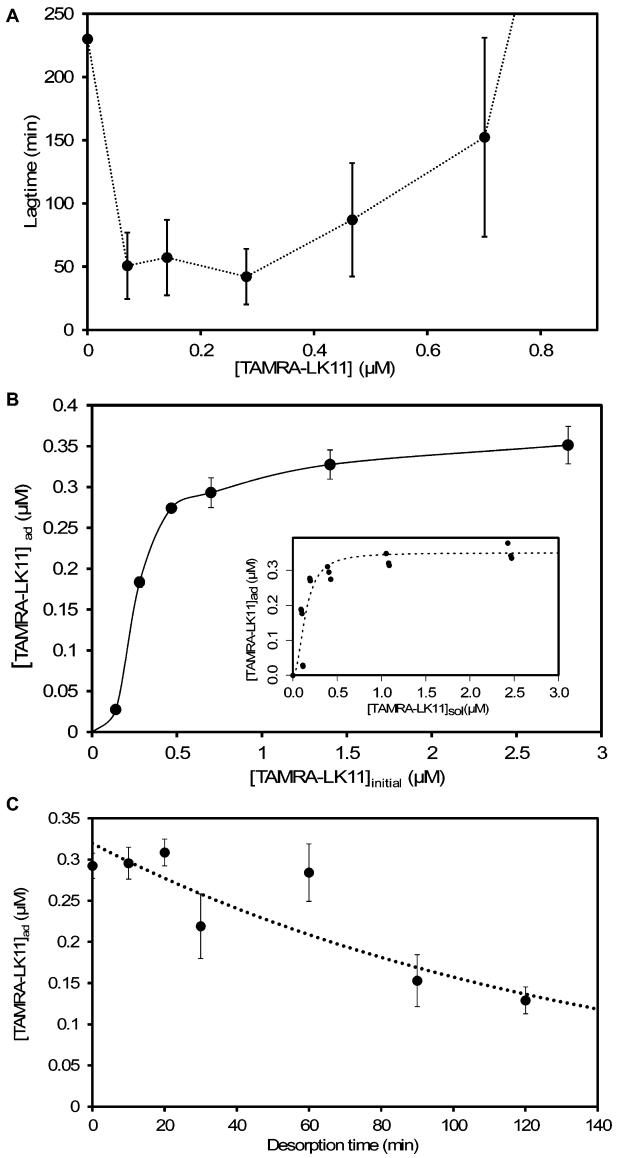

Figure 4. Stable and cooperative adsorption of TAMRA-LK11 on hydrophobic surfaces drives insulin amyloid aggregation. (A) Evolution of the lag time (circles) of HI aggregation as a function of the TAMRA-LK11 concentration. For easier reading, data points are joined by a hand-drawn dashed line. At 1.4 μM TAMRA-LK11, the lagtime is longer than 24 h. (B) Cooperative adsorption of TAMRA-LK11 on hydrophobic surfaces. The evolution of the amount of adsorbed peptide after 10 min incubation is shown as a function of the initial TAMRA-LK11 peptide concentration. The inset shows a fit using the Hill equation (dotted line) of the adsorbed TAMRA-LK11 peptide as a function of the peptide remaining in solution. (C) Desorption kinetics of TAMRA-LK11. TAMRA-LK11 (1.4 μM) was preadsorbed in TMN buffer (10 min, 1200 rpm, 37 °C), and the concentration of the peptide remaining adsorbed was measured by fluorescence as a function of time. Data were obtained with three replicates.

rinsed. Indeed, as shown in Figure 4B, at 0.3 μM, most LK11 is adsorbed in oligomers on the surface, while at 3 μM, an excess of peptide remains in solution. Then, the fibrillation has been monitored after adding HI and the peptide at the same concentration C in solution as used for the preadsorption (Figure 5, black bars) or after adding HI and LK11 in excess at 3 μM (Figure 5, gray bars). The lag times obtained were compared to those observed by directly mixing HI with LK11 at concentrations C.

Figure 5 shows that LK11 preadsorbed at 0.3 μM and added at the same concentration in solution can accelerate HI fibrillation. In that case, the lag times obtained are similar to those observed when directly mixing LK11 and HI (Figure 5, white and black bars at 0.3 μM). It suggests that, although insufficient amounts of peptide remain adsorbed on the surface during preadsorption (see Figure 3), the nucleation phase can be accelerated later thanks to the continued presence of the peptide in solution. In contrast, when the peptide is added in excess at 3 μM consecutively to the preadsorption at 0.3 μM, the accelerating effect of LK11 is abolished (Figure 5, gray bar at 0.3 μM).

Figure 5 confirms that, the accelerating effect, obtained by preadsorption of 0.3 μM LK11 peptide, can be blocked by inhibiting peptide concentrations in solution (3 μM). This clearly demonstrates that the peptide can interact with insulin and prevent it from aggregating into growing fibrils. This effect is strongly dependent on the free concentration of peptide in solution (≥3 μM, Figure 5). The inhibitory effect of the LK11 peptide on HI aggregation is probably driven by electrostatic interactions between the positively charged K side chains and HI (negatively charged at pH 7.4). Indeed, high NaCl concentrations (500 mM) reduce this effect drastically but do not affect the acceleration behavior at 0.3 μM (Figure 6).

Rotation is Not Necessary for the Preadsorption of the Peptide but for the Nucleation Step. In order to gain insight into the mechanism of LK seed formation, the influence of the rotation during the preadsorption of the peptide has been investigated.

Figure 7 shows that, at LK11 concentrations of 0.3 and 3 μM, agitation was not necessary to obtain the pro-amyloidogenic effect of LK11. Peptides thus efficiently adsorb on the hydrophobic surface by diffusion and form stable complexes. In contrast, rotation is necessary for the nucleation step: no aggregation was observed when the plates were not agitated after the preadsorption step. Moreover, incubation of LK11 at 0.3 μM in the presence of HI for several hours without agitation is not sufficient to create seeds as essayed with a fresh insulin solution. Thus, the transformation of HI and peptide complexes into active nuclei requires agitation.

Amyloid Prenuclei Can Be Observed by Microscopy. The nucleation and elongation phases of HI fibrillation can be monitored by different microscopy techniques. We used atomic force microscopy (AFM) to image amyloidogenic prenuclei in situ in the dry state. Glass coverslips were silanized to obtain hydrophobic surfaces and were subsequently incubated at 37 °C under rotation with HI solutions containing LK9 peptide or not (Figure 8).

Using AFM, no aggregates can be observed for the LK9 peptide alone after 2 h of incubation (Figure 8A) or HI alone after 1 h of incubation (Figure 8B). At this same time point, heterogeneous prenuclei can be observed on coverslips incubated with an HI solution mixed with LK9 peptide at 0.2 μM (Figure 8C). These complexes were diverse in shape and size, ranging from 10 nm to at least 35 nm in height and up to several hundred nanometers in width. Their distribution was rather dense after 1 h of incubation, when compared to the coverslips incubated with HI or peptide alone (Figure 8, panels A and B). After HI incubation, the surface rugosity varies from 0.5 nm without peptide to 6 nm in the presence of LK9. The

DOI: 10.1021/acs.jpcb.5b07365
J. Phys. Chem. B XXXX, XXX, XXX−XXX

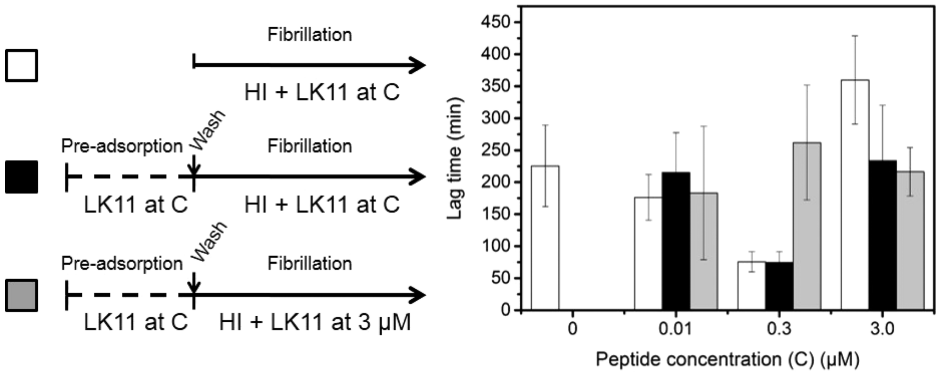

Figure 5. Excess of peptide LK11 in solution delays HI fibrillation. The peptide was incubated at concentrations C = 0.01, 0.3, or 3 μM with the hydrophobic surface and rinsed. Then, HI was added together with the peptide at the same concentration C to monitor the aggregation kinetics by ThT fluorescence (black columns). For comparison, HI was also supplemented with LK11 at C = 3 μM and ThT fluorescence was recorded (gray columns). The results have been compared with the effect of the peptide directly mixed with HI (white columns).

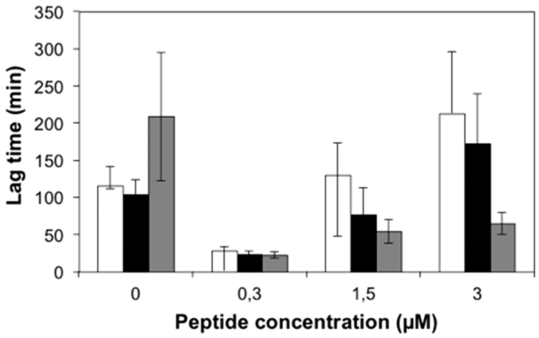

Figure 6. Effect of NaCl concentration on the lag time of HI aggregation. HI and ThT have been mixed with LK11 peptide at different concentrations in Tris buffer containing NaCl at 125 mM (white column), 250 mM (black column), or 500 mM (gray column). HI fibrillation was monitored by ThT fluorescence.

observed prenuclei in Figure 8C highly reduce the lag time of HI aggregation but do not abolish it, relative to the sample shown in Figure 8B.

ThT allows the labeling of amyloid structures and their observation by fluorescence microscopy (Figure 9). No specific fluorescence could be detected in the well incubated with HI and ThT for 120 min (Figure 9A). However, in wells incubated in the presence of LK9 at 0.2 μM, multiple small fluorescent objects, with different sizes up to 40 μm in diameter, could be observed at 120 min (Figure 9, panels B, C, and D).

Image analysis allows the determination of the size of the particles at the surface of the well with time. Fluorescent particles (up to 15 μm^2) were already identified after 30 min of incubation of HI mixed with LK9 (Figure 9C). The amount of such small particles increased dramatically after 120 min incubation (Figure 9D), and concomitantly bigger particles, up to 40 μm^2, were observed.

Together, the AFM and fluorescence microscopy observations confirm that LK peptides enhance the formation of surface-bound aggregative prenuclei that promote fibril growth.

DISCUSSION

In this paper, we use a series of (LK)nL peptides of various lengths as tools to investigate the mechanism of HI aggregation on hydrophobic surfaces. The results discussed here shed light on how amyloidogenic peptides cooperate with HI to either form stable aggregation nuclei on material surfaces, or, at higher concentration, block efficient fibril growth at the aggregation nucleus.

Cooperative Acceleration of Nuclei Formation at Low LK Peptide Concentration. Peptides (LK)nL, at low substoichiometric concentrations, accelerate the lag time of HI aggregation on hydrophobic surfaces and hence permit faster creation and maturation of amyloidogenic, surface-bound

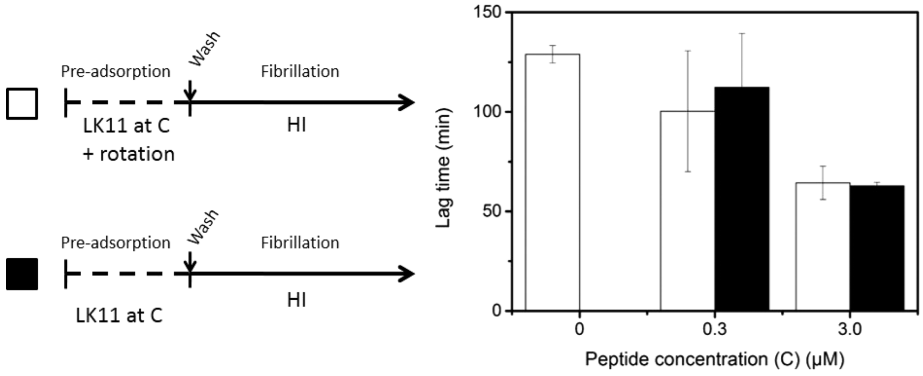

Figure 7. The agitation is not an important parameter for the preadsorption of the peptide. The LK11 peptide has been preadsorbed with (white bar) or without (black bar) agitation (1200 rpm) at a concentration of 0.3 or 3 μM and rinsed. HI and ThT were then added to monitor the aggregation kinetics by fluorescence measurements.

DOI: 10.1021/acs.jpcb.5b07365
J. Phys. Chem. B XXXX, XXX, XXX−XXX

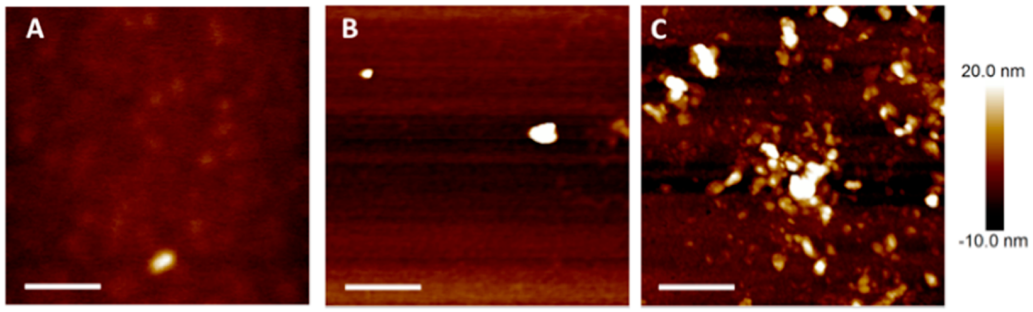

Figure 8. Observation of amyloid prenuclei. AFM (tapping mode) images of silanized glass coverslips incubated at 37 °C, 1200 rpm for 2 h with (A) LK9 peptide alone (0.2 μM), for 1 h with (B) HI solution without peptide, or with (C) HI solution containing 0.2 μM of LK9 peptide. Note that these time points correspond to the lag phase under these experimental conditions. The scale bar represents 500 nm. Images are representative of about 20 independent samples.

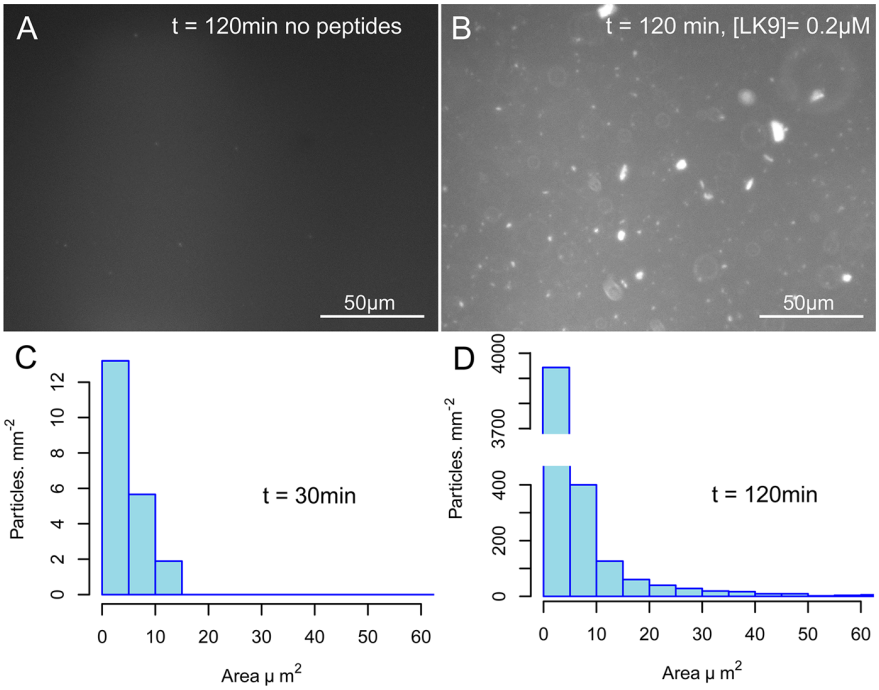

Figure 9. Fluorescence microscopy observation of insulin aggregates. HI was incubated at 37 °C and 1200 rpm and observed by fluorescence microscopy (DAPI filter) every 30 min. Images of the hydrophobic surface at 120 min are shown for (A) HI alone and for (B) HI in the presence of 0.2 μM LK9. The distribution of the particle size over a surface of 0.53 mm^2 is shown for HI + LK9 (0.2 μM) at (C) t = 30 min and (D) t = 120 min. Most particles are in focus and firmly adsorbed to the surface, some appear blurred and are not attached to the surface.

prenuclei (Figures 1 and 4A). This effect is most prominent with longer peptides (Figure 1 C), the fastest lag time (40−50 min) being recorded for LK11 and TAMRA-LK11 (Figures 1B and 4A). The increase of the accelerating effect with the length of the peptide is likely to be caused by stronger adsorption of long peptides onto hydrophobic surfaces. Indeed, the hydrophobic contribution to the adsorption energy increases with the number of hydrophobic amino acids. For LK5, which has the smallest hydrophobic contribution to its adsorption energy in the (LK)nL series tested here, higher peptide concentrations are needed to observe an acceleration of the nucleation step (Figure 1A). In line with the assumption that strong LK adsorption promotes faster aggregation, one expects that, for a peptide at a given concentration, the lag time decreases with longer surface contact times. This can be seen for example for LK11, for which the lag time is around 100 min if preadsorbed during 10 min but decreases to 50 min for longer contact times (Figure 3 black bar at 0.3 μM and Figure 1B). Furthermore, the results of Figures 3 and 4 demonstrate that, to obtain an accelerating effect, it is sufficient that peptides are stably adsorbed on the surface. After their surface adsorption, their presence in solution is no longer required to accelerate HI aggregation. This is due to the stability of their surface adsorption, as demonstrated with the fluorescently labeled TAMRA-LK11 (Figure 4C). This result confirms and strengthens the importance of a stable surface adsorption for peptides/proteins in order to promote the conformational changes that induce nuclei formation and fibrillation (Figure 10).

Plotting the lag time accelerating effect as a function of the LK peptide concentration, shows a sigmoidal behavior indicative of a cooperative effect of the peptides (Figure 1). Using the Hill equation (see Experimental and Theoretical Methods), we could determine a critical concentration and the

DOI: 10.1021/acs.jpcb.5b07365
J. Phys. Chem. B XXXX, XXX, XXX−XXX

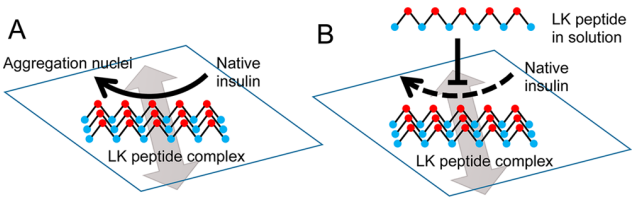

Figure 10. Dual effect of LK peptides on HI aggregation kinetics. (A) LK peptide complexes (represented with blue leucine and red lysine residues) cooperatively and stably adsorb on the hydrophobic surface (square) in β-sheet conformation. The hydrogen-bonding axis is represented by a gray transparent double-headed arrow. Upon integration of native insulin, they accelerate the formation of aggregation nuclei. (B) LK peptides in solution inhibit the formation of active aggregation nuclei.

Hill coefficient of each LK peptide concerning its effect on the lag time and for TAMRA-LK11 concerning its surface adsorption (Figure 1C and 4B). All peptides show a positive cooperative behavior and both critical concentrations and Hill coefficients decrease with peptide length (Figure 1C). This holds true for LK peptides that have less than 9 amino acids, and strongly indicates that stable complex formation relies on the local assembly of a defined number of peptides in time. The speed at which such complexes can be created depends on how quickly individual peptides can assemble at a given density on the surface. Using the fluorescently labeled TAMRA-LK11 peptide, we show that the peptide adsorption on the hydrophobic surface itself is positively cooperative (Figure 4B). Together with the demonstrated stability of their surface adsorption (Figure 4C), the cooperative binding of LKnL peptides to the surface is the driving force, accelerating the formation of surface-bound aggregation nuclei. Peptide length, and therefore occupied surface area, and the stability with which they adsorb on the surface determine their cooperative efficiency. For longer peptides less molecules are necessary because they reach higher surface coverage and/or bind more stably than smaller ones. The LK11 peptide shows slightly higher values for the Hill coefficient and the critical concentration than LK9 (Figure 1C), indicating that an optimal peptide length can be defined for efficient aggregation nuclei formation. The cooperative behavior demonstrates the strong potential of aggregative peptides to control aggregation kinetics on material surfaces.

Beyond stable surface adsorption, the conformation and spatial organization of LK peptides on a hydrophobic surface is paramount. DeGrado and Lear[16] have shown by circular dichroism and infrared spectroscopy that LK7 is structurally organized in antiparallel beta sheets in solution and at hydrophobic interfaces for micromolar concentrations and at neutral pH. Matthes et al.[18] determined the conformation of the HI B-chain-derived peptide LVEALYL and showed that it is organized in antiparallel beta sheets and the determination of the crystal structure of the same peptide (PDB: 2OMQ[19]) confirms this. The LVEALYL peptide is known to form the spine of the HI fibril[12] and to have accelerating effects similar to those of LK peptides when adsorbed in substoichiometric concentrations on hydrophobic surfaces.[14] We showed that beta-sheet conformation of peptides is essential to obtain accelerating effects, α helix conformations delaying aggregation.[14] Altogether these data strongly support the idea that the establishment of peptide complexes on hydrophobic surfaces effectively triggering nucleation requires the presence of antiparallel beta sheets (Figure 10). These are either formed by HI upon surface adsorption[15] or provided by adsorbed peptides or a combination of both. It is tempting to speculate that the lag time can be shortened because adsorbed peptides facilitate conformational changes on incoming HI for its incorporation into prenuclei (Figure 10). Electrostatic interactions between HI and solution-exposed K residues probably play only a minimal role. Indeed, in a previous study,[14] we have used a mutant of the B-chain LVEALYL peptide, in which we replaced the negative charge of the glutamate residue (E) by the neutral side chain of threonine (T). When adsorbed to a hydrophobic surface, the resulting LVTALYL peptide exhibits the side chains of amino acids L-T-L-L to the solution, instead of L-E-L-L for the wildtype peptide. Both peptides show similar, accelerated lag times in HI aggregation kinetics, indicating that charges are not the principle driving force for the accelerating effect of these adsorbed peptides. Also, we have used $(IS)_2I$ and $(IS)_3I$ peptides, which adsorb with their hydrophobic isoleucine side chain to the hydrophobic surface and expose a neutral serine side chain to the solution. Both $(IS)_2I$ and $(IS)_3I$ peptides show an accelerating effect,[14] and this effect is cooperative, similar to (LK)nL peptides (data not shown). Moreover high salt concentrations do not affect the accelerating effect of LK peptides (Figure 6).

Our results show that, in order to obtain an accelerating effect on the lag time of HI aggregation, LK peptides do not need to cover the entire material surface but are probably adsorbed in small discrete "islands" scattered over the hydrophobic surface. Indeed, at 0.2 μM, when LK11 reduces the lag time considerably (Figure 1B), there are not enough LK11 molecules in solution to cover the well surface uniformly. Assuming the peptide is a rectangle of width 2.5 Å and length 2 Å per amino acid, one LK11 molecule occupies approximately 55 Å^2. In order to cover the entire surface of a reaction well filled with 200 μL solution (0.02 dm^2) by a monolayer of peptides, 3.6×10^{14} LK11 molecules are needed. However, at 0.1 nMol (see Figure 4B), the number of LK11 peptide molecules adsorbed is 6×10^{13}, covering 17% of the surface. Therefore, LK peptides must be adsorbed in a discrete manner on hydrophobic surfaces, at the time when they accelerate nuclei formation. This is also documented by our microscopy results (Figures 8 and 9). In this context, it is relevant to note that DeGrado and Lear demonstrated that the LK7 peptide is organized in aggregates of 31 molecules at the water−air interface.[16] Nayak et al. have measured the kinetics of the formation of insulin aggregation nuclei in solution using small angle neutron scattering and proposed that aggregation nuclei are composed of 3 insulin dimers (6 monomers).[20] On a surface, however, this might be different, as peptide/protein adsorption increases their local concentration, and their interaction with surfaces is likely to stabilize the nucleation multimer. The stoichiometry of peptide/HI molecules in surface-bound aggregation nuclei is hitherto unknown, but amyloidogenic peptides are a valuable tool to investigate it.

Inhibition of HI Aggregation at High LK Peptide Concentration. The lag time decrease, observed for LK peptides at low concentrations, is reversed at higher peptide concentrations, albeit still substoichiometric (Figures 1 and 4A). For example, LK9 and LK11 lose their accelerating effect gradually when present in concentrations higher than 0.5 μM (Figure 1B). Moreover, we show that the delay in HI aggregation comes from an excess of peptide in solution (Figures 3 and 5). Our results presented in Figure 2 further

DOI: 10.1021/acs.jpcb.5b07365
J. Phys. Chem. B XXXX, XXX, XXX−XXX

show that none of the LK peptides have an effect on the fibrillation growth rate. It is therefore likely that nonadsorbed LK peptides remaining in solution interfere with efficient HI integration at growing prenuclei, either by interacting with preformed nuclei per se or by blocking the conformational changes that HI undergoes when incorporated into an aggregation nucleus (Figure 10). Because this inhibitory effect is observed at peptide concentrations in solution that are largely substoichiometric compared to the concentration of HI (86 μM), it is unlikely that the peptide interacts stably with HI before it reaches an aggregation nucleus. The mechanism of interaction of LK peptides with HI is unknown but probably based on hydrophobic or electrostatic interactions, given the nature of these peptides. Indeed, high ionic concentrations dampen the inhibitory effect (Figure 6), showing that the positively charged K residues and the negatively charged HI (pI = 5.3) could be electrostatically attracted.

The affinity of LK peptides for HI interaction at a growing nucleus is unknown, but the inhibitory effect is predominantly seen with longer peptides LK9 and LK11, suggesting a threshold for the size of the peptide. It is also possible that steric constraints present beyond a certain peptide size interfere with efficient incorporation of HI into a preformed surface-bound prenucleus. Along this line, the TAMRA tag, which is bulky, dramatically enhances the inhibitory effect of the TAMRA-LK11 (Figure 4A) at concentrations >0.7 μM. Finally LK peptides could also interfere with a domain in HI, exposed when HI is being integrated into the prenucleus, thereby hindering HI conformational changes. A comparative shielding mechanism has been shown to be efficient in preventing islet amyloid polypeptide (IAPP) aggregation during expression in *E. coli*.[21] Indeed, a recombinant protein tag using the HI18-binding domain, known to interact with a hydrophobic sequence in IAAP involved in aggregation, was used to sequester soluble IAAP monomers, thus preventing its aggregation. It is possible that LK peptides interact with partially unfolded HI thereby blocking further transition into the beta-sheet conformation found in the mature amyloid fiber.

CONCLUSIONS

In this paper, we demonstrate that small peptides consisting of alternate leucine and lysine amino acids of the type (LK)nL are capable to dramatically accelerate HI aggregation but also to inhibit it depending on their concentration. These effects are strictly dependent on the presence of hydrophobic material surfaces and highlight the importance of the impact of materials on protein stability. Indeed, we demonstrate that the cooperative effect on the acceleration of HI aggregation is based on a cooperative binding of the peptides to the surface. Beyond the results presented here, (LK)nL peptides clearly represent a versatile tool to study early stages of material-bound surface aggregation of proteins. As they are incorporated into aggregation nuclei, they are at the same time amyloid aggregation inducers and tools to investigate the aggregates they trigger.

AUTHOR INFORMATION

Corresponding Author

*Address: LMGP, Phelma Minatec, 3 parvis Louis Néel, CS50257, F-38016 Grenoble cedex1, France. Tel: ++ 33 4 56529335. Fax: ++ 33 4 56529301. E-mail: marianne.weidenhaupt@grenoble-inp.fr.

Notes

The authors declare no competing financial interest.

ACKNOWLEDGMENTS

This work was supported by a Ph.D. fellowship from the MENRT to K.C. We thank the CNRS for funding C.V. as a visiting researcher and acknowledge the Nanomonde facility of the CIME Nanotech and Sidali Bessa for assistance with the AFM experiments.

REFERENCES

(1) Eisenberg, D.; Jucker, M. The Amyloid State of Proteins in Human Diseases. *Cell* **2012**, *148* (6), 1188−203.
(2) Lougheed, W. D.; Albisser, A. M.; Martindale, H. M.; Chow, J. C.; Clement, J. R. Physical Stability of Insulin Formulations. *Diabetes* **1983**, *32* (5), 424−432.
(3) Ahmad, A.; Uversky, V. N.; Hong, D.; Fink, A. L. Early Events in the Fibrillation of Monomeric Insulin. *J. Biol. Chem.* **2005**, *280* (52), 42669−75.
(4) Brange, J.; Andersen, L.; Laursen, E. D.; Meyn, G.; Rasmussen, E. Toward Understanding Insulin Fibrillation. *J. Pharm. Sci.* **1997**, *86* (5), 517−25.
(5) Sluzky, V.; Tamada, J. A.; Klibanov, A. M.; Langer, R. Kinetics of Insulin Aggregation in Aqueous Solutions upon Agitation in the Presence of Hydrophobic Surfaces. *Proc. Natl. Acad. Sci. U. S. A.* **1991**, *88* (21), 9377−81.
(6) Ballet, T.; Brukert, F.; Mangiagalli, P.; Bureau, C.; Boulange, L.; Nault, L.; Perret, T.; Weidenhaupt, M. Dnak Prevents Human Insulin Amyloid Fiber Formation on Hydrophobic Surfaces. *Biochemistry* **2012**, *51* (11), 2172−80.
(7) Chabry, J.; Caughey, B.; Chesebro, B. Specific Inhibition of In Vitro Formation of Protease-Resistant Prion Protein by Synthetic Peptides. *J. Biol. Chem.* **1998**, *273* (21), 13203−7.
(8) Findeis, M. A.; Musso, G. M.; Arico-Muendel, C. C.; Benjamin, H. W.; Hundal, A. M.; Lee, J. J.; Chin, J.; Kelley, M.; Wakefield, J.; Hayward, N. J.; et al. Modified-Peptide Inhibitors of Amyloid Beta-Peptide Polymerization. *Biochemistry* **1999**, *38* (21), 6791−800.
(9) Kapurniotu, A.; Schmauder, A.; Tenidis, K. Structure-Based Design and Study of Non-Amyloidogenic, Double N-Methylated IAPP Amyloid Core Sequences as Inhibitors of IAPP Amyloid Formation and Cytotoxicity. *J. Mol. Biol.* **2002**, *315* (3), 339−50.
(10) Tjernberg, L. O.; Naslund, J.; Lindqvist, F.; Johansson, J.; Karlstrom, A. R.; Thyberg, J.; Terenius, L.; Nordstedt, C. Arrest of Beta-Amyloid Fibril Formation by a Pentapeptide Ligand. *J. Biol. Chem.* **1996**, *271* (15), 8545−8.
(11) Du, H. N.; Li, H. T.; Zhang, F.; Lin, X. J.; Shi, J. H.; Shi, Y. H.; Ji, L. N.; Hu, J.; Lin, D. H.; Hu, H. Y. Acceleration of Alpha-Synuclein Aggregation by Homologous Peptides. *FEBS Lett.* **2006**, *580* (15), 3657−64.
(12) Ivanova, M. I.; Sievers, S. A.; Sawaya, M. R.; Wall, J. S.; Eisenberg, D. Molecular Basis for Insulin Fibril Assembly. *Proc. Natl. Acad. Sci. U. S. A.* **2009**, *106* (45), 18990−5.
(13) Kim, J. R.; Murphy, R. M. Mechanism of Accelerated Assembly of Beta-Amyloid Filaments Into Fibrils by KLVFFK(6). *Biophys. J.* **2004**, *86* (5), 3194−203.
(14) Nault, L.; Vendrely, C.; Brechet, Y.; Bruckert, F.; Weidenhaupt, M. Peptides that Form Beta-Sheets on Hydrophobic Surfaces Accelerate Surface-Induced Insulin Amyloidal Aggregation. *FEBS Lett.* **2013**, *587* (9), 1281−6.
(15) Nault, L.; Guo, P.; Jain, B.; Brechet, Y.; Bruckert, F.; Weidenhaupt, M. Human Insulin Adsorption Kinetics, Conformational Changes and Amyloidal Aggregate Formation on Hydrophobic Surfaces. *Acta Biomater.* **2013**, *9* (2), 5070−9.
(16) DeGrado, W.; Lear, J. D. Induction of Peptide Conformation at Apolar/Water Interfaces. 1. A Study with Model Peptides of Defined Hydrophobic Periodicity. *J. Am. Chem. Soc.* **1985**, *107*, 7684−7689.

DOI: 10.1021/acs.jpcb.5b07365
J. Phys. Chem. B XXXX, XXX, XXX−XXX

(17) Meadows, D. L.; Shafer, J. S.; Schultz, J. S. Determining the Extent of Labeling for Tetramethylrhodamine Protein Conjugates. *J. Immunol. Methods* **1991**, *143* (2), 263−72.
(18) Matthes, D.; Daebel, V.; Meyenberg, K.; Riedel, D.; Heim, G.; Diederichsen, U.; Lange, A.; de Groot, B. L. Spontaneous Aggregation of The Insulin-Derived Steric Zipper Peptide VEALYL Results In Different Aggregation Forms with Common Features. *J. Mol. Biol.* **2014**, *426* (2), 362−76.
(19) Sawaya, M. R.; Sambashivan, S.; Nelson, R.; Ivanova, M. I.; Sievers, S. A.; Apostol, M. I.; Thompson, M. J.; Balbirnie, M.; Wiltzius, J. J.; McFarlane, H. T.; et al. Atomic Structures of Amyloid Cross-Beta Spines Reveal Varied Steric Zippers. *Nature* **2007**, *447* (7143), 453−7.
(20) Nayak, A.; Sorci, M.; Krueger, S.; Belfort, G. A Universal Pathway for Amyloid Nucleus and Precursor Formation for Insulin. *Proteins: Struct., Funct., Genet.* **2009**, *74* (3), 556−65.
(21) Mirecka, E. A.; Gremer, L.; Schiefer, S.; Oesterhelt, F.; Stoldt, M.; Willbold, D.; Hoyer, W. Engineered Aggregation Inhibitor Fusion For Production of Highly Amyloidogenic Human Islet Amyloid Polypeptide. *J. Biotechnol.* **2014**, *191*, 221−7.

DOI: 10.1021/acs.jpcb.5b07365
J. Phys. Chem. B XXXX, XXX, XXX−XXX

3.3 Extended discussion

In the absence of added peptide (Figure 1 in Article I), the long lag-times presenting extremely high variability contrast with the steady and fast aggregation occurring during the growth phase. This is evidence for a rare, unique and highly stochastic event of nucleation. The analysis of aggregation kinetics and their statistics can reveal how and what the peptides affect in this mechanism.

Minimum transition time to the amyloid state.

The lag time as a function of peptide concentration presents a horizontal asymptote at about 30min for $(LK)_nL$ peptides (Figure 1 in article). This incompressible lag-time suggests a minimum reaction time for the conformational transition into a ThT-positive form.

Of course the difference between the conventional lag-time (calculated by the intersection of the steepest tangent of the ThT signal with the base line) and the lag time sensu stricto (corresponding to the first appearance of a ThT-positive aggregate) contributes to the computed value of this incompressible reaction part.

In these kinetic experiments the first measure of ThT-positive aggregates (ThT-fluorescence intensity deviating from the baseline by more than 3σ) is rapidly (within 15 min) followed by measures of a high fluorescence intensity. This points towards a fast and dramatic growth, following the first fibril appearance, rather than towards a gradual aggregation.

Modeling of the influence of the nuclei number on the lag-time

We have here produced a simple model allowing a better understanding of the mechanisms involved in the pro-nucleation effects. We consider a simple nucleus as a mathematical object presenting a non-aging transition from the initial state (**I**) into the amyloid state (**A**). This transition is characterized by a half-life **λ**. We then consider a well, containing a collection of ***j*** nuclei through time: for this well, the lag-time will be defined as the duration until the transition of the first nucleus of this well into the **A** state. The evolution of a nuclei population will therefore follow an exponential decay distribution:

$$N(t) = N_0 \cdot e^{-\lambda t}$$

In the mathematical simulation, the transition time of each modeled nucleus was therefore randomly sampled according to the following negative exponential distribution: $P(x) = \lambda e^{-\lambda x}$. Then the lag-time of each individual well was determined by taking the minimum transition

time among the collection of ***j*** nuclei it contains. The resulting lag-times are plotted on Figure 42 A for each individual well.

In this model, it is clear that the increase in nuclei number results in a reduction of the lag-time (Figure 42 A). Here, contrary to the experimental data where the lag-time reaches a minimum (Figure 1 in the article), the simulated lag-time tends towards 0 as the number of nuclei increases. Moreover the variation of the lag-time also decreases with the number of nuclei as shown by the drastic reduction of the standard deviation (Figure 42 B). However this reduction is proportional to the mean duration of the lag-time as the **coefficients of variation (**i.e. the ratio between the standard deviation **σ** and the mean **μ**) remain stable with the increase of nuclei (Figure 42 C).

So in theory the increase of nucleation sites without any change in the individual rate of conformational transition (here without any change in **λ**) is sufficient to induce a dramatic reduction of the lag-time but not a reduction of their relative standard deviation.

Reduction of the lag-time coefficient of variation

One interesting point in our experimental data is the evolution of the **coefficients of variation** of the lag-times: at low peptide concentration the lag-times are long but also present extreme relative standard deviations. However when the lag-time decreases at efficient peptide concentrations, the coefficients of variation are drastically reduced (Figure 1 in article I, Figure 43). As shown by mathematical modeling (Figure 42) an increase of nucleation sites can account for a decrease of the lag-time but not for the decrease of its relative standard deviation.

However this reduction of the variation coefficient of the lag times might be the consequence of the existence of an incompressible reaction time presenting a low variation (cf. supra) that neither the peptides nor the increase in nucleation sites can reduce. Only the highly stochastic first nucleation phase is therefore reduced to its minimum due to the large amount of nucleation sites. As a consequence the coefficient of variation remains the same for the first nucleation phase but appears drastically reduced considering the entire lag-time (Figure 44).

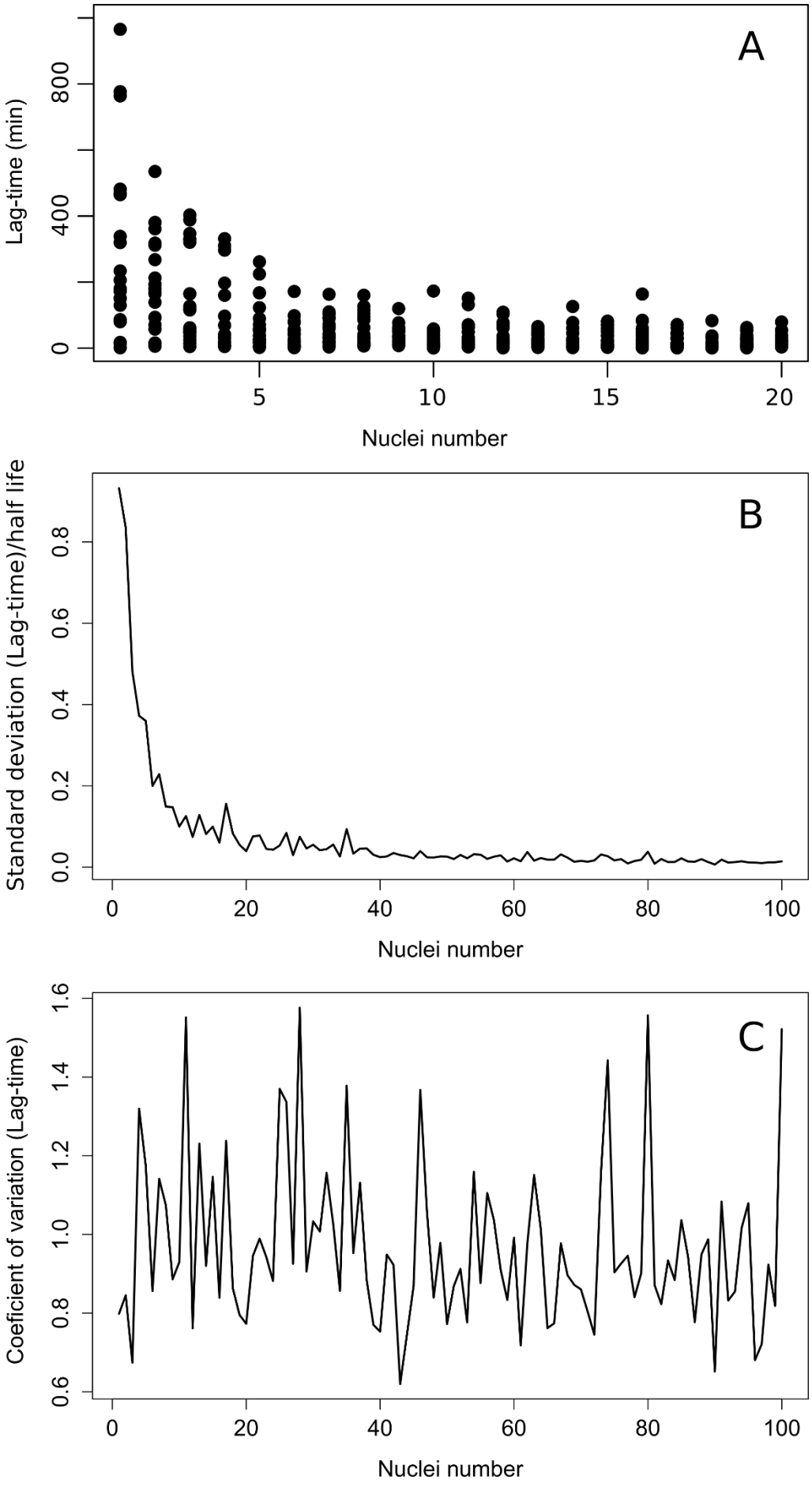

Figure 42. Simulation of lag-time duration and variation as a function of the nuclei number. Based on the mathematical model described in the text (n=21 wells per nuclei number condition; λ= 200 min). A: Aggregation lag-times of individual wells as a function of their nuclei number, B: Standard deviation of the lag-time expressed here as a fraction of the nucleus half-life (λ) as a function of the nuclei number, C: coefficient of variation of the lag-time (standard deviation divided by mean lag-time) as a function of the nuclei number.

Interestingly, the peptide-driven reduction of the lag-time does not present an "on-off" behavior, but rather presents an intermediate situation around a critical peptide concentration likely corresponding to a lower number of peptide patches forming nucleation sites.

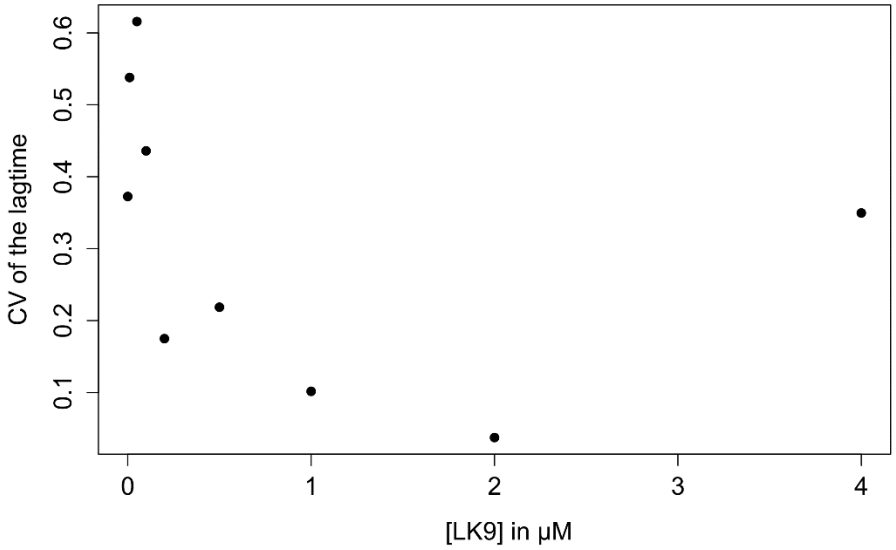

Figure 43 Coefficient of variation of the lag-time (experimental data) according to the concentration of LK9 peptide in µM (n=8).

In addition, the peptide patches might stabilize the nuclei intermediary state and reduce their transition time to the amyloid state to a minimal nucleation time. The reduction of the lag-time and the associated coefficient of variation would therefore result from a stabilization of nuclei transition states.

Both the nuclei stabilization and the increase in the number of nucleation sites likely contribute to the observed effects.

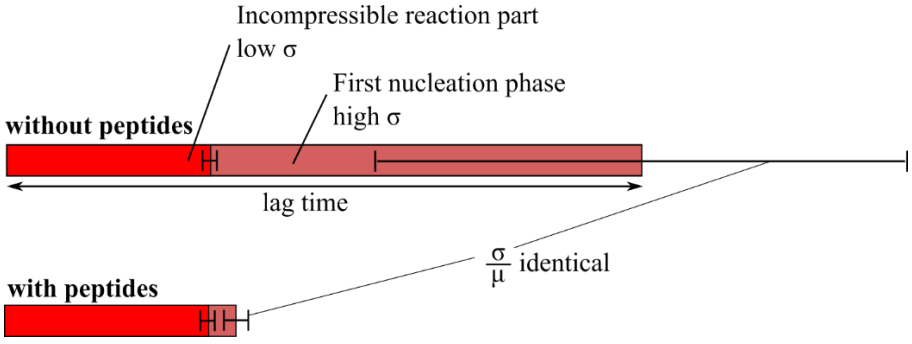

Figure 44. Explanation of the reduction of the lag-time coefficient of variation by the "reaction step hypothesis". If the lag-time can be divided into an incompressible part (typically a reaction time, in red) and a highly stochastic part (in pale red), the simple increase of the number of nuclei (in the presence of peptides) could explain the drastic reduction of the lag-time preceding the first appearance of aggregates, but also the apparent reduction of the coefficient of variation (σ/μ) of the total lag-time. Despite the fact that the coefficient of variation of the stochastic part remains identical whatever the number of nucleation sites the contribution to the overall variation is highly reduced for high numbers of nuclei.

Surface saturation

Interesting points in this article are the efficiency of the peptides on the surfaces at extremely low concentrations, but also their antagonist action in solution where they can only accumulate once the surface has been saturated. One fundamental concept to understand the behavior of these peptides is therefore their saturation of the surface. It is evident from our results that the adsorption of the peptides is cooperative however in a simplistic model we will here only consider the maximum occupied area according to the quantity of peptide in the well. Considering an inter β-strand distance of 4.7 Å (this distance is usually considered to lie between 3.5 Å and 5 Å) and an inter amino acid distance of 3.5 Å in an antiparallel β-sheet conformation[193], each peptide occupies an area of 16.45 Å² by amino acid. This area corresponds to 98.7 $mm^2.nmol^{-1}.amino\ acid^{-1}$.

An additional 4 Å spacing by peptide corresponds to the distance between the terminal $NH3^+$ and the terminal COO^- of different peptides. This corresponds to an additional area of 112.8 $mm^2.nmol^{-1}.peptide^{-1}$. The reaction is performed in a 200µL volume in contact with the 157 mm² surface of the well (from a 96 well plate, see Material and Methods). Simple calculations can therefore give us the maximum area that the peptides are able to cover and most interestingly, allow us to view these results in relation with the surface of the well (Table 6). In the experiment using TAMRA-LK11 to monitor the amount of peptides bound to the surface of a 200µL well (Figure 4B in article I), the surface begins to show saturation for initial concentrations above 0.5µM which, according to our estimations, correspond to a potential occupancy of 76% of the surface. More interestingly the critical concentration (K_A) observed at an initial concentration of 0.2µM (with a quasi-total adsorption) corresponds in our estimation to an occupancy of 31% of the surface. Eventually the adsorbed concentration reaches an asymptote at about 0.35µM (corresponding to 0.07nmol). This amount corresponds to a potential occupancy of 53%. These simple calculations prove therefore to be quite relevant to roughly estimate the maximal fraction of the surface occupied by peptides. As $(LK)_nL$ peptides have been described as forming monolayer patches, a supplementary distance separates individual peptide patches.

This fraction of occupied surface is

$$\theta = D \cdot A$$

with **D** the number of peptide patches per unit area and **A** the area of a patch. DeGrado and Lear[189] determined that each peptide patch of LK9 contained 30 peptides, corresponding to an

area of 5005 Å² per peptide patch. An occupancy of θ = 0.53 correspond to a density of 10 588 peptide patches by μm^2.

Assuming an ideal distribution of the peptide patches following a hexagonal lattice, the density of patches is

$$D = \frac{2}{\sqrt{5} \cdot d^2}$$

with **d** the distance separating the barycenter of two neighboring patches. With the previously calculated patch density of 10 588 μm^{-2} this distance is d = 20.55 nm.

The fact that the peptides presenting the highest affinity for the surface, LK9 and LK11, are active at concentrations where they cannot, even according to the most optimistic estimation, cover all the surface (below 0.1µM for LK11 corresponding to less than 15% of surface occupancy) supports the peptide patch model in which the critical concentration for lag-time reduction does not reflect the occupancy of the surface by the peptides but rather the stability of the peptide islets on the surface.

		LK5		LK7		LK9		LK11	
[Peptide]		max occupied area	surface fraction	max occupied area	surface fraction	max occupied area	surface fraction	max occupied area	surface fraction
0 µM	(0 nMol)	0 mm²	0	0 mm²	0	0 mm²	0	0 mm²	0
0,1 µM	(0,02 nMol)	12,1 mm²	0,08	16,0 mm²	0,10	20,0 mm²	0,13	24,0 mm²	0,15
0,35 µM	(0,07 nMol)	42,4 mm²	0,27	56,3 mm²	0,36	70,0 mm²	0,45	83,9 mm²	0,53
0,5 µM	(0,1 nMol)	60,6 mm²	0,39	80,4 mm²	0,51	100,1 mm²	0,64	119,9 mm²	0,76
1 µM	(0,2 nMol)	121,3 mm²	0,77	160,7 mm²	1,02	200,2 mm²	1,27	239,7 mm²	1,53
2 µM	(0,4 nMol)	242,5 mm²	1,54	321,5 mm²	2,05	400,4 mm²	2,55	479,4 mm²	3,05
5 µM	(1 nMol)	606,3 mm²	3,86	803,7 mm²	5,11	1001,1 mm²	6,37	1198,5 mm²	7,63
10 µM	(2 nMol)	1212,6 mm²	7,72	1607,4 mm²	10,23	2002,2 mm²	12,74	2397 mm²	15,25

Table 6: Maximum occupied area of hydrophobic surface by the peptides contained in a 200µL volume and corresponding fraction of the well surface (in a standard 96-well plate containing 200µL) by LK peptides in β-sheet conformation given according to their initial concentration in solution (and corresponding peptide amount for 200µL).

The protein nano-structures observed by AFM play a role in insulin aggregation.

The atomic force micrographs of hydrophobic glass surfaces incubated with peptides and/or insulin are shown in Figure 8 in Article I. These silanized glass surfaces, incubated for 30 min with 86µM HI, have the ability to reduce the aggregation lag time of a fresh insulin solution (Figure 45, circles). This reduction is even more dramatic when the surfaces have been pre-incubated with 86µM HI and 1µM LK9 peptides (Figure 45, squares). This indicates that the structures formed on the surfaces and visible by AFM have the ability to contribute to insulin

aggregation. Whether this mechanism involves seeding or a contribution to the nucleation process is difficult to ascertain with the current data.

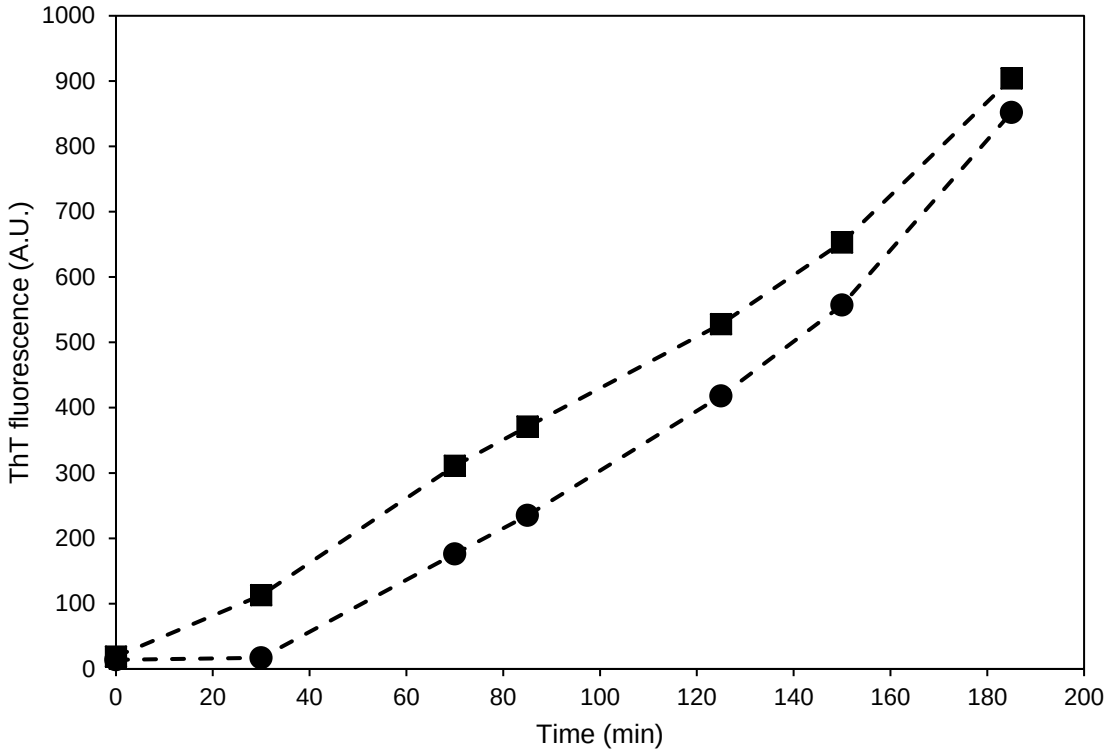

Figure 45. Kinetics of HI aggregation in contact with hydrophobic glass surfaces pre-incubated with 86µM HI (●) or 86µM HI plus 1µM LK9 (■) for 30 min.

Interaction mechanisms between peptide and HI

The formation of surface peptide patches stabilized by lateral inter-peptide β-sheets is suggested by the cooperativity of the adsorption as well as the previous ATR-FTIR results obtained by Nault et al[185] and De Grado & Lear[189]. They show a transition of the LK7 peptide conformation from random coil to anti-parallel β-sheet upon adsorption at interfaces. The interaction of insulin with these patches likely involves the lateral β-sheets of these peptide patches as the results presented by Nault et al.[185] and those obtained with Isoleucine-Serine peptides have shown that the accelerating effect of the peptides was independent of their specific sequence or exposed amino acids but only depends on their ability to present a β-sheet conformation on hydrophobic surfaces.

This article also provides evidence of inhibition of insulin aggregation at high peptide concentrations. We have shown that the peptides remaining in solution were responsible for this effect. As only the longer peptides with 9 and 11 amino acids presented this effect and

because this effect is stronger for longer peptides, the binding stability of these peptides with the insulin aggregates seems to be important.

As the LK peptides are positively charged at the experimental pH (7.4), the reduction of their inhibiting behavior at higher ionic strength shows that these charges are involved in this inhibition. The results obtained with the LD9 peptide in the next chapter (cf. 4.3.3) also confirm the importance of the positive charge of lysine in this inhibition mechanism.

Steric inhibition

Contrary to the other $(LK)_nL$ peptides, the duration of the lag-time in the presence of TAMRA-LK11 could not be determined for peptide concentrations above 0.7µM as it exceeds 48h at 1.4µM and even one week at 2.8µM. The plot of the lag-time presents therefore a vertical asymptote at 0.7µM TAMRA-LK11 (Figure 4 in article I). This indicates a complete inhibition of the early nucleation process as well as a null formation rate of insulin complexes able to deplete TAMRA-LK11 from the solution by binding (discussed in details in chapter 4). As the general behavior of this labeled peptide on surface-induced HI aggregation is similar to the other LK peptides, this extremely strong inhibition is likely the result of steric clashes induced by the TAMRA group at the N-terminus of the peptide.

Conclusion on the dual effect of $(LK)_nL$ peptides

The results presented in this chapter allow a precise representation of the mechanisms involved in the peptide-insulin interactions at the surface. In the absence of peptide, HI adsorbs on the surface where it forms highly unstable structures which rarely mature into a nucleus i.e. overcome the energy barrier. The $(LK)_nL$ peptides adsorb cooperatively on hydrophobic surfaces, where they are stabilized by inter molecular anti-parallel β-sheet forming a peptide patch (Figure 46-1). Then these patches stabilize the adsorption (as shown by Nault et al.) and nucleation of HI molecules, reducing the duration of the lag-phase (Figure 46-2). LK9 and LK11 peptides remaining in excess in solution however, prevent the nucleation (Figure 46-3) likely by an effect involving electrostatic interactions and steric hindrance, prolonging the lag-phase.

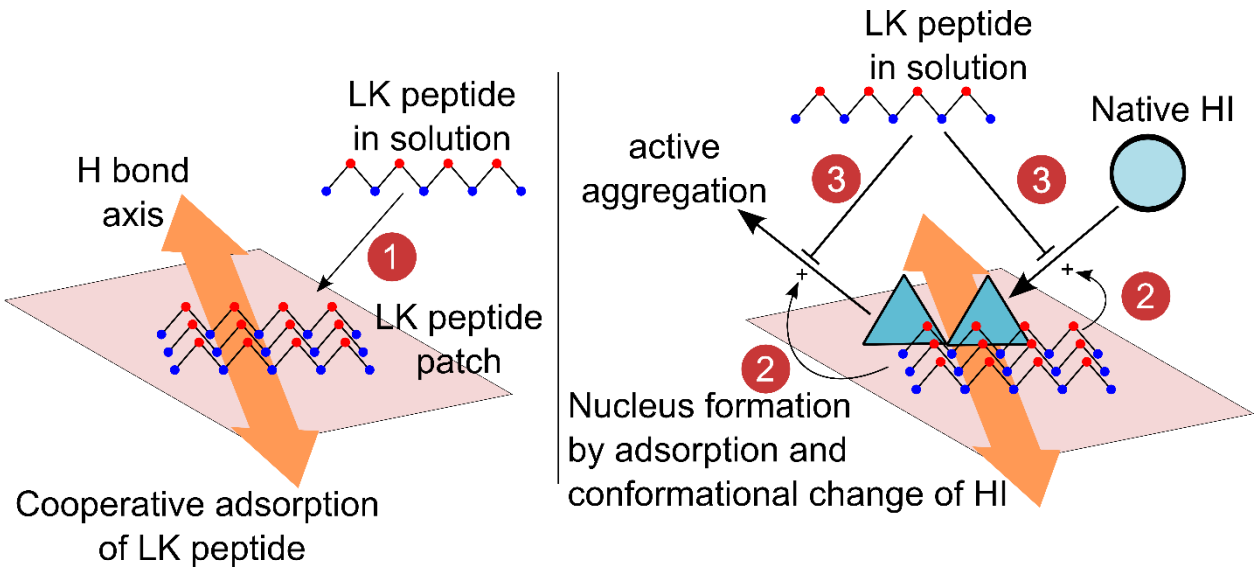

Figure 46: Dual effect of LK11 and LK9 peptides on insulin aggregation at hydrophobic surfaces. 1: cooperative adsorption of LK peptides in patches stabilized by intermolecular antiparallel β-sheets (the orange arrow indicate the orientation of the H bonds), the peptide patches then enhance insulin adsorption (2) and stabilize their conformational change towards the amyloid form. On the other hand (3) peptides remaining in solution prevent the nucleus formation.

4 Mechanism of the inhibition of insulin amyloid aggregation by $(LK)_nL$ peptides in solution

4.1 Context

In the first article (Article I) we demonstrate that the $(LK)_nL$ peptides are able to reduce the lag-time of surface-mediated insulin aggregation. But we also show the antagonistic inhibitory effect of the LK9 and LK11 peptides, remaining in solution, on the surface nucleation of insulin. However no effect on the growth rate could be characterized and the nature of the peptide-insulin interaction was not studied in details. In this chapter we therefore investigate in details the molecular interactions between $(LK)_nL$ peptide in solution and HI aggregates as well as the effect of peptides in solution on both HI nucleation and fibril growth.

The inhibitory effect of peptides in solution result in longer and more disperse (presenting higher coefficients of variation) lag-times. This lag-time is even longer than a week for the TAMRA-LK11 at 2.8 µM. This indicates an inhibition of nucleation by a steric effect. Moreover the role of the negatively charged group of the peptide in the inhibition mechanism was strongly suggested by experiments with varying ionic strength (125 to 500 mM NaCl) showing a reduction of the inhibitory effect (article I Figure 6).

4.2 $(LK)_nL$ peptide depletion from solution

The effect of the peptides on the growth rate is shown in Article I, Figure 2. In this figure no apparent effect of the $(LK)_nL$ peptide concentration on the growth rate is observed for any of the tested peptides. However these data result from kinetics of HI aggregation where the peptides were added at the beginning of the experiment.

This experiment does not take into account the depletion of peptides from solution occurring as peptides adsorb on the surface and later bind to insulin aggregates between the beginning of the kinetic and the beginning of the growth phase.

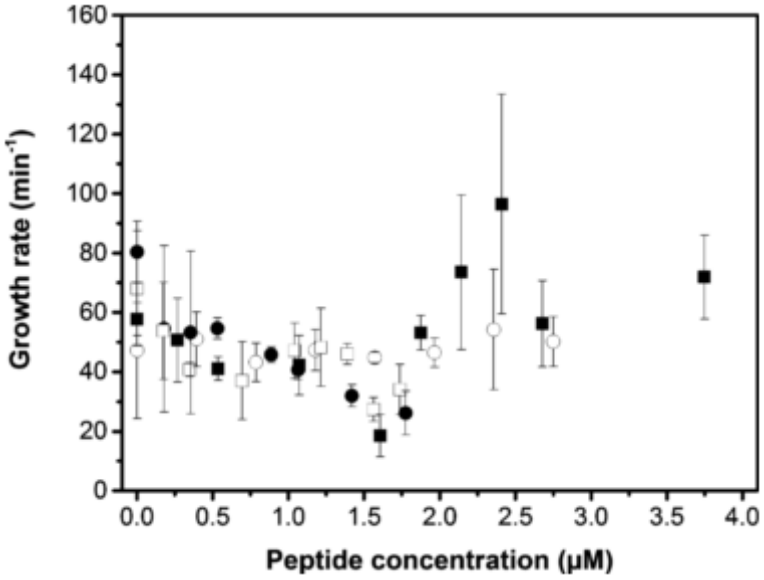

Figure 2 from article I. No influence of LK peptides on the growth rate of HI fibrillation. HI and ThT were mixed with LK5 (○), LK7 (●), LK9 (□) and LK11 (■) peptides at different concentrations, and HI fibrillation was monitored by ThT fluorescence.

In the article II the experiments were designed in order to obtain similar and comparable growth rates in the following way:

1. Pre-saturation of the surface with $(LK)_5L$, followed by a wash step, in order to drastically reduce the lag-time variation (to typically σ=3min) and limit the adsorption of the peptides added in solution.
2. In order to measure the impact of $(LK)_5L$ in solution on the growth rate of HI aggregation the peptides where added in solution 10 min before the measurement of the growth rate. This procedure allows the reduction of the continuous depletion by binding to HI aggregates.

Peptide depletion from solution.

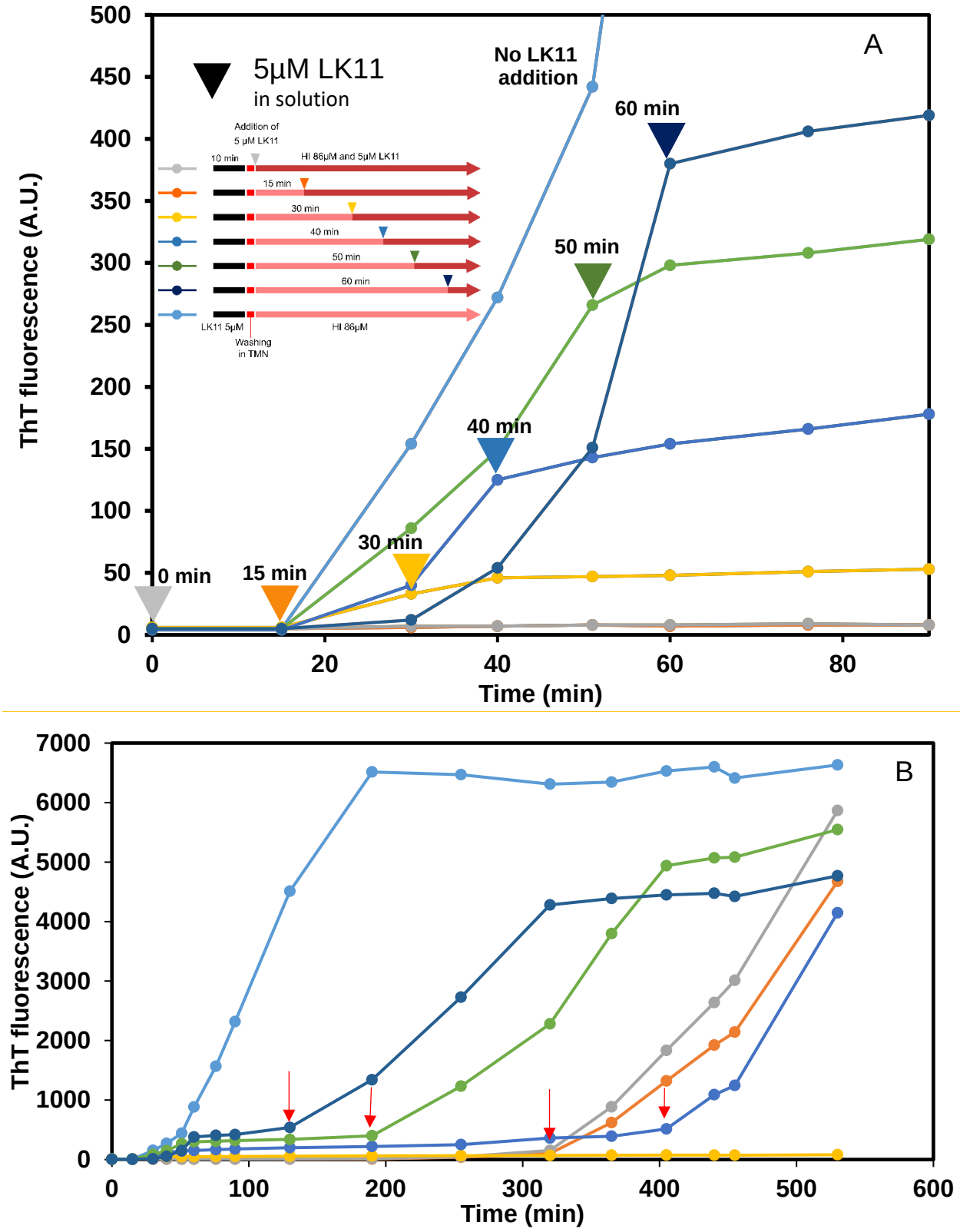

Figure 47. The depletion of LK11 peptides from solution, by binding to the fibrils, induces a new transition to a fast aggregation phase. After the introduction in solution of LK11 5µM at different time points (indicated by color arrow heads) during the aggregation kinetic on pre-saturated surfaces (A) the aggregation rate is drastically reduced; however after sufficient time, the reduction of the amount of LK peptides in solution allows the recovery of the aggregation rate (B :red arrows).

As observed in the article II Figure 4, the binding of the LK11 peptides on the insulin aggregates presents an important affinity resulting in the complete depletion of the initial concentration of peptides from solution. This depletion effect can be observed in Figure 47. After the addition of 5µM LK11 at various time points during a HI aggregation kinetic on an LK11-pre-saturated surface (Figure 47A), the rate of aggregation is drastically reduced. However, after several hours, we observe a rapid recovery of this aggregation rate to values close to the aggregation rate without inhibition (Figure 47 B). The duration of this depletion is shorter for the wells containing larger amount of insulin aggregates at the moment of the 5µM LK11 addition in solution (Figure 47). This is to link with the results obtained in the Figure 3 in article II showing that these larger amounts of insulin aggregates result in a significantly higher residual aggregation rate after the LK11 addition.

Pre-nuclei complexes are also likely to bind LK11 peptide in solution as this peptide completely inhibits insulin nucleation on hydrophobic surfaces (Figure 1 and Figure 5 Article II).

The same mechanisms could apply to aggregation kinetics presented in Figure 2 of article I: the first aggregates bind to the LK9 and LK11 peptides in solution, decreasing their concentration drastically. As a consequence the growth rates measured at mid-growth phase , when approx. 40µM of insulin molecules are under the state of aggregates (to compared with the initial peptide concentrations ranging from 0 to 4µM), appear unaffected by the initial concentration of peptides in solution.

4.3 Article II

Inhibition mechanisms of $(LK)_nL$ peptides in solution

4.3.1 Introduction

Numerous molecules are known to interfere with protein aggregation, most of them are unspecific small molecules that act by stabilization (e.g. trehalose, citruline, arginine) or destabilization (urea) of intramolecular interactions. These molecules are characterized by their efficiency at high stoichiometric ratio with respect to the protein. However some peptides and proteins exhibit specific activity on the kinetic of protein aggregation, usually presenting acceleration of aggregation at sub-stoichiometric concentrations and inhibition at higher peptide/protein ratio. Such peptides are often segments of amyloidogenic proteins. LVEALYLV, a segment of the insulin B chain, is able to accelerate the amyloid aggregation of its parent protein at low peptide / protein ratio (lower than 1/25) but inhibits its aggregation when this ratio exceeds 1/10. [123] In our previous work we characterized the properties of the $(LK)_nL$ peptides, which once adsorbed on hydrophobic surfaces, have the ability to greatly reduce the length as well as the variation of the insulin aggregation lag-time[194]. This phenomenon, different from seeding (in which misfolded proteins act as a template for a native one), can be explained by a stabilization of the aggregation nuclei[194] (cf. chapter 3). These stabilization mechanisms rely on the cooperative adsorption of the peptides at material surfaces. DeGrado and Lear[189] have described the self-association of an $(LK)_3L$ peptide into aggregates stabilized by anti-parallel β-sheets and presenting a high degree of association (n=30) at the air-solution interface. In solution, however, we have shown that $(LK)_5L$ and $(LK)_4L$ peptides inhibit the HI aggregate nucleation process and prolong the lag-time[194]. Here we further investigate this mechanism and show that the $(LK)_5L$ peptide inhibits both the insulin nucleation and its fibril growth.

4.3.2 Material and methods

Buffer

TMN (NaCl 125 mM, $MgCl_2$ 2 mM, Tris-HCl 25 mM, pH 7.4) buffer was prepared as a 10 fold concentrated solution (10X buffer). The desired masses of powder were weighed and dissolved in Milli-Q® pure water (filtered through a 0.22µm pore membrane; resistivity = 18 MOhm·cm at 25 °C). The pH was lowered to 7.4 by addition of HCl and the solution was filtered and stored at 4 °C.

Insulin solution

We purchased recombinant human insulin (HI) produced in *Saccharomyces cerevisiae* from Sigma-Aldrich (ref: I2643). HI solutions were solubilized in TMN buffer. In order to solubilize insulin, the pH of the solution was first lowered to 3.2 using 1 M HCl, then adjusted to pH 7.4 with 1 M NaOH using a pH electrode. The HI concentration was then precisely adjusted to 86 µM, measuring the 280 nm absorbance ($\varepsilon_{280\ nm}$(HI) = 5.53 mM^{-1} cm^{-1}). Once adjusted at the proper concentration, the solution was filtered through a 0.22 µm Millex-GV filter unit (ref: SLGV033SS). The solutions were stored at T = 4 °C for less than 2 weeks and re-filtered before use.

Peptides

In this study we used 3 peptides: LK11: $(LK)_5L$, LK9: $(LK)_4L$ and LD9: $(LD)_4L$ plus a tetra-methyl-rhodamine-labeled peptide TAMRA-LK11: TAMRA-$(LK)_5L$. We ordered these peptides from Genecust (Luxembourg) and solubilized them in 10 mM NaOH (LK11, LK9, TAMRA-LK11) or in 1mM NaOH (LD9), filtered them (0.22 µm Millex-GV filter unit) and stored them at -20°C in protein LoBind Eppendorf® tubes (ref:022431064). The exact concentration of peptides in solution was precisely determined with the QuantiPro™ BCA Assay Kit (Sigma®).

Insulin aggregation assays

Insulin aggregation assays were performed in polystyrene 96 well plates (Nunc™ ref: 237105), the reaction volume was 200µL. Routinely 3 replicas were analyzed per experimental condition and the results are presented as the mean values ± the standard deviation obtained from these replicas. A surface pre-saturation with peptide was achieved by incubation of the wells with 200µL of TMN containing 5µM LK11 at 37°C and 1200 rpm agitation on a Titramax 100. The wells were then rinsed for 30 seconds with filtered TMN buffer (37°C and 1200 rpm agitation on a Titramax 100) for 10 minutes. The buffer was then removed and the wells were incubated with 200µL of HI (86µM) in TMN buffer containing 20 µM ThT. Every 15 minutes the plates were removed from the shaker and the ThT fluorescence (λ_{ex}=450nm; λ_{em}=480nm) was recorded on a Tecan Infinite® plate reader in order to quantify the amount of amyloid aggregates in the wells. We have previously shown that under these conditions the release of surface-adsorbed peptides into solution is negligible for the duration of our assays[194].

Addition of LK11 during the aggregation kinetic

During the insulin aggregation assays described above (on LK11 pre-saturated surfaces) 0 to 5µM LK11 were added to the wells at the indicated time points. The HI aggregation kinetics was monitored every 15 min by ThT fluorescence as described before.

Co-precipitation of HI aggregates with TAMRA-LK11

A 20 min centrifugation at 13 500 rpm (in an Eppendorf® centrifuge 5415r; RCF = 16110g) allows the precipitation of more than 99% of ThT-positive HI aggregates. This property was used to measure the amount of TAMRA-LK11 bound to HI amyloid fibrils when 0.28µM TAMRA-LK11 are added to a 500µL TMN solution containing 0 to 44 µM of prepared amyloid HI aggregates as well as the same concentration of native insulin volume (eq. 0.56 nmol of TAMRA-LK11, 0 to 22 nmol of insulin fibrils and 0 to 22 nmol of native insulin).

An HI amyloid fiber solution was obtained in standard aggregation conditions after the addition of 1µM of an aggregated HI solution into 200µL of TMN containing 86µM HI. After 2h of incubation without ThT nor peptide (during the growth phase when 50% of the initial amount of insulin was aggregated), the HI solutions were collected and homogenized by inversion in non-binding tubes. To evaluate the amount of amyloid insulin in these solutions, 100µL were sampled in order to read their fluorescence at 450ex 480em in the presence of 20 µM ThT.

500µL of this suspension diluted in TMN buffer at the desired total HI concentration were then transferred in a low-bind tube (Eppendorf ref: 022431102) with 0.8µM of TAMRA-LK11. After brief and gentle mixing by one inversion, these tubes were centrifuged for 20 min at 16110g. The upper 400µL of the supernatant were then separated from the lower 100µL containing the aggregate pellet. The TAMRA fluorescence of 100µL from both fractions was then measured on a Tecan infinite 100 plate reader diluted in 200µL of TMN buffer (total volume) in the presence of 0.5% (v/v) SDS in a polystyrene 96 well plate (Nunc TM, ref :237105).

The fluorescence intensities of the pellet fraction were then subtracted from the corresponding supernatant fraction fluorescence value. The TAMRA fluorescence associated with peptide bound to HI aggregate was determined by:

$$F_b = F_p - F_{sn}$$

With F_b the TAMRA fluorescence of TAMRA-LK11 peptides bound to HI aggregates, F_{sn} the TAMRA fluorescence level for 100µL of the supernatant read in 200µL of TMN buffer in the

presence of 0.5%(v/v) SDS and F_p the TAMRA fluorescence level for 100µL of the pellet read in 200µL of TMN buffer in the presence of 0.5%(v/v) SDS.

Since no TAMRA fluorescence could be observed in the supernatant of the sample containing 44µM of amyloid insulin, the fraction of precipitated peptide associated with its F_b intensity was assigned to 1.

On the other hand the TAMRA-LK11 peptide concentration remaining in solution was quantified from the supernatant fluorescence (F_{sn}) by taking as a reference the F_{sn} of the sample without insulin fibrils assigned to 0.8µM.

The association constant is defined as follows:

$$K = \frac{[P] \cdot [F]}{[PF]}$$

With [P] the TAMRA-LK11 peptide concentration in solution, [F] the fibril concentration and [PF] the concentration of peptides associated with fibrils. It was determined by fitting the data using the nonlinear least-squares method with the following model:

$$[F_0] = [PF]\left(1 + \frac{K}{[P_0] - [PF]}\right)$$

Were [PF] represent the concentration of the peptides bound to the fibrils, $[P_0]$ the total concentration of TAMRA-LK11 peptide and $[F_0]$ the total concentration of HI fibrils.

Since the fluorescence data can only be biased by loss of fluorescence in the samples, the K was also determined for the point presenting the highest affinity using the following formula:

$$K = \frac{[P] \cdot [F]}{[PF]} = \frac{[P_0] - [PF] \cdot [F_0] - [PF]}{[PF]}$$

Nucleation inhibition and release

As seen in chapter 3, a surface pre-incubated with insulin has the ability to reduce the lag-time of insulin aggregation. We therefore wanted to investigate whether the complexes, formed on the surface at inhibiting concentrations of LK11 were able to subsequently reduce the insulin aggregation lag-time. We pre-incubated the wells during 60 min either with HI alone, HI with 5 µM LK11 or 5µM LK11 alone at 37° and 1200rpm agitation on a Titramax 100. After the pre-incubation time the liquid was removed and the wells were rinsed briefly with 200µL of filtered TMN buffer (under 1200 rpm agitation on a Titramax 100 at 37°). And a standard aggregation assay was performed on the pre-incubated surfaces.

4.3.3 Results

$(LK)_nL$ peptides in solution inhibit both nucleation and growth of amyloid fibers

Insulin aggregation on an LK11-pre-saturated surface presents shorter and significantly less disperse lag-times. We have therefore performed aggregation on such surfaces and added 5µM of LK11 in solution at various time points (Figure 1). This addition results in a strong reduction of the insulin aggregation rate when the peptide is added during the growth phase. Likewise when the peptide is added before the beginning of the growth phase, we observe a prolongation of the lag-time.

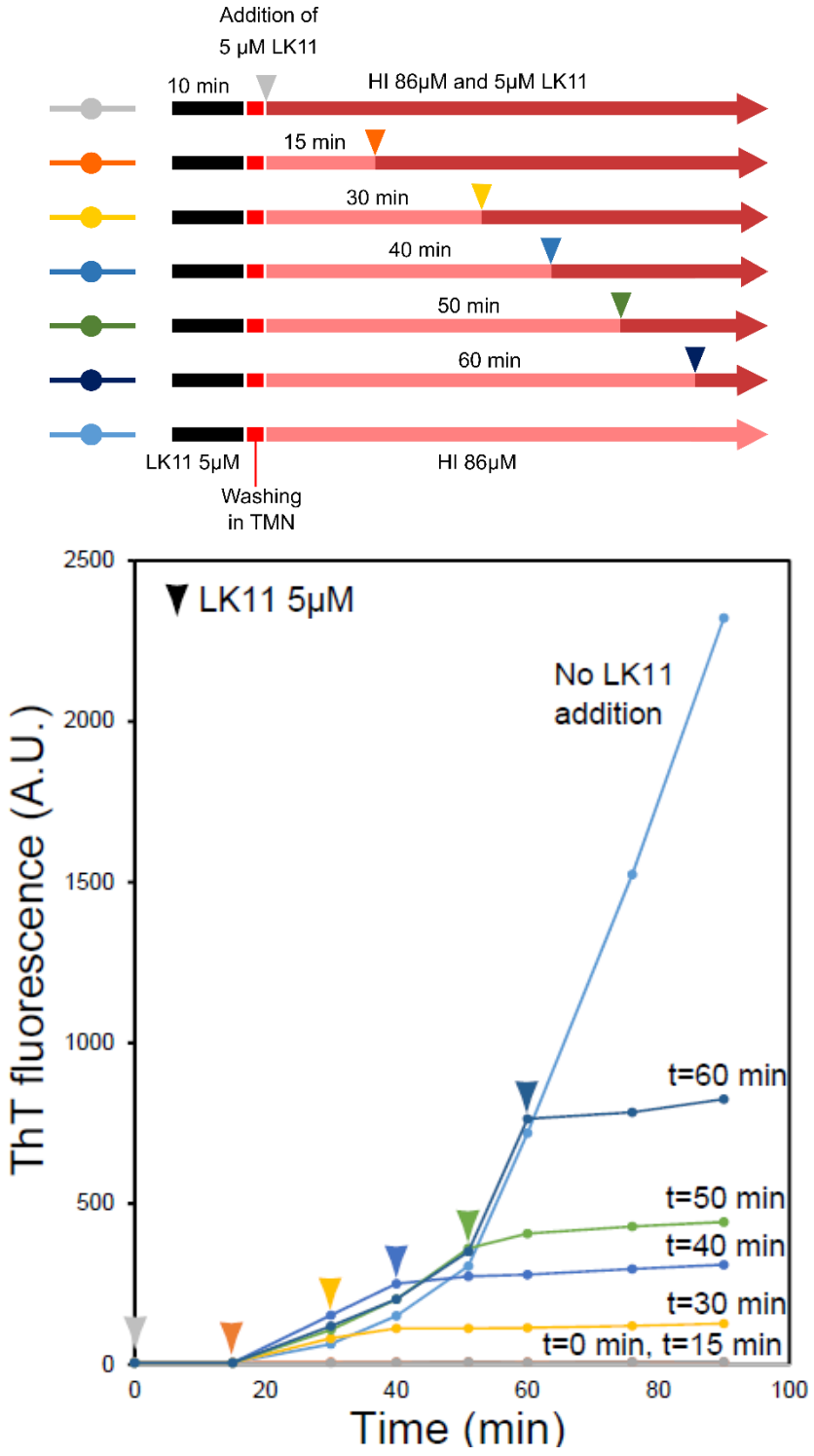

Figure 1. Inhibition of HI aggregation kinetics by addition of LK11 in solution. The arrowheads of the color of the curve mark the time point of addition of 5µM LK11 in the well during a standard insulin aggregation kinetics.

In order to understand the concentration-related effect of the nucleation inhibition, we have then added various concentrations of LK11 from the beginning of the incubation period (Figure 2). The peptides in solution induce a transition from short and low disperse lag-times to long

lag-times presenting increased relative variations. There is no evidence of cooperativity in this effect given the present data.

This inhibition of the nucleation effect can be extremely efficient indeed, as the TAMRA labeled-LK11 (which presents a cooperative reduction of the insulin aggregation lag-time similar to its unlabeled counterpart) dramatically prolongs the HI aggregation lag-time at concentrations superior to 0.74 µM (more than a week at 2.8µM).

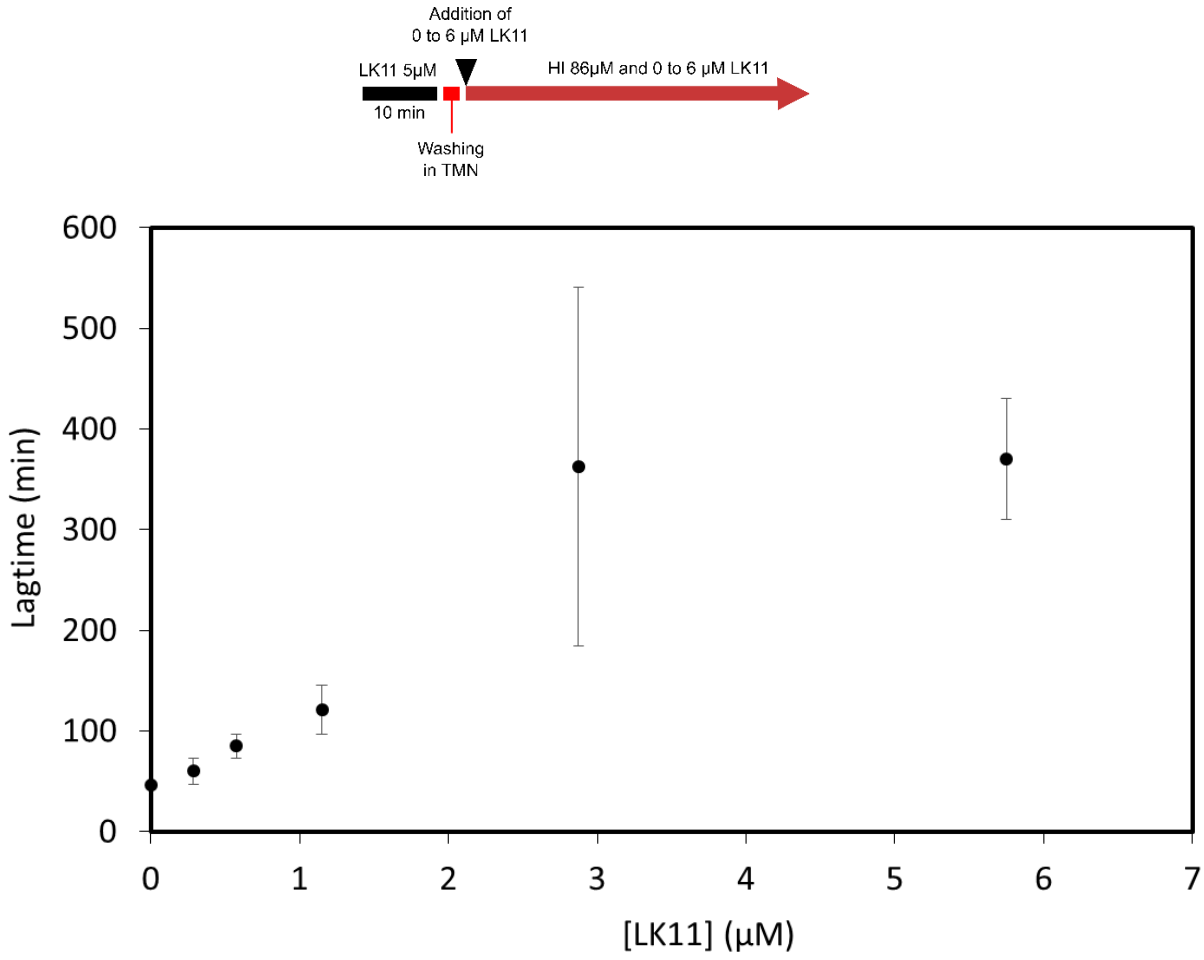

Figure 2. Insulin aggregation lag-time on a surface pre-saturated with LK11 as a function of the concentration of LK11 in solution during the nucleation step. Error bars present standard deviation (n=3).

LK11 peptides in solution inhibit growth

After the maturation of the nucleus into fast aggregating fibrils, we introduced various concentrations of LK11 in solution. The resulting aggregate growth rates were then plotted (Figure 3) as a function of the LK11 concentration for two time points of addition of the peptide at 60 min and 120 min. The growth rate is reduced when the peptide concentration in solution

increases, and both curves show a saturation at low aggregation rates. According to our model of aggregation during the growth phase, the concentration of native HI is higher at 60 min but the number of incorporation sites is lower.

The reduction of the growth rate at the lowest peptide concentration is more dramatic for the curve at 60 min than the curve at 120 min. This is likely the consequence of a fast inhibition of a lower number of incorporation sites. On the other hand, at 120min, the aggregation rate without peptide addition is lower (as a consequence of a lower concentration of native insulin) and the decrease in the growth rate with LK11 concentration is less pronounced.

The curve representing the growth rate after the addition of peptide at 120 min, thus presenting the highest amount of insulin aggregates, saturates at twice the growth rate of the curve inhibited at 60 min. This minimal growth rate value likely reflects the effects of a different mechanism: secondary processes. Even if, in high LK11 concentration, preexisting and newly created HI incorporation sites should be equally inhibited, the strong binding of the peptide on aggregates results in a reduction of its concentration in solution (Figure 47). Therefore the residual growth rate is likely the result of elongation at the newly created incorporation sites that cannot be efficiently inhibited due to the lack of available peptide in solution. Alternatively an HI incorporation mechanisms into growing fibers unaffected by the peptides (e.g. a hypothetical lateral growth mechanism) could also explain this residual aggregation.

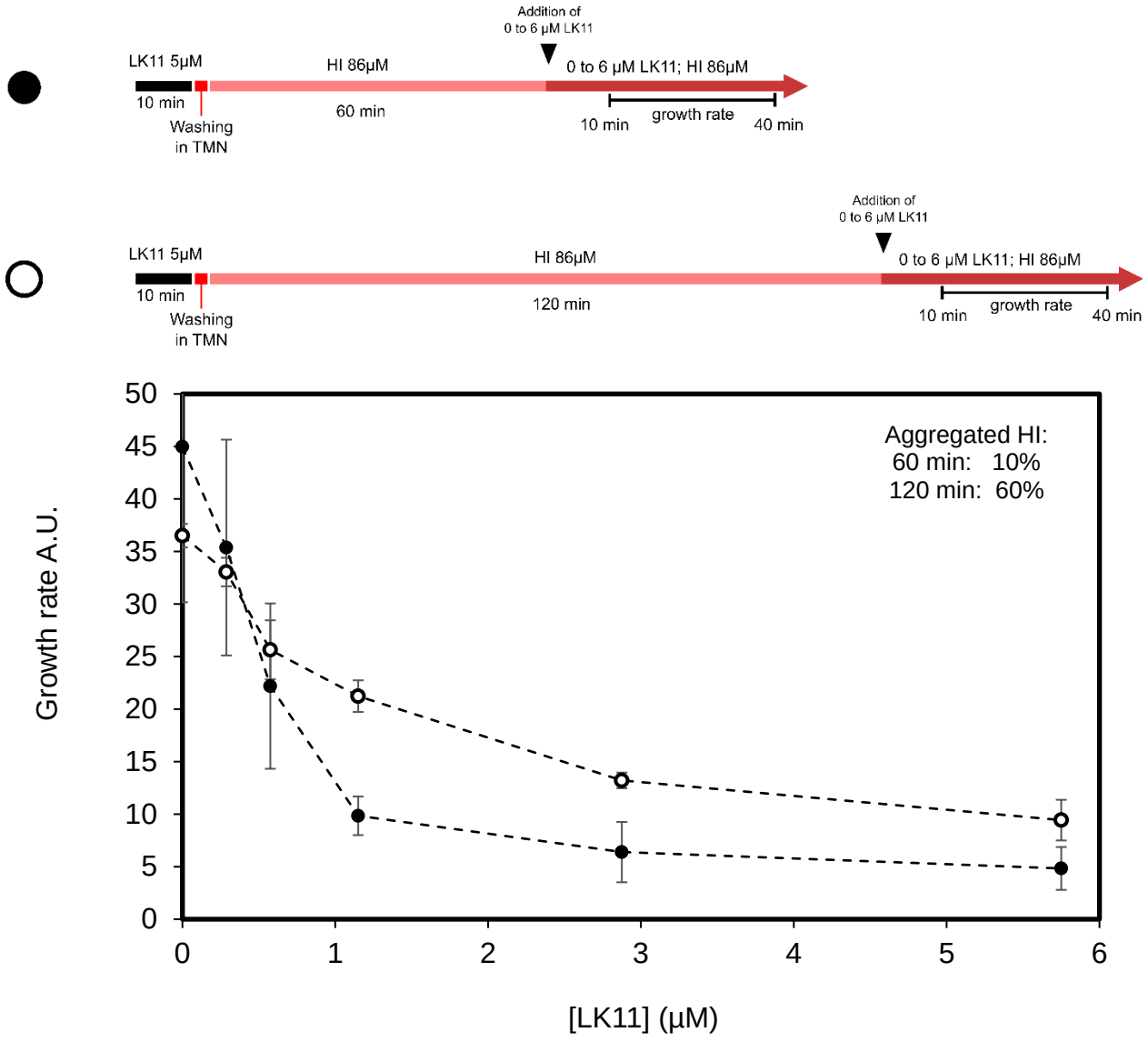

Figure 3. Insulin aggregation growth rate as a function of LK11 concentration in solution. LK11 was added during the exponential growth phase at t=60 min (filled circles) and t=120 min (empty circles). Error bars represent standard deviations (n=3), growth rates were measured between 10 and 40 min after the addition of LK11 peptide.

Binding of $(LK)_5L$ peptide to HI amyloid fibrils

Since the inhibition curve of fibril elongation during the growth phase suggests a binding and a stoichiometric inhibition phenomenon, this binding was further characterized. We performed co-precipitation experiments of HI amyloid aggregates with the fluorescently-labeled TAMRA-LK11. We determined the fraction of 0.28µM of TAMRA-LK11 precipitated with amyloid fibrils according to the concentration of available HI Amyloid fibers (Figure 4). We observe a strong affinity of the peptide for the fibril allowing a precipitation of close to 100% of the peptide in solution for 44µM of fibrils As no peptide remains in solution at high aggregate concentration, the binding affinity for native insulin is likely null or insignificant.

On the other hand, at low aggregate concentrations, the molar ratio of bound peptide over fibrillary insulin is superior to ¼ likely indicating a potential binding on every amyloid insulin molecule and not only to particular specific sites in the fibrils e.g. at their extremities.

The affinity constant:

$$K = \frac{[P] \cdot [F]}{[PF]}$$

is 3.73 µM according to the non-linear least squares fitting or 0.69 µM by using only to the point presenting the highest affinity. Note that the data point of the remaining TAMRA-LK11 peptide in solution as a function of total fibril concentration are symmetrical to the curve obtained with the point presenting the maximal affinity. We therefore consider that the affinity of the peptide for the fibril is 0.69µM and that about 1 peptide binds to 4-10 insulin monomers within an aggregate.

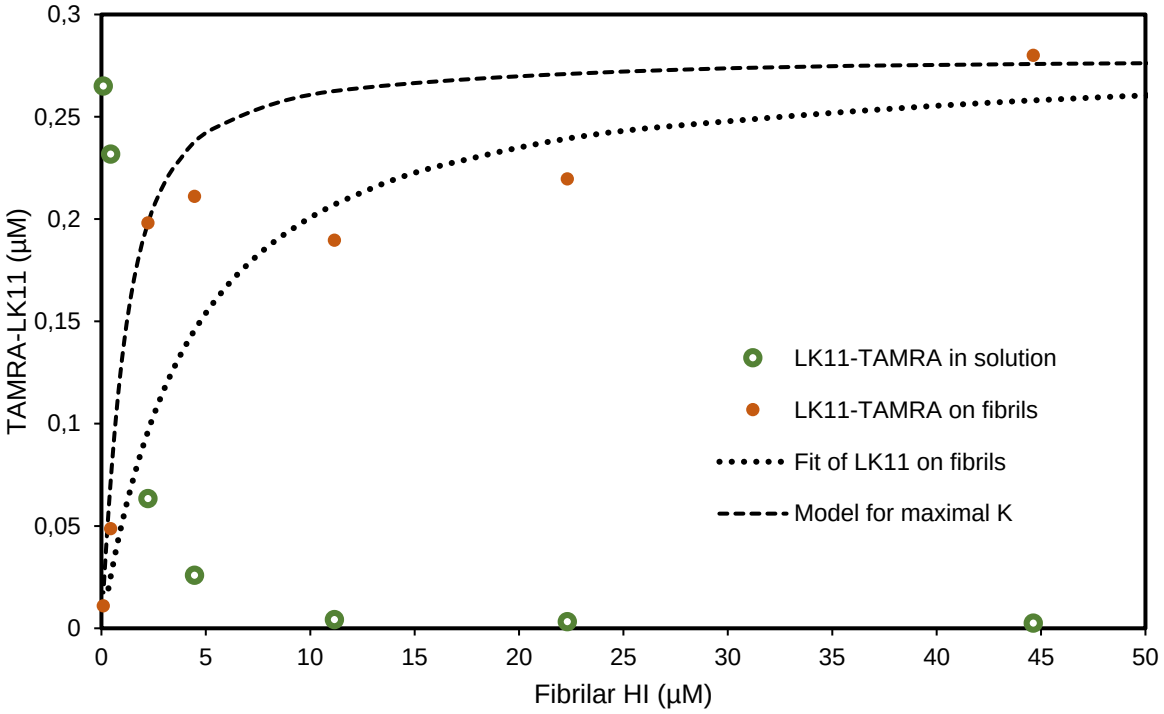

Figure 4. Binding of TAMRA-LK11 on insulin amyloid fibers. 0.28µM of TAMRA-LK11 were mixed with various concentrations of fibrillary insulin, then the insulin fibers were precipitated and the amount of TAMRA-LK11 peptide bound to the fibrils was quantified by fluorescence measurement in the supernatant and the pellet.

LK11 in solution can virtually abolish the nucleation process

Surfaces, pre-incubated with HI under agitation, present shorter lag-times than non-pre-incubated surfaces (chapter 3, Figure 45), providing evidence that at least the early steps in surface nucleation can be transferred as the foundation of subsequent nucleation after rinsing

of the surface and transfer into a fresh insulin solution. Here the pre-incubation of well surfaces with 5µM LK11 peptide and HI at 86µM for 60 min does not result in a reduction of the lag-time compared to a surface incubated with 5µM LK11 peptide alone (Figure 5). This means that no progress in the nucleation process has taken place during the pre-incubation time in the presence of inhibiting concentrations of peptide in solution. This implies either a strong reduction of the pre-nuclei complexes formation rate or an inactivation of the complexes by LK11 binding.

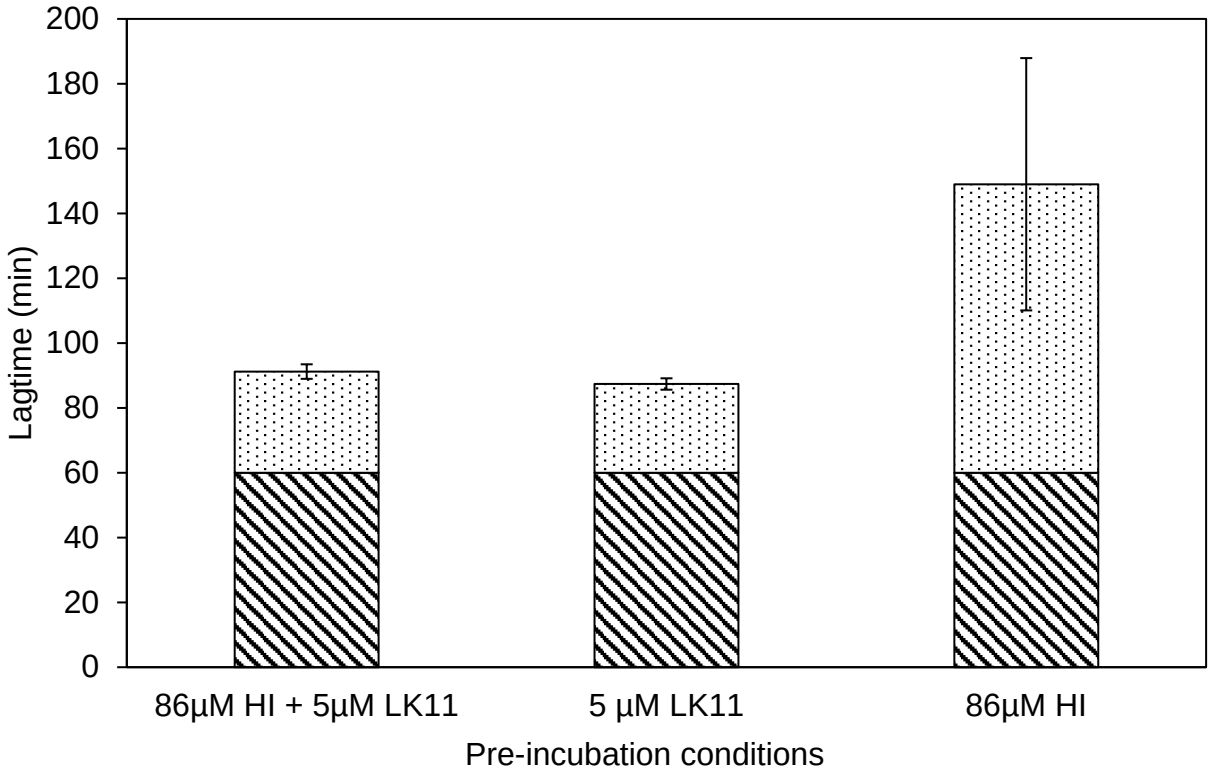

Figure 5. LK11 peptide in solution inhibits nucleation. The surface was pre-incubated during 60 min (hatched area) in different conditions then washed and subsequently incubated with 86µM HI (dotted area), mean values are shown, the error bars represent the standard deviation (n=3).

Negatively charged $(LD)_nL$ peptides do not inhibit nucleation or growth

We further tested the inhibiting properties of peptides using a similar sequence but with negatively charged amino acids, the LD9 peptide. The HI aggregation kinetics in the presence of this peptide presents a reduction of the lag-time similar to the effect observed in the presence of other alternating hydrophobic/hydrophilic sequence peptides[194], without any sign of inhibition at high concentration (Figure 6).

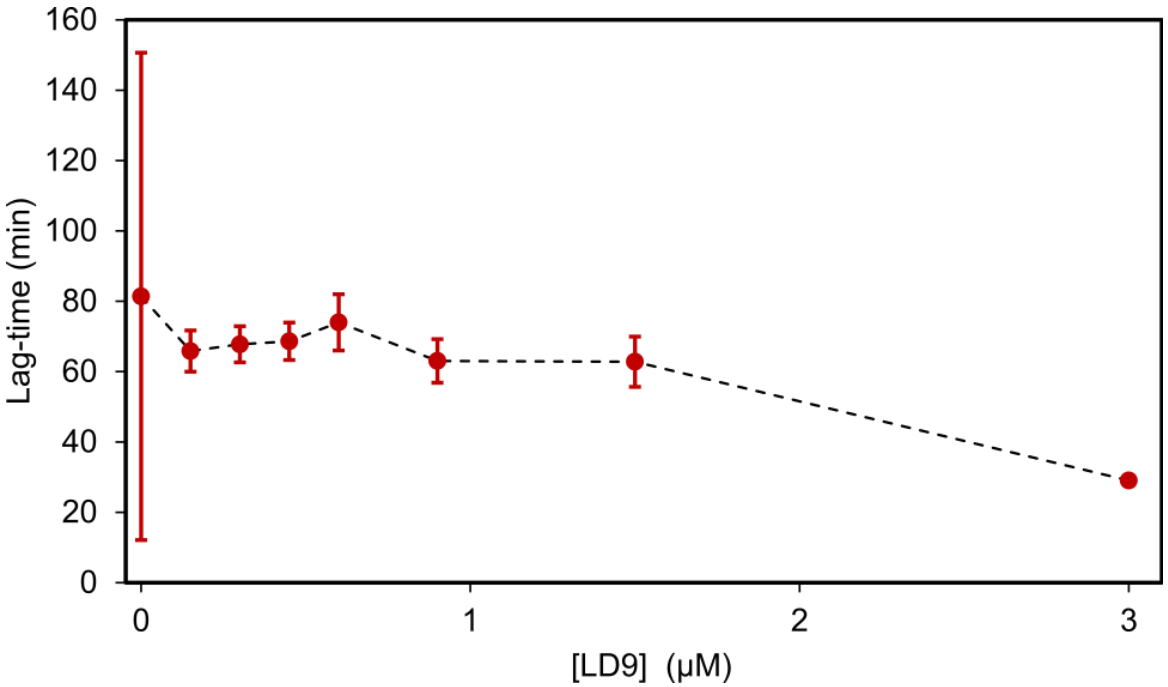

Figure 6. HI aggregation lag-time as a function of LD9 concentration. Mean values are shown, the error bars represent standard deviations (n=4).

4.3.4 Discussion

LK peptides in solution are able to inhibit surface-triggered amyloid aggregation of insulin either during nucleation (Figure 2 and 5) or during growth (Figure 1 and 3). This suggests that they are able to interact both with the fibrils and the pre-nucleus complexes.

Nucleation

The HI aggregation lag-time and their relative variations increase drastically with the LK11 concentration in solution (Figure 2). This peptide seems to inhibit nucleation from its very beginning. Indeed, as illustrated on Figure 5, the lag-time reduction expected from a pre-incubation of the surface in the presence of HI is inhibited by the presence of LK11 at 5µM during this pre-incubation. This suggests that the contribution of the pre-aggregation complexes created during this pre-incubation period is lost (Figure 5).

The inhibition of aggregation during the growth phase

During the growth phase the addition of LK11 peptide in solution induces a dramatic reduction of the aggregation rate. But not a destruction of the already formed fibrils. The mechanism of growth inhibition likely relies on the binding of LK11 to the fibrils preventing the incorporation of native insulin as suggested by the strong binding of TAMRA-LK11 on fibrillar insulin (Figure 4). This binding is apparently mediated by the charges as suggested by the reduction

of inhibition by LK peptide in higher salinity (Figure 6 in article I). The absence of inhibition observed with the negatively charged LD9 peptide compared to the LK9 peptide (Figure 6) also strongly suggests that this binding is mediated by the positive lateral charge of lysine.

During the growth phase the instantaneous growth rate $\left(\frac{dA}{dt}\right)$ is proportional to the amount of native protein (here **[HI]**) and to the amount of incorporation sites (**S**):

$$\frac{dA}{dt} \propto S \cdot [HI]$$

At 120 min the concentration of native insulin in solution is lower than at 60 min, but since the number of incorporation sites is higher the two initial aggregation rates (45 and 36 A.U.) are quite similar (Figure 3).

At the lower peptide concentrations the reduction of the aggregation rate is proportional to the amount of peptide in solution. This reduction is theoretically proportional to the number of native HI incorporation sites, which is in accordance with the more gradual reduction at 120 min, with approx. half of the slope of the curve at 60 min (m_{120min} = -25,7 and m_{60min} = -46,1; Figure 3).

At high peptide concentration both curves reach a minimum growth rate which is higher for the curve at 120 min (twice the minimum aggregation rate than for the one at 60 min). The existence of this significant residual aggregation rate even at high LK11 peptide concentrations in solution suggests the existence of at least two different aggregation mechanisms.

The role of Secondary processes

During the growth phase the amount of aggregates increases via 3 main mechanisms: elongation, monomer dependent secondary processes (e.g. secondary nucleation) and monomer independent secondary processes (e.g. fiber fragmentation). Secondary processes create new native protein incorporation sites at a rate which is proportional to the amount of aggregates in solution.

In addition, as shown on Figure 4, a significant depletion of LK11 peptides from solution exists because of their strong binding to the aggregates. At later stages during the aggregation process, newly created HI incorporation sites are therefore much less likely to undergo inhibition by LK11 peptide binding. The aggregation mechanism apparently unaffected by LK11 peptides likely corresponds to HI incorporation at these newly created sites.

The variation of incorporation sites by fiber fragmentation with time is:

$$\frac{dS}{dt} = \overrightarrow{\boldsymbol{k_{frag}}} \cdot \vec{\boldsymbol{a}} = \sum_{i=1}^{n} k_{frag_i} \cdot a_i$$

Where $\vec{\boldsymbol{a}}$ is the vector of the number of aggregate of size $\boldsymbol{i}$ and $\overrightarrow{\mathbf{k_{frag}}}$ the vector of the rate of new incorporation sites creation by the fragmentation of a fiber of the size $\boldsymbol{i}$. This implies that, without elongation, a certain quantity of aggregates with size distribution $\boldsymbol{a}$ can only generate a limited quantity of new incorporation sites by fragmentation (Figure 7).

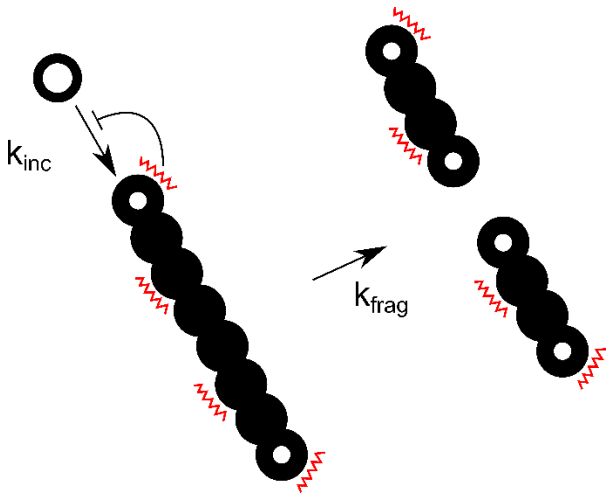

Figure 7. Model of interaction of the LK11 peptide with amyloid fibril during the elongation phase. The peptide binds amyloid fibrils inhibiting the incorporation of new native proteins and preventing possible secondary nucleation. The fibril fragmentation, however, creates new incorporation sites.

The inhibition of HI aggregation by LK11 is likely due to steric hindrance

The insulin aggregation lag-time in the presence of 2.8 µM TAMRA-LK11 exceeds a week. This shows the ability of LK11 peptide-driven mechanisms to completely abolish nucleation. This higher efficiency observed for the labeled peptide is likely attributable to steric hindrance.

The LK9 and LK11 binding is mediated by the charges of lysine lateral chains

The absence of inhibition observed with LK5 and LK7 peptides,[194] points towards the requirement of at least 4 positively charged lateral chain charges in order to stably bind to the HI fibrils. The stronger inhibition observed with the TAMRA-LK11 is unlikely due to a more efficient binding induced by the TAMRA-moiety since the other effects of the labeled peptide on HI aggregation kinetic are comparable with that of unlabeled LK11 peptide (similar cooperative adsorption on hydrophobic surface, and similar effects on both cooperative reduction of HI aggregation lag-time and inhibition of aggregation).

Interestingly the $(LKKLLKL)_2$ peptide, which adopts an α-helix conformation on hydrophobic interfaces[189], also prolongs the insulin aggregation lag-time for more than 30h at sub-

stoichiometric concentrations (1:10) [185]. Nault *et al.* attributed this effect to a stabilization of the HI native conformation by the adsorbed peptides, however this effect could result from a binding of the peptides in solution to the pre-nucleus complexes similar to the effect observed here for LK9 and LK11 peptides.

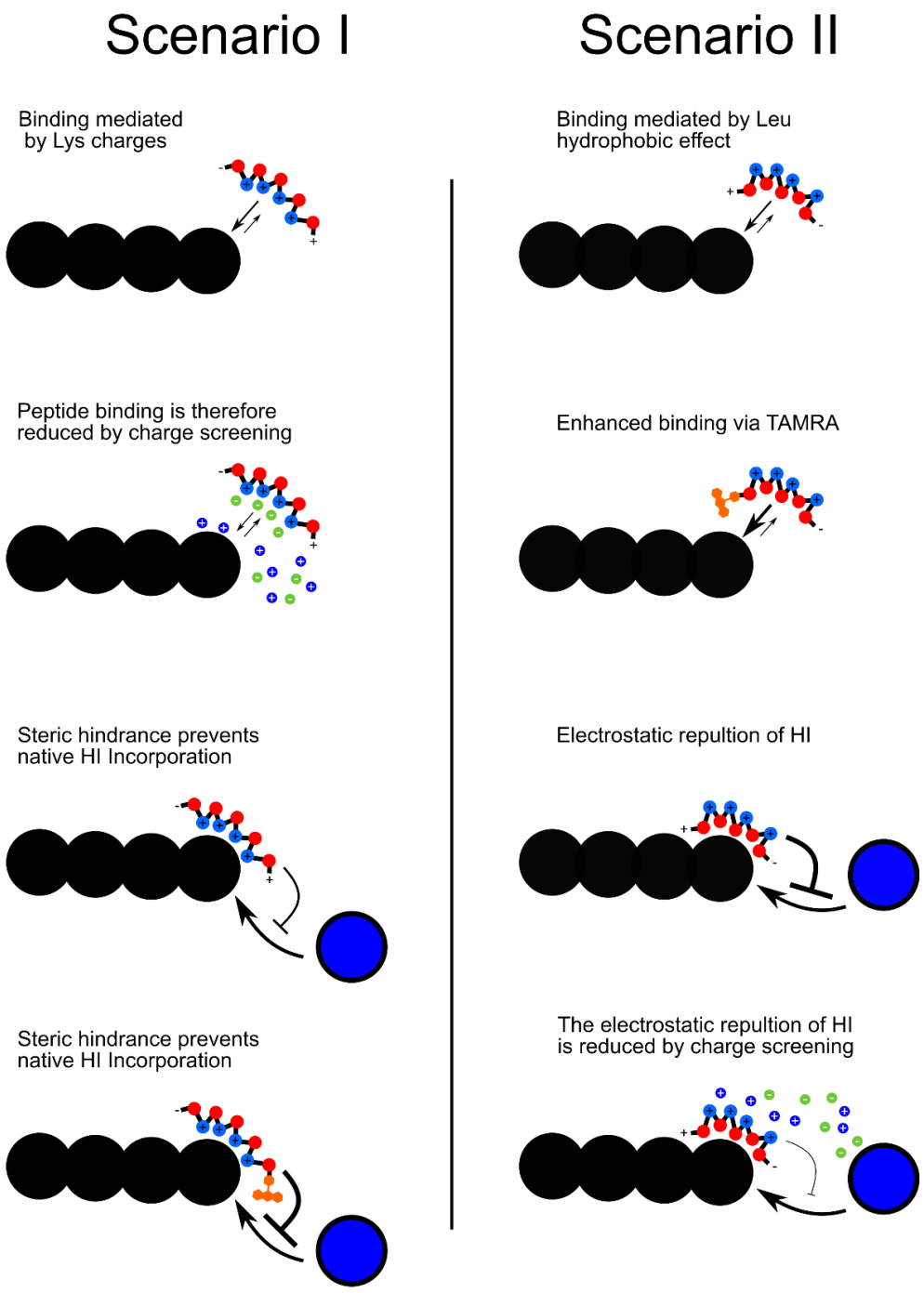

Figure 8. Model of LK11 binding to HI amyloid aggregate during the elongation phase. The favored hypothesis (scenario I) involves a binding mediated by positive lysine positive charges and a prevention of HI incorporation by steric hindrance. Alternatively (scenario II) the binding could be mediated by hydrophobic effects via leucine, the lysine positive charges would then prevent HI incorporation by charge repultion.

Localization

As the ratio of bound peptide over the amount of HI aggregates is higher than expected for a binding only localized on fiber extremities, and the addition of a fluorophore drastically increases the inhibition of insulin nucleation, the peptide can probably bind an allosteric site near the incorporation site of insulin (or on the edges of this site), and prevent the incorporation of native HI by steric hindrance (Scenario I on Figure 8). This binding is unlikely to occur directly by incorporation at the extremity of the β-sheet spine, blocking the incorporation of subsequent Native HI monomers, as similar but negatively charged peptides (LD peptides) do not inhibit HI aggregation. Alternatively the $(LK)_nL$ peptides could bind HI aggregates by hydrophobic effect and prevent the incorporation of native HI by electrostatic repulsion (Scenario II on Figure 8). Since HI is expected to be negatively charged at pH 7.4 and the LD9 peptides does not inhibits HI aggregation, this second scenario is extremely unlikely.

Competitive inhibition?

The elongation by incorporation of native HI can be considered analogous to a Michaelis-Menten reaction mechanism under the hypothesis of a 2-steps reaction divided into a reversible binding of the native insulin to the incorporation site and a subsequent conformational change (Figure 9). The peptide inhibition mechanism could therefore be classified either as competitive (i on Figure 9) if it binds only to the fiber, uncompetitive (ii on Figure 9) if it binds only to the intermediary state or non-competitive (i and ii on Figure 9) if it bind to both.

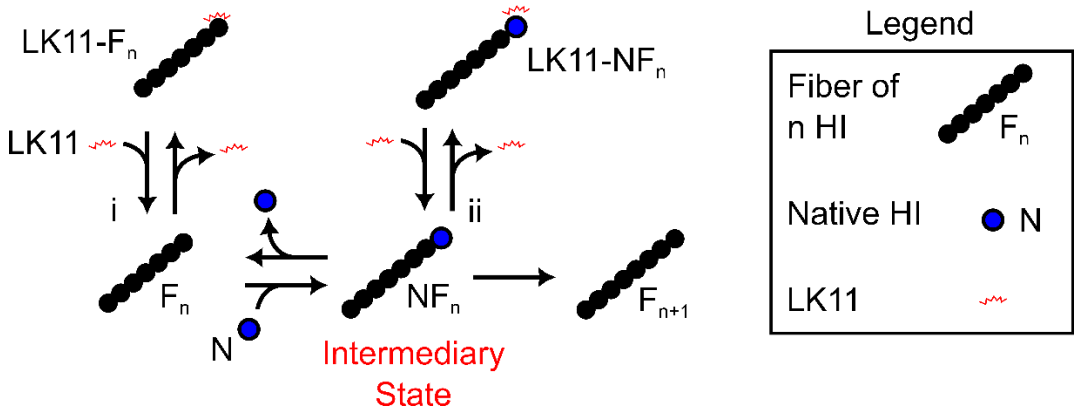

Figure 9. Hypothetical Michaelis-Menten-like incorporation mechanism. An inhibitior of this mechanism can either bind to the fiber (i), the intermediary state (ii) or both (i and ii).

In practice, the determination of the mode of inhibition of the LK11 peptide with native HI is difficult due to the peptide depletion from solution (adsorption on well surfaces and the stable binding on HI aggregates likely both in and outside the incorporation area) and the exponential

(logistic) character of the HI aggregation kinetics. In other words neither the number of reaction sites nor the number of inhibiting molecules are constant during the experiment.

Experiments of kinetic inhibition at various HI and LK11 concentrations with low amounts of initial aggregates, compared to native insulin and LK11 (preventing depletion from solution) and upon lower agitation (reducing aggregation rate and likely aggregates fragmentation) could resolve this competition issue at incorporation sites.

If the peptide inhibits insulin aggregation by competitive inhibition it likely binds on or most likely very close to the native insulin binding site on the aggregates preventing its incorporation into the growing fiber by steric hindrances (As proposed Figure 8 scenario I). Alternatively, a possible non-competitive mechanism could involve the binding of the peptide in the vicinity of the insulin aggregation site without preventing the binding of a native insulin molecule but blocking its conformational change into amyloid state.

Pre-nuclei complexes are unstable due to their high conformational energy. If an LK11 binding prevents the incorporation of new insulin molecules into the complex, the inactivated structure is likely to present an important dissociation rate. This explains the absence of lag-time reduction when a surface is incubated with insulin in the presence of 5µM LK11 (Figure 5).

Variation of the lag-time coefficient of variation

A reduction of the relative variation of the lag-time similar to the reduction observed in chapter 3 (between effective concentration of peptides and insulin alone) is observed in Figure 2. We have discussed that these changes could be due to an increase in the number of nucleation sites and/or a thermodynamic stabilization leading to a catalysis of the nucleation steps. Here once again these changes could be triggered by a destabilization of the nuclei (thermodynamic inhibition) and/or the preferential formation of non amyloidogenic complexes (kinetic inhibition).

Further characterization of peptide effect on nucleation by AFM

The formation of approx. 20 nm structures at the surface of hydrophobic glass coverslips incubated with HI has been characterized in the chapter 3. Surfaces presenting such structures have the ability to seed for amyloid aggregation in a fresh insulin solution. The next experiment would be to perform the same characterization in inhibiting concentrations of LK11. As LK11 inhibits nucleation the presence or absence of these structures can reveal if the mechanism of inhibition leads to a dissociation of the pre-nuclei HI complexes or to their inactivation.

5 Light induced insulin aggregation and location of the nucleation area

5.1 Introduction

The microscopy experiments have been conducted in order to observe in situ the appearance of the first aggregates. In order to do so we had to design a specific device allowing the direct observation of a surface on which insulin nucleation and aggregation could take place. We therefore developed an experimental set-up consisting of a chamber combined with a continuously agitation by a rotating glass rod for agitation. The bottom of the chamber, consisting in a borosilicate coverslip, is illuminated and observed by a fluorescence microscope. With the purpose of observing the insulin nucleation and earlier aggregation processes described in the two preceding chapters, which occur on hydrophobic surfaces under strong agitation we monitored the level of ThT fluorescence at this surface.

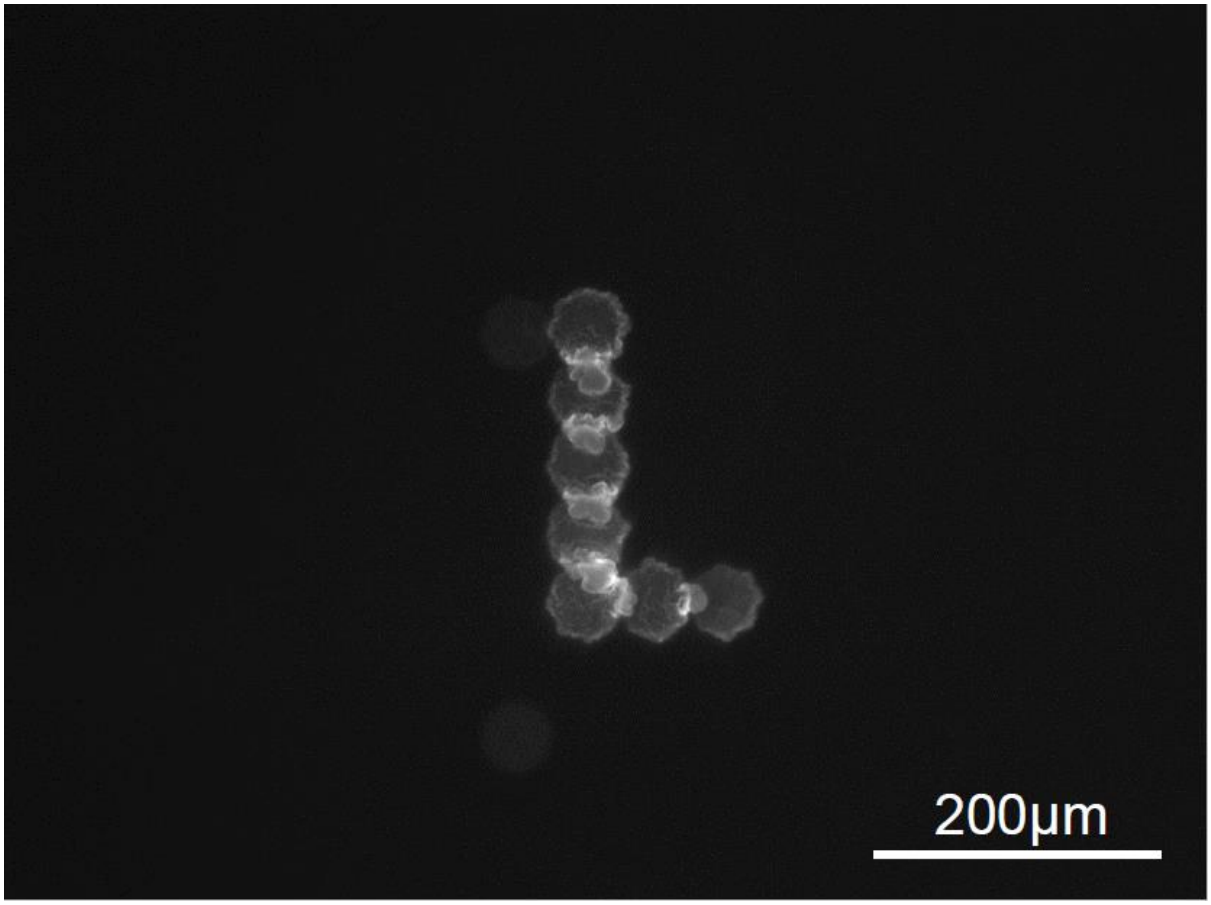

Figure 48 "L" pattern obtained by Light induced aggregation on glass coverslip.

The predominant process observed during these studies was a Light-Induced Aggregation (LIA) of HI at material surfaces in the area of illumination. The interesting mechanisms governing this processes have been extensively investigated in the following article.

LIA depends on the following parameters: agitation, surfaces and light, three factors known to induce protein denaturation and aggregation. This phenomenon, allows the controlled formation and growth of insulin aggregates on surfaces, restricted to the illuminated area. In the following paper, this illumination area has the shape of the octagonal microscope diaphragm. The process could allow the formation of desired patterns, provided an appropriate mask is used. The L pattern illustrated in Figure 48 was obtained by displacement of the glass surface by the microscope stage allowing a temporary illumination of each location of the surface (20 min per octagon).

5.2 Article III

Visible light-induced insulin aggregation on surfaces

Karim Chouchane, Isabelle Pignot-Paintrand, Franz Bruckert, Marianne Weidenhaupt[1]

Univ. Grenoble Alpes, CNRS, Grenoble INP*, LMGP, F-38000 Grenoble, France

*Institute of Engineering Univ. Grenoble Alpes
[1]Corresponding author:
Marianne Weidenhaupt
LMGP, Phelma Minatec, 3 parvis Louis Néel, CS50257, F-38016 Grenoble cedex1
Tel: + 33 4 56529335
FAX: + 33 4 56529301
email: marianne.weidenhaupt@grenoble-inp.fr

Abstract

Insulin, the most produced therapeutic protein is known to form amyloid aggregates induced by hydrophobic material surfaces. Here we describe the thioflavin T-mediated and material-dependent induction of thioflavin T-positive insulin fibrils on hydrophobic surfaces by visible light, in the presence of strong shear stress and at physiological pH. Light-induced insulin aggregation kinetics does not present a nucleation phase and is based on an energy transfer from visible light to the protein via thioflavin T. This process allows the formation of local surface-bound aggregation patterns.

Keywords

insulin amyloid aggregation, light-induced aggregation, Thioflavin T, surface-induced aggregation, agitation-dependent aggregation

Abbreviation[1]

[1] AOI: Area Of Interest

HI: Human Insulin

LIA: Light-Induced Aggregation

ND: Neutral Density

ThT: Thioflavin T

ThT_F : fluorescent Thioflavin T inside the aggregates

Introduction

In solution, the folding and conformational stability of proteins are mainly affected by temperature, pH, ionic strength, intermolecular interactions, agitation and exposure to electromagnetic radiation[1]. Protein aggregation usually results from conformational transition states or chemical degradations promoting a structural stabilization by inter-protein interactions[2].

Ultraviolet radiations for instance can directly excite aromatic amino acids, inducing protein denaturation. In particular, it has been shown for cutinase that an UV-excited tryptophan can disrupt an adjacent disulfide bridge via the ejection of an electron[3]. Moreover, the release of the energy of an absorbed UV photon as vibrational energy has been proposed as the mechanisms of reversible denaturation and subsequent aggregation of β-crystallin[4].

By contrast, the effect of visible light on protein stability is seldom described in the scientific literature, because most soluble proteins do not absorb radiations from this part of the spectrum. Light-induced functions in proteins are therefore based on the excitation of a bound chromophore and are mediated either by a change in the chromophore structure (e.g. rhodopsin[5]) or via a chemical reaction of the chromophore with the protein (e.g. LOV domain[6]). In addition, porphyrins, among other molecules, are known to be able to bind to proteins and oxidize them photochemically, directly or indirectly, via reactive oxygen species production[7,8].

Amyloid fibers are a class of highly ordered aggregates[9] in which the proto-filaments are stabilized by inter-protein β-sheets and the bundling of proto filaments into fibrils is in turn stabilized by the hydrophobic effect. Thioflavin T (ThT) undergoes a fluorescence shift when bound to amyloid fibrils, a state referred to as ThT-positive. Due to their high activation energy, the amyloid fibril formation usually follows a nucleated aggregation kinetic characterized by a lag-time[10].

Insulin, the most used protein drug, forms such amyloid aggregates at low pH and high temperature[11]. In addition amyloid-like aggregates can be formed at physiological conditions upon agitation by nucleation on hydrophobic surfaces, which raises formulation as well as possible iatrogenic issues[12,13]. Previous studies have shown that the rapid adsorption of an insulin layer on hydrophobic surfaces was triggering the slow conformational transition towards its amyloid state[14–16]. Heterogeneous nucleation of insulin on hydrophobic and rough surfaces present a much higher rate than homogeneous nucleation in solution[17].

Here we present a setup allowing the constant agitation of a protein solution above a continuously illuminated surface in the presence of ThT. We demonstrate, for the first time, that the energy transfer from visible light to insulin, mediated by ThT, triggers light-induced aggregation (LIA) of human insulin at a hydrophobic surface. The formation of these ThT-positive aggregates is restricted to the illumination area, which could be used for patterning strategies. Interestingly the aggregation kinetics follows a quasi-exponential growth without any observable lag-time which is unusual for amyloid-like aggregation[18].

Materials and Methods

Insulin and Thioflavin T preparation

Recombinant human insulin (HI) produced in *Saccharomyces cerevisiae* was purchased from Sigma-Aldrich (ref: I2643). HI solutions were prepared in TN buffer (25 mM Tris-HCl pH 7.4, 125 mM NaCl), using Milli-Q® deonized water (resistivity = 18 MΩ.cm at 25°C). In order to fully solubilize insulin, the pH of the solution was first lowered to 3.2 using 1 M HCl then adjusted to pH 7.4 with 1 M NaOH using a pH electrode. The HI concentration was then precisely adjusted to 86 µM, using the 280 nm absorbance ($\varepsilon_{280\ nm}$ = 5.53 mM^{-1} cm^{-1}). Once adjusted at the proper concentration, the HI solution was filtered through a 0.22 µm Millex-GV filter unit (ref: SLGV033SS). The solutions were stored at T = 4 °C for less than 2 weeks and filtered again before use.

Upon binding to amyloid fibers, Thioflavin T (ThT) undergoes a fluorescence shift from (λex= 342 nm; λem= 430 nm) to (λex= 450 nm; λem= 482 nm). This property allows the direct quantification of amyloid fibers by fluorescence since the fluorescence of bound ThT is proportional to the amount of amyloid fibers. Thioflavin T (from Sigma-Aldrich, ref: T3516) was solubilized in TN buffer. The ThT concentration was then adjusted to 1 mM by absorbance measurement ($\varepsilon_{416\ nm}$ = 26.6 $mM^{-1}.cm^{-1}$ in ethanol). Finally, ThT solutions were filtered through a 0.22 µm Millex-GV filter and stored at 4°C protected from light for less than 2 weeks.

Material surface treatment

Borosilicate glass coverslips (VWR international 631-0162) were used either without surface treatment (water contact angle = 60°) or after etching in 14M NaOH for 30 min (water contact angle = 30°). As the same rotating glass rod was used for every experiment, it was cleaned with sodium hypochlorite to remove any adsorbed protein, then etched in the same manner as described before to prevent protein adsorption and aggregation on its surface.

Experimental setup

The experimental setup consists of a home-made chamber installed on the microscope stage of an inverted microscope (Figure 1A). The microscope provides both the illumination for the photoactivation process and the monitoring of ThT fluorescence. The chamber was built using a 5 mm diameter tube cut from the top of a 1200 µL polypropylene pipette tip (Sorenson 34000), sealed over a borosilicate glass coverslip using melted Parafilm M®. It was filled with 750 µL of a protein and ThT solution, continuously stirred with a 1.5mm diameter cylindrical glass rod rotating at 1200 rpm thanks to a 6mm diameter DC gear motor (Nano Planetary 16mm Type ref: 206-102). The chamber was then placed on the stage of an Olympus IX71 inverted microscope and illuminated by episcopic illumination at the ThT excitation wavelength through a 60 x magnification objective (1.25 numerical aperture). The microscope is fitted with a mercury short arc bulb (Osram cb1915239) and a Chroma DEAC filter cube (ref. U-N31036v2 C108867). The spectroscopic parameters of the illumination and the fluorescence recording were: excitation wavelength λ_{ex} = 436 nm, bandwidth 20 nm, long-pass dichroic mirror cutoff wavelength λ_{cutoff} = 455 nm, emission wavelength λ_{em} = 480 nm, bandwidth 30 nm. The illuminating light intensity was modulated using neutral density (ND) filters and the area of illumination was delimited using the field diaphragm (Figure 1C). The time lapse imaging of the ThT fluorescence distribution at the surface was performed with an Olympus DP30BW camera (256 grey levels). The exposure time is set depending on the illumination irradiance.

The illumination irradiance was determined in the following manner. The radiant flux falling on the illuminated area (1725 µm²) was measured at 440nm using a photodiode detector (18I27 Lasermate Q, Coherent, USA) with each ND filter used in this study. From these measurements we determined that the radiant flux (P) within the total illuminated area was given by $P = 3.3187 \cdot \tau$ (mW), where τ is the ND filter transmittance. This corresponds to an irradiance $I = 1920 \cdot \tau$ nW.µm^{-2}.

For insulin aggregation assays on plain surfaces, the protein solution contained 86 µM HI and 20 µM ThT in TN buffer (unless otherwise specified). The field diaphragm aperture was set to its minimum resulting in an octagonal illumination area (50 µm diameter, Figure 1C). The illumination was continuous, at different light intensities, and the surface fluorescence was measured every 30 sec.

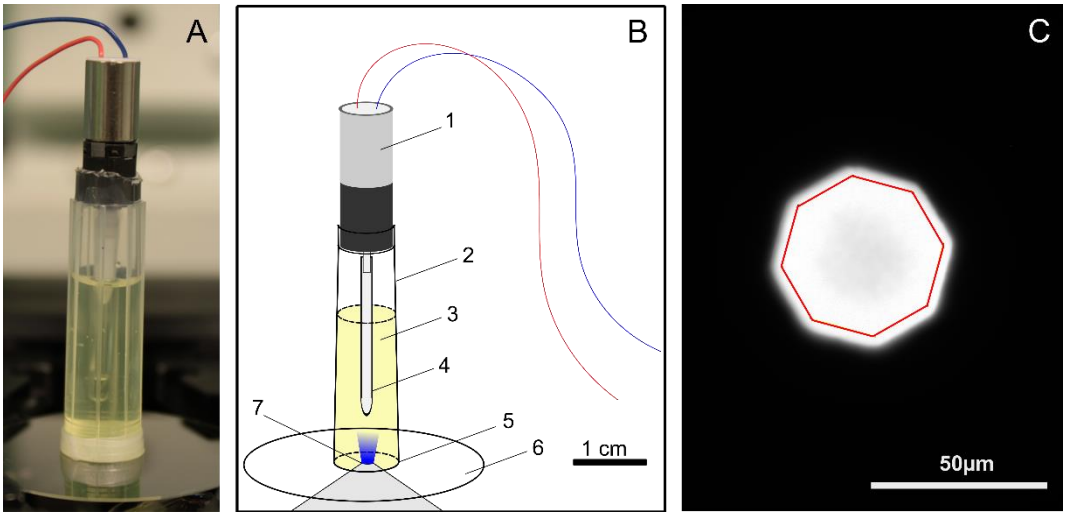

Figure 1: Experimental setup. A: Photograph of the experimental setup on the fluorescence microscope stage while the motor is under tension (exposure time = 160ms). B: Scheme of the experimental setup: electrical motor (1), polypropylene well (2), protein solution (3), rotating glass rod (4), Parafilm gasket (5), glass coverslip (6), inverted microscope objective (7). C: Microscope image taken during a representative light-induced insulin aggregation assay using the minimum aperture of the field diaphragm. The red polygon defines the area of interest (AOI) used for image analysis.

Light-induced aggregation at bead surfaces

For insulin aggregation assays on beads, red fluorescent carboxylate-modified polystyrene beads (0.5 µm diameter, $4.87 \cdot 10^7$ beads.mL^{-1}) were purchased from Sigma-Aldrich (L3280) and diluted 100 times in TN buffer. Then 10 µL of the diluted suspension were added to the protein solution containing 86 µM HI and 20 µM ThT in TN buffer. The suspension was observed under red fluorescence conditions (λ_{ex} = 575 nm; λ_{em} = 610 nm) for 10 min, until about 10 beads had been stably adsorbed on the surface in the field of view. The illumination was then switched to the ThT fluorescence conditions and the aggregation kinetics was recorded as described above.

Peptide addition during exponential growth of the aggregates

In order to test the effect of peptides in solution on the kinetic of light-induced aggregation, we constructed a chamber fitted with an injection hole allowing the direct addition of small volumes to the solution during the imaging process. We tested the effect of peptides on the growth rate via the addition of 5µM $(LK)_5L$ peptide and observed peptide localization via the addition of 0.42µM TAMRA-$(LK)_5L$ peptide. The two peptide solutions were prepared as described in [19].

Image processing and data analysis

We defined an area of interest (AOI) located in the center of the illumination field (Figure 1C). The fluorescence intensity of each image was obtained by averaging the value of the pixels in

this region: average raw fluorescence intensity. The saturation of the CCD camera limits the linear range of fluorescence recordings. We therefore excluded from analysis images presenting saturated pixels. In addition, we observed, after sufficient time, that ThT-positive objects grow rapidly extending in height above the coverslip surface. This results in defocusing of the fluorescent zone and therefore a reduction of its measured fluorescence intensity. Images that were not well focused were therefore removed from the quantitative analysis.

To compare fluorescence intensities measured with different exposure times t_{exp} (s), at different irradiances $I_0 = 1920 \cdot \tau$ (nW.µm^{-2}), where τ is the ND filter transmittance, and at different ThT concentrations [ThT] (µM), the average raw fluorescence intensity is divided by the following coefficient $H = \tau \cdot t_{exp} \cdot [ThT]/0.6$ s^{-1}µM^{-1}, resulting in F, the normalized surface fluorescence intensity. The following experimental conditions have been used as a standard for normalization: 86 µM HI, 20 µM ThT, I_0 = 57.7 nW.µm^{-2}, t_{exp}= 1 s, τ =0.03. In these conditions H=1. The initial kinetics of aggregate growth under continuous agitation and illumination are then fitted with a first order exponential (Eq. 1) using a non-linear least squares method (Gauss-Newton algorithm) to determine A, k_{app} and B.

$$F = Ae^{k_{app}t} + B \qquad \text{(Eq. 1)}$$

To analyze the fluorescence increase on beads' surfaces, an AOI was defined around the beads, large enough to encompass the maximum extent of the ThT fluorescence recorded around individual beads. Another AOI was defined in the background region, to measure the (very slow) fluorescence increase at the coverslip surface. The fluorescence levels were subtracted from the initial values to obtain the normalized fluorescence with respect to the initial fluorescence.

Sample preparation for confocal laser scanning microscopy and scanning electron microscopy

For confocal laser scanning microscopy (CLSM), the protein solution contained 86 µM HI and 130 µM ThT in TN buffer. The field diaphragm aperture was set to its maximum resulting in a circular illumination area (425 µm diameter). The illumination was continuous, at 960 nW.µm^{-2} irradiance during 1 hour. The sample was then imaged using a 63x / 1.4 numerical aperture oil immersion objective on a LSM700 ZEISS confocal microscope.

To prepare samples for scanning electron microscopy, the protein solution contained 86 µM HI and 20 µM ThT in TN buffer. In the fluorescence microscope, the field diaphragm aperture was

set to its maximum resulting in a circular illumination area (425 µm diameter). The illumination was continuous, at I = 57.7 nW.µm^{-2} irradiance during 1 hour.

The coverslip was then separated from the chamber, rinsed in pure H_2O, fixed 1hour in glutaraldehyde (2.5% in 0.1 M sodium cacodylate buffer pH=7.2) rinsed 3 times in 0.1M sodium cacodylate buffer pH 7.2 and eventually dehydrated in successive ethanol baths of increasing concentrations (70%, 90%, 95%, 100%). After a platinum deposition, the sample was then observed on a Quanta FEG 250 (FEI) scanning electron microscope in secondary electron detection, using an Everhart-Thornley detector (voltage= 5.00kV; magnification 20 000 X; working distance: 9.2mm; spot size: 3.0 nm).

Results

Light-induced insulin aggregation

The experimental setup is described in Materials and Methods and Figure 1. A home-made chamber is built on a borosilicate glass coverslip and filled with a solution containing insulin and Thioflavin T (ThT). The solution is continuously stirred and illuminated at ThT excitation wavelength (436 nm) with calibrated light intensities. The field diaphragm of the microscope is used to restrict the illumination to a 50 µm diameter octagonal area. ThT fluorescence at 480 nm is used to monitor the formation of insulin aggregates at the coverslip surface (focused fluorescence). To estimate the amount of insulin aggregates, the fluorescence intensity is divided by the illuminating light intensity, the exposure time and the ThT concentration (normalized fluorescence intensity).

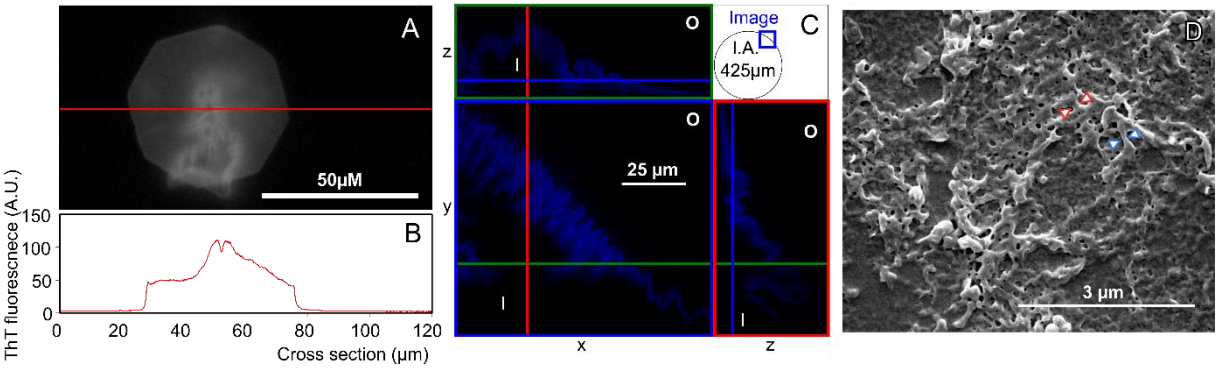

Figure 2: Microscopic characterization of light-induced ThT-positive insulin aggregates. A: Image of the ThT fluorescent pattern after 2h of incubation at I_0 = 7.2 nW.µm^{-2}. Scale bar = 50 µm. Note that the image is obtained with a full aperture of the field diaphragm; B: Fluorescence intensity profile of image A along the red line; C: Confocal laser scanning microscopy of light induced insulin aggregates (1h illumination, [ThT]= 130µM, I_0 = 960 nW.µm^{-2}). The image displays a slice (z =0.4 µm) of the edge of the protein aggregate which presents the highest ThT fluorescence signal. Two orthogonal vertical slices (xz and yz, green and red lines, respectively) and a horizontal slice (xy, blue lines) are displayed. I.A. illumination area (diameter =425 µm), I:interior of the protein aggregate, O: solution; D: Scanning electron microscopy of the surface of the light aggregated structure (1 h illumination, I_0 = 57.7 nW.µm^{-2}). The image

displays the edge of the protein aggregate. The arrows point to fibrillary material of 100nm (blue) and 150 nm (red) diameter.

After illumination of the surface, a ThT-fluorescent octagon is clearly visible, that matches the illumination area. No ThT fluorescence is visible outside the illumination area (Figure 2A and B). When the setup was illuminated at 475 nm (at the cyan-end of the bound ThT excitation peak), the aggregation rate was drastically reduced. No light-induced aggregation phenomenon appears when the surface was illuminated at 535nm (at a wavelength beyond the bound ThT excitation peak). The light aggregation efficiency therefore matches the bound ThT excitation spectrum.

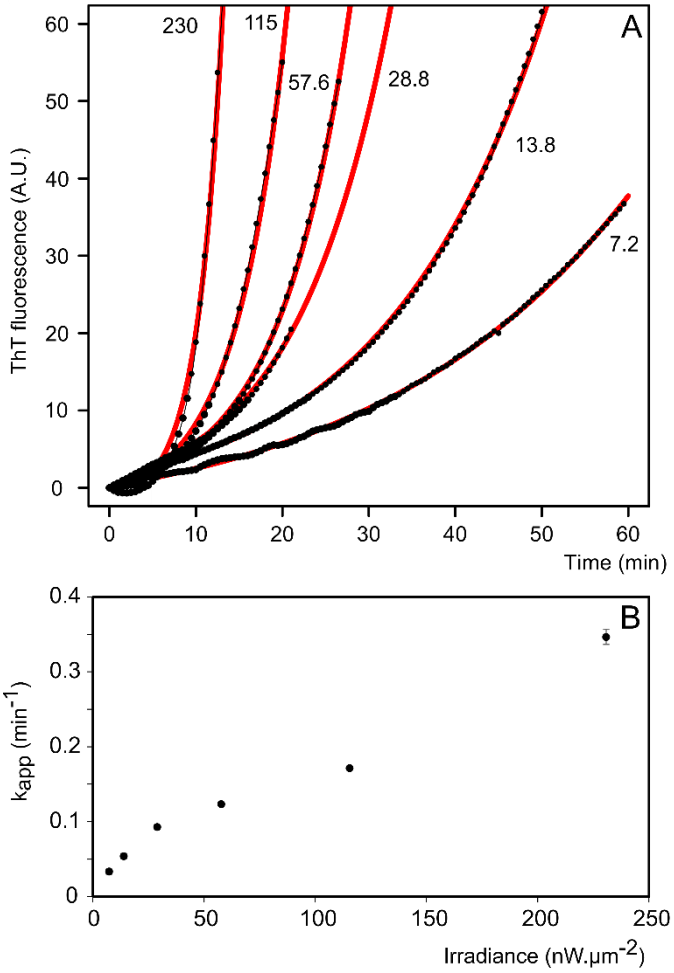

Figure 3: Exponential increase of ThT surface fluorescence under constant illumination. In this experiment, an insulin solution (86 µM HI, 20 µM ThT) is constantly illuminated under stirring. The surface fluorescence is recorded as a function of time and normalized to the illumination intensity. A: Evolution of the normalized fluorescence intensity as a function of time in the area of interest for the indicated irradiances I_0 in nW.µm^{-2}. Dots: experimental points, red solid line : fit with Eq. 1. B: k_{app} as a function of irradiance. Error bars: standard error on k_{app}.

The time course of surface ThT fluorescence evolution is first studied at different illuminating light intensities. In the dark, no ThT fluorescence increase is observed. At intermediate light

levels (7-200 nW.µm^{-2}), the surface ThT fluorescence increases immediately after the illumination is turned on, and displays exponential growth (Figure 3A). The initial kinetics of aggregation have been fitted with Equation 1. The resulting growth rate (k_{app}) increases with the light irradiance (Figure 3.B). Furthermore, during the early time course of the experiment, no diffuse fluorescence appears in solution. The formation of ThT-positive aggregates is therefore restricted to the illuminated area on the surface, and neither takes place in the bulk solution nor in the non-illuminated area.

Before any illumination, the surface is slightly fluorescent (Figure S1A). We attribute this fluorescence to adsorbed HI, which is indeed able to bind ThT as shown by Nault et al.[14] (Figure S1A). For irradiances above 250 nW.µm^{-2}, this initial fluorescent layer is rapidly bleached in the illumination area (Figure S1B). As a consequence, we observe another growth pattern: a faster initiation of aggregation at the edges, where a light gradient creates lower irradiances, allowing the formation of sufficient insulin aggregate prior to the photo-bleaching of the initial ThT layer (Figure S2, 0min and 5min). These aggregates subsequently invade the center from the margins (Figure S2, 7.5min and 10 min). These results demonstrate that a competition exists at the level of adsorbed HI and ThT layer between photobleaching and light induced aggregation. Because of this complex growth pattern kinetic, data obtained at I_0>250nW.µm^{-2} were not taken into consideration for quantitative analysis.

The ThT-fluorescent structure initially grows on the glass surface, then above the surface as a 3D structure presenting micro-convolutions on its surface. Such a structure obtained after 1h illumination in conditions allowing a rapid growth (I_0 = 960 nW.µm^{-2}, [ThT]=130µM, [HI]=86µM) was studied by confocal laser scanning microscopy (Figure 2C). It reveals that, when the aggregate has grown in height, ThT fluorescence localizes at the surface of the structure, where fresh ThT and proteins are constantly supplied by the fluid agitation. After fixation and dehydration, scanning electron microscopy reveals the presence of an interconnected network of 100 to 150 nm-wide filaments at the surface of the aggregate (Figure 2D).

Light-induced insulin aggregation strongly depends on material surface chemistry

We then investigate the dependence of light-induced insulin aggregation on the material surface chemistry. Purchased glass cover slips exhibit a water contact angle of 60°, which is reduced to 30° after treatment with 14 M NaOH. This is due to the etching and hydroxylation of the glass surface[20]. In contact with insulin and ThT, these hydrophilic surfaces exhibit less initial ThT fluorescence than more hydrophobic ones (Figure 4 and S1A). Upon illumination at

intermediate levels, insulin aggregation is strongly delayed on hydrophilic surfaces (Figure 4A), compared to the more hydrophobic ones (Figure 4B). Moreover, ThT fluorescence appears in a spatially inhomogeneous manner on the more hydrophilic surface (Figure 4A, t = 40 min and 50 min). This inhomogeneity is likely due to local hydrophobic surface contaminants where insulin aggregation could be promoted.

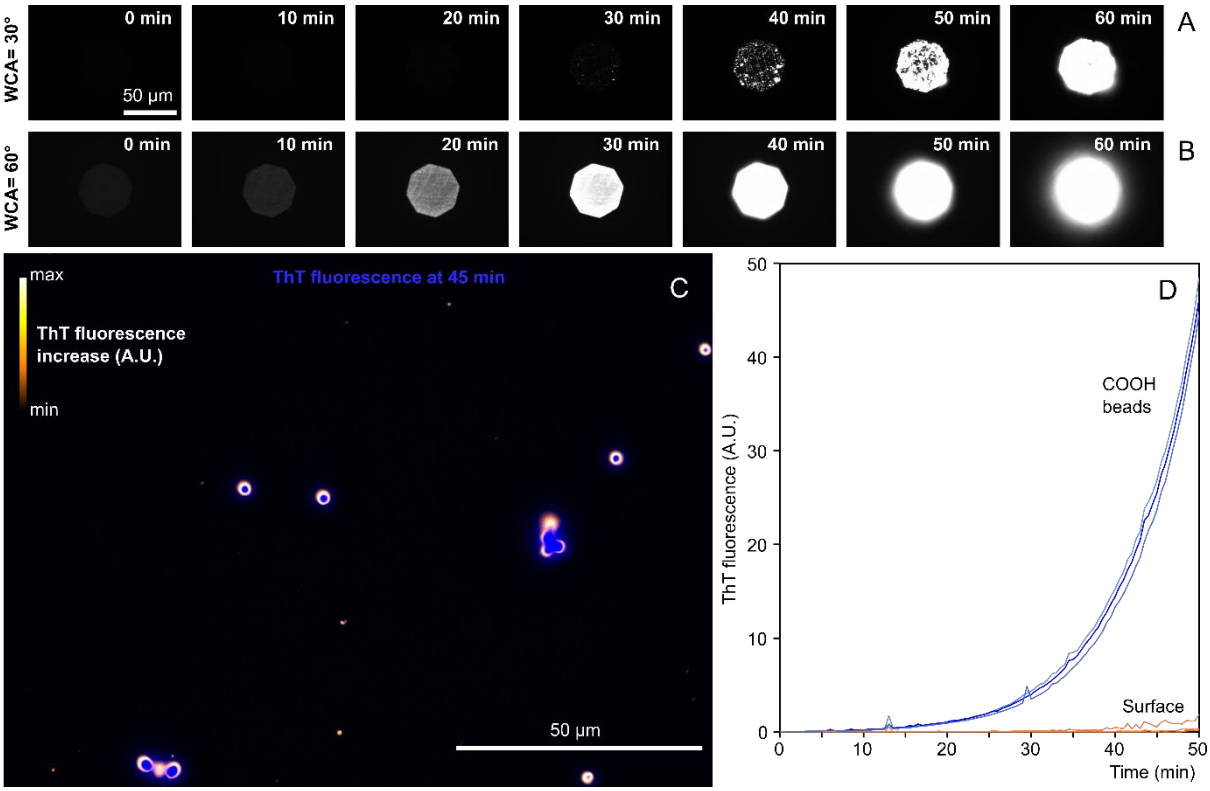

Figure 4: Light-induced insulin aggregation depends on material surface chemistry. Time course of light-induced insulin aggregation on NaOH-treated (A) or untreated (B) glass surface. The experimental conditions are : 86 µM HI, 20 µM ThT, I_0 = 115.2 nW.µm^{-2}, scale bar 50 µm. C: Light-induced insulin aggregation is performed on a NaOH treated glass coverslip in the presence of COOH-functionalized microbeads. The experimental conditions are: 86 µM HI, 20 µM ThT, I_0 = 115.2 nW.µm^{-2}, scale bar 50 µm. The blue image corresponds to a ThT surface fluorescence image at 45 min of illumination and the yellow image to the ThT fluorescence increase between 45 min and 45.5 min. D: Kinetics of light-induced insulin aggregation on three beads (blue curves) and on the glass surface (orange curves), measured in the recording of Figure 4C.

To investigate the effect of surface chemistry, red-fluorescent, 500 nm diameter, polystyrene beads were dispersed into the insulin + ThT solution, in an illumination chamber made on top of a highly hydrophilic NaOH-treated glass coverslip. These hydrophobic microbeads are functionalized with a few carboxylic groups to prevent their clustering. During the time course of the experiment, some of them stably adsorb on the hydrophilic glass surface. As soon as polystyrene beads reach the illuminated zone, ThT fluorescence appears at their surface and continuously increases with time. The total fluorescence around one bead can be integrated and representative fluorescence kinetics are shown in Figure 4D, which demonstrates reproducible

exponential growth around the hydrophobic microbeads, similarly to the one observed on untreated glass surfaces. Furthermore, by comparing ThT-fluorescence at two different time points (45 and 45.5 min), it is clear that ThT-fluorescent structures grow eccentrically (Figure 4C). This confirms that hydrophobic surfaces are prone to light-induced insulin aggregation.

Effect of physical and chemical parameters on light-induced insulin aggregation

Two key parameters of chemical reactions are temperature and mixing. The experiments reported above were performed at room temperature (22-25°C) and under constant agitation (1200 rpm). In the following part, we investigate the effect of heating and stirring on the reaction kinetics. In addition, we demonstrate that light illumination is absolutely required for fiber growth.

In order to study the effect of temperature on light-induced aggregation, a new experimental setup was built where a water jacket surrounds the reaction chamber to maintain it at the desired temperature. As shown in supplementary information (Figure S3), light-induced aggregation is strikingly reduced at 0°C, indicating that insulin conformational changes are blocked at this low temperature. In contrast, the aggregation kinetics presents little acceleration between 23°C and 45°C, showing that the fiber growth is not temperature-limited under these conditions.

Interrupting the rotation of the stirring rod during the experiment results in an immediate, but partial and reversible decrease of ThT fluorescence to a new equilibrium, at approx. 60% of the fluorescence level attained when the agitation was switched off (Figure 5A). This reduced ThT fluorescence level, without agitation, depends on the amount of HI aggregates.

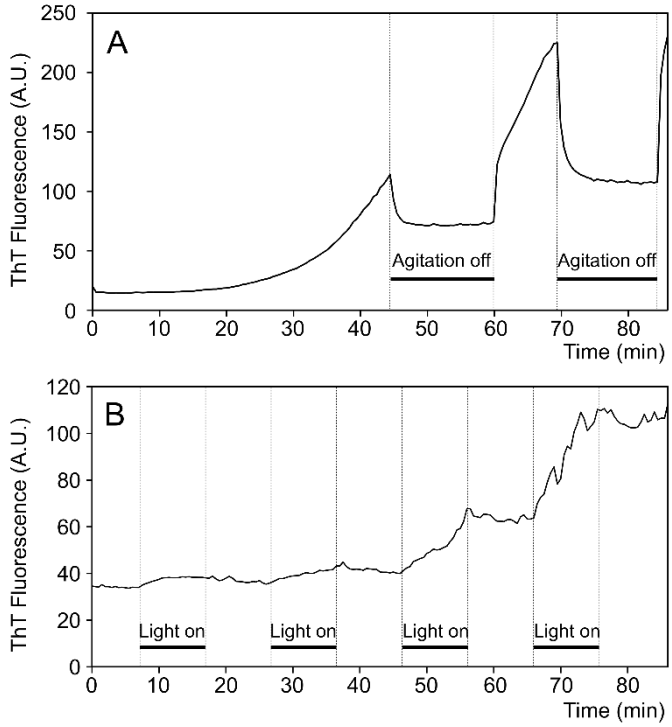

Figure 5: Effect of stirring (A) and illumination (B) on light-induced insulin aggregation kinetics. Light-induced aggregation assays are performed under standard conditions: 86 µM HI, 20 µM ThT, I_0 = 57.7 nW.µm^{-2} with the indicated temporary interruption of stirring (A) or illumination (B). The normalized fluorescence intensity is plotted as a function of time.

After restoration of stirring, the ThT fluorescence returns rapidly to its previous value, and starts increasing again in the continuity of the signal acquired before the interruption of stirring. This proves that fibers formed beforehand do not disappear when the HI and ThT supply is reduced in the absence of stirring. The fluorescent ThT content of the aggregates is therefore decreased to 60% of the value at the time point when stirring was stopped.

In another set of experiments, we examine whether continuous illumination is necessary for fiber growth. It could indeed be possible that light would help native insulin to overcome the nucleation barrier to form fibrils that would later grow in the absence of illumination. Figure 5B demonstrates that this is not the case. When the illuminating light is switched off, except briefly (exposure = 1s at I_0 = 57.7 nW.µm^{-2}) to measure surface ThT fluorescence, insulin fibers stop growing, and growth resumes only when the light is turned on again.

We then examine the influence of HI and ThT concentrations on light-induced aggregation. The HI aggregation rate increases with ThT concentration (Figure 6A), as shown by the evolution of the apparent first order kinetic coefficient, k_{app}, with the ThT concentration (Figure 6B). This is in accordance with the results shown in Figure S1C, which demonstrate that the level of ThT fluorescence of an aggregate increases with the concentration of ThT in solution within the range used in this study. Furthermore, in the absence of ThT, no HI aggregates (that could later

be revealed by ThT addition) grow on the material surface. This confirms the essential role of ThT as a mediator between light and adsorbed insulin. The aggregation rate strongly depends on the insulin concentration. As expected, no ThT fluorescence increase is observed in the absence of protein. More surprisingly, at insulin concentrations below 43 µM, light-induced insulin aggregates do not grow exponentially but instead gradually increase, whereas exponential growth is observed at 54 µM (Figure 6C).

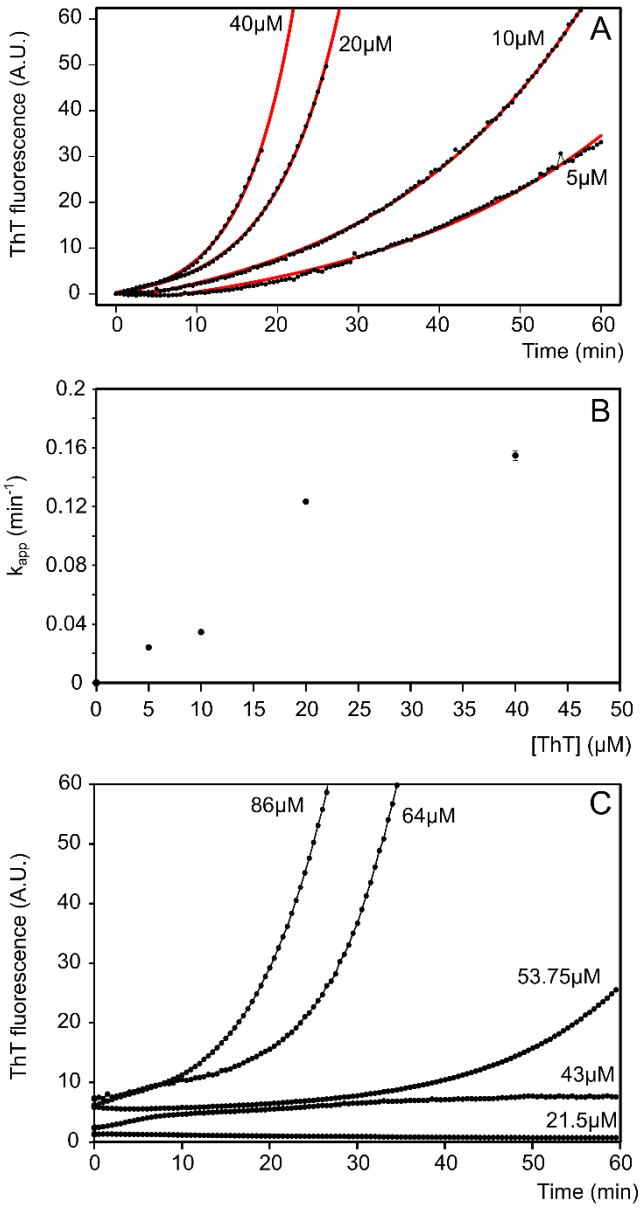

Figure 6: Effect of Thioflavin T and insulin concentrations on light-induced insulin aggregation kinetics. A: Kinetics of light-induced insulin aggregation at the indicated ThT concentration. I_0 = 57.7 nW.µm^{-2}. Dots : experimental normalized fluorescence values, red lines : fit with Eq. 1. B: Apparent kinetic coefficient k_{app}, as a function of ThT concentration. Error bars: standard error on k_{app}. C: Kinetics of light-induced insulin aggregation at the indicated HI concentration. ThT = 20 µM, I_0 = 57.7 nW.nm^{-2}.

We recently demonstrated that sub-stoichiometric concentrations of $(LK)_5L$, a short polypeptide with alternating hydrophobic and hydrophilic amino acids, has a dual effect on

insulin aggregation kinetics[19]. At low concentrations (< 0.1 µM), it decreases the lag time of insulin aggregation on hydrophobic surfaces, thanks to the formation of peptide patches stabilized by intermolecular β-sheets on hydrophobic surfaces, that promote insulin aggregate nucleation. This effect is not relevant here because light-induced aggregation has no observable lag time. At larger concentrations however (> 2 µM), the peptides remaining in excess in solution prevent insulin aggregation on hydrophobic surfaces. We conducted experiments to test whether light-induced insulin aggregation was also sensitive to the action of this peptide. Addition of $(LK)_5L$ peptide at 3 µM during the exponential phase of light-induced insulin aggregation gradually reduces the growth rate until a complete block after 30 min (Figure 7A). Moreover, the addition of 0.42 µM of TAMRA-labeled $(LK)_5L$ peptide in solution after the formation of a tridimensional insulin aggregate results in the localization of a strong TAMRA fluorescence at the surface of the aggregate (Figure 7B). This demonstrates that $(LK)_5L$ peptides bind to the light-induced HI aggregates, likely preventing native insulin incorporation.

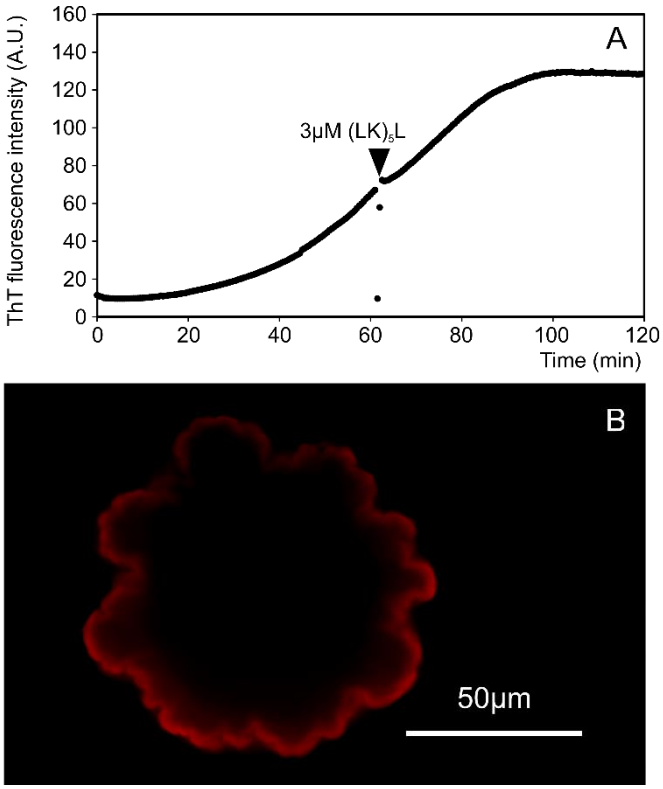

Figure 7: Effect of the $(LK)_5L$ peptide on light-induced aggregation. A: After the addition of 3µM $(LK)_5L$ in solution (triangle), the aggregation rate is progressively reduced until a complete stop of aggregation (90 min). The abnormal points below the arrowhead correspond to an injection artefact. B: TAMRA-$(LK)_5L$ localisation on light-induced HI aggregate, 0.42µM of TAMRA-$(LK)_5L$ was added in solution during LIA. The TAMRA fluorescence signal is located at the surface of the aggregate and its intensity is approx. 10 times that of the ThT fluorescence signal (t=60 min, [HI]=86µM, [ThT] = 40µM, I_0 = 960 nW.µm^{-2}).

Discussion

We have discovered and described a process allowing patterned growth of amyloid-like insulin aggregates. Furthermore we have characterized the surface specificity and the kinetic of this process and investigated its underlying thermodynamic requirements.

Since the observed aggregation process requires the presence of ThT and light at the bound ThT absorption wavelength, the observed process does not result from a direct excitation of HI. Furthermore, even after the formation of light-induced aggregates, aggregation stops in the absence of illumination (Figure 5B). This is in contrast with other classical protocols for insulin aggregation in metastable conditions (e.g. pH 2, 63°C[11,21,22]) where the initiation of aggregation is the limiting step.

Initiation of aggregation

One of the most striking aspects of LIA is that its kinetics overcome the thermodynamic requirement for a lag-time, usually observed before the first primary nucleation (Figure 3A). Therefore the transition from the native state to the aggregated form of HI occurs directly rather than through a nucleation phase usually required in order to stabilize conformational intermediates (nucleated conformational conversion[23]).

We have shown that hydroxylated borosilicate glass coverslip surfaces delay LIA (Figure 4) and present lower initial ThT_F fluorescence levels (Figure S1A). This lower initial ThT_F fluorescence level likely results from the absence of an insulin layer, which induces a low ThT-positive fluorescence signal on non-hydrophilic surfaces. In the absence of this initial layer LIA is strongly delayed demonstrating that the formation of an initial insulin layer presenting a low ThT-positive signal is necessary for the initiation of LIA. Similarly the fast photo-bleaching of this initial layer before the formation of enough aggregate material (Figure S2) also induces a delay in the initiation of growth.

HI incorporation.

By contrast with irradiance and ThT concentration, the exponential behavior of LIA disappears at low insulin concentrations (Figure 6C). In amyloid aggregation, an exponential growth of the total amount of aggregates is the consequence of secondary processes increasing the number of HI incorporation sites. In secondary nucleation typically, the rate of creation of new aggregation sites depends on the monomer concentration[24]. Hence the loss of the exponential behavior observed at low insulin concentration can indicate that aggregate growth presents a high

reaction order with respect to insulin, for instance, the insulin incorporation could be cooperative and/or dominated by secondary nucleation-like processes.

Similarly, in the absence of agitation the aggregation rate is null (Figure 5A), yet the ThT fluorescence level stabilizes at a lower but still important value (40% decrease compared to the value when agitation was turned off, Fig. 5A). This lower density of fluorescent ThT inside the fibril, resulting from the interruption of agitation is sufficient to induce LIA as seen in the experiments performed at lower ThT concentrations (Figure 6A curve at 5µM and 10µM). This shows that if stirring is important for ThT renewal, the limiting factor in the absence of agitation is the insulin supply.

In aggregation of insulin triggered by hydrophobic surfaces upon agitation, the addition of the $(LK)_5L$ peptide in solution inhibits aggregation likely via steric hindrance[19]. The complete arrest of light-induced aggregation, 30 min after the addition of 3µM $(LK)_5L$ in solution, indicates that the light-induced aggregation mechanism is also inhibited by the $(LK)_5L$ peptide. This suggests a partially common mechanism of insulin incorporation. In contrast to hydrophobic surface-induced aggregates however, the HI aggregates produced by LIA do not present any observable growth in the absence of illumination at ThT excitation wavelength.

Aggregate morphology

Once bound to an amyloid fibril, a ThT molecule undergoes a fluorescence shift and shows an increased quantum yield. This fluorescence transition presents a high specificity for amyloid aggregates, albeit not an absolute one [25,26]. Although the scanning electron microscopy micrograph (Figure 2D) does not present the well-organized, fibrillary structures, characteristic of the amyloid state, we obtain insulin aggregates presenting strong ThT-fluorescence, indicating that they most likely present amyloid or β-sheet rich amyloid-like structures. After sufficient growth the aggregate presents a compact structure with a surface exhibiting fractal patterns (Figure 2C), which are typical of a reaction-limited aggregation process. Spherulite superstructures were observed in acidic conditions for bovine insulin amyloid fibrils showing that these protein fibrils are able to aggregate in higher order assemblies [27].

Mechanism of aggregation

We first examine whether the formation of insulin aggregates could be explained by a trivial elevation of the temperature of the insulin layer due to light absorption by ThT. On the one hand, the energy of absorbed photons is mostly dissipated as heat, resulting in a local heating.

On the other hand, the surrounding water dissipates this heat, reducing the local temperature increase.

The light power adsorbed is equal to $P = I_0 - I$, where I_0 and I are the irradiances of the incident and transmitted light, respectively. Using the Beer-Lambert law, the maximal heat generated by the absorption of the incident blue light, per unit area and unit time, is:

$$P_{absorbed} = I_0 - I_0 \cdot 10^{-\epsilon \cdot l \cdot [ThT_F]} \quad \text{(eq. 2)}$$

Where **ε** is ThT absorption coefficient, $[ThT_F]$ the ThT concentration in insulin amyloid fibers and ***l*** the thickness of the fluorescent zone in the building amyloid material. This power is dissipated at a rate determined by the water heat transfer coefficient (***h***) and the temperature difference between the illuminated zone and the surroundings (***ΔT***). The heat dissipated per unit area and unit time is thus:

$$P_{dissipated} = h \cdot \Delta T \quad \text{(eq. 3)}$$

This system evolve towards a stable equilibrium where $P_{absorbed} = P_{dissipated}$. One can combine eq.2 and eq.3 to calculate the maximum heating due to the energy purely released by light absorption:

$$\Delta T = \frac{I_0 - I_0 \cdot 10^{-\epsilon \cdot l \cdot [ThT_F]}}{h} \qquad \text{(eq. 4)}$$

The saturating ThT concentration in insulin amyloid fibers at pH 7.5 is one tenth of the HI concentration[28,29], and thus $[ThT_F]$ is at most 20 mM. For a height of the aggregate layer of l = 1µm which is a typical value during the kinetics presented Figure 3 (at the initiation a thinner layer is present), since ε = 26.6 $mM^{-1}.cm^{-1}$, and h = 4000 $W.m^{-2}.K^{-1}$ under stirring[30], the local temperature increase is comprised between 0.2 and 13.8 K, from the lowest to the highest irradiance used in the kinetic study (7 to 480 $kW.m^{-2}$). It is therefore unlikely that this modest temperature increase would be sufficient to unfold insulin and lead to its aggregation at low irradiance. It is indeed known that both low pH (<4) and high temperatures (65°C) are necessary to trigger the formation of insulin amyloid fibers[11,31].

However, the interior of the aggregates represents a hydrophobic and at least a partially dehydrated environment. The bound ThT could therefore directly transfer its fluorescence energy, bypassing the energy dissipation of water, to the neighboring insulin molecules inducing their direct denaturation. Such direct denaturation has been for instance suggested for the light-induced aggregation of β-cristallins in solution induced by the excitation of tryptophan[4].The amyloid-bound ThT fluorescence at (λ_{ex}= 440 nm; λ_{em}= 482 nm) results in a

dissipation of an energy of 23.7 kJ per mole of emitted photon by non-radiative transitions. Moreover since amyloid-bound ThT does not present a high quantum yield[32], the adsorbed photon energy is frequently released by non-radiative decay, most likely under the form of heat which would correspond to an energy of 272 $kJ.mol^{-1}$. This last value largely exceed the typical protein folding energy supporting the hypothesis of a local photon energy transfer associated to a stabilization by adsorption.

To conclude, the time it takes to dissipate the heat emitted by a ThT non-radiative decay has to match the timescale of conformational changes in HI in order for LIA to be based on a local heat transfer from ThT to HI.

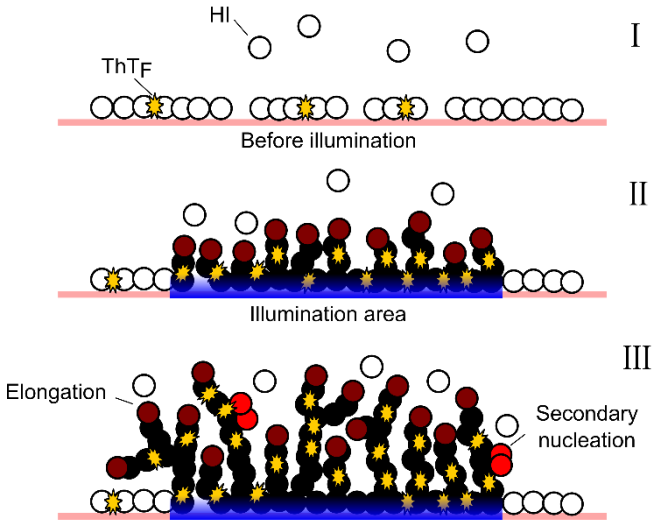

Figure 8: Model of light-induced insulin aggregation and growth on hydrophobic surfaces. On hydrophobic surfaces (orange line), HI (white circle) adsorption results in a ThT-positive protein layer (I). ThT$_F$ is denoted by a star. Upon illumination at 440 nm (blue) the ThT molecules are photoexcited and transmit part of their excitation energy to the surrounding HI molecules allowing them to change their conformation and form protofibrils (black, II). The resulting aggregates present strong ThT fluorescence allowing further HI incorporation via elongation (brown) or secondary nucleation (red) (III).

Conclusion

The initial layer of adsorbed HI presents low ThT fluorescence before illumination (Figure 8 I). The photo-excitation of these ThT molecules then results in the aggregation of the surrounding HI. Inside the aggregate the ThT fluorescence level is, at equilibrium, proportional to the ThT concentration in solution and to the aggregate size. The aggregation rate is proportional to the ThT fluorescence of the fibers and as a consequence the growth displays an exponential behavior (Figure 8 II). A secondary nucleation-like mechanism depending on a cooperative HI incorporation can explain both the reduction of aggregation at low insulin concentration and the tridimensional shape of the aggregates (Figure 8 III).

We have reported a method for the production of localized ThT-positive insulin aggregates on illuminated surfaces were HI is able to adsorb. We have shown that this phenomenon is mediated by the ThT contained in insulin layers and involves an energy transfer from visible light to the protein. Contrary to most amyloid-like aggregations, the kinetics of LIA is devoid of a lag-time but presents an exponential growth from an initial adsorbed HI/ThT layer. Agitation is a critical parameter for HI supply to the incorporation area.

Acknowledgment

This work was supported by a Ph.D. fellowship from the MENRT to K.C. We thank Thibaut Frachon who worked jointly on the Olympus microscope shutter automation and Mikhail Anikin for his technical assistance with the electrical gear motor.

References

[1] W. Wang, S. Nema, D. Teagarden, Protein aggregation-Pathways and influencing factors, Int. J. Pharm. 390 (2010) 89–99. doi:10.1016/j.ijpharm.2010.02.025.

[2] C.M. Dobson, Principles of protein folding, misfolding and aggregation, Semin. Cell Dev. Biol. 15 (2004) 3–16. doi:10.1016/j.semcdb.2003.12.008.

[3] M.T. Neves-Petersen, Z. Gryczynski, J. Lakowicz, P. Fojan, S. Pedersen, E. Petersen, S. Bjørn Petersen, High probability of disrupting a disulphide bridge mediated by an endogenous excited tryptophan residue, Protein Sci. 11 (2009) 588–600. doi:10.1110/ps.06002.

[4] E. Chelnokov, L. Soustov, N. Sapogova, M. Ostrovsky, N. Bityurin, Nonreciprocal XeCl laser-induced aggregation of beta-crystallins in water solution., Opt. Express. 16 (2008) 18798–18803. doi:10.1364/OE.16.018798.

[5] T. Okada, M. Sugihara, A.N. Bondar, M. Elstner, P. Entel, V. Buss, The retinal conformation and its environment in rhodopsin in light of a new 2.2 Å crystal structure, J. Mol. Biol. 342 (2004) 571–583. doi:10.1016/j.jmb.2004.07.044.

[6] J.P. Zayner, T.R. Sosnick, Factors that control the chemistry of the LOV domain photocycle, PLoS One. 9 (2014). doi:10.1371/journal.pone.0087074.

[7] S.C. Afonso, R. Enriquez De Salamanca, A.M. Del, The photodynamic and non-photodynamic actions of porphyrins, Brazilian J. Med. Biol. Res. 32 (1999) 255–266. doi:10.1590/S0100-879X1999000300002.

[8] B. Il Lee, S. Lee, Y.S. Suh, J.S. Lee, A.K. Kim, O.Y. Kwon, K. Yu, C.B. Park, Photoexcited Porphyrins as a Strong Suppressor of β-Amyloid Aggregation and Synaptic Toxicity, Angew. Chemie - Int. Ed. 54 (2015) 11472–11476. doi:10.1002/anie.201504310.

[9] T.P.J. Knowles, M.J. Buehler, Nanomechanics of functional and pathological amyloid materials, Nat Nano. 6 (2011) 469–479. http://dx.doi.org/10.1038/nnano.2011.102.

[10] R. Wetzel, Kinetics and thermodynamics of amyloid fibril assembly, Acc. Chem. Res. 39 (2006) 671–679. doi:10.1021/ar050069h.

[11] M.I. Ivanova, S.A. Sievers, M.R. Sawaya, J.S. Wall, D. Eisenberg, Molecular basis for insulin fibril assembly, Proc. Natl. Acad. Sci. 106 (2009) 18990–18995. doi:10.1073/pnas.0910080106.

[12] S. Grudzielanek, A. Velkova, A. Shukla, V. Smirnovas, M. Tatarek-Nossol, H. Rehage, A.

Kapurniotu, R. Winter, Cytotoxicity of Insulin within its Self-assembly and Amyloidogenic Pathways, J. Mol. Biol. 370 (2007) 372–384. doi:10.1016/j.jmb.2007.04.053.

[13] M.P.S. Sie, H.E. van der Wiel, F.M.M. Smedts, A.C. de Boer, Human recombinant insulin and amyloidosis: An unexpected association, Neth. J. Med. 68 (2010) 138–140.

[14] L. Nault, P. Guo, B. Jain, Y. Bréchet, F. Bruckert, M. Weidenhaupt, Human insulin adsorption kinetics, conformational changes and amyloidal aggregate formation on hydrophobic surfaces., Acta Biomater. 9 (2013) 5070–9. doi:10.1016/j.actbio.2012.09.025.

[15] J.S. Sharp, J.A. Forrest, R.A.L. Jones, Surface denaturation and amyloid fibril formation of insulin at model lipid-water interfaces, Biochemistry. 41 (2002) 15810–15819. doi:10.1021/bi020525z.

[16] M.I. Smith, J.S. Sharp, C.J. Roberts, Nucleation and growth of insulin fibrils in bulk solution and at hydrophobic polystyrene surfaces., Biophys. J. 93 (2007) 2143–51. doi:10.1529/biophysj.107.105338.

[17] A. Nayak, A.K. Dutta, G. Belfort, Surface-enhanced nucleation of insulin amyloid fibrillation., Biochem. Biophys. Res. Commun. 369 (2008) 303–7. doi:10.1016/j.bbrc.2008.01.159.

[18] S.I.A. Cohen, M. Vendruscolo, C.M. Dobson, T.P.J. Knowles, From macroscopic measurements to microscopic mechanisms of protein aggregation, J. Mol. Biol. 421 (2012) 160–171. doi:10.1016/j.jmb.2012.02.031.

[19] K. Chouchane, C. Vendrely, M. Amari, K. Moreaux, F. Bruckert, M. Weidenhaupt, Dual Effect of (LK)nL Peptides on the Onset of Insulin Amyloid Fiber Formation at Hydrophobic Surfaces, J. Phys. Chem. B. 119 (2015) 10543–10553. doi:10.1021/acs.jpcb.5b07365.

[20] N.P. Mellott, S.L. Brantley, J.P. Hamilton, C.G. Pantano, Evaluation of surface preparation methods for glass, Surf. Interface Anal. 31 (2001) 362–368. doi:10.1002/sia.971.

[21] C.-C. Lee, A. Nayak, A. Sethuraman, G. Belfort, G.J. McRae, A three-stage kinetic model of amyloid fibrillation., Biophys. J. 92 (2007) 3448–3458. doi:10.1529/biophysj.106.098608.

[22] A. Nayak, M. Sorci, S. Krueger, G. Belfort, A universal pathway for amyloid nucleus and precursor formation for insulin, Proteins Struct. Funct. Bioinforma. 74 (2009) 556–565. doi:10.1002/prot.22169.

[23] T.R. Serio, A.G. Cashikar, A.S. Kowal, G.J. Sawicki, J.J. Moslehi, L. Serpell, M.F. Arnsdorf, S.L. Lindquist, Nucleated Conformational Conversion and the Replication of Conformational Information by a Prion Determinant, Science (80-.). 289 (2000) 1317–1321. doi:10.1126/science.289.5483.1317.

[24] G. Meisl, J.B. Kirkegaard, P. Arosio, T.C.T. Michaels, M. Vendruscolo, C.M. Dobson, S. Linse, T.P.J. Knowles, Molecular mechanisms of protein aggregation from global fitting of kinetic models, Nat. Protoc. 11 (2016) 252–272. doi:10.1038/nprot.2016.010.

[25] L.S. Wolfe, M.F. Calabrese, A. Nath, D. V Blaho, A.D. Miranker, Y. Xiong, Protein-induced photophysical changes to the amyloid indicator dye thioflavin T., Proc. Natl. Acad. Sci. U. S. A. 107 (2010) 16863–16868. doi:10.1073/pnas.1002867107.

[26] H. Levine, Thioflavine T interaction with synthetic Alzheimer's disease β-amyloid peptides: Detection of amyloid aggregation in solution, Protein Sci. 2 (2008) 404–410. doi:10.1002/pro.5560020312.

[27] M.R.H. Krebs, C.E. Macphee, A.F. Miller, I.E. Dunlop, C.M. Dobson, A.M. Donald, The formation of spherulites by amyloid fibrils of bovine insulin., Proc. Natl. Acad. Sci. U. S. A. 101 (2004) 14420–14424. doi:10.1073/pnas.0405933101.

[28] M. Groenning, M. Norrman, J.M. Flink, M. van de Weert, J.T. Bukrinsky, G. Schluckebier, S. Frokjaer, Binding mode of Thioflavin T in insulin amyloid fibrils, J. Struct. Biol. 159 (2007) 483–497. doi:10.1016/j.jsb.2007.06.004.

[29] M. Groenning, Binding mode of Thioflavin T and other molecular probes in the context of amyloid fibrils-current status, J. Chem. Biol. 3 (2010) 1–18. doi:10.1007/s12154-009-0027-5.

[30] Y. Xuan, Q. Li, Investigation on convective heat transfer and flow features of nanofluids, J. Heat Transfer. 125 (2003) 151. doi:10.1115/1.1532008.

[31] R. Jansen, W. Dzwolak, R. Winter, Amyloidogenic self-assembly of insulin aggregates probed by high resolution atomic force microscopy, Biophys. J. 88 (2005) 1344–1353. doi:10.1529/biophysj.104.048843.

[32] A.I. Sulatskaya, I.M. Kuznetsova, K.K. Turoverov, Interaction of thioflavin T with amyloid fibrils: Fluorescence quantum yield of bound dye, J. Phys. Chem. B. 116 (2012) 2538–2544. doi:10.1021/jp2083055.

Supplementary figures

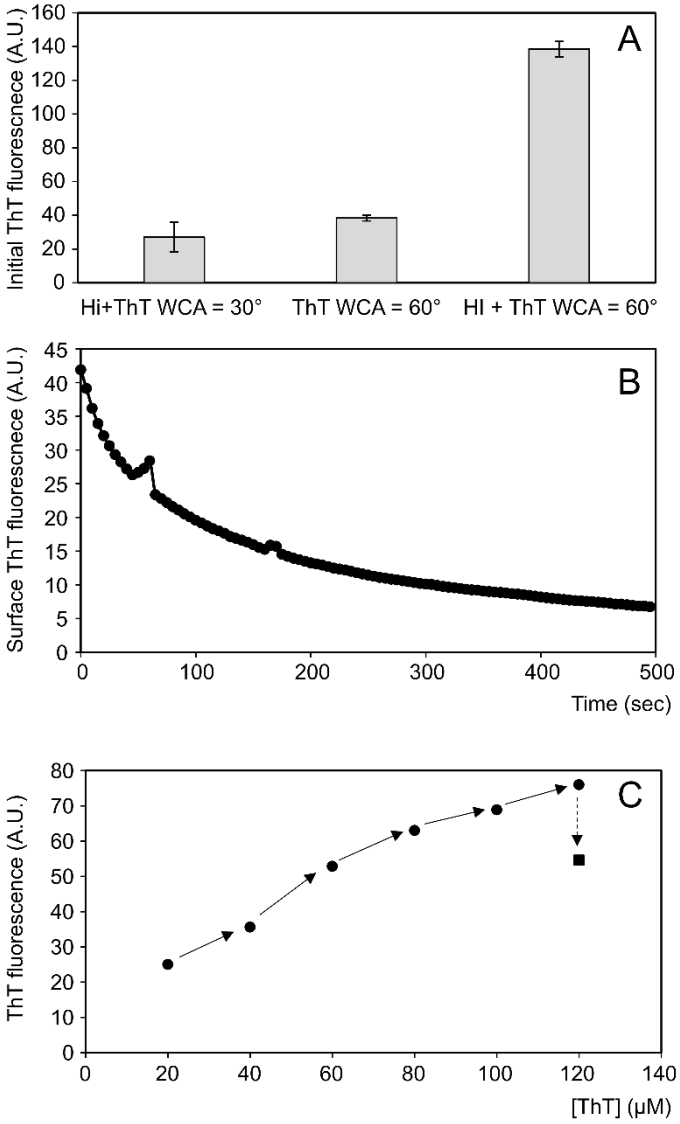

Figure S1. Evolution of ThT fluorescence in aggregates and in pre-aggregate protein layers. A: Mean fluorescence value of the initial ThT layer upon agitation before any illumination. These values are given for NaOH etched glass: WCA=30° and for untreated glass: WCA= 60° at 0µM or 86µM of HI. [ThT]= 20µM, n=3. B: Photo-bleaching of the original HI and ThT layer. Evolution of the ThT fluorescence level of the initial surface layer prior to any growth, imaged without agitation at HI= 86µM, ThT= 20µM, I_0= 480 nW.µm^{-2}. C: Fluorescence of an HI aggregate obtained by LIA as a function of ThT concentration in solution without illumination (circles) or upon illumination (square). After the growth of an aggregate structure by LIA, the light was turned off to prevent any growth and the ThT concentration in solution was gradually increased by successive ThT addition followed by a short agitation (solid arrows). The coresponding overall fluorescence intensity of the aggregate was measured (by brief exposure to light (0.5s) in the absence of agitation). The light (I_0 =480 nW.µm^{-2}) was then turned on (dotted arrow) and the fluorescence measured once the new equilibrium was reached.

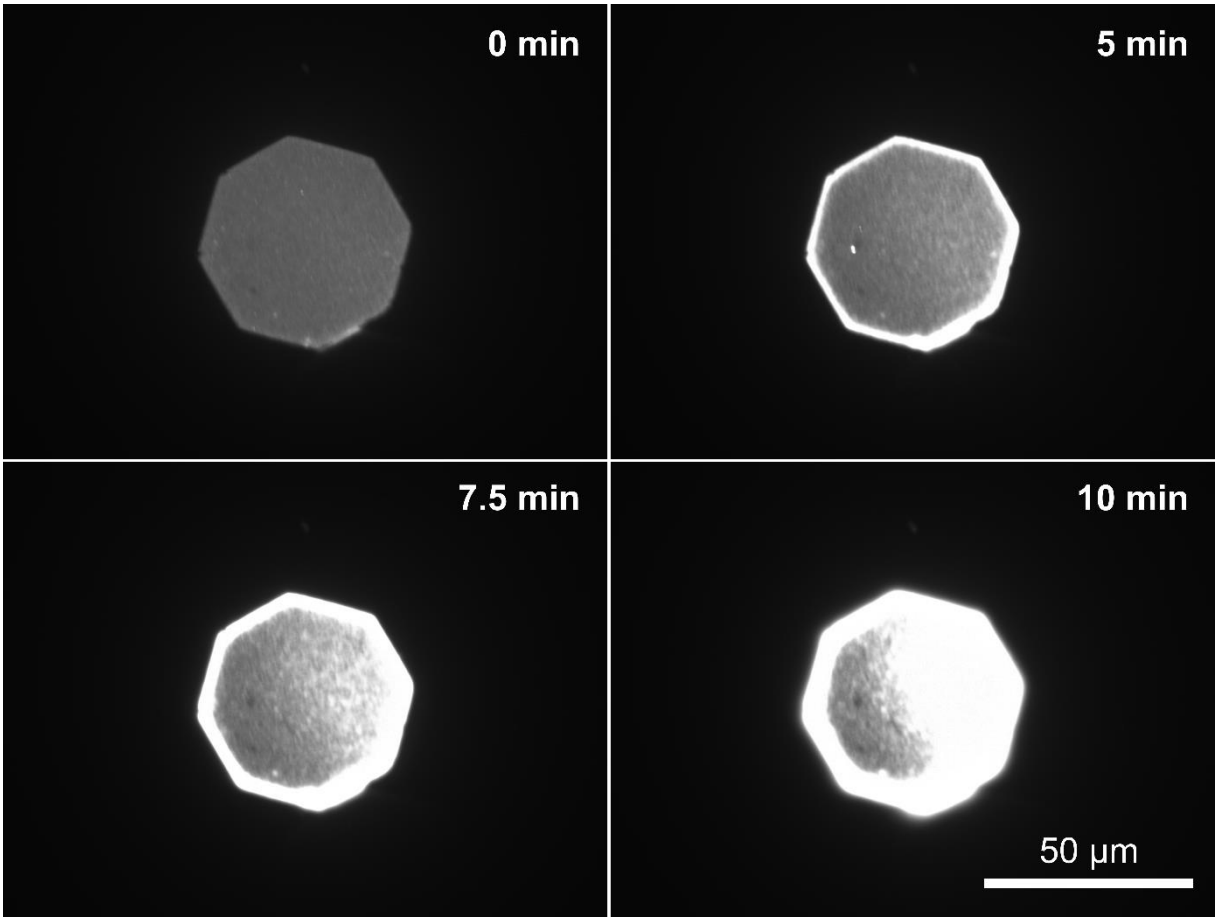

Figure S2: Evolution of the ThT fluorescence pattern at I_0= 480nW.µm^{-2} with time. The light-induced aggregation phenomenon is first located on the edges of the illumination area (5min), with a subsequent invasion of the center (7.5 and 10 min). The imaging is performed at the minimum field diaphragm aperture.

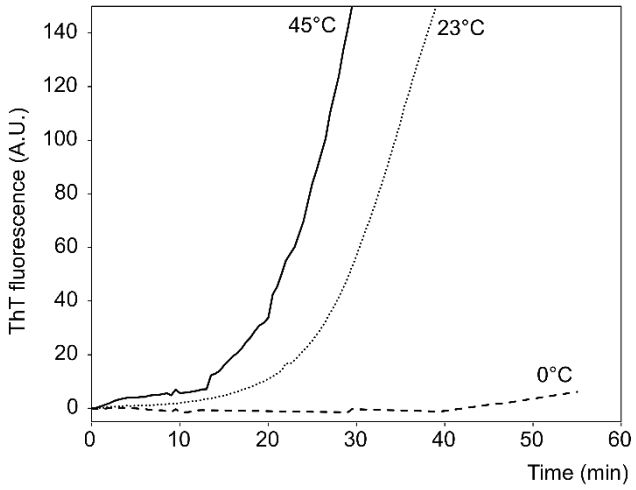

Figure S3. Effect of temperature on light-induced insulin aggregation kinetics. Kinetic of light-induced insulin aggregation at 0°C, 23°C and 45°C. Experimental conditions are 86 µM HI, ThT = 40µM, I_0 = 57.7 nW.nm^{-2}.

5.1 Extended discussion of the Article III

5.1.1 Nature of the aggregates produced by LIA

The insulin aggregates produced by LIA on surfaces are ThT-positive and their growth can be inhibited by LK11 peptides in solution (Figure 7 in Article III). Figure 49 shows that the HI aggregates formed in surface induced aggregation under agitation saturate with ThT at 20µM, which is coherent with the affinity of ThT for amyloid fibrils described in the literature[195].

However, contrary to the aggregates produced in standard plate assays on hydrophobic surfaces (SIA) in the Article I and Article II, the light-induced aggregates do not saturate with ThT at 20µM (Figure S2C in article III). The two aggregates type must therefore present different affinity for ThT.

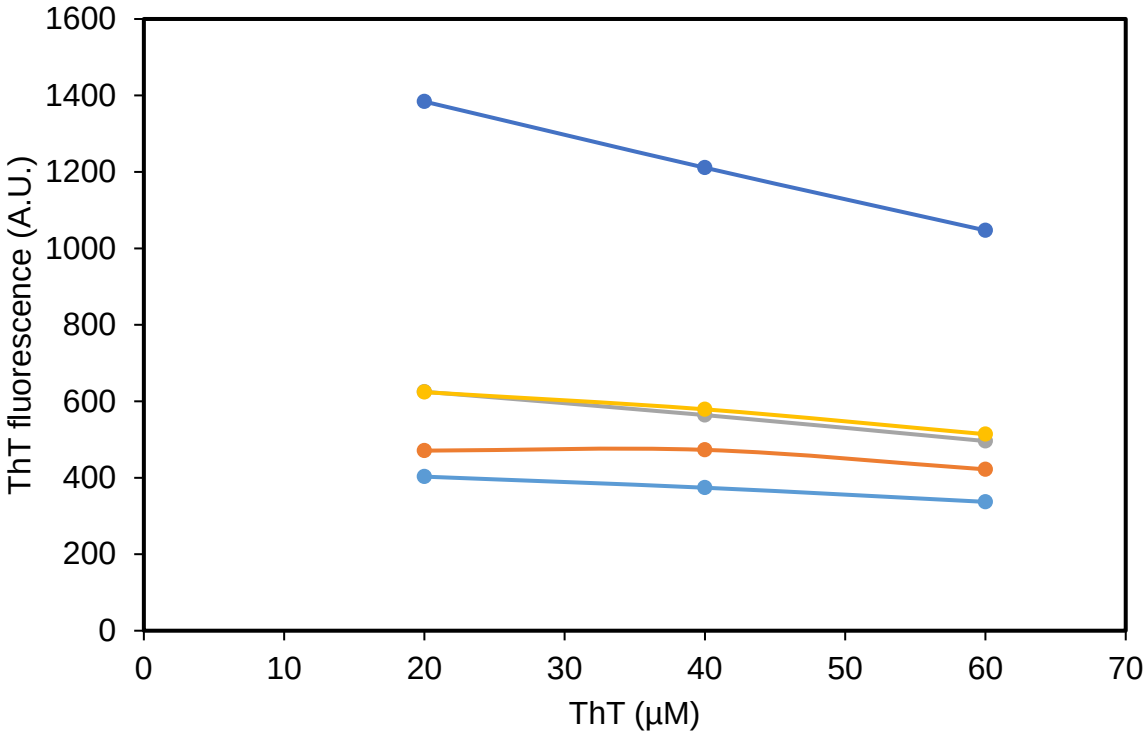

Figure 49: Evolution of the ThT fluorescence intensity of insulin aggregates produced by hydrophobic surface-induced aggregation as a function of the ThT concentration in solution. Shown for n=5 samples (presenting diferent aggregates quantity), aggregated in standard condition for 1h. Then their ThT fluorescence was read on a Tecan infinite in increasing ThT concentrations. Each curve coresponds to one well.

The aggregation kinetics of LIA is exponential without any lag-time, while SIA kinetics presents a clear lag-time and a much less exponential behavior in its early growth. The latter point can however be explained by the experimental conditions of LIA in which the amount of aggregate is extremely reduced and not limited by the concentration of native HI in solution.

Moreover the aggregates produced by LIA do not present any residual growth under agitation in the absence of illumination at a ThT exciting wavelength. On the other hand SIA grow under agitation providing that the rate limiting nucleation step is overcome.

One last point is that in our experimental setup SIA could only be observed at the triple interface and never at the bottom of our chamber.

These elements suggest important differences in the nature of the aggregates produced by LIA compared to SIA. LIA are probably less amyloid like as they present no lag-time nor fibrillary structure under the scanning electron microscope and an overall fractal structure

5.1.2 Mathematical modeling of LIA

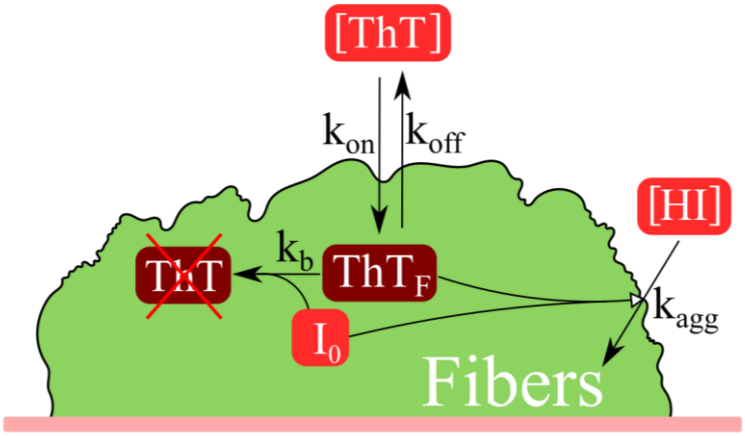

Figure 50 Extended: Model of light induced insulin aggregation and growth on hydrophobic surfaces. Reaction and kinetic model of LIA. In red the 3 main expetrimental parameters investigated here: the 440nm photon irradiance I_0, the ThT concentration [ThT] and HI concentration [HI]. k_{on} is the rate constant of ThT diffusion into the aggregate, k_{off} the rate constant of ThT diffusion outside the aggregate, k_b the rate constant of the ThT inside the fibrils (ThT_F) bleaching and k_{agg} the apparent rate constant of HI aggregation.

Using the data collected with all the various parameters, we constructed a mathematical model describing the kinetic relationship observed. This model represents the evolution of the total amount of HI aggregates (**A)** and ThT bound to these fibrils (**ThT_F)**, starting from the chemical equations of ThT diffusion, ThT photo-bleaching and HI incorporation into the aggregates (Figure 50).

Density of ThT inside the aggregates

We have seen in the Article III that an aggregate of fixed size (**A** in mol of aggregated HI) can present a homogenous ThT fluorescence intensity (corresponding to a quantity of ThT mol) varying according to the experimental conditions (Figure 5 and S1C in article III). We therefore introduce the density **D** and the maximal density $\mathbf{D_{max}}$ of ThT_F inside the aggregates

$$D = \frac{ThT_F}{A} \text{ and } D_{max} = \frac{ThT_{F\,max}(A)}{A}$$

D_{max} is a constant characteristic of this HI aggregate type. The fraction of unoccupied ThT binding sites ***θ*** in an aggregate of size **A** is therefore defined by:

$$\theta = \left(\frac{D_{max} - D}{D_{max}}\right)$$

Since a ThT in solution cannot be incorporated in a site already occupied by a ThT_F, we introduce **A_{free}** the part of the aggregates of size **A** unoccupied by ThT:

$$A_{free} = A \cdot \theta = A - A_{bond}$$

The number of molecule of HI aggregates occupied by a bound ThT_F molecule is

$$\alpha = \frac{1}{D_{max}}$$

This coefficient represents the number of aggregated HI molecules saturated by molecule of ThT_F. The aggregates A are not in solution, α only represents a stoichiometric constant not the reaction order of A.

Model of insulin incorporation

The ThT inside the fibrils (**ThT_F**), transfers the energy from the 436nm light at the irradiance I_0 to the native insulin to form aggregates **A**. However the stoichiometry of insulin incorporation into the aggregate is not clear from the present data (Figure 6C in Article III), this reaction is likely a complex reaction with adsorption of native insulin and possible secondary nucleation at the aggregate surface. The aggregation kinetics can therefore be modeled by the following chemical equation:

$$ThT_F + I_0 \xrightarrow{k_{agg}([HI])} ThT_F + A \qquad \text{(Chem. Eq. of aggregate growth)}$$

Where A is the total amount of aggregates, $k_{agg}([HI])$ the kinetic constant of HI incorporation into the aggregates as a function of HI concentration, ThT_F the fluorescent ThT bound to the aggregates and I_0 the irradiance. The corresponding differential equation of aggregate growth is:

$$\frac{dA}{dt} = k_{agg}([HI]) \cdot I_0 \cdot ThT_F$$

Model of ThT equilibrium inside the aggregates

The density of ThT inside the aggregates is determined by its diffusion and photo-bleaching. In the following chemical equations

$$[ThT_F;\ S_{occ}] = [ThT_F;\ \alpha \cdot A_{occ}]$$

Refers to the complex of ThT_F and its associated HI aggregate molecules. Please note that during the initiation of the LIA the adsorbed ThT + protein layer do present low ThT_F fluorescence despite the absence of fibrils. Moreover the density of ThT_F inside an aggregate can also vary. This two points justify the distinction between ThT inside the fibrils and fluorescent fibrils.

The evolution of the fluorescent ThT bound to the aggregate can be described by the following chemical equation:

Chem. Eq. of ThT diffusion into the aggregates:

$$ThT + S_{free} \xrightarrow{^{s}k_{on}} [ThT_F;\ S_{occ}]$$

Chem. Eq. of ThT_F diffusion out of the aggregates:

$$[ThT_F;\ S_{occ}] \xrightarrow{k_{off}} ThT + S_{free}$$

Chem. Eq. of ThT_F photo-bleaching:

$$[ThT_F;\ S_{occ}] + \mathrm{I}_0 \xrightarrow{k_b} ThT_{bleached} + \alpha \cdot A_{free}$$

Where k_{on} is the kinetic constant of ThT diffusion in the aggregate, k_{off} is the kinetic constant of ThT_F diffusion out of the aggregate and k_b the kinetic constant of ThT photo-bleaching.

The corresponding differential equation of ThT_F is:

$$\frac{dThT_F}{dt} = {}^{s}k_{on} \cdot S_{free} \cdot [ThT] - k_{off} \cdot ThT_F - k_b \cdot ThT_F \cdot \mathrm{I}_0$$

With the kinetic constant relative to the number of HI molecules:

$$k_{on} = \frac{{}^{s}k_{on}}{\alpha}$$

We obtain:

$$\frac{dThT_F}{dt} = k_{on} \cdot A_{free} \cdot [ThT] - k_{off} \cdot ThT_F - k_b \cdot ThT_F \cdot \mathrm{I}_0$$

However aggregate growth and ThT equilibrium do not occur at the same time scales: k_{on}, k_{off}, $k_b >> k_{agg}$ which means that ThT_F reaches rapidly a steady state for a given fibril quantity.

In stationary conditions:

$$\frac{dThT_F}{dt} = k_{on} \cdot A_{free} \cdot [ThT] - k_{off} \cdot ThT_F - k_b \cdot ThT_F \cdot I_0 = 0$$

$$\Leftrightarrow ThT_F = \frac{k_{on} \cdot A_{free} \cdot [ThT]}{k_{off} + k_b \cdot I_0}$$

Units used in the mathematical model

Quantities	Units
A; A_{free}; A_{occ}	mol of HI
S; S_{free}; S_{occ}	mol of binding site = α·mol of HI
[HI]	M of HI
ThT_F	mol of ThT
[ThT]	M of ThT
I_0	nW.µm^{-2}
k_{on}; $^s k_{on}$	M^{-1}.s^{-1}
k_{off}	s^{-1}
k_b	µm^2.nW^{-1}.s^{-1}
$k_{agg(HI)}$	µm^2.nW^{-1}.s^{-1}

Table 7 Units used in the mathematical model

Model without saturation

Since the ThT fluorescence of the aggregates does not exhibit saturation with [ThT] below 100µM (Figure S1C in article III), i.e. Dmax>>D, we can consider $\boldsymbol{A_{free}}$ to be approximately equal to ***A***. The ThT_F input becomes therefore proportional to the total amount of fibril (A). The amount of ThT_F at steady state can therefore be approximated as:

$$ThT_F = \frac{k_{on} \cdot A_{free} \cdot [ThT]}{k_{off} + k_b \cdot I_0} \approx \frac{k_{on} \cdot A \cdot [ThT]}{k_{off} + k_b \cdot I_0}$$

As the ThT equilibrium inside the aggregates is relatively fast compared to aggregation (Figure 5 in article III), we can consider the ThT inside the fibrils (ThT_F) to be at equilibrium in the differential equation describing the evolution of aggregates:

$$\frac{dA}{dt} = k_{agg}([HI]) \cdot I_0 \cdot \frac{k_{on} \cdot A \cdot [ThT]}{k_{off} + k_b \cdot I_0}$$

During the experiment one determines the apparent kinetic constant of aggregate growth ($\mathbf{k_{app}}$) which is defined as:

$$\frac{dA}{dt} = k_{app} \cdot A$$

Hence:

$$k_{app} = k_{agg}([HI]) \cdot \mathrm{I}_0 \cdot \frac{k_{on} \cdot [ThT]}{k_{off} + k_b \cdot \mathrm{I}_0}$$

As the flux of ThT into the aggregate is reduced in the absence of agitation this entails a reduction of k_{on} but also likely, in a lesser extent, a reduction of k_{off}. The stirring therefore affects the density of ThT fluorescence inside the fibril by affecting:

$$\aleph = \frac{k_{on}}{k_{off} + k_b \cdot \mathrm{I}_0}$$

Model with saturation

A more exact model taking into account the saturation of ThT_F inside the aggregate can be detailed if saturation becomes significant (which is not the case in our experimental conditions). The part of aggregates accessible to ThT was defined earlier as:

$$A_{free} = A \cdot \theta = A \cdot \left(\frac{D_{max} - D}{D_{max}}\right)$$

The evolution of ThT_F is therefore:

$$\frac{dThT_F}{dt} = k_{on} \cdot A \cdot \left(\frac{D_{max} - D}{D_{max}}\right) \cdot [ThT] - k_{off} \cdot \ ThT_F - k_b \cdot \ ThT_F \cdot \mathrm{I}_0$$

In stationary conditions:

$$\frac{dThT_F}{dt} = k_{on} \cdot A \cdot \left(\frac{D_{max} - D}{D_{max}}\right) \cdot [ThT] - k_{off} \cdot \ ThT_F - k_b \cdot \ ThT_F \cdot \mathrm{I}_0 = 0$$

$$\Leftrightarrow k_{on} \cdot A \cdot [ThT] - \frac{D}{D_{max}} \cdot k_{on} \cdot A \cdot [ThT] - k_{off} \cdot \ ThT_F - k_b \cdot \ ThT_F \cdot \mathrm{I}_0 = 0$$

$$\Leftrightarrow k_{on} \cdot A \cdot [ThT] - \frac{ThT_F}{D_{max}} \cdot k_{on} \cdot [ThT] - k_{off} \cdot \ ThT_F - k_b \cdot \ ThT_F \cdot \mathrm{I}_0 = 0$$

$$\Leftrightarrow ThT_F = \frac{k_{on} \cdot A \cdot [ThT]}{\left(\frac{k_{on} \cdot [ThT]}{D_{max}}\right) + k_{off} + k_b \cdot \ \mathrm{I}_0}$$

Evolution of the total amount of aggregates with saturation:

$$\frac{dA}{dt} = k_{agg}([HI]) \cdot \gamma \cdot \frac{k_{on} \cdot A \cdot [ThT]}{\left(\frac{k_{on} \cdot [ThT]}{D_{max}}\right) + k_{off} + k_b \cdot I_0}$$

Kinetic constant of aggregate growth with saturation:

$$k_{app} = k_{agg}([HI]) \cdot \gamma \cdot \frac{k_{on} \cdot [ThT]}{\left(\frac{k_{on} \cdot [ThT]}{D_{max}}\right) + k_{off} + k_b \cdot I_0}$$

Implication

With these assumptions, it is possible to plot the light-induced aggregate growth rate as a function of the irradiance (I_0) or the ThT concentration in solution (**[ThT]**):

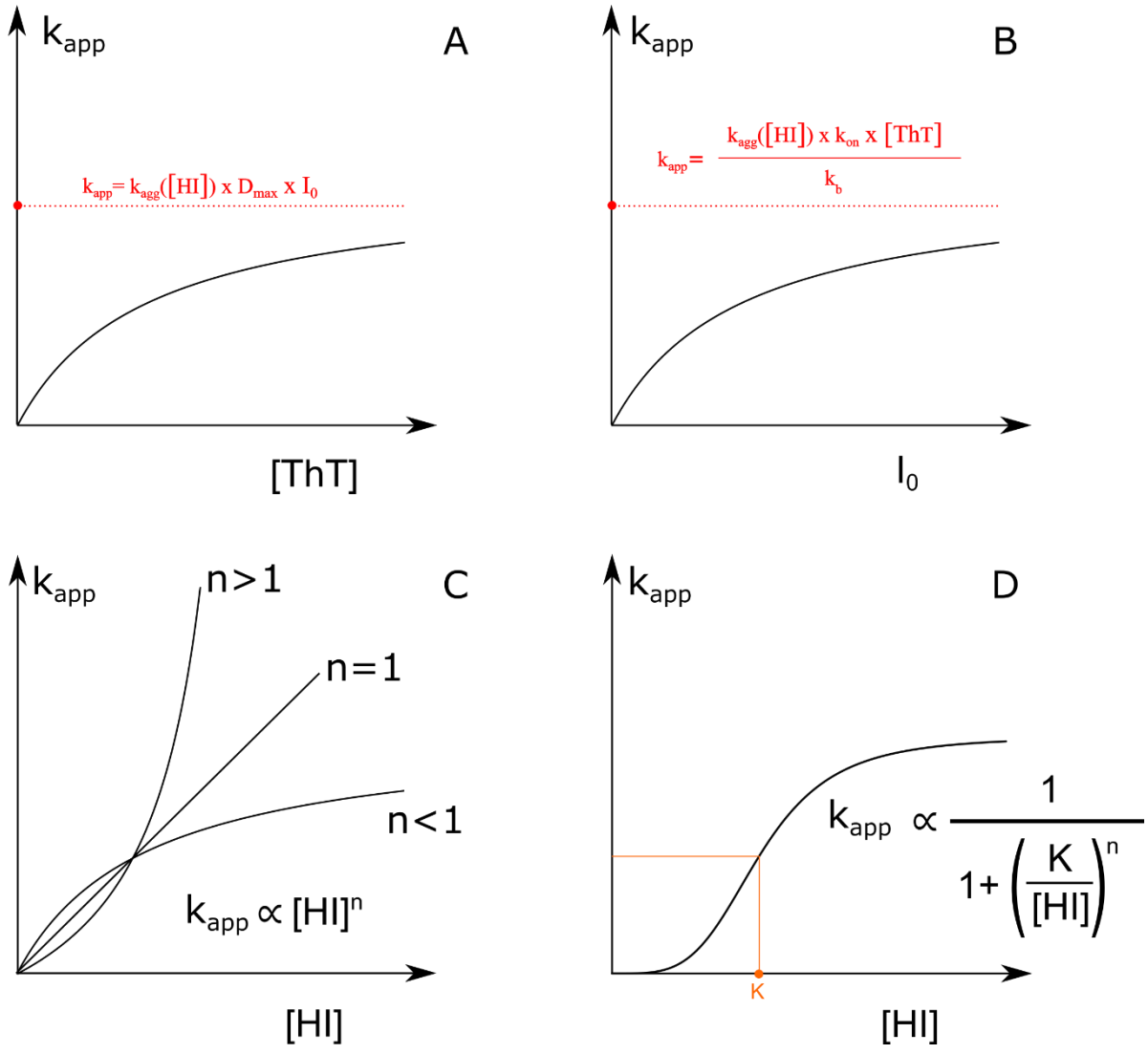

Figure 51. Evolution of the growth rate of HI light-induced insulin aggregates as a function of the ThT concentration in solution (A) and as a function of the irradiance (B) according to the mathematical model. Two hypothesis concerning

the effect of [HI] on the kagg are presented: a reaction order n for native HI in solution (C) and a cooperative beheaviour of HI (D).

In our experimental condition, the saturation point of ThT is not reached and the bleaching of the initial ThT fluorescence layer on the surface makes it difficult to visualize the saturation of the growth rate due to the ThT_F bleaching inside the aggregates.

Insulin

Under the hypothesis of a stoichiometric coefficient of insulin *n* (which can be a non-integer) the chemical equation of HI incorporation is:

$$ThT_F + \boldsymbol{n} \cdot HI + \mathrm{I}_0 \xrightarrow{k_{agg}} ThT_F + A$$

Which corresponds to the following differential equation of aggregate growth:

$$\frac{dA}{dt} = k_{agg} \cdot [HI]^n \cdot \mathrm{I}_0 \cdot ThT_F$$

In this specific case, k_{agg} expressed in $M^{-\mathbf{n}}.\mu m^2.nW^{-1}.s^{-1}$, with n corresponding to the stoichiometric coefficient of HI. Such kinetic relationship results in kapp following a power law (Figure 51C). Alternatively, and maybe more coherent with our results, the cooperative adsorption of native HI at the surface of the aggregate can represent a limiting step. In this case the evolution of the k_{app} can results in a sigmoid (Figure 51D).

Eventually as the reaction loses its exponential behavior at low HI concentration, and completely stop in the absence of agitation,

Fitting of kinetic constant

We have define k_{app} by:

$$\frac{dA}{dt} = k_{app} \cdot A$$

Under the approximations that k_{app} is proportional to irradiance (i.e. bleaching is negligible in ThT equilibrium under agitation which is verified in our experimental conditions) and proportional to [ThT] (i.e. saturation of the aggregates with ThT is negligible in the ThT equilibrium which also is verified in our experimental conditions), we can also define the kinetic constant k_c:

$$\frac{dA}{dt} = k_c \cdot \mathrm{I}_0 \cdot [ThT] \cdot A$$

$$\Leftrightarrow \mathrm{k_{app}}(\mathrm{I}_0, [ThT]) = k_c \cdot \mathrm{I}_0 \cdot [ThT]$$

With k_c in $\mu m^2.min^{-1}.M^{-1}$ of ThT.nW^{-1}.

According to the fit obtained Figure 2B in article III, the k_{app} in s^{-1} as a function of γ expressed in nW.μm^{-2} (at [ThT] = 20µM and [HI] = 86µM) is given by:

$$k_{app}(\gamma, 20\mu M) = 2{,}66 \cdot 10^{-5} \cdot I_0$$

$$\Leftrightarrow k_c = 1{,}33 \cdot 10^{6}\ \mu m^2 \cdot s^{-1} \cdot M^{-1} \cdot nW^{-1}$$

On the other hand, according to the fit obtained Figure 6B in article III, the k_{app} in s^{-1} as a function of [ThT] (at γ = 57.7nW.μm^{-2} and [HI] = 86µM) is given by:

$$k_{app}(57.7 nW.\mu m^{-2}, [ThT]) = 7{,}33 \cdot 10^{-5} \cdot [THT]$$

$$\Leftrightarrow k_c = 1{,}27 \cdot 10^{-6}\ \mu m^2 \cdot s^{-1} \cdot M^{-1} \cdot nW^{-1}$$

The two determined k_c are close allowing a precise determination of the reaction rate for given irradiance and ThT concentration

5.1.3 **Fractal dimension**

The fractal dimension of an object can be determined by the ball covering method, fractal objects scale. Here we use this technique in order to describe the scaling dimension in a section of the outline of the light-induced aggregate. From the confocal micrograph presented in Figure 3C, we have hand-drawn the outline of the aggregates, we have then covered this surface with circles of increasing size and record the minimal number of circles necessary to cover all the path: Figure S4. The resulting Hausdorff dimension of a section of the aggregate perimeter is 1.49. This fractal pattern is likely the result of the extreme experimental conditions (Strong agitation 1h illumination,[ThT]= 130µM, I_0 = 960 nW.μm^{-2}) in which the high illumination and ThT concentration allows a rapid diffusion and conversion of native HI into aggregate. One could expect variations of the aggregate fractal dimensions as a function of the aggregation rate.

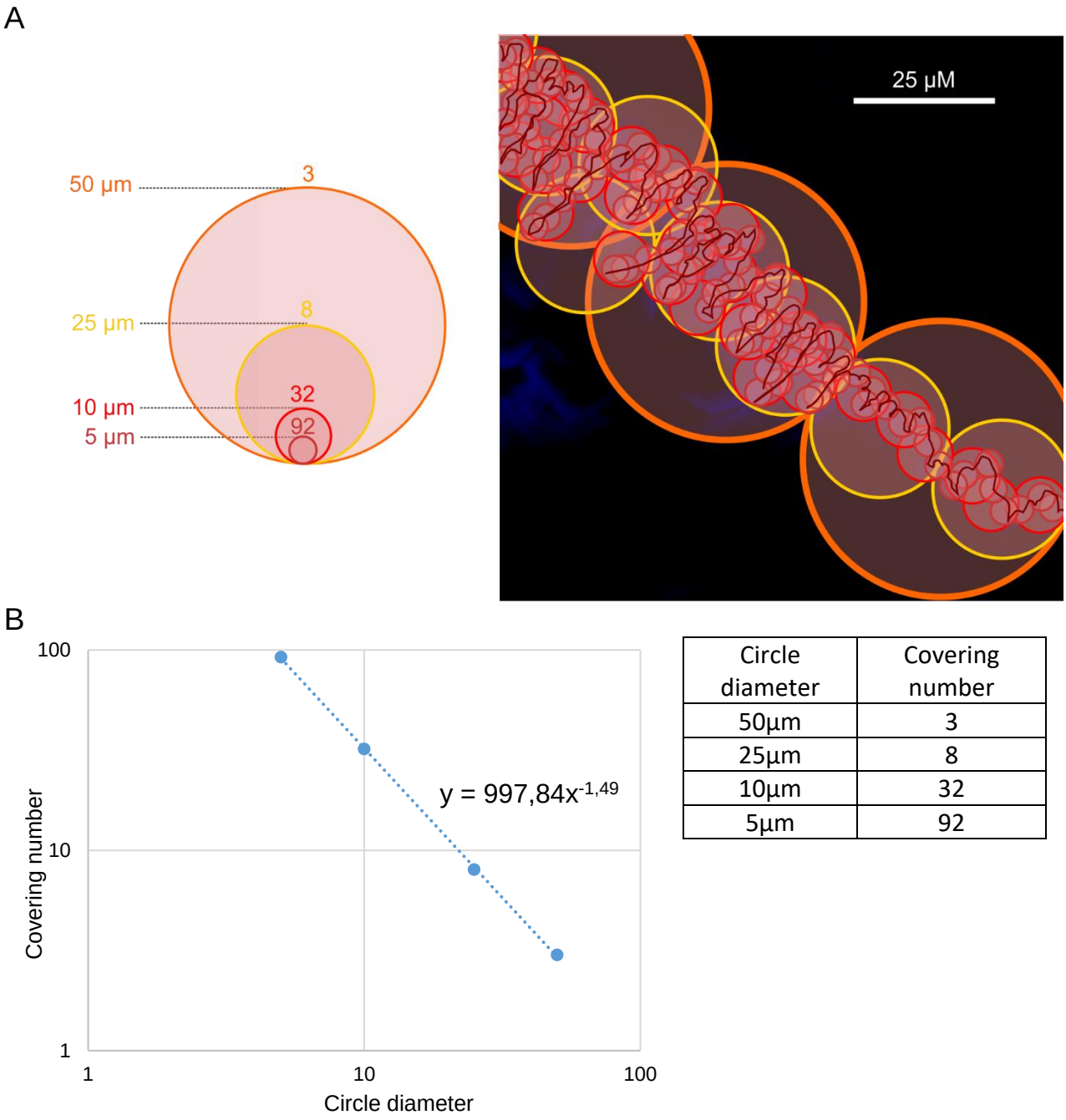

Circle diameter	Covering number
50µm	3
25µm	8
10µm	32
5µm	92

Figure S4. Fractal dimension of light-induced aggregate surface in horizontal section. A: circle covering of the aggregate surface section (burgundy line) by circles of 5µm, 10µm; 25µm and 50µm; the image used is the confocal image from Figure 3C (1h illumination,[ThT]= 130µM, I_0 = 960 nW.µm^{-2}). B: Logarithmic representation of the covering number as a function of the circle diameter and a fitting of the data with a power function showing the fractal dimension: 1.49.

5.2 Agitation in the experimental set-up

The effect of agitation on protein denaturation and aggregation is usually attributed to 3 effects in the scientific literature: i) increase of the protein diffusion, ii) shear stress and iii) formation of dynamic triple points. As LIA is observed at the bottom of our chamber in the absence of air bubbles, our experimental design allow us to rule out the role of dynamic triple points in.

As with classical surface induced aggregation (Chapter 3 and 4), agitation is paramount for the growth of light induced aggregates (Article III). As ThT renewal inside the aggregates is not the limiting factor in LIA, ThT diffusion is not reason for this agitation dependency.

5.2.1 Details of the gear motor performances

The performances of the gear motor used in this study are shown Figure 52, the rotation speed of the rod was controlled to be around 1200 rpm in our experimental condition by short exposure microscope imaging. The absence of significant precession (distance of the spin axis to the axis of precession inferior to the diameter of the rod) of the rod was also controlled by microscopy imaging and long exposure single-lens reflex camera photography.

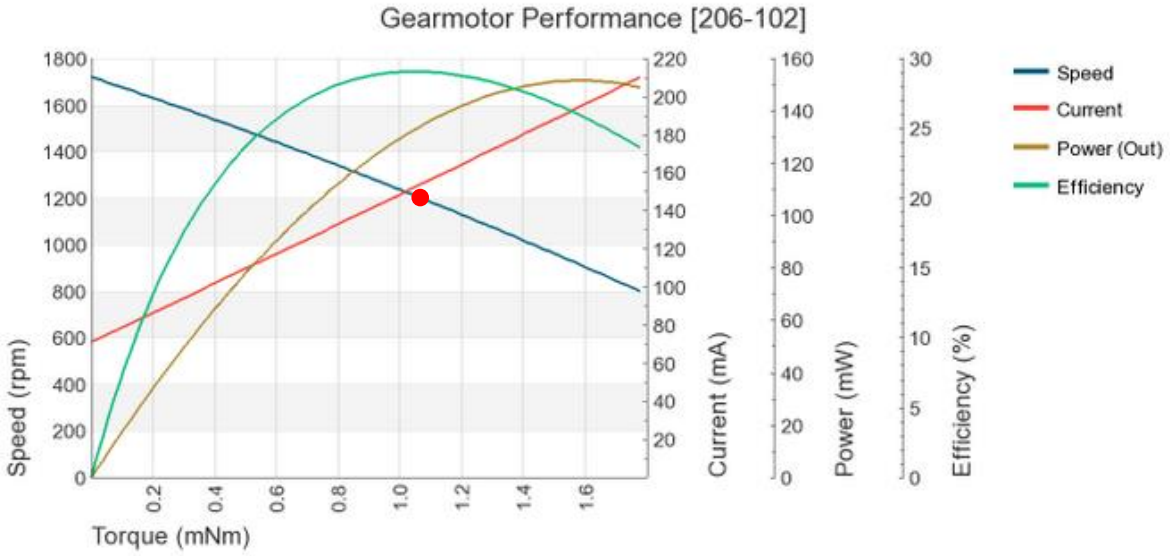

Figure 52. Performance of the electrical motor used in the light-induced aggregation assays. The red point indicates the set point used in the study.

5.2.2 Shear stress at the surface

The shear stress above a surface in the case of a Newtonian fluid is given by:

$$\tau = \mu \frac{\partial u}{\partial Z}$$

With **τ** the shear stress in mPa, **μ** the dynamic viscosity of the fluid in mPa.s , **u** the velocity of the fluid parallel to the surface in μm.s^{-1} and **Z** the height above the surface in μm. The 0.5μm beads observed in the Z= 0 - 5μm region above the surface (Figure 53.A) present a velocity comprised between 0 and 100μm.s^{-1}. Considering the fluid to present a laminar flow with a linear profile near the surface (Figure 53.B) and the dynamic viscosity of the solution at room

temperature to be equal to that of water at 20°C (μ=1.002 mPa·s), one can estimate the shear stress at the surface:

$$\tau = \mu \frac{\Delta u}{\Delta Z}$$

With $\Delta u = 100 \mu m.s^{-1}$; $\Delta Z = 5\ \mu m$ and $\mu = 1.002\ \text{mPa} \cdot \text{s}$

$$\tau = 20.04\ mPa$$

The shear rate is

$$\frac{\Delta u}{\Delta Z} = 20 s^{-1}$$

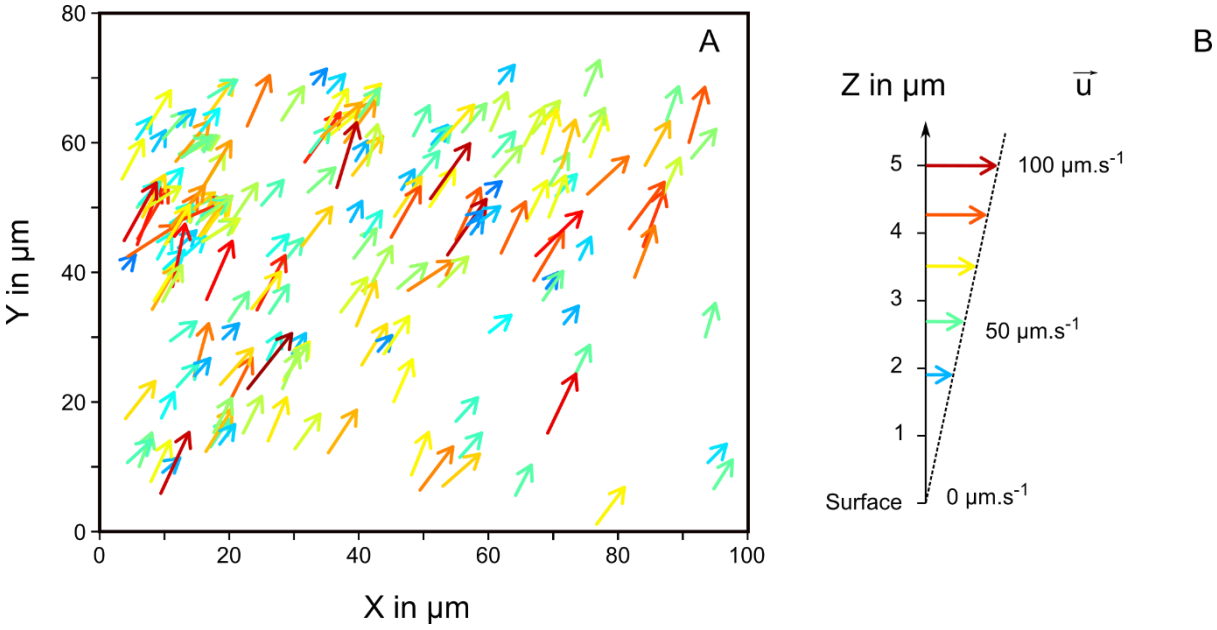

Figure 53. Determination of the fluid velocity above the surface in our experimental conditions. Fluorecent polystyrene beads d = 0.5 µm were imaged in solution under agitation by the glass rod at 1200 rpm. The depth of field of the 60X objective allows the imaging of beads in a focused region of 5µm just above the glass surface of our experimental chamber. A: The vectors represent the displacement of each individual bead during the 100ms exposure time. X and Y are dimensions parallel to the surface; B: Velocity profile of the fluid under the hypothesis of a laminar flow with a linear profile. Z is the height above the surface and $\vec{u}$ is the velocity of the fluid. The maximal velocity measured ($\vec{u} = \mathbf{100}\mu \boldsymbol{m.s^{-1}}$) was asigned to the maximal height above the surface observable (Z=5µm).

5.2.3 Flow regime

The Reynolds number (**Re**) is a dimensionless number indicating the flow regime, it is given by:

$$Re = \frac{u \cdot l}{\nu}$$

With **u** the fluid velocity, **l** the characteristic dimension and $\boldsymbol{\nu}$ the kinematic viscosity of the fluid. In our experimental setup:

$$\mathrm{u} = 100\mu\mathrm{m}\cdot\mathrm{s}^{-1}; \mathrm{l} = 2000\ \mu\mathrm{m}; \nu = 1.002\cdot 10^{6}\mu\mathrm{m}^{2}\cdot\mathrm{s}^{-1}$$

$$Re = \frac{u\cdot l}{\nu} = \frac{100\ \mu\mathrm{m}.\mathrm{s}^{-1}\ \cdot 2000\ \mu\mathrm{m}}{1.002\cdot 10^{6}\mu\mathrm{m}^{2}\cdot\mathrm{s}^{-1}} = 0.2$$

As Re < 1 the viscous forces are preponderant over inertial forces. One therefore expect no turbulence, the flow regime corresponds to a laminar flow or even to a Stokes flow at lower scale (e.g. around the 50µm wide aggregate) characteristic of microfluidic systems.

5.2.4 HI diffusion in the absence of agitation

In the absence of agitation the flux of HI molecules received by a surface in contact with the solution is determined only by Brownian motion. The diffusivity is defined by the Stokes–Einstein equation:

$$D = \frac{k_B T}{6\pi\mu r}$$

With **D** the diffusion constant in m^2s^{-1}, $\mathbf{k_B}$ the Boltzmann constant ($1.3806503\cdot10^{-23}$ J·mol^{-1}·K^{-1}), **T** the temperature in Kelvin (T = 293.15 K), **µ** the water viscosity in ($1.0016\cdot10^{-3}$ Pa.s at 20°C) and **r** the hydrodynamic radius of an insulin molecule ($1.7\cdot10^{-9}$ m). In our experimental conditions D_{HI} = 126 µm².s^{-1}. The flux of HI due to Brownian motion is determined by the Fick's laws:

$$\vec{J} = D\cdot\vec{\nabla}\,[HI]$$

At the surface $\vec{\nabla}\,[HI] = [HI]\cdot\mu m^{-1}$

The flux of HI molecules received by a surface by Brownian motion is therefore:

$$J = D\cdot\ [HI]\cdot\mu m^{-1} = \ 126\ \mu\mathrm{m}^{2}.\mathrm{s}^{-1}\cdot 86\cdot 10^{-21} mol.\,\mu m^{-4} = \ 1.0836\cdot 10^{-17}\ mol.\,\mu m^{-2}$$

5.2.5 Flux of HI and ThT in the displaced fluid

Expectation

As agitation dramatically increases the incorporation of both HI and ThT (which presents higher diffusivity) into the aggregates (Cf. Article III), the flux of HI due to fluid velocity must be at least of comparable scale with the HI flux induced by Brownian motion:

$$\overrightarrow{J_{HI}} = [HI]\cdot\vec{u} \sim \cdot\ 10^{-17} mol.\,\mu m^{-2}$$

with $\overrightarrow{J_{HI}}$ the flux of HI contained in the fluid flux and $\vec{u}$ the velocity of the fluid.

Calculation according to the measured fluid velocity

The flux of HI generated by agitation is:

$$J_{HI} = [HI] \cdot u$$

With J the flux of HI in mol.µm^{-2} [HI] the HI concentration in mol.µm^{-3} and u the solution velocity in µm.s^{-1}. At [HI] = 86µM = $86 \cdot 10^{-21}$ mol.µm^{-3} with a velocity comprised between 0 and 100 µm.s^{-1}, J_{HI} is comprised between 0 and $8{,}6 \cdot 10^{-18}$ mol. µm^{-2}.The same calculation can be applied to ThT, At 20µM ($20 \cdot 10^{-21}$ mol.µm^{-3}) with a liquid velocity comprised between 0 and 10 µm.s^{-1}, J_{ThT} is comprised between 0 and $2{,}0 \cdot 10^{-18}$ mol. µm^{-2}.

The estimation of HI flux induced by fluid displacement near the observed surface is inferior to the flux determined by calculation of the diffusion by Brownian motion alone, albeit they are of comparable scale.

5.3 Aggregation at the material-liquid-air triple interface

Apart from the LIA mechanism, the observation of the surface of this device in the absence of illumination i.e. by short exposure (t=0.5s every 30s) and in strong agitation (U= 2V equivalent to approx. 1200 rpm) shows the progressive appearance of small aggregates (0-3µm) on the surface. These ThT-fluorescent particles do not originate on the observed surface but appear progressively in solution after 90min of incubation and subsequently adsorb on the surface. Moreover the size of the adsorbed particles remains stable for the duration of the experiment. We therefore observe an aggregation pattern similar to that of article 1 (Figure 9 in article 1), however we were not able to locate nor observe the first aggregation steps.

As we suspected these early events in insulin aggregation to take place on the surface of the glass rod, which presents the highest shear stress as well as a triple interface, we performed an assay in which a silanized glass rod is rotating in an insulin solution inside a hydrophilic glass container. The only surface allowing protein adsorption in this experimental setup is the surface of the silanized hydrophobic glass rod (WCA~100°), which was imaged in 20µM ThT (Figure 54). After 120min of incubation in 86µM HI in TN buffer, the ThT fluorescence pattern on the surface of the rod ise striking: a few ThT-positive spots can be observed on the permanently immerged surface but most of the fluorescence is concentrated along the triple interface solution/air/glass rod (Figure 54). Other work performed by our team have shown that the dynamic triple line is the trigger of insulin aggregation in experimental set-up presenting intermittent wetting [196].

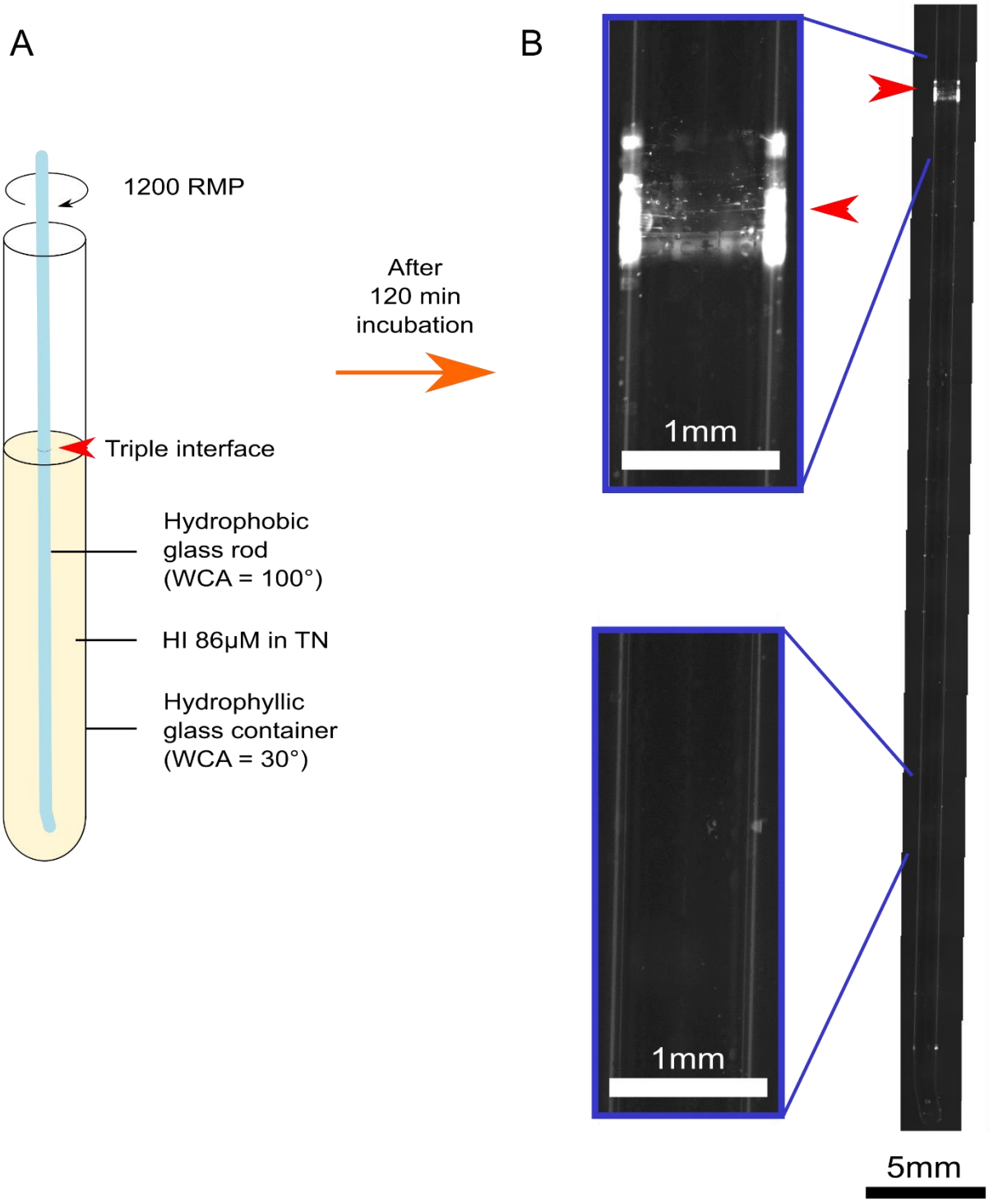

Figure 54. Pattern of ThT-positive aggregates on the agitation glass rod. A: Scheme of the experimental setup with a DMDCS functionalized glass rod; B: ThT fluorescence on the glass rod after 120 min incubation at 1200 rpm, the red arrowheads indicate the triple interface.

5.4 The mechanism of LK peptides is independent from the triple interface

In our preliminary results, no differences in the duration of the lag-time were observed between wells in which the pre-incubation of 5µM LK11 were performed in a 100µL volume and wells in which the pre-incubation was performed in a 200µL volume. Hence the accelerating mechanism of the peptide is not dependent on the formation of peptide patches at the triple interface.

5.5 Use of TAMRA-LK11 for high shutter speed imaging

The high intensity of TAMRA fluorescence obtained at the surface of the HI aggregate (Figure 7B in article III) allows the imaging of HI aggregates at high shutter speed (10ms, 1X gain on our experimental setup for the Figure 7B in article III). This short exposure time allow the visualization of large aggregate under strong agitation with an extreme reduction of their motion blur. We tested this approach in preliminary assays on large light-induced aggregates in order to observe their mechanical response to shear stress. The Figure 55 presents recorded positions of a light-induced aggregate under agitation in our experimental dispositive. This result indicates an important bending of the aggregate. Moreover the anisotropy in the displacement indicates an anisotropy in the mechanical stresses.

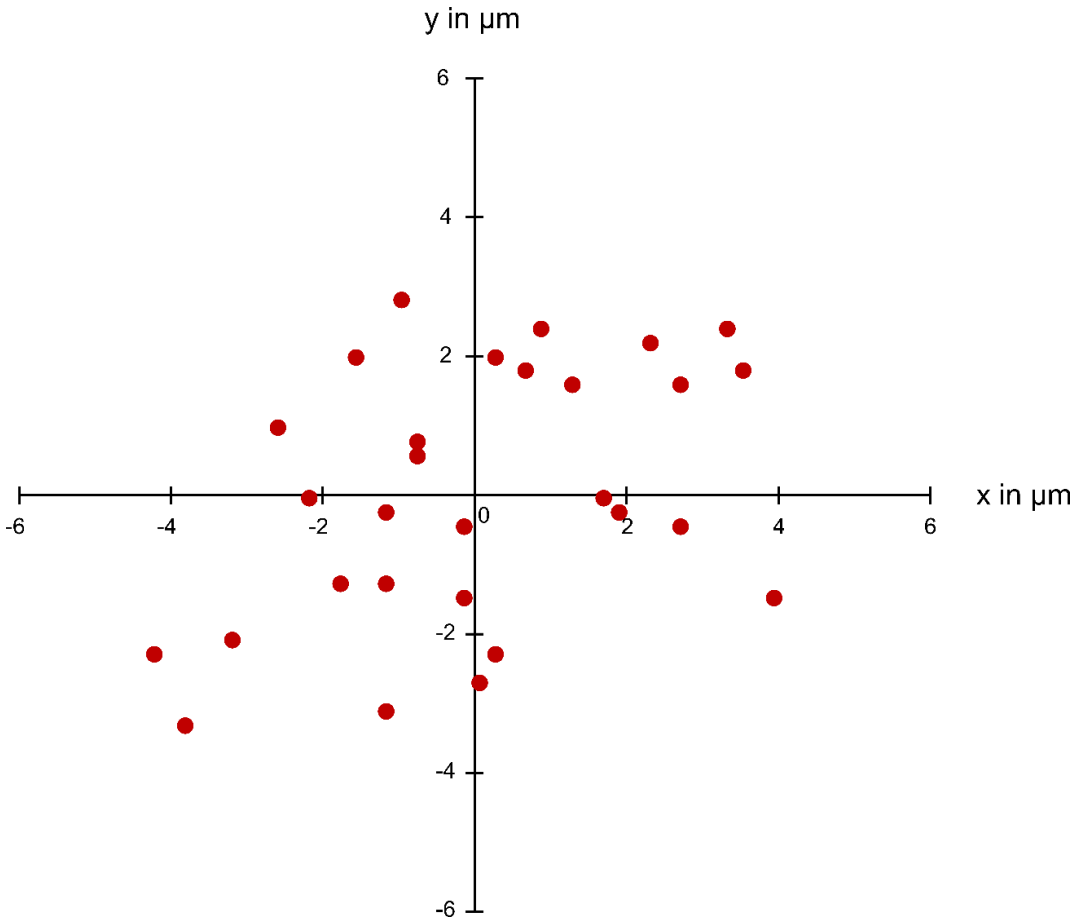

Figure 55 Displacement of the 50 µm wide and approx 40µm high light-induced aggregate under agitation in our experimental conditions. The centered coordinates are extracted from high shutter speed imaging (exp = 10 ms) of the TAMRA-LK11 peptides bound to the aggregate.

6 Discussion and conclusion

6.1 Location of nucleation

The location of first ThT fluorescence associated with surface-bound HI aggregates is studied in the last chapter. We determined that in a rod-agitated solution, the surface of the rod in contact with the liquid surface i.e. the triple interface, hence maximizing the shear stress as well as the dehydration stress (dynamic triple interface), was the preferential site for the first ThT fluorescence appearance. In peptide assays, however, the pre-incubation of peptide only in the bottom half of the well (100µL solution), did not impact the lag-time duration of an HI solution occupying the whole well (200µL). If the **dynamic triple interface** is likely the preferential nucleation site in insulin aggregation without peptide, (as shown by the striking pattern of ThT positive aggregates obtained on the hydrophobic glass rod) the insulin nucleation mechanism in the presence of peptide complexes is therefore largely independent from such effects.

6.2 Importance of agitation

No aggregation can be observed in the absence of agitation neither in the assays in 96 well plates nor in light-induced aggregation. This requirement necessary for both nucleation and growth could be explained either by the need of an important HI flux to the nucleation site or by the requirement for a mechanical stress in the aggregation process. This second point is often refuted in the literature, at least at the molecular level on the basis of the low scales of fluid mechanical forces on nanometric objects. A minimal shear rate of 10^7 s^{-1} would be necessary to denature small globular proteins in water[131] while in our LIA experiments the shear rate at the observed surface was estimated at 20 s^{-1}. However during the growth phase micrometric aggregates could indeed be affected by shear stress and for instance be detached from the surface to the solution. The minimal size of the aggregates observed in solution during surface induced HI aggregation were 200nm aggregates[197], this size corresponds to aggregates large enough to be detached from the surface by shear stress.

The scientific literature however contains numerous examples of shear stress-induced protein denaturation [198] and aggregation, including insulin. Shear rates comprised between 200 and 600 s^{-1} are reported to accelerate the amyloid aggregation of insulin at low pH as well as influencing the aggregate overall structure [199,200]. These reports however do not rule out the hypothesis of effects induced by mixing or dynamic triple interface formation and are performed in experimental conditions inducing amyloid aggregation in the absence of agitation. Our experimental condition differ in that not even residual aggregation rate can be

measured in the absence of agitation (Figure 56). One should therefore remain extremely prudent in the interpretation of the role of shear stress in the denaturation of protein either in solution or adsorbed on surface. On the other hand the shear stress is certainly responsible to the detachment of larger aggregates from the surface to the solution.

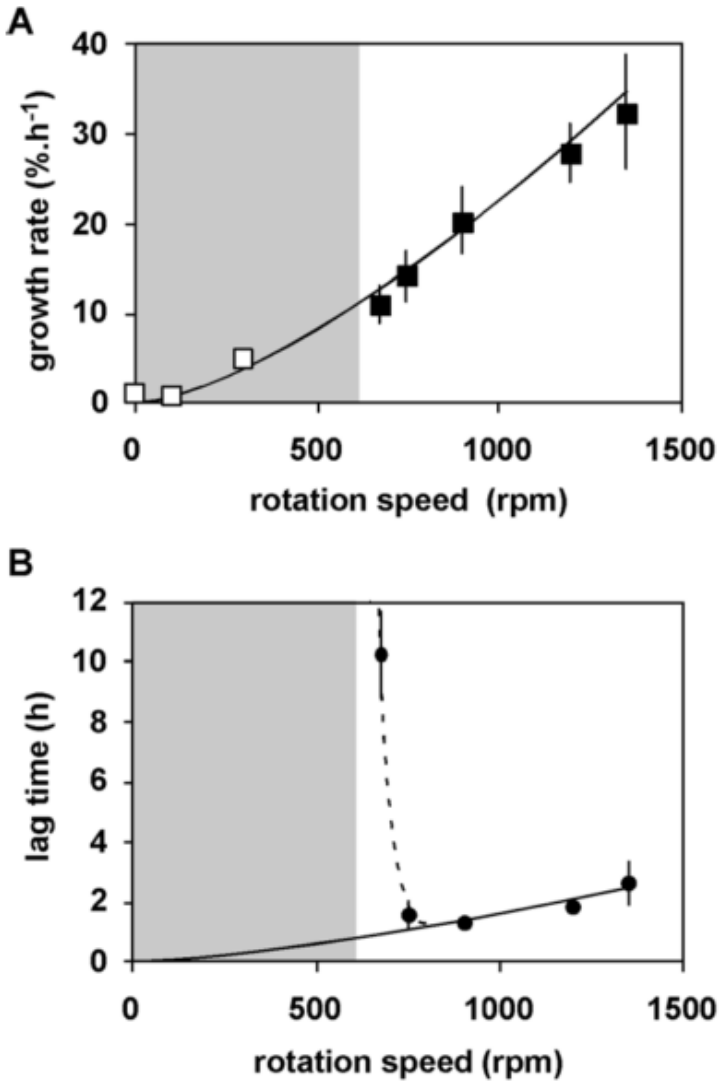

Figure 56. Effect of agitation on the growth rate (A) and lag-time (B) of HI aggregation in plate assays (From Nault PhD Thesis[201])

6.3 Peptide accelerating effect

Prior to this work, Nault et al. have shown that some peptides were able to accelerate insulin aggregation at hydrophobic surfaces via the formation of β-sheet[185]. We have here further investigated this mechanism and demonstrate that these peptides were able to cooperatively adsorb on hydrophobic surfaces where they enhance insulin aggregation.

This cooperative adsorption is most likely mediated by the formation of an antiparallel inter peptide β-sheet on the surface as described in the work of DeGrado and Lear[189]. The intermolecular hydrogen bonds stabilize the peptides forming "peptide patches" on two of their sides which would otherwise be exposed to the solution. (Figure 57). The shortest LK peptide presents a higher cooperativity index underlining its stronger requirement for inter molecular stabilization. Molecular dynamics simulations show that the $(LK)_7L$ peptide adsorption on a hydrophobic layer is mainly entropy driven[202], with entropy gains from the displaced solvent molecules counterbalancing the loss of peptide configurational entropy (-4.0 kJ/mol.K).

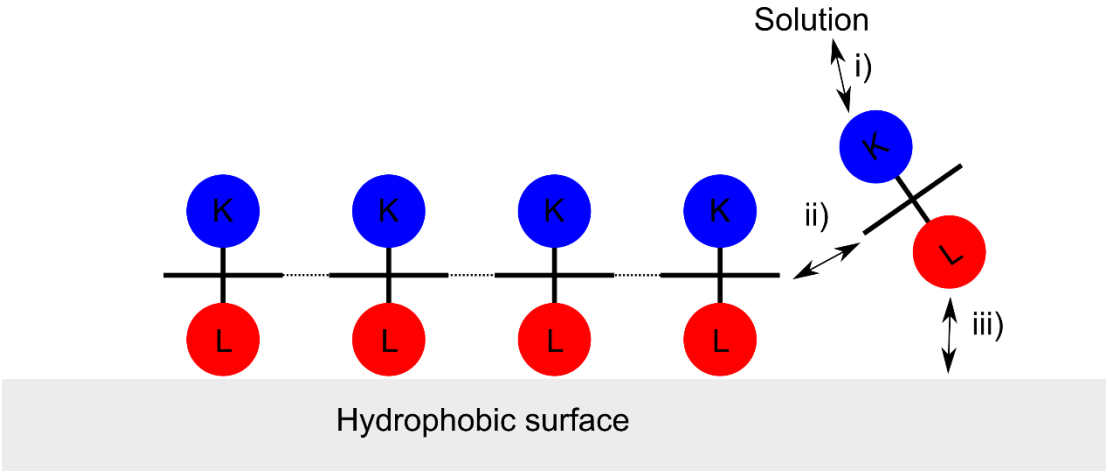

Figure 57 Principle of $(LK)_nL$ peptide's cooperative adsorption. The peptides are here represented in transversal view with hydrogen bonds represented by a thin dotted line. In a peptide patch a peptide is stabilized by i) polar interactions of the lysines with the solution, ii) inter-peptide hydrogen bonds involved in the antiparalel β-sheet formation and iii) the hydrophobic effect at the leucine/hydrophobic surface interaction.

The adsorbed $(LK)_nL$ peptides expose the amine groups of lysine towards the solution, yet amine-functionalized surfaces accelerate the nucleation rate of insulin aggregation[203]. This effect has also been observed during this PhD with amine functionalized plates as well as amine functionalized microbeads, both presenting lower lag-times than hydrophobic surfaces (data not shown), which could lead one to attribute the accelerating effect of these peptides to these exposed amine groups. Howbeit this interpretation is not consistent with the previous observations from other peptides. First ISISI and ISISISI both present the same cooperative effect on HI lag-time reduction while only exposing uncharged polar residues toward the solution. What is more, the LKKLLKLLKKLLKL peptide adopting an α-helix conformation at hydrophobic interfaces[189,204] also presents amine groups towards the solution but prolongs the lag-time of insulin aggregation for up to 30h[185]. Finally, Nault et al. have shown that the accelerating effect of the peptide on insulin aggregation was independent from a specific

sequence or motive and only depends to their ability to form a β-sheets on hydrophobic surfaces.

As the mechanisms by which these peptides increase the adsorption of insulin molecules and accelerate their conformational change[181,194] is independent from their sequence[185] but only relies on the formation of β-sheets on the hydrophobic surfaces, it is likely that the lateral hydrogen bonds of the peptide patches (Figure 46) are responsible for the stabilization of nucleation.

The model of the insulin intermediary state proposed by Millican et al.[205](Figure 58) is interesting in that the exposed hydrophobic domain, hence likely stabilized by the hydrophobic surface, would place the LVEALYLV (B11-18) segment of the insulin B chain exactly facing the hydrogen bond of the surface peptide β-sheet. Molecular dynamic studies have suggested the formation of a parallel β-sheet between the LVEALYL peptide and B22-27 segment of insulin[206]. It is possible that this segment (also implied in the formation of β-sheet between two insulin molecules in the dimer) forms the first attachment to a peptide patch via an intermolecular β-sheet with simultaneous adsorption of insulin on the surface on the exposed hydrophobic domain (Figure 58).

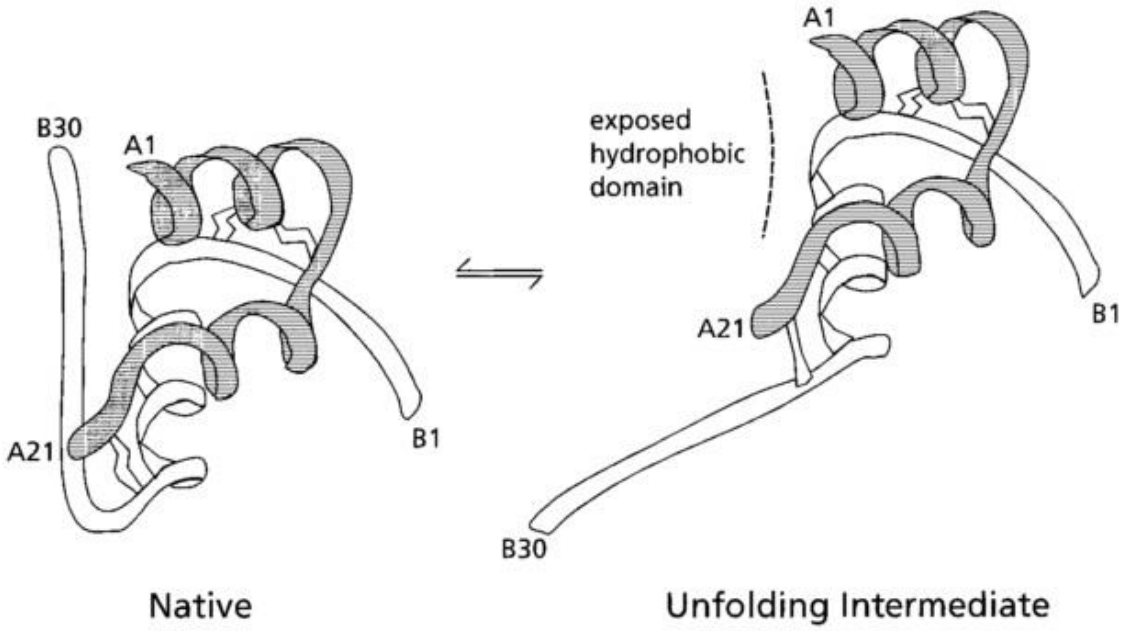

Figure 58: Model of insulin unfolding at material surfaces as proposed by Millican et al. [205](From Brange et al. [207])

6.4 Aggregate growth

The two most important issues concerning the general mechanisms of the surface-induced aggregation of insulin are: (i) does the aggregate growth only occur on suitable surfaces or also in the bulk solution? and (ii)what is the elongation unit of the aggregates?

The fact that the first ThT positive aggregates are generated on the surfaces from where they are subsequently detached to the solution is well documented[171,184,201]. The absence of HI aggregates below 100nm in solution indicates that all the early aggregates are formed on the surfaces from which they cannot be detached due to their minute size[184,197]. This however is not incompatible with a subsequent growth of these aggregates in the bulk solution.

The microscopic observations of 96-well plates content throughout the procedure of HI aggregation (chapter 3) reveals a continuous increase of the aggregate particle size (Figure 9 in article I). If the aggregation is restricted to the surface then these particles could be conglomerates of smaller aggregates released in solution or the result of detachment of larger aggregates from the surface.

Moreover the observation of a surface under agitation by short intermittent illumination (hence preventing LIA), leads to the gradual appearance of micro ThT-positive aggregate particles in solution subsequently adsorbing on the observed glass surface, where they do not present observable growth. This indicates that because of the surface chemistry and/or local shear stress the bottom of the observation chamber is not the location of the nucleation nor the place for the growth of the aggregates.

On the other hand the ability of HI aggregates in solution to seed a fresh insulin solution, indicates that the aggregates released in solution contribute to the aggregation growth phase. Whether they do so after a reabsorption or directly in solution is not certain, however this growth strictly requires strong agitation.

Vestergaard et al. present the HI amyloid elongation unit in acidic conditions as a helical hexamer of insulin[159]. For Sluzky et al. the elongation units are insulin monomers unfolded on hydrophobic surfaces and released in solution. Such an elongation unit consisting in partially unfolded insulin could be in favor of a surface-dependent aggregate growth.

6.5 Peptide inhibition in solution

The other effect observed for the two longest LK peptides (LK9 and LK11) is their ability to inhibit insulin aggregation at higher concentrations. We have in chapter 3, demonstrated that

this effect results from their presence in excess (to the surface) in solution. The model presented in Figure 59 describes the dual effect of LK11 and LK9 peptides, as shown in the article I[194]. The saturation of the surface by LK peptides results in the accumulation of peptides in excess in solution. These peptides in solution can then bind both amyloid and pre-amyloid insulin complexes, involving the lateral charges of lysine residues, and block the native insulin incorporation by steric hindrance. The pre-nucleus + peptide complexes are likely to dissociate rapidly if they present a high conformational energy and if they cannot attain a stable conformation by the incorporation of new insulin molecules. On the other hand, if the amyloid state is already attained, the peptides bound near or on the incorporation sites, prevent the aggregate growth. But as the peptides also bind with great affinity on other parts of the aggregates, the concentration of peptides in solution can be dramatically reduced. In particular, the low residual aggregation rates, resulting in part from secondary processes (hence presenting a rate of new incorporation site formation proportional to the amount of aggregates), is responsible for the production of new aggregates continuously depleting the peptides from the solution and eventually restoring a normal aggregation rate.

The inhibition of amyloid aggregation as well as the reduction of the toxicity of amyloid aggregates have generated significant research interests. One must distinguish the approaches based on small molecules from approaches based on specific peptide interactions.

Small molecules inhibiting amyloid aggregation

Saha et al.[208,209] have shown that glycerol inhibited both primary and secondary processes in insulin amyloid aggregation at pH 1.6. Several polyphenols found in consumed plants have been shown to interfere with amyloid aggregation (Figure 59) both in vitro and in vivo, providing possible therapeutic approaches[210]. Epigallocatechin gallate (EGCG), a polyphenol found in Tea (*Camellia sinensis*) inhibits amyloid-β fibrillation and even dissolves preformed Aβ and transthyretin aggregates[211]. Curcumin is a di-phenol produced by *Curcuma longa* which inhibits the fibrillation of transthyretin by stabilizing its tetramers and promoting the formation of non-fibrillar aggregates [212]. Because of its non-toxicity and the modulation of its bioavailability by piperine[212], curcumin is regularly investigated in amyloid inhibition studies.

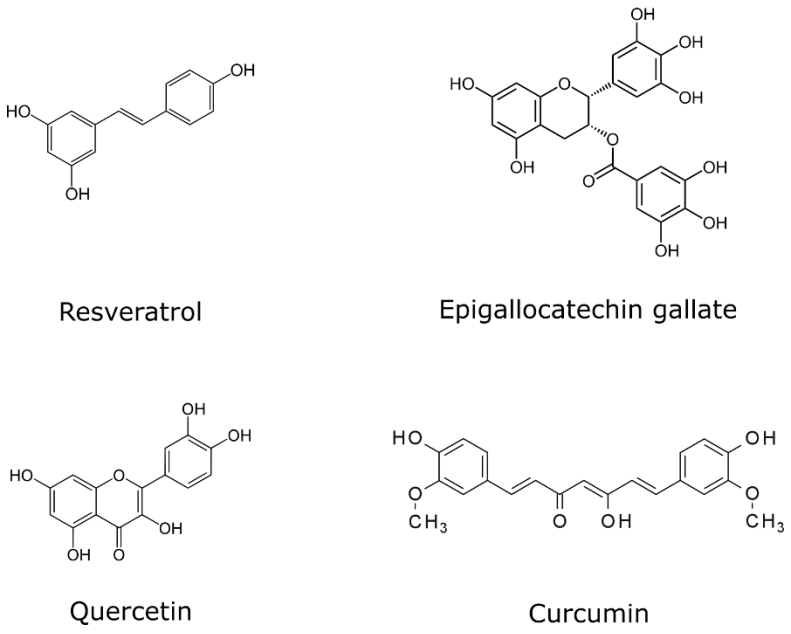

Figure 59: Polyphenols known to interfer with amyloid aggregation.

Moreover curcumin, quercetin and resveratrol are known to interfere with ThT fluorescence in amyloid fibrils by non-spectral interactions most likely by competitive binding to amyloid fibrils[213]. It is likely that the mechanisms of these small molecules rely on a binding to the fibril, similar to that of ThT, subsequently inducing a destabilization of the aggregate structure. Necula et al. have shown that small peptide inhibitors of Aβ aggregation could be classed as inhibitor of oligomerization, inhibitor of fibrillation or inhibitor of both[214], indicating that oligomerization is not a necessary intermediate in Aβ fibrillation. Interestingly some of the inhibitors of oligomerization present pro-fibrillation activities at sub-stoichiometric concentrations (1:100 of Aβ concentration) indicating a pro-nucleation effect.

The formation of off pathways oligomers by binding of the native protein is a frequently reported mechanism of amyloid aggregation inhibition by both small molecules and peptides. However the binding of a native protein can also trigger its aggregation. The ring-fused 2-pyridone FN075 for instance inhibits the aggregation of the bacterial curli protein CsgA but promotes the aggregation of α-synuclein[215].

Peptides inhibiting amyloid aggregation

More related to the results presented in Article I and II, small peptides can also inhibit amyloid aggregation. The so called β-breaker peptides both prevent aggregation and dissociate amyloid fibrils reducing their toxicity[216–221]. This dissociation of both oligomers and mature fibrils has never been observed with (LK)nL peptides; on the contrary, there is evidence that the

aggregates formed beforehand are not broken down after the addition of LK11 (Figure 47, Figure 7 in Article III).

The mechanism of the NF11 peptide (NAVRWSLMRPF) consists in the derivation of oligomeric intermediates from the Aβ aggregation pathway via the formation of off pathway NF11-Aβ complexes[216]. Moreover this peptide binds Aβ in amyloid fibrils resulting in the dissociation and reduction of the toxicity of preformed aggregates. This peptide can bind both native and amyloid Aβ which is not the case of LK11 peptide which uniquely binds HI aggregates and not native HI in solution (Article II).

A penta-peptide fragment of amyloid-β, KLVFF (Aβ16–20) can bind the full length Aβ peptide and prevent its amyloid aggregation[222]. The authors show that the KLXXF motive is critical for this binding. Peptides containing this motive are able to stop the aggregation of Aβ, allegedly by binding to monomeric Aβ in solution. These amino acids belong to the first beta spine in a model based on an NMR structure[68,223]. The addition of a poly-lysine Cterm tail, at the end of this minimal peptide (KLVFFKKKKKK), resulted in the acceleration of Aβ aggregation with significant changes in aggregate morphology as well as a reduced cellular toxicity[114,224,225].

Efforts to develop peptide sequences partially homologous to the Aβ16–20 sequence but comprising proline residues preventing a β-sheet conformation have yielded interesting results: the RDLPFFPVPID peptide prevents Aβ fibrillation and partially disaggregates preformed fibrils[218]. The trehalose conjugated LPFFD peptide also presents inhibiting activity on Aβ(1–42) aggregation[219].

One of the key strategies in the design of peptides for amyloid aggregation inhibition is the targeting of the steric zipper region, with the purpose of preventing the incorporation of new proteins[217]. As LK11 prevents the growth of HI aggregate without disaggregating preformed fibrils, this inhibition mode is the most likely.

The core sequence from syrian golden hamster (*Mesocricetus auratus)* prion protein HaPrP106-141 can inhibit the conversion of native PrP into PrPres[226], with a critical role of the amino acid 119 and 120 in these phenomena. These amino acids belong to a highly hydrophobic region, which however does not seem to be involved in the formation of a β-sheet in prion fibrils[227].

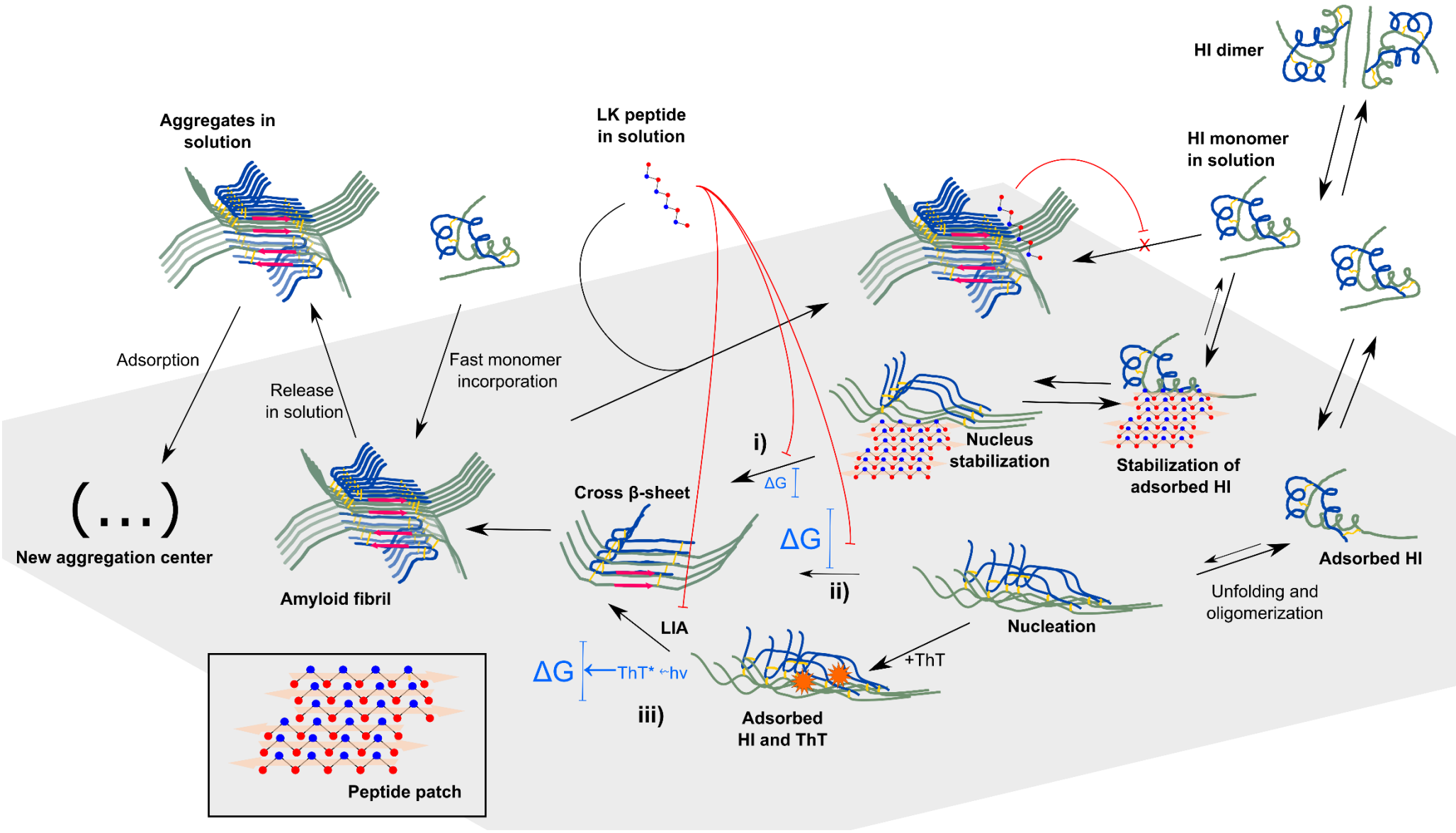
HI dimer
HI monomer in solution
Aggregates in solution
LK peptide in solution
Adsorption
Release in solution
Fast monomer incorporation
(...)
New aggregation center
Amyloid fibril
Cross β-sheet
i)
ΔG
Nucleus stabilization
Stabilization of adsorbed HI
ΔG
ii)
Nucleation
Adsorbed HI
Unfolding and oligomerization
LIA
ΔG ← ThT* ↜ hv
iii)
+ThT
Adsorbed HI and ThT
Peptide patch

Figure 60 Model of insulin aggregation mechanisms triggered by surfaces. Three different pathways are illustrated: i) aggregation stabilized by peptide patch reducing the activation energy to attain the amyloid form; ii) normal surface induced aggregation only stabilized by the surface which presents a high activation energy barrier and iii) light induced aggregation which overcomes this barrier by the transfer of energy from the excited ThT to the protein. These three pathways are inhibited by LK9 and LK11 peptides in solution. The gray area represents a hydrophobic surface; the peptide represented is LK9 with leucine side chains in red and lysine side chains in blue; the red and pale orange arrows represent a region in β-sheet conformation on the backbone of an HI and a peptide respectively; the ΔG in blue and their associated scales represent the relative value of the free energy barrier for the irreversible, rate-limiting steps; the size of the reaction arrows represents their associated reaction constants; orange stars represent protein-bound ThT molecules; bar-headed lines represent an inhibition.

Another approach consists in the N-methylation of two amide groups from the backbone of a peptide originating from the core sequence of an amyloidogenic protein with the purpose of preventing the formation of a cross β-sheet structure. 5 to 10 amino acid long peptides from the β-sheet forming region of islet amyloid polypeptide, IAPP20-29, are able to prevent the amyloid aggregation of their un-methylated counterpart and of the full length protein [228].

However in our system the peptide inhibition of insulin aggregation does not seem to be sequence specific but only driven by the lateral charges, they are therefore unlikely to interact directly with the core cross beta sheet structure nor to be involved in the formation of a steric zipper.

6.6 Light induced aggregation

The light induced aggregation mechanism described here is similar to the standard technique used in chapter 3 and 4 in its dependency on surfaces where insulin is able to absorb, in its inhibition of aggregate growth by the LK11 peptide, in the ThT-positive states of the resulting aggregates and in the dependency on strong agitation. However, this growth mechanism is strictly dependent on light illumination at a wavelength allowing ThT_F excitation. Another difference lies in the structure of these aggregates presenting much higher ThT-saturation, hence much lower ThT affinity. It is clear from our results that the ThT molecules in the aggregates absorb the radiant light and transfer its energy by a non-radiative ways to the surrounding insulin molecules. This energy then allows the structural transition of adsorbed native insulin to the aggregated state.

The aggregation rate is, as predicted by our model, proportional to irradiance and to ThT concentration. However, this rate is not proportional to the HI concentration, as aggregation is drastically reduced and loses its exponential behavior below a critical HI concentration (50µM). This indicates a growth mechanism that is more complex than a simple one step incorporation. This growth mechanism likely involves native protein-dependent secondary processes such as secondary nucleation, which is also in agreement with the tridimensional structure of the aggregates.

In the absence of agitation the aggregation completely stops while the fibrils maintain an overall ThT fluorescence level and a ThT density (ratio of the ThT fluorescence to the amount of aggregates) allowing LIA. This is either the result of a shortage of insulin supply to the aggregate, preventing growth, or might be the result of a shear stress-dependent mechanism.

Light-induced protein conformational changes

The control of biological processes by light are the foundation of some of the most promising techniques in biological research: optogenetics, in particular, allows the direct activation of single neurons by light as well as specific cell signaling pathways[229]. In recent years, multiple applications of surface patterning with proteins have emerged such as cell culture[230] (including cell patterning and differentiation) or protein arrays[231]. The methods of surface patterning with proteins includes classical microdeposition[232], patterning of light sensitive gels[233] and covalent immobilization of proteins on the surface by photo-active chemical groups[234,235].

Light induced protein aggregation is seldom described in the literature. Among the scarce examples available, light in excess induces the reversible aggregation in 2 dimensions of photosystem II and light-harvesting complex II in the thylakoid membrane[236]. Light has also been shown to accelerate the chemical degradation and subsequent aggregation of antibodies[237]. More relevant Chelnokov et al. have shown that a pulsed UV (308 nm) laser induces the abrupt aggregation of β-crystallins after an exposure of 100 $J.cm^{-2}$. The proposed mechanism is a photo-excitation of tryptophan with subsequent conversion of this energy into vibrational energy leading to a high local temperature and thermal denaturation of the crystalline. The exposure energy at which the initiation of the fast aggregation phase is observed decreases with the frequency of the laser pulse, indicating a relaxation of this reversible "photo-activated state".

Except for the Green Fluorescent Protein (GFP) family in which the tripeptide His-Tyr-Gly spontaneously react to form a conjugate system, light-sensitive proteins usually rely on external chromophores. Kaede is one of the photoactivable fluorescent proteins from the GFP family, which undergoes a transition from green to red fluorescence upon UV adsorption and subsequent reaction forming a larger conjugate system[238,239].

Protein conformational changes induced by light are usually the result of the isomerization or chemical reaction of a bound chromophore. In rhodopsins, the retinal chromophore is covalently bound to the protein via a Schiff base[§], the retinal isomerization by the absorption of a photon induces conformational changes in the protein[240].

Flavoproteins form a wide class of proteins characterized by their binding to a flavin mononucleotide (FMN) or a flavin adenine dinucleotide (FAD). Several flavoproteins are

[§] A **Schiff base** is a functional group of the form $R_2C=NR$

photo-sensitive (cryptochrome, photolyase), relying on chemical reaction induced by the absorbtion of a photon by their flavin chromophore. Light-oxygen-voltage (LOV) domains are light-sensitive domains containing a FMN chromophore[241]. In particular the Oat LOV2 domain undergoes conformational changes upon blue light illumination via the formation of a flavin-cysteine adduct[241,242]. This last example, could be similar to the effect observed in Light induced HI aggregation, as suggested in Article III, excited ThT could reduce insulin disulfide bonds resulting in a loss of stability and unfolding of the individual peptide chain. These individual chains, known to be amyloidogenic, would then aggregate and bind more ThT. There are other examples of flavin reaction on protein, formylmethylflavin for instance reacts with Nterm cysteine in peptide via the formation of an heterocycle[243].

An increase in the size of surface-induced HI aggregates has been observed by optical microscopy under continuous illumination. This phenomenon corresponds to a degradation of the preexisting aggregates by the light as it only occurs in the illumination area and persists after the replacement of the solution by a protein-free buffer. This subsequent light degradation (increase of the particle size without any protein incorporation) could be the reason of the difference of structure (lower protein density, higher saturation with ThT) observed in light induced aggregates.

6.7 Amyloid aggregation?

Despite the publications available on surface-induced insulin aggregation, the structural data of these aggregates remain scarce. No electron nor atomic force micrograph have revealed the highly organized structure, typical of the amyloids. Hitherto, no X-ray diffraction experiment has ever been performed on such aggregates. This experiment could revealed the typical amyloid diffraction pattern. However, the numerous kinetic studies detailed in this work and in earlier works of our team or others have revealed a seeded aggregation mechanisms typical of the amyloid-like aggregation mode (cf. chapter I). Additionally, the ThT fluorescence of these aggregates is characteristic of their β-sheet-rich content (cf. discussion on ThT staining specificity in chapter I). Insulin aggregation in acidic conditions, however, has received detailed structural characterization: these aggregates show all the characteristic structural features of amyloid fibrils: the fibril structure [163] and the typical X-ray diffraction pattern[123]. Ballet reported the abolition of lag-time in acidic condition and at high temperature by insulin aggregates formed on surface in physiological conditions[184]. This direct seeding is a solid evidence for a common structure. So the aggregation mechanism studied here is largely

amyloid-like in kinetics, secondary structure and seeding ability without definitive structural proof for the moment.

6.8 Future directions

6.8.1 Grazing-incidence small-angle X-ray scattering, GISAXS

Grazing-incidence small-angle X-ray scattering (GISAXS), is a powerful technique to characterize surface nanostructures. We had the privilege to obtain 48h of beam time on the European Synchrotron Research Facility. Preliminary results obtained on early HI aggregation complexes on hydrophobic cover slips (using an identical protocol to that described for AFM in the article I[194]) exhibit differences in surface roughness between samples obtained at different incubation times, with significant increased surface structures as a function of incubation time. The mean particle size was estimated at 10nm which represent the same order of magnitude as particles observed by AFM (chapter 3). This technique allows the analysis of important surface area, but the determination of mean particles size by model fitting can be hampered by the variability of these particles.

6.8.2 Mass spectroscopy

One of the initial objectives of this PhD was to characterize the protein-peptide interaction from a structural point of view. We therefore studied the approach and feasibility of cross-linking and subsequent characterization by MALDI-TOF mass spectroscopy of peptide-insulin complexes.

The target of this crosslinking could therefore be either the nucleation complexes or the fibrils.

Even if the numerous structures observed in AFM (Chapter 3) can be considered as pre nucleation complexes, the kinetic nucleus itself is a rare and ephemeral event. So if the surface complexes are to be crosslinked, most of the signal would likely result from these structures which do not necessarily all belong to the pathways of insulin amyloid nucleation.

In the case of a peptide pre-saturated surface however, the number of nuclei is drastically increased as well as the reproducibility of their kinetics (chapter 3). Furthermore the amount of peptide released in solution is negligible, hence reducing the signal resulting from interaction of peptides in solution with these complexes. $(LK)_nL$-pre-saturated surfaces are therefore an invaluable tool in this approach as they define reproducible conditions and increase the number of surface HI nuclei, most of which presenting the peptide-insulin interaction of interest.

Concerning the interaction of HI aggregates with the LK11 and LK9 peptide from the solution, the coupled cross-linking and mass spectroscopy approach is even more promising, as the number of objects is not a limiting constraint.

6.8.3 Förster resonance energy transfer

The interaction between two molecules can be characterized by taking advantage of Förster resonance energy transfer (FRET). The two molecules that interact (or even each of the two regions of the same macromolecule) should be labeled with two different fluorophores, the first fluorophore being able to transfer its fluorescence energy to the second. As FRET is only effective at nanometric range, the efficiency of the resulting fluorescence quenching or fluorescence transfer indicates interaction. The TAMRA labeling of the LK11 peptide has been specifically chosen in order for its potential fluorescence transfer with FITC. However attempts to obtain surface-mediated aggregation complexes with FITC-labeled bovine insulin have failed. Furthermore the TAMRA-labeled LK11 peptide loses its fluorescence once adsorbed on polystyrene plates.

6.8.4 Total internal reflection fluorescence microscopy

Thanks to its high resolution in height this technique would be extremely promising to investigate the nucleation on glass surfaces. The development of an incubation chamber presenting low surface hydrophobicity combined with localized and patterned hydrophobic area could be used for observation in TIRF. Moreover the imaging mode of scanning laser microscopes would be extremely efficient at reducing LIA.

The early nucleation events are not ThT-positive so fluorescently labeled insulin must be used to visualize these early steps. The adsorption of LK peptides on the surface likely forms patches rather than a continuous monolayer. The nucleation of insulin on the edges of these patches will likely also form discrete spots of fluorescence rather than a continuous layer.

7 Bibliography

1. Zhang, L., Li, N., Gao, F., Hou, L. & Xu, Z. Insulin amyloid fibrils: An excellent platform for controlled synthesis of ultrathin superlong platinum nanowires with high electrocatalytic activity. *J. Am. Chem. Soc.* **134,** 11326–11329 (2012).
2. Kyte, J. & Doolittle, R. F. A simple method for displaying the hydropathic character of a protein. *J. Mol. Biol.* **157,** 105–132 (1982).
3. Lehninger, A., Nelson, D. & Cox, M. *Principles of Biochemistry*. *Book* (2008).
4. Cross, L. C. & Klyne, W. *Rules for the Nomenclature of Organic Chemistry Section E : Stereochemistry*. *Pure & Applied Chemistry* **45,** (Elsevier Science, 1976).
5. Mor, A., Amiche, M. & Nicolas, P. Enter a new post-translational modification: d-amino acids in gene-encoded peptides. *Trends Biochem. Sci.* **17,** 481–485 (1992).
6. Dasuri, K. *et al.* Amino acid analog toxicity in primary rat neuronal and astrocyte cultures: Implications for protein misfolding and TDP-43 regulation. *J. Neurosci. Res.* **89,** 1471–1477 (2011).
7. Merrifield, R. B. Solid Phase Peptide Synthesis. I. The Synthesis of a tetrapeptide. *J. Am. Chem. Soc.* **85,** 2149 (1963).
8. Lesk, A. *Introduction to Protein Science: Architecture, Function, and Genomics*. (OUP Oxford, 2010).
9. Cantor, C. R. & Schimmel, P. R. *Biophysical Chemistry: Part I: The Conformation of Biological Macromolecules*. (W. H. Freeman, 1980).
10. Ramachandran, G. N., Ramakrishnan, C. & Sasisekharan, V. Stereochemistry of polypeptide chain configurations. *J. Mol. Biol.* **7,** 95–99 (1963).
11. Daggett, V. Alpha-sheet: The toxic conformer in amyloid diseases? *Acc. Chem. Res.* **39,** 594–602 (2006).
12. Cao, A., Hu, D. & Lai, L. Formation of amyloid fibrils from fully reduced hen egg white lysozyme. *Protein Sci.* **13,** 319–324 (2004).
13. Alberts, B. *et al. Molecular Biology of the Cell. 5th Edition, New York* (2007).
14. Berg, J. M., Tymoczko, J. L. & Stryer, L. *Biochemistry*. (W. H. Freeman, 2007).
15. Van Holde, K. E. *Physical biochemistry*. (Prentice-Hall, 1985).
16. Zimmerman, S. B. & Trach, S. O. Estimation of macromolecule concentrations and excluded volume effects for the cytoplasm of Escherichia coli. *J. Mol. Biol.* **222,** 599–620 (1991).
17. Minton, A. P. Implications of macromolecular crowding for protein assembly. *Curr. Opin. Struct. Biol.* **10,** 34–39 (2000).
18. White, D. A., Buell, A. K., Knowles, T. P. J., Welland, M. E. & Dobson, C. M. Protein aggregation in crowded environments. *J. Am. Chem. Soc.* **132,** 5170–5175 (2010).
19. Munishkina, L. A., Ahmad, A., Fink, A. L. & Uversky, V. N. Guiding protein aggregation with macromolecular crowding. *Biochemistry* **47,** 8993–9006 (2008).
20. Sukenik, S. *et al.* Crowding alone cannot account for cosolute effect on amyloid

aggregation. *PLoS One* **6,** (2011).

21. Holde, K. E. Van, Johnson, W. C. & Ho, P. S. *Principles of Physical Biochemistry*. *Education* (Pearson/Prentice Hall, 2006). doi:10.1021/ed076p474.1
22. Martin, T. W. & Derewenda, Z. S. The name is bond--H bond. *Nature structural biology* **6,** 403–406 (1999).
23. Tanford, C. *The hydrophobic effect: formation of micelles and biological membranes*. (Wiley, 1973).
24. Meyer, E. E., Rosenberg, K. J. & Israelachvili, J. Recent progress in understanding hydrophobic interactions. *Proc. Natl. Acad. Sci. U. S. A.* **103,** 15739–15746 (2006).
25. Fernández, A. Epistructural tension promotes protein associations. *Phys. Rev. Lett.* **108,** 1–5 (2012).
26. Fernández, A. *et al.* Correction for Fernandez et al., Structural defects and the diagnosis of amyloidogenic propensity. *Proc. Natl. Acad. Sci.* **108,** 16133–16133 (2011).
27. Fernández, A. Keeping dry and crossing membranes. *Nat. Biotechnol.* **22,** 1081–1084 (2004).
28. Pietrosemoli, N., Crespo, A. & Fernández, A. Dehydration propensity of order-disorder intermediate regions in soluble proteins. *J. Proteome Res.* **6,** 3519–3526 (2007).
29. Fernandez, A. & Crespo, A. Protein wrapping: a molecular marker for association, aggregation and drug design. *Chem. Soc. Rev.* **37,** 2373–2382 (2008).
30. Norde, W. My voyage of discovery to proteins in flatland ...and beyond. *Colloids Surfaces B Biointerfaces* **61,** 1–9 (2008).
31. Dill, K. a & Chan, H. S. From Levinthal to pathways to funnels. *Nat. Struct. Biol.* **4,** 10–19 (1997).
32. Anfinsen, C. B. Principles that Govern the Folding of Protein Chains. *Science (80-.).* **181,** 223–230 (1973).
33. Dunker, A. K., Silman, I., Uversky, V. N. & Sussman, J. L. Function and structure of inherently disordered proteins. *Curr. Opin. Struct. Biol.* **18,** 756–764 (2008).
34. Lee, R. Van Der *et al.* Classi fi cation of Intrinsically Disordered Regions and Proteins. *Prog Biophys Mol Biol* (2015).
35. Ward, J. J., Sodhi, J. S., McGuffin, L. J., Buxton, B. F. & Jones, D. T. Prediction and Functional Analysis of Native Disorder in Proteins from the Three Kingdoms of Life. *J. Mol. Biol.* **337,** 635–645 (2004).
36. Brylinski, M., Konieczny, L. & Roterman, I. Hydrophobic collapse in (in silico) protein folding. *Comput. Biol. Chem.* **30,** 255–267 (2006).
37. Arai, M. & Kuwajima, K. Rapid formation of a molten globule intermediate in refolding of α-lactalbumin. *Fold. Des.* **1,** 275–287 (1996).
38. Dill, K. a *et al.* Principles of protein folding--a perspective from simple exact models. *Protein Sci.* **4,** 561–602 (1995).
39. Jaremko, M. *et al.* Cold denaturation of a protein dimer monitored at atomic resolution. *Nat. Chem. Biol.* **9,** 264–70 (2013).
40. Dias, C. L. *et al.* The hydrophobic effect and its role in cold denaturation. *Cryobiology*

60, 91–99 (2010).

41. Bekard, I. B. & Dunstan, D. E. Tyrosine autofluorescence as a measure of bovine insulin fibrillation. *Biophys. J.* **97,** 2521–2531 (2009).

42. Chi, E. Y., Krishnan, S., Randolph, T. W. & Carpenter, J. F. Physical Stability of Proteins in Aqueous Solution: Mechanism and Driving Forces in Nonnative Protein Aggregation. **20,** (2003).

43. Fink, A. L. Protein aggregation: Folding aggregates, inclusion bodies and amyloid. *Fold. Des.* **3,** 9–23 (1998).

44. Invernizzi, G., Papaleo, E., Sabate, R. & Ventura, S. Protein aggregation: Mechanisms and functional consequences. *Int. J. Biochem. Cell Biol.* **44,** 1541–1554 (2012).

45. Wang, W., Nema, S. & Teagarden, D. Protein aggregation-Pathways and influencing factors. *International Journal of Pharmaceutics* **390,** 89–99 (2010).

46. Fast, J. L., Cordes, A. A., Carpenter, J. F. & Randolph, T. W. Physical instability of a therapeutic Fc fusion protein: Domain contributions to conformational and colloidal stability. *Biochemistry* **48,** 11724–11736 (2009).

47. Zimm, B. H. Application of the Methods of Molecular Distribution to Solutions of Large Molecules. *J. Chem. Phys.* **14,** 164 (1946).

48. Neal, B. L., Asthagiri, D. & Lenhoff, A. M. Molecular Origins of Osmotic Second Virial Coefficients of Proteins. *Biophys. J.* **75,** 2469–2477 (1998).

49. Senesi, N. & Wilkinson, K. J. *Biophysical Chemistry of Fractal Structures and Processes in Environmental Systems*. (Wiley, 2008).

50. Horne, D. S. Determination of the fractal dimension using turbidimetric techniques. Application to aggregating protein systems. *Faraday Discuss. Chem. Soc.* **83,** 259 (1987).

51. Lin, M. Y. *et al.* Universality in colloid aggregation. *Nature* **339,** 360–362 (1989).

52. Lin, M. Y. *et al.* Universal reaction-limited colloid aggregation. *Phys. Rev. A* **41,** 2005–2020 (1990).

53. De Young, L. R., Fink, A. L. & Dill, K. A. Aggregation of globular proteins. *Acc. Chem. Res.* **26,** 614–620 (1993).

54. Gavira, J. A. Current trends in protein crystallization. *Arch. Biochem. Biophys.* (2015). doi:10.1016/j.abb.2015.12.010

55. McPherson, A. & Gavira, J. A. Introduction to protein crystallization. *Acta Crystallogr. Sect. FStructural Biol. Commun.* **70,** 2–20 (2014).

56. Gertz, M. A. & Rajkumar, S. V. *Amyloidosis: Diagnosis and Treatment*. (Humana Press, 2010).

57. Fitzpatrick, A. W. P. Atomic structure and hierarchical assembly of a cross-β amyloid fibril - Supplementary Info. *Proc Natl Acad Sci U S A* **5590,** 5468–5473 (2013).

58. Zandomeneghi, G., Krebs, M. R. H., McCammon, M. G. & Fändrich, M. FTIR reveals structural differences between native beta-sheet proteins and amyloid fibrils. *Protein Sci.* **13,** 3314–21 (2004).

59. Peim, A. *et al.* Mutagenic exploration of the cross-seeding and fibrillation propensity of Alzheimer's beta-amyloid peptide variants. *Protein Sci.* **15,** 1801–1805 (2006).

60. Andersen, C. B. *et al.* Branching in amyloid fibril growth. *Biophys. J.* **96,** 1529–1536 (2009).

61. Assarsson, A., Hellstrand, E., Cabaleiro-Lago, C. & Linse, S. Charge dependent retardation of amyloid amyloid β aggregation by hydrophilic proteins. *ACS Chem. Neurosci.* **5,** 266–274 (2014).

62. Goldsbury, C., Frey, P., Olivieri, V., Aebi, U. & Müller, S. A. Multiple assembly pathways underlie amyloid-beta fibril polymorphisms. *J. Mol. Biol.* **352,** 282–298 (2005).

63. Sunde, M. *et al.* Common Core Structure of Amyloid Fibrils by Synchrotron X-ray Diffraction. *Diversity* (1997).

64. Petkova, A., Yau, W.-M. & Tycko, R. Experimental Constraints on Quaternary Structure in Alzheimer's β-Amyloid Fibrils. *Biochemistry* **45,** 498–512 (2006).

65. Comellas, G. & Rienstra, C. M. Protein Structure Determination by Magic-Angle Spinning Solid-State NMR, and Insights into the Formation, Structure, and Stability of Amyloid Fibrils. *Annu. Rev. Biophys.* **42,** 515–36 (2013).

66. Wasmer, C. *et al.* Amyloid Fibrils of the HET-s(218-289) Prion Form a β Solenoid with a Triangular Hydrophobic Core. *Science (80-.).* **319,** 1523–1526 (2008).

67. Nielsen, J. T. *et al.* Unique identification of supramolecular structures in amyloid fibrils by solid-state NMR spectroscopy. *Angew. Chemie - Int. Ed.* **48,** 2118–2121 (2009).

68. Eisenberg, D. S. & Sawaya, M. R. Implications for Alzheimer's disease of an atomic resolution structure of amyloid-β(1-42) fibrils. *Proc. Natl. Acad. Sci. U. S. A.* **113,** 9398–400 (2016).

69. Biancalana, M. & Koide, S. Molecular mechanism of Thioflavin-T binding to amyloid fibrils. *Biochim. Biophys. Acta - Proteins Proteomics* **1804,** 1405–1412 (2010).

70. Wolfe, L. S. *et al.* Protein-induced photophysical changes to the amyloid indicator dye thioflavin T. *Proc. Natl. Acad. Sci. U. S. A.* **107,** 16863–16868 (2010).

71. Sulatskaya, A. I., Kuznetsova, I. M. & Turoverov, K. K. Interaction of thioflavin T with amyloid fibrils: Fluorescence quantum yield of bound dye. *J. Phys. Chem. B* **116,** 2538–2544 (2012).

72. Khurana, R. *et al.* Mechanism of thioflavin T binding to amyloid fibrils. *J. Struct. Biol.* **151,** 229–238 (2005).

73. Levine, H. Thioflavine T Interaction with Amyloid β-Sheet Structures. *AMYLOID-INTERNATIONAL J. Exp. Clin. Investig.* **2,** 1–6 (1995).

74. Groenning, M. *et al.* Binding mode of Thioflavin T in insulin amyloid fibrils. *J. Struct. Biol.* **159,** 483–497 (2007).

75. Maskevich, A. A. *et al.* Spectral properties of thioflavin T in solvents with different dielectric properties and in a fibril-incorporated form. *J. Proteome Res.* **6,** 1392–1401 (2007).

76. Maskevich, A. A., Lavysh, A. V., Kuznetsova, I. M., Sulatskaya, A. I. & Turoverov, K. K. Spectral Manifestations of Thioflavin T Aggregation. *J. Appl. Spectrosc.* **82,** 33–39 (2015).

77. Groenning, M. *et al.* Study on the binding of Thioflavin T to β-sheet-rich and non-β-sheet cavities. *J. Struct. Biol.* **158,** 358–369 (2007).

78. Sabate, R., Rodriguez-Santiago, L., Sodupe, M., Saupe, S. J. & Ventura, S. Thioflavin-T excimer formation upon interaction with amyloid fibers. *Chem. Commun. (Camb).* **49,** 5745–7 (2013).

79. Voropai, E. S. *et al.* Spectral properties of thioflavin T and its complexes with amyloid fibrils. *J. Appl. Spectrosc.* **70,** 868–874 (2003).

80. Bucciantini, M. *et al.* Inherent toxicity of aggregates implies a common mechanism for protein misfolding diseases. *Nature* **416,** 507–511 (2002).

81. Kumar, S., Singh, A. K., Krishnamoorthy, G. & Swaminathan, R. Thioflavin T displays enhanced fluorescence selectively inside anionic micelles and mammalian cells. *J. Fluoresc.* **18,** 1199–1205 (2008).

82. Howie, A. J., Brewer, D. B., Howell, D. & Jones, A. P. Physical basis of colors seen in Congo red-stained amyloid in polarized light. *Lab. Investig.* **88,** 232–242 (2008).

83. Sipe, J. D. & Cohen, A. S. Review: History of the Amyloid Fibril. *J. Struct. Biol.* **130,** 88–98 (2000).

84. Guijarro, J. I., Sunde, M., Jones, J. A., Campbell, I. D. & Dobson, C. M. Amyloid fibril formation by an SH3 domain. *Proc Natl Acad Sci USA* **95,** 4224–4228 (1998).

85. Chiti, F. *et al.* Designing conditions for in vitro formation of amyloid protofilaments and fibrils. *Proc. Natl. Acad. Sci. U. S. A.* **96,** 3590–4 (1999).

86. Dobson, C. M. Protein misfolding, evolution and disease. *Trends Biochem. Sci.* **24,** 329–332 (1999).

87. Balbirnie, M., Grothe, R. & Eisenberg, D. S. An amyloid-forming peptide from the yeast prion Sup35 reveals a dehydrated beta-sheet structure for amyloid. *Proc. Natl. Acad. Sci. U. S. A.* **98,** 2375–2380 (2001).

88. Nelson, R. *et al.* Structure of the cross-β spine of amyloid-like fibrils. *Nat. Cell Biol.* **435,** 773–778 (2005).

89. Sawaya, M. R. *et al.* Atomic structures of amyloid cross-beta spines reveal varied steric zippers. *Nature* **447,** 453–7 (2007).

90. Jansen, R., Grudzielanek, S., Dzwolak, W. & Winter, R. High pressure promotes circularly shaped insulin amyloid. *J. Mol. Biol.* **338,** 203–206 (2004).

91. Randolph, T. W., Seefeldt, M. & Carpenter, J. F. High hydrostatic pressure as a tool to study protein aggregation and amyloidosis. *Biochim. Biophys. Acta - Protein Struct. Mol. Enzymol.* **1595,** 224–234 (2002).

92. Trovato, A., Seno, F. & Tosatto, S. C. E. The PASTA server for protein aggregation prediction. *Protein Eng. Des. Sel.* **20,** 521–523 (2007).

93. Kallberg, Y., Gustafsson, M., Persson, B., Thyberg, J. & Johansson, J. Prediction of Amyloid Fibril-forming Proteins *. **276,** 12945–12950 (2001).

94. Tartaglia, G. G. *et al.* Prediction of Aggregation-Prone Regions in Structured Proteins. *J. Mol. Biol.* **380,** 425–436 (2008).

95. Pawar, A. P. *et al.* Prediction of ‘aggregation-prone’ and ‘aggregation- susceptible’ regions in proteins associated with neurodegenerative diseases. *J. Mol. Biol.* **350,** 379–392 (2005).

96. Varga, J., Flinn, M. S. M., Shirahama, T., Rodgers, O. G. & Cohen, A. S. The induction

of accelerated murine amyloid with human splenic extract - Probable role of amyloid enhancing factor. *Virchows Arch. B Cell Pathol. Incl. Mol. Pathol.* **51,** 177–185 (1986).

97. Ono, K., Takahashi, R., Ikeda, T. & Yamada, M. Cross-seeding effects of amyloid β-protein and α-synuclein. *J. Neurochem.* **122,** 883–890 (2012).

98. Meisl, G. *et al.* Molecular mechanisms of protein aggregation from global fitting of kinetic models. *Nat. Protoc.* **11,** 252–272 (2016).

99. Kashchiev, D. & van Rosmalen, G. M. Review: Nucleation in solutions revisited. *Cryst. Res. Technol.* **38,** 555–574 (2003).

100. Sear, R. P. Nucleation: theory and applications to protein solutions and colloidal suspensions. *J. Phys. Condens. Matter* **19,** 33101–28 (2007).

101. Schmelzer, J. W. P. *Nucleation Theory and Applications*. (Wiley, 2006).

102. Kalikmanov, V. *Nucleation Theory*. (Springer Netherlands, 2012).

103. Sear, R. P. Nucleation: theory and applications to protein solutions and colloidal suspensions. *J. Phys. Condens. Matter* **19,** 33101 (2007).

104. Wetzel, R. Kinetics and thermodynamics of amyloid fibril assembly. *Acc. Chem. Res.* **39,** 671–679 (2006).

105. Žerovnik, E. Amyloid-fibril formation: Proposed mechanisms and relevance to conformational disease. *European Journal of Biochemistry* **269,** 3362–3371 (2002).

106. Xue, W.-F., Homans, S. W. & Radford, S. E. Systematic analysis of nucleation-dependent polymerization reveals new insights into the mechanism of amyloid self-assembly. *Proc. Natl. Acad. Sci. U. S. A.* **105,** 8926–31 (2008).

107. Cohen, S. I. A. *et al.* Proliferation of amyloid-β42 aggregates occurs through a secondary nucleation mechanism. *Proc. Natl. Acad. Sci. U. S. A.* **110,** 9758–63 (2013).

108. Cohen, S. I. A., Vendruscolo, M., Dobson, C. M. & Knowles, T. P. J. From macroscopic measurements to microscopic mechanisms of protein aggregation. *J. Mol. Biol.* **421,** 160–171 (2012).

109. Morris, A. M., Watzky, M. A. & Finke, R. G. Protein aggregation kinetics, mechanism, and curve-fitting: a review of the literature. *Biochim. Biophys. Acta* **1794,** 375–97 (2009).

110. Walsh, D. M., Lomakin, A., Benedek, G. B., Condron, M. M. & Teplow, D. B. Amyloid β-Protein Fibrillogenesis. *J. Biol. Chem.* **272,** 22364–22372 (1997).

111. Kirkitadze, M. D., Condron, M. M. & Teplow, D. B. Identification and characterization of key kinetic intermediates in amyloid beta-protein fibrillogenesis. *J. Mol. Biol.* **312,** 1103–19 (2001).

112. Kelly, J. W. Mechanisms of amyloidogenesis. *Nat. Struct. Biol.* **7,** 824–826 (2000).

113. Serio, T. R. *et al.* Nucleated Conformational Conversion and the Replication of Conformational Information by a Prion Determinant. *Science (80-.).* **289,** 1317–1321 (2000).

114. Pallitto, M. M. & Murphy, R. M. A mathematical model of the kinetics of beta-amyloid fibril growth from the denatured state. *Biophys. J.* **81,** 1805–1822 (2001).

115. Giurleo, J. T., He, X. & Talaga, D. S. β-Lactoglobulin Assembles into Amyloid through Sequential Aggregated Intermediates. *J. Mol. Biol.* **381,** 1332–1348 (2008).

116. Hills, R. D. & Brooks, C. L. Hydrophobic Cooperativity as a Mechanism for Amyloid Nucleation. *J. Mol. Biol.* **368,** 894–901 (2007).

117. Armen, R. S., Bernard, B. M., Day, R., Alonso, D. O. V & Daggett, V. Characterization of a possible amyloidogenic precursor in glutamine-repeat neurodegenerative diseases. *Proc. Natl. Acad. Sci. U. S. A.* **102,** 13433–8 (2005).

118. Muta, H. *et al.* Supersaturation-limited Amyloid fibrillation of Insulin revealed by ultrasonication. *J. Biol. Chem.* **289,** 18228–18238 (2014).

119. So, M., Hall, D. & Goto, Y. Revisiting supersaturation as a factor determining amyloid fibrillation. *Curr. Opin. Struct. Biol.* **36,** 32–39 (2016).

120. Zhang, L. *et al.* Mapping hydration dynamics around a protein surface. *Proc. Natl. Acad. Sci. U. S. A.* **104,** 18461–6 (2007).

121. Dyson, H. J., Wright, P. E. & Scheraga, H. a. The role of hydrophobic interactions in initiation and propagation of protein folding. *Proc. Natl. Acad. Sci. U. S. A.* **103,** 13057–13061 (2006).

122. Lashuel, H. A., Wurth, C., Woo, L. & Kelly, J. W. The most pathogenic transthyretin variant, L55P, forms amyloid fibrils under acidic conditions and protofilaments under physiological conditions. *Biochemistry* **38,** 13560–13573 (1999).

123. Ivanova, M. I., Sievers, S. A., Sawaya, M. R., Wall, J. S. & Eisenberg, D. Molecular basis for insulin fibril assembly. *Proc. Natl. Acad. Sci.* **106,** 18990–18995 (2009).

124. Souillac, P. O. *et al.* Elucidation of the molecular mechanism during the early events in immunoglobulin light chain amyloid fibrillation. Evidence for an off-pathway oligomer at acidic pH. *J. Biol. Chem.* **277,** 12666–12679 (2002).

125. Hekstra, D. R. *et al.* Electric-field-stimulated protein mechanics. *Nature* **540,** 400–405 (2016).

126. Astumian, R. D. & Robertson, B. Nonlinear effect of an oscillating electric field on membrane proteins. *J. Chem. Phys.* **91,** 4891–4900 (1989).

127. Ball, P. & Hallsworth, J. E. Water structure and chaotropicity: their uses, abuses and biological implications. *Phys. Chem. Chem. Phys.* **17,** 8297–8305 (2015).

128. Collins, K. D. Ions from the Hofmeister series and osmolytes : e V ects on proteins in solution and in the crystallization process. **34,** 300–311 (2004).

129. Crowe, J. H. Trehalose as a 'chemical chaperone': Fact and fantasy. *Adv. Exp. Med. Biol.* **594,** 143–158 (2007).

130. Jayamani, J., Shanmugam, G., Ramaprasad, E. & Singam, A. Inhibition of insulin amyloid fibril formation by ferulic acid , a natural compound found in many vegetables and fruits. *RSC Adv.* **4,** 62326–62336 (2014).

131. Jaspe, J. & Hagen, S. J. Do protein molecules unfold in a simple shear flow? *Biophys. J.* **91,** 3415–3424 (2006).

132. Norde, W. Protein adsorption at solid surfaces: A thermodynamic approach. *Pure Appl. Chem.* (1994).

133. Mollmann, S. H. *et al.* Interfacial adsorption of insulin: Conformational changes and reversibility of adsorption. *Eur. J. Pharm. Sci.* **27,** 194–204 (2006).

134. Bauer, H. H., Muller, M., Goette, J., Merkle, H. P. & Fringeli, U. P. Interfacial

adsorption and aggregation associated changes in secondary structure of human calcitonin monitored by ATR-FTIR spectroscopy. *Biochemistry* **33,** 12276–12282 (1994).

135. Ball, V. *et al.* Kinetics of Exchange Processes in the Adsorption of Proteins on Solid Surfaces. *Proc. Natl. Acad. Sci. Nat. Acad. Sci. U.S.A.* **91,** 7330–7334 (1994).

136. Schladitz, C., Vieira, E. P., Hermel, H. & Mohwald, H. Amyloid-β-sheet formation at the air-water interface. *Biophys. J.* **77,** 3305–3310 (1999).

137. Holdgate, G. a. Thermodynamics of binding interactions in the rational drug design process. *Expert Opin. Drug Discov.* **2,** 1103–14 (2007).

138. Alexandrescu, A. T. Amyloid accomplices and enforcers. *Protein Sci.* **14,** 1–12 (2005).

139. Maynard, C. J., Bush, A. I., Masters, C. L., Cappai, R. & Li, Q.-X. Metals and amyloid-beta in Alzheimer's disease. *Int. J. Exp. Pathol.* **86,** 147–159 (2005).

140. Eury, H., Bijani, C., Faller, P. & Hureau, C. Copper(II) coordination to amyloid β: Murine versus human peptide. *Angew. Chemie - Int. Ed.* **50,** 901–905 (2011).

141. Hureau, C. Coordination of redox active metal ions to the amyloid precursor protein and to amyloid-β peptides involved in Alzheimer disease. Part 1: An overview. *Coord. Chem. Rev.* **256,** 2164–2174 (2012).

142. Alies, B. *et al.* Zinc(II) modulates specifically amyloid formation and structure in model peptides. *J. Biol. Inorg. Chem.* **16,** 333–340 (2011).

143. Ma, J., Yee, A., Brewer, H. B., Das, S. & Potter, H. Amyloid-associated proteins α1-antichymotrypsin and apolipoprotein E promote assembly of Alzheimer β-protein into filaments. *Nature* **372,** 92–94 (1994).

144. Eriksson, S., Janciauskiene, S. & Lannfelt, L. Alpha 1-antichymotrypsin regulates Alzheimer beta-amyloid peptide fibril formation. *Proc Natl Acad Sci U S A* **92,** 2313–2317 (1995).

145. Pallarès, I., Vendrell, J., Avilés, F. X. & Ventura, S. Amyloid fibril formation by a partially structured intermediate state of α-chymotrypsin. *J. Mol. Biol.* **342,** 321–331 (2004).

146. Wisniewski, T., Castaño, E. M., Golabek, A., Vogel, T. & Frangione, B. Acceleration of Alzheimer's fibril formation by apolipoprotein E in vitro. *Am. J. Pathol.* **145,** 1030–5 (1994).

147. Evans, K. C., Berger, E. P., Cho, C. G., Weisgraber, K. H. & Lansbury, P. T. Apolipoprotein E is a kinetic but not a thermodynamic inhibitor of amyloid formation: implications for the pathogenesis and treatment of Alzheimer disease. *Proc. Natl. Acad. Sci. U. S. A.* **92,** 763–7 (1995).

148. McLaurin, J., Yang, D., Yip, C. M. & Fraser, P. E. Review: modulating factors in amyloid-β fibril formation. *J Struct Biol* **130,** 259–270 (2000).

149. Mayer, J. P., Zhang, F. & DiMarchi, R. D. Insulin structure and function. *Biopolym. - Pept. Sci. Sect.* **88,** 687–713 (2007).

150. Treacy, G. B., Shaw, D. C., Griffiths, M. E. & Jeffrey, P. D. Purification of a marsupial insulin: amino-acid sequence of insulin from the Eastern grey kangaroo Macropus giganteus. *Biochim. Biophys. Acta - Gen. Subj.* **990,** 263–268 (1989).

151. Wintersteiner, O. & Abramson, a. Isoelectric Point of Insulin. *J. Biol. Chem.* **99,** 741–

753 (1933).

152. Frank, B. H., Pekar, A. H. & Veros, A. J. Insulin and Proinsulin Conformation in Solution. *Diabetes* **21,** 486–491 (1972).

153. Holladay, L. A., Ascoli, M. & Puett, D. Conformational stability and self-association of zinc-free bovine insulin at neutral pH. *BBA - Protein Struct.* **494,** 245–254 (1977).

154. Hvidt, S. Insulin association in neutral solutions studied by light scattering. *Biophys. Chem.* **39,** 205–213 (1991).

155. Waugh, D. F. A fibrous modification of insulin. I. The heat precipitate of insulin. *J. Am. Chem. Soc.* **68,** 247–50 (1946).

156. Waugh, D. F., Thompson, R. E. & Weimer, R. J. Assay of insulin in vitro by fibril elongation and precipitation. *J. Biol. Chem.* **185,** 85–95 (1950).

157. Garriques, L. N., Frokjaer, S., Carpenter, J. F. & Brange, J. The effect of mutations on the structure of insulin fibrils studied by Fourier transform infrared (FTIR) spectroscopy and electron microscopy. *J. Pharm. Sci.* **91,** 2473–2480 (2002).

158. Lee, C.-C., Nayak, A., Sethuraman, A., Belfort, G. & McRae, G. J. A three-stage kinetic model of amyloid fibrillation. *Biophys. J.* **92,** 3448–3458 (2007).

159. Vestergaard, B. *et al.* A helical structural nucleus is the primary elongating unit of insulin amyloid fibrils. *PLoS Biol.* **5,** 1089–1097 (2007).

160. Nielsen, L. *et al.* Effect of Environmental Factors on the Kinetics of Insulin Fibril Formation. *Biochemistry* **40,** 6036–6046 (2001).

161. Bouchard, M., Zurdo, J., Nettleton, E. J., Dobson, C. M. & Robinson, C. V. Formation of insulin amyloid fibrils followed by FTIR simultaneously with CD and electron microscopy. *Protein Sci.* **9,** 1960–1967 (2000).

162. Dutta, C., Yang, M., Long, F., Shahbazian-Yassar, R. & Tiwari, A. Preformed Seeds Modulate Native Insulin Aggregation Kinetics. *J. Phys. Chem. B* **119,** 15089–15099 (2015).

163. Jiménez, J. L. *et al.* The protofilament structure of insulin amyloid fibrils. *Proc. Natl. Acad. Sci. U. S. A.* **99,** 9196–201 (2002).

164. Mauro, M. *et al.* Kinetics of Different Processes in Human Insulin Amyloid Formation. *J. Mol. Biol.* **366,** 258–274 (2007).

165. Manno, M., Craparo, E. F., Martorana, V., Bulone, D. & San Biagio, P. L. Kinetics of insulin aggregation: disentanglement of amyloid fibrillation from large-size cluster formation. *Biophys. J.* **90,** 4585–4591 (2006).

166. Nayak, A., Dutta, A. K. & Belfort, G. Surface-enhanced nucleation of insulin amyloid fibrillation. *Biochem. Biophys. Res. Commun.* **369,** 303–7 (2008).

167. Waugh, D. A mechanism for the formation of fibrils from protein molecules. *J. Cell. Comp. Physiol.* 145–164 (1957). doi:10.1002/jcp.1030490415

168. Sefton, M. V. & Antonacci, G. M. Adsorption isotherms of insulin onto various materials. *Diabetes* **33,** 674–680 (1984).

169. Lougheed, W. D., Albisser, A. M., Martindale, H. M., Chow, J. C. & Clement, J. R. Physical stability of insulin formulations. *Diabetes* **32,** 424–432 (1983).

170. Feingold, V; Jenkins, A B; Kraegen, E. W. Effect of contact material on vibraction-

induced insulin aggregation. *Diabetologia* 373–378 (1984).

171. Sluzky, V., Tamada, J. a, Klibanov, a M. & Langer, R. Kinetics of insulin aggregation in aqueous solutions upon agitation in the presence of hydrophobic surfaces. *Proc. Natl. Acad. Sci. U. S. A.* **88,** 9377–81 (1991).

172. Irsigler, K. *et al.* Long-term continuous intraperitoneal insulin infusion with an implanted remote-controlled insulin infusion device. *Diabetes* **30,** 1072–1075 (1981).

173. Kritz, H., Hagmüller, G., Lovett, R. & Irsigler, K. Implanted constant basal rate insulin infusion devices for type 1 (Insulin-dependent) diabetic patients. *Diabetologia* **25,** 78–81 (1983).

174. Irsigler, K. & Kritz, H. Long-term continuous intravenous insulin therapy with a portable insulin dosage-regulating apparatus. *Diabetes* **28,** 196–203 (1979).

175. W.D., L. *et al.* Insulin aggregation in artificial delivery systems. *Diabetologia* **19,** 1–9 (1980).

176. Yeo, S. D., Debenedetti, P. G., Patro, S. Y. & Przybycien, T. M. Secondary structure characterization of microparticulate insulin powders. *J. Pharm. Sci.* **83,** 1651–1656 (1994).

177. Swift, B. & Hawkins, P. Examination of insulin injection sites: an unexpected finding of localized amyloidosis. *Diabet. Med.* 881–886 (2002).

178. Shikama, Y. *et al.* Localized Amyloidosis at the Site of Repeated Insulin Injection in a Diabetic Patient. *Intern. Med.* **49,** 397–401 (2010).

179. Grudzielanek, S. *et al.* Cytotoxicity of Insulin within its Self-assembly and Amyloidogenic Pathways. *J. Mol. Biol.* **370,** 372–384 (2007).

180. Sluzky, V., Klibanov, a M. & Langer, R. Mechanism of insulin aggregation and stabilization in agitated aqueous solutions. *Biotechnol. Bioeng.* **40,** 895–903 (1992).

181. Nault, L. *et al.* Human insulin adsorption kinetics, conformational changes and amyloidal aggregate formation on hydrophobic surfaces. *Acta Biomater.* **9,** 5070–9 (2013).

182. Mauri, S. *et al.* Bovine and human insulin adsorption at lipid monolayers: a comparison. *Front. Phys.* **3,** 1–6 (2015).

183. Mollmann, S. H. *et al.* Interfacial adsorption of insulin: Conformational changes and reversibility of adsorption. *Eur. J. Pharm. Sci.* **27,** 194–204 (2006).

184. Ballet, T. Stabilité des protéines thérapeutiques au contact des matériaux: Agrégation induite par les surfaces et détection des changements de conformation à l'aide de protéines chaperonnes. (2010).

185. Nault, L., Vendrely, C., Bréchet, Y., Bruckert, F. & Weidenhaupt, M. Peptides that form β-sheets on hydrophobic surfaces accelerate surface-induced insulin amyloidal aggregation. *FEBS Lett.* **587,** 1281–6 (2013).

186. Engelman, D. M., Steitz, T. A. & Goldman, A. Identifying nonpolar transbilayer helices in amino acid sequences of membrane proteins. *Annu. Rev. Biophys. Biophys. Chem.* **15,** 321–353 (1986).

187. LeVine, H. Quantification of β-sheet amyloid fibril structures with thioflavin T. *Methods Enzymol.* **309,** 274–284 (1999).

188. Pace, C. N. *et al.* How to measure and predict the molar absorption coefficient of a protein. *Protein Sci.* **4,** 2411–2423 (1995).

189. DeGrado, W. & Lear, J. Induction of peptide conformation at apolar water interfaces. 1. A study with model peptides of defined hydrophobic periodicity. *J. Am. Chem. Soc.* **107,** 7684–7689 (1985).

190. Khurana, R. & Fink, A. L. Do Parallel β-Helix Proteins Have a Unique Fourier Transform Infrared Spectrum? *Biophys. J.* **78,** 994–1000 (2000).

191. Cerf, E. *et al.* Antiparallel β-sheet: a signature structure of the oligomeric amyloid β-peptide. *Biochem. J.* **421,** 415–423 (2009).

192. Demirdöven, N. *et al.* Two-dimensional infrared spectroscopy of antiparallel beta-sheet secondary structure. *J. Am. Chem. Soc.* **126,** 7981–7990 (2004).

193. Dubey, R. C. *Advanced Biotechnology*. (S Chand, 2014).

194. Chouchane, K. *et al.* Dual Effect of (LK)nL Peptides on the Onset of Insulin Amyloid Fiber Formation at Hydrophobic Surfaces. *J. Phys. Chem. B* **119,** 10543–10553 (2015).

195. Sulatskaya, A. I., Kuznetsova, I. M. & Turoverov, K. K. Interaction of thioflavin T with amyloid fibrils: Stoichiometry and affinity of dye binding, absorption spectra of bound dye. *J. Phys. Chem. B* **115,** 11519–11524 (2011).

196. Frachon, T., Bruckert, F., Le Masne, Q., Monnin, E. & Weidenhaupt, M. Insulin aggregation at a dynamic solid-liquid-air triple interface. *Langmuir* acs.langmuir.6b03314 (2016). doi:10.1021/acs.langmuir.6b03314

197. Dathe, M., Gast, K., Zirwer, D., Welfle, H. & Mehlis, B. Insulin aggregation in solution. *Int. J. Pept. Protein Res.* **36,** 344–349 (1990).

198. Teoh, C. L. *et al.* Shear flow induced changes in apolipoprotein C-II conformation and amyloid fibril formation. *Biochemistry* **50,** 4046–4057 (2011).

199. Bekard, I. B. & Dunstan, D. E. Shear-Induced deformation of bovine insulin in couette flow. *J. Phys. Chem. B* **113,** 8453–8457 (2009).

200. McBride, S. A., Tilger, C. F., Sanford, S. P., Tessier, P. M. & Hirsa, A. H. Comparison of Human and Bovine Insulin Amyloidogenesis under Uniform Shear. *J. Phys. Chem. B* **119,** 10426–10433 (2015).

201. Nault, L. Mécanismes moléculaires de l'agrégation de l'insuline induite par la surface des matériaux. (2013).

202. Sprenger, K. G. & Pfaendtner, J. Strong Electrostatic Interactions Lead to Entropically Favorable Binding of Peptides to Charged Surfaces. *Langmuir* **32,** 5690–5701 (2016).

203. Pandey, L. M. *et al.* Surface chemistry at the nanometer scale influences insulin aggregation. *Colloids Surf. B. Biointerfaces* **100,** 69–76 (2012).

204. Dalgicdir, C., Globisch, C., Peter, C. & Sayar, M. Tipping the Scale from Disorder to Alpha-helix: Folding of Amphiphilic Peptides in the Presence of Macroscopic and Molecular Interfaces. *PLoS Comput. Biol.* **11,** 1–24 (2015).

205. Millican, R. L. & Brems, D. N. Equilibrium intermediates in the denaturation of human insulin and two monomeric insulin analogs. *Biochemistry* **33,** 1116–1124 (1994).

206. Chiang, H. L., Ngo, S. T., Chen, C. J., Hu, C. K. & Li, M. S. Oligomerization of Peptides LVEALYL and RGFFYT and Their Binding Affinity to Insulin. *PLoS One* **8,** (2013).

207. Brange, J., Andersen, L., Laursen, E. D., Meyn, G. & Rasmussen, E. Toward understanding insulin fibrillation. *J. Pharm. Sci.* **86,** 517–525 (1997).

208. Saha, S. & Deep, S. Glycerol inhibits the primary pathways and transforms the secondary pathway of insulin aggregation. *Phys. Chem. Chem. Phys.* **18,** 18934–18948 (2016).

209. Saha, S., Sharma, A. & Deep, S. Differential influence of additives on the various stages of insulin aggregation. *RSC Adv.* **6,** 28640–28652 (2016).

210. Belluti, F., Rampa, A., Gobbi, S. & Bisi, A. Small-molecule inhibitors/modulators of amyloid-β peptide aggregation and toxicity for the treatment of Alzheimer's disease: a patent review (2010 - 2012). *Expert Opin. Ther. Pat.* **23,** 581–96 (2013).

211. Ferreira, N. *et al.* Binding of epigallocatechin-3-gallate to transthyretin modulates its amyloidogenicity. *FEBS Lett.* **583,** 3569–3576 (2009).

212. Ferreira, N., Santos, S. A. O., Domingues, M. R. M., Saraiva, M. J. & Almeida, M. R. Dietary curcumin counteracts extracellular transthyretin deposition: Insights on the mechanism of amyloid inhibition. *Biochim. Biophys. Acta - Mol. Basis Dis.* **1832,** 39–45 (2013).

213. Hudson, S. A., Ecroyd, H., Kee, T. W. & Carver, J. A. The thioflavin T fluorescence assay for amyloid fibril detection can be biased by the presence of exogenous compounds. *FEBS J.* **276,** 5960–5972 (2009).

214. Necula, M., Kayed, R., Milton, S. & Glabe, C. G. Small molecule inhibitors of aggregation indicate that amyloid beta-oligomerization and fibrillization pathways are independent and distinct. *J. Biol. Chem.* **282,** 10311–10324 (2007).

215. Horvath, I. *et al.* Mechanisms of protein oligomerization: Inhibitor of functional amyloids templates α-synuclein fibrillation. *J. Am. Chem. Soc.* **134,** 3439–3444 (2012).

216. Ghosh, A. *et al.* Inhibition and Degradation of Amyloid Beta (Aβ40) Fibrillation by Designed Small Peptide: A Combined Spectroscopy, Microscopy, and Cell Toxicity Study. *ACS Chem. Neurosci.* **8,** 718–722 (2017).

217. Sievers, S. A. *et al.* Structure-based design of non-natural amino-acid inhibitors of amyloid fibril formation. *Nature* **475,** 96–100 (2011).

218. Soto, C., Kindy, M. S., Baumann, M. & Frangione, B. Inhibition of Alzheimer's Amyloidosis by Peptides That Prevent β-Sheet Conformation. *Biochem. Biophys. Res. Commun.* **226,** 672–680 (1996).

219. De Bona, P. *et al.* Design and synthesis of new trehalose-conjugated pentapeptides as inhibitors of Aβ(1-42) fibrillogenesis and toxicity. *J. Pept. Sci.* **15,** 220–228 (2009).

220. Viet, M. H., Ngo, S. T., Lam, N. S. & Li, M. S. Inhibition of aggregation of amyloid peptides by beta-sheet breaker peptides and their binding affinity. *J. Phys. Chem. B* **115,** 7433–7446 (2011).

221. Richman, M. *et al.* In vitro and mechanistic studies of an antiamyloidogenic self-assembled cyclic D, l-$α$-peptide architecture. *J. Am. Chem. Soc.* **135,** 3474–3484 (2013).

222. Tjernberg, L. O. *et al.* Arrest of beta-amyloid fibril formation by a pentapeptide ligand. *J. Biol. Chem.* **271,** 8545–8548 (1996).

223. Wälti, M. A. *et al.* Atomic-resolution structure of a disease-relevant Aβ(1-42) amyloid

fibril. *Proc. Natl. Acad. Sci. U. S. A.* **113,** E4976-84 (2016).

224. Pallitto, M. M., Ghanta, J., Heinzelman, P., Kiessling, L. L. & Murphy, R. M. Recognition sequence design for peptidly modulators of ß-amyloid aggregation and toxicity. *Biochemistry* **38,** 3570–3578 (1999).

225. Lowe, T. L., Strzelec, A., Kiessling, L. L. & Murphy, R. M. Structure - Function relationships for inhibitors of beta-Amyloid toxicity containing the recognition sequence KLVFF. *Biochemistry* **40,** 7882–7889 (2001).

226. Chabry, J., Caughey, B. & Chesebro, B. Specific inhibition of in vitro formation of protease-resistant prion protein by synthetic peptides. *J Biol Chem* **273,** 13203–13207 (1998).

227. Nyström, S. & Hammarström, P. Generic amyloidogenicity of mammalian prion proteins from species susceptible and resistant to prions. *Sci. Rep.* **5,** 10101 (2015).

228. Kapurniotu, A., Schmauder, A. & Tenidis, K. Structure-based design and study of non-amyloidogenic, double N-methylated IAPP amyloid core sequences as inhibitors of IAPP amyloid formation and cytotoxicity. *J. Mol. Biol.* **315,** 339–350 (2002).

229. Govorunova, E. G., Sineshchekov, O. A., Li, H. & Spudich, J. L. Microbial Rhodopsins: Diversity, Mechanisms, and Optogenetic Applications. *Annu. Rev. Biochem.* **86,** 15–31 (2017).

230. Khan, S. & Newaz, G. A comprehensive review of surface modification for neural cell adhesion and patterning. *J Biomed Mater Res A* **93,** 1209–1224 (2010).

231. Zhu, H. & Snyder, M. Protein arrays and microarrays. *Current Opinion in Chemical Biology* **5,** 40–45 (2001).

232. Roda, A., Guardigli, M., Russo, C., Pasini, P. & Baraldini, M. Protein microdeposition using a conventional ink-jet printer. *Biotechniques* **28,** 492–496 (2000).

233. Nishimura, T. *et al.* A Light Sensitive Self-Assembled Nanogel as a Tecton for Protein Patterning Materials. *Chem. Commun.* **52,** 1222–1225 (2015).

234. Grunwald, C. *et al.* In situ assembly of macromolecular complexes triggered by light. *Proc. Natl. Acad. Sci. U. S. A.* **107,** 6146–6151 (2010).

235. DeForest, C. A. & Tirrell, D. A. A photoreversible protein-patterning approach for guiding stem cell fate in three-dimensional gels. *Nat. Mater.* **14,** 523–531 (2015).

236. Duffy, C. D. P., Valkunas, L., Ruban, A. V, Valkūnas, L. & Ruban, A. V. Light-harvesting processes in the dynamic photosynthetic antenna. *Phys. Chem. Chem. Phys.* **15,** 18752–70 (2013).

237. Hernández-Jiménez, J. *et al.* The Effects of Light-Accelerated Degradation on the Aggregation of Marketed Therapeutic Monoclonal Antibodies Evaluated by Size-Exclusion Chromatography with Diode Array Detection. *J. Pharm. Sci.* **105,** 1405–1418 (2016).

238. Mizuno, H. *et al.* Photo-induced peptide cleavage in the green-to-red conversion of a fluorescent protein. *Mol. Cell* **12,** 1051–1058 (2003).

239. Ando, R., Hama, H., Yamamoto-Hino, M., Mizuno, H. & Miyawaki, A. An optical marker based on the UV-induced green-to-red photoconversion of a fluorescent protein. *Proc. Natl. Acad. Sci. U. S. A.* **99,** 12651–12656 (2002).

240. Okada, T. *et al.* The retinal conformation and its environment in rhodopsin in light of a

new 2.2 Å crystal structure. *J. Mol. Biol.* **342,** 571–583 (2004).

241. Zayner, J. P. & Sosnick, T. R. Factors that control the chemistry of the LOV domain photocycle. *PLoS One* **9,** (2014).

242. Renicke, C., Schuster, D., Usherenko, S., Essen, L. O. & Taxis, C. A LOV2 domain-based optogenetic tool to control protein degradation and cellular function. *Chem. Biol.* **20,** 619–626 (2013).

243. Morikawa, M. *et al.* Formation of a flavin-linked cysteine. *Proc. 17th Int. Electron. Conf. Synth. Org. Chem.* b002 (2013). doi:10.3390/ecsoc-17-b002

French summary

1 Introduction

1.1 Introduction générale

Avant les années 1980, l'unique manière d'obtenir des protéines était l'extraction à partir d'organismes vivant. La biotechnologie offre désormais des possibilités de produire purifier et modifier les protéines à grande échelle ce qui bénéficie grandement à la recherche et aux industries pharmaceutiques. Le développement des protéines thérapeutiques met à la disposition des patients de nouveaux traitements présentant une efficacité augmentée ainsi que des effets secondaires réduits. La stabilité et l'agrégation des protéines et de leur agrégation sont des problématiques complexes qui préoccupent de nombreux domaines scientifiques, industriels et médicaux. Si le cout des protéines recombinantes a été considérablement réduit, leur valeur reste encore très élevée justifiant pleinement les besoins en termes de minimisation des pertes au cours des procédés de production et de formulation. Mais les études de l'agrégation des protéines in vitro ne permettent pas seulement de comprendre et d'augmenter la stabilité des protéines thérapeutiques, c'est également une précieuse source d'information pour comprendre les phénomènes plus complexe d'agrégation in vivo qui sont impliquées dans un certain nombre de pathologies humaines.

Cette thèse s'intéresse en particulier à l'agrégation de l'insuline humaine induite par la surface des matériaux. Cette molécule est un modèle de premier plan d'une part du fait de sa considérable valeur thérapeutique mais également du fait de l'abondance de littérature scientifique disponible sur ses mécanismes d'agrégation et de l'intérêt possible de l'exploitation de ses fibrilles pour la nanotechnologie.[1]

1.2 Les protéines: prolégomènes

1.2.1 Acides aminés et peptides

Les acides aminés sont des molécules organiques possédant à la fois un groupe acide carboxylique et un groupe amine, le premier servant de référence pour la dénomination des carbones de la chaine principale. Le premier carbone attaché à l'acide carboxylique est donc appelé le carbone alpha, le second : carbone beta et ainsi de suite. Les acides aminés protéogènes possédant une fonction amine sur leur carbone alpha ils sont dénommé acides alpha aminées. Ce carbone alpha est un centre stéréogène chez tous les acides protéogènes excepté la glycine, ces acides aminées existent donc sous deux énantiomère nommé par convention L ou D par analogie avec l'énantiomère levrorotatoire ou dextrorotatoire du glycéraldéhyde.

(Chem. Eq. I)

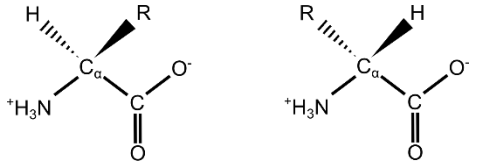

L amino acid D amino acid

Ce système est plus pertinent en biologie que les règles de Cahn–Ingold–Prelog associant des priorités aux groupe chimiques sur la base de leurs numéros atomiques et donc associe à la cystéine et la sélénocystéine une conformation (R) différente des autres acides aminées (S)[2]. Seul les énantiomère L peuvent être insérés dans les protéines, des acides aminés D peuvent cependant être formés par des modifications post-traductionnelles[3].

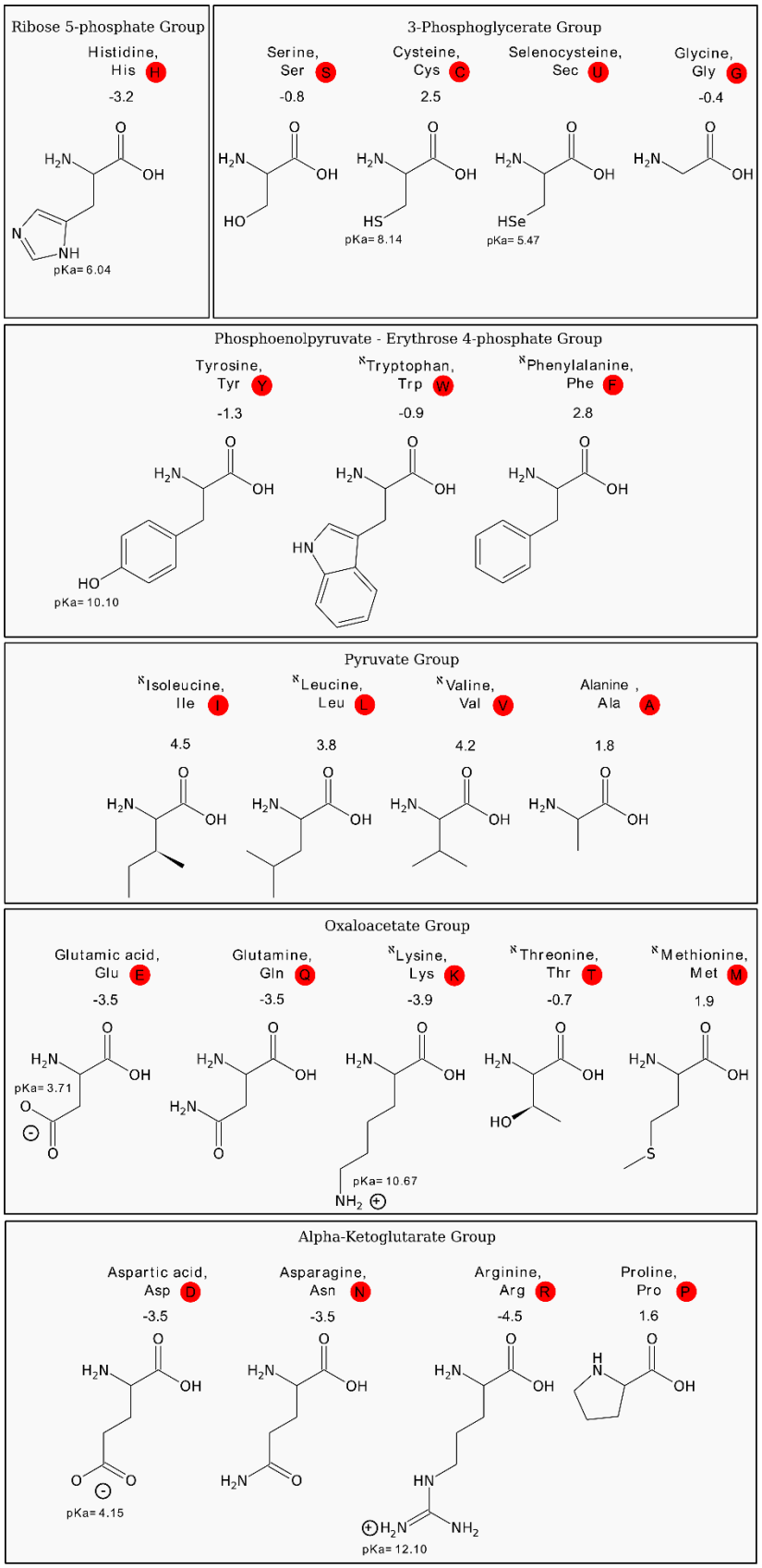

Figure 1. les 21 acides aminées proteinogenes. Ordonées selon leur voie anabolique chez les animaux avec une mention de leur indice d'hydrophobicité[4], du pKa de leur chaines latérale, ϰ:acide aminé essentiel chez *Homo sapiens*[5]**.**

Les acides aminés sont impliqués in vivo dans une grande diversité de fonctions biologiques (neurotransmetteurs, toxines[6], métabolisme de l'azote, etc.) et constituent les éléments de base pour la synthèse des protéines via la formation d'une liaison peptidique. Cette liaison peptidique consiste en la condensation du groupe carboxyle de l'acide aminé n avec un groupe amine de l'acide aminé n+1 libérant une molécule d'H2O et formant une liaison covalente :

(Chem. Eq. II)

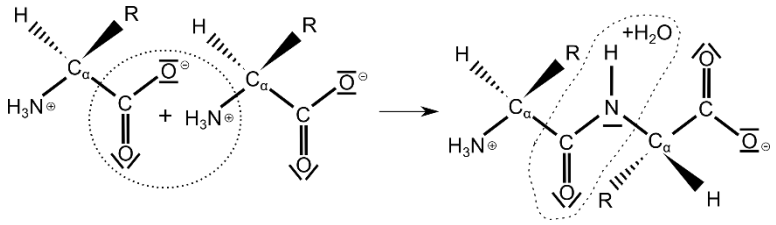

La chaine hétéropolymérique d'acide amine résultante est appelée un peptide. La diversité de peptides issue de la combinaison de multiples acides aminés leur permet d'assurer une diversité de fonctions biologiques (toxines, paroi cellulaire, hormone, neurotransmetteur, etc.).

La formation d'une liaison peptidique est défavorisée thermodynamiquement et est spontanément hydrolysée même si la vitesse de réaction est extrêmement réduite dans des conditions physiologiques. Chez les organismes vivants les peptides peuvent être synthétisées de multiples manière habituellement classifiées en tant que voies ribosomales et voies non ribosomales. Mais les peptides peuvent aussi être synthétisés in vitro, particulièrement grâce à la synthèse en phase solide[7], ce qui permet la conception de peptides spécifique en vue d'applications scientifiques ou industrielles.

1.2.2 Description et structure des protéines

Les protéines sont des macromolécules biologiques, qui consistent en au moins en une chaine linéaire et hétéropolymérique d'acides L- α-aminés liée par des liaisons peptidiques. Elle sont synthétisées in vivo par les ribosomes[5,8] à partir les 21 acides aminées protéogènes (22 si on inclus la Pyrrolysine limitée à certaine eubactéries et achées méthanogènes ou 23 en incluant la N-Formylmethionine) qui sont représentées Figure 1. La structure des protéines peut être décrite à 4 différents niveaux. La structure primaire consiste en la séquence brute d'acides aminés qui est écrite par convention du N-terminal au C-terminal ce qui correspond à l'ordre de traduction de la protéine. La structure secondaire consiste en l'arrangement des angles dièdre entre les atomes de la chaine principale. Pour chaque résidu on peut définir 3 angles φ, ψ et ω (sauf l'acide aminé C-terminal qui ne possède pas d'angle dièdre ω) [9]. La liaison peptidique est plane en raison de sa stabilisation par mesmérisme provenant de la délocalisation des doublets non liant de l'atome d'azote :

(Chem. Eq. III)

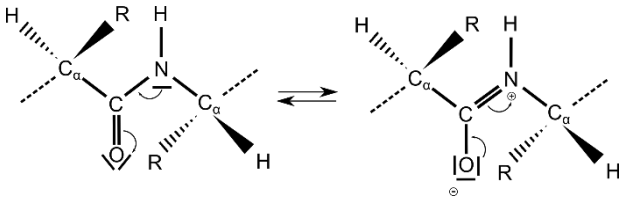

En conséquence la rotation de cette liaison n'est pas libre mais alterne entre une conformation cis (ω =0°) et trans (ω =180°). En revanche les angles φ et ψ ne sont pas fixe et peuvent adopter une valeur préférentielle. Un diagramme de Ramachandran[10] représente la distribution des combinaison d'angle φ et ψ adoptées par chaque acide aminé dans la structure des protéines(Figure 2).

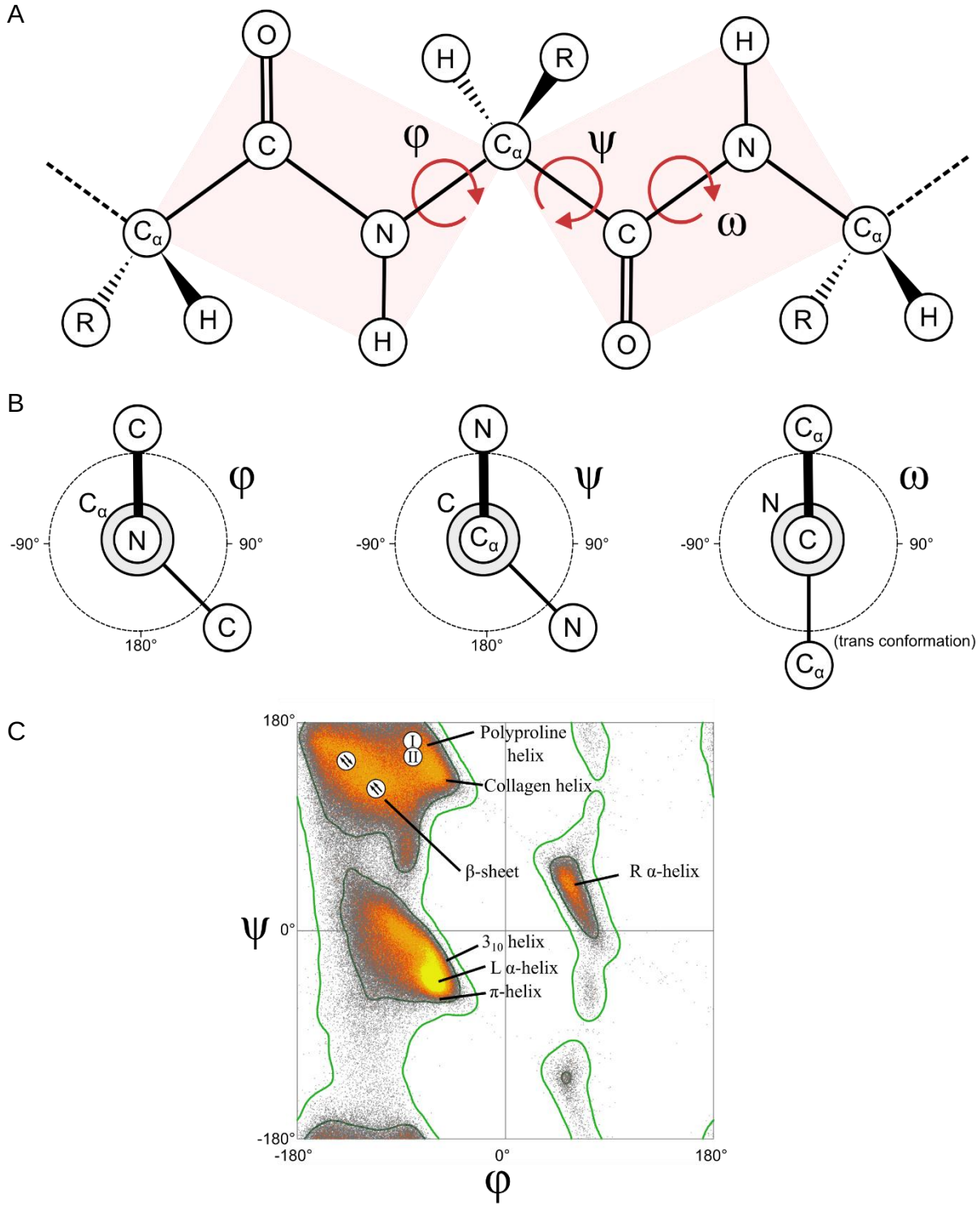

Figure 2. Principe de la structure secondaire des proteines. A: Definition des axes de rotation pour les angles dièdre φ, ψ et ω; B: Convention habituellement utilisé pour les valeurs des angle φ, ψ et ω, C: Diagramme de Ramachandran montrant les domaines spécifiques de structure secondaire: feuillet β parallèle (II), feuillet β antiparallele (II),Hélice de polyproline I (I), hélice de polyproline II (II). Pour les feuillets α les angles dièdresthe ne sont pas constant mais alternent entre hélice α R et hélice α D (C: Modifiée à partir de Jane S. Richardson, Proteopedia url: http://proteopedia.org/wiki/index.php/Ramachandran_Plots).

Les deux structures secondaires les plus fréquemment observées sont l'hélice alpha et le feuillet béta qui sont représentées Figure 3. Dans une hélice alpha la chaine principale forme une hélice comprenant 3.6 acides aminé par tour, avec toutes les chaines latérales exposées vers l'extérieur. Cette structure est stabilisée par la formation d'une liaison hydrogène entre le groupement C=O de l'acide aminé i et le groupe N-H de l'acide aminé i+4 ($N_{i+4} \rightarrow O_i$). Selon la nomenclature R_h des hélices où R est le nombre de résidus par tour et h est le nombre d'atomes dans l'anneau par les atomes autour de chaque liaison hydrogène, ce motif est appelé une hélice 3.6_{13}. D'autres motifs en hélice moins communs dans la structure des protéines incluent l'hélice 3_{10} et l'hélice π (ou hélice 4.4_{16}) ces motifs de liaisons hydrogènes respectivement en $N_{i+3} \rightarrow O_i$ et en $N_{i+5} \rightarrow O_i$. Les contraintes stériques imposées par les chaines latérales imposent un pas gauche aux hélices alpha, excepté les hélices de polyglycine qui peuvent parfois adopter un pas droit.

Dans les feuillets béta la chaine principale forme une structure plane avec les chaines latérales exposées alternativement vers la face supérieure et vers la face inferieure ce qui correspond approximativement à un angle de 180° entre l'orientation de la chaine latérale d'un résidu et celle de l'acide aminé suivant. Ce motif est stabilisé latéralement par la formation d'une liaison hydrogène perpendiculaire à la chaine latérale entre deux brins β. La structure formée par cet assemblage de brin β est appelée un feuillet β. Puisque les différents brins constituant un feuillet β peuvent appartenir à deux parties distantes de la chaine peptidique ou même à des chaines peptidiques différentes (par exemple un feuillet béta intermoléculaire), l'orientation $N_{term} \rightarrow C_{term}$ de deux brin adjacents peut être soit identique (feuillet β parallèle) soit dans des directions opposées (feuillet β antiparallèle). En conséquence la distribution des liaisons hydrogènes peut-être soit régulière (chaque acide aminé est lié à un unique autre acide aminé de la chaine opposé) dans le cas d'un feuillet β antiparallèle soit en quinconce dans le cas d'un feuillet β parallèle (chaque acide aminé est lié à deux acides aminés de la chaine opposée).

Un autre type de feuillet atypique et énergétiquement défavorisé mérite ici une description particulière : le feuillet alpha consiste en un assemblage de brins similaire aux brins β mais dans les quels tous les groupements C=O sont exposées dans la même direction avec les groupements N-H dans la direction opposée ce qui induit une polarité du feuillet. Bien que très rarement observée dans les protéines natives les feuillets alpha ont été proposés en tant que conformation intermédiaire entre les hélices alpha et les feuillets béta dans les processus d'amyloidogenèse et est observée dans la structure native du lysozyme de blanc d'œuf de poule[11] (la forme réduite de cette protéines peu former des fibres amyloïdes et des protéines homologues sont amyloidogène).

Il existe d'autres structures secondaires plus spécifiques ou locales tell que les tours, les hélices de polyproline I et II et leur analogue en polyglycine. Les motifs secondaires peuvent également s'assembler en structure super secondaire tell que les hélices béta ou les superhélices.

La structure tertiaire représente la structure tridimensionnelle de la protéine incluant les orientations des chaines latérales et les arrangements en domaines structuraux. Enfin, les protéines fonctionnelles consistent fréquemment en un assemblage de sous unités protéiques qui définissent la structure quaternaire.

1.2.3 Les protéines dans un contexte biologique

Les protéines sont la principale classe de macromolécules biologiquement actives et jouent un nombre important de rôles in vivo (structuraux, régulateurs, transports, signalisation, moteurs, catalytiques, etc.[12]). Elles sont avec les ribosomes la seule classe de molécules biologique capable de biocatalyse (enzymes), elles forment le cytosquelette et la matrice extracellulaire

(animale) ainsi que les transporteurs membranaires. Chez les eucaryotes, les gènes encodés dans l'ADN nucléaire sont transcrit en ARN messagers qui sont ensuite exporté via les pores nucléaires du noyau vers le cytoplasme ou ils sont ensuite traduits en protéines par les ribosomes. Les modifications post-traductionnelles sont toutes les modifications chimiques subies par les protéines après leurs traductions. Elles peuvent en particulier affecter la séquence par clivage de la chaine peptidique (en particulier les peptides signaux), des modifications des acides aminés, la formation de ponts disulfures, etc.

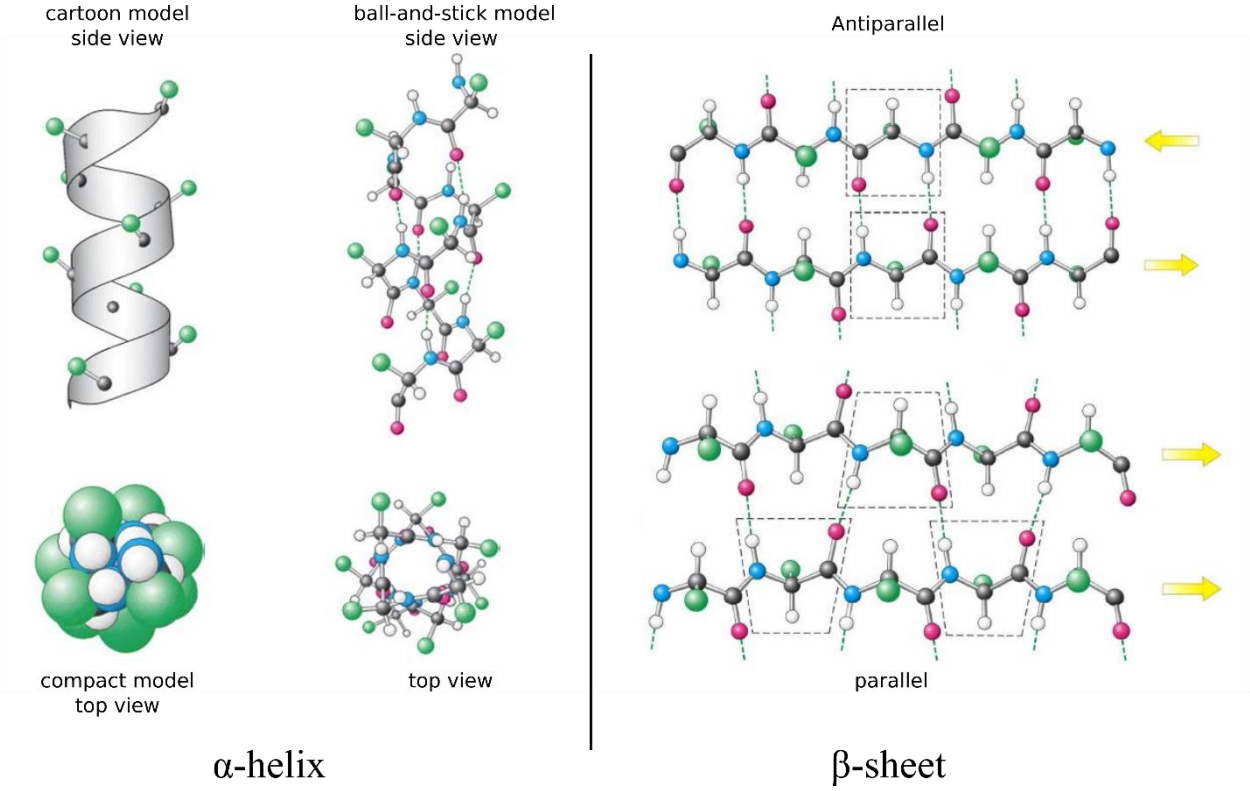

Figure 3. Structure de l'hélice α et du feuillet β. Coloration des atomes selon la convention cpk (figure modifié depuis Berg et al.[13]).

1.2.4 Protéines en solution

Les comportements des protéines en solution peuvent être affectées par les conditions physicochimiques de la solution (température, pH, force ionique, etc.). Les macromolécules en solution diffusent en marche aléatoire par mouvement Brownien[14]. La loi de Fick décrit le flux d'un soluté possédant une concentration locale φ par

$$\vec{J} = -D \cdot \nabla\varphi$$

Avec D la diffusivité du soluté. L'équation de Stokes–Einstein définie la diffusivité pour une particule sphérique dans un liquide de bas nombre de Reynolds par :

$$D = \frac{k_b T}{6\pi\mu r}$$

Avec $\mathbf{k_b}$ la constante de Boltzmann, **T** la température, **μ** la viscosité dynamique et **r** le rayon de la particule.

La diffusivité définit la vitesse à laquelle une molécule peu interagir avec d'autres molécules en solution. L'assemblement de protéines peu mener à la formation de complexe présentant un haut poids moléculaire, si le mouvement brownien ne suffit plus à maintenir ces oligomères en solution ils sédimentent.

A forte concentration de protéine (typiquement les concentrations observées dans les cellules vivantes ∽ 300 mg/ml)[15], le volume d'exclusion élevé de la solution entraine une réduction du volume accessible à une protéine et, en conséquence, augmente leur activité thermodynamique*. Ce phénomène porte le nom de *crowding* macromoléculaire. Ces conditions sont rencontrées dans les cellules vivantes et peuvent en particulier favoriser l'agrégation des protéines[16–19].

1.3 Repliement des protéines

1.3.1 Interactions non covalentes

En solution, les groupements chimiques des chaines latérales et des chaines principales d'une protéine sont sujets à des interactions intramoléculaire et intermoléculaire non covalentes. Ces interactions peuvent être électrostatique, stérique ou des effets émergeant des propriétés de la solution. Une interaction peut être définie par une énergie et par la manière dont cette énergie varie en fonction de la distance séparant les deux atomes concernés[20].

Force et énergie d'interactions

Le travail (W en J) d'une force ($\vec{F}$ en N) appliquée à un objet correspond à la contribution de cette force au déplacement de cet objet.

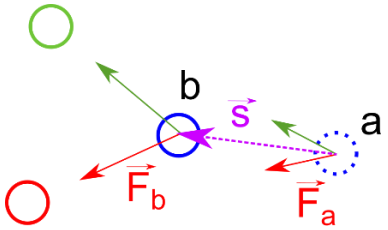

Figure 4. Scheme of the forces exerted by a green and a red particle on a blue particle throughout its displacement $\vec{s}$ from the point a to the point b. $\vec{F}_a$ and $\vec{F}_b$ represent the force exerted by the red particle on the blue particle at the position a and b, respectively.

Sur l'exemple présenté Figure 4, le travail exercé par la particule rouge sur la particule bleu durant son déplacement du point a au point b corresponds au produit scalaire de la force par le vecteur infinitésimal de déplacement (en m) intégré sur l'intégralité du déplacement :

$$W_{rouge\ sur\ bleue} = \int_a^b \vec{F}_i \cdot d\vec{s}$$

L'énergie (en J) de l'interaction particule rouge-particule bleu correspond à la quantité de travail de la force $\vec{F}$ pour un déplacement de l'infinité au point b :

$$E_{rouge-bleue} = \int_\infty^b \vec{F}_i \cdot d\vec{s}$$

L'énergie totale de l'interaction représentée Figure 4 correspond donc à la quantité de travail nécessaire pour déplacer la particule bleu du point b à l'infini étant donné le présent champ de force :

$$E_{tot} = E_{rouge-bleue} + E_{verte-bleue} = \int_\infty^b \vec{F}_i \cdot d\vec{s} + \int_\infty^b \vec{F}_i' \cdot d\vec{s}$$

* **Thermodynamic activity:** Effective concentration of a chemical species in solution

Le champ de force d'un système définit donc son état énergétique.

Fonctions d'état

Une fonction d'état représente une propriété d'un système qui est indépendante de la voie par laquelle le système a accédé à son état actuel. Ici nous allons brièvement passer en revue 4 fonctions d'états d'intérêt pour la thermodynamique du repliement des protéines : l'énergie interne, l'enthalpie, entropie et l'énergie libre de Gibbs.

La variation d'énergie interne (**ΔU**) d'un système est la différence entre la chaleur (Q) absorbée par ce système et le travail (W) fournit par ce système :

$$\Delta U = Q - W$$

Toutes les quantités sont exprimées en J. U est une fonction d'état de l'énergie contenue dans le système, en particulier de l'énergie définie par les champs de forces internes mais pas l'énergie définie par les champs de forces extérieur au système ni l'énergie cinétique du système.

Une autre fonction d'état, l'enthalpie (H exprimé en J) est définie par :

$$H = U + PV$$

Avec P la pression en $J.m^{-3}$ et V le volume du système en m^3.

L'entropie S qui n'est pas exprimée en joules mais en $J.K^{-1}$ est une fonction d'état reliée au nombre de configuration accessible pour un système dans un état donné :

$$S = k_B \cdot \ln(\Omega)$$

Avec **Ω** le nombre d'états équiprobable et $\mathbf{k_{B\ la}}$ constante de Boltzmann en $J.K^{-1}$.

En thermodynamique une question fondamentale est la spontanéité d'un procédé chimique dans des conditions données, c'est la variation d'énergie libre de Gibbs (G) qui permet de répondre à cette question elle est définie par :

$$G = \mathrm{H} - \mathrm{T\,S}$$

La variation d'énergie libre de Gibbs correspond à la variation d'énergie au cours d'une transformation à température et pression constante ce qui est relativement approprié pour les systèmes biologiques. Cette variation correspond à :

$$\Delta G = \Delta\mathrm{H} - \mathrm{T}\,\Delta S$$

Avec ΔH la variation d'enthalpie (en J), ΔS est la variation d'entropie (en $J.K^{-1}$) et T la température absolue en K. un **ΔG** négatif est nécessaire pour une transformation spontanée à pression et température constante.

Interactions électrostatiques

Les interactions électrostatiques sont une des 4 interactions fondamentales. La loi de coulomb décrit les forces entre deux charges statique par :

$$\overrightarrow{\mathrm{F}_{ij}} = \frac{1}{4\pi\varepsilon_0}\frac{Z_i \cdot Z_j}{r^2}\vec{r}$$

Où $\overrightarrow{\mathbf{F_{ij}}}$ est la force électrostatique d'une particule chargée i possédant une charge $\boldsymbol{Z_i}$ sur une particule chargée J présentant une charge $\boldsymbol{Z_j}$, $\boldsymbol{\varepsilon_0}$ est la permittivité du vide. La quantité de travail nécessaire pour amener la particule chargée de l'infinité au point r est l'énergie de l'interaction.

Les interactions électrostatiques incluent les liaisons hydrogènes (en partie), les interactions charge-charge, les interactions charge-dipôle induit, le π–π stacking et les interactions de Van Der Waals. Les interactions de Van Der Waals incluent les interactions dipôle-dipôle, les interactions dipôle-dipôle induit et les forces de dispersion de London.

Les liaisons hydrogènes sont un type particulier d'interaction dipôle-dipôle entre un groupe donneur et un groupe accepteur dans lequel l'énergie de liaison est principalement le résultat d'une interaction électrostatique mais également dans une moindre mesure (typiquement 10% de l'énergie totale), du partage de l'atome d'hydrogène[21]. Le groupe donneur consiste dans un atome d'hydrogène lié de manière covalente à un atome électronégatif (typiquement un oxygène ou un azote dans les macromolécules biologiques) et le groupe accepteur est un autre atome électronégatif. L'énergie mise en jeu dans une liaison hydrogène est d'autant plus forte que la distance entre les deux groupe est courte, cette distance peut être inférieure à la somme du rayon de Van Der Waals des deux atomes. Dans les protéines, l'énergie d'interaction des liaisons hydrogène est comprise entre 1 et 5 kcal.mol^{-1}.

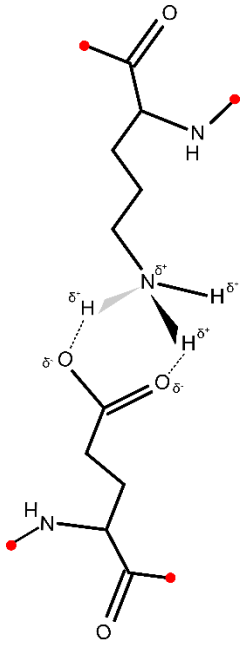

Figure 5. Pont salin entre un résidu glutamate et un résidu lysine. Les charges globales (respectivment -1 et +1) des deux groupes chargés sont dristibués en tant que charge partiel entre les différents atomes menant à la formation de liaison hydrogène et d'interactions electrostatique entre charges partielles opposées. Les point rouges corespondent au reste de la chaine peptidique.

Les ponts salins sont un autre type de liaisons présentes dans les protéines qui impliquent une combinaison de liaison hydrogène et d'interaction électrostatique entre charge (ou charges partielles) opposées. Un exemple typique est l'interaction entre un groupe amine primaire et un groupe carboxylate (Figure 5). Premièrement les charges globales opposées des deux groupes permettent une interaction électrostatique à distance, le pont est ensuite stabilisé à courte distance par une ou plusieurs liaison hydrogène.

	Interaction	Energie	Ordre de grandeur (kcal.mol^{-1})
	Ion-ion	$E \propto \frac{Z_i \cdot Z_j}{\varepsilon r}$	10-100
	Ion- dipôle induit	$E \propto \frac{Z_i \cdot \alpha_j}{\varepsilon r^4}$	1-10
Van Der Waals	Dipôle-Dipôle (Keesom)	$E \propto \frac{\mu_i \cdot \mu_j}{\varepsilon r^6}$	1
	Dipôle-dipôle induit (Debye)	$E \propto \frac{\mu_i \cdot \alpha_j}{\varepsilon r^6}$	1
	Dispersion (London)	$E \propto \frac{\alpha_i \cdot \alpha_j}{\varepsilon r^6}$	1

Table 1. Ordre de grandeur et variation en fonction de la distance de l'energie des interactions electrostatiques. Avec Z_i et Z_j la charge permanente des particules i et j; μ_i et μ_j les charges partielles des particules i et j; α_i and α_j la polarizabilité des particule i et j ; ε est la permitivité du vide ; E l'energie de l'interaction et r la distance interparticule.

Effet stérique

Les effets stériques proviennent d'une superposition des orbitales électroniques de deux atomes. Puisque les électrons sont des fermions, ils obéissent au principe d'exclusion de Pauli. Chaque atome occupant son propre volume d'espace repousse donc les autres atomes à courte distance de manière à réduire les conflits de superposition de leurs orbitales électroniques.

Interactions avec le solvant et effet hydrophobes

Puisque l'eau est un solvant polaire, les molécules d'eau interagissent avec l'une l'autre via la formation de liaisons hydrogènes, expliquant leurs forte cohésion. De même les groupements polaires des macromolécules créent des interactions électrostatiques avec les molécules environnantes qui vont augmenter sa solvatation. La couche de solvatation ou couche d'hydratation d'une macromolécule représente l'ensemble des molécules d'eau impliquée dans l'interface aqueuse avec cette macromolécule.

D'autre part les groupements apolaires ne forment pas d'interactions d'haute énergie avec cette interface aqueuse et vont donc en conséquence tendre à réduire leurs contacts avec cette couche de solvatation. En plus des effets enthalpiques qui résultent de la cohésion du liquide, la réduction de l'entropie associée à la perte de dégrées de libertés pour les molécules d'eau de la couche d'hydratation a été avancée comme une source majeur de l'effet hydrophobe [22]. En effet l'absence de liaisons hydrogènes entre les molécules d'eau et les groupements apolaires d'une macromolécule en solution implique une réduction du nombre d'orientation possible pour les molécules d'eau et donc une perte d'entropie [23].

Les groupements, domaines, molécules ou surfaces avec lesquelles l'eau tend à minimiser les contacts sont désigné comme hydrophobes ; par opposition les molécules chargées ou polaire qui forment des interactions plus énergétiques avec les molécules d'eau sont dénommé hydrophiles.

Dans les conformations natives des protéines les chaines latérales apolaires ont donc tendance à être enfouies au cœur de la structure afin de minimiser leur interaction avec la solution, ce qui aboutit généralement à la formation d'un cœur hydrophobe. La tension interfaciale ou

tension épistructurale dans le cas spécifique des macromolécules, est définie comme le changement d'énergie libre par unité de surface nécessaire pour envelopper une macromolécule de sa couche de solvatation. Le calcul de la tension épistructurale de la surface d'une structure de protéine peut apporter de précieuses informations pour l'identification de sites de liaison ou d'interaction [24].

Un autre bénéfice de la déshydratation est la protection des interactions électrostatiques de l'écrantage quelles subissent en solution, l'énergie impliquée dans les interaction électrostatique est donc significativement plus élevé dans un environnement anhydre [25–27]

Les concepts de « *protein wrapping* » (ang. Recouvrement de protéine) et de dehydron sont particulièrement intéressant pour la compréhension et la prédiction des interactions intermoléculaires. Un dehydron est une liaison hydrogène d'une protéine partiellement exposée au solvant (incomplètement recouverte), en conséquence cette région aura tendance à lier des ligands afin d'accroitre son recouvrement et donc de minimiser son énergie libre [28].

1.3.2 Conformation des protéines

La conformation des protéines dépend des conditions physicochimiques de leur environnement, leurs groupes fonctionnels interagissant entre eux ainsi qu'avec la solution. La stabilité structurelle d'une protéine est donc définie par l'énergie impliquée dans ses interactions internes ainsi que l'énergie impliquée dans les interactions protéine-solvant. De plus le nombre de ponts disulfures a une grande influence sur la stabilité conformationnelle d'une protéine. Les protéines avec une grande stabilité conformationnelle sont appelées *hard proteins* (ang. « Protéines dures ») alors que les protéines facilement déformables par contact intermoléculaire ou par adoption sont appelée *soft protéins* (ang. « Protéine molles ») [29].

1.3.3 Paysage énergétique et repliement natif : le dogme d'Anfinsen et le paradoxe de Levinthal

On peut représenter l'enthalpie d'une protéine (soit son nombre de conformations accessibles) pour un niveau d'énergie donnée comme un paysage énergétique[30] (Figure 6). Dans cette représentation le nombre de conformation accessible pour une protéine diminue à mesure que le niveau énergétique baisse et ces différentes conformations deviennent séparées par d'importantes barrières énergétiques. Selon l'hypothèse thermodynamique d'Anfinsen, une protéine dépliée émergent d'un ribosome se replie spontanément dans son état natif qui correspond à la conformation accessible présentant le niveau d'énergie libre le plus bas [31]. Avec cependant comme exception notable les protéine intrinsèquement désordonnées [32–34] dont la conformation reste dépliée et instable dans des condition physiologique.

Le paradoxe de Levinthal [35] souligne l'immense quantité de conformation possible pour une protéine et l'impossibilité de les parcourir toutes aléatoirement avant d'atteindre la plus stable (celle présentant le niveau énergétique le plus bas) dans un temps finit relativement court. Puisque les protéines se replient spontanément dans leur état natif dans des échelles de temps relativement courtes [36], ce repliement doit s'effectuer via des voies préférentielles avec un repliement en domaine structurel par intermédiaire de repliement. La théorie de l'effondrement hydrophobe avance qu'un intermédiaire de repliement présentant des structures secondaires similaire à la forme native atteint ensuite sa conformation tertiaire par regroupement des chaines latérales apolaire au sein d'un cœur hydrophobe [37–39]. Les *molten globules* (ang. « Globules fundus ») sont un état conformationnel métastable dans lequel les protéines conservent leur structure secondaire alors que les chaines latérales restent dynamiques. Cet état qui peut être obtenue dans des conditions modérément dénaturantes est analogue aux états intermédiaires rencontrés au cours du repliement des protéines.

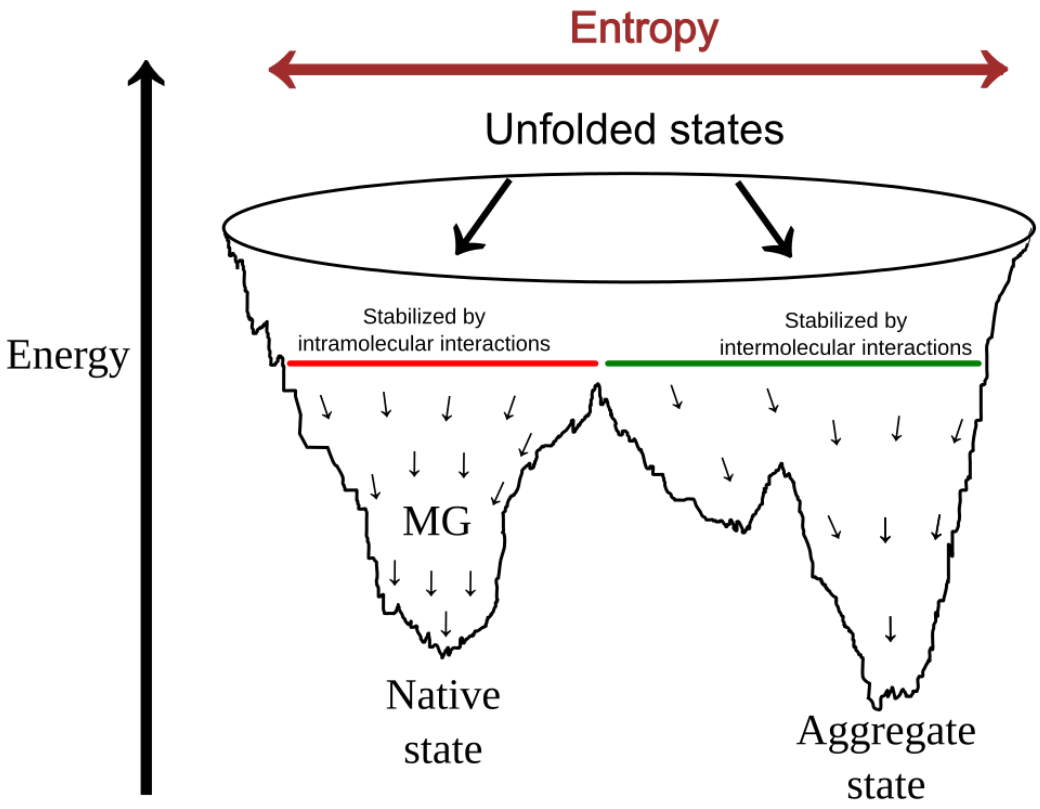

Figure 6. Paysage energétique du repliment des protéines. MG: molten globule**.**

1.4 Stabilité des protéines et agrégation

La stabilité d'une protéine désigne sa propension à maintenir sa structure native. La stabilité peut être définie à 3 niveaux : stabilité chimique, stabilité conformationnel et stabilité en solution. Une perte de stabilité chimique peu par exemple induire une perte de conformation (dénaturation partielle ou totale) qui peu elle-même affecter la stabilité en solution et mener à une agrégation.

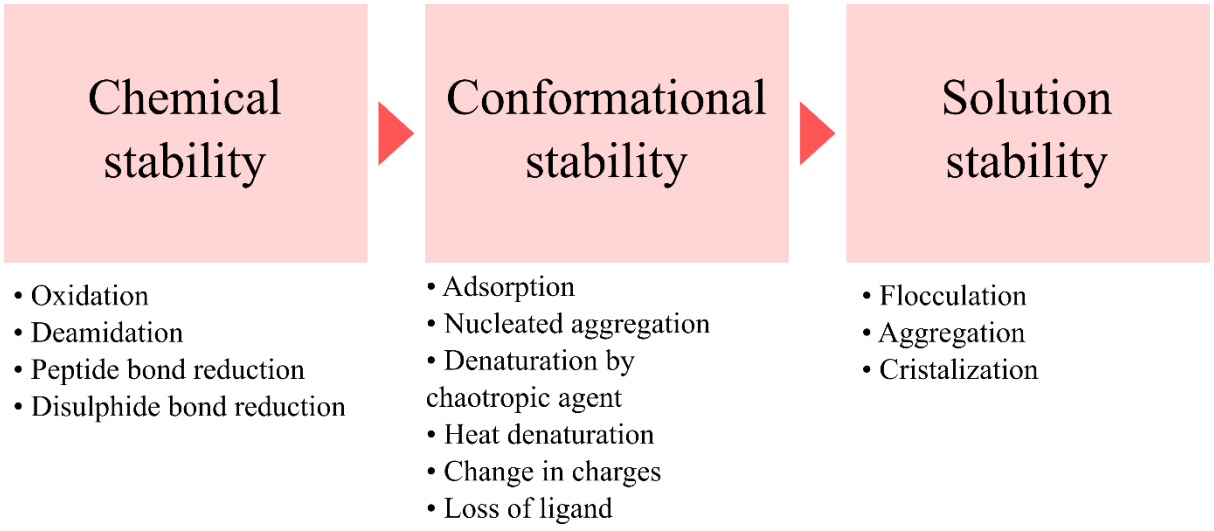

Figure 7. Principaux méchanismes de perte de stabilité des protéines.

1.4.1 Dénaturation chimique

Les molécules organiques sont sujettes à de nombreuses dégradations chimiques, les protéines peuvent subir en particulier une déamidation de leurs chaines latérales. Ces dégradations peuvent engendrer d'importantes pertes de stabilité conformationnel et une agrégation. La réduction des ponts disulfure ou l'hydrolyse des liaisons peptidiques est évidement extrêmement déstabilisante pour la conformation des protéines.

1.4.2 Dénaturation structural des protéines

La dénaturation est la perte de la structure native d'une macromolécule, elle intervient lorsque les conditions physicochimiques de la solution ne stabilisent plus son état conformationnel. A haute température la dénaturation résulte principalement de la rupture des liaisons hydrogènes. A basse température également une « dénaturation froide » [40,41] peut provenir d'effets entropiques tell que des effets hydrophobes.

Les changements conformationnel des protéines peuvent être suivit par des techniques de fluorescence basées sur des fluorophores se liant de manière préférentiel aux régions hydrophobes des protéines tell que l'Acide 8-Anilinonaphthalene-1-sulfonique (ANS) ou le SYPRO orange. Cette approche est particulièrement utilisée pour le suivit d'agrégation amorphe tell que les dénaturations thermiques ce qui est à l'origine de techniques de criblage haut débit pour la recherche de médicaments

De plus les changements dans la structure d'une protéine peuvent affecter son auto-fluorescence par exemple la fluorescence de la tyrosine (l'insuline ne possédant pas de tryptophane) a été utilisée pour le suivit des changements conformationnel de l'insuline[42].

1.4.3 Agrégation des protéines

Si la structure d'une protéine n'est plus stabilisée par le solvant, d'autres interactions entre protéine peuvent se mettre en place stabilisant les protéines dans une nouvelle structure. Ces interactions intermoléculaires sont habituellement dirigées par des effets hydrophobes entre les résidus apolaires nouvellement exposées [43–45].

Wang et al. [46] ont proposé une classification générale des voies d'agrégation (Figure 8). Ces voies sont divisées en 3 catégories (1) agrégation via un état intermédiaire, (2) agrégation directe depuis un état natif (2a et 2b) ou dénaturé (2a' et 2b') et (3) dégradation chimique induisant une potentiel agrégation.

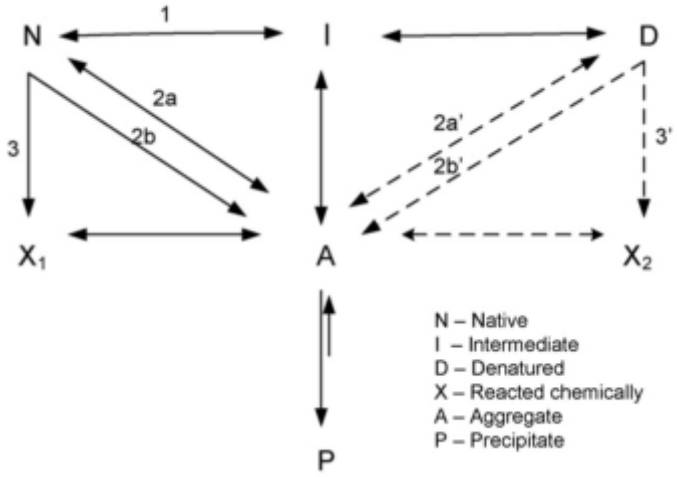

Figure 8. Voie de dénaturation des protéines d'après Wang et al. 2010. Cette classification distingue l'aggrégation reversible depuis un état natif (2a) ou dénaturé (2a') de l'agrégation irreversible (2b and 2b').

Agrégation spontanée.

Une agrégation spontanée (voie 2 dans la classification de Wang et al.) est habituellement le résultat d'une perte soudaine de la stabilité en solution après un changement dans les conditions physicochimiques de la solution (température, pH, dénaturant, etc.) ou d'une dénaturation de la protéine. Les agrégats formés dans ces conditions présentent habituellement une structure peu ordonnée : précipité ou agrégat amorphe. De plus ces agrégats peuvent être composés de plusieurs espèces de protéine ou macromolécules.

La Figure 9 présente les domaines de solubilité d'une protéine en fonction de sa concentration et d'un autre paramètre (tell que la concentration d'un agent de précipitation). Dans le domaine de solubilité c'est-à-dire à a basse concentration de protéine ou d'agent précipitant (par exemple), l'agrégation directe peut intervenir par dénaturation de la protéine (voies 2a' et 2b'). Au-dessus de la super-saturation les protéines ne sont plus soluble et floculent voies 2a et 2b.

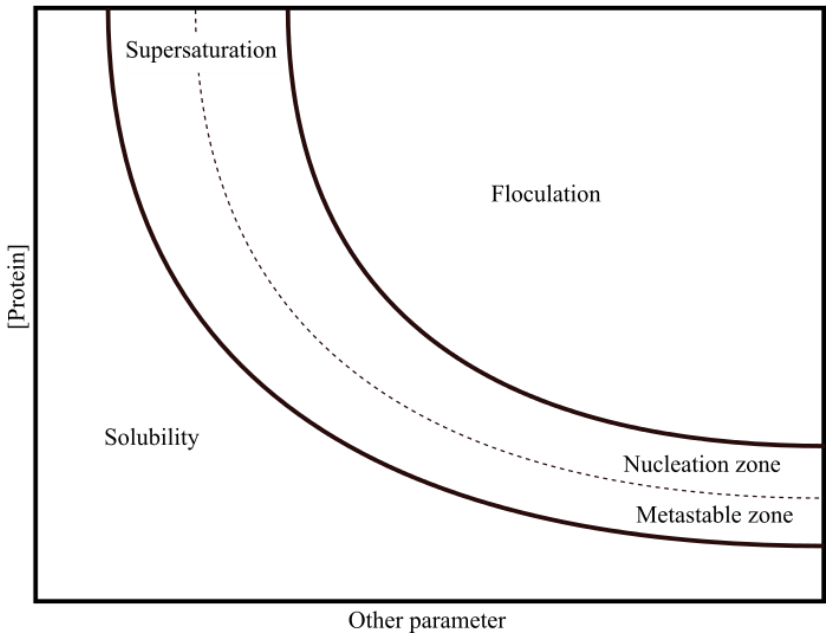

Figure 9. Profil de solubilité d'une protéine présantant les 3 principaux domaines. Dans le domaine de solubilité l'agrégation directe intervient par dénaturation, dans le domaine de supersaturation les cristaux de protéine peuvent

croitre (les noyaux de cristaux ne peuvent cepenant que se former dans la zone de nucléation) enfin dans le domaine de floculation les protéine précipitent spontanément.

Mécanisme de floculation

La propension d'une protéine à floculer peut être estimer à l'aide de leur second coefficient du viriel osmotique ainsi que leur potentiel Zeta [47]. L'expansion viriel de la pression osmotique [48] est :

$$\Pi = \mathrm{RT}\left(\frac{1}{Mw}\cdot \mathrm{c}_p + B_{22}\cdot {\mathrm{c}_p}^2 + B_{23}\cdot {\mathrm{c}_p}^3 + \cdots\right)$$

Où **R** est la constant des gaz parfaits, **T** la température absolue en K, $\mathbf{M_w}$ est la masse moléculaire en Da, $\mathbf{c_p}$ est la concentration de la protéine en M et B_{22} le second coefficient du viriel osmotique [49] est donné par:

$$B_{22} = \frac{2\pi}{{M_w}^2}\int_0^\infty {r_{12}}^2\left(1 - e^{-\frac{W(r_{12})}{k_B T}}\right) dr_{12}$$

Où $\mathbf{r_{12}}$ est la distance intermoléculaire de centre à centre, $W(\mathbf{r_{12}})$ est le potentiel de force moyen, k_B est la constant de Boltzmann constant et T la température absolue en K. Les coefficients du viriel osmotique sont responsables de la déviation d'une solution idéale : Dans le cas de coefficients positifs la pression osmotique est plus élevée que la solution idéale avec une dominance des interactions intermoléculaires répulsives. Des coefficients fortement négatifs entrainent donc habituellement une précipitation rapide.

Morphologie des superstructures d'agrégats

La morphologie des agrégats peut être déterminée par des mécanismes d'agrégation spécifique : une agrégation limitée par la diffusion (Figure 10) produit des motifs de dimension fractals inferieure à ceux des agrégations limitée par la réaction [50–54]. La détermination de la dimension fractale d'un agrégat est donc importante pour la détermination des mécanismes de croissance par exemple par comparaison avec des données générées par des modèles informatiques

		Wang et al.	Nucleation	Domain	Structure
	Crystallization		Usually nucleated	Supersaturation	Ordered
Aggregation	Via intermediate	1		Solubility	Ordered
	Flocculation	2a, 2b	Direct	Flocculation	Amorphous
	By denaturation	2a', 2b'		Solubility	Amorphous
	By chemical degradation	3		Solubility	Amorphous

Table 2. Summary of protein association mechanisms. With coresponding pathways in Wang et al. clasification, nucleation dependancy, solubility domain of occurance and level of order of their structures.

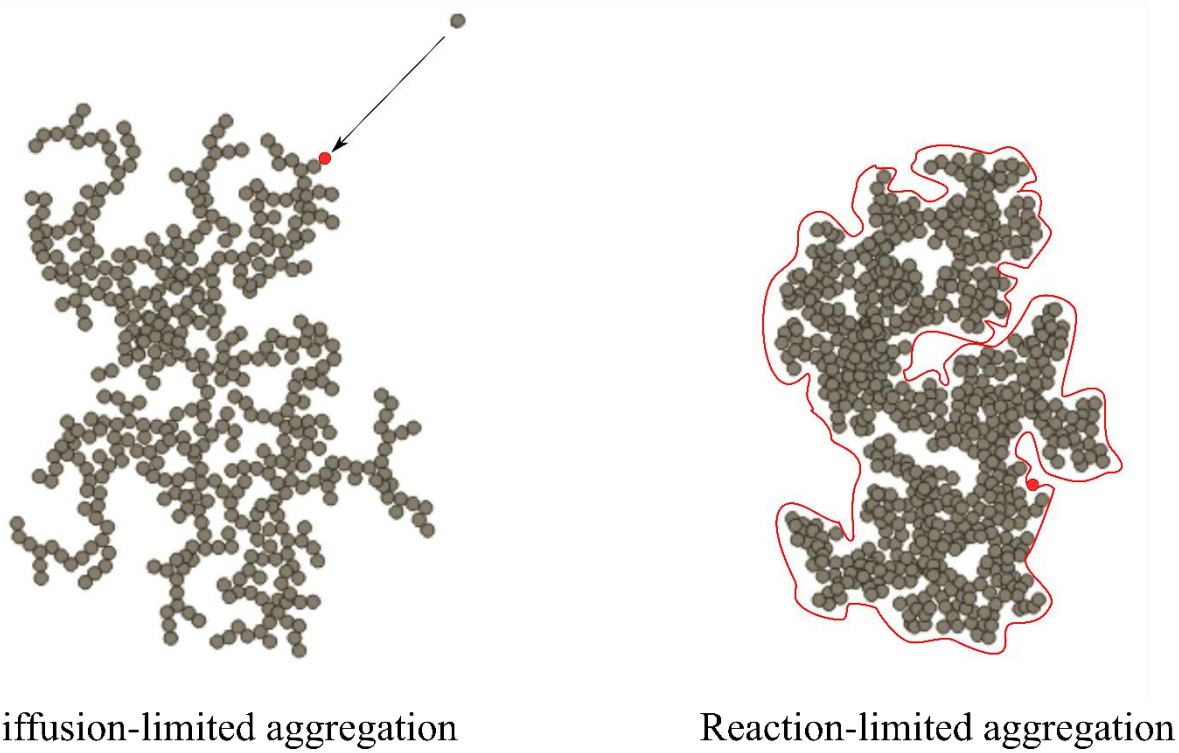

Figure 10. Mechanisme de croissance d'agrégats limité par la difusion et limitée (DLA) par la réaction (RLA).. Pour la DLA les particules difisant depuis l'infini sont incorporé imédiatement par contact avec l'agrégat. Au contraire pour la RLA chaque point de la surface est équiprobable pour l'incorporation d'une nouvelle particule (modifiée depuis wikimedia commons : https://commons.wikimedia.org/wiki/File:ParticleAggregationDLCAvsRLCA1.png)

Agrégation via des états intermédiaires

Les mécanismes d'agrégation impliquant un état intermédiaire (voie d'agrégation de type 1 dans la classification de Wang et al.) peuvent se rencontrer dans le domaine de solubilité. L'importante barrière énergétique qui existe entre la protéine native et agrégée (Figure 6) autorise les deux formes à être stable (ou métastable) dans les même conditions. Les agrégats formés via des états intermédiaires peuvent présenter un haut niveau d'organisation (Table 2).

Cristallisation

Lorsque la concentration de la protéine augmente ou sa solubilité diminue, la solution passe dans le domaine de sursaturation **(**Figure 9**)**. Dans des conditions de supersaturation et de pureté élevée, des cristaux protéiques peuvent nucléer. Ces cristaux sont monopécifiques et très ordonné et les protéines conservent la plus grande partie de leur structure native sous cet État [55,56]. Contrairement à la nucléation amyloïde qui se produit dans le domaine de la solubilité, la nucléation des cristaux de protéine n'a lieu que dans la zone de nucléation au sein du domaine de supersaturation. La croissance de ces cristaux est alors thermodynamiquement favorable dans tout le domaine de supersaturation.

1.4.4 **Agrégation amyloïde**

Description et structure

Les agrégats amyloïdes sont un cas particulier d'agrégats de protéique fibrillaire monopécifique et très organisé, qui sont caractérisés par leurs propriétés structurales uniques [57] (Figure 11). La caractéristique principale des fibres amyloïdes est l'empilement d'une protéine le long l'axe de la fibre maintenue ensemble par une colonne vertébrale de feuillet β intermoléculaire [58]. Les liaisons hydrogène de ces feuillets β étant orientées le long de l'axe

principale de la fibrille et présentent généralement une plus faible dispersion des angles φ et ψ que les feuillets β des protéines natives [59]. Malgré cette stabilisation par la chaine principale des protéines, l'agrégation amyloïde est hautement séquence spécifique puisque seules des séquences apparentées peuvent être incorporé au sein d'une même fibrille [60] l'agrégation amyloïde s'effectue principalement via des oligomères d'intermédiaires conformationnels et au cours d'une phase de nucléation.

La morphologie des finales fibrilles est régulière et non ramifié (ou généralement non ramifié[61]). Les charges sont censées jouer un rôle important dans la formation des fibrilles ainsi que dans leur stabilité [62].

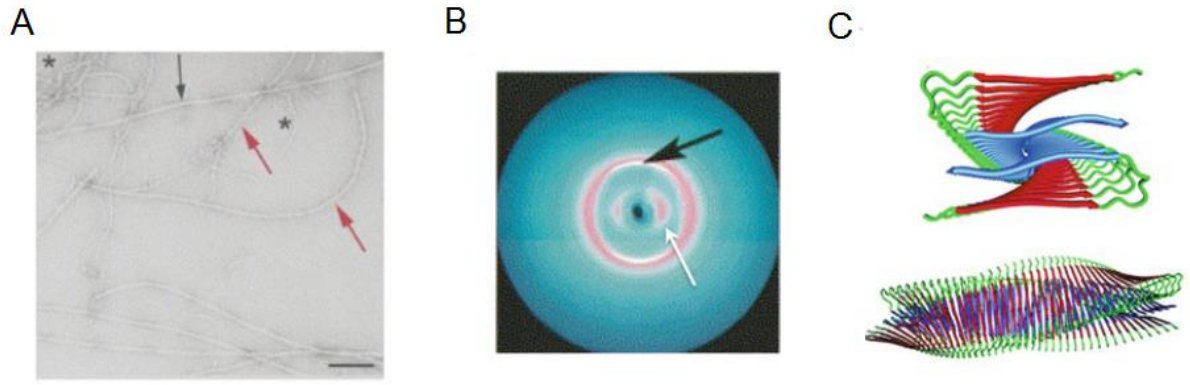

Figure 11. Structural characterization of amyloid fibrils by 3 biophysical methods.

A: micrographie électronique en transmission d'Aβ$_{1-40}$ imagés après coloration au formate d'uranyle, l'astérisque indique une proto-fibrille tandis que les flèches indiquent des fibrilles, B: schéma de difraction au rayon x synchrotron de fibrilles amyloïdes d'un patient présentant amylose familiale; cette figure de difraction présente un espacement inter-brin de 4.7 Å (flèche blanche) et espacement inter-feuille de 10 Å (flèche noire) typique des fibres amylmoides, C: modèle de fibrilles d' Aβ$_{1-40}$ provenant de données RMN magic angle à l'état. Modifié d'après Martin et al. [63] adapté à l'origine de Goldsbury et al.[64] (A), Sunde et al.[65](B) et Petkova et al.[66] (C).

Les données structurelles détaillées sur les fibres amyloïdes sont rares en raison de l'incapacité d'obtenir des cristaux amyloïde, la pluparts des structures détaillée sont habituellement obtenues par RMN (en particulier par *magic angle spinning solid-state nuclear magnetic resonance* [67–69]) souvent conjuguée à la cryo-microscopie électronique et suivit d'optimisation des modèles par minimisation d'énergie assistée par ordinateur [70].

La Thioflavine T

La thioflavine T (ThT) est un colorant constitué d'une partie benzothiazol et d'une partie dimethylaminobenzyl qui est capable de se lier spécifiquement aux les fibrilles amyloïdes dans le sillon formé par les feuillets bêta intermoléculaires [71].

Dans un solvant protique[†] la ThT présente un pic d'absorption à 342nm et un pic d'émission de fluorescence à 430nm [72]. Cependant, une fois lié à une fibrille amyloïde, les molécules de ThT subissent une transition de fluorescence vers pic d'absorption à 450 nm et un pic d'émission à 480nm ainsi qu'une augmentation de leur rendement quantique de fluorescence ([73–77]. Les agrégats de protéines induisant une telle transition de fluorescence sont appelés ThT-positif dans la littérature.

[†] **Solvant protique**: solvant capable de donner un H^+ (e.g. H_2O)

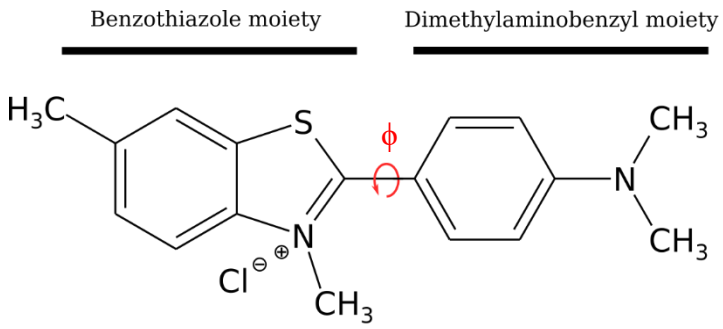

Figure 12. Structure de la thioflavine T montrant l'angle dièdre entre les deux portions (angle ϕ).

Certaines études suggèrent la formation d'un excimère de ThT [78] (c.-à-d. un dimère de thioflavine T excité) dans les cavités capables de lier deux molécules de ThT [79,80]. Un tel système permettrait une conjugaison intermoléculaire entraînant un changement de fluorescence. Ces dimères de molécules de ThT empilés de manière colinéaire ont été observées dans des structures cristallines [71,72] mais l'absence de déplacement du spectre d'émission vers le rouge associé [72] et non coopérativité de la liaison de la ThT aux fibres amyloïdes [75] montrent qu'il est peu probable que la formation d'un excimère soit à l'origine de l'état ThT-positif.

La barrière d'énergétique de la rotation de la liaison entre les deux portions de la ThT (angle ϕ). est de 2,2 kcal/mol [81]. Dans un micro-environnement rigide, empêchant cette rotation, la ThT subit sa transition de fluorescence vers des longueurs d'onde plus élevée.

Les sillons formés entre les chaînes latérales des feuilles bêta fournissent un environnement rigide de ce type empêchant la libre rotation de l'angle dièdre ϕ et donc augmente la fluorescence à λ_{ex} = 450nm. L'incorporation de la ThT à l'intérieur de la fibrille pourrait être limitée par l'accessibilité du site de liaison ; en effet, la présence de ThT au cours de la phase d'élongation résulte en une fluorescence plus élevé comparativement à l'addition de ThT à la fin de l'agrégation.

La ThT est considéré comme un colorant spécifique de la structure amyloïde, cependant des états ThT-positifs ont été observés pour des agrégats ne présentant pas de structures fibrillaires en microscopie électronique et donc qualifiée d'amorphe, quoique possédant une augmentation de la structuration en feuillet β [82]. Dans une moindre mesure, un rendement quantique accru et une transition de longueur d'onde de fluorescence ont également été observés dans des membranes et des micelles[83].

D'autres produits chimiques sont connus pour colorer les agrégats amyloïdes, le rouge Congo en particulier est un colorant spécifique des fibres amyloïdes qui présente une biréfringence vert pomme sous une lumière polarisée lorsqu'il est lié à des fibrilles amyloïdes [84].

Le terme amyloïde (amylum + oid «lat. de type amidon ») a été présenté par Rudolf Virchow en 1854 en raison de la coloration positive à l'iode de ces agrégats extracellulaires [85]. Cette définition à l'origine purement histologique est maintenant étendue aux propriétés structurale des protéines dans ces agrégats. La structure commune des agrégats amyloïdes permet l'exploitation des données acquises sur une protéine pour éclairer l'agrégation amyloïde des autres protéines.

Étant donné que les structures fibrillaires amyloïdes s'appuient sur une stabilisation par la chaine latérale des protéines qui la compose et non les chaines latérale et que les protéines amyloïdogènes ne sont pas limités à une séquence particulière mais au contraire sont largement

rependues au seins de diverses familles, il a été suggéré que l'agrégation amyloïde était une propriété commune des chaînes polypeptidiques [86–88].

Si les interactions inter-protéines par feuillet β intermoléculaire le long de l'axe des fibrilles sont bien connues, ce n'est pas le cas pour les interactions inter-protéines perpendiculaires à cet axe. Et pourquoi les agrégats amyloïdes sont-ils si séquence-spécifique, malgré cette stabilisation par la chaine principale de la protéine ? Nombreux données obtenus avec de courts peptides formant des fibres amyloïde ont mis en évidence des interactions de leurs chaînes latérales perpendiculairement à l'axe principale de la fibre formant une interface déshydratée appelée *steric zipper* [89–91]. Cette interaction étroite des chaînes latérales est stabilisée principalement par l'effet hydrophobe et/ou les interactions électrostatiques. Par ailleurs, la déshydratation du centre des fibrilles augmente l'énergie des interactions électrostatiques [25]. Sous haute pression hydrostatique les vides anisotropes créés par ces interfaces déshydratés peuvent conduire à la déformation de la fibrille par courbure. Ces vides contribuent à réduire le potentiel thermodynamique de leur formation dans des conditions de haute pression hydrostatique [92,93].

La formation d'un steric zipper peut donc expliquer la spécificité de séquence de l'agrégation amyloïde et nuancer son universalité. Il suggère en outre que seule une section spécifique de la protéine est impliquée dans la formation des fibrilles. Par conséquent, pour chaque protéine amyloïdogène un peptide minimal capable de former des fibrilles amyloïdes par lui-même doit exister. Des tentatives de prédiction de la propension des séquences polypeptidiques à agréger de manière amyloïdes ont même été avancées. Par exemple les régions riches en arginine sont bien connues pour leur propension à former des agrégats amyloïdes [94–97].

1.4.5 Cinétique d'agrégation amyloïde

Les agrégations amyloïdes suivent habituellement une cinétique d'agrégation nucléée typique qui se divise en trois phases (Figure 13): dans un premier temps, le taux d'agrégation reste nul pour une longue période de temps (généralement plusieurs heures). Ce temps de latence précédant l'apparition des premiers agrégats est la phase de nucléation au cours de laquelle les protéines doivent surmonter l'importante barrière d'énergétique entre leur forme soluble et leur forme agrégées via la formation de structures oligomériques très instables appelées noyaux. L'apparition des premières fibrilles initie ensuite une phase d'agrégation exponentielle dont la vitesse d'agrégation est rapidement atténuée par l'épuisement des protéines natives en solution, entraînant une phase de croissance logistique[‡]. Finalement l'agrégation atteint un plateau lorsque toutes les protéines natives en solution ont été convertis en agrégats amyloïdes.

L'ajout de fibrilles amyloïdes au début d'une cinétique abolit le temps de latence et induit une transition rapide vers la phase de croissance, cette action est appelée *seeding* (ang. « ensemencement ») [98]. Le seeding et la croissance des fibrilles sont séquence-spécifique [60]. De véritable interseeding entre différents peptides possédant des séquences indépendante ont pourtant été signalés ce qui est d'une haute importance médicale [99].

Un moyen simple de disséquer les processus cinétiques de l'agrégation amyloïde est de distinguer la nucléation primaire, c'est-à-dire le processus conduisant à l'apparition des premier agrégats des processus secondaires (ou ensemencées, *seeded aggregation* en anglais) qui ont lieu durant la phase de croissance. Puisque les agrégats amyloïdes sont remarquablement

[‡] Croissance logistique : une croissance exponentielle (dont la croissance est proportionnelle à la sa taille et à une ressource) dans un environnement ou les ressource sont limité, ici un nombre limité de protéines natives, conduit à une cinétique sigmoïde.

efficaces pour ensemencer une solution de protéines native, ces procédés secondaires deviennent largement prédominants, dès l'apparition des premiers agrégats dans la solution.

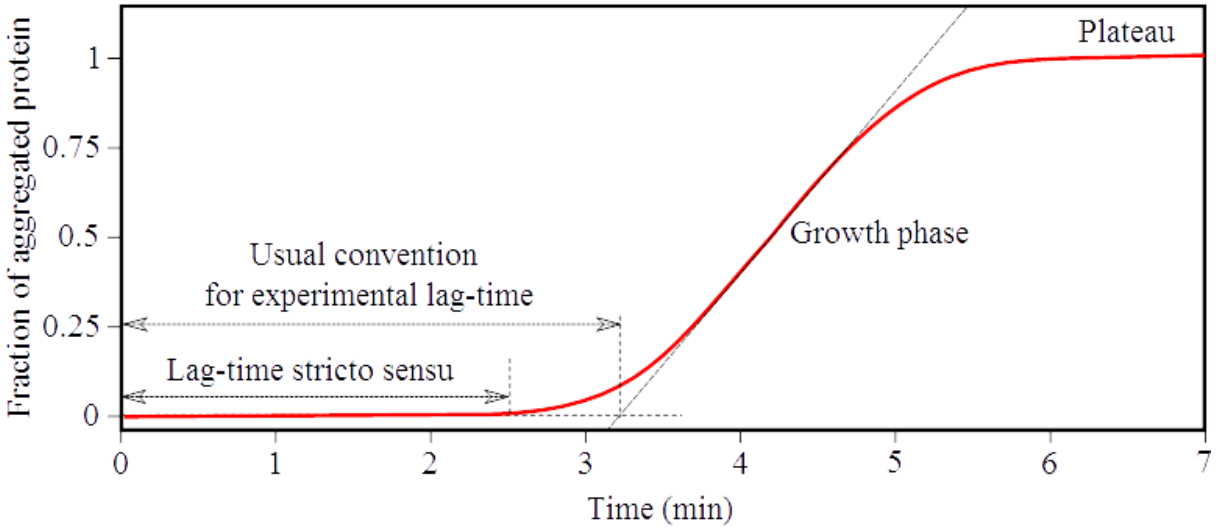

Figure 13 Cinétique théorique d'une agrégation amyloïde in vitro avec une quantité limitée de protéines natives.

La cinétique d'agrégation amyloïde est généralement contrôlée par quantification de fluorescence en utilisant le colorant fluorescent spécifique thioflavine T. Les points expérimentaux ne sont pas forcément assez réguliers dans le temps pour couvrir avec assez de précision la transition rapide entre la phase de latence et la croissance rapide pour permettre la détermination exacte du point d'apparition de la première fibre ThT positive (temps de latence stricto sensu). Les temps de latence expérimentaux sont donc généralement définis comme l'intersection de la tangente plus raide de la quantité d'agrégats durant la phase de croissance avec les abscisses (ou avec la ligne de base de la fluorescence ThT, Figure 13).

Les cinétiques d'agrégation amyloïde et d'agrégation des protéines en général ont reçu beaucoup d'attention car ils permettent la déduction des mécanismes d'agrégation [100] ; ces mécanismes recevront une attention particulière dans les sections suivantes.

1.4.6 Principes de la nucléation

La nucléation est le processus menant à la première formation d'une nouvelle phase ou structure à partir de particules individuelles. Elle diffère d'un assemblement spontané par la présence d'un temps de latence précédant l'assemblement rapide. La nucléation est connue dans de nombreux processus impliquant un auto-assemblement tels que la formation de glace ou la cristallisation [101]. Une distinction est faite entre la nucléation hétérogène qui se produit au contact d'une surface (ou d'une interface) et la nucléation homogène et qui se produit dans un milieu homogène (par exemple en solution). La nucléation des protéines a été observée à la fois sur des surfaces et en solution. La théorie classique de la nucléation est le principal modèle utilisé pour décrire un changement de phase thermodynamiques et a également été utilisée afin de comprendre la nucléation des protéines [102].

La théorie classique de la nucléation (TCN) met l'accent sur la variation changement d'énergie libre associée à la surface et d'énergie libre associée au volume d'un noyau sphérique de rayon r [103–105]. Le résultat de la tension interfaciale (σ) de ce noyau est une énergie libre de surface proportionnelle à sa surface ($4\pi r^2$). Cette contribution positive à l'énergie libre totale du noyau est donc défavorable à nucléation. En revanche, l'énergie libre associée au transfert

d'un monomère depuis solution vers le cœur du noyau (Δg_{trans}) crée un terme d'énergie de volume proportionnel au volume du noyau ($4\pi\ r^3/3$). Cette contribution négative à l'énergie libre totale est favorable à la nucléation. La somme de ces deux les contributions antagonistes à l'énergie libre totale définit la taille critique du noyau, sa variation d'énergie libre en fonction de son rayon étant :

$$\Delta G = \Delta G_{bulk} + \Delta G_{surf}$$

$$\Delta G = \frac{4}{3}\pi r^3\ \Delta g_{trans} + 4\pi r^2 \sigma$$

Pour les petits noyaux ($r < r^*$), l'augmentation de l'énergie de surface associé à l'ajout d'un nouveau monomère dépasse la libération d'énergie résultant des interactions dans le volume. La croissance du noyau est donc thermodynamiquement défavorable en premier lieu. Mais la contribution de la surface étant proportionnelle à r^2, cette instabilité sera bientôt compensée par la contribution du volume qui est proportionnelle à r^3. Le noyau peu donc atteindre par la suite un rayon critique r* correspondant au rayon où ΔG atteint un maximum :

$$\frac{d}{dr}\Delta G\Big|_{r^*} = 0$$

avec

$$r^* = \frac{-2\sigma}{\Delta g_{trans}}$$

Où l'ajout de monomère cesse d' accroître l'énergie libre du noyau mais, au contraire, commence à le stabiliser (Figure 14).

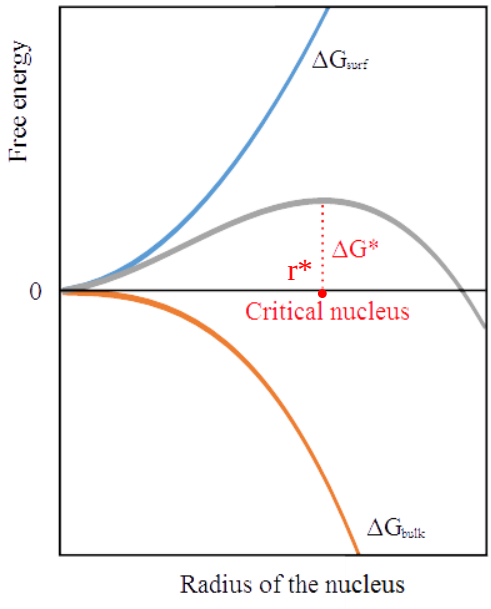

Figure 14. Evolution de la contribution de l'énergie libre de volume et de surface à l'énergie libre totale du noyau.

La théorie classique de la nucléation cependant ne tient pas compte des transitions conformationnelles des protéines ni les changements de ΔG associée à ces transitions. Par ailleurs, ce modèle considère les noyaux comme des sphères ayant une énergie de volume et une énergie de surface ce qui peut être une hypothèse assez incertaine pour les petits noyaux comprenant un nombre discret de molécules. Néanmoins cette théorie nous permet de visualiser les concepts de base de la nucléation : les premiers oligomères sont instables et les noyaux ne

pourront gagner en stabilité après la réalisation d'un état critique après un certain nombre d'États de transition.

En outre, la prédominance de la nucléation hétérogène sur la nucléation homogène en présence d'une surface pour laquelle les monomères ont une affinité est assez évidente : les noyaux qui poussent sur une interface physique auront une plus faible surface exposée au liquide et donc une ΔG_{surf} plus basse

1.4.7 Mécanisme de nucléation amyloïde

Puisque les protéines sont des molécules complexes, avec de nombreux groupes fonctionnels ayant entre eux des énergies d'interaction spécifique et puisque la conformation des protéines est capable de changer en particulier par des interactions intermoléculaires, la stabilité des noyaux de protéine n'est pas limitée aux simples considérations d'une énergie de volume par rapport à une énergie de surface. En outre, l'assemblage de structures aussi complexes que des fibres amyloïdes matures est divisé en plusieurs états intermédiaires avec au moins l'un d'entre eux étant thermodynamiquement limitant.

Comme dans le modèle de la théorie classique de la nucléation, les noyaux critiques représentent la forme oligomérique avec l'énergie libre la plus haute sur la voie d'agrégation menant à la formation d'une fibrille amyloïde. D'un point de vue cinétique, la vitesse de nucléation correspond à la vitesse de formation du premier oligomère pour lequel l'ajout d'un monomère est plus favorable que son désassemblement.

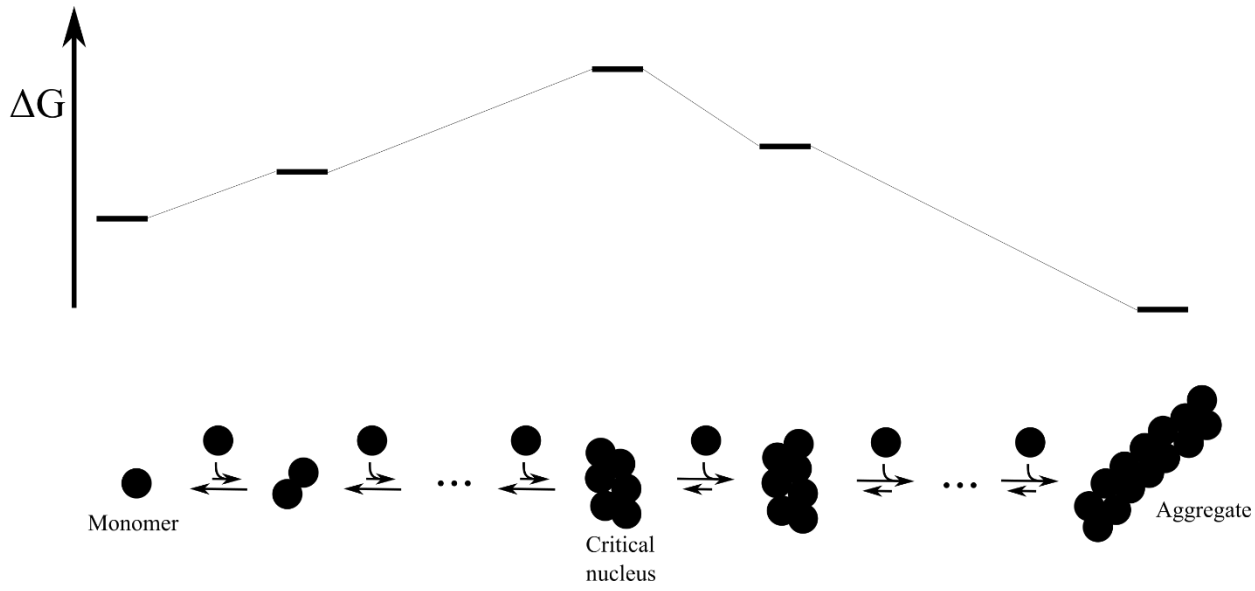

Figure 15. Modèle themodynamic le plus simple d'une nucléation amyloïde.

La cinétique d'agrégation amyloïde a reçu beaucoup d'attention ces dernières années, [106–111] aboutissent à l'obtention de nombreux modèles thermodynamiques et cinétiques tels que: le modèle de *template-assembly* [112,113], la *nucleated polymerization*, la *monomer-directed conversion*[114], la *nucleated conformational conversion* [115] (Figure 16) et le *off-pathway folding* model[116].

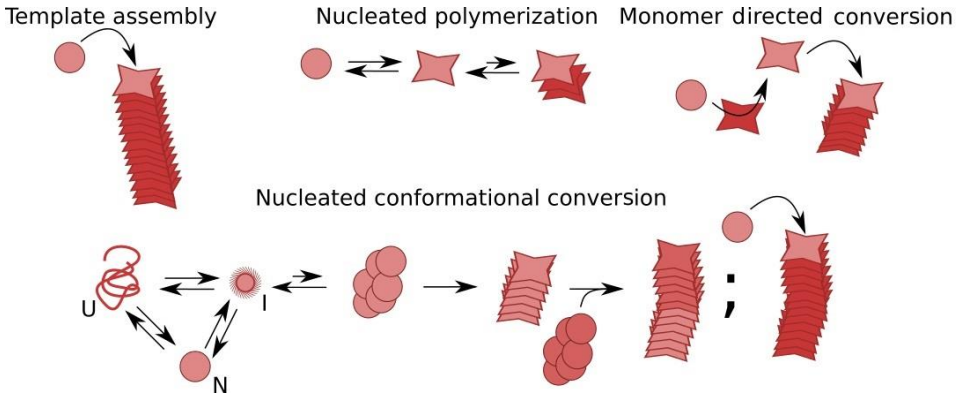

Figure 16. modèle de mechanisme d'agrégation amyloide (adapté d'après Serio et al.[115])

Dans le modèle de *template assembly* (Figure 16), les monomères natifs subissent des changements conformationnels directement lors de leur incorporation dans l'agrégat amyloïde. Ce changement conformationnel constitue l'étape limitante. Ce modèle n'inclut pas une étape de nucléation, mais peut s'appliquer au mécanisme d'allongement des fibrilles. Dans le modèle de *monomer-directed conversion*, l'étape cinétiquement limitante est la conversion en solution d'une protéine native par un monomère à l'état amyloïde ; les monomères amyloïdes agrégeant ultérieurement lors d'une étape non limitante. Dans le modèle de *nucleated polymerization* il existe un équilibre en solution entre monomère natifs et amyloïde, l'étape limitante consiste ensuite en l'association des monomères amyloïdes rares en solution.

Le modèle de *Nucleated conformational conversion* a été ensuite proposé par Serio et al. [115] après des expériences sur le prion fongique sup 35. Ils ont montré que la conversion conformationnelle est cinétiquement limitante imposant une vitesse maximum de nucléation primaire. Dans ce modèle les noyaux proviennent de monomères partiellement dépliés, ils se développent ensuite par l'addition de monomères natifs ou partiellement dépliés jusqu'à stabiliser suffisamment la transition structurale vers un état amyloïde. A partir ce point, la croissance par addition de monomères sera prédominant par rapport au désassemblement.

Avec la *nucleated conformational conversion* le mécanisme de nucléation ne repose pas sur un effet d'action de masse, mais plutôt sur des changements de conformation. La transition de la constante thermodynamique associée à un ajout de monomère s'explique donc par une augmentation qualitative plutôt que par une quantitative des interactions intermoléculaires à l'intérieur du noyau. En effet, les fibrilles amyloïdes finales sont des objets extrêmement allongées avec un rapport surface/volume élevé.

Un modèle cinétique général de la nucléation amyloïde est donc du type :

$$(1) \qquad N \rightleftarrows I$$

$$(2) \qquad \left(I_{n-1} + N \rightleftarrows I_n\right)_{n \text{ times}}$$

$$(3) \qquad I_n \rightleftarrows A_n$$

$$(4) \qquad N + A_n \rightleftarrows A_{n+1}$$

Où N est un monomère natif en solution, I est une protéine dans un état intermédiaire et A est une protéine à l'état amyloïde. Protéine dans un état intermédiaire est ici un terme qui peut s'appliquer à plusieurs états qui sont distinct de à l'état natif, de l'état déplié (U dans la classification de Wang) et de l'état amyloïde. En particulier, les protéines formant le noyau

sont appelées ici intermédiaires mais ne sont pas nécessairement tous dans la même conformation. Par analogie au modèle proposé par Serio et al., la protéine native (1) subit une transition vers un état intermédiaire (par exemple par adsorption sur une surface), cette protéine dans un état intermédiaire est alors capable d'agir comme un centre thermodynamiquement instable d'oligomérisation formant un noyau $\mathbf{I_n}$ composé de n monomères (2). Ce noyau présente une forte propension au désassemblement jusqu'à ce qu'il atteigne un état critique $\mathbf{A_n}$ de transition conformationnelle (3) à partir duquel la propension à l'incorporation de monomère sera plus grande que la propension au désassemblement (4).

En raison de la forte instabilité conformationnelle élevée des noyaux, les événements de nucléation primaire sont extrêmement rares : les durées typiques de nucléation (c'est-à-dire la durée précédant l'apparition du premier agrégat amyloïde en solution) varient de plusieurs minutes à plusieurs jours. Les événements de nucléation présentent un comportement stochastique très prononcé avec de très fortes variations de la durée de la période de latence entre des échantillons semblables.

Il faut cependant souligner que la voie d'agrégation d'un monomère jusqu'aux fibrilles amyloïdes appartient généralement à un réseau plus large d'agrégation [117] dans lequel plus d'une voie peut conduire à la formation de fibrilles amyloïdes et dans lequel les différentes réactions d'addition de monomère peuvent être en compétition. Un obstacle supplémentaire à la nucléation peut donc consister dans son inhibition cinétique par la formation de structures oligomériques concurrentes hors de la voie de formation d'agrégats amyloïdes (formation de complexes *off pathway*).

Un des modèles de noyau amyloïde proposé est une structure micellaire, stabilisée par l'effet hydrophobe. Des simulations de dynamique moléculaire, en particulier, ont souligné l'importance de la coopérativité hydrophobe dans la nucléation amyloïde [118]. Par la suite des changements conformationnels se produisent dans ce noyau, stabilisés par des interactions intermoléculaires. Le feuillet α a été proposée comme un conformation intermédiaire entre la conformation native et le feuillet β [119] intermoléculaire des fibres amyloïdes. Cette conformation intermédiaire a été proposée pour le lysozyme et est suspectée d'être impliqué dans la toxicité cellulaire des agrégats amyloïdes [11].

La nucléation amyloïde dépend (au moins en partie) de la concentration de monomère, par conséquent l'augmentation de la concentration de monomère augmentera la vitesse de nucléation. Cependant, contrairement à la cristallisation des protéines, la nucléation amyloïde est principalement décrite comme ne nécessitant ne pas des conditions de supersaturation [101,120,121].

1.4.8 La phase de croissance

La phase d'élongation consiste en l'incorporation rapide de monomères aux extrémités des fibrilles amyloïdes (Figure 17). Selon le modèle « *template* », les monomères natifs (ou dimères natifs) sont facilement convertis et intégrées aux extrémités de la fibrille. Dans d'autres modèles proposés cependant, l'élongation se poursuit par l'incorporation des protéines d'état de transition ou de noyaux à l'état de transition.

Les Fibrilles amyloïdes sont non ramifiées, ce qui signifie que leur élongation ne peut procéder que par l'incorporation de protéines à une ou deux de leurs extrémités. En supposant que les événements de nucléation primaire sont extrêmement rares et pour k_{inc}, la constante de vitesse de l'incorporation des protéines par site, le vitesse d'agrégation $\frac{dA}{dt}$ peut-être écrite comme :

$$\frac{dA}{dt} = a \cdot k_{inc} \cdot S \cdot [P_{inc}]$$

Avec **a** le coefficient stœchiométrique correspondant au nombre d'unités de protéines sous la forme incorporée (1 pour un monomère, 2 pour un dimère, et ainsi de suite) [P_{inc}] est la concentration de protéine dans l'état qui peut être incorporé dans les fibrilles et S le nombre de sites d'incorporation. S est constante en l'absence de nucléation primaire et de processus secondaires. À concentration élevée en protéines et sous l'hypothèse où S est constante, cette loi de vitesse se traduit par une cinétique linéaire. En revanche, dans des conditions où la concentration de la protéine précurseur est limitée, cette loi de vitesse donne une agrégation cinétique sous la forme :

$$A(t) = [P]_0 \cdot (1 - e^{-a \cdot k_{inc} \cdot S \cdot t})$$

Où A(t) est le nombre de mole de protéines à l'état agrégé et $[P]_0$ est la concentration initiale de protéine (en supposant une conversion rapide entre les différentes formes de protéines en solution).

En revanche si la nucléation primaire n'est pas si rare et se produit à un rythme significatif alors le nombre de sites d'élongation augmentera avec le temps. Conduisant à une agrégation suivant une cinétique en $A(t) \propto t^n$.

Le comportement exponentiel de la cinétique d'agrégation au cours de la phase de croissance ne peut donc que provenir d'une multiplication des sites d'incorporation par procédés secondaires. Ces processus secondaires incluent des phénomènes indépendants des monomères tels que la fragmentation des fibres ou des processus dépendant de la concentration en monomères que la nucléation secondaire (Figure 17).

Cependant en cas d'élongation par incorporation de formes intermédiaires ou d'oligomères de protéine (par exemple un allongement par addition de noyaux), le taux de formation de ces intermédiaires peut devenir un facteur limitant qui ralentit l'élongation.

La vitesse de nucléation primaire et secondaire peut être obtenu d'après les données cinétiques d'agrégation à différentes concentrations en protéine native en utilisant la formule suivante [110]:

$$T_{1/2} \propto [\text{monomère}]^{\gamma}$$

Où $T_{1/2}$ est le temps nécessaire pour réaliser l'agrégation de la moitié de la concentration initiale de protéine [monomère] et γ est le coefficient exponentiel d'échelle. Selon les mécanismes dominants le coefficient γ permet la détermination des taux de nucléation :

(Nucléation primaire) $\gamma = -\frac{n_c}{2}$

(Processus secondaires) $\gamma = -\frac{1+n_2}{2}$

Avec n_c: le taux de nucléation primaire et n_2 : le taux de nucléation secondaire.

Parmi la diversité des mécanismes d'agrégation amyloïde décrits dans la littérature (Figure 18) la prévalence de chacun des mécanismes individuels peut grandement différer selon la protéine et les conditions expérimentales.

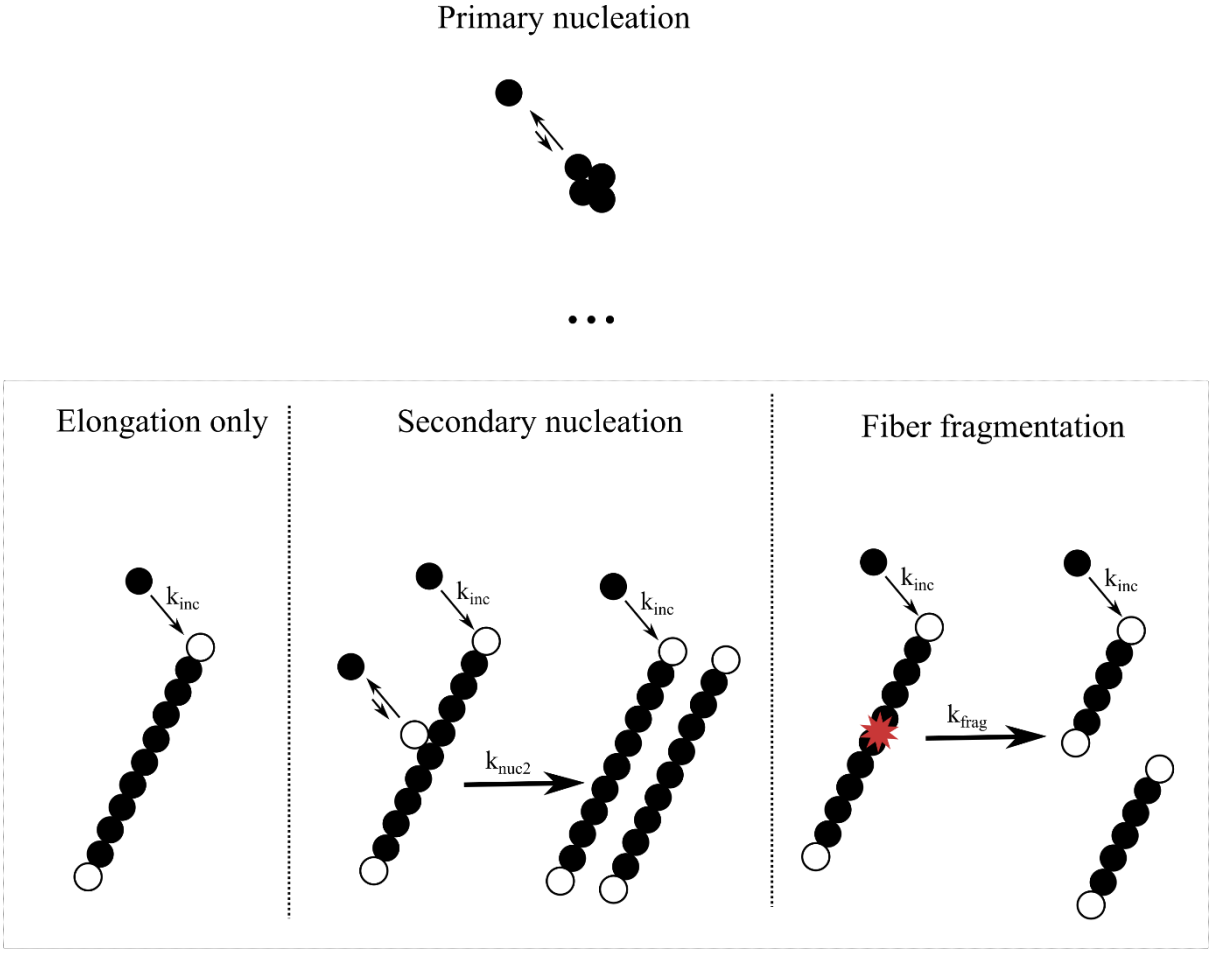

Figure 17: Modèle cinétique présentant l'étape de nucléation primaire conduisant à l'apparition de la première fibrille et les mécanismes de croissance ulterieurs observés dans les cinétiques amyloïdes. Les cercles pleins représentent les protéines, les cercles vides représentent les sites d'incorporation de protéine dans fibrilles amyloïdes.

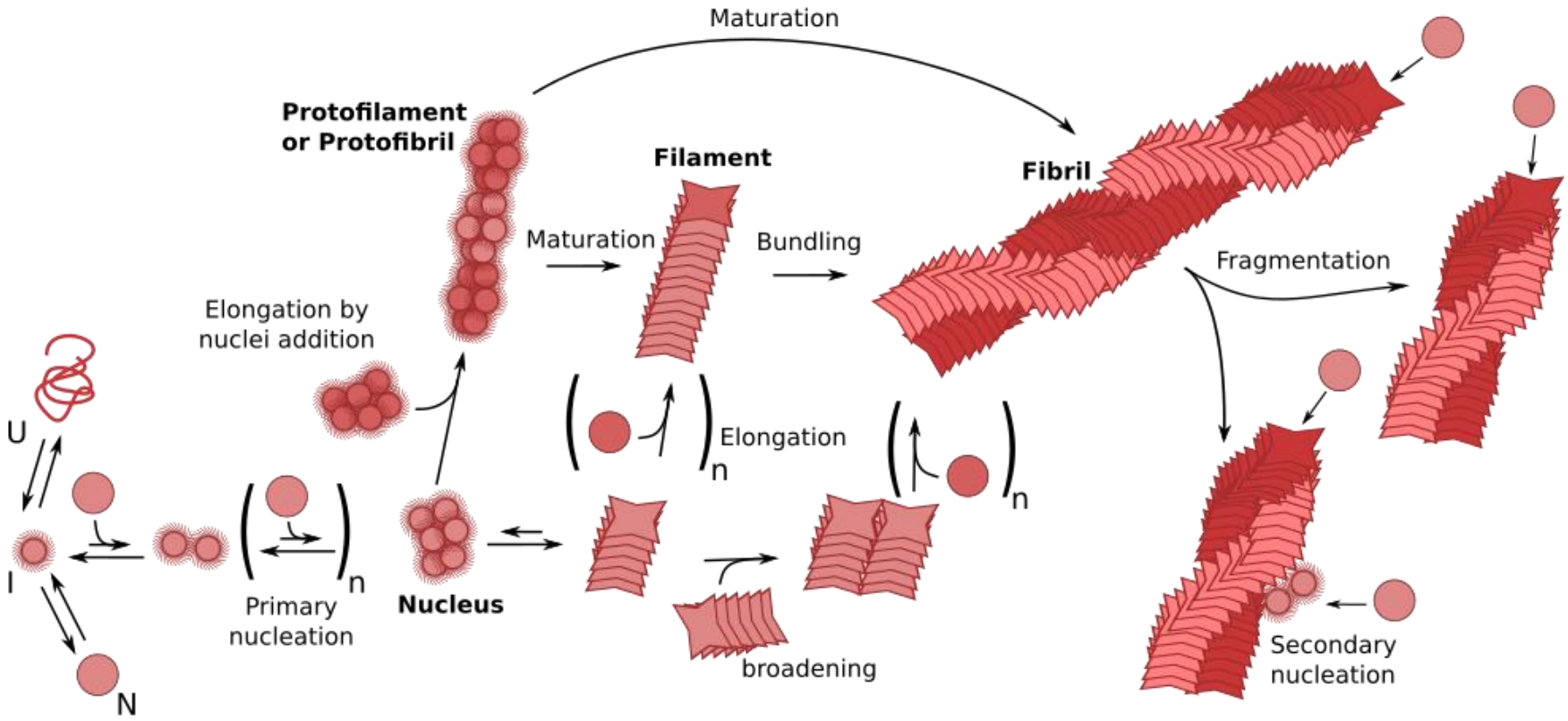

Figure 18: Vue d'enssemble des mécanismes d'agrégation amyloïde décrits dans la littérature. Le rôle de chaque mécanisme individuel varie selon les cas spécifiques et dans la plupart des cas est encore discuté. Le noyau représente ici un noyau critique à partir duquel l'ajout d'un monomère devient thermodynamiquement favorisée par rapport à son désassemblement. Fibrilles peuvent inclure plus de deux filaments (généralement 2 à 4), afin de maintenir le réseau aussi simple que possible les processus secondaires sont détaillés dans la Figure 19.

Un résumé des processus secondaires mettant l'accent sur les processus qui pourrait conduire à une ramification des fibrilles amyloïdes a été proposé par Andersen et al. (Figure 19)

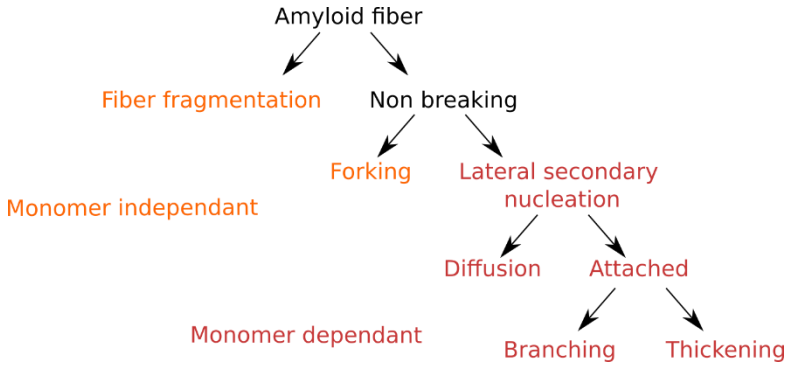

Figure 19. Classification de 5 processus secondaires selon Andersen et al.[61] dans les processus indépendant des monomères (ici en orange) le taux de création de nouveaux sites de rassemblement ne dépend que de la quantité d'agrégats. En revanche, dans les processus dépendants des monomère (ici en rouge) la vitesse de la création de nouveaux sites de d'incorporation dépend de la quantité d'agrégats et de la concentration de monomères en solution.

1.5 Paramètres influençant la stabilité des protéines

Dans cette section, nous examinerons les principales sources d'instabilité des protéines en mettant l'accent sur les phénomènes d'agrégation amyloïde. Premièrement les conditions physico-chimiques de la solution comme le pH, température, force ionique, la concentration des agents chaotropiques ou kosmotropiques, potentiel red/Ox, la concentration de protéines, etc. [46] sont déterminants pour la stabilité chimique et en solution des protéines. L'absorption de photons fournit de l'énergie supplémentaire aux les protéines ou leurs environnement qui peut induire une perte de stabilité chimique ou en solution.

Des stress résultant de l'agitation ou de la formation d'interfaces air-liquide tels que : la déshydratation, cisaillement, la formation de bulles ou d'émulsions sont bien connus pour être des déclencheurs de l'agrégation des protéines et posent des défis majeurs à l'industrie pharmaceutique. Finalement des interactions non spécifiques avec petites molécules, des macromolécules ou des surfaces ainsi que des interactions spécifiques avec des peptides et des protéines peuvent contrôler la formation de structures multimériques de protéines [122].

1.5.1 Paramètres physicochimiques de la solution

Température

La température influe sur la stabilité des protéines de multiples façons : l'augmentation de la température augmente la diffusion, la vitesse de réaction et l'énergie moyenne des particules. C'est pourquoi la cinétique et la thermodynamique des réactions chimiques sont affectées par la température. Selon la Loi d'Arrhenius, la constante de vitesse d'une réaction chimique est définie par :

$$k = A \cdot e^{\frac{-E‡}{k_B T}}$$

Où A est le facteur pré-exponentiel, E‡ est l'énergie d'activation par molécule, k_B est la constante de Boltzmann et T est la température. Mais le facteur pré-exponentiel et l'énergie d'activation peuvent être également être influencés par la température.

Les interactions hydrophobes en particulier dépendent fortement de la température, des températures plus élevées entrainant plus de dynamisme dans le réseau de liaisons hydrogènes, augmentant ainsi de la solubilité des groupes apolaires et réduisant en conséquence, l'importance des effets hydrophobes et donc la stabilité des protéines [123].

pH

Le pH de la solution définit les groupes chimiques qui seront chargés ou non en fonction leur pKa. Affectant par conséquent la charge globale de la protéine ainsi que les charges locales. Outre l'effet de floculation, entraînée par la réduction du potentiel zêta, le changement des charges de groupes particuliers peut permettre des interactions autrement impossibles, en raison de la répulsion électrostatique. L'agrégation amyloïde de plusieurs protéines est influencée par le pH en particulier dans des conditions acides, (p. ex. la transthyrétine (L55P) [124], l'insuline [125] et la chaine légère des immunoglobuline [126]. Une des explications réside dans le fait que la répulsion entre charge de même signe peut prévenir la formation du *steric zipper* et donc l'apparition des fibrilles amyloïdes. C'est le cas de l'insuline pour laquelle l'absence de charge des résidus acide glutamique située face à face dans le modèle de *steric zipper* proposé par Ivanova et al. Semble être la raison de l'agrégation amyloïde rapide de l'insuline à pH 2.

Forces ionique et champs electriques

La force ionique désigne la capacité d'une solution à former une « atmosphère ionique » de contre-ions autour de groupements chargés. Elle est définie comme :

$$I = \frac{1}{2}\sum_{i=1}^{n} c_i \cdot z_i^2$$

Où c_i and z_i sont la concentration et la charge de l'ion i, respectivement. La force ionique est responsable de l'écrantage des charges en solution, donc de la réduction l'effet de ces charges dans les interactions macromoléculaires. La force ionique et la charge nette de la protéine sont impliquées dans le potentiel zêta qui est le potentiel d'une particule et ses ions associées sur le *slipping plane* (c'est-à-dire l'interface entre la couche de solution stationnaire autour de la particule et le reste de la solution). Comme le potentiel zêta est impliqué dans la stabilité de la solution, floculation peut se produire lorsqu'il s'approche de zéro. Mais, comme décrit dans la section suivante, les ions sont également en mesure d'affecter de manière plus spécifique la solubilité et la conformation des protéines.

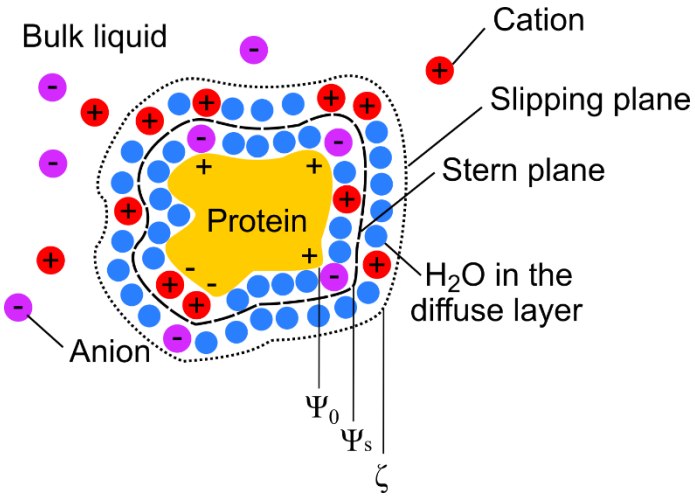

Figure 20. Definition of the planes and potentials around a solute protein. The surface potential (Ψ_0), Stern potential (Ψ_s) and Zeta potential (ξ) of the protein are defined at the protein surface, at the Stern plane and at the slipping plane respectively.

Les protéines sont des molécules chargées et donc migrent sous l'influence de champs électriques par électrophorèse. Les champs électriques peuvent également induire des changements conformationnels dans une structure protéique. Au sein de cristaux du domaine PDZ humain la conformation induites par un champ-électrique imite la conformation du domaine lors de la liaison d'un ligand [127]. Cependant, ces effets restent rares dans les conditions physiologiques en dehors des protéines membranaires [128].

1.5.2 Agents chaotropiques et kosmotropiques

Les molécules de chaotropiques sont des espèces chimiques, déstabilisant la structure conformationnelle des macromolécules [129] par exemple en diminuant l'effet hydrophobe. D'autre part les molécules kosmotropiques abaissent la solubilité des groupes apolaires. L'effet de Hofmeister décrit la capacité des ions à influer sur la solubilité des protéines et la stabilité structurelle [130]. Les ions interagissent avec les molécules d'eau de la couche de solvatation et directement avec les macro-molécules, modifiant leur tension interfaciale et les interactions hydrophobes à son tour. La série Hofmeister classifie les anions et les cations du plus *out salting* (diminuant la solubilité de la protéine avec sa concentration) au plus *in salting* (augmentant la solubilité de la protéine avec sa concentration) (Figure 21). Les ions *out salting* augmentent l'effet hydrophobe, augmentant par conséquent la tendance de protéines à agréger. Mais ces ions stabilisent également la structure de la protéine probablement par le biais de la stabilisation de leur cœur hydrophobe.

D'autre part les ions *in salting* améliorent la solubilité des groupes polaires, augmentant la solubilité des protéines mais favorisant de ce fait la forme dépliée de la protéine.

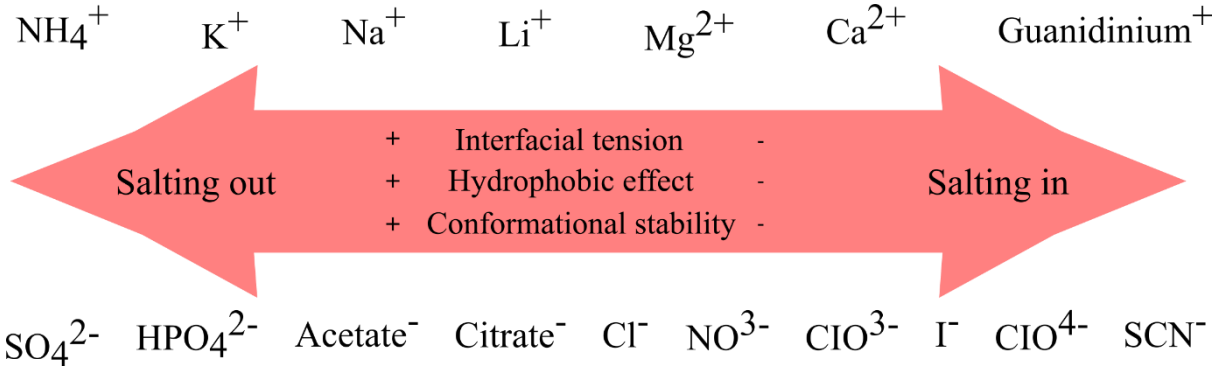

Figure 21: Série de Hofmeister présentant les séries des anions et des cations.

En dehors des ions, d'autres molécules présentent des comportements chaotropes ou kosmotropes, l'urée par exemple est connue depuis longtemps pour dénaturer les protéines.

En revanche, le tréhalose, la bétaïne et la citruline sont parmi les exemples les plus connus de kosmotropes, certaines de ces molécules même parfois appelés chaperonnes chimiques par analogie avec les protéines chaperonnes [131] . L'acide férulique par exemple inhibe la nucléation d'insuline [132].

1.5.3 Radiations électromagnétique

Les photons peuvent être absorbés par les électrons des molécules augmentant leur énergie du niveau d'énergie du photon :

$$E = h \cdot \nu$$

Où h est la constante de Planck et ν la fréquence du photon. Les molécules sont capables d'absorber un photon présentant une énergie correspondant à la différence entre une orbitale moléculaire occupée et une orbitale inoccupée d'énergie plus élevée (Figure 22).

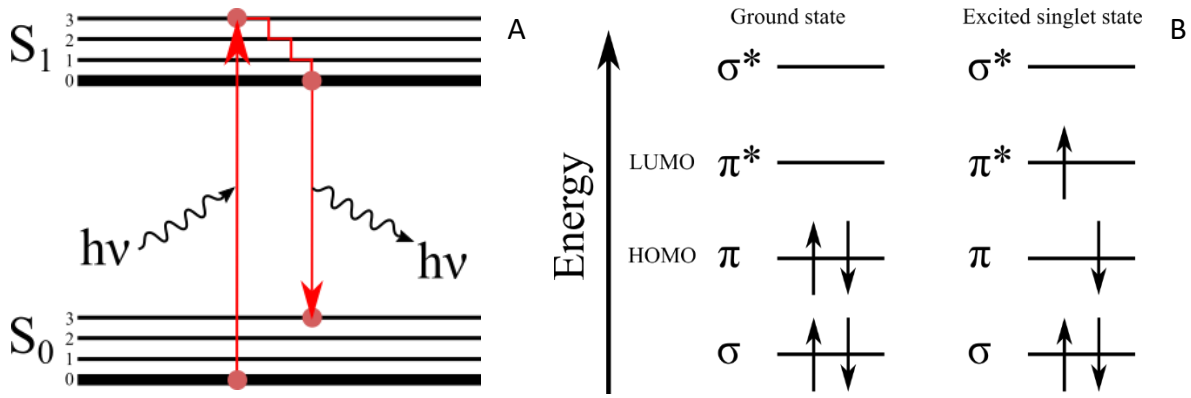

Figure 22. Jablonski diagram (A) and diagram of electron orbital ocupancy before and after a π→π* transition induced by a photon absorbtion (B).

La théorie des orbitales moléculaires frontières décrit le passage de l'orbitale moléculaire occupée la plus haute à la plus basse orbitale moléculaire inoccupé par l'absorption d'un photon d'énergie correspondant. Les électrons π en particulier ont une propension supérieure à absorber le rayonnement électromagnétique en raison du faible écart d'énergie entre leur état fondamental et leur état excité. Après relaxation vibrationnelle interne aboutissant à la dissipation d'énergie sous forme de chaleur, l'électron regagne son état fondamental en émettant un photon d'énergie plus faible que le photon d'excitation. Mais cette relaxation radiative n'est pas le seul moyen de libérer l'énergie absorbée. Tout d'abord la molécule excitée peut réagir en particulier via les réactions d'oxydation conduisant à sa dégradation chimique. Les voies de relaxation non radiatives incluent la libération d'énergie sous forme de chaleur. A distance nanométrique, le transfert d'énergie de résonance de Förster (FRET) permet le transfert direct de l'énergie de la molécule excitée à une molécule présentant une énergie d'excitation correspondant à son énergie d'émission.

Dans les protéines, les acides aminés aromatiques (Phe, Trp, Tyr) ainsi que les His sont capables d'absorber des photons dans l'ultraviolet. L'énergie absorbée par les protéines ou à les molécules à proximité peut entraîner un chauffage locale permettant des changements de conformations ou pouvant entraîner leur dégradation chimique.

1.5.4 Stress mécaniques

Les contraintes mécaniques sont connues pour être un facteur d'accélération dans l'agrégation des protéines : agitation peut accroître la diffusion et en conséquence augmenter la vitesse de réaction, surtout dans le cas des réactions localisées sur les surfaces. Les contraintes de cisaillement sont généralement associée à l'agrégation protéique dans la littérature malgré leur incapacité à dénaturer les protéines [133]. En revanche la fragmentation mécanique d'agrégats particulièrement de fibrilles conduisant à une augmentation des sites d'incorporation de protéines natives peut être autre explication quant à la dépendance vis à vis de l'agitation observée dans les cinétiques d'agrégation des protéines. Alternativement, stress mécanique pourrait conduire à la formation de triple interface (air-solution-matériau) dynamique conduisant à des phases répétées d'hydratation / déshydratation des protéines adsorbés sur à la surfaces du matériau à triple interface (cf. section 1.5.5).

1.5.5 Interactions des protéines avec les surfaces et les interfaces

L'adsorption des protéines est le processus menant à la liaison d'une protéine à la surface d'un matériau ou une interface (par exemple interface liquide-air, interface polaire-apolaire, etc.).

Au contact d'une surface, en particulier les surfaces hydrophobes ou qui sont chargées, les interactions non covalentes entre la protéine et la surface peuvent conduire à une déshydratation de l'interface protéine-matériel [134]. La différence d'énergie de cette interaction interfaciale par rapport à l'interaction solvant protéine définit la stabilité de cette adsorption. En raison de la diversité de leurs groupes chimiques et leur caractère amphiphile, les protéines sont capables d'interagir avec un large éventail de surfaces et d'interfaces physiques. Souvent, l'adsorption des protéines à la surface des matériaux et à l'interface air-liquide est signalée comme formant des monocouches. Dans ce cas, l'adsorption d'une protéine sur une surface peut être modélisée à l'aide de l'équation suivante :

$$\theta = \frac{1}{1 + \left(\frac{K}{[P]}\right)^n}$$

Où θ, la fraction de surface occupée dépend de la concentration de la protéine [P], la constante d'affinité K et l'indice de coopérativité n de la protéine. L'indice de coopérativité reflète la stabilisation d'une protéine à la surface par d'autres molécules de protéine adsorbé. En effet les interactions protéine-protéine peuvent stabiliser les protéines adsorbées et faciliter l'adsorption de nouvelles protéines (Figure 23). Cette coopération positive se traduirait par un indice de coopérativité supérieur à 1.

Cependant si le pH est éloigné du point isoélectrique de la protéine, la répulsion électrostatique qui en résulte peut défavorisez son adsorption à proximité d'autres protéines à la surface. Dans un tel cas, de coopérativité négative, où l'adsorption d'une première protéine défavorise l'adsorption d'une autre protéine à proximité, n est inférieur à 1. Pour un indice de coopérativité égal à 1, l'équation devient identique à l'équation de Langmuir.

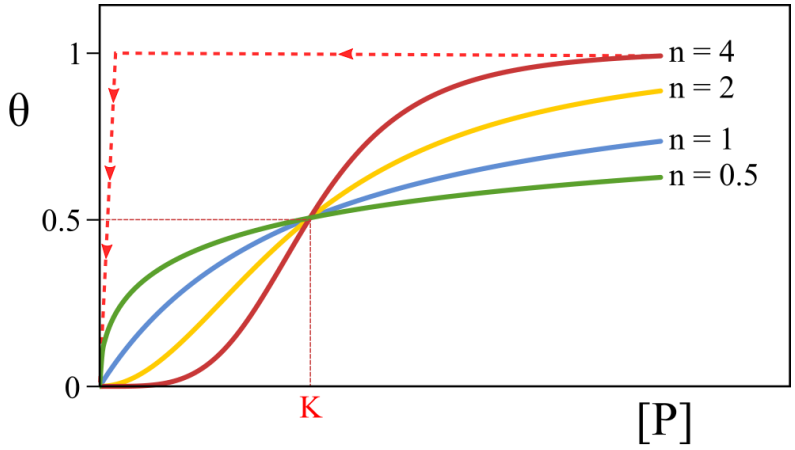

Figure 23. Adsorption isotherm for cooperative (n=2 and n=4), non-cooperative (n=1) and anti cooperative adsorption(n=0.5). The red doted curve also shows desorption hysteresis after the sudden reduction of protein concentration in solution.

L'énergie impliquée dans l'interaction non covalente protéine-surface définit l'affinité K de la protéine pour la surface. Ces interactions vont, comme les interactions internes de la protéine et les interactions solvant-protéine, influer sur la conformation de la protéine. Au moment de l'adsorption, la conformation des macromolécules subit donc une transition rapide afin de renforcer l'interaction protéine surface, augmentant la surface de contact et stabilisant l'interaction. En particulier une augmentation de *random coil* et une modification de la stabilité thermique des protéines adsorbés sont souvent observés [135,136]. Cet État peut représenter le premier intermédiaire menant à la formation d'agrégats de protéines [136]. L'affinité pour la

surface et la formation d'intermédiaires conformationnels explique pourquoi les voies de nucléation hétérogène dominent en présence de surfaces adaptées (comme décrit section 1.4).

L'effet Vroman explique la succession de molécules adsorbées sur une surface, nouvellement exposée à la solution. Les protéines ou peptides plus petits sont les premiers à s'adsorber sur la surface en raison de leur plus grande mobilité. Ils sont suivis plus tard et souvent remplacés par des protéines plus grosses qui ont par conséquent des constantes de diffusion moins élevées mais possèdent généralement une plus haute affinité pour la surface [137].

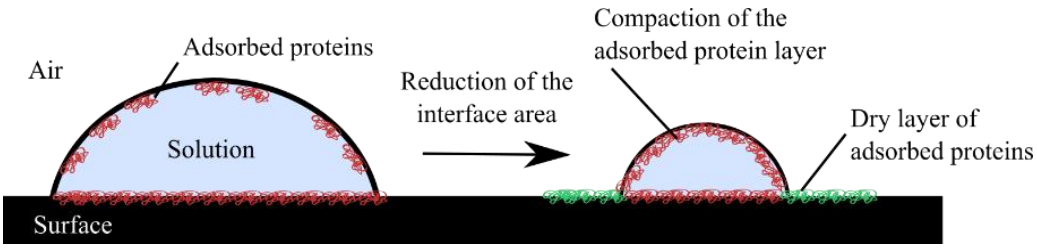

Figure 24. Effect of triple interface point variation and surface reduction on the interfacial layer of proteins.

L'interface air-liquide est également d'une grande importance pour l'agrégation des protéines et en particulier pour l'agrégation amyloïde. Par exemple, les peptides amyloïdes bêta forment à cette interface des monocouches dont la structure contient une grande proportion de feuillets β [138]. La région de la triple interface est souvent désignée comme essentielle pour la stabilité des protéines pour plusieurs raisons. Premièrement l'aire de l'interface air-liquide peut être rapidement contractée ou étendue, conduisant à des variations rapides de la densité de la protéine à l'interface. En outre, la ligne de triple interface peut varier le long de la surface du matériau et éventuellement exposer les protéines adsorbées à l'air. Et donc a stress de déshydratation.

1.5.6 **Interactions spécifiques**

Tout d'abord la liaison d'un ligand augmente le nombre d'interactions totales de l'ensemble formant le complexe et a donc tendance à stabiliser la structure de la protéine, en particulier le complexe protéine-ligand reste généralement stable à des températures plus élevées que la protéine seule. Cette propriété générale est le fondement des méthodes criblage pour la recherche de molécules thérapeutiques par *thermal shift assays* dans lesquels la température de dénaturation d'une protéine (ou point de fusion de la protéine, qui est la température à laquelle 50% des protéines en solution sont dénaturées) est évaluée en présence de différents ligands potentiels [139].

Puis, dans le contexte particulier d'amyloïdes, nombreuses petites molécules présentent des mécanismes d'interférence l'agrégation amyloïde ou interagissent spécifiquement avec des fibrilles amyloïdes, y compris des métaux, des glycosaminoglycanes et d'autres protéines [140].

C'est particulièrement le cas pour l'agrégation d'Aβ(1-42) pour laquelle plusieurs cas d'interactions avec les ions des métaux sont bien documentés [141]. En particulier les ions Cu^{2+} lient le motif N-terminale de liaison au cuivre et au nickel (Nterm-X-X - H-) du peptide Aβ(11-23) [142,143] ce qui réduit le nombre de liaisons hydrogènes inter brins et en conséquence inhibe l'agrégation [144].

Si l'introduction de *seeds* amyloïdes d'une protéine dans une nouvelle solution de cette protéine spécifique est bien connue pour induire une transition rapide vers une phase rapide de l'agrégation, d'autres chaînes polypeptidiques peuvent inhiber spécifiquement les cinétiques d'agrégation amyloïde. L'Alpha 1-antichymotrypsine, par exemple, est connu soit pour

promouvoir agrégation de l'Aβ à un bas rapport molaire (1/200) [145] ou au contraire l'inhiber à un rapport molaire de 1/10 [146] et désagrège même les fibres amyloïde déjà formées. Cette protéine peut également former des agrégats amyloïdes d'elle-même dans des conditions spécifiques [147]. De même, l'apolipoprotéine E accélère l'agrégation d'Aβ avec un rapport molaire de 1: 100 [145,148] mais inhibe cinétiquement l'étape de nucléation à des concentrations inférieures [149].

Outre le double effet de ces deux protéines, de nombreuses molécules sont connus comme inhibitrices ou comme accélératrice de l'agrégation d'Aβ notamment des protéines, des phospholipides, des gangliosides, etc [150].

On considère généralement que seule une courte séquence de la protéine est responsable de cet effet de seeding dans l'agrégation amyloïde : la section de la protéine impliquée dans la formation du feuillet β intermoléculaire. Ivanova et al [125] ont montré qu'un petit peptide provenant de la séquence de l'insuline pouvait considérablement interférer avec la cinétique d'agrégation de l'insuline. Soit en accélérant la phase de nucléation et de croissance à des concentrations sub-stœchiométrique (rapports molaires de 1/40 et 1/25) ou empêcher l'agrégation des ratios équimolaire.

Nous observons donc des mécanismes affectant l'agrégation qui, contrairement aux agents chaotropiques, interviennent à des concentrations sub-stœchiométriques. Ceci indique une interaction de ces peptides avec un intermédiaire constituant une étape limitante sur la voie d'agrégation amyloïde et suggère fortement un effet sur la phase de nucléation. En revanche, inhibition près de concentration équimolaire suggère une inhibition de l'incorporation des protéines natives.

1.6 Contexte scientifique et approche

Dans la présente thèse, nous nous concentrerons sur les questions d'agrégation de l'insuline induite par les surfaces hydrophobes.

1.6.1 L'insuline

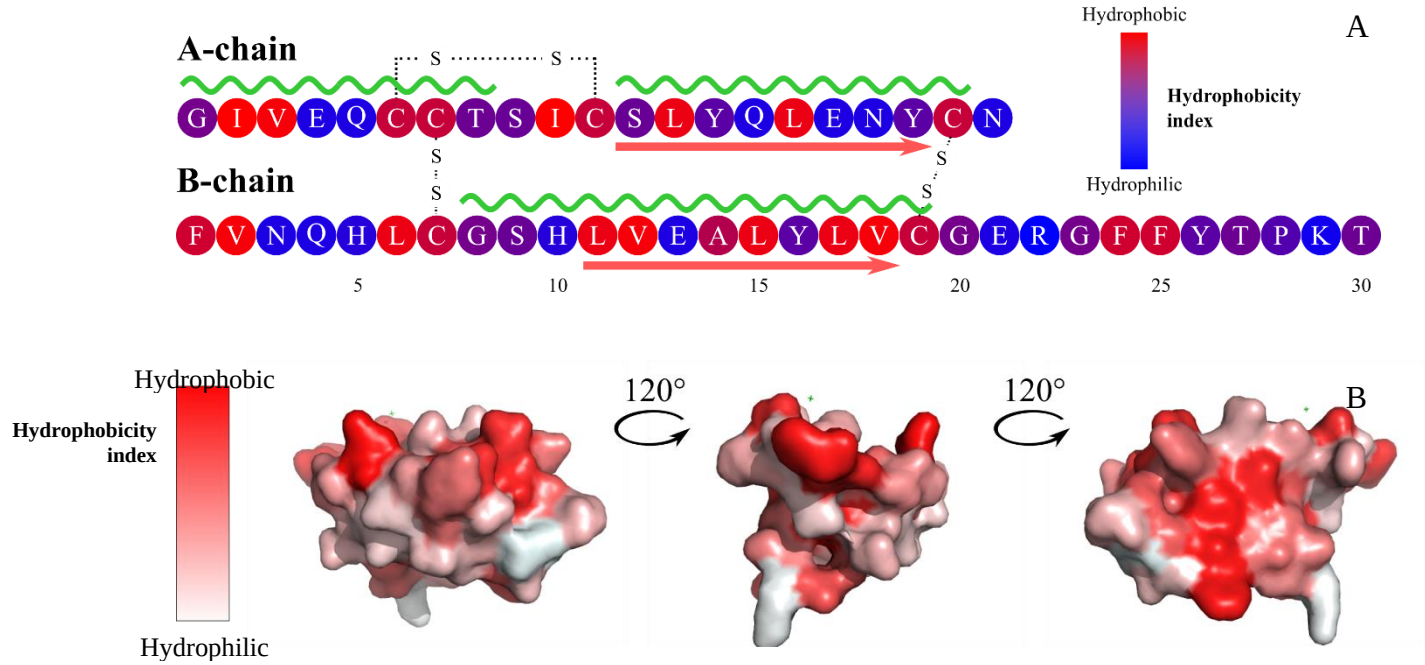

Figure 25. A : séquence des chaînes A et B de l'insuline humaine et l'hydrophobicité [4] **de leurs acides aminés. La ligne ondulée verte marque les hélices alpha dans la structure native. Flèches rouges marquent les β-feuilles dans la structure**

amyloïde. B : modèle de surface de insuline native de porc (*Sus scrofa*) coloré en utilisant une échelle hydrophobicité (PDB acces number 4INS).

L'insuline est une hormone protéique sécrétée par les cellules β des îlots de Langerhans dans le pancréas (d'où son nom du lat. insula « île ») qui présente un effet important sur la régulation du métabolisme et de la glycémie et est donc utilisé comme une protéine thérapeutique dans le traitement du diabète sucré [151].

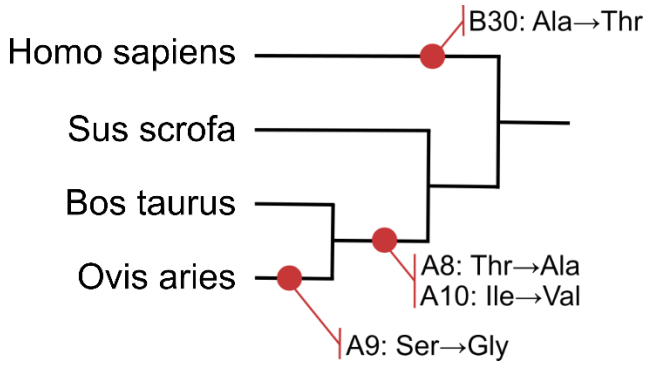

Figure 26. Évolution de la séquence d'acides aminés de l'insuline entre les quatre espèces les plus utilisées dans la littérature sur l'insuline.

L'insuline est une petite protéine d'environ 5800 Da, sa structure est essentiellement globulaire et comprend 3 ponts disulfures qui sont des éléments conservés caractéristiques de la famille des protéines insulin-like.

Deux de ces liaisons relient les deux chaînes peptidiques et un pont de disulfure est intrachaîne dans la chaîne de A (Figure 25).

Sa séquence est hautement conservée chez les vertébrés [152]: l'insuline d'espèce très distantes peut donc induire des réponses cliniques. L'insuline porcine et humaine ne diffèrent que d'un seul acide aminé (Figure 26) permettant l'utilisation généralisée de l'insuline de *Sus scrofa* dans la thérapie du diabète avant l'émergence des biotechnologies basées sur l'ADN recombinant. Plus récemment, l'ingénierie des protéiques a conduit au développement d'analogues de l'insuline présentant des profils d'absorption, distribution, métabolisation et excrétion modifiées. En particulier ces analogues ont été développés afin d'obtenir les constantes d'association choisies et les propriétés pharmacocinétiques correspondantes.

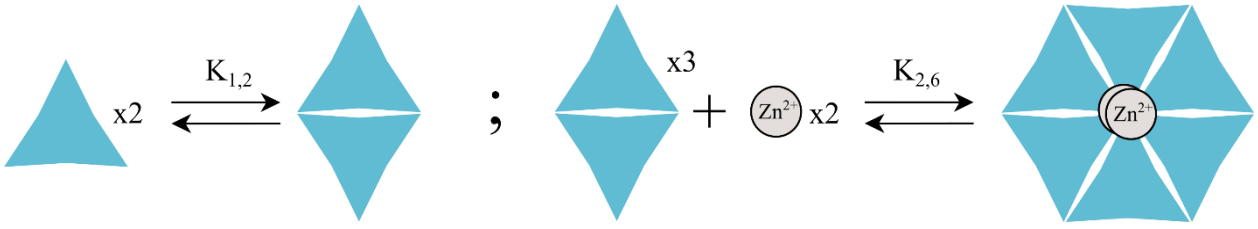

Figure 27. Auto-association des monomères d' insuline en dimère et auto-association de ces dimère en hexamères par association avec 2 ions Zn^{2+}

L'insuline peut former des dimères et hexamères en solution augmentant sa stabilité conformationnelle grâces aux interactions intermoléculaires. Les hexamères d'insuline sont formés par l'association de 3 dimères via la formation d'un complexe avec 2 ions Zn^{2+} (Figure 27). Le point isoélectrique de l'insuline humaine est de 5.3-5,35 [153] (Figure 28).

Forme de l'insuline	$K_{1,2}$ (M^{-1})	$K_{2,6}$ (M^{-2})
Sus scrofa Zn-free[154]	$14 \cdot 10^4$	$4 \cdot 10^8$
Bos taurus Zn-free[155]	$1 \cdot 10^4$	$1 \cdot 10^8$
Sus scrofa Zn[156]	$14 \cdot 10^4$	$15 \cdot 10^{10}$

Table 3: Constante d'équilibre pour la formation des dimère ($K_{1,2}$) et des hexamère ($K_{2,6}$) pour différentes molécules d'insuline.

1.6.2 Agrégation amyloïde de l'insuline

Deux conditions principales sont connues pour induire la formation d'agrégats amyloïdes d'insuline : (i) en solution à haute température et à pH faible (> 70° C ; pH 2) et (ii) sur des surfaces hydrophobes en conditions physiologiques (37° C, pH 7) et sous agitation importante.

Agrégation fibrillaire de l'insuline à faible pH et à température élevée en solution est connue depuis longtemps [157,158]. La plupart des données disponibles sur l'agrégation de l'insuline mécanistes provient de ces conditions. les fibrilles résultant de cette agrégation sont linéaires non branchées et caractérisée par des feuillets β intermoléculaire [159].

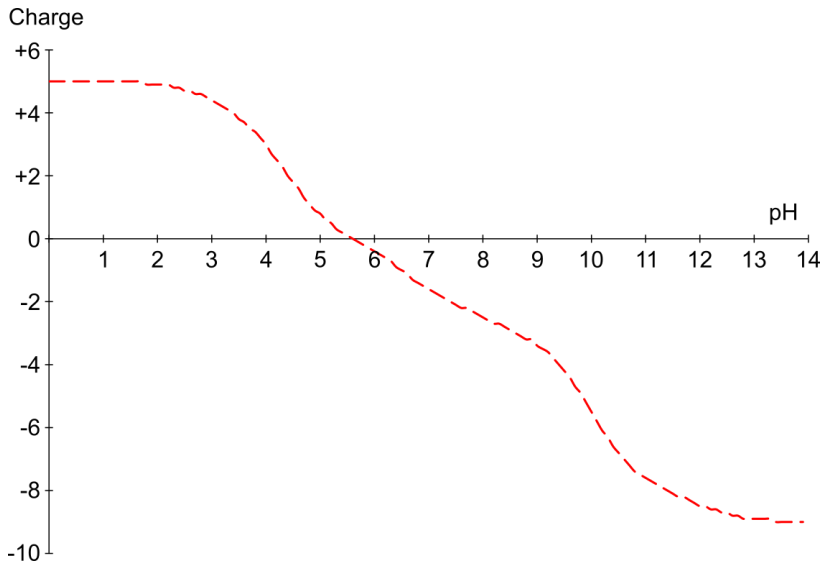

Figure 28. Charge nette théorique de l'insuline humaine en fonction du pH.

Lee et al. ont présenté un modèle cinétique divisé en trois phases : mauvais repliement, nucléation et élongation [160]. Selon ce modèle, qui est semblable au modèle général développé précédemment, l'hexamère se dissocie en monomères, qui, après un changement de conformation, s'oligomerizent dans les noyaux selon un processus d'association énergétiquement défavorable. Au-delà d'une taille critique de noyau, l'ajout de monomère devient thermodynamiquement favorable permettant l'allongement rapide des fibrilles. Les premières étapes de la fibrillation insuline bovine peuvent être suivit par le biais de fluorescence intrinsèque de la tyrosine (l'insuline bovine présente quatre tyrosines situés aux mêmes positions que l'insuline humaine mais ne possède pas de tryptophane cf. Figure 25). Cette approche combinée avec un suivit de la fluorescence de la ThT ou de l'ANS a montré que la dissociation des dimère, la coalescence et le dérepliement (État ANS positif) précédait l'état ThT positif [42].

La technique de *Small angle X-ray scattering en solution* a permis d'obtenir des structures en basse résolution du monomère, de la fibrilles et de manière plus intéressante d'un oligomère composé de 5-6 monomères d'insuline [161]. Les auteurs présentent ces oligomères comme des noyaux, qui constitueraient également l'unité d'élongation des fibrilles d'insuline. Nielsen et al [162] ont effectué un criblage de l'effet des facteurs environnementaux sur l'agrégation de l'insuline, présentant un modèle dans lequel des intermédiaires monomériques partiellement repliés forment des noyaux qui deviennent des fibrilles amyloïdes. Ils observent une dépendance à des températures élevées pour la fibrillation de l'insuline qu'ils attribuent à la formation d'intermédiaires « fibrillation-compétente » qui représenteraient l'étape cinétiquement limitante. En outre, ils soulignent le rôle positif de l'agitation mécanique sur la nucléation qui ils expliquent par la formation d'une zone d'interface air-eau plus étendue.

Les étapes d'agrégation amyloïde de l'insuline étudiées par dichroïsme circulaire et par microscopie électronique sont d'abord la formation d'agrégats non fibrillaire, menant à l'élaboration de protofilaments qui s'assemblent ensuite en fibrilles et se réorganisent finalement en structure entortillé très ordonnée présentant un répétition hélicoïdale de 450 Å [163]. Pendant ce temps, le spectre FTIR révèle une augmentation progressive du pique à 1628cm^{-1}caractéristique des feuillets β.

Dutta et al. considèrent les agrégats d'insuline ThT positifs obtenus après seeding à pH neutre et en présence d' agents de réduction des disulfures, comme amorphe [164] En raison de leur morphologie globale observée par microscopie électronique ainsi que par microscopie à force atomique. Seules leurs « seeds intermediaires » ont la capacité d'amorcer la formation d'agrégats de type fibrillaire mais instable dans le temps.

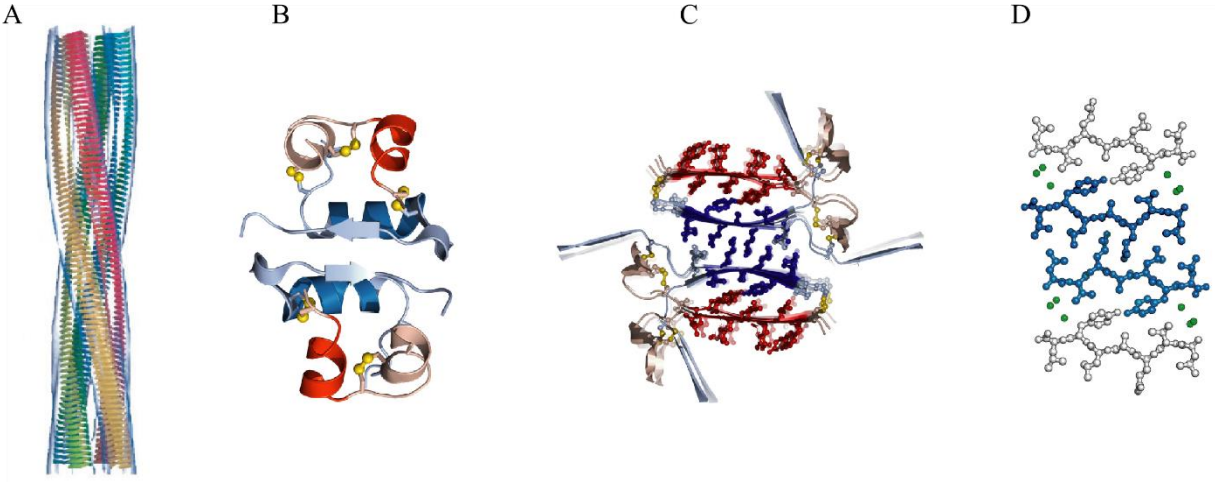

Figure 29. Structure of insulin amyloid fibril. A fibril, B structure of the native insulin dimer, C model of amyloid insulin dimer, D structure of region involved in the β sheet formation with formation of a steric zipper. Modified from Jimenez et al.[165] (A) and Ivanova et al.[125] (B, C, D).

En 2002 Jimenez et al. [165]ont étudié la structure des fibrilles amyloïdes d'insuline par cryo-microscopie électronique, une fois de plus, à haute température et à pH faible. Ils ont observé des fibrilles contenant 2, 4 ou 6 protofilaments (Figure 31). Manno et al. ont caractérisé la croissance cinétique d'un point de vue morphologique et décrit la phase de croissance comme une combinaison d'élongation et d'élargissement par nucléation secondaire [166,167]. Ivanova [125] ont également étudié les mécanismes de la formation de fibrilles amyloïdes d'insuline et produit un modèle détaillé des changements de conformation de l'insuline pendant la fibrillation. Ils ont caractérisé les sections de la protéine impliquées dans la formation des feuillets β intermoléculaire en cherchant les peptides minimaux issus de la séquence de

l'insuline humaine capable d'agréger d'eux même. L'un de ces peptides impliqués dans la formation du feuillet β intermoléculaire est en mesure d'influer sur la cinétique d'agrégation de l'insuline de manière concentration dépendante. Nayak et al.[168] a fait observer la corrélation entre l'hydrophobie ou la rugosité des surfaces et leur capacité à réduire le temps de latence de l'agrégation de l'insuline. Même à pH 1.6, les surfaces hydrophobes et rugueuses ont été en mesure d'accroître sensiblement la nucléation. En revanche, ils n'ont pas observé une influence de la surface sur la vitesse de croissance des agrégats.

Toutes ces données sont d'un grand intérêt pour notre thématique de de recherche, mais ne sont pas facilement rattachables. Premièrement, même si la nucléation (et pas de croissance) est la seule étape nécessitant une température élevée [169], le faible pH modifie les charges de l'insuline permettant des interactions autrement très défavorable en conditions physiologiques.

Une autre condition connue pour provoquer l'agrégation de l'insuline est sous agitation à la surface des matériaux. Le développement de l'insulinothérapie pour le diabète sucré, à rapidement amené la question de son adsorption sur les surfaces des systèmes de stockage et d'injections [170] pouvant ultérieurement induire son agrégation [171,172]. Le rôle du stress mécanique dans cette perte de stabilité a aussi été mis en avant [171,173], soulevant des obstacles au développement des dispositifs d'administration de l'insuline [174–177] et des poudre d'insuline en microparticules [178]. En outre des amylose iatrogène localisée ont été observé dans les sites d'injection régulière d'insuline [179,180]. Les agrégats amorphes et amyloïdes d'insuline présentent tous deux une cytotoxicité pour les cellules cultivées d'insulinome de rats [181]. Cette cytotoxicité est plus élevée pour les agrégats amyloïdes et augmente la durée d'agrégation.

Sluzky et al. [173,182] ont étudié la cinétique et les mécanismes d'agrégation de l'insuline sous contraintes mécaniques et sur les surfaces hydrophobes. Ils ont proposé un modèle dans lequel les monomères d'insuline monomère s'adsorbent sur des surfaces hydrophobes, où elles subissent des transitions structurelles vers l'état déplié. Ces monomères à l'état déplié sont ensuite libérés dans la solution où ils agrègent par la suite (Figure 32). Ils ont également observé que les hexamères d'insuline participaient à la stabilité de la solution en interagissant avec la surface hydrophobe. Agrégation de l'insuline à 37° C est promue par l'agitation, l'hydrophobicité de surface et augmente avec la zone de surface hydrophobe au contact de la solution.

Plus récemment, notre équipe s'est penchée (en particulier par le biais de deux thèse par Thomas Ballet et Laurent Nault) sur les changement conformationnel subi par l'insuline adsorption à surfaces de matériaux [183]. L'adsorption rapide de l'insuline est associée à un premier changement conformationnel (Figure 30) qui est suivi d'un deuxième conformationnel changement de et beaucoup plus lent présentant une augmentation présumée de sa teneur en feuillet β et un signal ThT positif. La teneur en feuillet β du stade « amyloïde » de Nault (Figure 30) basée sur l'augmentation d'un pic de 1700cm^{-1}, a été mise en doute par Mauri et al.[183,184]. Il reste toutefois claire grâce à la signature infrarouge qu'un changement de conformation important survient après adsorption de l'‘insuline. Mollmann et al. et Mauri et al. ont rapporté une perte de proportion d'hélice α et une augmentation de *random coils* [184,185] au cours de l'adsorption de l'insuline.

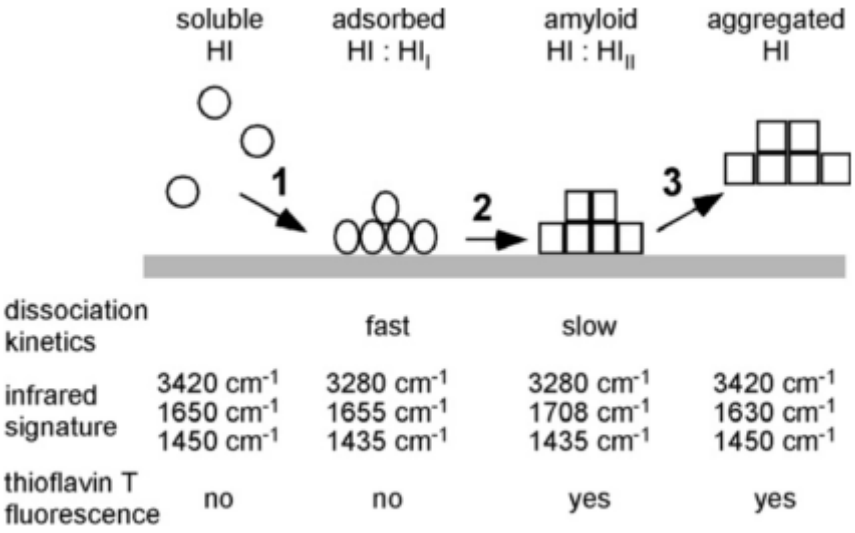

Figure 30. fluorescence Modèle de Nault pour les stades de changements de conformation de l'insuline induits par la surface. Avec les signatures FTIR et la fluorescence ThT.

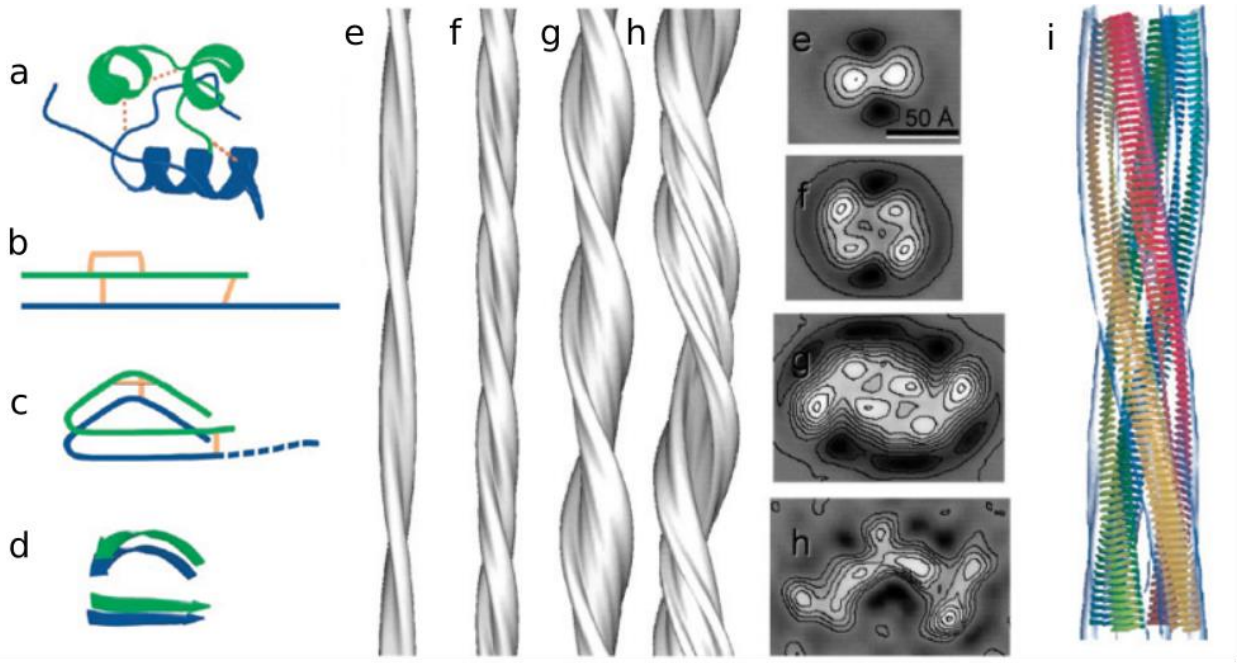

Figure 31.

Structure de la fibrille d'insuline d'après Jimenez [165] (a) structure native d'insuline montrant la chaîne A en vert et la chaîne B en bleu ; b) localisation des ponts disulfures; c) modèle proposé pour insuline amyloïde ; d) feuillet β dans le modèle de l'insuline amyloïde. Structure et coupe transversale de fibrilles observées contenant 1 filament (e), 2 filaments (f), 4 filaments (g) ou 6 filaments (h). Modèle de la fibrille amyloïde d'insuline présentant la structure des feuillet β intermoléculaires (i)

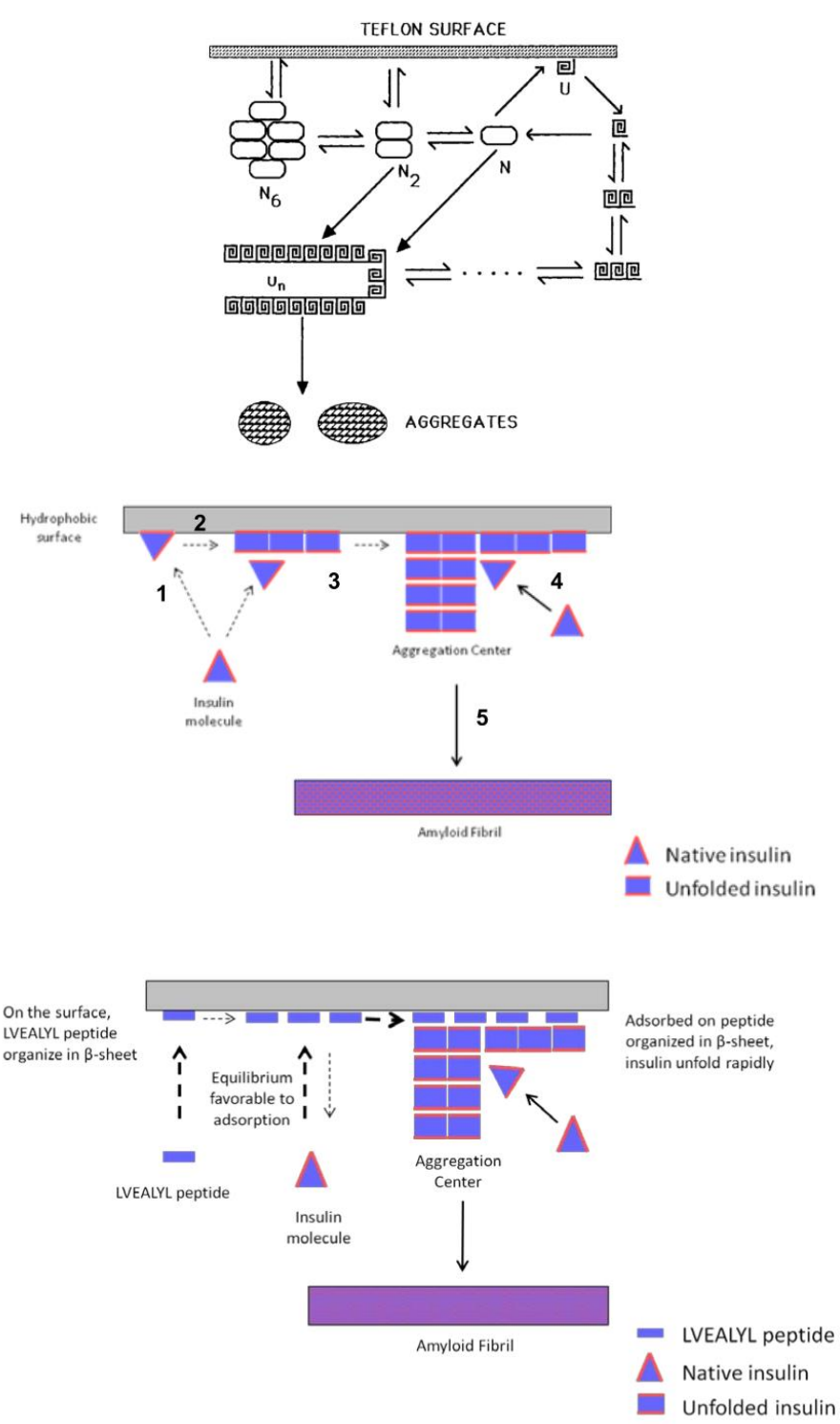

Figure 32. Modèle d'agrégation de l'insuline humaine induite par la surface proposée par Sluzky et al. (A), Ballet et al. (B) et Nault et al. (C). Selon le modèle de Sluzky, les molécules d'insuline se déplient sur les surfaces hydrophobes et sont libérées dans la solution où ils s'oligomerizent jusqu'à former des oligomères de grande taille capables d'intégrer des monomères natifs. Selon le modèle de Ballet, l'insuline est adsorbé et se déplie sur des surfaces hydrophobes, où elle nucléent pour former des centres d'agrégation incorporant des monomères natifs. Les fibrilles amyloïdes sont ensuite libérés dans la solution. Enfin, dans modèle de Nault les peptides agissent comme activateurs de nucléation et déplient l'insuline sur la surface.

Au cours de son doctorat Ballet a signalé la réduction du temps de latence de l'agrégation l'insuline à pH 2 et à 60 ° C par des seeds formées dans les mêmes conditions ou sur une surface hydrophobe à pH 7.4 et 37 ° C. Avec des seeds formées dans cette dernière condition, le temps de latence est même complètement aboli ce qui indiquerait un seeding direct alors même que les agrégats formés à pH 2 et 60 ° C présente un temps de latence d'environ 1 H 30 [186]. Ces résultats si ils sont exacts, montreraient que les agrégats d'insuline formés sur des surfaces hydrophobes et par la suite relâchés en solution dans des conditions physiologiques seraient des agrégats amyloïdes semblables à ceux formés dans des conditions acides et à haute température.

1.6.3 Interaction des péptides avec l'agrégation de l'insuline.

Afin de déterminer les sections de l'insuline humaine impliquée dans la formation des feuillet β formant la colonne vertébrale des fibres amyloïdes, Ivanova et al [125] ont cherché le peptide minimal capable à la fois s'agréger en fibrilles amyloïdes et d'accélérer l' agrégation amyloïde de l'insuline native. Ils ont montré que deux peptides SLYQLENY et LVEALYLV, présents dans la séquence de la chaîne A et de la chaîne B de l'insuline respectivement, pouvaient former des fibres amyloïdes. Par ailleurs, LVEALYLV a pu modifier la cinétique de l'agrégation de l'insuline (Figure 33). A des concentrations sub-stœchiométriques (1/40), elle accélère agrégation de l'insuline, mais à un rapport molaire de 1/10 ou équimolaire le peptide inhibe cette agrégation.

D'après la cinétique présentée (Figure 33) les peptides LVEALYLV peuvent probablement ensemencer l'agrégation des fibrilles amyloïdes d'insuline puisque le temps de latence semble aboli à des concentrations de peptide très faibles. Mais à des concentrations plus élevée la nucléation et la croissance semblent toute deux impactés

Les auteurs ont donc proposé un modèle structurel pour l'agrégation amyloïde insuline (Figure 29 C and D) dans lequel ces deux sections de peptide forment un *steric zipper* à la base de la colonne vertébrale des fibrilles amyloïdes. Néanmoins cette étude ni met l'accent sur le rôle potentiel joué par les surfaces sur l'agrégation de l'insuline, ni sur les interactions entre l'insuline et les peptides absorbés qui pourraient être adsorbés.

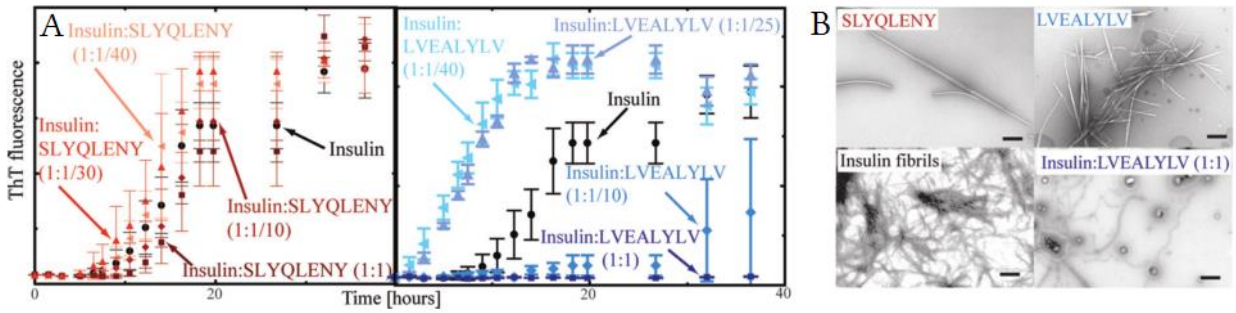

Figure 33. Deux peptides, extraits de la séquence de l'insuline sont capables de s'agréger en fibrilles amyloïdes. A: effet de SLYQLENY et LVEALYLV sur la cinétique d' agrégation de l'insuline, B : fibres de SLYQLENY et LVEALYLV (en haut) et réduction de la fibrillation de l'insuline à ratio équimolaire insuline/LVEALYLV (en bas). (Chiffres tirés du ivanova (Ivanova et al 2009)) (Figure issues d'ivanova et al.[125])

Récemment, notre équipe [187] a étudié l'effet des peptides sur l'agrégation de l'insuline en mettant l'accent sur les phénomènes qui se produisent à la surface des matériaux. Nault à utilise différentes séquences de petits peptides et suivit leurs effets sur la cinétique d'agrégation de l'insuline. Il a démontré que les peptides formant feuillet β sur les surfaces hydrophobes pouvaient accélérer significativement la nucléation de l'agrégation de l'insuline induite par la surface des matériaux surfaces et ce à concentrations sub-stœchiométriques. La résonance

plasmonique de surface a révélé que ces peptides une fois adsorbés à la surface, augmentaient la masse de l'insuline adsorbée.

En outre, en comparant le spectre infrarouge de peptides en solution par FTIR en transmission et de peptides adsorbés sur la surface de par ATR FTIR, il a démontré que les peptides présentant une conformation en feuillet β sur des surfaces hydrophobes, pouvaient réduire le temps de latence de l'agrégation de l'insuline quelle que soit leur séquence en acide aminée. Comme ces peptides ont été conçus par l'alternance d'acides aminés hydrophobes et hydrophiles, leur adsorption entraîne la formation d'un feuillet β sur la surface par l'adsorption d'une chaine hydrophobe tous deux les acides aminés. Ce phénomène suggère que les liaisons hydrogène latérales sont responsables de l'effet de nucléation. D'autre part un peptide formant une hélice alpha sur des surfaces hydrophobes présente un comportement complètement différent, retardant considérablement l'apparition d'agrégats d'insuline ThT positifs.

1.6.4 **Objectifs**

Le présent travail consiste à comprendre les différents effets sur l'agrégation de l'insuline de peptides présentant une séquence avec une alternance d'acides aminés hydrophobes et hydrophiles et leur comportement en solution ou sur des surfaces hydrophobes. En outre, on a tenté de caractériser et d'observer l'emplacement de nucléation de l'insuline sur des surfaces hydrophobes.

Dans la première partie (chapitre 3), nous examinons l'effet des peptides avec une séquence alternant entre les acides aminés hydrophobes et hydrophiles, en particulier les peptides $(LK)_nL$, sur la cinétique de l'agrégation de l'insuline. Nous avons démontré que les peptides $(LK)_nL$ s'adsorbaient de manière collaborative sur les surfaces hydrophobes, où ils favorisent la nucléation de l'insuline. Un deuxième effet antagoniste a été observé avec les peptides les plus longs ($(LK)_4L$ and $(LK)_5L$): les peptides restant en solution prolongent le temps de latence de l'agrégation de l'insuline.

Dans la seconde partie (chapitre 4), nous caractérisons les mécanismes de cet effet inhibiteur dans le détail et la nature de l'interaction agrégat-peptide en solution. Le peptide LK11 se lie avec une haute affinité aux agrégats d'insuline et empêche leur croissance probablement par des effets stériques. Cette liaison est médiée par les charges des chaînes latérales du peptide et inhibe la nucléation et la croissance des agrégats d'insuline. Dans la dernière partie (chapitre 5) nous étudions l'emplacement des sites de nucléation de l'insuline sur les surfaces, en particulier l'interface triple entre le matériau, l'air et la solution maximisant la contrainte de cisaillement, mais aussi le stress de la déshydratation. On observe une présence maximale des premiers objets ThT positifs à cette triple interface.

Sur des surfaces éclairées un mécanisme d'agrégation différent a été découvert : en présence de ThT la lumière induit localement l'agrégation de l'insuline a la surface. Nous avons mis en lumière la dépendance de ce mode d'agrégation aux surfaces permettant l'adsorption de l'insuline ainsi que sa dépendance à une forte agitation. En outre, nous étudions le rôle de la ThT comme un médiateur de l'énergie entre la lumière à 436nm et l'insuline. Cette induction localisée de croissance d'agrégats ThT positifs, dans des conditions où l'emplacement et la vitesse d'agrégation peuvent être entièrement contrôlés, est d'un intérêt particulier pour des tests (ou même des criblages) de l'effet de composés chimiques sur l'agrégation des protéines.

Effet des peptides $(LK)_nL$ sur l'agrégation de insuline

1.7 Peptides hydrophile/hydrophobe

Les principes fondamentaux derrière la recherche du peptide minimal, capable à la fois s'agréger et d'ensemencer l'agrégation de la protéine reposent sur l'hypothèse que cette séquence constitue les brins β de la colonne vertébrale des fibrilles amyloïdes et est impliquée dans la formation du steric zipper. Cependant, tel qu'illustré par les œuvres de Nault et al. il existe des différences entre ensemencement pur (dans laquelle l'agrégation se produit à partir de fibrilles préexistants) et nucléation amélioré de (où le taux de nucléation primaire est augmenté) surtout quand des interactions avec les interfaces sont impliqués. Au pH physiologique, le peptide LVEALYLV est incapable de former des fibrilles amyloïdes [187] de lui-même. Nault et al. ont cependant montré qu'il est tout de même capable d'accélérer l'agrégation de l'insuline, plus précisément sur les surfaces hydrophobes. Ses expériences n'ont toutefois été menées qu'à une seule concentration de peptide.

Des essais avec des variations de cette séquence peptidique a prouvé que, contrairement à l'expérience de seeding effectué par Ivanova et al. en conditions acides [125] à un pH faible, la séquence des peptides n'est pas impliquée dans ce mécanisme. Seule leur capacité à former des feuillets β lors de leurs adsorption sur des surfaces hydrophobes détermine leur capacité à réduire (mais pas à supprimer) le temps de latence d'agrégation de l'insuline [187]. Contrairement à ce que ces auteurs annoncent, les peptides ne sont donc probablement pas des « seeds » pour l'agrégation « amyloïde » de l'insuline induite par la surface, amyloïdes mais jouent plutôt un rôle dans la nucléation de l'insuline.

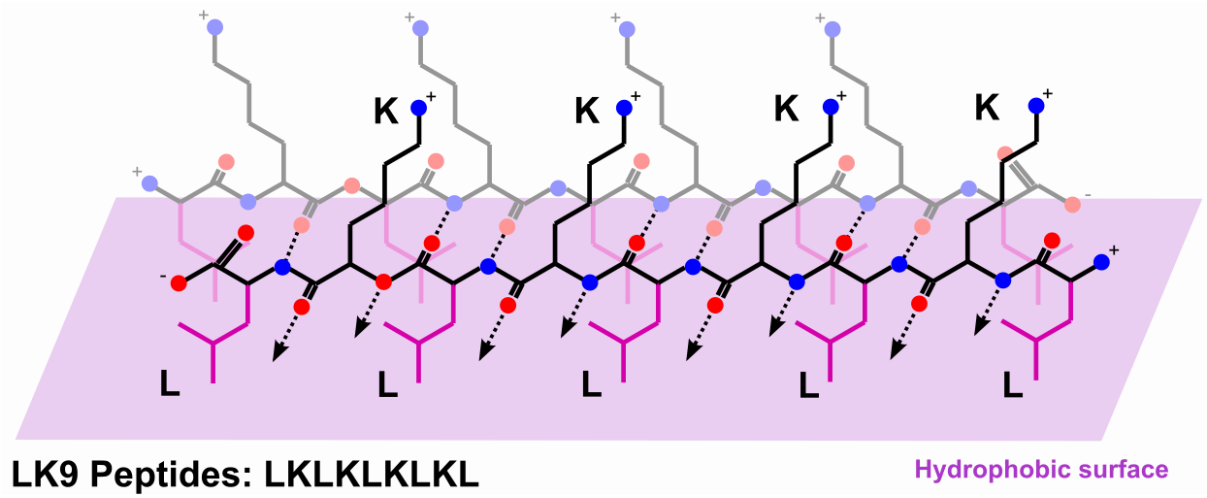

Figure 34. Peptide LK9 dont la séquence alterne entre acide aminé hydrophile et acide aminé hydrophobe remplaçant formant un feuillet β antiparallèle sur une surface hydrophobe. Les lignes pointillées représentent les liaisons hydrogène intermoléculaires. Nous utilisons la coloration CPK une couleur violette pour des chaînes latérales apolaire en contact avec la surface hydrophobe

Le plus efficace des peptides utilisé par Nault est $(IS)_3I$, un peptide présentant dans sa séquence une alternance entre isoleucine, hydrophobe et sérine, hydrophiles. Ces peptides peuvent s'adsorber sur des surfaces hydrophobes où ils adoptent une conformation β-feuille, résultant de l'exposition des chaînes latérales hydrophobes vers la surface et les chaînes latérales hydrophile vers la solution[188]. Les premières expériences que nous avons effectuées avec ce peptide et le peptide plus court $(IS)_2I$ ont montré leur capacité à réduire de manière

collaborative le temps de latence de l'agrégation de l'insuline. La plus faible concentration critique a été trouvée pour le $(IS)_3I$. Des peptides similaires, mais chargées alternant leucine et lysine ont été décrits dans la littérature comme faisant des feuillet β antiparallèles feuilles sur les surfaces hydrophobes [188](Figure 35).

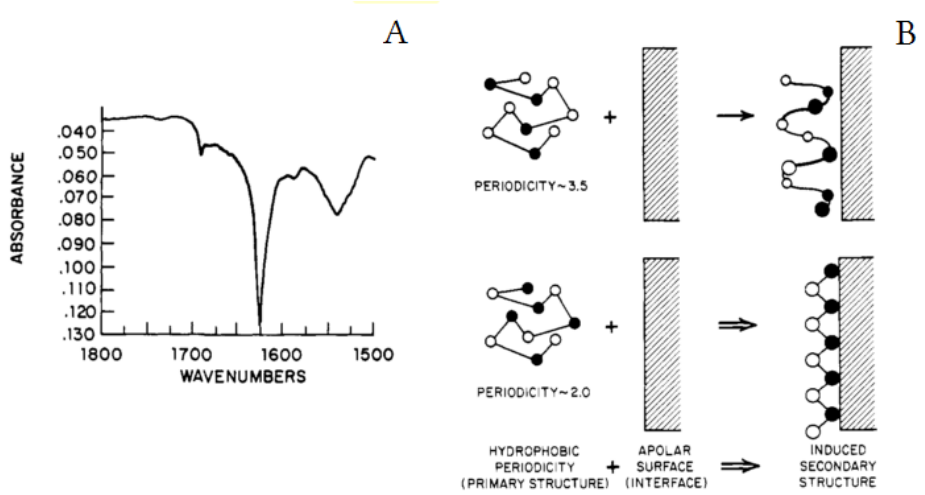

Figure 35. Conformation des peptides présentant une alternance d'acides aminés hydrophobes et hydrophiles sur des surfaces hydrophobes. A: spectre infrarouge ATIR d'une monocouche adsorbée LK7 peptide montrant le pic à 1700 cm^{-1} la caractéristique des feuillet β antiparallèles, B: structure secondaire induite par l'adsorption sur une surface hydrophobe en fonction de la periodicité des acides aminées hydrophobe des peptides. Des acides aminés hydrophobes sont représentés par des cercles pleins et des résidus hydrophiles avec des cercles vides. Modifié d'après Degrado et Lear [188].

***Cette interprétation du spectre semble cohérente avec la littérature scientifique [189–191] définissant la région de l'amide I pour les feuillets β antiparallele comme suit : "In antiparallel β-sheet structures, the amide I region displays two typical components. The major component has an average wavenumber located at ~1630 cm^{-1}, whereas the minor component, approx. 5-fold weaker than the major one, is characterized by an average wavenumber at 1695 cm^{-1}." Cerf et al. 2009[190]. Cette interprétation a toutefois été contestée par des membres du jury de défense de thèse sur la base (i) la largeure du pic principale principale à ~1625 cm^{-1} et (ii) de l'absence d'un autre pic.**

Dans le premier article, nous avons utilisé des peptides LK pour démontrer que ces petits peptides possédaient deux effets antagonistes sur la cinétique de l'agrégation de l'insuline, en fonction de leur concentration. Le premier effet dont sont responsable les peptides absorbés consiste en l'accélération de la nucléation de l'insuline sur des surfaces hydrophobes. En revanche, les peptides restant en excès dans la solution des peptides l'agrégation.

1.8 Nucléation sur les surfaces

Durée minimale de la transition ver l'état ThT positif

En l'absence de peptide ajouté (Figure 1 dans l'Article I), les temps de latence sont longs et présentent une variabilité extrêmement élevé ce qui contraste nettement avec l'agrégation stable et rapide se produisant au cours de la phase de croissance. Ceci plaide donc très fortement pour un événement rare, unique et hautement stochastique de nucléation. L'analyse statistique des cinétiques d'agrégations peut révéler comment les peptides affectent ce mécanisme. Le temps de latence en fonction de la concentration de peptide présente une asymptote horizontale à environ 30min pour les peptides $(LK)_nL$ (Figure 1 à l'article). Ce délai incompressible suggère un temps de réaction minimum pour la transition conformationnelle vers un état de ThT-positif. Bien sûr, la différence entre le temps de latence conventionnel (calculé par l'intersection entre la tangente plus pentue du signal ThT avec la ligne de base) et le temps de latence sensu stricto (correspondant à la première apparition d'un agrégat de ThT-positif) contribue à une petite partie de ce temps.

Dans ces expériences cinétiques la première mesure d'agrégats ThT-positifs (Intensité de fluorescence s'écartant de la ligne de base de plus de 3σ) est rapidement (en moins de 15 min) suivie par des mesures d'une intensité de fluorescence élevée. Il pointe vers une croissance rapide, après la première apparition de la fibrille, plutôt que vers une agrégation progressive.

Les nanostructures protéiques observées par AFM jouent un rôle dans l'agrégation de l'insuline.

Les micrographies par force atomique des surfaces de verre hydrophobe incubées en présence de peptides et/ou d'insuline sont présentées dans la Figure 8 Article I. Ces surfaces de verre silanisée, incubés pendant 30 min avec 86µM d'insuline ont la capacité de réduire le temps de latence de l'agrégation d'une nouvelle solution fraîche d'insuline (Figure 37, cercles). Cette réduction est encore plus dramatique lorsque les surfaces ont été préalablement incubées avec 86µM HI et 1µM LK9 peptides (Figure 37, carrés). Ceci indique que les structures formées sur les surfaces et visibles par AFM ont la capacité de contribuer à l'agrégation de l'insuline. S'agit-il seulement d'un mécanisme de seeding direct ou réellement d'une contribution au processus de nucléation ? La question reste difficile à trancher avec les données actuelles.

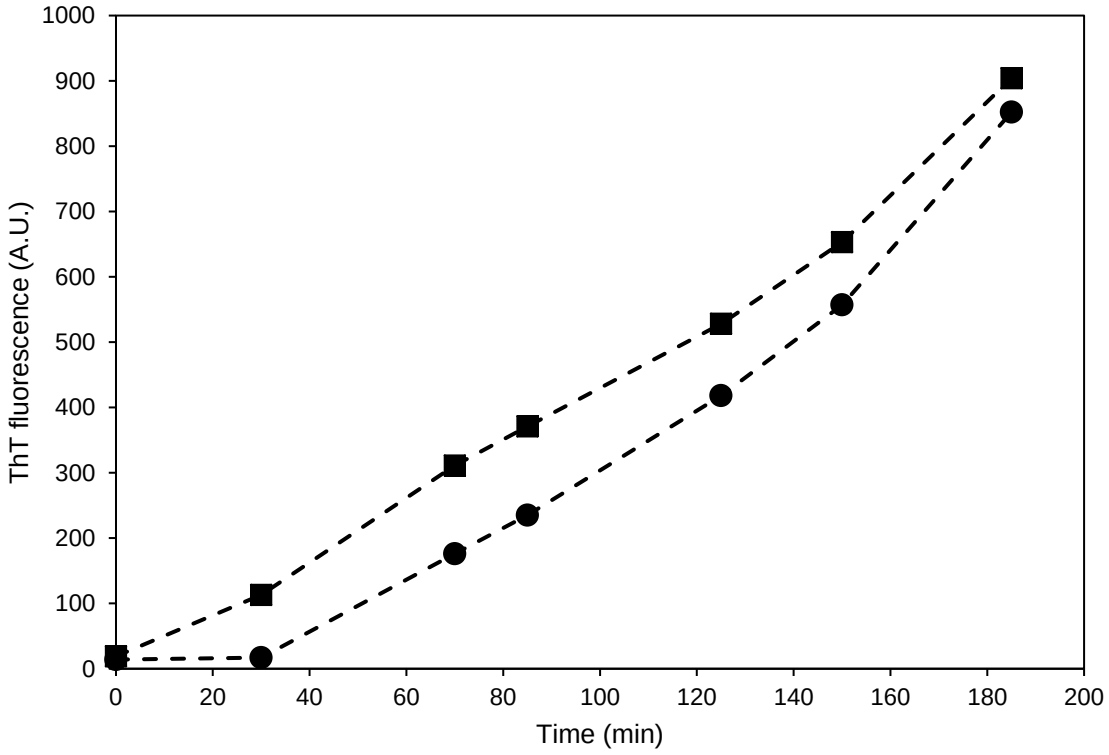

Figure 36. Cinétique d'agrégation de l'insuline en contact avec des surfaces de verre hydrophobe préalablement incubées avec 86µM d'insuline (●) ou 86µM plus 1µM de LK9 (■) durant 30 min.

1.9 Mécanismes des peptides adsorbées sur les surface sur la nucléation de l'insuline

La formation de patches de peptide à la surface stabilisée par des feuillets β latéraux inter-peptides est suggérée par la coopérativité de l'adsorption ainsi que les précédents résultats de TIRF obtenus par Nault et al [187] et De Grado & Lear [188]. Ils montrent une transition de la conformation de peptide LK7 de *random coil* vers des feuillets β antiparallèle lors de leur adsorption aux interfaces. L'interaction de l'insuline avec ces patchs implique probablement les feuillets β latéraux de ces îlots de peptide puisque que les résultats présentés par Nault et

al., [187] et ceux obtenus précédemment avec des peptides de Isoleucine-Sérine ont montré que l'effet d'accélération des peptides été indépendamment de séquences spécifiques ou des acides aminés exposés mais dépendait seulement de leur capacité à présenter une conformation en feuillets β sur les surfaces hydrophobes.

1.10 Mécanisme d'inhibition

Cet article fournit également des preuves d'un mécanisme d'inhibition de l'agrégation de l'insuline à des concentrations de peptide élevé. Nous avons démontré que les peptides restant en solution sont responsables de cet effet. Cet effet n'est observé qu'avec les peptides les plus longs avec 9 et 11 acides aminés ce qui suggère que la stabilité de la liaison de ces peptides avec les agrégats d'insuline est importante

Inhibition de la Nucleation

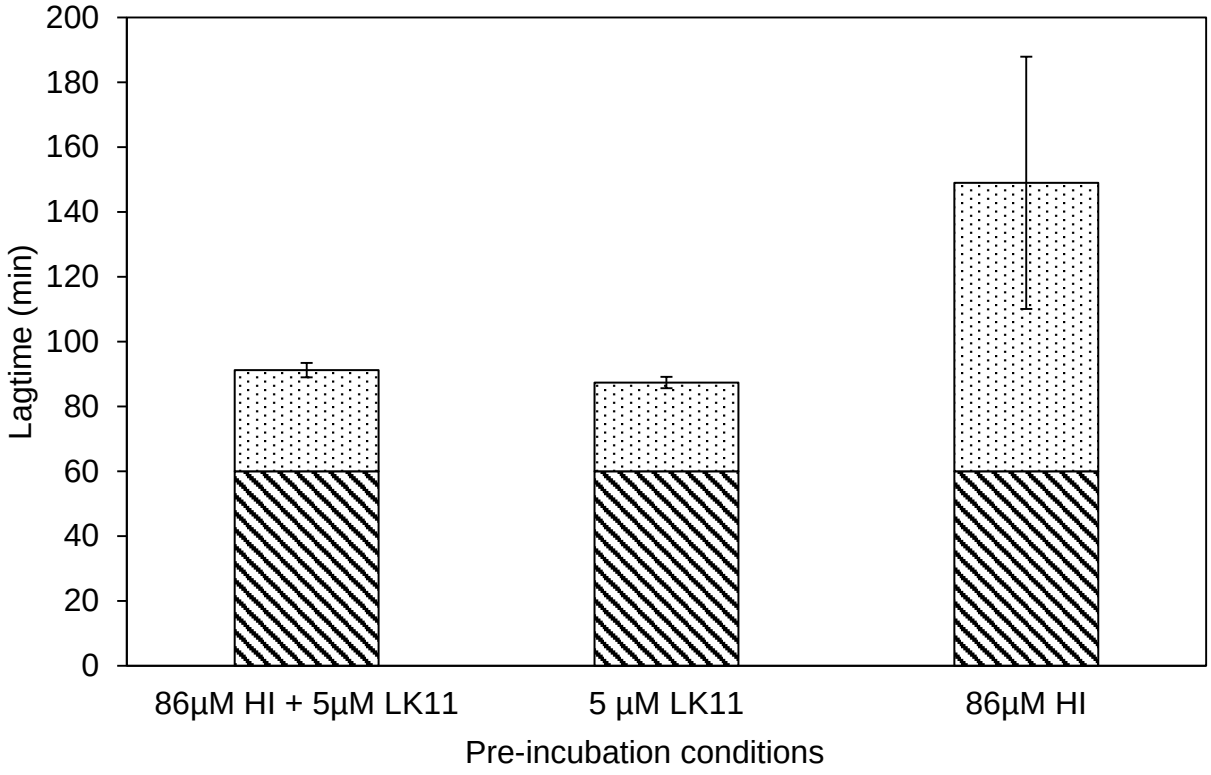

Figure 37. Les Peptides LK11 en solution inhibent totalement la nucléation. La surface a été préalablement incubée pendant 60 min (zone hachurée) dans différentes conditions puis lavés et incubés avec 86µM d'insuline (zone en pointillé), les valeurs moyennes de temps de latence sont affichées, les barres d'erreur représentent l'écart-type (n = 3).

Le temps de latence de l'agrégation de HI et leurs variations relatives augmentent considérablement avec la concentration de LK11 en solution (Figure 38). Ce peptide semble inhiber la nucléation depuis ses tout débuts. En effet, tel qu'illustré sur la Figure 5, la réduction du temps de latence attendue lors d'une incubation préalable de la surface en présence de HI est totalement inhibée par la présence de LK11 à 5 µM pendant ce temps d'incubation préalable. Ces résultats suggèrent que la contribution des complexes pré-agrégation créée au cours de cette période d'incubation préalable est perdue (Figure 37).

Le rôle des charges

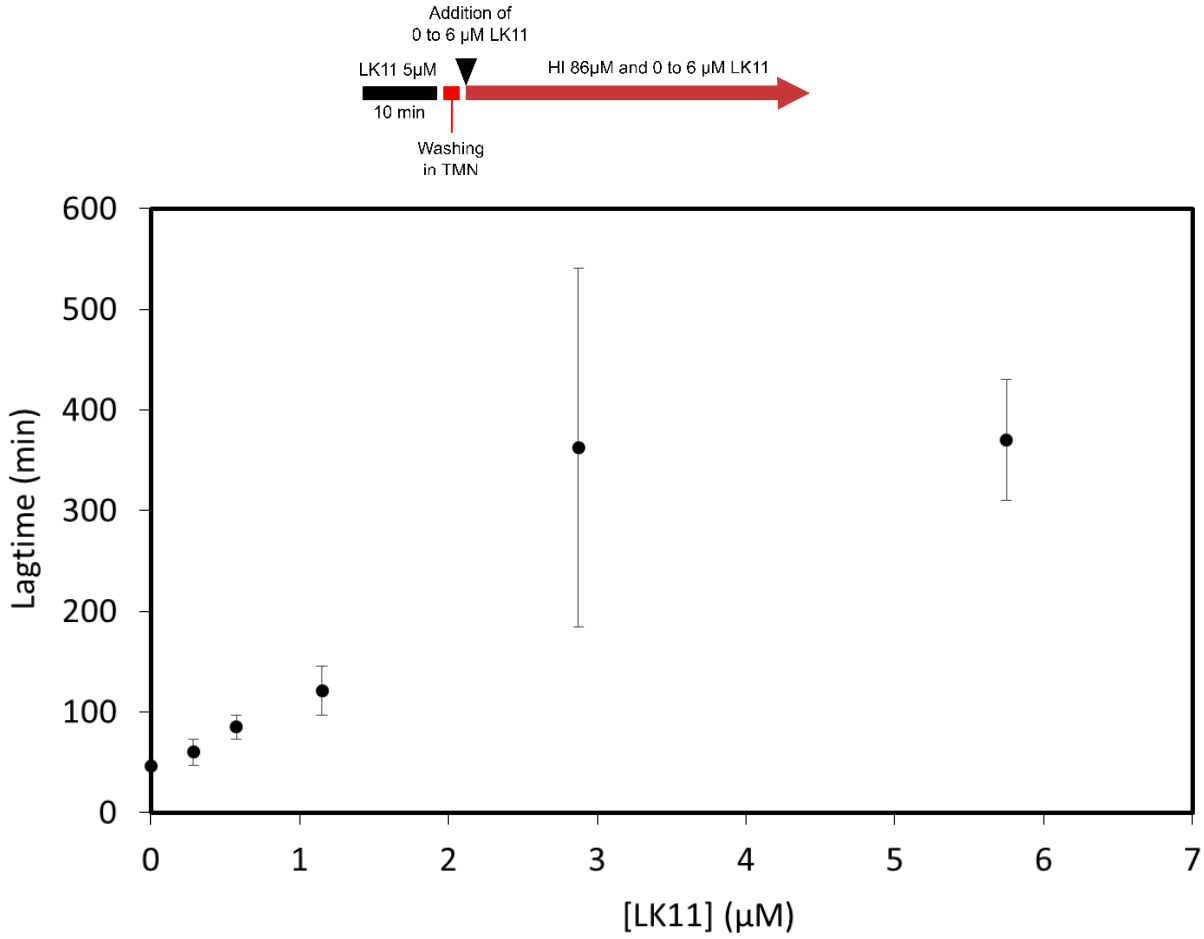

Figure 38. Temlps de latence de l' agrégation de l'insuline en fonction du temps sur une surface préalablement saturée avec LK11 en fonction de la concentration de LK11 en solution au cours de l'étape de nucléation. Barres d'erreur présentent déviation standard (n = 3).

Comme les peptides LK sont chargés positivement au pH expérimental (7.4), la réduction de leur comportement inhibiteur à force ionique plus élevée montre que ces charges sont impliquées dans cette inhibition. Les résultats obtenus avec le peptide LD9 Figure 39 confirment également l'importance de la charge positive de la lysine dans le mécanisme de cette inhibition.

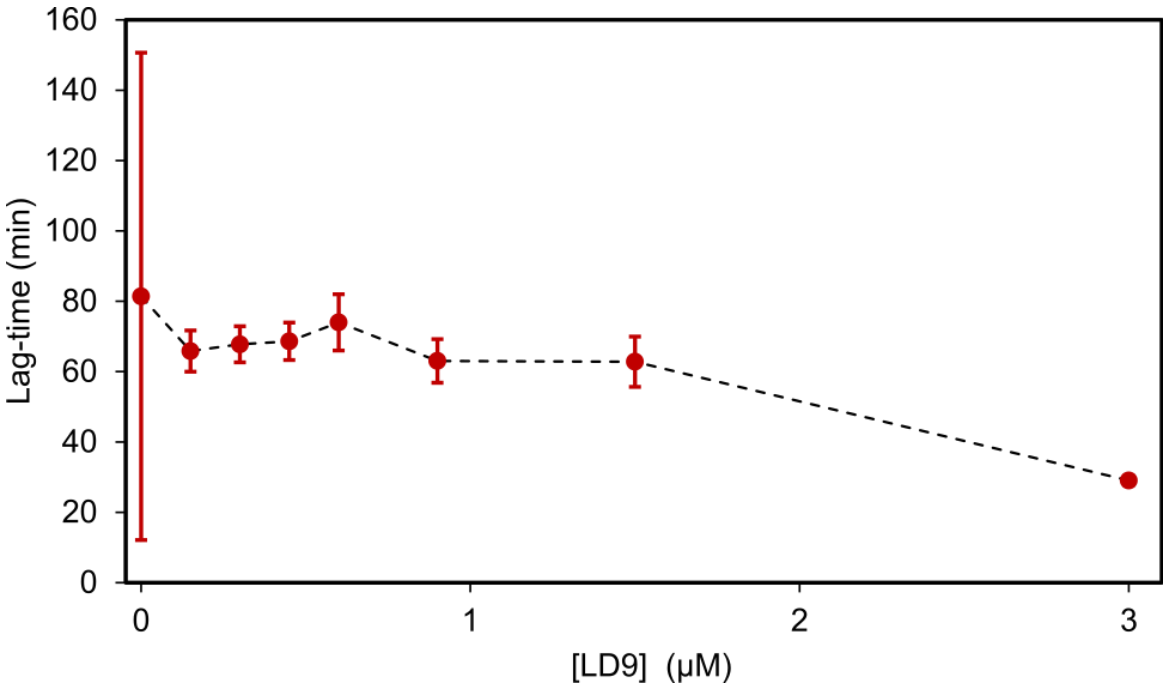

Figure 39. Temps de latence pour l'agrégation de l'insuline en fonction de la concentration de LD9. Les valeurs moyennes sont affichés, les barres d'erreur représentent les écarts-types (n = 4).

Mécanisme d'inhibition stérique

Contrairement à d'autres peptides $(LK)_nL$, la durée de la période de latence en présence de TAMRA-LK11 pas pu être déterminée pour les concentrations de peptide au-dessus de 0.7µM car il excède 48 h à 1.4µM et même une semaine à 2.8µM. La période de latence présente donc une asymptote verticale à 0.7µM TAMRA-LK11 (Figure 4 dans l'article I). Ceci indique une inhibition complète du processus de nucléation précoce ainsi qu'un taux quasi nul de formation de complexes d'insuline capables d'épuiser le TAMRA-LK11 en solution en le liant. Comme le comportement général de ce peptide marqué sur l'agrégation HI induite sur la surface est similaire aux autres peptides LK, cette très forte inhibition est probablement le résultat d'affrontements stériques induite par le groupe TAMRA à l'extrémité N-terminale du peptide.

Conclusion sur l'effet double des peptides sur la nucléation de l'insuline

Les résultats présentés dans ce chapitre permettent une représentation précise des mécanismes impliqués dans les interactions peptide-insuline à la surface. En l'absence de peptide, l'insuline est adsorbé sur la surface où elle forme des structures très instable qui se transforment rarement en un noyau, c'est-à-dire qu'elle surmonte très rarement la barrière d'énergétique vers un état agrégé.

Les peptides LK eux s'adsorbent de manière coopérative sur des surfaces hydrophobes, où elles sont stabilisées par feuillet β antiparallèle inter moléculaire formant ainsi un patch de peptide (Figure 40-1). Puis ces patchs stabilisent l'adsorption (tel que montré par Nault et al.) et la nucléation des molécules d'insuline, réduisant la durée de la phase de latence (Figure 40-2). Les peptides LK9 et LK11 restant en excès dans la solution, au contraire empêchent la nucléation (Figure 40-3) probablement par un effet impliquant des interactions électrostatiques et un encombrement stérique, prolongeant la phase de latence.

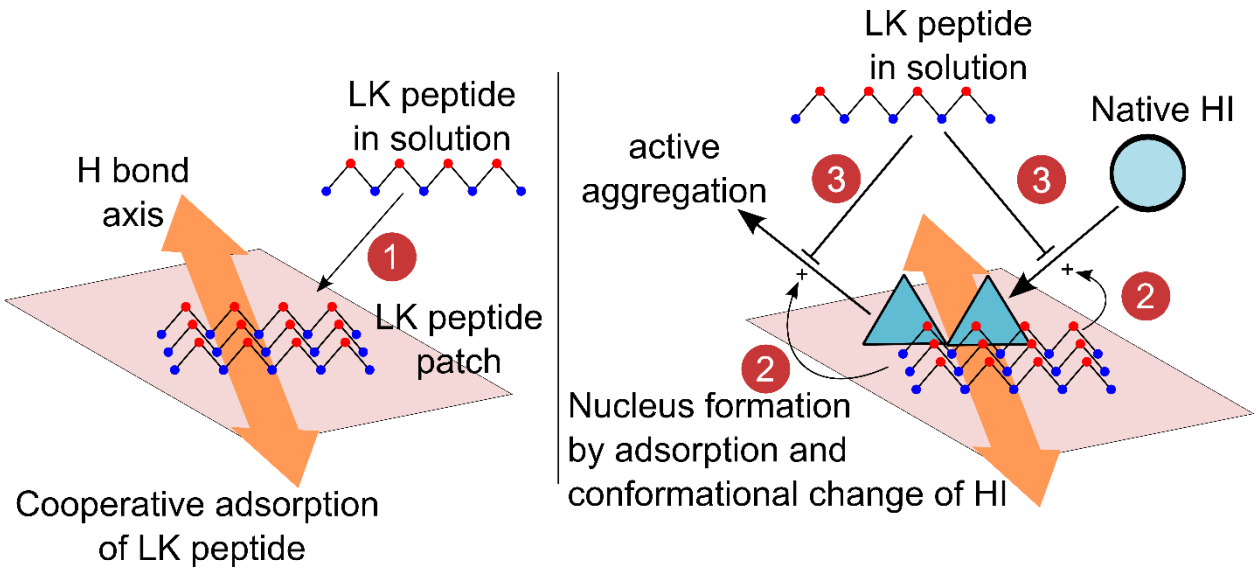

Figure 40: Double effet des peptides LK11 et LK9 sur l'agrégation de l'insuline sur surfaces hydrophobes. 1 : adsorption coopérative de peptides de LK en plaques stabilisées par des feuillet β antiparallèles intermoléculaires (la flèche orange indique l'orientation des liaisons H), les patchs de peptides améliorent ensuite l'adsorption de l'insuline (2) et stabilisent son changement de conformation vers la forme agrégée. D'autre part (3) peptides restant en solution empêchent la formation de noyau.

1.11 Effet des peptides sur la phase de croissance.

Au cours de la phase de croissance, l'ajout du peptide LK11 en solution induit une réduction spectaculaire du taux d'agrégation. Mais pas une destruction des fibrilles déjà formés. Le mécanisme d'inhibition de la croissance probable s'appuie sur la liaison du LK11 pour les fibrilles empêchant l'incorporation d'insuline indigène comme le suggère la liaison forte de TAMRA-LK11 insuline fibrillaire. Cette liaison est apparemment médiée par les charges comme suggéré par la réduction de l'inhibition des peptides de LK à salinité plus élevée (Figure 6 de l'article I). L'absence d'inhibition observée avec le peptide LD9 chargé négativement par rapport au peptide LK9 (Figure 39) suggère également fortement que cette liaison est médiée par les charges latérales positives de la lysine.

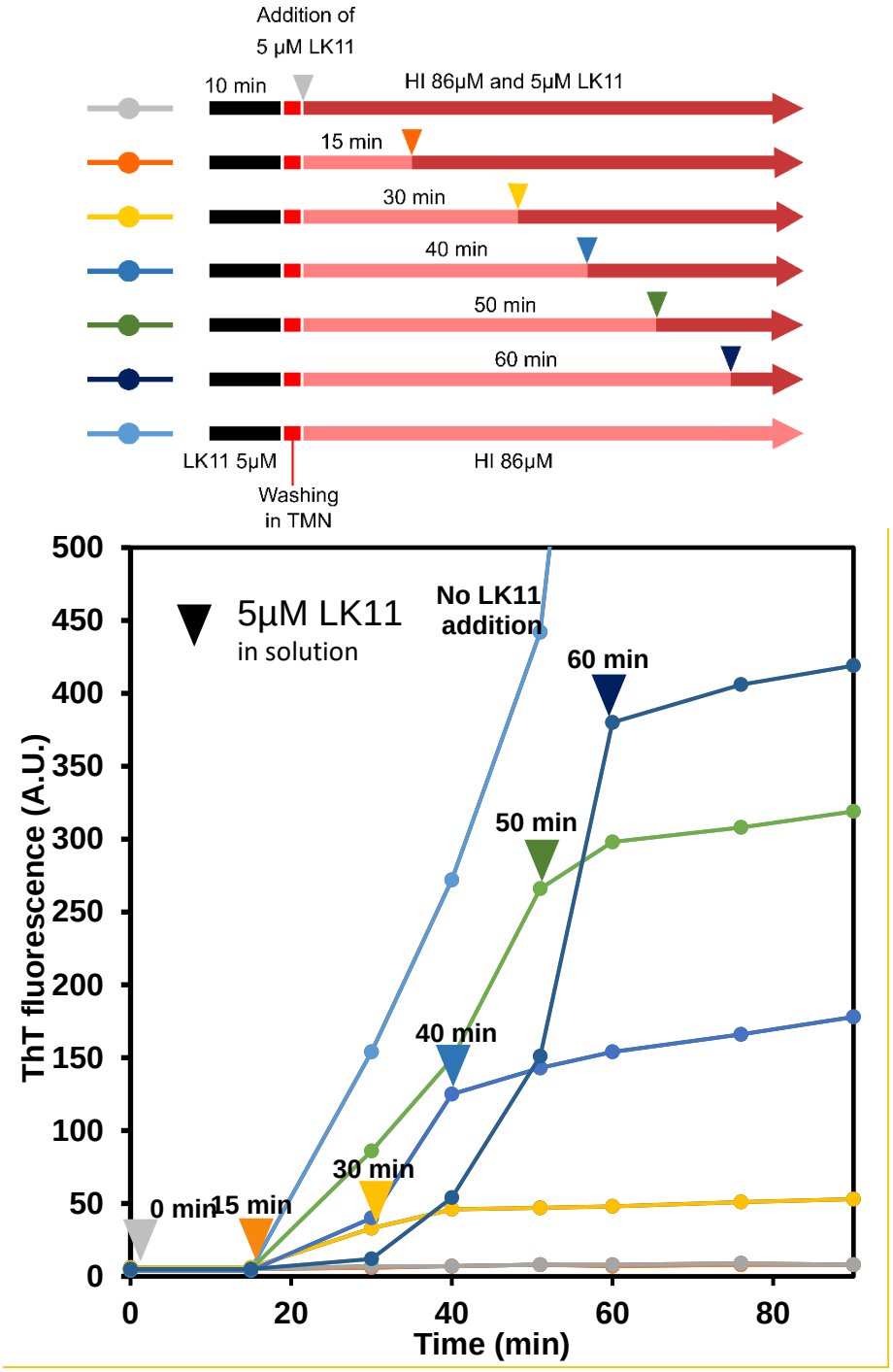

Figure 41. Après l'introduction dans la solution de 5µM de LK11 à diférent temps d'agrégation (indiqué par les flèches couleur) au cours de cinétique d'agrégation sur surfaces préalablement saturées l'agrégation est considérablement réduite.

Localisation

comme le ratio de peptide lié par rapport à la quantité d'agrégats d'insuline est plus élevé que prévu pour une liaison uniquement localisée sur les extrémités de la fibre et que l'ajout d'un fluorophore augmente considérablement l'inhibition de la nucléation de l'insuline, le peptide peut sans doute lier à un site allostérique près du site de l'incorporation de l'insuline (ou sur les bords de ce site) et prévenir l'incorporation de HI native par effet stérique (scénario I sur la Figure 42).Il est assez invraisemblable que la liaison du peptide procède par incorporation à l'extrémité de la fibre directement en prolongement du feuillet β bloquant ainsi l'incorporation

des monomères de insuline native, puisque les peptides (peptides LD) semblables, mais négativement chargés des n'inhibent pas l'agrégation de l'insuline.

Alternativement les peptides (LK)nL pourraient lier les agrégats d'insuline par effet hydrophobe et empêcher l'intégration d'insuline native par répulsion électrostatique (scénario II sur la Figure 42). Puisque l'insuline est censée être chargé négativement à pH 7.4 et que les peptides LD9 n'inhibent pas l'agrégation, ce second scénario est extrêmement peu probable.

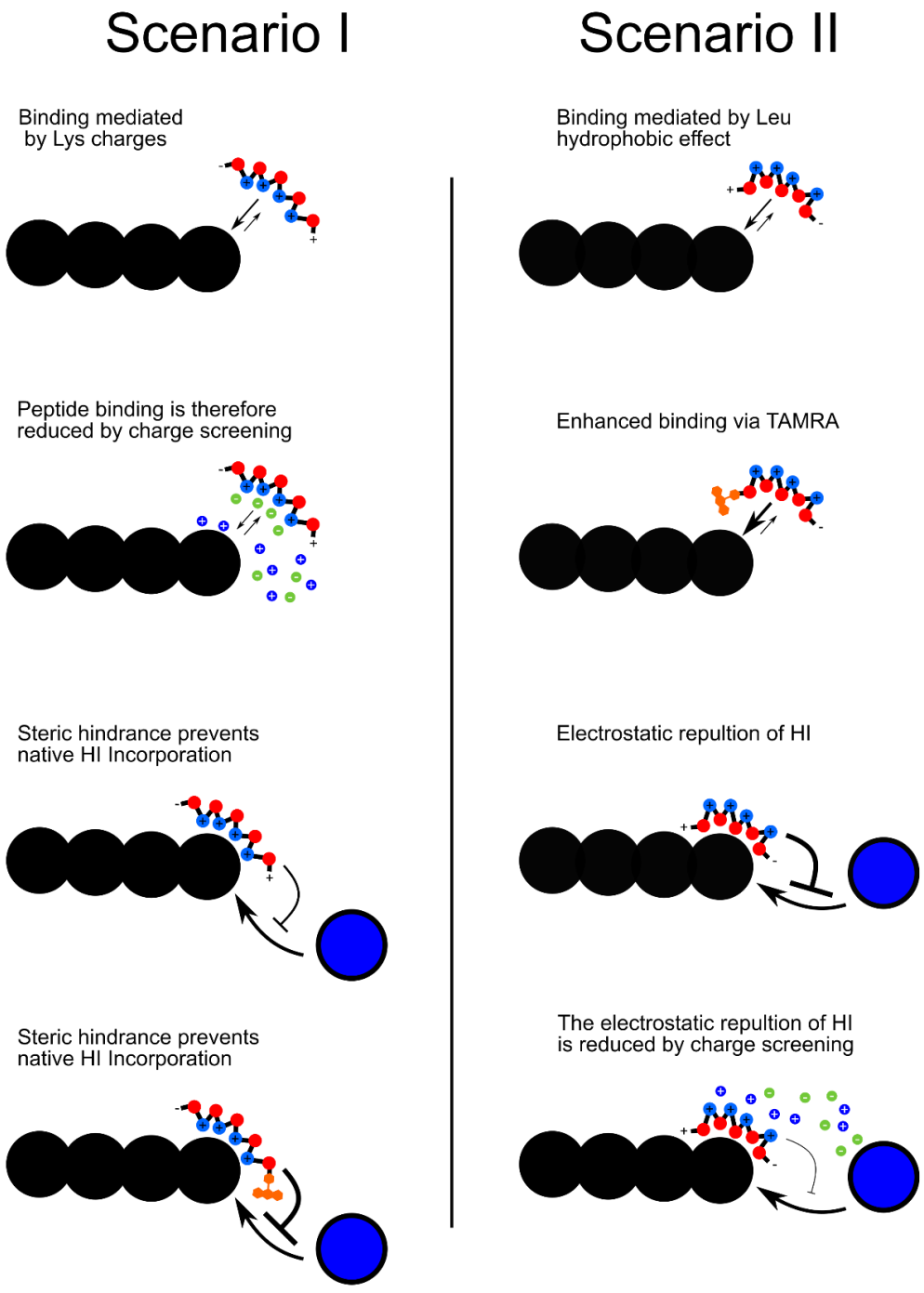

Figure 42. Modèle de liaison du LK11 sur une fibre d'amyloïde d'insuline au cours de la phase d'élongation. L'hypothèse privilégiée (scénario I) implique une liaison médiée par les charges positives des lysine et une inhibition de l'incorporation de l'insuline par encombrement stérique. Alternativement (scénario II) la liaison pourrait être médiée

par des effets hydrophobes par l'intermédiaire de leucine, les charges positives de la lysine empêcherait ensuite incorporation d'insuline.

Inhibition compétitive ?

L'allongement par incorporation d'insuline native peut être considérée comme analogue à un mécanisme de réaction de type Michaelis-Menten dans l'hypothèse d'une réaction en 2 étapes divisé en une liaison réversible de l'insuline native sur le site d'intégration et un changement de conformation (Figure 43). Le mécanisme d'inhibition de peptide pourrait donc être classés soit comme compétitif (i sur la Figure 43) si il lie uniquement à la fibre, non compétitif (ii sur la Figure 43) s'il ne relie que à l'état l'intermédiaire ou incompétitif (i et ii sur la Figure 43) si il lie aux deux à la fois.

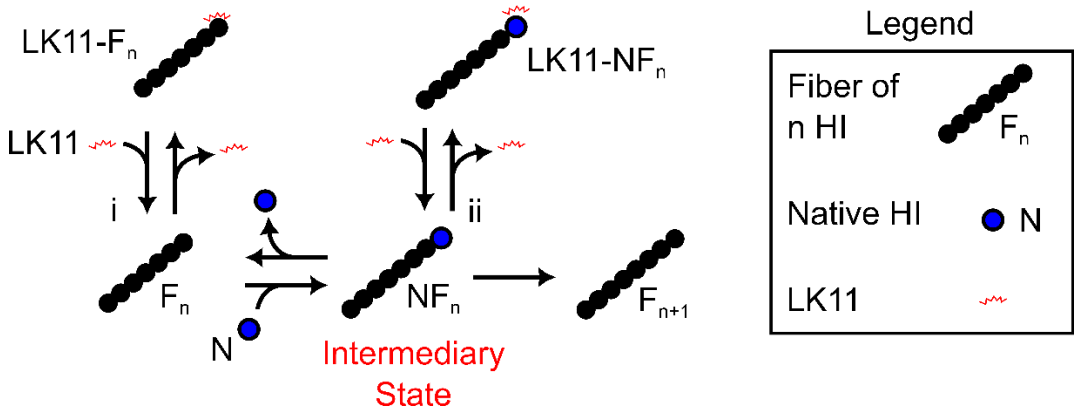

Figure 43. Mécanisme hypothétique d'incorporation de type Michaelis-Menten. Un inhibiteur de ce mécanisme peut soit se lier à la fibre (i), soit à l'état intermédiaire (ii) ou aux deux (i et ii).

En pratique, la détermination du mode d'inhibition du peptide LK11 est difficile en raison de l'épuisement de peptide en solution (adsorption sur des surfaces et la liaison stable sur les agrégats d'insuline) d'incorporation et du caractère exponentiel (logistique) de la cinétique de l'agrégation. En d'autres termes ni le nombre de sites de réaction ni sur le nombre d'inhibition de molécules d'inhibition ne sont constants au cours de l'expérience. Quoi qu'il en soit il convient de ne pas confondre inhibition par liaison avec inhibition compétitrice qui représente un cas particulier (quoi que probable si les conditions énoncés précédemment sont exactes).

Si le peptide inhibe l'agrégation insuline par inhibition compétitive il se lie probablement très près du site de liaison de l'insuline native sur les agrégats empêchant son incorporation dans la fibre croissante par encombrement stériques (comme proposé Figure 42 scénario I). Alternativement, un mécanisme non concurrentiel pourrait impliquer la liaison du peptide à proximité du site d'agrégation de l'insuline sans empêcher la fixation d'une molécule d'insuline native mais bloquant son changement conformationnel vers un état amyloïde.

2 Agrégation in situ

2.1 Localisation des premières étapes de l'agrégation

Les expériences de microscopie ont été menées afin d'observer in situ l'apparition des premiers agrégats. Pour ce faire, nous devions concevoir un dispositif spécifique permettant l'observation directe de la surface sur laquelle la nucléation et agrégation de l'insuline pourraient avoir lieu. Nous avons donc mis au point un système expérimental consistant en une chambre combinée avec une agitation continuellement par une tige de verre tournante pour agitation. Le fond de la chambre, consistant en une lamelle de borosilicate, est illuminé et observé par un microscope à fluorescence. Dans le but d'observer la nucléation de l'insuline et les processus d'agrégation plus tôt décrit dans les deux chapitres précédents, qui se produisent sur des surfaces hydrophobes sous forte agitation, que nous avons mesuré le niveau de la ThT fluorescence à cette surface.

2.1 Agrégation induite par la lumière

Le processus prédominant observé au cours de ces études est une agrégation de l'insuline induite par la lumière à la surface du matériau dans le domaine de l'éclairage. Mécanismes intéressants qui régissent ce processus ont été étudiés dans l'article suivant. LIA dépend des paramètres suivants : agitation, surfaces et lumière, trois facteurs connus pour provoquer la dénaturation des protéines et agrégation. Ce phénomène, permet la formation contrôlée et la croissance des agrégats de l'insuline sur des surfaces limitées à la zone éclairée. Dans le document suivant, ce domaine de l'éclairage a la forme du diaphragme microscope octogonale. Le processus pourrait permettre la formation de motifs souhaités, pourvu qu'un masque d'illumination approprié soit fourni. Le motif en L illustré à la Figure 44 a été obtenu par le déplacement de la surface du verre par la platine du microscope permettant un éclairage temporaire de chaque endroit de la surface (20 min par octogone).

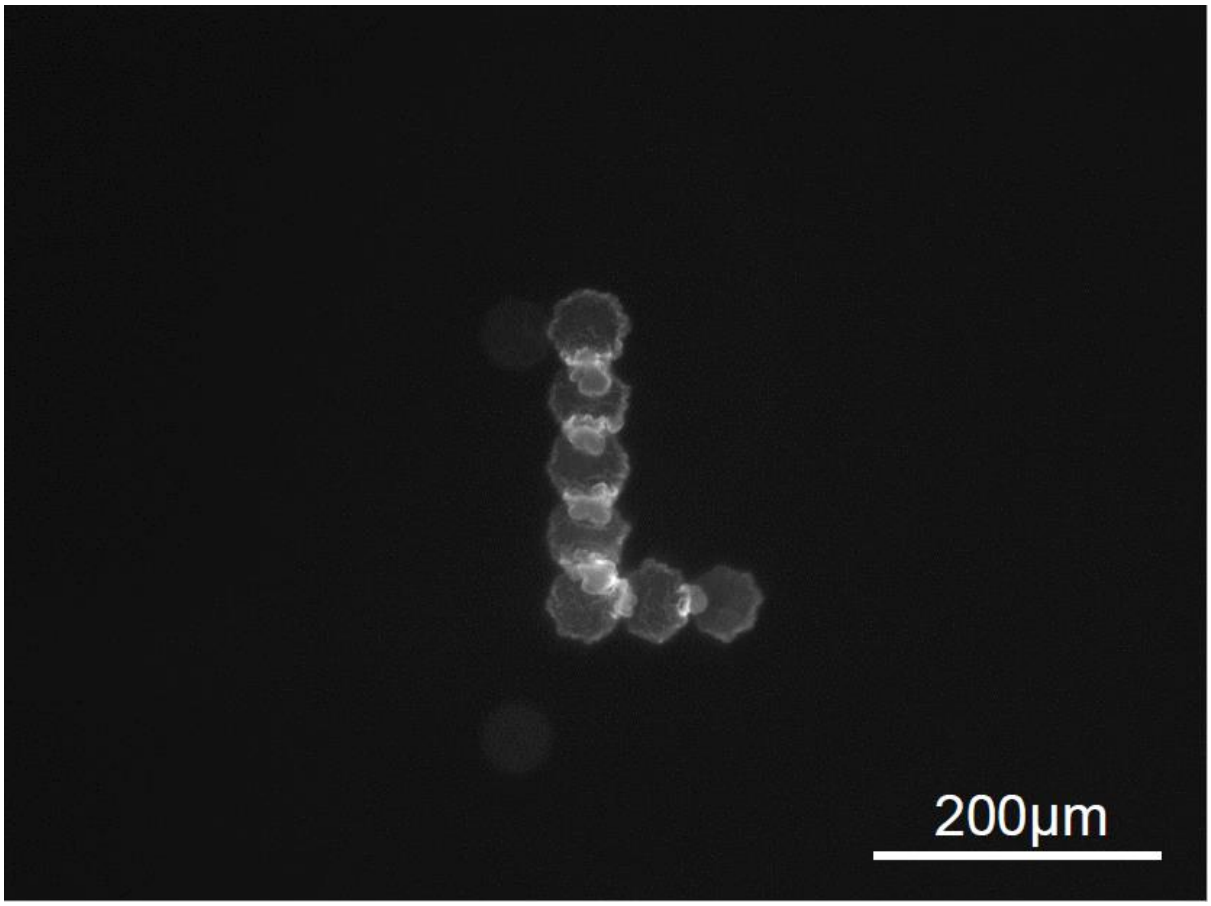

Figure 44 "L" obtenu par agrégation induite par la lumière sur une lamelle de verre.

2.2 Agrégation à l'interface triple air-liquide-matériel dynamique

Mis à part le mécanisme LIA, l'observation de la surface de cet appareil en l'absence d'éclairage, c'est-à-dire par d'exposition courte (t = 0.5s toutes les 30 s) et sous forte agitation (U = 2V équivaut à environ 1200 tr/min) montre l'apparition progressive de petits agrégats (0-3µm) sur la surface. Ces particules fluorescentes ThT ne sont pas créés sur la surface observée mais apparaissent progressivement en solution après 90min d'incubation et s'adsorbent par la suite sur la surface. En outre, la taille des particules adsorbées reste stable pendant la durée de l'expérience. Nous observons donc un mode d'agrégation similaire à celui de l'article I (Figure 9 dans l'article I), toutefois nous n'étions pas en mesure de localiser ni observer les premières étapes de l'agrégation.

Comme nous l'avions soupçonné ces événements précoces agrégation d'insuline se déroulent à la surface de la tige de verre, qui présente les contraintes de cisaillement plus élevée ainsi qu'une interface triple dynamique. Nous avons effectué un test dans lequel un barreau de verre silanisée tourne dans une solution d'insuline à l'intérieur d'un récipient en verre hydrophile. La seule surface permettant l'adsorption de protéines dans ce dispositif expérimental est la surface de la tige de verre hydrophobe silanisée (angle de contact de l'eau~ 100°), qui a été photographiée sur 20µM ThT (Figure 45).

Après 120min d'incubation dans une solution d'insuline à 86µM la répartition de la fluorescence de la ThT sur la surface du barreau est frappante: quelques taches ThT-positives peuvent être observées à la surface en permanence immergée, mais la plupart de la fluorescence

est concentrée le long de l'interface triple dynamique solution/air/verre tige (Figure 45). D'autre travaux effectués par notre équipe ont montré que la triple dynamique est le déclencheur d'agrégation de l'insuline dans la présentation du montage expérimental intermittente humidifiant [192].

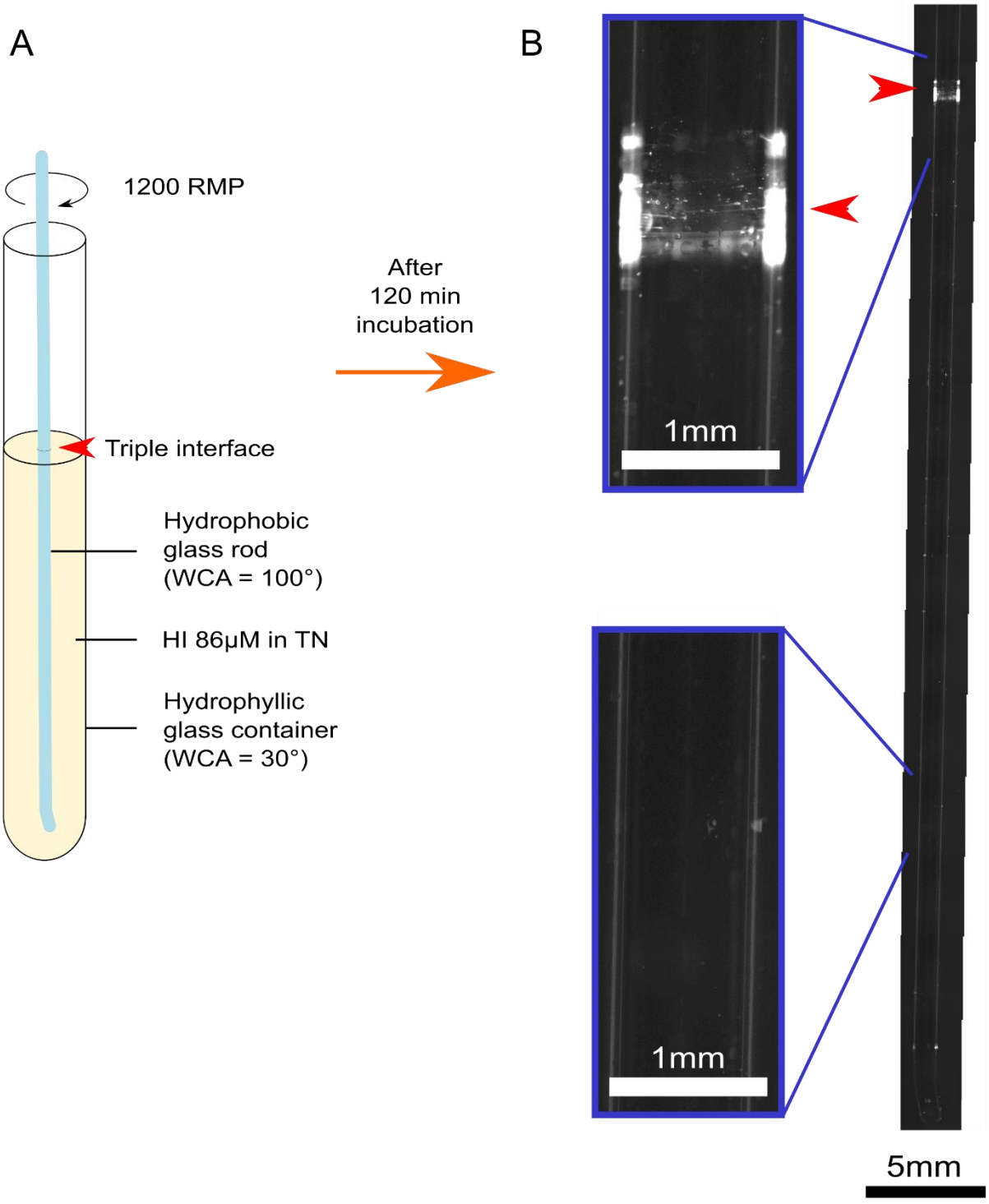

Figure 45. Répartition des agrégats ThT-positifs sur la tige de verre d'agitation. A: schéma de l'installation expérimentale avec une baguette de verre fonctionnalisés hydrophobe; B: fluorescence ThT sur la tige de verre après 120 min d'incubation à 1200 tr/min, les flèches rouges indiquent l'interface triple.

3 Discussion et conclusion

3.1 Localisation de la nucléation

La localisation des premiers agrégats positifs à la ThT a été étudiée dans le dernier chapitre. Nous avons déterminé que dans le cas d'une solution agitée par un barreau de verre, la surface du barreau en contact avec la surface du liquide c'est-à-dire la triple interface qui maximise le stress de cisaillement ainsi que le stress de déshydratation pour les protéines adsorbées (triple interface dynamique sous agitation), était le site privilégié d'apparition des premiers agrégats positifs à la ThT. Pour les incubations en présence de peptide LK en revanche, la pré-incubation de peptide LK11 uniquement au fond des puits (100µL de solution), n'impacte pas la durée du temps de latence pour 200µL d'une solution de HI occupant donc l'intégralité du puits. Si la triple interface dynamique est probablement le site de nucléation préférentiel en l'absence de peptide (comme le montre le motif obtenu à la surface du barreau hydrophobe immergé dans une solution d'HI), l'effet accélérateur des peptides sur la nucléation de l'insuline est probablement indépendant de cette zone.

3.2 Importance de l'agitation

Aucune agrégation d'insuline n'a pu être observée en l'absence d'agitation ni au cours des incubations dans des plaques 96 puits ni pour le phénomène d'agrégation induit par la lumière. L'agitation est requise à la fois pour la nucléation et pour la croissance des agrégats. Les effets d'une agitation peuvent être triples : une diffusion augmentée des espèces chimiques, un stress mécanique (principalement stress de cisaillement) ou la formation de triple interface dynamique.

Le stress de cisaillement est pourtant habituellement réfuté dans la littérature en raison de la faible magnitude des forces exercé par le fluide sur des objets nanométrique. Un taux de cisaillement minimal de of 10^7 s^{-1} serait nécessaire pour dénaturer une protéine globulaire dans l'eau [133] alors que dans le dispositif d'agrégation induite par la lumière ce taux de cisaillement à la surface observé est estimé à seulement 20 s^{-1}. Cependant durant la phase de croissance des agrégats de taille micrométrique pourraient effectivement être affecté par le stress de cisaillement et par exemple être arraché de la surface des puits. La taille minimale d'agrégats pouvant être observé en solution dans le cas d'agrégation induite par la surface est de 200nm [193], cette taille correspond à des agrégats assez gros pour être détacher de la surface par le stress de cisaillement.

La littérature scientifique contient pourtant de nombreux exemple de dénaturation [194] ou d'agrégation induite par stress de cisaillement, y compris l'insuline. Des taux de cisaillement compris entre 200 et 600 s^{-1} seraient responsables d'une accélération de l'agrégation amyloïde de l'insuline à bas pH et haute température ainsi que d'une influence sur la superstructure des agrégats [195,196]. Ces observations cependant n'excluent pas que les effets observes résultent simplement d'un mélange plus rapide de la solution (ou encore dans certains cas de la formation d'une triple interface dynamique) puisque elles proviennent toutes de conditions expérimentale déclenchant l'agrégation des protéines y compris en l'absence d'agitation.

En cela nos condition expérimentale diffère totalement puisque pas même des taux d'agrégation résiduels ne peuvent être observées en l'absence d'agitation (Figure 46). Il convient donc de rester extrêmement prudent quant à l'interprétation de ces résultats expérimentaux, avant de conclure à un rôle du stress de cisaillement dans la dénaturation des protéines. En revanche le stress de cisaillement est certainement responsable du détachement des agrégats de la surface.

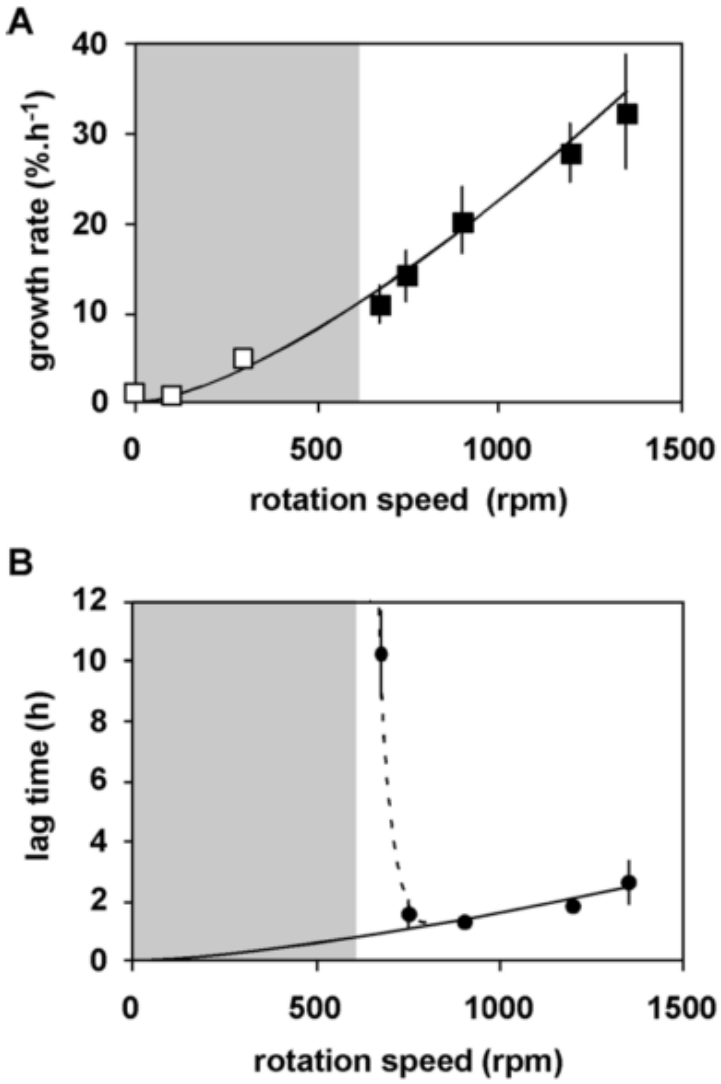

Figure 46. Effet de l'agitation sur taux de croissance (A) et du temps de latence (B) de l'agrégation de l'insuline humaine en plaque 96 puits (d'après la thèse de Laurent Nault [197]**).**

3.3 Effet accélérateur des peptides

Avant ce travail de thèse, Nault et al. avaient montré que certain peptides formant des feuillets β sur les surfaces hydrophobe avaient la capacité d'accélérer l'agrégation de l'insuline [187]. De manière générale l'effet des peptides adsorbés résultant uniquement en la réduction du temps de latence et leur effet à des concentrations très largement sub-stœchiométriques traduisent clairement un effet sur la nucléation.

Nous avons ici approfondi la connaissance de ces mécanismes et démontré que ces peptides sont capables de se lier de manière coopérative aux surfaces hydrophobes. Une fois adsorbés ces peptides exercent un effet pro agrégatif réduisant drastiquement le temps de nucléation ainsi que sa dispersion. Cette adsorption coopérative résulte vraisemblablement de la formation sur les interfaces hydrophobes de feuillet β antiparallèles entre les peptides tel que décrits dans les travaux de DeGrado and Lear [188].

Dans cette configuration les liaisons hydrogènes stabilisent le peptide latéralement au sein du « patch » (Figure 47). Ce cette façon l'addition d'un peptide supplémentaire sur le bord d'un patch stabilisent protègent de la solution le coté de deux peptides via la formation des liaisons hydrogène ii) et la chaine latérale apolaire des leucines par adsorption.

Le plus court peptide LK présente une coopérativité (nombre de Hill) plus élevé ce qui souligne son besoin de stabilisation intermoléculaire pour la formation d'un patch. Des simulations de dynamique moléculaire montent que sur une couche hydrophobe l'adsorption de peptides $(LK)_7L$ est principalement dirigé par l'entropie [198], le gain d'entropie qui résulte du déplacement des molécules du solvant contrebalance la perte d'entropie conformationnelle pour le peptide (-4.0 kJ/mol.K).

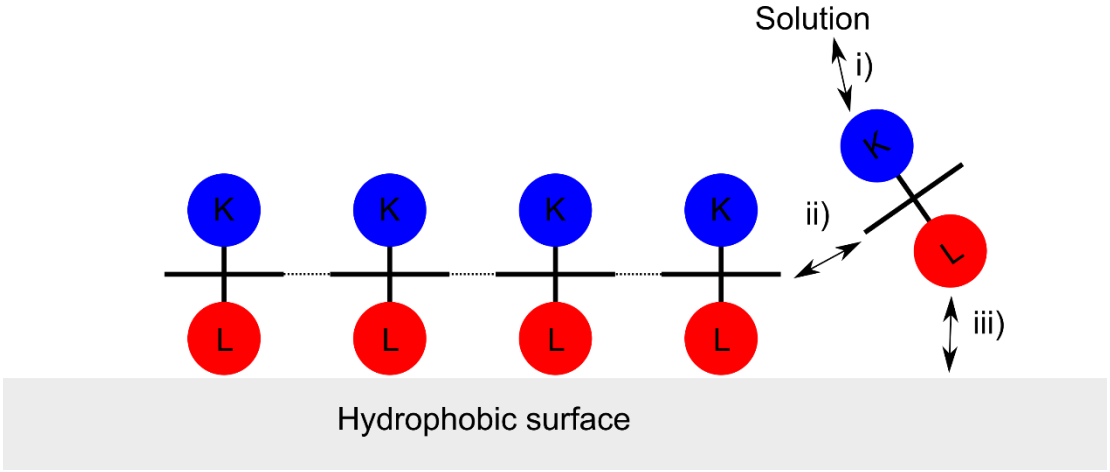

Figure 47. Principe de l'adsorption coopérative des peptides $(LK)_nL$. Les peptides sont ici représenté en vu transversale avec les liaisons hydrogènes sous forme de lignes pointillées. Au sein d'un patche de peptides un peptide est stabilisé par i) des interaction polaires des lysines avec la solution (ces interactions existant evidemment également lorsque le peptide est en solution), ii) des liaisons hydrogènes inter-peptide impliquées dans la formation du feuillet β antiparalele et iii) l'effet hydrophobe pour l'interaction leucine/surface hydrophobe.

Les peptides $(LK)_nL$ adsorbés exposent les groupes amines de leurs lysine vers la solution, or les surfaces fonctionnalisé avec des groupements amine accélèrent la vitesse de nucléation pour l'agrégation de l'insuline[199]. Cet effet a également été observé au cours de cette thèse avec des billes de polystyrènes fonctionnalisé avec des amines primaires ou des plaques multi-puits fonctionnalisées avec des amines qui présentent toutes deux des temps de latence significativement inferieures au surfaces hydrophobes. Ceci pourrait nous pousser à attribuer l'effet accélérateurs des peptides LK à ces groupes amines exposées, pourtant cette interprétation n'est pas cohérente avec les précédentes observations avec d'autres types de peptides. Premièrement les peptides ISISI et ISISISI présentent tous deux le même effet coopératif de réduction du temps de latence de l'agrégation de l'insuline alors qu'ils n'exposent que des chaines latérales apolaires (Isoleucines) vers la solution. De plus le peptide LKKLLKLLKKLLKL qui lui adopte une conformation en hélice α aux interfaces hydrophobes avec également des groupements amines vers la solution [188,200] prolonge pourtant le temps de latence de l'agrégation de l'insuline de plus de 30h [187]. Enfin Nault et al. ont montré que les effets accélérateurs des peptides sur l'agrégation de l'insuline étaient indépendants d'une séquence ou d'un motif spécifique mais dépendait uniquement de leurs tendance à former des feuillets β sur les surfaces hydrophobes. Puisque l'effet par lequel ces peptides augmentent l'adsorption des molécules d'insulines ainsi que leurs changements conformationnels [183,201] sont indépendants de leur séquence [187] mais dépend uniquement de leur capacité à former des feuillets β sur les surfaces hydrophobes, il est probable que la formation de liaisons hydrogènes latérales (Figure 40) soient responsable de l'effet stabilisateur sur la nucléation.

Le modèle d'un état intermédiaire de l'insuline proposé par Millican et Brems [202](Figure 48) possède un domaine hydrophobe exposé qui si il était adsorbé sur une surface hydrophobe placerait le segment LVEALYLV (B11-18) de la chaine B de l'insuline en face des groupements donneurs et accepteur de liaison hydrogène d'un patch de peptides.

Des études de dynamique moléculaires ont suggérées la formation d'un feuillet béta parallèle entre le peptide LVEALYL et le segment B22-27 de l'insuline [203]. Il est possible que ce segment également impliqué dans la formation de feuillet β entre les deux molécules d'insuline dans un dimère forme la première attache à un patch de peptides via un feuillet β intermoléculaire, avec une adsorption simultanée du domaine hydrophobe exposée (Figure 48).

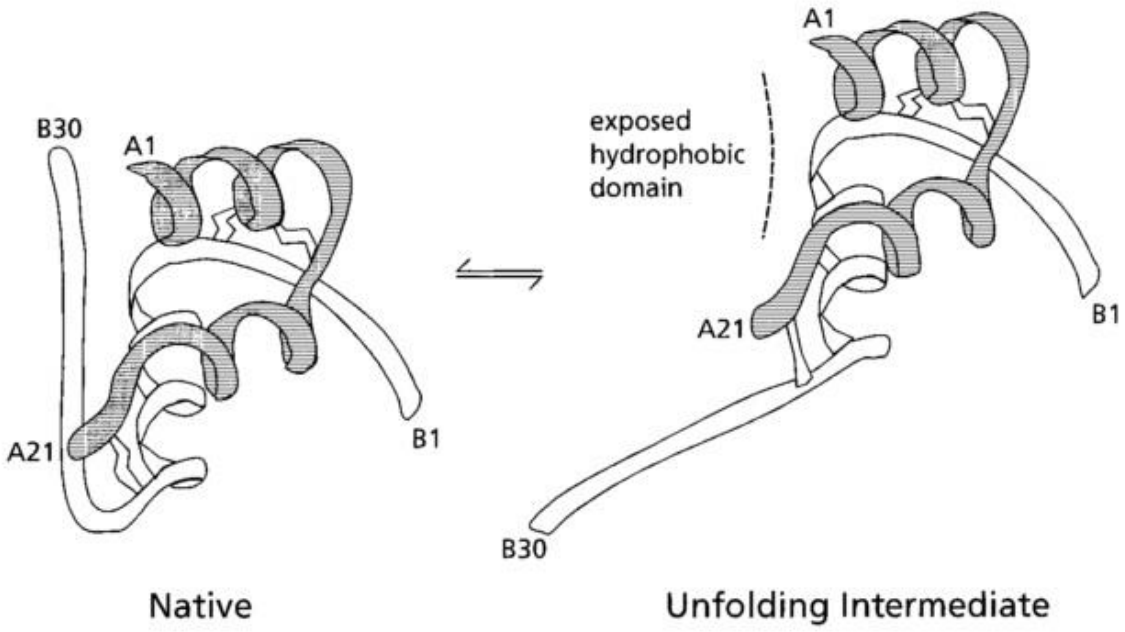

Figure 48: Modèle de dépliment de l'insuline à la surface des materiaux tel que proposé par Millican et al. [202](From Brange et al. [204])

3.4 Croissance des agrégats

Les deux plus importantes questions concernant les mécanismes généraux d'agrégation de l'insuline induite par les surfaces sont (i) es ce que la croissance des agrégats ne se produit qu'à la surface ou également en solution ? Et (ii) quel est l'unité d'élongation des agrégats ?

Le fait que les premier agrégats ThT positifs sont généré sur les surfaces d'où elle se détachent par la suite vers la solution est très bien documenté dans les travaux précédents [173,186,197] et par cette thèse. L'absence de particules d'agrégats inferieur à 100nm en solution indique clairement que les premiers agrégats sont formés sur les surfaces d'où ils ne peuvent être arrachés par le stress de cisaillement en raison de leur petite taille [186,193]. Ce point n'est en revanche pas incompatible avec une croissance ultérieure de ces agrégats en solution.

L'observation microscopique de la population de particules d'agrégats en solution en plaques 96 puits au cours d'une procédure standard d'agrégation révèle un accroissement continu de la taille des particules d'agrégats en suspension. (Figure 9 dans l'Article I).

Si l'agrégation est restreinte à la surface, alors ces particules pourraient être des conglomérats de particules plus petites ou provenir du détachement de particules de plus en plus grosses depuis la surface.

De plus l'observation d'une surface sous agitation par illumination intermittente et courte (pour empêcher les phénomènes d'agrégation induite par la lumière), montre l'apparition progressive de micro agrégats ThT positif en solution s'adsorbant par la suite sur la surface de verre observée ou il ne présentent pas de croissance observable. Cela indique que dans nos condition expérimentales le fond de notre chambre d'observation (Chapitre 5) n'est (soit pour des raisons de chimie de surface soit pour des raisons d'agitation insuffisante) pas l'emplacement ni de la nucléation ni de la croissance des agrégats.

D'un autre côté, les expériences de « seedings » montrent la possibilité pour des agrégats en solution de réduire **dans certains cas** le lag-time mais que la vitesse de croissance n'est pas proportionnel à la quantité d'agrégats en solution. Cela montre bien que le seeding est un phénomène complexe qui nécessite sans doute une réadsorption des agrégats ou une nucléation secondaire. Quoi qu'il en soit la croissance est strictement dépendante d'une agitation forte (Figure 46).

Vestergaard et al. Décrivent l'unité d'élongation des fibre amyloïde d'insuline dans des conditions acides comme un hexamère présentant une conformation hélicoïdale[161]. Pour Sluzky et al. l'unité d'élongation dans des conditions expérimentales proches des nôtres consiste en des monomères d'insuline dépliés par adsorption sur des surfaces hydrophobes puis relâchées en solution. Une unité d'élongation de ce type consistant en une protéine dépliée dans un état intermédiaire peut-être en faveur d'un mécanisme de croissance dépendant de la surface. Bien qu'il soit plus probable que l'incorporation se produisent au niveau de la surface [186,197].

3.5 Inhibition de l'agrégation par les peptides en solution.

Le second effet observe avec les deux peptides LK les plus long (LK9 et LK11) est leurs capacité à inhiber l'agrégation de l'insuline à des concentrations un peu plus élevées mais toujours nettement sub-stœchiométriques. Nous avons démontré dans le chapitre 3 que cet effet résulte de leur présence en excès (par rapport à la surface) en solution. Le modèle présenté Figure 50 démontre l'effet double des peptide LK11 et LK9 tell que démontré dans l'article I [201].

La saturation de la surface par les peptides LK engendre une accumulation des peptides en excès en solution. Ces peptides peuvent ensuite se lier aux complexes prés et post nucléation grâce aux charges latérales de la lysine et bloquer l'incorporation de nouvelles molécules d'insuline par encombrement stérique. Les complexes pré-nucléation bloquées par une telle liaison de peptides ne peuvent évoluer que vers une dissociation rapide puisqu'ils possèdent une très importante énergie conformationnelle et qu'ils ne peuvent atteindre un état plus stable par incorporation de nouvelles molécules. Pour les complexes post nucléation, la liaison d'un peptide proche d'un site d'incorporation a pour effet d'empêcher l'addition de nouvelles molécules. Cependant comme la liaison du peptide n'est pas spécifique au site d'incorporation mais qu'il peut se lier avec une grande affinité ailleurs sur les agrégats en solution, la concentration de peptide en solution peut être drastiquement réduite. En particulier la production d'agrégats par les taux résiduels d'agrégations observées à forte concentration de peptides sont responsable d'une déplétion graduelle de la concentration de peptides en solution jusqu'à aboutir à la restauration d'un taux d'agrégation normal.

L'inhibition de l'agrégation amyloïde ainsi que la réduction de la toxicité des agrégats amyloïdes ont suscité un intérêt de recherche particulier. Il convient de distinguer les approches non séquences spécifiques souvent basées sur des petites molécules des approches plus spécifiques souvent basées sur des peptides.

Inhibition de l'agrégation amyloïde par des petites molécules

Saha et al. [205,206] ont montré que le glycérol inhibait les processus primaires et secondaires dans agrégation amyloïde de l'insuline à pH 1.6. Plusieurs polyphénols trouvés dans des plantes consommées ont démontré leur capacité à interférer avec les mécanismes d'agrégation amyloïde (Figure 49) à la fois in vitro et in vivo, apportant de possibles une approches thérapeutiques [207]. Le gallate d'Epigallocatechin (EGCG), un polyphénol présent dans le thé (*Camellia sinensis*) inhibe la fibrillation d'Aβ et dissout même les agrégats d'Aβ et de transthyrétine préexistants [208]. La curcumine, un di-phénol produite par *Curcuma longa*, inhibant la fibrillation de transthyrétine [209] en stabilisant ses tétramères et en favorisant la formation d'agrégats non fibrillaire (*off pathway*). En raison de sa non-toxicité et de la modulation de sa biodisponibilité, grâce à la pipérine [209], la curcumine est régulièrement étudiée dans des études d'inhibition amyloïde.

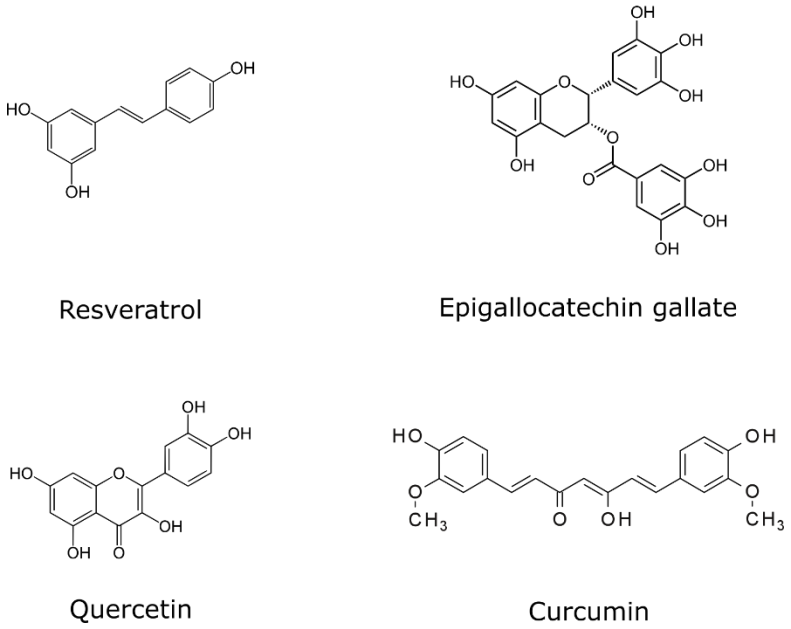

Figure 49: Polyphénols connus pour interférer avec l'agrégation amyloïde.

En outre, la curcumin, la quercétine et le resvératrol sont connus pour interférer avec la fluorescence de la ThT dans fibres amyloïdes par des interactions non spectrales très probablement par compétition pour la liaison aux fibres [210]. Il est donc probable que les mécanismes de ces petites molécules reposent sur une liaison à la fibre, semblable à celle de la ThT, provoquant par la suite une déstabilisation de la structure globale. Necula et al. ont montré que les petit peptides inhibant l'agrégation de l'Aβ pouvaient être classés comme inhibiteur de l'oligomérisation, inhibiteur de la fibrillation ou inhibiteur de ces deux [211], indiquant que l'oligomérisation n'est pas un intermédiaire nécessaire pour la fibrillation d'Aβ. Fait intéressant, certains des inhibiteurs d'oligomérisation présentent une activité pro-fibrillation à des concentrations sub-stœchiométriques (1/100 de la concentration d'Aβ) indiquant un effet de pro-nucléation.

La formation d'oligomères *off pathway* par liaison à la protéine native est un mécanisme fréquemment signalé d'inhibition de l'agrégation amyloïde par des petites molécules ou des peptides. Toutefois, la liaison à une protéine native peut aussi déclencher son agrégation. Par exemple, le FN075 fusionnés avec l'anneau 2-pyridone inhibe l'agrégation de la protéine bactérienne curli ACPS mais favorise l'agrégation de l'α-synucléine [212].

Peptides inhibant l'agrégation amyloïde

Plus en rapport avec les résultats présentés dans l'Article I et II, des peptides peuvent aussi inhiber l'agrégation amyloïde. Les peptides « β-breaker » empêchent l'agrégation et dissocient des fibrilles amyloïdes réduisant leur toxicité [213–218]. Cette dissociation des oligomères et fibrilles matures n'a cependant jamais été observée avec des peptides $(LK)_nL$; au contraire, il existe de nombreuses preuves expérimentales que les agrégats préalablement formés ne sont pas décomposées après l'ajout de LK11 (Figure 41, Figure 7 in Article III).

Le mécanisme du peptide NF11 (NAVRWSLMRPF) consiste en la dérivation des oligomères intermédiaires de la voie de l'agrégation d'Aβ via la formation de complexes *off pathway* NF11- Aβ [213]. En outre ce peptide peut lier Aβ en conformation amyloïde, ce qui entraîne la dissociation et la réduction de la toxicité des agrégats préformés. Ce peptide peut lier à la fois l'Aβ natif et amyloïde Aβ ce qui n'est pas le cas du peptide LK11 qui se lie uniquement aux agrégats d'insuline et non aux insulines natives en solution (Article II).

Un de penta-peptide fragment d'Aβ, KLVFF (Aβ16 – 20) peut lier le peptide Aβ complet et empêcher son agrégation amyloïde [219]. Les auteurs montrent que le motif KLXXF est critique pour cette liaison. Les peptides contenant ce motif sont en mesure d'arrêter l'agrégation de l'Aβ, supposément en se liant aux monomères en solution. Ces acides aminés font partie de la section impliquée dans la formation du premier feuillet bêta intermoléculaire d'après un modèle basé sur une structure de RMN [70,220]. L'addition d'une queue poly-lysine C-terminale, à la fin de ce peptide minimal (KLVFFKKKKKK), a provoqué l'accélération de l'agrégation de l' Aβ avec des changements significatifs dans la morphologie globale des agrégats ainsi qu'une toxicité cellulaire réduite [116,221,222].

Les efforts visant à développer des séquences peptidiques partiellement homologues à la séquence de l'Aβ16 – 20, mais comprenant les résidus de proline empêchant une conformation en feuillet β ont donné des résultats intéressants : le peptide RDLPFFPVPID empêche la fibrillation d'Aβ et désagrège partiellement des fibrilles préformées [215]. Le peptide LPFFD conjugué au tréhalose présente également une activité inhibitrice sur l'agrégation de Aβ(1–42) [216]. Une des stratégies clés dans la conception des peptides pour l'inhibition de l'agrégation amyloïde est le ciblage de la région du steric zipper, dans le but de prévenir l'incorporation de nouvelles protéines [214]. Comme LK11 empêche la croissance de l'agrégat de HI sans fibrilles préformées désagréer, ce mode d'inhibition est le plus probable.

La séquence HaPrP106-141 de la protéine prion du hamster doré (*Mesocricetus auratus*) peut inhiber la transformation de la PrP native en PrPres [223], avec un rôle essentiel des acides aminés 119 et 120 dans ces phénomènes. Ces acides aminés font partie d'une région fortement hydrophobe, qui toutefois ne semble pas être impliqués dans la formation d'un feuillet β dans les fibrilles de prion [224].

Une autre approche consiste en la N-méthylation de deux groupes amide de la chaine principale d'un peptide provenant de la séquence de base d'une protéine amyloïdogène dans le but de prévenir la formation d'un feuillet β intermoléculaire. Des peptides long de 5 à 10 acides aminés issues de la région impliquée dans la formation du feuillet β intermoléculaire des fibres d' Amylin (IAPP20-29), sont en mesure d'empêcher l'agrégation amyloïde de leurs homologues non méthylé et de la protéine complète [225].

Toutefois, dans notre système, l'inhibition de l'agrégation de l'insuline ne semble pas être séquence spécifique mais seulement induite par les charges latérales, elles sont donc peu de chances d'interagir directement avec la chaine principale au niveau du feuillet béta intermoléculaire, ni de participer à la formation d'un *steric zipper*.

.

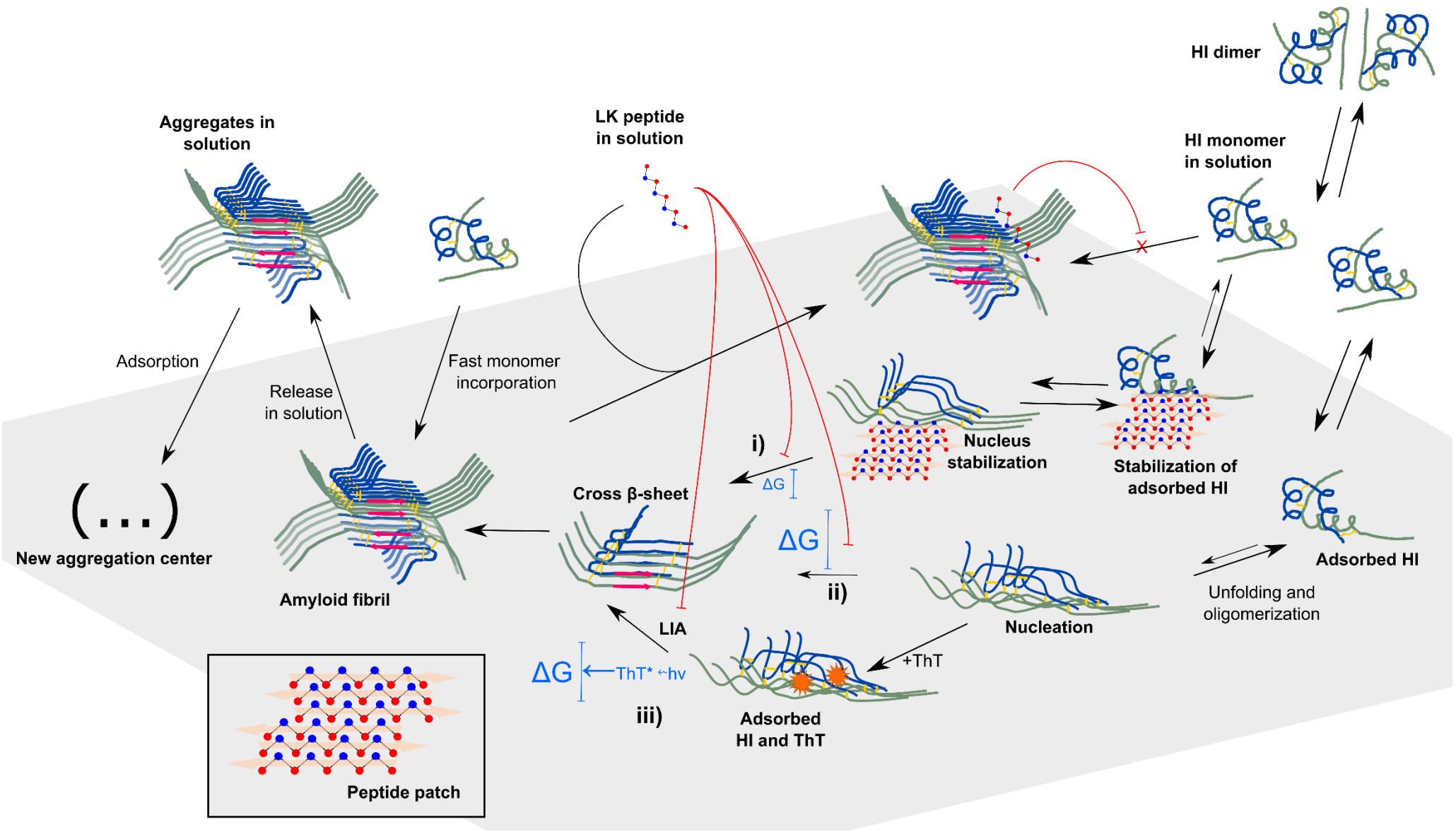
HI dimer
HI monomer in solution
Aggregates in solution
LK peptide in solution
Adsorption
Release in solution
Fast monomer incorporation
(...)
New aggregation center
Amyloid fibril
Cross β-sheet
i)
ΔG
ΔG
ii)
Nucleus stabilization
Stabilization of adsorbed HI
Adsorbed HI
Unfolding and oligomerization
Nucleation
LIA
ΔG ← ThT* ↜ hv
iii)
+ThT
Adsorbed HI and ThT
Peptide patch

Figure 50. Modéle du mechanisme d'aggrégation de l'insuline induit par la surface des materiaux .Trois diférentes voie d'aggrégation sont illustrées i) agrégation stabilisé par des patches de peptides diminuant l'énergie d'activation pour atteindre la forme amyloïde; ii) agrégation induite par la lumière ; iii) voie normale d'agrégation induite par surface, seulement stabilisée par la surface et qui présente une barrière d'énergie d'activation élevée et iii) induite par l'agrégation qui permet de surmonter cet obstacle par le transfert d'énergie de la ThT excité à la protéine. Ces trois voies sont inhibées par des peptides LK9 et LK11 en solution. La zone grise représente une surface hydrophobe ; le peptide représenté est LK9 avec des chaînes latérales des leucines en rouge et celles des lysines en bleu ; les flèches orange pâles et rouges représentent une région en feuillet β pour la chaine principale de l'insuline et les peptides respectivement ; le ΔG en bleu et leurs échelles associées représentent la valeur relative de la barrière d'énergie libre pour les étapes irréversibles, cinétiquement limitante ; la taille des flèches de réaction représente leur constante de réaction; les étoiles orange représentent les molécules de ThT liées aux protéines.

3.6 Agrégation induite par la lumière

Le mécanisme d'agrégation induite par la lumière décrit ici est similaire à la technique standard utilisée dans les chapitres 3 et 4 par sa dépendance aux surfaces sur lesquelles l'insuline est capable de s'absorber mais aussi par l'inhibition de sa croissance par le peptide LK11, par l'état ThT-positif des agrégats formées et par la dépendance vis-à-vis d'une forte agitation. Toutefois, ce mécanisme de croissance est strictement dépendant de l'illumination lumineuse à une longueur d'onde permettant l'excitation de la ThT_F. Une autre différence réside dans la structure de ces agrégats saturant en ThT à des concentrations beaucoup plus élevées (ayant donc une affinité beaucoup plus faible pour la ThT). Il ressort de nos résultats que les molécules de ThT dans les agrégats absorbent la lumière incidente et transfèrent son énergie par voie non-radiative vers les molécules d'insuline environnantes. Cette énergie permet alors la transition structurelle d'une insuline adsorbée native vers un état agrégé.

La vitesse d'agrégation est, comme prédit par notre modèle, proportionnelle à l'irradiance et à la concentration de ThT. Toutefois, ce taux n'est pas proportionnel à la concentration d'insuline, l'agrégation est considérablement réduite, et perd son comportement exponentiel au-dessous d'une concentration critique de 50µM. Cela indique un mécanisme de croissance qui est plus complexe qu'une simple incorporation en une seule étape. Ce mécanisme de croissance probable implique des procédés secondaires dépendants des protéines natives de type nucléation secondaire, qui est également en accord avec la structure tridimensionnelle des agrégats.

En l'absence d'agitation l'agrégation s'arrête complètement tandis que les fibrilles maintiennent un niveau de fluorescence ThT_F global et une densité de ThT_F (ratio de la fluorescence de ThT_F sur la quantité d'agrégats) permettant l'AIL. Cet effet résulte probablement de la réduction de l'approvisionnement en insuline native au niveau de l'agrégat (en d'autre terme de son activité chimique), empêchant les mécanismes de croissance, ou bien (moins vraisemblablement) d'un mécanisme dépendant de la contrainte de cisaillement.

Intérêt du patterning de surface dirigé par la lumière avec des protéines

Ces dernières années, plusieurs applications des techniques de *surface patterning* avec des protéines sont apparus par exemple pour la culture de cellulaires [226] (y compris le *cell patterning* ou différenciation cellulaire) ou pour les *protein arrays* [227]. Les méthodes de *surface patterning* avec des protéines comprennent la microdeposition classique[228], patterning de gels photosensibles [229] et immobilisation covalente de protéines à la surface par des groupes chimiques photo-actif [230,231].

Changements de conformation de protéines induites par la lumière

Le contrôle des processus biologiques par la lumière sont à la base de certaines des techniques plus prometteuses dans la recherche biologique : l'optogenetique, en particulier, permet l'activation directe de cellules neuronales unique par la lumière mais également l'activation de voie de signalisation spécifiques [232].

L'agrégation de protéines induite par la lumière est rarement décrite dans la littérature. Parmi les rares exemples disponibles, la lumière en excès provoque l'agrégation réversible en 2 dimensions du photosystème II et des antennes collectrices II dans la membrane des thylakoïdes [233]. La lumière a également la capacité d'accélérer la dégradation chimique et l'agrégation ultérieure des anticorps. Plus pertinentes Chelnokov et al. ont montré qu'un laser à UV (308 nm) pulsé induit l'agrégation brusque des β-cristallines après une exposition de 100 $J.cm^{-2}$. Le mécanisme proposé est une photo-excitation du tryptophane avec une conversion ultérieure de cette énergie en énergie vibrationnelle, conduisant à une haute température locale et la

dénaturation thermique de la cristalline. L'énergie d'exposition à laquelle on observe l'initiation de la phase d'agrégation rapide diminue avec la fréquence de l'impulsion laser, indiquant une relaxation cet «état photo-activé » réversible.

À l'exception notable de la famille de la Green Fluorescent Protein (GFP) dans laquelle le tripeptide His-Tyr-Gly réagit spontanément pour former un système conjugué, les protéines sensibles à la lumière dépendent généralement de chromophores externes. La Kaede (jap. « érable ») est une protéine fluorescentes photoactivable de la famille de la GFP, qui subit une transition fluorescence du vert vers le rouge par l'adsorption d'un photon dans les ultraviolets qui induit une réaction chimique formant un système conjugué plus vaste [234,235].

Les changements de conformation de protéines induites par la lumière sont habituellement le résultat d'une isomérisation ou d'une réaction chimique d'un chromophore lié. Chez les rhodopsines, le rétinal (chromophore) est lié de manière covalente à la protéine via une base de Schiff[4], c'est son isomérisation par l'absorption d'un photon induit le changements de conformation de la protéine [236].

Les flavoproteins forment une importante classe de protéines caractérisées par leur liaison à une flavine mononucléotide (FMN) ou une flavine adénine dinucléotide (FAD). Plusieurs flavoproteins sont photosensibles (cryptochrome, photolyase), s'appuyant sur une réaction chimique induite par l'absorption d'un photon par leur chromophore de type flavine. Les domaines Light-Oxygen-Voltage (LOV) sont des domaines sensibles à la lumière contenant un chromophore FMN [237]. En particulier le domaine LOV2 de l'avoine subit des changements de conformation induit par illumination avec de la lumière bleu via la formation d'un adduit flavine-cystéine [237,238]. Ce dernier exemple, pourrait être semblable à l'effet observé dans le cas d'agrégation induite par la lumière.

Une théorie avancée dans l'article III au moment de la soutenance, voudrait que la ThT excité puisse réduire les ponts disulfures de l'insuline entraînant une perte de stabilité et un dépliement des chaînes peptidique individuelles. Ces chaînes individuelles, connus pour être amyloïdogènes, agrégeraient alors et lieraient plus de ThT. Il y a d'autres exemples de réaction de flavines sur des protéine, la formylmethylflavine par exemple réagit avec la cystéine Nterminale de peptides via la formation d'un hétérocycle [239].

Une augmentation de la taille des agrégats d'insuline induite uniquement par la surface a observé au microscope optique sous un éclairement continu. Comme ce phénomène ne se produit que dans la zone d'illumination et persiste après le remplacement de la solution par un tampon sans protéines, il correspond à une dégradation des agrégats préexistants par la lumière. Cette dégradation par la lumière (augmentation de la taille des particules sans aucune incorporation de protéine) pourrait être la raison de la différence de structure (densité plus faible de protéines, saturation en ThT à des concentrations plus élevées) observée chez les agrégats induits par la lumière.

3.7 Agrégation Amyloïde?

Malgré les publications disponibles sur l'agrégation de l'insuline induite par les surfaces, les données structurales sur ces agrégats restent rares. Aucun micrographie électronique ni par force atomique n'ont révélé la structure hautement organisée, typique des amyloïdes. Jusqu'à présent, aucune expérience de diffraction des rayons x n'a effectué sur ces agrégats. Cette expérience pourrait révéler le motif de diffraction typique des agrégats amyloïdes. Cependant, les nombreuses études cinétiques détaillées dans cet ouvrage et dans les premières réalisations

[4] A **Schiff base** is a functional group of the form $R_2C=NR$

de notre équipe, ou d'autres ont révélé une cinétique d'agrégation typique des agrégations de type amyloïde (cf. chapitre I). En outre, la fluorescence ThT de ces agrégats est caractéristique de leur teneur en β-feuillet (cf. discussion sur la spécificité du marquage ThT dans le chapitre I).

L'agrégation de l'insuline dans des conditions acides, en revanche, a reçu une caractérisation structurale détaillée : ces agrégats montrent toutes les caractéristiques structurelles de fibres amyloïdes : la structure des fibrilles [165] et le motif de diffraction au rayons-X typique des fibres amyloïdes [125]. Ballet a signalé la suppression des temps de latence à pH acide et à température élevée par seeding avec des agrégats d'insuline formés sur la surface dans des conditions physiologiques [186]. Ce seeding direct (si ce résultat est vrai) est une preuve très forte en faveur d'une structure commune ou très similaire. Le mécanisme d'agrégation étudié ici est donc en grande partie de type amyloïde quant à sa cinétique, sa structure secondaire et sa capacité de seeding, sans preuve structurelle définitive pour le moment.

4 Bibliographie

[1] L. Zhang, N. Li, F. Gao, L. Hou, Z. Xu, Insulin amyloid fibrils: An excellent platform for controlled synthesis of ultrathin superlong platinum nanowires with high electrocatalytic activity, J. Am. Chem. Soc. 134 (2012) 11326–11329. doi:10.1021/ja302959e.

[2] L.C. Cross, W. Klyne, Rules for the Nomenclature of Organic Chemistry Section E : Stereochemistry, Elsevier Science, 1976. doi:10.1351/pac197645010011.

[3] A. Mor, M. Amiche, P. Nicolas, Enter a new post-translational modification: d-amino acids in gene-encoded peptides, Trends Biochem. Sci. 17 (1992) 481–485. doi:10.1016/0968-0004(92)90333-5.

[4] J. Kyte, R.F. Doolittle, A simple method for displaying the hydropathic character of a protein, J. Mol. Biol. 157 (1982) 105–132. doi:10.1016/0022-2836(82)90515-0.

[5] A. Lehninger, D. Nelson, M. Cox, Principles of Biochemistry, 2008. citeulike-article-id:3823091%5Cnhttp://www.amazon.ca/exec/obidos/redirect?tag=citeulike09-20&#38%5Cnpath=ASIN/1429224169.

[6] K. Dasuri, P.J. Ebenezer, R.M. Uranga, E. Gavilán, L. Zhang, S.O.K. Fernandez-Kim, A.J. Bruce-Keller, J.N. Keller, Amino acid analog toxicity in primary rat neuronal and astrocyte cultures: Implications for protein misfolding and TDP-43 regulation, J. Neurosci. Res. 89 (2011) 1471–1477. doi:10.1002/jnr.22677.

[7] R.B. Merrifield, Solid Phase Peptide Synthesis. I. The Synthesis of a tetrapeptide, J. Am. Chem. Soc. 85 (1963) 2149. doi:10.1021/ja00897a025.

[8] A. Lesk, Introduction to Protein Science: Architecture, Function, and Genomics, OUP Oxford, 2010. https://books.google.com/books?hl=en&lr=&id=QVScAQAAQBAJ&pgis=1.

[9] C.R. Cantor, P.R. Schimmel, Biophysical Chemistry: Part I: The Conformation of Biological Macromolecules, W. H. Freeman, 1980. https://books.google.com/books?id=Jb0fQH1Eto0C&pgis=1.

[10] G.N. Ramachandran, C. Ramakrishnan, V. Sasisekharan, Stereochemistry of polypeptide chain configurations., J. Mol. Biol. 7 (1963) 95–99. doi:10.1016/S0022-2836(63)80023-6.

[11] V. Daggett, Alpha-sheet: The toxic conformer in amyloid diseases?, Acc. Chem. Res. 39 (2006) 594–602. doi:10.1021/ar0500719.

[12] B. Alberts, A. Johnson, J. Lewis, M. Raff, K. Roberts, P. Walter, Molecular Biology of the Cell, 2007. http://www.ncbi.nlm.nih.gov/books/NBK21054/.

[13] J.M. Berg, J.L. Tymoczko, L. Stryer, Biochemistry, W. H. Freeman, 2007. https://books.google.fr/books?id=Uhm_ngEACAAJ.

[14] K.E. Van Holde, Physical biochemistry, Prentice-Hall, 1985. https://books.google.fr/books?id=bdpqAAAAMAAJ.

[15] S.B. Zimmerman, S.O. Trach, Estimation of macromolecule concentrations and excluded volume effects for the cytoplasm of Escherichia coli, J. Mol. Biol. 222 (1991) 599–620. doi:10.1016/0022-2836(91)90499-V.

[16] A.P. Minton, Implications of macromolecular crowding for protein assembly, Curr.

Opin. Struct. Biol. 10 (2000) 34–39. doi:10.1016/S0959-440X(99)00045-7.

[17] D.A. White, A.K. Buell, T.P.J. Knowles, M.E. Welland, C.M. Dobson, Protein aggregation in crowded environments, J. Am. Chem. Soc. 132 (2010) 5170–5175. doi:10.1021/ja909997e.

[18] L.A. Munishkina, A. Ahmad, A.L. Fink, V.N. Uversky, Guiding protein aggregation with macromolecular crowding, Biochemistry. 47 (2008) 8993–9006. doi:10.1021/bi8008399.

[19] S. Sukenik, R. Politi, L. Ziserman, D. Danino, A. Friedler, D. Harries, Crowding alone cannot account for cosolute effect on amyloid aggregation, PLoS One. 6 (2011). doi:10.1371/journal.pone.0015608.

[20] K.E. Van Holde, W.C. Johnson, P.S. Ho, Principles of Physical Biochemistry, Pearson/Prentice Hall, 2006. doi:10.1021/ed076p474.1.

[21] T.W. Martin, Z.S. Derewenda, The name is bond--H bond., Nat. Struct. Biol. 6 (1999) 403–406. doi:10.1038/8195.

[22] C. Tanford, The hydrophobic effect: formation of micelles and biological membranes, Wiley, 1973. https://books.google.fr/books?id=ndpqAAAAMAAJ.

[23] E.E. Meyer, K.J. Rosenberg, J. Israelachvili, Recent progress in understanding hydrophobic interactions., Proc. Natl. Acad. Sci. U. S. A. 103 (2006) 15739–15746. doi:10.1073/pnas.0606422103.

[24] A. Fernández, Epistructural tension promotes protein associations, Phys. Rev. Lett. 108 (2012) 1–5. doi:10.1103/PhysRevLett.108.188102.

[25] A. Fernández, J. Kardos, R. Scott, Y. Goto, R.S. Berry, A. Fernandez, R.S. Berry, G. Guaitoli, D. Tondi, G. Marverti, D. Guerrieri, A. Ligabue, C. Pozzi, S. Mangani, D. Fessas, Correction for Fernandez et al., Structural defects and the diagnosis of amyloidogenic propensity, Proc. Natl. Acad. Sci. 108 (2011) 16133–16133. doi:10.1073/pnas.1112740108.

[26] A. Fernández, Keeping dry and crossing membranes, Nat. Biotechnol. 22 (2004) 1081–1084. doi:10.1038/nbt0904-1081.

[27] N. Pietrosemoli, A. Crespo, A. Fernández, Dehydration propensity of order-disorder intermediate regions in soluble proteins, J. Proteome Res. 6 (2007) 3519–3526. doi:10.1021/pr070208k.

[28] A. Fernandez, A. Crespo, Protein wrapping: a molecular marker for association, aggregation and drug design, Chem. Soc. Rev. 37 (2008) 2373–2382. doi:10.1039/b804150b.

[29] W. Norde, My voyage of discovery to proteins in flatland ...and beyond, Colloids Surfaces B Biointerfaces. 61 (2008) 1–9. doi:10.1016/j.colsurfb.2007.09.029.

[30] K. a Dill, H.S. Chan, From Levinthal to pathways to funnels., Nat. Struct. Biol. 4 (1997) 10–19. doi:10.1038/nsb0197-10.

[31] C.B. Anfinsen, Principles that Govern the Folding of Protein Chains, Science (80-.). 181 (1973) 223–230. doi:10.1126/science.181.4096.223.

[32] A.K. Dunker, I. Silman, V.N. Uversky, J.L. Sussman, Function and structure of inherently disordered proteins, Curr. Opin. Struct. Biol. 18 (2008) 756–764. doi:10.1016/j.sbi.2008.10.002.

[33] R. Van Der Lee, M. Buljan, B. Lang, R.J. Weatheritt, G.W. Daughdrill, A.K. Dunker, M. Fuxreiter, J. Gough, J. Gsponer, D.T. Jones, P.M. Kim, R.W. Kriwacki, C.J. Old, R. V Pappu, P. Tompa, V.N. Uversky, P.E. Wright, M.M. Babu, Classi fi cation of Intrinsically Disordered Regions and Proteins, Prog Biophys Mol Biol. (2015).

[34] J.J. Ward, J.S. Sodhi, L.J. McGuffin, B.F. Buxton, D.T. Jones, Prediction and Functional Analysis of Native Disorder in Proteins from the Three Kingdoms of Life, J. Mol. Biol. 337 (2004) 635–645. doi:10.1016/j.jmb.2004.02.002.

[35] C. Levinthal, Are there pathways for protein folding?, J. Chim. Phys. 65 (1968) 44–45. doi:10.1051/jcp/1968650044.

[36] A.N. Naganathan, V. Muñoz, Scaling of folding times with protein size, J. Am. Chem. Soc. 127 (2005) 480–481. doi:10.1021/ja044449u.

[37] M. Brylinski, L. Konieczny, I. Roterman, Hydrophobic collapse in (in silico) protein folding, Comput. Biol. Chem. 30 (2006) 255–267. doi:10.1016/j.compbiolchem.2006.04.007.

[38] M. Arai, K. Kuwajima, Rapid formation of a molten globule intermediate in refolding of α-lactalbumin, Fold. Des. 1 (1996) 275–287. doi:10.1016/S1359-0278(96)00041-7.

[39] K. a Dill, S. Bromberg, K. Yue, K.M. Fiebig, D.P. Yee, P.D. Thomas, H.S. Chan, Principles of protein folding--a perspective from simple exact models., Protein Sci. 4 (1995) 561–602. doi:10.1002/pro.5560040401.

[40] M. Jaremko, Ł. Jaremko, H.-Y. Kim, M.-K. Cho, C.D. Schwieters, K. Giller, S. Becker, M. Zweckstetter, Cold denaturation of a protein dimer monitored at atomic resolution., Nat. Chem. Biol. 9 (2013) 264–70. doi:10.1038/nchembio.1181.

[41] C.L. Dias, T. Ala-Nissila, J. Wong-ekkabut, I. Vattulainen, M. Grant, M. Karttunen, The hydrophobic effect and its role in cold denaturation, Cryobiology. 60 (2010) 91–99. doi:10.1016/j.cryobiol.2009.07.005.

[42] I.B. Bekard, D.E. Dunstan, Tyrosine autofluorescence as a measure of bovine insulin fibrillation, Biophys. J. 97 (2009) 2521–2531. doi:10.1016/j.bpj.2009.07.064.

[43] E.Y. Chi, S. Krishnan, T.W. Randolph, J.F. Carpenter, Physical Stability of Proteins in Aqueous Solution: Mechanism and Driving Forces in Nonnative Protein Aggregation, 20 (2003).

[44] A.L. Fink, Protein aggregation: Folding aggregates, inclusion bodies and amyloid, Fold. Des. 3 (1998) 9–23. doi:10.1016/S1359-0278(98)00002-9.

[45] G. Invernizzi, E. Papaleo, R. Sabate, S. Ventura, Protein aggregation: Mechanisms and functional consequences, Int. J. Biochem. Cell Biol. 44 (2012) 1541–1554. doi:10.1016/j.biocel.2012.05.023.

[46] W. Wang, S. Nema, D. Teagarden, Protein aggregation-Pathways and influencing factors, Int. J. Pharm. 390 (2010) 89–99. doi:10.1016/j.ijpharm.2010.02.025.

[47] J.L. Fast, A.A. Cordes, J.F. Carpenter, T.W. Randolph, Physical instability of a therapeutic Fc fusion protein: Domain contributions to conformational and colloidal stability, Biochemistry. 48 (2009) 11724–11736. doi:10.1021/bi900853v.

[48] B.H. Zimm, Application of the Methods of Molecular Distribution to Solutions of Large Molecules, J. Chem. Phys. 14 (1946) 164. doi:doi: 10.1063/1.1724116.

[49] B.L. Neal, D. Asthagiri, A.M. Lenhoff, Molecular Origins of Osmotic Second Virial

Coefficients of Proteins, Biophys. J. 75 (1998) 2469–2477. doi:10.1016/S0006-3495(98)77691-X.

[50] N. Senesi, K.J. Wilkinson, Biophysical Chemistry of Fractal Structures and Processes in Environmental Systems, Wiley, 2008. https://books.google.fr/books?id=tz4g10vI8LoC.

[51] D.S. Horne, Determination of the fractal dimension using turbidimetric techniques. Application to aggregating protein systems, Faraday Discuss. Chem. Soc. 83 (1987) 259. doi:10.1039/dc9878300259.

[52] M.Y. Lin, H.M. Lindsay, D.A. Weitz, R.C. Ball, R. Klein, P. Meakin, Universality in colloid aggregation, Nature. 339 (1989) 360–362. doi:10.1038/339360a0.

[53] M.Y. Lin, H.M. Lindsay, D.A. Weitz, R.C. Ball, R. Klein, P. Meakin, Universal reaction-limited colloid aggregation, Phys. Rev. A. 41 (1990) 2005–2020. doi:10.1103/PhysRevA.41.2005.

[54] L.R. De Young, A.L. Fink, K.A. Dill, Aggregation of globular proteins, Acc. Chem. Res. 26 (1993) 614–620. doi:10.1021/ar00036a002.

[55] J.A. Gavira, Current trends in protein crystallization, Arch. Biochem. Biophys. (2015). doi:10.1016/j.abb.2015.12.010.

[56] A. McPherson, J.A. Gavira, Introduction to protein crystallization, Acta Crystallogr. Sect. FStructural Biol. Commun. 70 (2014) 2–20. doi:10.1107/S2053230X13033141.

[57] M.A. Gertz, S. V Rajkumar, Amyloidosis: Diagnosis and Treatment, Humana Press, 2010. https://books.google.fr/books?id=-SyuFzJOKPwC.

[58] A.W.P. Fitzpatrick, Atomic structure and hierarchical assembly of a cross-β amyloid fibril - Supplementary Info, Proc Natl Acad Sci U S A. 5590 (2013) 5468–5473. doi:10.1073/pnas.1219476110/-/DCSupplemental.www.pnas.org/cgi/doi/10.1073/pnas.1219476110.

[59] G. Zandomeneghi, M.R.H. Krebs, M.G. McCammon, M. Fändrich, FTIR reveals structural differences between native beta-sheet proteins and amyloid fibrils., Protein Sci. 13 (2004) 3314–21. doi:10.1110/ps.041024904.

[60] A. Peim, P. Hortschansky, T. Christopeit, V. Schroeckh, W. Richter, M. Fändrich, Mutagenic exploration of the cross-seeding and fibrillation propensity of Alzheimer's beta-amyloid peptide variants., Protein Sci. 15 (2006) 1801–1805. doi:10.1110/ps.062116206.

[61] C.B. Andersen, H. Yagi, M. Manno, V. Martorana, T. Ban, G. Christiansen, D.E. Otzen, Y. Goto, C. Rischel, Branching in amyloid fibril growth, Biophys. J. 96 (2009) 1529–1536. doi:10.1016/j.bpj.2008.11.024.

[62] A. Assarsson, E. Hellstrand, C. Cabaleiro-Lago, S. Linse, Charge dependent retardation of amyloid amyloid β aggregation by hydrophilic proteins, ACS Chem. Neurosci. 5 (2014) 266–274. doi:10.1021/cn400124r.

[63] D.J. Martin, E.G. Randles, M. Ramirez-Alvarado, Fibril Structure and Fibrillogenesis, Amyloidosis: (2010). doi:10.1007/978-1-60761-631-3.

[64] C. Goldsbury, P. Frey, V. Olivieri, U. Aebi, S.A. Müller, Multiple assembly pathways underlie amyloid-beta fibril polymorphisms, J. Mol. Biol. 352 (2005) 282–298. doi:10.1016/j.jmb.2005.07.029.

[65] M. Sunde, L.C. Serpell, M. Bartlam, P.E. Fraser, M.B. Pepys, C.C.F. Blake, Common

Core Structure of Amyloid Fibrils by Synchrotron X-ray Diffraction, Diversity. (1997).

[66] A. Petkova, W.-M. Yau, R. Tycko, Experimental Constraints on Quaternary Structure in Alzheimer's β-Amyloid Fibrils, Biochemistry. 45 (2006) 498–512. http%5Cn//pubs.acs.org/doi/abs/10.1021/bi051952q.

[67] G. Comellas, C.M. Rienstra, Protein Structure Determination by Magic-Angle Spinning Solid-State NMR, and Insights into the Formation, Structure, and Stability of Amyloid Fibrils, Annu. Rev. Biophys. 42 (2013) 515–36. doi:10.1146/annurev-biophys-083012-130356.

[68] C. Wasmer, A. Lange, H. Van Melckebeke, A. Siemer, R. Riek, B.H. Meier, Amyloid Fibrils of the HET-s(218-289) Prion Form a β Solenoid with a Triangular Hydrophobic Core, Science (80-.). 319 (2008) 1523–1526. doi:10.1126/science.1151839.

[69] J.T. Nielsen, M. Bjerring, M.D. Jeppesen, R.O. Pedersen, J.M. Pedersen, K.L. Hein, T. Vosegaard, T. Skrydstrup, D.E. Otzen, N.C. Nielsen, Unique identification of supramolecular structures in amyloid fibrils by solid-state NMR spectroscopy, Angew. Chemie - Int. Ed. 48 (2009) 2118–2121. doi:10.1002/anie.200804198.

[70] D.S. Eisenberg, M.R. Sawaya, Implications for Alzheimer's disease of an atomic resolution structure of amyloid-β(1-42) fibrils., Proc. Natl. Acad. Sci. U. S. A. 113 (2016) 9398–400. doi:10.1073/pnas.1610806113.

[71] M. Biancalana, S. Koide, Molecular mechanism of Thioflavin-T binding to amyloid fibrils, Biochim. Biophys. Acta - Proteins Proteomics. 1804 (2010) 1405–1412. doi:10.1016/j.bbapap.2010.04.001.

[72] L.S. Wolfe, M.F. Calabrese, A. Nath, D. V Blaho, A.D. Miranker, Y. Xiong, Protein-induced photophysical changes to the amyloid indicator dye thioflavin T., Proc. Natl. Acad. Sci. U. S. A. 107 (2010) 16863–16868. doi:10.1073/pnas.1002867107.

[73] A.I. Sulatskaya, I.M. Kuznetsova, K.K. Turoverov, Interaction of thioflavin T with amyloid fibrils: Fluorescence quantum yield of bound dye, J. Phys. Chem. B. 116 (2012) 2538–2544. doi:10.1021/jp2083055.

[74] R. Khurana, C. Coleman, C. Ionescu-Zanetti, S.A. Carter, V. Krishna, R.K. Grover, R. Roy, S. Singh, Mechanism of thioflavin T binding to amyloid fibrils, J. Struct. Biol. 151 (2005) 229–238. doi:10.1016/j.jsb.2005.06.006.

[75] H. Levine, Thioflavine T Interaction with Amyloid β-Sheet Structures, AMYLOID-INTERNATIONAL J. Exp. Clin. Investig. 2 (1995) 1–6.

[76] M. Groenning, M. Norrman, J.M. Flink, M. van de Weert, J.T. Bukrinsky, G. Schluckebier, S. Frokjaer, Binding mode of Thioflavin T in insulin amyloid fibrils, J. Struct. Biol. 159 (2007) 483–497. doi:10.1016/j.jsb.2007.06.004.

[77] A.A. Maskevich, V.I. Stsiapura, V.A. Kuzmitsky, I.M. Kuznetsova, O.I. Povarova, V.N. Uversky, K.K. Turoverov, Spectral properties of thioflavin T in solvents with different dielectric properties and in a fibril-incorporated form, J. Proteome Res. 6 (2007) 1392–1401. doi:10.1021/pr0605567.

[78] A.A. Maskevich, A. V. Lavysh, I.M. Kuznetsova, A.I. Sulatskaya, K.K. Turoverov, Spectral Manifestations of Thioflavin T Aggregation, J. Appl. Spectrosc. 82 (2015) 33–39. doi:10.1007/s10812-015-0060-9.

[79] M. Groenning, L. Olsen, M. van de Weert, J.M. Flink, S. Frokjaer, F.S. Jørgensen, Study on the binding of Thioflavin T to β-sheet-rich and non-β-sheet cavities, J. Struct. Biol.

158 (2007) 358–369. doi:10.1016/j.jsb.2006.12.010.

[80] R. Sabate, L. Rodriguez-Santiago, M. Sodupe, S.J. Saupe, S. Ventura, Thioflavin-T excimer formation upon interaction with amyloid fibers., Chem. Commun. (Camb). 49 (2013) 5745–7. doi:10.1039/c3cc42040j.

[81] E.S. Voropai, M.P. Samtsov, K.N. Kaplevskii, A.A. Maskevich, V.I. Stepuro, O.I. Povarova, I.M. Kuznetsova, K.K. Turoverov, A.L. Fink, V.N. Uverskii, Spectral properties of thioflavin T and its complexes with amyloid fibrils, J. Appl. Spectrosc. 70 (2003) 868–874. doi:10.1023/B:JAPS.0000016303.37573.7e.

[82] M. Bucciantini, E. Giannoni, F. Chiti, F. Baroni, L. Formigli, J. Zurdo, N. Taddei, G. Ramponi, C.M. Dobson, M. Stefani, Inherent toxicity of aggregates implies a common mechanism for protein misfolding diseases., Nature. 416 (2002) 507–511. doi:10.1038/416507a.

[83] S. Kumar, A.K. Singh, G. Krishnamoorthy, R. Swaminathan, Thioflavin T displays enhanced fluorescence selectively inside anionic micelles and mammalian cells, J. Fluoresc. 18 (2008) 1199–1205. doi:10.1007/s10895-008-0378-2.

[84] A.J. Howie, D.B. Brewer, D. Howell, A.P. Jones, Physical basis of colors seen in Congo red-stained amyloid in polarized light, Lab. Investig. 88 (2008) 232–242. doi:10.1038/labinvest.3700714.

[85] J.D. Sipe, A.S. Cohen, Review: History of the Amyloid Fibril, J. Struct. Biol. 130 (2000) 88–98. doi:10.1006/jsbi.2000.4221.

[86] J.I. Guijarro, M. Sunde, J.A. Jones, I.D. Campbell, C.M. Dobson, Amyloid fibril formation by an SH3 domain, Proc Natl Acad Sci USA. 95 (1998) 4224–4228.

[87] F. Chiti, P. Webster, N. Taddei, A. Clark, M. Stefani, G. Ramponi, C.M. Dobson, Designing conditions for in vitro formation of amyloid protofilaments and fibrils., Proc. Natl. Acad. Sci. U. S. A. 96 (1999) 3590–4. doi:10.1073/pnas.96.7.3590.

[88] C.M. Dobson, Protein misfolding, evolution and disease, Trends Biochem. Sci. 24 (1999) 329–332. doi:10.1016/S0968-0004(99)01445-0.

[89] M. Balbirnie, R. Grothe, D.S. Eisenberg, An amyloid-forming peptide from the yeast prion Sup35 reveals a dehydrated beta-sheet structure for amyloid., Proc. Natl. Acad. Sci. U. S. A. 98 (2001) 2375–2380. doi:10.1073/pnas.041617698.

[90] R. Nelson, M.R. Sawaya, M. Balbirnie, A.Ø. Madsen, C. Riekel, R. Grothe, D. Eisenberg, Structure of the cross-β spine of amyloid-like fibrils, Nat. Cell Biol. 435 (2005) 773–778. doi:10.1038/nature03680.

[91] M.R. Sawaya, S. Sambashivan, R. Nelson, M.I. Ivanova, S.A. Sievers, M.I. Apostol, M.J. Thompson, M. Balbirnie, J.J.W. Wiltzius, H.T. McFarlane, A.Ø. Madsen, C. Riekel, D. Eisenberg, Atomic structures of amyloid cross-beta spines reveal varied steric zippers., Nature. 447 (2007) 453–7. doi:10.1038/nature05695.

[92] R. Jansen, S. Grudzielanek, W. Dzwolak, R. Winter, High pressure promotes circularly shaped insulin amyloid, J. Mol. Biol. 338 (2004) 203–206. doi:10.1016/j.jmb.2004.02.056.

[93] T.W. Randolph, M. Seefeldt, J.F. Carpenter, High hydrostatic pressure as a tool to study protein aggregation and amyloidosis, Biochim. Biophys. Acta - Protein Struct. Mol. Enzymol. 1595 (2002) 224–234. doi:10.1016/S0167-4838(01)00346-6.

[94] A. Trovato, F. Seno, S.C.E. Tosatto, The PASTA server for protein aggregation

prediction, Protein Eng. Des. Sel. 20 (2007) 521–523. doi:10.1093/protein/gzm042.

[95] Y. Kallberg, M. Gustafsson, B. Persson, J. Thyberg, J. Johansson, Prediction of Amyloid Fibril-forming Proteins *, 276 (2001) 12945–12950. doi:10.1074/jbc.M010402200.

[96] G.G. Tartaglia, A.P. Pawar, S. Campioni, C.M. Dobson, F. Chiti, M. Vendruscolo, Prediction of Aggregation-Prone Regions in Structured Proteins, J. Mol. Biol. 380 (2008) 425–436. doi:10.1016/j.jmb.2008.05.013.

[97] A.P. Pawar, K.F. DuBay, J. Zurdo, F. Chiti, M. Vendruscolo, C.M. Dobson, Prediction of "aggregation-prone" and "aggregation- susceptible" regions in proteins associated with neurodegenerative diseases, J. Mol. Biol. 350 (2005) 379–392. doi:10.1016/j.jmb.2005.04.016.

[98] J. Varga, M.S.M. Flinn, T. Shirahama, O.G. Rodgers, A.S. Cohen, The induction of accelerated murine amyloid with human splenic extract - Probable role of amyloid enhancing factor, Virchows Arch. B Cell Pathol. Incl. Mol. Pathol. 51 (1986) 177–185. doi:10.1007/BF02899027.

[99] K. Ono, R. Takahashi, T. Ikeda, M. Yamada, Cross-seeding effects of amyloid β-protein and α-synuclein, J. Neurochem. 122 (2012) 883–890. doi:10.1111/j.1471-4159.2012.07847.x.

[100] G. Meisl, J.B. Kirkegaard, P. Arosio, T.C.T. Michaels, M. Vendruscolo, C.M. Dobson, S. Linse, T.P.J. Knowles, Molecular mechanisms of protein aggregation from global fitting of kinetic models, Nat. Protoc. 11 (2016) 252–272. doi:10.1038/nprot.2016.010.

[101] D. Kashchiev, G.M. van Rosmalen, Review: Nucleation in solutions revisited, Cryst. Res. Technol. 38 (2003) 555–574. doi:10.1002/crat.200310070.

[102] R.P. Sear, Nucleation: theory and applications to protein solutions and colloidal suspensions, J. Phys. Condens. Matter. 19 (2007) 33101–28. doi:10.1088/0953-8984/19/3/033101.

[103] J.W.P. Schmelzer, Nucleation Theory and Applications, Wiley, 2006. https://books.google.fr/books?id=1V2lUqF7kKAC.

[104] V. Kalikmanov, Nucleation Theory, Springer Netherlands, 2012. https://books.google.fr/books?id=GKC5BQAAQBAJ.

[105] R.P. Sear, Nucleation: theory and applications to protein solutions and colloidal suspensions, J. Phys. Condens. Matter. 19 (2007) 33101. doi:10.1088/0953-8984/19/3/033101.

[106] R. Wetzel, Kinetics and thermodynamics of amyloid fibril assembly, Acc. Chem. Res. 39 (2006) 671–679. doi:10.1021/ar050069h.

[107] E. Žerovnik, Amyloid-fibril formation: Proposed mechanisms and relevance to conformational disease, Eur. J. Biochem. 269 (2002) 3362–3371. doi:10.1046/j.1432-1033.2002.03024.x.

[108] W.-F. Xue, S.W. Homans, S.E. Radford, Systematic analysis of nucleation-dependent polymerization reveals new insights into the mechanism of amyloid self-assembly., Proc. Natl. Acad. Sci. U. S. A. 105 (2008) 8926–31. doi:10.1073/pnas.0711664105.

[109] S.I.A. Cohen, S. Linse, L.M. Luheshi, E. Hellstrand, D.A. White, L. Rajah, D.E. Otzen, M. Vendruscolo, C.M. Dobson, T.P.J. Knowles, Proliferation of amyloid-β42 aggregates occurs through a secondary nucleation mechanism., Proc. Natl. Acad. Sci. U. S. A. 110 (2013) 9758–63. doi:10.1073/pnas.1218402110.

[110] S.I.A. Cohen, M. Vendruscolo, C.M. Dobson, T.P.J. Knowles, From macroscopic measurements to microscopic mechanisms of protein aggregation, J. Mol. Biol. 421 (2012) 160–171. doi:10.1016/j.jmb.2012.02.031.

[111] A.M. Morris, M.A. Watzky, R.G. Finke, Protein aggregation kinetics, mechanism, and curve-fitting: a review of the literature., Biochim. Biophys. Acta. 1794 (2009) 375–97. doi:10.1016/j.bbapap.2008.10.016.

[112] D.M. Walsh, A. Lomakin, G.B. Benedek, M.M. Condron, D.B. Teplow, Amyloid β-Protein Fibrillogenesis, J. Biol. Chem. 272 (1997) 22364–22372. doi:citeulike-article-id:1477308 doi: 10.1074/jbc.272.35.22364.

[113] M.D. Kirkitadze, M.M. Condron, D.B. Teplow, Identification and characterization of key kinetic intermediates in amyloid beta-protein fibrillogenesis., J. Mol. Biol. 312 (2001) 1103–19. doi:10.1006/jmbi.2001.4970.

[114] J.W. Kelly, Mechanisms of amyloidogenesis., Nat. Struct. Biol. 7 (2000) 824–826. doi:10.1038/82815.

[115] T.R. Serio, A.G. Cashikar, A.S. Kowal, G.J. Sawicki, J.J. Moslehi, L. Serpell, M.F. Arnsdorf, S.L. Lindquist, Nucleated Conformational Conversion and the Replication of Conformational Information by a Prion Determinant, Science (80-.). 289 (2000) 1317–1321. doi:10.1126/science.289.5483.1317.

[116] M.M. Pallitto, R.M. Murphy, A mathematical model of the kinetics of beta-amyloid fibril growth from the denatured state., Biophys. J. 81 (2001) 1805–1822. doi:10.1016/S0006-3495(01)75831-6.

[117] J.T. Giurleo, X. He, D.S. Talaga, β-Lactoglobulin Assembles into Amyloid through Sequential Aggregated Intermediates, J. Mol. Biol. 381 (2008) 1332–1348. doi:10.1016/j.jmb.2008.06.043.

[118] R.D. Hills, C.L. Brooks, Hydrophobic Cooperativity as a Mechanism for Amyloid Nucleation, J. Mol. Biol. 368 (2007) 894–901. doi:10.1016/j.jmb.2007.02.043.

[119] R.S. Armen, B.M. Bernard, R. Day, D.O. V Alonso, V. Daggett, Characterization of a possible amyloidogenic precursor in glutamine-repeat neurodegenerative diseases., Proc. Natl. Acad. Sci. U. S. A. 102 (2005) 13433–8. doi:10.1073/pnas.0502068102.

[120] H. Muta, Y.H. Lee, J. Kardos, Y. Lin, H. Yagi, Y. Goto, Supersaturation-limited Amyloid fibrillation of Insulin revealed by ultrasonication, J. Biol. Chem. 289 (2014) 18228–18238. doi:10.1074/jbc.M114.566950.

[121] M. So, D. Hall, Y. Goto, Revisiting supersaturation as a factor determining amyloid fibrillation, Curr. Opin. Struct. Biol. 36 (2016) 32–39. doi:10.1016/j.sbi.2015.11.009.

[122] L. Zhang, L. Wang, Y.-T. Kao, W. Qiu, Y. Yang, O. Okobiah, D. Zhong, Mapping hydration dynamics around a protein surface., Proc. Natl. Acad. Sci. U. S. A. 104 (2007) 18461–6. doi:10.1073/pnas.0707647104.

[123] H.J. Dyson, P.E. Wright, H. a Scheraga, The role of hydrophobic interactions in initiation and propagation of protein folding., Proc. Natl. Acad. Sci. U. S. A. 103 (2006) 13057–13061. doi:10.1073/pnas.0605504103.

[124] H.A. Lashuel, C. Wurth, L. Woo, J.W. Kelly, The most pathogenic transthyretin variant, L55P, forms amyloid fibrils under acidic conditions and protofilaments under physiological conditions, Biochemistry. 38 (1999) 13560–13573. doi:10.1021/bi991021c.

[125] M.I. Ivanova, S.A. Sievers, M.R. Sawaya, J.S. Wall, D. Eisenberg, Molecular basis for insulin fibril assembly, Proc. Natl. Acad. Sci. 106 (2009) 18990–18995. doi:10.1073/pnas.0910080106.

[126] P.O. Souillac, V.N. Uversky, I.S. Millett, R. Khurana, S. Doniach, A.L. Fink, Elucidation of the molecular mechanism during the early events in immunoglobulin light chain amyloid fibrillation. Evidence for an off-pathway oligomer at acidic pH, J. Biol. Chem. 277 (2002) 12666–12679. doi:10.1074/jbc.M109229200.

[127] D.R. Hekstra, K.I. White, M.A. Socolich, R.W. Henning, V. Šrajer, R. Ranganathan, Electric-field-stimulated protein mechanics, Nature. 540 (2016) 400–405. doi:10.1038/nature20571.

[128] R.D. Astumian, B. Robertson, Nonlinear effect of an oscillating electric field on membrane proteins, J. Chem. Phys. 91 (1989) 4891–4900. doi:10.1063/1.456728.

[129] P. Ball, J.E. Hallsworth, Water structure and chaotropicity: their uses, abuses and biological implications, Phys. Chem. Chem. Phys. 17 (2015) 8297–8305. doi:10.1039/C4CP04564E.

[130] K.D. Collins, Ions from the Hofmeister series and osmolytes : e V ects on proteins in solution and in the crystallization process, 34 (2004) 300–311. doi:10.1016/j.ymeth.2004.03.021.

[131] J.H. Crowe, Trehalose as a "chemical chaperone": Fact and fantasy, Adv. Exp. Med. Biol. 594 (2007) 143–158. doi:10.1007/978-0-387-39975-1-13.

[132] J. Jayamani, G. Shanmugam, E. Ramaprasad, A. Singam, Inhibition of insulin amyloid fibril formation by ferulic acid , a natural compound found in many vegetables and fruits, RSC Adv. 4 (2014) 62326–62336. doi:10.1039/C4RA11291A.

[133] J. Jaspe, S.J. Hagen, Do protein molecules unfold in a simple shear flow?, Biophys. J. 91 (2006) 3415–3424. doi:10.1529/biophysj.106.089367.

[134] W. Norde, Protein adsorption at solid surfaces: A thermodynamic approach, Pure Appl. Chem. (1994). http://www.degruyter.com/view/j/pac.1994.66.issue-3/pac199466030491/pac199466030491.xml (accessed August 11, 2016).

[135] S.H. Mollmann, L. Jorgensen, J.T. Bukrinsky, U. Elofsson, W. Norde, S. Frokjaer, Interfacial adsorption of insulin: Conformational changes and reversibility of adsorption, Eur. J. Pharm. Sci. 27 (2006) 194–204. doi:10.1016/j.ejps.2005.09.010.

[136] H.H. Bauer, M. Muller, J. Goette, H.P. Merkle, U.P. Fringeli, Interfacial adsorption and aggregation associated changes in secondary structure of human calcitonin monitored by ATR-FTIR spectroscopy, Biochemistry. 33 (1994) 12276–12282. doi:10.1021/bi00206a034.

[137] V. Ball, P. Huetz, A. Elaissari, J.P. Cazenave, J.-C. Voegel, P. Schaaf, Kinetics of Exchange Processes in the Adsorption of Proteins on Solid Surfaces, Proc. Natl. Acad. Sci. Nat. Acad. Sci. U.S.A. 91 (1994) 7330–7334. doi:10.1073/pnas.91.15.7330.

[138] C. Schladitz, E.P. Vieira, H. Hermel, H. Mohwald, Amyloid-β-sheet formation at the air-water interface, Biophys. J. 77 (1999) 3305–3310. doi:10.1016/S0006-3495(99)77161-4.

[139] G. a Holdgate, Thermodynamics of binding interactions in the rational drug design process., Expert Opin. Drug Discov. 2 (2007) 1103–14. doi:10.1517/17460441.2.8.1103.

[140] A.T. Alexandrescu, Amyloid accomplices and enforcers., Protein Sci. 14 (2005) 1–12.

doi:10.1110/ps.04887005.

[141] C.J. Maynard, A.I. Bush, C.L. Masters, R. Cappai, Q.-X. Li, Metals and amyloid-beta in Alzheimer's disease., Int. J. Exp. Pathol. 86 (2005) 147–159. doi:10.1111/j.0959-9673.2005.00434.x.

[142] H. Eury, C. Bijani, P. Faller, C. Hureau, Copper(II) coordination to amyloid β: Murine versus human peptide, Angew. Chemie - Int. Ed. 50 (2011) 901–905. doi:10.1002/anie.201005838.

[143] C. Hureau, Coordination of redox active metal ions to the amyloid precursor protein and to amyloid-β peptides involved in Alzheimer disease. Part 1: An overview, Coord. Chem. Rev. 256 (2012) 2164–2174. doi:10.1016/j.ccr.2012.03.037.

[144] B. Alies, V. Pradines, I. Llorens-Alliot, S. Sayen, E. Guillon, C. Hureau, P. Faller, Zinc(II) modulates specifically amyloid formation and structure in model peptides, J. Biol. Inorg. Chem. 16 (2011) 333–340. doi:10.1007/s00775-010-0729-8.

[145] J. Ma, A. Yee, H.B. Brewer, S. Das, H. Potter, Amyloid-associated proteins α1-antichymotrypsin and apolipoprotein E promote assembly of Alzheimer β-protein into filaments, Nature. 372 (1994) 92–94. doi:10.1038/372092a0.

[146] S. Eriksson, S. Janciauskiene, L. Lannfelt, Alpha 1-antichymotrypsin regulates Alzheimer beta-amyloid peptide fibril formation, Proc Natl Acad Sci U S A. 92 (1995) 2313–2317. doi:10.1073/pnas.92.6.2313.

[147] I. Pallarès, J. Vendrell, F.X. Avilés, S. Ventura, Amyloid fibril formation by a partially structured intermediate state of α-chymotrypsin, J. Mol. Biol. 342 (2004) 321–331. doi:10.1016/j.jmb.2004.06.089.

[148] T. Wisniewski, E.M. Castaño, A. Golabek, T. Vogel, B. Frangione, Acceleration of Alzheimer's fibril formation by apolipoprotein E in vitro., Am. J. Pathol. 145 (1994) 1030–5. http://www.pubmedcentral.nih.gov/articlerender.fcgi?artid=1887417&tool=pmcentrez&rendertype=abstract.

[149] K.C. Evans, E.P. Berger, C.G. Cho, K.H. Weisgraber, P.T. Lansbury, Apolipoprotein E is a kinetic but not a thermodynamic inhibitor of amyloid formation: implications for the pathogenesis and treatment of Alzheimer disease., Proc. Natl. Acad. Sci. U. S. A. 92 (1995) 763–7. doi:10.1073/pnas.92.3.763.

[150] J. McLaurin, D. Yang, C.M. Yip, P.E. Fraser, Review: modulating factors in amyloid-β fibril formation, J Struct Biol. 130 (2000) 259–270. doi:10.1006/jsbi.2000.4289.

[151] J.P. Mayer, F. Zhang, R.D. DiMarchi, Insulin structure and function, Biopolym. - Pept. Sci. Sect. 88 (2007) 687–713. doi:10.1002/bip.20734.

[152] G.B. Treacy, D.C. Shaw, M.E. Griffiths, P.D. Jeffrey, Purification of a marsupial insulin: amino-acid sequence of insulin from the Eastern grey kangaroo Macropus giganteus, Biochim. Biophys. Acta - Gen. Subj. 990 (1989) 263–268. doi:10.1016/S0304-4165(89)80043-1.

[153] O. Wintersteiner, a Abramson, Isoelectric Point of Insulin, J. Biol. Chem. 99 (1933) 741–753. http://www.jbc.org/content/99/3/741.full.pdf.

[154] B.H. Frank, A.H. Pekar, A.J. Veros, Insulin and Proinsulin Conformation in Solution, Diabetes. 21 (1972) 486–491. doi:10.2337/diab.21.2.S486.

[155] L.A. Holladay, M. Ascoli, D. Puett, Conformational stability and self-association of

zinc-free bovine insulin at neutral pH, BBA - Protein Struct. 494 (1977) 245–254. doi:10.1016/0005-2795(77)90152-0.

[156] S. Hvidt, Insulin association in neutral solutions studied by light scattering, Biophys. Chem. 39 (1991) 205–213. doi:10.1016/0301-4622(91)85023-J.

[157] D.F. Waugh, A fibrous modification of insulin. I. The heat precipitate of insulin., J. Am. Chem. Soc. 68 (1946) 247–50. doi:10.1021/ja01206a030.

[158] D.F. Waugh, R.E. Thompson, R.J. Weimer, Assay of insulin in vitro by fibril elongation and precipitation., J. Biol. Chem. 185 (1950) 85–95.

[159] L.N. Garriques, S. Frokjaer, J.F. Carpenter, J. Brange, The effect of mutations on the structure of insulin fibrils studied by Fourier transform infrared (FTIR) spectroscopy and electron microscopy, J. Pharm. Sci. 91 (2002) 2473–2480. doi:10.1002/jps.10238.

[160] C.-C. Lee, A. Nayak, A. Sethuraman, G. Belfort, G.J. McRae, A three-stage kinetic model of amyloid fibrillation., Biophys. J. 92 (2007) 3448–3458. doi:10.1529/biophysj.106.098608.

[161] B. Vestergaard, M. Groenning, M. Roessle, J.S. Kastrup, M. Van De Weert, J.M. Flink, S. Frokjaer, M. Gajhede, D.I. Svergun, A helical structural nucleus is the primary elongating unit of insulin amyloid fibrils, PLoS Biol. 5 (2007) 1089–1097. doi:10.1371/journal.pbio.0050134.

[162] L. Nielsen, R. Khurana, A. Coats, S. Frokjaer, J. Brange, S. Vyas, V.N. Uversky, A.L. Fink, Effect of Environmental Factors on the Kinetics of Insulin Fibril Formation, Biochemistry. 40 (2001) 6036–6046. doi:Doi 10.1021/Bi002555c.

[163] M. Bouchard, J. Zurdo, E.J. Nettleton, C.M. Dobson, C. V Robinson, Formation of insulin amyloid fibrils followed by FTIR simultaneously with CD and electron microscopy., Protein Sci. 9 (2000) 1960–1967. doi:10.1110/ps.9.10.1960.

[164] C. Dutta, M. Yang, F. Long, R. Shahbazian-Yassar, A. Tiwari, Preformed Seeds Modulate Native Insulin Aggregation Kinetics, J. Phys. Chem. B. 119 (2015) 15089–15099. doi:10.1021/acs.jpcb.5b07221.

[165] J.L. Jiménez, E.J. Nettleton, M. Bouchard, C. V Robinson, C.M. Dobson, H.R. Saibil, The protofilament structure of insulin amyloid fibrils., Proc. Natl. Acad. Sci. U. S. A. 99 (2002) 9196–201. doi:10.1073/pnas.142459399.

[166] M. Mauro, E.F. Craparo, A. Podestà, D. Bulone, R. Carrotta, V. Martorana, G. Tiana, P.L. San Biagio, Kinetics of Different Processes in Human Insulin Amyloid Formation, J. Mol. Biol. 366 (2007) 258–274. doi:10.1016/j.jmb.2006.11.008.

[167] M. Manno, E.F. Craparo, V. Martorana, D. Bulone, P.L. San Biagio, Kinetics of insulin aggregation: disentanglement of amyloid fibrillation from large-size cluster formation., Biophys. J. 90 (2006) 4585–4591. doi:10.1529/biophysj.105.077636.

[168] A. Nayak, A.K. Dutta, G. Belfort, Surface-enhanced nucleation of insulin amyloid fibrillation., Biochem. Biophys. Res. Commun. 369 (2008) 303–7. doi:10.1016/j.bbrc.2008.01.159.

[169] D. Waugh, A mechanism for the formation of fibrils from protein molecules, J. Cell. Comp. Physiol. (1957) 145–164. doi:10.1002/jcp.1030490415.

[170] M. V. Sefton, G.M. Antonacci, Adsorption isotherms of insulin onto various materials, Diabetes. 33 (1984) 674–680. doi:10.2337/diabetes.33.7.674.

[171] W.D. Lougheed, A.M. Albisser, H.M. Martindale, J.C. Chow, J.R. Clement, Physical stability of insulin formulations, Diabetes. 32 (1983) 424–432. doi:10.2337/diabetes.32.5.424.

[172] E.W. Feingold, V; Jenkins, A B; Kraegen, Effect of contact material on vibraction-induced insulin aggregation, Diabetologia. (1984) 373–378.

[173] V. Sluzky, J. a Tamada, a M. Klibanov, R. Langer, Kinetics of insulin aggregation in aqueous solutions upon agitation in the presence of hydrophobic surfaces., Proc. Natl. Acad. Sci. U. S. A. 88 (1991) 9377–81. http://www.pubmedcentral.nih.gov/articlerender.fcgi?artid=52720&tool=pmcentrez&rendertype=abstract.

[174] K. Irsigler, H. Kritz, G. Hagmüller, M. Franetzki, K. Prestele, H. Thurow, K. Geisen, Long-term continuous intraperitoneal insulin infusion with an implanted remote-controlled insulin infusion device., Diabetes. 30 (1981) 1072–1075.

[175] H. Kritz, G. Hagmüller, R. Lovett, K. Irsigler, Implanted constant basal rate insulin infusion devices for type 1 (Insulin-dependent) diabetic patients, Diabetologia. 25 (1983) 78–81. doi:10.1007/BF00250891.

[176] K. Irsigler, H. Kritz, Long-term continuous intravenous insulin therapy with a portable insulin dosage-regulating apparatus, Diabetes. 28 (1979) 196–203.

[177] L. W.D., W.-F. H., C. J.R., A. A.M., W.D. Lougheed, H. Woulfe-Flanagan, J.R. Clement, A.M. Albisser, Insulin aggregation in artificial delivery systems, Diabetologia. 19 (1980) 1–9. doi:10.1007/BF00258302.

[178] S.D. Yeo, P.G. Debenedetti, S.Y. Patro, T.M. Przybycien, Secondary structure characterization of microparticulate insulin powders, J. Pharm. Sci. 83 (1994) 1651–1656. doi:10.1002/jps.2600831203.

[179] B. Swift, P. Hawkins, Examination of insulin injection sites: an unexpected finding of localized amyloidosis, Diabet. Med. (2002) 881–886. http://onlinelibrary.wiley.com/doi/10.1046/j.1464-5491.2002.07581.x/abstract (accessed April 22, 2014).

[180] Y. Shikama, J. Kitazawa, N. Yagihashi, O. Uehara, Y. Murata, N. Yajima, R. Wada, S. Yagihashi, Localized Amyloidosis at the Site of Repeated Insulin Injection in a Diabetic Patient, Intern. Med. 49 (2010) 397–401. doi:10.2169/internalmedicine.49.2633.

[181] S. Grudzielanek, A. Velkova, A. Shukla, V. Smirnovas, M. Tatarek-Nossol, H. Rehage, A. Kapurniotu, R. Winter, Cytotoxicity of Insulin within its Self-assembly and Amyloidogenic Pathways, J. Mol. Biol. 370 (2007) 372–384. doi:10.1016/j.jmb.2007.04.053.

[182] V. Sluzky, a M. Klibanov, R. Langer, Mechanism of insulin aggregation and stabilization in agitated aqueous solutions., Biotechnol. Bioeng. 40 (1992) 895–903. doi:10.1002/bit.260400805.

[183] L. Nault, P. Guo, B. Jain, Y. Bréchet, F. Bruckert, M. Weidenhaupt, Human insulin adsorption kinetics, conformational changes and amyloidal aggregate formation on hydrophobic surfaces., Acta Biomater. 9 (2013) 5070–9. doi:10.1016/j.actbio.2012.09.025.

[184] S. Mauri, R. Pandey, I. Rzeźnicka, H. Lu, M. Bonn, T. Weidner, Bovine and human insulin adsorption at lipid monolayers: a comparison, Front. Phys. 3 (2015) 1–6. doi:10.3389/fphy.2015.00051.

[185] S.H. Mollmann, L. Jorgensen, J.T. Bukrinsky, U. Elofsson, W. Norde, S. Frokjaer, Interfacial adsorption of insulin: Conformational changes and reversibility of adsorption, Eur. J. Pharm. Sci. 27 (2006) 194–204. doi:10.1016/j.ejps.2005.09.010.

[186] T. Ballet, Stabilité des protéines thérapeutiques au contact des matériaux: Agrégation induite par les surfaces et détection des changements de conformation à l'aide de protéines chaperonnes, 2010.

[187] L. Nault, C. Vendrely, Y. Bréchet, F. Bruckert, M. Weidenhaupt, Peptides that form β-sheets on hydrophobic surfaces accelerate surface-induced insulin amyloidal aggregation., FEBS Lett. 587 (2013) 1281–6. doi:10.1016/j.febslet.2012.11.036.

[188] W. DeGrado, J. Lear, Induction of peptide conformation at apolar water interfaces. 1. A study with model peptides of defined hydrophobic periodicity, J. Am. Chem. Soc. 107 (1985) 7684–7689. doi:10.1021/ja00311a076.

[189] R. Khurana, A.L. Fink, Do Parallel β-Helix Proteins Have a Unique Fourier Transform Infrared Spectrum?, Biophys. J. 78 (2000) 994–1000. doi:10.1016/S0006-3495(00)76657-4.

[190] E. Cerf, R. Sarroukh, S. Tamamizu-Kato, L. Breydo, S. Derclaye, Y.F. Dufrêne, V. Narayanaswami, E. Goormaghtigh, J.-M. Ruysschaert, V. Raussens, Antiparallel β-sheet: a signature structure of the oligomeric amyloid β-peptide, Biochem. J. 421 (2009) 415–423. doi:10.1042/BJ20090379.

[191] N. Demirdöven, C.M. Cheatum, H.S. Chung, M. Khalil, J. Knoester, A. Tokmakoff, Two-dimensional infrared spectroscopy of antiparallel beta-sheet secondary structure, J. Am. Chem. Soc. 126 (2004) 7981–7990. doi:10.1021/ja049811j.

[192] T. Frachon, F. Bruckert, Q. Le Masne, E. Monnin, M. Weidenhaupt, Insulin aggregation at a dynamic solid-liquid-air triple interface, Langmuir. (2016) acs.langmuir.6b03314. doi:10.1021/acs.langmuir.6b03314.

[193] M. Dathe, K. Gast, D. Zirwer, H. Welfle, B. Mehlis, Insulin aggregation in solution., Int. J. Pept. Protein Res. 36 (1990) 344–349.

[194] C.L. Teoh, I.B. Bekard, P. Asimakis, M.D.W. Griffin, T.M. Ryan, D.E. Dunstan, G.J. Howlett, Shear flow induced changes in apolipoprotein C-II conformation and amyloid fibril formation, Biochemistry. 50 (2011) 4046–4057. doi:10.1021/bi2002482.

[195] I.B. Bekard, D.E. Dunstan, Shear-Induced deformation of bovine insulin in couette flow, J. Phys. Chem. B. 113 (2009) 8453–8457. doi:10.1021/jp903522e.

[196] S.A. McBride, C.F. Tilger, S.P. Sanford, P.M. Tessier, A.H. Hirsa, Comparison of Human and Bovine Insulin Amyloidogenesis under Uniform Shear, J. Phys. Chem. B. 119 (2015) 10426–10433. doi:10.1021/acs.jpcb.5b04488.

[197] L. Nault, Mécanismes moléculaires de l'agrégation de l'insuline induite par la surface des matériaux, 2013.

[198] K.G. Sprenger, J. Pfaendtner, Strong Electrostatic Interactions Lead to Entropically Favorable Binding of Peptides to Charged Surfaces, Langmuir. 32 (2016) 5690–5701. doi:10.1021/acs.langmuir.6b01296.

[199] L.M. Pandey, S. Le Denmat, D. Delabouglise, F. Bruckert, S.K. Pattanayek, M. Weidenhaupt, Surface chemistry at the nanometer scale influences insulin aggregation., Colloids Surf. B. Biointerfaces. 100 (2012) 69–76. doi:10.1016/j.colsurfb.2012.05.022.

[200] C. Dalgicdir, C. Globisch, C. Peter, M. Sayar, Tipping the Scale from Disorder to Alpha-

helix: Folding of Amphiphilic Peptides in the Presence of Macroscopic and Molecular Interfaces, PLoS Comput. Biol. 11 (2015) 1–24. doi:10.1371/journal.pcbi.1004328.

[201] K. Chouchane, C. Vendrely, M. Amari, K. Moreaux, F. Bruckert, M. Weidenhaupt, Dual Effect of (LK)nL Peptides on the Onset of Insulin Amyloid Fiber Formation at Hydrophobic Surfaces, J. Phys. Chem. B. 119 (2015) 10543–10553. doi:10.1021/acs.jpcb.5b07365.

[202] R.L. Millican, D.N. Brems, Equilibrium intermediates in the denaturation of human insulin and two monomeric insulin analogs., Biochemistry. 33 (1994) 1116–1124. doi:10.1021/bi00171a010.

[203] H.L. Chiang, S.T. Ngo, C.J. Chen, C.K. Hu, M.S. Li, Oligomerization of Peptides LVEALYL and RGFFYT and Their Binding Affinity to Insulin, PLoS One. 8 (2013). doi:10.1371/journal.pone.0065358.

[204] J. Brange, L. Andersen, E.D. Laursen, G. Meyn, E. Rasmussen, Toward understanding insulin fibrillation, J. Pharm. Sci. 86 (1997) 517–525. doi:10.1021/js960297s.

[205] S. Saha, S. Deep, Glycerol inhibits the primary pathways and transforms the secondary pathway of insulin aggregation, Phys. Chem. Chem. Phys. 18 (2016) 18934–18948. doi:10.1039/C6CP02906J.

[206] S. Saha, A. Sharma, S. Deep, Differential influence of additives on the various stages of insulin aggregation, RSC Adv. 6 (2016) 28640–28652. doi:10.1039/C5RA27206H.

[207] F. Belluti, A. Rampa, S. Gobbi, A. Bisi, Small-molecule inhibitors/modulators of amyloid-β peptide aggregation and toxicity for the treatment of Alzheimer's disease: a patent review (2010 - 2012)., Expert Opin. Ther. Pat. 23 (2013) 581–96. doi:10.1517/13543776.2013.772983.

[208] N. Ferreira, I. Cardoso, M.R. Domingues, R. Vitorino, M. Bastos, G. Bai, M.J. Saraiva, M.R. Almeida, Binding of epigallocatechin-3-gallate to transthyretin modulates its amyloidogenicity, FEBS Lett. 583 (2009) 3569–3576. doi:10.1016/j.febslet.2009.10.062.

[209] N. Ferreira, S.A.O. Santos, M.R.M. Domingues, M.J. Saraiva, M.R. Almeida, Dietary curcumin counteracts extracellular transthyretin deposition: Insights on the mechanism of amyloid inhibition, Biochim. Biophys. Acta - Mol. Basis Dis. 1832 (2013) 39–45. doi:10.1016/j.bbadis.2012.10.007.

[210] S.A. Hudson, H. Ecroyd, T.W. Kee, J.A. Carver, The thioflavin T fluorescence assay for amyloid fibril detection can be biased by the presence of exogenous compounds, FEBS J. 276 (2009) 5960–5972. doi:10.1111/j.1742-4658.2009.07307.x.

[211] M. Necula, R. Kayed, S. Milton, C.G. Glabe, Small molecule inhibitors of aggregation indicate that amyloid beta-oligomerization and fibrillization pathways are independent and distinct, J. Biol. Chem. 282 (2007) 10311–10324. doi:10.1074/jbc.M608207200.

[212] I. Horvath, C.F. Weise, E.K. Andersson, E. Chorell, M. Sellstedt, C. Bengtsson, A. Olofsson, S.J. Hultgren, M. Chapman, M. Wolf-Watz, F. Almqvist, P. Wittung-Stafshede, Mechanisms of protein oligomerization: Inhibitor of functional amyloids templates α-synuclein fibrillation, J. Am. Chem. Soc. 134 (2012) 3439–3444. doi:10.1021/ja209829m.

[213] A. Ghosh, N. Pradhan, S. Bera, A. Datta, J. Krishnamoorthy, N.R. Jana, A. Bhunia, Inhibition and Degradation of Amyloid Beta (Aβ40) Fibrillation by Designed Small Peptide: A Combined Spectroscopy, Microscopy, and Cell Toxicity Study, ACS Chem.

Neurosci. 8 (2017) 718–722. doi:10.1021/acschemneuro.6b00349.

[214] S.A. Sievers, J. Karanicolas, H.W. Chang, A. Zhao, L. Jiang, O. Zirafi, J.T. Stevens, J. Münch, D. Baker, D. Eisenberg, Structure-based design of non-natural amino-acid inhibitors of amyloid fibril formation, Nature. 475 (2011) 96–100. doi:10.1038/nature10154.

[215] C. Soto, M.S. Kindy, M. Baumann, B. Frangione, Inhibition of Alzheimer's Amyloidosis by Peptides That Prevent β-Sheet Conformation, Biochem. Biophys. Res. Commun. 226 (1996) 672–680. doi:10.1006/bbrc.1996.1413.

[216] P. De Bona, M.L. Giuffrida, F. Caraci, A. Copani, B. Pignataro, F. Attanasio, S. Cataldo, G. Pappalardo, E. Rizzarelli, Design and synthesis of new trehalose-conjugated pentapeptides as inhibitors of Aβ(1-42) fibrillogenesis and toxicity, J. Pept. Sci. 15 (2009) 220–228. doi:10.1002/psc.1109.

[217] M.H. Viet, S.T. Ngo, N.S. Lam, M.S. Li, Inhibition of aggregation of amyloid peptides by beta-sheet breaker peptides and their binding affinity, J. Phys. Chem. B. 115 (2011) 7433–7446. doi:10.1021/jp1116728.

[218] M. Richman, S. Wilk, M. Chemerovski, S.K.T.S. Wärmländer, A. Wahlström, A. Gräslund, S. Rahimipour, In vitro and mechanistic studies of an antiamyloidogenic self-assembled cyclic D, l-$α$-peptide architecture, J. Am. Chem. Soc. 135 (2013) 3474–3484.

[219] L.O. Tjernberg, J. Näslund, F. Lindqvist, J. Johansson, a R. Karlström, J. Thyberg, L. Terenius, C. Nordstedt, Arrest of beta-amyloid fibril formation by a pentapeptide ligand., J. Biol. Chem. 271 (1996) 8545–8548. doi:10.1074/jbc.271.15.8545.

[220] M.A. Wälti, F. Ravotti, H. Arai, C.G. Glabe, J.S. Wall, A. Böckmann, P. Güntert, B.H. Meier, R. Riek, Atomic-resolution structure of a disease-relevant Aβ(1-42) amyloid fibril., Proc. Natl. Acad. Sci. U. S. A. 113 (2016) E4976-84. doi:10.1073/pnas.1600749113.

[221] M.M. Pallitto, J. Ghanta, P. Heinzelman, L.L. Kiessling, R.M. Murphy, Recognition sequence design for peptidly modulators of ß-amyloid aggregation and toxicity, Biochemistry. 38 (1999) 3570–3578.

[222] T.L. Lowe, A. Strzelec, L.L. Kiessling, R.M. Murphy, Structure - Function relationships for inhibitors of beta-Amyloid toxicity containing the recognition sequence KLVFF, Biochemistry. 40 (2001) 7882–7889. doi:10.1021/bi002734u.

[223] J. Chabry, B. Caughey, B. Chesebro, Specific inhibition of in vitro formation of protease-resistant prion protein by synthetic peptides., J Biol Chem. 273 (1998) 13203–13207.

[224] S. Nyström, P. Hammarström, Generic amyloidogenicity of mammalian prion proteins from species susceptible and resistant to prions, Sci. Rep. 5 (2015) 10101. doi:10.1038/srep10101.

[225] A. Kapurniotu, A. Schmauder, K. Tenidis, Structure-based design and study of non-amyloidogenic, double N-methylated IAPP amyloid core sequences as inhibitors of IAPP amyloid formation and cytotoxicity., J. Mol. Biol. 315 (2002) 339–350. doi:10.1006/jmbi.2001.5244.

[226] S. Khan, G. Newaz, A comprehensive review of surface modification for neural cell adhesion and patterning, J Biomed Mater Res A. 93 (2010) 1209–1224. doi:10.1002/jbm.a.32698.

[227] H. Zhu, M. Snyder, Protein arrays and microarrays, Curr. Opin. Chem. Biol. 5 (2001) 40–45. doi:10.1016/S1367-5931(00)00170-8.

[228] A. Roda, M. Guardigli, C. Russo, P. Pasini, M. Baraldini, Protein microdeposition using a conventional ink-jet printer, Biotechniques. 28 (2000) 492–496.

[229] T. Nishimura, M. Takara, S. Mukai, S. Sawada, Y. Sasaki, K. Akiyoshi, A Light Sensitive Self-Assembled Nanogel as a Tecton for Protein Patterning Materials., Chem. Commun. 52 (2015) 1222–1225. doi:10.1039/C5CC08416D.

[230] C. Grunwald, K. Schulze, A. Reichel, V.U. Weiss, D. Blaas, J. Piehler, K.-H. Wiesmüller, R. Tampé, In situ assembly of macromolecular complexes triggered by light., Proc. Natl. Acad. Sci. U. S. A. 107 (2010) 6146–6151. doi:10.1073/pnas.0912617107.

[231] C.A. DeForest, D.A. Tirrell, A photoreversible protein-patterning approach for guiding stem cell fate in three-dimensional gels., Nat. Mater. 14 (2015) 523–531. doi:10.1038/nmat4219.

[232] E.G. Govorunova, O.A. Sineshchekov, H. Li, J.L. Spudich, Microbial Rhodopsins: Diversity, Mechanisms, and Optogenetic Applications, Annu. Rev. Biochem. 86 (2017) 15–31.

[233] C.D.P. Duffy, L. Valkunas, A. V Ruban, L. Valkūnas, A. V Ruban, Light-harvesting processes in the dynamic photosynthetic antenna., Phys. Chem. Chem. Phys. 15 (2013) 18752–70. doi:10.1039/c3cp51878g.

[234] H. Mizuno, T.K. Mal, K.I. Tong, R. Ando, T. Furuta, M. Ikura, A. Miyawaki, Photo-induced peptide cleavage in the green-to-red conversion of a fluorescent protein, Mol. Cell. 12 (2003) 1051–1058. doi:10.1016/S1097-2765(03)00393-9.

[235] R. Ando, H. Hama, M. Yamamoto-Hino, H. Mizuno, A. Miyawaki, An optical marker based on the UV-induced green-to-red photoconversion of a fluorescent protein., Proc. Natl. Acad. Sci. U. S. A. 99 (2002) 12651–12656. doi:10.1073/pnas.202320599.

[236] T. Okada, M. Sugihara, A.N. Bondar, M. Elstner, P. Entel, V. Buss, The retinal conformation and its environment in rhodopsin in light of a new 2.2 Å crystal structure, J. Mol. Biol. 342 (2004) 571–583. doi:10.1016/j.jmb.2004.07.044.

[237] J.P. Zayner, T.R. Sosnick, Factors that control the chemistry of the LOV domain photocycle, PLoS One. 9 (2014). doi:10.1371/journal.pone.0087074.

[238] C. Renicke, D. Schuster, S. Usherenko, L.O. Essen, C. Taxis, A LOV2 domain-based optogenetic tool to control protein degradation and cellular function, Chem. Biol. 20 (2013) 619–626. doi:10.1016/j.chembiol.2013.03.005.

[239] M. Morikawa, T. Senda, M. Suzuki, T. Kobayashi, H. Miyazawa, K. Kino, Formation of a flavin-linked cysteine, Proc. 17th Int. Electron. Conf. Synth. Org. Chem. (2013) b002. doi:10.3390/ecsoc-17-b002.

Contrôler l'agrégation de l'insuline à la surface des matériaux via des interactions avec des peptides et la lumière.

Le repliement et la stabilité des protéines dépendent des conditions physico-chimiques de leur environnement. En particulier, le pH, la température, l'agitation et les interactions avec d'autres macromolécules ou avec les interfaces (liquide–surfaces des matériaux ; air-liquide ; etc.) sont connues pour induire des phénomènes de dénaturation et d'agrégation des protéines.

Le contrôle de la stabilité des protéines thérapeutiques représente un enjeu médical et économique pour l'industrie pharmaceutique. L'insuline, qui est la protéine thérapeutique la plus produite, est connue in vitro pour former des fibres amyloïdes induites par les surfaces hydrophobes. Les agrégations amyloïdes sont également impliquées dans un certain nombre de pathologies, notamment humaines et animales présentant de forts enjeux de santé publique et économiques.

Cette thèse traite en particulier de l'agrégation amyloïde à la surface des matériaux en utilisant l'insuline comme protéine modèle. Les travaux précédents réalisés par notre équipe ont démontré que des peptides de courte longueur avaient la capacité de modifier très significativement la cinétique d'agrégation induite par la surface des matériaux, et ce à des concentrations sub-stœchiométriques par rapport à l'insuline. En particulier les peptides adoptant une conformation secondaire en feuillet beta une fois adsorbés sur les surfaces hydrophobes, induisent une réduction drastique de la durée de nucléation de fibres amyloïdes d'insuline.

Dans les travaux présentés ici nous avons découvert des séquences peptidiques présentant, toujours à des concentrations sub-stœchiométriques, deux effets antagonistes sur la cinétique de l'agrégation amyloïde de l'insuline. Le premier effet, coopératif et localisé à la surface de matériaux hydrophobes, résulte en une accélération de la nucléation. A l'inverse le second effet provient des peptides en solution et résulte en une puissante inhibition à la fois de la nucléation et de l'élongation des fibres.

Nous avons premièrement caractérisé quantitativement ces effets pour un ensemble de peptides possédant des séquences de type (LK)nL, et investigué les mécanismes à l'origine du phénomène accélérateur. Des mesures quantitatives de fluorescence (Thioflavine T, marquage fluorescent du peptide) ont permis de montrer que l'adsorption coopérative des peptides sur la surface du matériau était responsable de l'accélération de la vitesse de nucléation. Pour l'effet inhibiteur, provenant des peptides en solution, nous avons démontré que cet effet résulte de la liaison des peptides sur l'insuline fibrillaire et qu'il est médié par les charge.

De surcroit nous avons étudié la localisation de la nucléation et de l'apparition des premiers agrégats par microscopie à fluorescence. Nous avons observé que les zones situées à l'interface triple matériau-air-solution et subissant une contrainte de cisaillement élevé étaient les sites préférentiels d'apparition des premiers agrégats amyloïdes et donc très probablement les régions dominantes en termes de nucléation.

Nous avons enfin développé une technique permettant une croissance localisée, patternable et induite par la lumière d'agrégats amyloïde d'insuline sur une surface de verre. Cette voie d'agrégation singulière ne présente pas de phase de nucléation apparente et dépend strictement de la présence de Thioflavine T. Nous avons montré que la Thioflavine T insérée entre les feuillets béta et qui peut être excitée à 440 nm fournit localement l'énergie nécessaire pour la transition de conformation de l'insuline native adsorbée vers l'état agrégé. Cette méthode permet d'obtenir une croissance différentielle entre des zones de surface hydrophile et hydrophobe.

Controlling surface mediated insulin aggregation by peptides and light

The folding and stability of proteins depend on the physico-chemical conditions of their environment. Especially pH, temperature, stirring and interactions with other macromolecules or with interfaces (liquid-material surfaces; air-liquid; etc.) are known to induce protein denaturation and aggregation phenomena.

The control of therapeutic protein stability represents a medical and economic challenge for the pharmaceutic industry. For instance insulin, which is the most s model produced therapeutic protein, is known to form amyloid aggregates in vitro induced by hydrophobic surfaces. Amyloid aggregates are also involved in several pathologies including human and animal diseases of high economic and public health impact.

This thesis focuses on amyloid aggregation at material surfaces using insulin as a model protein. Previous work from our team have demonstrated that short peptides have the ability to significantly interfere with the kinetics of surface-driven amyloid aggregation and this at sub-stoichiometric concentrations with respect to insulin. In particular peptides adopting a beta-sheet secondary structure when adsorbed on hydrophobic surfaces, were able to reduce the nucleation time of insulin aggregation.

In the present work we have discovered peptide sequences presenting, again at sub-stoichiometric concentrations, two antagonistic effects on insulin aggregation kinetics. The first consists in a cooperative reduction of the nucleation time and operates via peptides bound to the material surface. The second, on the other hand, results in a powerful inhibition of both nucleation and fiber elongation via peptides remaining in solution.

We have first quantitatively characterized these effects on a set of peptides presenting alternate primary sequences of the type (LK)nL, and investigated the underlying mechanisms promoting insulin nucleation. Quantitative fluorescence measurements (Thioflavin T, fluorescent labelling of the peptide) have shown that the cooperative adsorption of peptides on hydrophobic material surfaces was responsible for the reduction of the insulin nucleation time. We have then shown that the inhibitory effect results from the binding of peptides in solution to fibrillar insulin aggregates and that this effect is mediated by charges.

In addition we studied the localization of the insulin nucleation and of the appearance of the first aggregates using fluorescence microscopy. We observed the preferential appearance of the first ThT positive aggregates at the solid-liquid-air triple interface undergoing high shear stress, making these regions the predominant nucleation sites.

We eventually developed a technique allowing a localized and patterned growth of light-induced insulin aggregates on glass surfaces. This atypical aggregation pathway does not present any observable lag time and depends strictly on Thioflavin T. We have shown that the ThT inserted between the cross beta-sheets and which can be excited at 440 nm locally provides the energy required for the conformational transition of the native insulin into the aggregated one. This method can be used to obtain a differential amyloid growth between surface area of different hydrophobicity.